

DEVELOPMENT OF WIND SPEED CONTOURS FOR 2017 ATLANTIC BASIN LAND FALLING HURRICANES

Hurricane Harvey
Hurricane Irma
Hurricane Maria
Hurricane Nate

March 2019



FEMA

Page intentionally left blank.

CREDITS

Prepared by:

Lauren A. Mudd, Ph.D., P.E., Applied Research Associates (ARA), Inc., a member of Compass PTS JV

Peter J. Vickery, Ph.D., P.E., ARA Inc., a member of Compass PTS JV

Fangqian Liu, Ph.D., P.E., ARA Inc., a member of Compass PTS JV

Francis M. Lavelle, Ph.D., P.E., ARA Inc., a member of Compass PTS JV

Charles “Chip” Isetts, Project Manager, ABSG Consulting, a member of Compass PTS JV

Edited by:

Zachary Henry, Technical Editor, ABSG Consulting, a member of Compass PTS JV

Reviewed by:

Casey Zuzak, GISP, Senior Risk Analyst, FEMA – Natural Hazards Risk Assessment Program

Prepared by request of the National Hazards Risk Assessment Program (NHRAP).

For any questions or feedback, please send an email to fema-nhrap@fema.dhs.gov.

Master Services Agreement No.16S-17353-DC18

Contract No. HSFE60-15-D-0003

Task Order No. 04

Delivery Order No. 70FA6018F00000034

TABLE OF CONTENTS

LIST OF TABLES.....	V
LIST OF FIGURES.....	V
1 INTRODUCTION	1
2 WIND FIELD MODELING	1
2.1 MODEL OVERVIEW	1
2.2 MODEL UNCERTAINTY AND EVALUATION	2
2.2.1 <i>Uncertainty in Modeling</i>	2
2.2.2 <i>Goodness of Fit Statistic</i>	3
3 METHODOLOGY.....	3
3.1 DATA COLLECTION	3
3.1.1 <i>NHC Best Track</i>	3
3.1.2 <i>Surface Observations</i>	3
3.2 DATA CORRECTIONS	4
3.2.1 <i>Correction for Height and Averaging Period</i>	5
3.2.2 <i>Correction for Surrounding Terrain</i>	6
3.3 UNCERTAINTY IN DATA CORRECTIONS	7
3.3.1 <i>Uncertainty in Anemometer Height Correction</i>	8
3.3.2 <i>Uncertainty in Averaging Period Correction</i>	8
3.3.3 <i>Uncertainty in Surrounding Terrain Correction</i>	9
4 HURRICANE HARVEY	11
4.1 EVENT BACKGROUND.....	11
4.2 DATA COLLECTION	12
4.2.1 <i>Track</i>	12
4.2.2 <i>Observations</i>	12
4.3 DATA CORRECTIONS (DEVIATION FROM STANDARD PROCEDURES)	14
4.4 DISCUSSION OF SELECT STATION TIME HISTORIES	15
4.5 ERRORS AND UNCERTAINTY.....	31
4.6 WIND FIELD MAP	34
5 HURRICANE IRMA (CONUS).....	36
5.1 EVENT BACKGROUND.....	36
5.2 DATA COLLECTION	36
5.2.1 <i>Track</i>	36
5.2.2 <i>Observations</i>	37
5.3 DATA CORRECTIONS (DEVIATION FROM STANDARD PROCEDURES)	38
5.4 DISCUSSION OF SELECT STATION TIME HISTORIES	39
5.5 ERRORS AND UNCERTAINTY.....	58
5.6 WIND FIELD MAP	61
6 HURRICANE IRMA (OCONUS)	63
6.1 EVENT BACKGROUND.....	63
6.2 DATA COLLECTION	63
6.2.1 <i>Track</i>	63

6.2.2	Observations	64
6.3	DATA CORRECTIONS (DEVIATION FROM STANDARD PROCEDURES)	65
6.4	DISCUSSION OF SELECT STATION TIME HISTORIES	68
6.5	ERRORS AND UNCERTAINTY	85
6.6	WIND FIELD MAPS	88
7	HURRICANE MARIA	92
7.1	EVENT BACKGROUND	92
7.2	DATA COLLECTION	92
7.2.1	Track	92
7.2.2	Observations	93
7.3	DATA CORRECTIONS (DEVIATION FROM STANDARD PROCEDURES)	94
7.4	DISCUSSION OF SELECT STATION TIME HISTORIES	97
7.5	ERRORS AND UNCERTAINTY	112
7.6	WIND FIELD MAPS	114
8	HURRICANE NATE	118
8.1	EVENT BACKGROUND	118
8.2	DATA COLLECTION	119
8.2.1	Track	119
8.2.2	Observations	119
8.3	DISCUSSION OF SELECT STATION TIME HISTORIES	120
8.4	ERRORS AND UNCERTAINTY	136
8.5	WIND FIELD MAP	138
9	SUMMARY	140
10	REFERENCES	140
APPENDIX A.	HURRICANE HARVEY	A-1
APPENDIX A.1	SURFACE OBSERVATION STATION DETAILS	A-1
APPENDIX A.2	MODELED AND OBSERVED STATION TIME HISTORIES	A-2
APPENDIX A.3	STATION DIRECTIONAL SURFACE ROUGHNESS VALUES	A-43
APPENDIX A.4	AERIAL IMAGERY OF STATIONS WITH VISUALLY ESTIMATED SURFACE ROUGHNESS	A-45
APPENDIX B.	HURRICANE IRMA (CONUS)	B-1
APPENDIX B.1	SURFACE OBSERVATION STATION DETAILS	B-1
APPENDIX B.2	MODELED AND OBSERVED STATION TIME HISTORIES	B-3
APPENDIX B.3	STATION DIRECTIONAL SURFACE ROUGHNESS VALUES	B-64
APPENDIX B.4	AERIAL IMAGERY OF STATIONS WITH VISUALLY ESTIMATED SURFACE ROUGHNESS	B-66
APPENDIX C.	HURRICANE IRMA (OCONUS)	C-1
APPENDIX C.1	SURFACE OBSERVATION STATION DETAILS	C-1
APPENDIX C.2	MODELED AND OBSERVED STATION TIME HISTORIES	C-2
APPENDIX C.3	STATION DIRECTIONAL SURFACE ROUGHNESS VALUES	C-26
APPENDIX C.4	AERIAL IMAGERY OF STATIONS WITH VISUALLY ESTIMATED SURFACE ROUGHNESS	C-27
APPENDIX D.	HURRICANE MARIA	D-1
APPENDIX D.1	SURFACE OBSERVATION STATION DETAILS	D-1
APPENDIX D.2	MODELED AND OBSERVED STATION TIME HISTORIES	D-2

APPENDIX D.3	STATION DIRECTIONAL SURFACE ROUGHNESS VALUES.....	D-19
APPENDIX D.4	AERIAL IMAGERY OF STATIONS WITH VISUALLY ESTIMATED SURFACE ROUGHNESS	D-20
APPENDIX E.	HURRICANE NATE.....	E-1
APPENDIX E.1	SURFACE OBSERVATION STATION DETAILS	E-1
APPENDIX E.2	MODELED AND OBSERVED STATION TIME HISTORIES	E-3
APPENDIX E.3	STATION DIRECTIONAL SURFACE ROUGHNESS VALUES.....	E-54

LIST OF TABLES

TABLE 3-1.	PARAMETERS FOR CUBIC WIND SPEED TERRAIN ADJUSTMENT FACTOR VERSUS $\ln(z_0)$	7
TABLE 4-1.	ERRORS IN MODELED PEAK GUST WIND SPEED IN HURRICANE HARVEY WHEN OBSERVATIONS ARE CORRECTED FOR HEIGHT ONLY AND FOR HEIGHT AND TERRAIN. ALL WIND SPEED VALUES ARE PRESENTED AT 10 M ELEVATION IN OPEN TERRAIN.	33
TABLE 5-1.	ERRORS IN MODELED PEAK GUST WIND SPEED IN HURRICANE IRMA WHEN OBSERVATIONS ARE CORRECTED FOR HEIGHT ONLY AND FOR HEIGHT AND TERRAIN. ALL WIND SPEED VALUES ARE PRESENTED AT 10 M ELEVATION IN OPEN TERRAIN.	60
TABLE 6-1.	ERRORS IN MODELED PEAK GUST WIND SPEED IN HURRICANE IRMA OCONUS WHEN OBSERVATIONS ARE CORRECTED FOR HEIGHT ONLY AND FOR HEIGHT AND TERRAIN. ALL WIND SPEED VALUES ARE PRESENTED AT 10 M ELEVATION IN OPEN TERRAIN.....	88
TABLE 7-1.	ERRORS IN MODELED PEAK GUST WIND SPEED IN HURRICANE MARIA WHEN OBSERVATIONS ARE CORRECTED FOR HEIGHT ONLY AND FOR HEIGHT AND TERRAIN. ALL WIND SPEED VALUES ARE PRESENTED AT 10 M ELEVATION IN OPEN TERRAIN.	113
TABLE 8-1.	ERRORS IN MODELED PEAK GUST WIND SPEED IN HURRICANE NATE WHEN OBSERVATIONS ARE CORRECTED FOR HEIGHT ONLY AND FOR HEIGHT AND TERRAIN. ALL WIND SPEED VALUES ARE PRESENTED AT 10 M ELEVATION IN OPEN TERRAIN.	137

LIST OF FIGURES

FIGURE 3-1.	DIRECTIONAL EFFECTIVE SURFACE ROUGHNESS LENGTH FOR NAPLES MUNICIPAL AIRPORT COMPUTED IN MASTERS ET AL. (2010) AND USED HEREIN.	4
FIGURE 3-2.	(LEFT TO RIGHT) NDBC STATIONS 42020, RSJT2, AND ANPT2 WITH ANEMOMETERS LOCATED AT HEIGHTS OF 4, 10, AND 14.22 M ABOVE SEA LEVEL.	5
FIGURE 3-3.	GUST WIND SPEED ADJUSTMENT FACTORS FOR VARIOUS ANEMOMETER HEIGHTS WITH TYPICAL EFFECTIVE AIRPORT SURFACE ROUGHNESS VALUES.	8
FIGURE 3-4.	GUST FACTOR VS. GUST DURATION FOR OPEN TERRAIN.	9
FIGURE 3-5.	GUST WIND SPEED CORRECTION FACTOR AT A HEIGHT OF 10 M DUE TO SURFACE ROUGHNESS AS A FUNCTION OF THE EFFECTIVE UPSTREAM SURFACE ROUGHNESS.	10
FIGURE 4-1.	BEST-TRACK INFORMATION OF HURRICANE HARVEY (2017) COLLECTED FROM THE NHC ATLANTIC HURRICANE DATABASE (HURDAT2).	12
FIGURE 4-2.	ASOS AND NDBC STATIONS WITH SURFACE OBSERVATIONS DURING THE LIFESPAN AND WITHIN 150 MILES OF HURRICANE HARVEY.	13
FIGURE 4-3.	NDBC STATIONS LOCATED NEAR THE PERIOD OF HIGH WINDS PRIOR TO AND DURING LANDFALL OF HURRICANE HARVEY (2017).....	14
FIGURE 4-4.	NDBC STATION PTAT2 LOCATED VERY NEARSHORE WITH A BEACH PARK LOCATED TO THE NORTH AND RESIDENTIAL STRUCTURES LOCATED TO THE WEST.	15
FIGURE 4-5.	MODELED AND OBSERVED METEOROLOGICAL TIME SERIES AT NDBC STATION 42002: 207 NM EAST OF BROWNSVILLE, TEXAS.....	17
FIGURE 4-6.	MODELED AND OBSERVED METEOROLOGICAL TIME SERIES AT NDBC STATION 42045: TGLO TABS BUOY K.....	18

FIGURE 4-7. MODELED AND OBSERVED METEOROLOGICAL TIME SERIES AT NDBC STATION 42020: 60NM SSE OF CORPUS CHRISTI, TEXAS.	19
FIGURE 4-8. MODELED AND OBSERVED METEOROLOGICAL TIME SERIES AT THE TEXAS COASTAL OBSERVING NETWORK’S STATION IRDT2: SOUTH BIRD ISLAND, TEXAS.	20
FIGURE 4-9. MODELED AND OBSERVED METEOROLOGICAL TIME SERIES AT THE TEXAS COASTAL OBSERVING NETWORK’S STATION ANPT2: ARANSAS PASS, TEXAS.	21
FIGURE 4-10. MODELED AND OBSERVED METEOROLOGICAL TIME SERIES AT ASOS STATION KRKP: ARANSAS COUNTY AIRPORT.	22
FIGURE 4-11. MODELED AND OBSERVED METEOROLOGICAL TIME SERIES AT THE TEXAS COASTAL OBSERVING NETWORK’S STATION AWRT2: ARANSAS WILDLIFE REFUGE, TEXAS.	23
FIGURE 4-12. MODELED AND OBSERVED METEOROLOGICAL TIME SERIES AT THE TEXAS COASTAL OBSERVING NETWORK’S STATION VCAT2: PORT LAVACA, TEXAS.	24
FIGURE 4-13. MODELED AND OBSERVED METEOROLOGICAL TIME SERIES AT NDBC STATION 42019: 60 NM SOUTH OF FREEPORT, TEXAS.	25
FIGURE 4-14. MODELED AND OBSERVED METEOROLOGICAL TIME SERIES AT ASOS STATION KPIL: PORT ISABEL CAMERON COUNTY AIRPORT.	26
FIGURE 4-15. MODELED AND OBSERVED METEOROLOGICAL TIME SERIES AT ASOS STATION KALI: ALICE INTERNATIONAL AIRPORT.	27
FIGURE 4-16. MODELED AND OBSERVED METEOROLOGICAL TIME SERIES AT ASOS STATION KSAT: SAN ANTONIO INTERNATIONAL AIRPORT.	28
FIGURE 4-17. MODELED AND OBSERVED METEOROLOGICAL TIME SERIES AT ASOS STATION KBMQ: BURNET MUNICIPAL AIRPORT – KATE CRADDOCK FIELD.	29
FIGURE 4-18. MODELED AND OBSERVED METEOROLOGICAL TIME SERIES AT ASOS STATION KLBX: TEXAS GULF COAST REGIONAL AIRPORT.	30
FIGURE 4-19. MODELED AND OBSERVED MAXIMUM PEAK GUST WIND SPEED CORRECTED ONLY FOR HEIGHT (LEFT) AND CORRECTED FOR HEIGHT AND TERRAIN (RIGHT).	31
FIGURE 4-20. MODELED AND OBSERVED MINIMUM CENTRAL PRESSURE.	32
FIGURE 4-21. AERIAL VIEW OF TEXAS COASTAL OBSERVING NETWORK STATION CPNT2.	32
FIGURE 4-22. AERIAL VIEW OF TEXAS COASTAL OBSERVING NETWORK STATION AWRT2.	33
FIGURE 4-23. PEAK GUST WIND SPEED CONTOUR MAP FOR HURRICANE HARVEY (2017) SHOWING ESTIMATED 3-SECOND PEAK GUST WIND SPEEDS (MPH) AT 10 M ABOVE GROUND OVER OPEN TERRAIN. MODEL OUTPUT OBTAINED FROM ARA WIND FIELD MODEL FIT TO SURFACE LEVEL OBSERVATIONS USING NHC BEST TRACK AND CENTRAL PRESSURES.	35
FIGURE 5-1. BEST-TRACK INFORMATION OF HURRICANE IRMA (2017) COLLECTED FROM THE NHC ATLANTIC HURRICANE DATABASE (HURDAT2).	37
FIGURE 5-2. ASOS, NDBC AND UNIVERSITY OF FLORIDA MOBILE STATIONS WITH SURFACE OBSERVATIONS IN AND NEAR THE CONTIGUOUS UNITED STATES DURING THE LIFESPAN AND WITHIN 150 MILES OF HURRICANE IRMA.	38
FIGURE 5-3. NOAA NATIONAL OCEAN SERVICE STATION VCAF1 LOCATED VERY NEARSHORE WITH CONDOMINIUMS, RESIDENTIAL STRUCTURES, AND AN UNINHABITED ISLAND LOCATED TO THE EAST AND SOUTH.	39
FIGURE 5-4. MODELED AND OBSERVED METEOROLOGICAL TIME SERIES AT NDBC STATION PLSF1: PULASKI SHOALS LIGHT, FLORIDA.	41
FIGURE 5-5. MODELED AND OBSERVED METEOROLOGICAL TIME SERIES AT NDBC STATION VCAF1: VACA KEY, FLORIDA.	42
FIGURE 5-6. MODELED AND OBSERVED METEOROLOGICAL TIME SERIES AT NDBC STATION FWYF1: FOWEY ROCK, FLORIDA.	43
FIGURE 5-7. MODELED AND OBSERVED METEOROLOGICAL TIME SERIES AT ASOS STATION KRSW: SOUTHWEST FLORIDA INTERNATIONAL AIRPORT.	44
FIGURE 5-8. MODELED AND OBSERVED METEOROLOGICAL TIME SERIES AT ASOS STATION KSRQ: SARASOTA-BRADENTON INTERNATIONAL AIRPORT.	45
FIGURE 5-9. MODELED AND OBSERVED METEOROLOGICAL TIME SERIES AT ASOS STATION KOPF: MIAMI-OPA LOCKA EXECUTIVE AIRPORT.	46
FIGURE 5-10. MODELED AND OBSERVED METEOROLOGICAL TIME SERIES AT ASOS STATION KPBI: PALM BEACH INTERNATIONAL AIRPORT.	47
FIGURE 5-11. MODELED AND OBSERVED METEOROLOGICAL TIME SERIES AT ASOS STATION KFPR: TREASURE COAST INTERNATIONAL AIRPORT AND BUSINESS PARK.	48

FIGURE 5-12. MODELED AND OBSERVED METEOROLOGICAL TIME SERIES AT ASOS STATION KGIF: WINTER HAVEN REGIONAL AIRPORT.	49
FIGURE 5-13. MODELED AND OBSERVED METEOROLOGICAL TIME SERIES AT ASOS STATION KORL: ORLANDO EXECUTIVE AIRPORT.	50
FIGURE 5-14. MODELED AND OBSERVED METEOROLOGICAL TIME SERIES AT ASOS STATION KDAB: DAYTONA BEACH INTERNATIONAL AIRPORT.	51
FIGURE 5-15. MODELED AND OBSERVED METEOROLOGICAL TIME SERIES AT ASOS STATION KCRG: JACKSONVILLE EXECUTIVE AT CRAIG AIRPORT.	52
FIGURE 5-16. MODELED AND OBSERVED METEOROLOGICAL TIME SERIES AT ASOS STATION KVLD: VALDOSTA REGIONAL AIRPORT.	53
FIGURE 5-17. MODELED AND OBSERVED METEOROLOGICAL TIME SERIES AT ASOS STATION KDHN: DOTHAN REGIONAL AIRPORT.	54
FIGURE 5-18. MODELED AND OBSERVED METEOROLOGICAL TIME SERIES AT ASOS STATION KGZH: MIDDLETON FIELD.	55
FIGURE 5-19. MODELED AND OBSERVED METEOROLOGICAL TIME SERIES AT ASOS STATION KSAV: SAVANNAH/HILTON HEAD INTERNATIONAL AIRPORT.	56
FIGURE 5-20. MODELED AND OBSERVED METEOROLOGICAL TIME SERIES AT ASOS STATION KAHN: ATHENS-BEN EPPS AIRPORT.	57
FIGURE 5-21. MODELED AND OBSERVED MAXIMUM PEAK GUST WIND SPEED CORRECTED ONLY FOR HEIGHT (LEFT) AND CORRECTED FOR HEIGHT AND TERRAIN (RIGHT).	58
FIGURE 5-22. MODELED AND OBSERVED MINIMUM CENTRAL PRESSURE.	59
FIGURE 5-23. AERIAL VIEW OF NDBC STATION VCAF1.	59
FIGURE 5-24. PEAK GUST WIND SPEED CONTOUR MAP FOR HURRICANE IRMA (2017) SHOWING ESTIMATED 3-SECOND PEAK GUST WIND SPEEDS (MPH) AT 10 M ABOVE GROUND OVER OPEN TERRAIN. MODEL OUTPUT OBTAINED FROM ARA WIND FIELD MODEL FIT TO SURFACE LEVEL OBSERVATIONS USING NHC BEST TRACK AND CENTRAL PRESSURES.	62
FIGURE 6-1. BEST-TRACK INFORMATION OF HURRICANE IRMA (2017) COLLECTED FROM THE NHC ATLANTIC HURRICANE DATABASE (HURDAT2).	64
FIGURE 6-2. ASOS AND NDBC STATIONS IN AND NEAR THE VIRGIN ISLANDS AND PUERTO RICO WITH SURFACE OBSERVATIONS DURING THE LIFESPAN AND WITHIN 150 MILES OF HURRICANE IRMA.	65
FIGURE 6-3. NOAA NATIONAL OCEAN SERVICE STATION LTBV3 LOCATED VERY NEARSHORE WITH A REFINERY, SHIPPING PORT, AND POPULATED COMMUNITIES LOCATED TO THE NORTH.	66
FIGURE 6-4. MAXIMUM TOPOGRAPHIC SPEED-UP FACTORS FOR THE U.S. VIRGIN ISLANDS.	67
FIGURE 6-5. MAXIMUM TOPOGRAPHIC SPEED-UP FACTORS FOR PUERTO RICO.	68
FIGURE 6-6. MODELED AND OBSERVED METEOROLOGICAL TIME SERIES AT NDBC STATION CHSV3: CHRISTIANSTED HARBOR, ST. CROIX, USVI.	70
FIGURE 6-7. MODELED AND OBSERVED METEOROLOGICAL TIME SERIES AT NDBC STATION 41052: SOUTH OF ST. JOHN, USVI.	71
FIGURE 6-8. MODELED AND OBSERVED METEOROLOGICAL TIME SERIES AT NDBC STATION CHAV3: CHARLOTTE AMALIE, USVI.	72
FIGURE 6-9. MODELED AND OBSERVED METEOROLOGICAL TIME SERIES AT ASOS STATION TIST: CYRIL E KING AIRPORT, ST. THOMAS, USVI.	73
FIGURE 6-10. MODELED AND OBSERVED METEOROLOGICAL TIME SERIES AT NDBC STATION 41058: NORTH OF ST. THOMAS, USVI.	74
FIGURE 6-11. MODELED AND OBSERVED METEOROLOGICAL TIME SERIES AT NDBC STATION ESPP4: ESPERANZA, VIEQUES ISLAND, PUERTO RICO.	75
FIGURE 6-12. MODELED AND OBSERVED METEOROLOGICAL TIME SERIES AT NDBC STATION 41056: VIEQUES ISLAND, PUERTO RICO.	76
FIGURE 6-13. MODELED AND OBSERVED METEOROLOGICAL TIME SERIES AT NDBC STATION FRDP4: FAJARDO, PUERTO RICO.	77
FIGURE 6-14. MODELED AND OBSERVED METEOROLOGICAL TIME SERIES AT ASOS STATION TJNR: ROOSEVELT ROADS NAVAL STATION, PUERTO RICO.	78
FIGURE 6-15. MODELED AND OBSERVED METEOROLOGICAL TIME SERIES AT NDBC STATION SJNP4: SAN JUAN, LA PUNTILLA, SAN JUAN BAY, PUERTO RICO.	79
FIGURE 6-16. MODELED AND OBSERVED METEOROLOGICAL TIME SERIES AT NDBC STATION AROP4: ARECIBO, PUERTO RICO.	80
FIGURE 6-17. MODELED AND OBSERVED METEOROLOGICAL TIME SERIES AT NDBC STATION YABP4: YABUCOA HARBOR, PUERTO RICO.	81
FIGURE 6-18. MODELED AND OBSERVED METEOROLOGICAL TIME SERIES AT NDBC STATION 42085: SOUTHEAST OF PONCE, PUERTO RICO.	82
FIGURE 6-19. MODELED AND OBSERVED METEOROLOGICAL TIME SERIES AT NDBC STATION IMG4: ISLA MAGUEYES, PUERTO RICO.	83

FIGURE 6-20. MODELED AND OBSERVED METEOROLOGICAL TIME SERIES AT NDBC STATION MGZP4: 9759394 - MAYAGUEZ, PUERTO RICO.	84
FIGURE 6-21. MODELED AND OBSERVED MAXIMUM PEAK GUST WIND SPEED CORRECTED ONLY FOR HEIGHT (LEFT) AND CORRECTED FOR HEIGHT AND TERRAIN (RIGHT).....	85
FIGURE 6-22. MODELED AND OBSERVED MINIMUM CENTRAL PRESSURE.	86
FIGURE 6-23. AERIAL VIEW OF NDBC STATION FRDP4.	86
FIGURE 6-24. NDBC STATION FRDP4: VIEW FROM DOCK TOWARDS ANEMOMETER.....	87
FIGURE 6-25. AERIAL VIEW OF NDBC STATION YABP4.	87
FIGURE 6-26. PEAK GUST WIND SPEED MAP FOR HURRICANE IRMA (2017) SHOWING ESTIMATED 3-SECOND PEAK GUST WIND SPEEDS (MPH) AT 10 M ABOVE GROUND OVER OPEN TERRAIN. MODEL OUTPUT OBTAINED FROM ARA WIND FIELD MODEL FIT TO SURFACE LEVEL OBSERVATIONS USING NHC BEST TRACK AND CENTRAL PRESSURES. MODELED GUST WIND SPEEDS INCLUDE THE EFFECTS OF TOPOGRAPHY.	89
FIGURE 6-27. PEAK GUST WIND SPEED MAP FOR HURRICANE IRMA (2017) IN ST. THOMAS AND ST. JOHN, USVI, SHOWING ESTIMATED 3-SECOND PEAK GUST WIND SPEEDS (MPH) AT 10 M ABOVE GROUND OVER OPEN TERRAIN. MODEL OUTPUT OBTAINED FROM ARA WIND FIELD MODEL FIT TO SURFACE LEVEL OBSERVATIONS USING NHC BEST TRACK AND CENTRAL PRESSURES. MODELED GUST WIND SPEEDS INCLUDE THE EFFECTS OF TOPOGRAPHY.	90
FIGURE 6-28. PEAK GUST WIND SPEED MAP FOR HURRICANE IRMA (2017) IN ST. CROIX, USVI, SHOWING ESTIMATED 3-SECOND PEAK GUST WIND SPEEDS (MPH) AT 10 M ABOVE GROUND OVER OPEN TERRAIN. MODEL OUTPUT OBTAINED FROM ARA WIND FIELD MODEL FIT TO SURFACE LEVEL OBSERVATIONS USING NHC BEST TRACK AND CENTRAL PRESSURES. MODELED GUST WIND SPEEDS INCLUDE THE EFFECTS OF TOPOGRAPHY.	91
FIGURE 7-1. BEST-TRACK INFORMATION OF HURRICANE MARIA (2017) COLLECTED FROM THE NHC ATLANTIC HURRICANE DATABASE (HURDAT2).	93
FIGURE 7-2. ASOS AND NDBC STATIONS WITH SURFACE OBSERVATIONS DURING THE LIFESPAN AND WITHIN 150 MILES OF HURRICANE MARIA.....	94
FIGURE 7-3. NOAA NATIONAL OCEAN SERVICE STATION LTBV3 LOCATED VERY-NEAR SHORE WITH A REFINERY, SHIPPING PORT, AND POPULATED COMMUNITIES LOCATED TO THE NORTH.	95
FIGURE 7-4. MAXIMUM TOPOGRAPHIC SPEED-UP FACTORS FOR THE U.S. VIRGIN ISLANDS.	96
FIGURE 7-5. MAXIMUM TOPOGRAPHIC SPEED-UP FACTORS FOR PUERTO RICO.	97
FIGURE 7-6. MODELED AND OBSERVED METEOROLOGICAL TIME SERIES AT NDBC STATION CHSV3: CHRISTIANSTED HARBOR, ST. CROIX, USVI.....	100
FIGURE 7-7. MODELED AND OBSERVED METEOROLOGICAL TIME SERIES AT ASOS STATION TIST: CYRIL E KING AIRPORT, ST. THOMAS, USVI.....	101
FIGURE 7-8. MODELED AND OBSERVED METEOROLOGICAL TIME SERIES AT NDBC STATION VQSP4: ISABEL SEGUNDA, VIEQUES ISLAND, PUERTO RICO.....	102
FIGURE 7-9. MODELED AND OBSERVED METEOROLOGICAL TIME SERIES AT NDBC STATION 41056: VIEQUES ISLAND, PUERTO RICO....	103
FIGURE 7-10. MODELED AND OBSERVED METEOROLOGICAL TIME SERIES AT NDBC STATION FRDP4: FAJARDO, PUERTO RICO.	104
FIGURE 7-11. MODELED AND OBSERVED METEOROLOGICAL TIME SERIES AT NDBC STATION YABP4: YABUCA HARBOR, PUERTO RICO.	105
FIGURE 7-12. MODELED AND OBSERVED METEOROLOGICAL TIME SERIES AT ASOS STATION TJSJ: LUIS MUÑOZ MARÍN INTERNATIONAL AIRPORT, PUERTO RICO.	106
FIGURE 7-13. MODELED AND OBSERVED METEOROLOGICAL TIME SERIES AT NDBC STATION 41053: SAN JUAN, PUERTO RICO.	107
FIGURE 7-14. MODELED AND OBSERVED METEOROLOGICAL TIME SERIES AT NDBC STATION AROP4: ARECIBO, PUERTO RICO.....	108
FIGURE 7-15. MODELED AND OBSERVED METEOROLOGICAL TIME SERIES AT NDBC STATION 42085: SOUTHEAST OF PONCE, PUERTO RICO.	109
FIGURE 7-16. MODELED AND OBSERVED METEOROLOGICAL TIME SERIES AT NDBC STATION MGIP4: MAGUEYES ISLANDS, PUERTO RICO.	110
FIGURE 7-17. MODELED AND OBSERVED METEOROLOGICAL TIME SERIES AT NDBC STATION MGZP4: 9759394 - MAYAGUEZ, PUERTO RICO.	111

FIGURE 7-18. MODELED AND OBSERVED MAXIMUM PEAK GUST WIND SPEED CORRECTED ONLY FOR HEIGHT (LEFT) AND CORRECTED FOR HEIGHT AND TERRAIN (RIGHT).....	112
FIGURE 7-19. MODELED AND OBSERVED MAXIMUM PEAK GUST WIND SPEED CORRECTED ONLY FOR HEIGHT (LEFT) AND CORRECTED FOR HEIGHT AND TERRAIN (RIGHT) EXCLUDING NDBC STATION 41056.	113
FIGURE 7-20. MODELED AND OBSERVED MINIMUM CENTRAL PRESSURE.	113
FIGURE 7-21. PEAK GUST WIND SPEED MAP FOR HURRICANE MARIA (2017) IN PUERTO RICO SHOWING ESTIMATED 3-SECOND PEAK GUST WIND SPEEDS (MPH) AT 10 M ABOVE GROUND OVER OPEN TERRAIN. MODEL OUTPUT OBTAINED FROM ARA WIND FIELD MODEL FIT TO SURFACE LEVEL OBSERVATIONS USING NHC BEST TRACK AND CENTRAL PRESSURES. MODELED GUST WIND SPEEDS INCLUDE THE EFFECTS OF TOPOGRAPHY.	115
FIGURE 7-22. PEAK GUST WIND SPEED MAP FOR HURRICANE MARIA (2017) IN St. THOMAS AND St. JOHN, USVI, SHOWING ESTIMATED 3-SECOND PEAK GUST WIND SPEEDS (MPH) AT 10 M ABOVE GROUND OVER OPEN TERRAIN. MODEL OUTPUT OBTAINED FROM ARA WIND FIELD MODEL FIT TO SURFACE LEVEL OBSERVATIONS USING NHC BEST TRACK AND CENTRAL PRESSURES. MODELED GUST WIND SPEEDS INCLUDE THE EFFECTS OF TOPOGRAPHY.	116
FIGURE 7-23. PEAK GUST WIND SPEED MAP FOR HURRICANE MARIA (2017) IN St. CROIX, USVI, SHOWING ESTIMATED 3-SECOND PEAK GUST WIND SPEEDS (MPH) AT 10 M ABOVE GROUND OVER OPEN TERRAIN. MODEL OUTPUT OBTAINED FROM ARA WIND FIELD MODEL FIT TO SURFACE LEVEL OBSERVATIONS USING NHC BEST TRACK AND CENTRAL PRESSURES. MODELED GUST WIND SPEEDS INCLUDE THE EFFECTS OF TOPOGRAPHY.	117
FIGURE 8-1. BEST-TRACK INFORMATION OF HURRICANE NATE (2017) COLLECTED FROM THE NHC ATLANTIC HURRICANE DATABASE (HURDAT2).	119
FIGURE 8-2. ASOS AND NDBC STATIONS WITH SURFACE OBSERVATIONS DURING THE LIFESPAN AND WITHIN 150 MILES OF HURRICANE NATE.	120
FIGURE 8-3. MODELED AND OBSERVED METEOROLOGICAL TIME SERIES AT NDBC STATION 42001: MID GULF LOCATED 180NM SOUTH OF SOUTHWEST PASS, LOUISIANA.	122
FIGURE 8-4. MODELED AND OBSERVED METEOROLOGICAL TIME SERIES AT NDBC STATION SPL1: SOUTH TIMBALIER BLOCK 52, LOUISIANA.	123
FIGURE 8-5. MODELED AND OBSERVED METEOROLOGICAL TIME SERIES AT ASOS STATION KNEW: NEW ORLEANS LAKEFRONT AIRPORT.	124
FIGURE 8-6. MODELED AND OBSERVED METEOROLOGICAL TIME SERIES AT ASOS STATION KHBG: HATTIESBURG BOBBY L. CHAIN MUNICIPAL AIRPORT.	125
FIGURE 8-7. MODELED AND OBSERVED METEOROLOGICAL TIME SERIES AT NDBC STATION BURL1: SOUTHWEST PASS, LOUISIANA.	126
FIGURE 8-8. MODELED AND OBSERVED METEOROLOGICAL TIME SERIES AT ASOS STATION KGPT: GULFPORT-BILOXI INTERNATIONAL AIRPORT.	127
FIGURE 8-9. MODELED AND OBSERVED METEOROLOGICAL TIME SERIES AT NDBC STATION 42040: LUKE OFFSHORE TEST PLATFORM 63NM SOUTH OF DAUPHIN ISLAND, ALABAMA.	128
FIGURE 8-10. MODELED AND OBSERVED METEOROLOGICAL TIME SERIES AT NDBC STATION DKCM6: DOCK C, PORT OF PASCAGOULA, MISSISSIPPI.	129
FIGURE 8-11. MODELED AND OBSERVED METEOROLOGICAL TIME SERIES AT NDBC STATION FMOA1: FORT MORGAN, ALABAMA.	130
FIGURE 8-12. MODELED AND OBSERVED METEOROLOGICAL TIME SERIES AT ASOS STATION KMOB: MOBILE REGIONAL AIRPORT.	131
FIGURE 8-13. MODELED AND OBSERVED METEOROLOGICAL TIME SERIES AT ASOS STATION KGZH: MIDDLETON FIELD.	132
FIGURE 8-14. MODELED AND OBSERVED METEOROLOGICAL TIME SERIES AT ASOS STATION KTCL: TUSCALOOSA REGIONAL AIRPORT.	133
FIGURE 8-15. MODELED AND OBSERVED METEOROLOGICAL TIME SERIES AT ASOS STATION KMSL: NORTHWEST ALABAMA REGIONAL AIRPORT.	134
FIGURE 8-16. MODELED AND OBSERVED METEOROLOGICAL TIME SERIES AT ASOS STATION KDCU: PRYOR FIELD AIRPORT.	135
FIGURE 8-17. MODELED AND OBSERVED MAXIMUM PEAK GUST WIND SPEED CORRECTED ONLY FOR HEIGHT (LEFT) AND CORRECTED FOR HEIGHT AND TERRAIN (RIGHT).....	136
FIGURE 8-18. MODELED AND OBSERVED MINIMUM CENTRAL PRESSURE.	136
FIGURE 8-19. PEAK GUST WIND SPEED CONTOUR MAP FOR HURRICANE NATE (2017) SHOWING ESTIMATED 3-SECOND PEAK GUST WIND SPEEDS (MPH) AT 10 M ABOVE GROUND OVER OPEN TERRAIN. MODEL OUTPUT OBTAINED FROM ARA WIND FIELD MODEL FIT TO SURFACE LEVEL OBSERVATIONS USING NHC BEST TRACK AND CENTRAL PRESSURES.	139

1 INTRODUCTION

The objective of this project is to develop wind field maps for the 2017 Atlantic hurricanes that made landfall—Hurricane Harvey (Texas only), Hurricane Irma (U.S. and territories), Hurricane Maria (U.S. territories), and Hurricane Nate (U.S. only)—by fitting the Applied Research Associates’ (ARA) wind field model using available track and meteorological surface observations.

The hurricane hazard model used by ARA for this project has been developed over a twenty-two year period beginning in 1996. The first model, published in 2000 (Vickery et al. 2000), was used to define the hurricane wind hazard as given in ASCE 7-98 (American Society of Civil Engineers Standard 7, 1998), which was used to specify the design wind speed for buildings constructed in the United States. The model from 2000 was the first hurricane simulation model employing an approach that simulated the full track of a hurricane, allowing for storms to vary in both size and intensity along the track.

The model went through significant updates in 2006, including an improved wind field model (Vickery et al., 2009a), and new models for the radius to maximum winds (RMW) and the Holland B parameter (Vickery and Wadhera, 2008). The final hazard model is described in Vickery et al. (2009b) and Vickery et al. (2010), and the results of the revised hurricane simulation model were used to develop the wind load provisions given in ASCE 7-10 and ASCE 7-16.

This report details the methodology for creating the wind field maps. Section 2 outlines the wind field model and associated uncertainties. The methodology for modeling the wind field of a specific storm is presented in Section 3, including collecting data and converting it to a 3-second gust wind speed at 10 m height over open terrain. Uncertainties associated with converting the wind speeds to the standardized format are also discussed. Sections 4-7 present storm specific information on Hurricanes Harvey, Irma in the Contiguous United States (CONUS), Irma Outside the Contiguous United States (OCONUS), Maria, and Nate, respectively. Each section includes event background, historical data, discussion of model results, errors and uncertainties, and the wind field map. A corresponding appendix is provided for each modeled storm that includes a table of surface observation station information, and meteorological time series figures for all stations utilized in the modeling process. A summary is presented in Section 9.

2 WIND FIELD MODELING

2.1 MODEL OVERVIEW

The hurricane wind field model developed by ARA is described in detail in Vickery et al. (2000). The vortex model uses the numerical solution of the two-dimensional, vertically integrated equations of motion for a translating hurricane. The asymmetries in a moving storm are a function of the translation speed of the storm and the nonlinear interactions between the wind velocity vectors and the frictional effects of the surface of the earth. The numerical solutions of the equations of motion of the hurricane have been solved separately for a storm translating over the ocean and for a storm translating over land because the surface drag coefficients are different. When the storm is over water, the magnitude of the surface drag coefficient is a function of the wind speed itself (Powell et al. 2005), whereas, when the storm is over land, the magnitude of the surface drag coefficient is wind speed independent. The numerical solutions represent the integrated, boundary-layer averaged wind speeds, which are

representative of a long duration average wind, taken as having an averaging time of one hour. The mean, 1-hour average, integrated wind speeds are combined with a boundary layer model to produce estimates of wind speeds for any height and averaging time. The variation of wind speed with height used in this hurricane model is described in Vickery et al. (2009a).

Key inputs to the hurricane wind field model include the central pressure, translation speed, radius of maximum winds, and the Holland B pressure profile parameter. Solutions have been pre-computed for 12 values of central pressure, 10 values of translational velocity, 13 values of radius of maximum wind, and 9 values of B, for a total of 14,040 pre-computed solutions. For each pre-computed solution, the u and v components of wind speed were converted into Fourier series and the coefficients were recalled as needed for modeling the event. Wind speeds for the model were generated in 15-minute increments between input observations, which were typically recorded every 6 hours. When generating incremental winds, the profile parameters were interpolated in time—as opposed to interpolating between the wind fields themselves—and a new solution was obtained.

The values of central pressure and storm translation speed are defined by the best track information obtained from the National Hurricane Center (NHC) hurricane database (HURDAT2). An iterative process is used to adjust the values of radius of maximum wind and the Holland B parameter to obtain the best fit to the observed values of wind speed, wind direction, and atmospheric pressure at the location of all stations with valid surface observations.

Surface roughness is a critical component in the time series modeling of the hurricane wind field at a single point. As the ground surface becomes rougher, the wind speeds near the ground decrease while the upper-level wind speeds remain the same. In the rapid transition of surface level gusts from a marine environment to smooth open terrain, more than half of the reduction occurs within 100 m of the coast, and approximately 80% of the reduction occurs within 1 km of the coast. Mean wind speeds transition more slowly, so a distance of 300 km is required to achieve a fully transitioned overland wind field within the model. For each station used in the wind field model validation, distances to the coast are tabulated for 36 wind directions at 10° intervals.

2.2 MODEL UNCERTAINTY AND EVALUATION

2.2.1 Uncertainty in Modeling

The model results include the effect of uncertainties in both wind speed and direction. The wind speed uncertainty terms are the same as that used in the development of the ASCE 7 wind speed maps. The uncertainty increases the 100-year return period wind speed by a few percent. The effect of the error term on the percentage increase of the nominal wind speed increases with increasing return period. The wind speed uncertainty term is modeled using a multiplicative term with a mean of 1.0 and a standard deviation, σ , of 0.10. The wind speed uncertainty term is normally distributed and truncated at $\pm 2\sigma$. The wind direction uncertainty term is modeled using a normally distributed term with a mean of zero and a standard deviation, σ , of 20 degrees. The wind direction uncertainty term is truncated at $\pm 2\sigma$. Single values of the wind speed and wind direction uncertainty terms are applied to the wind speed and wind direction, respectively, for each time series, both for surface-level and upper-level wind speeds for each time step of the storm. New values are sampled for the subsequent storm.

2.2.2 Goodness of Fit Statistic

Time series of modeled and observed wind speeds, wind direction, and central pressure at select meteorological observation stations located within the wind field of Hurricanes Harvey, Irma, Maria, and Nate are presented in this report. For each station, the bias and scatter index (SI) are calculated as measures of model performance using all observations during which the hurricane was of tropical storm strength or greater, that is, a threshold of sustained wind speed of 40 mph. The SI is typically presented as a percentage where lower values indicate better model performance. The SI was developed in the U.S. Army Corps of Engineers Coastal and Hydraulics Engineering Technical Note I-91 Evaluation Statistics Computed for the Wave Information Studies (Bryant et al., 2016). The SI is calculated as in

$$SI = \frac{RMSE}{\bar{X}} \quad \text{Eq. 1}$$

where \bar{X} is the mean of the observed parameter and $RMSE$ is the root-mean-square error obtained from

$$RMSE = \sqrt{\frac{1}{N} \sum (Y_i - X_i)^2} \quad \text{Eq. 2}$$

where N is the number of observations, and Y_i and X_i are the modeled and observed parameters at time step i .

The model bias, b , is calculated from

$$b = \frac{1}{N} \sum (Y_i - X_i) \quad \text{Eq. 3}$$

3 METHODOLOGY

3.1 DATA COLLECTION

3.1.1 NHC Best Track

In May 2018, the NHC updated the Atlantic hurricane database (HURDAT2) to include the best tracks of the 2017 hurricane season events. Track information contained in HURDAT2 is reanalyzed and revised as necessary at the completion of the hurricane season using an enhanced collection of historical meteorological data. The best-track information was used for the wind field modeling of all hurricanes presented herein.

3.1.2 Surface Observations

Surface wind and pressure measurements were collected in order to validate the wind field model. Land-based observations were obtained from a real-time repository of Automated Surface Observing System (ASOS) networks maintained by Iowa State University. Offshore and very nearshore observations were obtained from the National Data Buoy Center (NDBC), which maintains observations from several networks in addition to their own (e.g., Coastal-Marine Automated Network and Texas Coastal Ocean Observing Network).

Further detail of stations used to model each storm is presented in the storm-specific sections later in the report.

3.2 DATA CORRECTIONS

Wind speeds output from the hurricane simulation model correspond to a gust wind speed (3-second averaging time) at 10 m height over open terrain (ASCE 7 Surface Roughness Category C). When observations are not reported in the same format, the Engineering Sciences Data Unit (ESDU) (1982, 1983) models for atmospheric turbulence were used to convert the wind speeds to standard conditions. The adjustment for height is performed with the assumption that the lower 50 m of the hurricane boundary layer can be described using the logarithmic law for neutral flow conditions (Vickery and Skerlj, 2005). These same models were also used in the development of the methodology given in ASCE 7-16 to determine in what terrain category a building is located, as well as the methodology given in ASCE 7-10 and ASCE 7-16 to compute intermediate terrains. A brief outline of adjustments made using the ESDU methodology is presented later in this section.

Most stations in the ASOS network report wind speed observations as 3-second gust wind speeds at 10 m height and are located on airport grounds. While the immediate terrain of the sensor location can typically be characterized as open terrain, a wide spectrum of terrain conditions exist beyond the airport perimeter. Previous research was performed (Masters et al., 2010) to estimate directional effective roughness length (z_0) values from averages of neutrally stratified mean gust factors at ASOS stations located in hurricane-prone areas. Directional effective roughness lengths were determined for 16 sectors surrounding each station; those computed for the Naples Municipal Airport (KAPF) in Florida are shown in Figure 3-1. These pre-computed values of z_0 serve as input to the ESDU methodology.

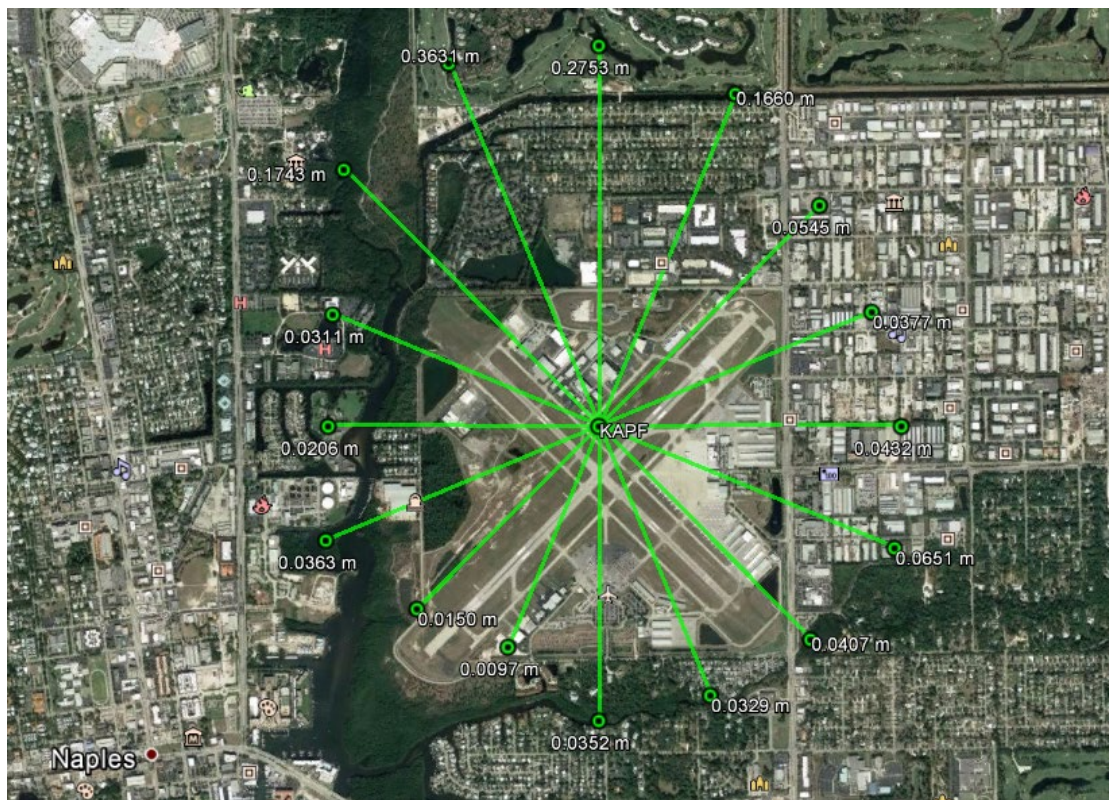


Figure 3-1. Directional effective surface roughness length for Naples Municipal Airport computed in Masters et al. (2010) and used herein.

NDBC gust wind speed observations typically correspond to a 5- or 8-second averaging period, depending on the payload in operation. The height of the wind speed observations in the NDBC network can vary significantly between sensors located on buoys, towers, or platforms as shown in Figure 3-2.



Figure 3-2. (left to right) NDBC Stations 42020, RSJT2, and ANPT2 with anemometers located at heights of 4, 10, and 14.22 m above sea level.

3.2.1 Correction for Height and Averaging Period

The height conversion to 10 m is performed by first converting the wind speed observation to a 1-hour mean wind speed and then adjusting it to a 10 m height. The 1-hour averaged wind speed is then converted to a 3-second averaged gust wind speed.

The expression for the peak wind speed using the ESDU model is

$$\hat{U}(\tau, z) = U(T_0, z)[1 + g(v, \tau, z)I_u(z)] \quad \text{Eq. 4}$$

where τ is the desired averaging time in seconds, $U(T_0, z)$ is the T_0 -second averaged wind speed at a height z , $g(v, \tau, z)$ is a peak factor, and $I_u(z)$ is the turbulence intensity defined as the ratio of the standard deviation of the wind speed at a height z to the T_0 -second averaged wind speed at a height z . The standard deviation is calculated using

$$\sigma_u(z) = \frac{u_* 7.5 \eta [0.538 + 0.09 \cdot \ln(z/z_0)]^{\eta^{1.6}}}{1 + 0.156 \cdot \ln\left(\frac{u_*}{f z_0}\right)} \quad \text{Eq. 5}$$

where u_* is the friction velocity, f is the Coriolis parameter, z_0 is the surface roughness, and η is a scaling parameter. The friction velocity—a measure of surface shear stress having units of velocity—is obtained using Eq. 6. The Coriolis parameter accounts for the apparent deflection of a moving object when observed from a rotating point of reference and is obtained using Eq. 7. The empirical scaling parameter η is obtained using Eq. 8. The surface roughness parameter is a measure of the aerodynamic roughness of a surface and theoretically the height at which the wind profile is equal to zero. For open terrain conditions (ASCE Exposure C), z_0 is equal to 0.03 m (~1.18 inches). The friction velocity, u_* , is computed using the logarithm law as in

$$u_* = \frac{k \cdot U(3600, z)}{\ln(z/z_0)} \quad \text{Eq. 6}$$

where k is the von Karman constant equal to 0.4. The Coriolis parameter is given by

$$f = 2\omega \cdot \sin(\varphi) \quad \text{Eq. 7}$$

where ω is the angular rotation of the Earth equal to 7.29×10^{-5} radians/second, and φ is the latitude of the site of interest. The scaling parameter, η , is calculated as

$$\eta = 1 - 6fz/u_* \quad \text{Eq. 8}$$

The peak factor, using the ESDU model, is calculated using

$$g(v, \tau, z) = \left[\sqrt{2 \ln(T_0 \cdot v)} + \frac{0.577}{\sqrt{2 \ln(T_0 \cdot v)}} \right] \cdot \frac{\sigma_u(z, \tau)}{\sigma_u(z)} \quad \text{Eq. 9}$$

where T_0 is the averaging time of the wind speed in seconds, and v is the up-crossing frequency. In ESDU (1982), $\sigma_u(z, \tau)$ is approximated using

$$\sigma_u(z, \tau) = \int_0^\infty S(n) \cdot \psi(n, \tau, T_0) dn \cong \sigma_u(z) \left[1 - 0.193 \left(\frac{T_u}{\tau} + 0.1 \right)^{-0.68} \right] \quad \text{Eq. 10}$$

The zero up-crossing frequency is approximated by

$$v = \frac{0.007 + 0.213 \left[\frac{T_u}{\tau} \right]^{0.654}}{T_u} \quad \text{Eq. 11}$$

where T_u is the integral time scale given as

$$T_u = 3.13z^{0.2} \quad \text{Eq. 12}$$

Finally, the ESDU representation of the gust factor is calculated using

$$C_g(T_0, z, U, \tau) = 1 + g(v, \tau, z)I_u(z) \quad \text{Eq. 13}$$

Given values of $\hat{U}(\tau, z)$, τ , z , f , and z_0 , an iterative approach is used to solve for a value of u_* that satisfies Eq. 4. The logarithmic law presented in Eq. 6 is then used with z equal to 10 to obtain a value of the hourly averaged wind speed at a height of 10 m as in

$$U(3600, 10) = U(3600, z) \cdot \frac{\ln(10/z_0)}{\ln(z/z_0)} \quad \text{Eq. 14}$$

The hourly averaged wind speed at a height of 10 m is then converted to a 3-second gust wind speed, or a 10-minute mean wind speed, at a height of 10 m using the value of u_* already computed from the iterative solution.

3.2.2 Correction for Surrounding Terrain

The standardization process for conversion of a gust or sustained wind speed observation to an equivalent value for open terrain is detailed in Vickery and Skerlj (2005) and Masters et al. (2010). Given the wind speed and surface roughness, the value of friction velocity is computed using the logarithmic law. This value of friction velocity is then converted to its equivalent value in open terrain, and the new open terrain wind speed is computed with the logarithmic law.

The wind speed terrain adjustment factor is taken as the ratio of the raw wind speed to the open terrain wind speed. Cubic functions of the terrain adjustment factor versus surface roughness in natural logarithm space have been pre-computed to simplify the process. The cubic functions are specific to wind speed averaging period as shown below.

For each station location, surrounding values of surface roughness are tabulated for 16 wind directions at 22.5° intervals. The tabulated values of surface roughness were estimated from in situ measurements (Masters et al., 2010) or estimated from aerial imagery. The surface roughness for a given wind direction is interpolated from these tabulated values as in

$$z_{o,\theta_i} = z_{o,\theta_{i+1}} - (z_{o,\theta_{i+1}} - z_{o,\theta_{i-1}}) * \left(\frac{\theta_{i+1} - \theta_i}{\theta_{i+1} - \theta_{i-1}} \right) \quad \text{Eq. 15}$$

where z_{o,θ_i} is the surface roughness for the given wind direction θ_i , and $z_{o,\theta_{i+1}}$ and $z_{o,\theta_{i-1}}$ are the tabulated values of surface roughness for the bounding values of wind direction θ_{i+1} and θ_{i-1} , respectively.

To convert from the local surface roughness conditions to open terrain, a cubic function is first used to obtain a multiplicative term as a function of $\ln(z_{o,\theta_i})$ as in

$$f_o = a_1 + a_2 * x + a_3 * x^2 + a_4 * x^3 \quad \text{Eq. 16}$$

where

$$x = \ln(z_{o,\theta_i}) \quad \text{Eq. 17}$$

and the coefficients a_i vary by the wind speed averaging period as shown in Table 3-1.

Table 3-1. Parameters for cubic wind speed terrain adjustment factor versus $\ln(z_o)$.

Averaging Period	a_1	a_2	a_3	a_4
3-Second	0.703357258	-0.115278821	-0.010363251	-0.000470714
1-minute	0.605568493	-0.147627874	-0.011755497	-0.000504765
Hourly	0.517562649	-0.176740684	-0.013008461	-0.000535410

The terrain adjustment factor used to obtain design wind speeds of ASCE 7 has been halved as in

$$f = \begin{cases} \left(\frac{f_o - 1}{2} \right) + 1 & \text{for } f > 1 \\ 1 - \left(\frac{1 - f_o}{2} \right) & \text{for } f < 1 \end{cases} \quad \text{Eq. 18}$$

The reduced terrain adjustment factor is also used herein to obtain the open terrain equivalent wind speed observations as in

$$V = \frac{V_o}{f} \quad \text{Eq. 19}$$

where V is the equivalent wind speed in open terrain and V_o is the wind speed observation.

3.3 UNCERTAINTY IN DATA CORRECTIONS

Uncertainties in the wind field validation may include uncertainty in:

- Correcting observations for anemometer height
- Correcting observations for gust duration
- Correcting observations for the roughness of the surrounding terrain

3.3.1 Uncertainty in Anemometer Height Correction

The ESDU models for atmospheric turbulence (ESDU, 1982, 1983) can be used to generate gust wind speed height corrections factors. These height correction factors are applied by dividing the gust wind speed recorded at height z by the correction factor to yield an estimate of the wind speed at a height of 10 m. These correction factors are given for three different terrains (as defined by z_0) in Figure 3-3. As indicated in Powell et al. (1996), visual estimates of the surface roughness is somewhat subjective, and differences of factors of 2 obtained when experienced persons estimate z_0 are not uncommon. It is unrealistic to believe that we can visually distinguish between roughness lengths of 0.03 and 0.05 m. Figure 3-3 shows that if the value of surface roughness is off by a factor of 2, then the uncertainty in the anemometer height correction is on the order of 5%.

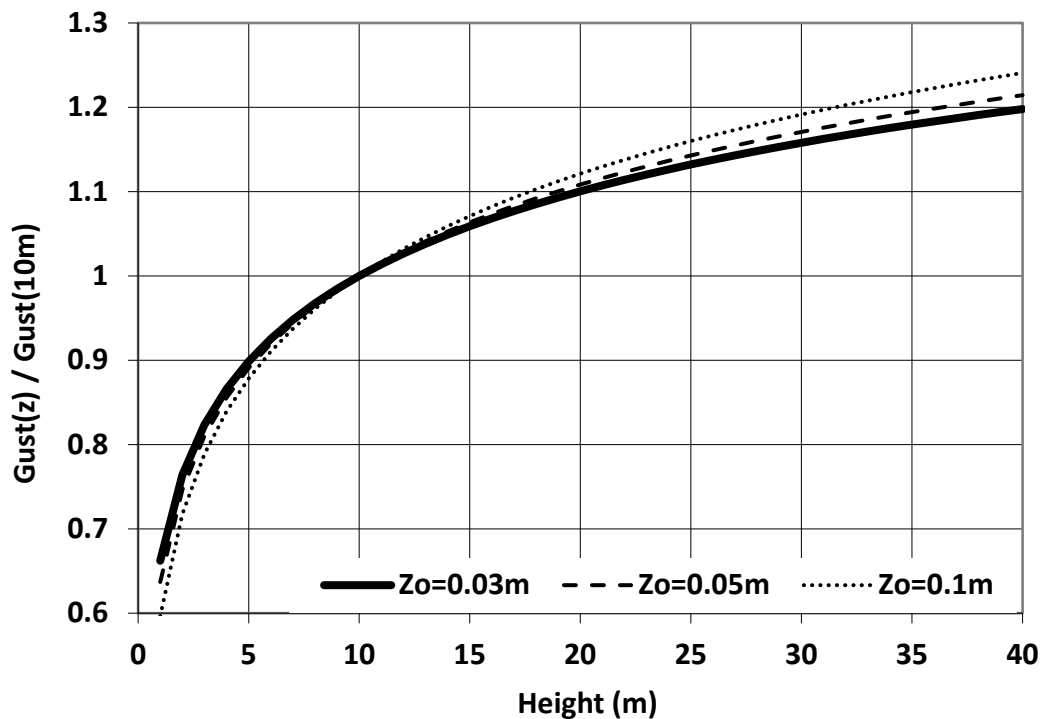


Figure 3-3. Gust wind speed adjustment factors for various anemometer heights with typical effective airport surface roughness values.

3.3.2 Uncertainty in Averaging Period Correction

In the United States, the anemometry system on most ASOS locations from the mid-2000s and later transitioned to ice-free ultrasonic anemometers using a system that reports a 3-second running average peak gust wind speed. The gust factor curve for open terrain conditions shown in Figure 3-4 was used to develop the uncertainties associated with gust duration corrections. The gust factor shown in Figure 3-4 is the ratio of the peak gust wind speed associated with the indicated average divided by the mean wind speed averaged over 3,600 seconds. Assuming that the nominal gust wind speed averaging time is 3 seconds, the potential uncertainty is found to have a coefficient of variation (CoV) of only 3%. This yields a 1 standard deviation range of 0.97 to 1.03, or a gust averaging time range of about 1 second.

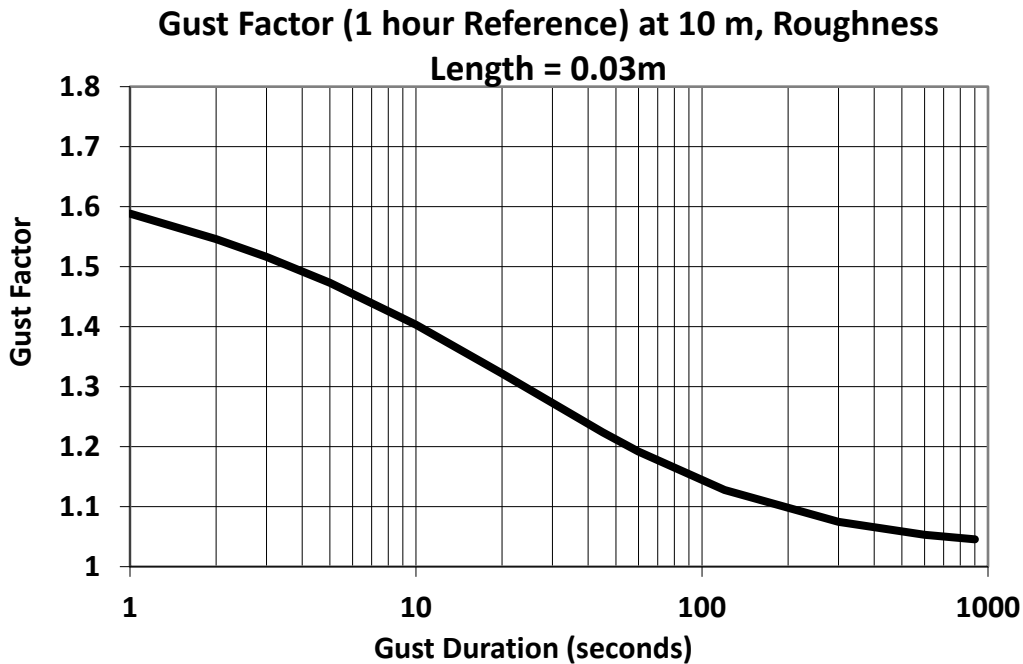


Figure 3-4. Gust factor vs. gust duration for open terrain.

3.3.3 Uncertainty in Surrounding Terrain Correction

The effect of the upstream terrain on wind speed measurements at airport locations is discussed in Masters et al. (2010) where it is indicated that few U.S. airport anemometer sites (located along the hurricane prone coastline) are associated with true open terrain ($z_0=0.03$ m). Instead, the median effective value of z_0 was found to be 0.07 m. A site-specific effective surface roughness can be obtained by examining aerial imagery of the airport sites, attempting to find the location of the anemometer, and then assessing the effective value of the surface roughness at the site. The coefficient of variation can be estimated using a combination of experience and the actual surrounding terrain as indicated in the aerial photographs. Typically, sites have estimated nominal z_0 values in the range of 0.06 m or so (Masters et al., 2010). A 100% CoV yields a $\pm 1.0\sigma$ range of $0.027 \text{ m} < z_0 < 0.138 \text{ m}$. This range seems reasonable with the lower bound (-1.0σ) near the “true” open terrain and the upper bound ($+1.0 \sigma$) less than suburban terrain (ASCE Exposure B) which is defined using $z_0 = 0.15$ m. In the Australian wind loading provisions, open terrain is associated with an aerodynamic roughness length of 0.02 m, and suburban terrain is characterized by a z_0 of 0.2 m. In the U.K. building code, open and suburban terrains are defined as having a surface roughness equal to 0.03 and 0.3 m, respectively. The Eurocode defines open terrain (Terrain Category II) with a surface roughness of 0.05 m and suburban terrain (Terrain Category III) with a surface roughness of 0.30 m.

Figure 3-5 presents relationships between the effective surface roughness and the gust wind speed correction factor. One of the relationships given in Figure 3-5 was derived using the ESDU (1982, 1983) models for atmospheric turbulence, and the other was derived using the approach given in Simiu and Scanlan (1996). As indicated in Figure 3-5 for a typical range, say, $0.010 \text{ m} < z_0 < 0.20 \text{ m}$, depending on the direction, the correction factor ranges between 0.94 and 1.16.

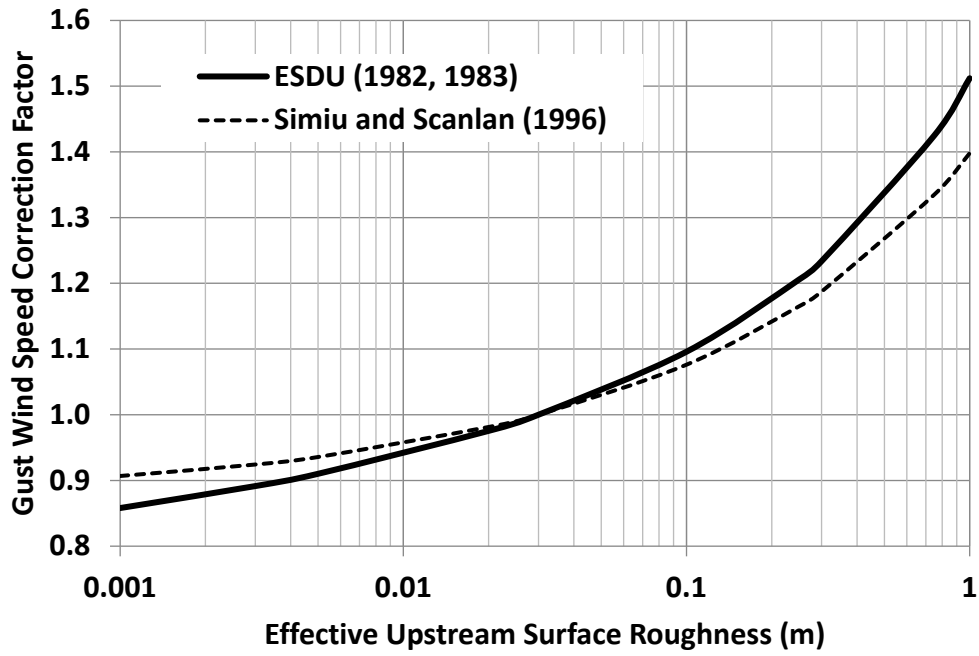


Figure 3-5. Gust wind speed correction factor at a height of 10 m due to surface roughness as a function of the effective upstream surface roughness.

4 HURRICANE HARVEY

4.1 EVENT BACKGROUND

A brief background for Hurricane Harvey (2017) is presented in this section. For a full narrative of the storm, including synoptic history, meteorological statistics, casualty and damage statistics, and forecast and warning critique, see the National Hurricane Center's Tropical Cyclone Report on Hurricane Harvey (Blake and Zelinsky, 2018) available at https://www.nhc.noaa.gov/data/tcr/AL092017_Harvey.pdf.

Hurricane Harvey was a Category 4 hurricane that made landfall along the Texas coastline northeast of Corpus Christi near the city of Rockport during the 2017 hurricane season. According to the NHC, Harvey produced a maximum 1-minute sustained wind speed of 115 knots (132 mph) occurring over water just prior to making landfall on San Jose Island on August 26 3:00 UTC. (The NHC best track wind speed data is reported to the nearest 5 knots.) The estimated central pressure at landfall was 937 mbar. After crossing the narrow island, Harvey made a second landfall three hours later on August 26 6:00 UTC on the mainland Texas coast. The maximum 1-minute sustained wind speed and central pressure during the second landfall were estimated by the NHC to be 105 knots (~121 mph) and 948 mbar, respectively.

After making landfall, Harvey weakened to tropical storm status rapidly; its center remained over or near land for the following four days. The storm moved offshore to the southeast on August 28 3:00 UTC and slightly intensified, although it never regained hurricane strength due to the presence of strong vertical wind shear. The storm's trajectory turned to the northeast, and it made a third landfall in southwestern Louisiana on August 30 8:00 UTC. The stalling of the storm over land and the change in storm heading just off the coast resulted in historic amounts of rainfall over much of the Texas coastal region. Harvey continued on a northeastern trajectory, weakening to a tropical depression by August 31, transforming into an extratropical cyclone by September 1 6:00 UTC, and finally dissipating on September 2 12:00 UTC.

The highest observed sustained wind speed over land was 96 knots (110 mph) at the Texas Coastal Observing Network's Port Aransas Sentinel (ANPT2) site at a height of 14.2 m. The highest observed gust wind speed over land was 122 knots (140 mph) as recorded by a University of Florida research tower located at the Aransas County Airport (KRKP) at a height of 15 m using a wind monitor sensor. The University of Florida had two additional ultrasonic sensors in place at the Aransas County Airport that recorded maximum gust winds of 116 knots (134 mph) and 119 knots (137 mph) at heights of 10 and 15 m, respectively. It is likely that the true maximum gust wind speed at 10 m height was slightly greater than 134 mph as the ultrasonic sensors tend to miss observations in high winds. However, the observations at KRKP used herein are based on the ultrasonic observations at 10 m in lieu of converting the 15 m height wind monitor to 10 m equivalent wind speeds. Additionally, Hurricane Harvey made landfall with its front right quadrant located over uninhabited areas (e.g., Aransas National Wildlife Refuge, San Jose Island, and Matagorda Island) where no meteorological observation networks were in place, making it likely that the true maximum wind speeds were not observed.

Maximum storm surge and tide inundation levels of 6 to 10 feet were estimated near the coast to the north and east of Harvey's Texas landfalls. Further to the northeast near Port Arthur, maximum rainfall totals of approximately 60 inches were reported near the cities of Nederland and Groves; 36-48 inches were reported in the Houston Metro area. Harvey produced the highest rainfall rate and total accumulation from a tropical cyclone on record.

4.2 DATA COLLECTION

4.2.1 Track

A portion of the best track of Hurricane Harvey is shown in Figure 4-1 as the storm approached and made landfall along the Texas coastline.

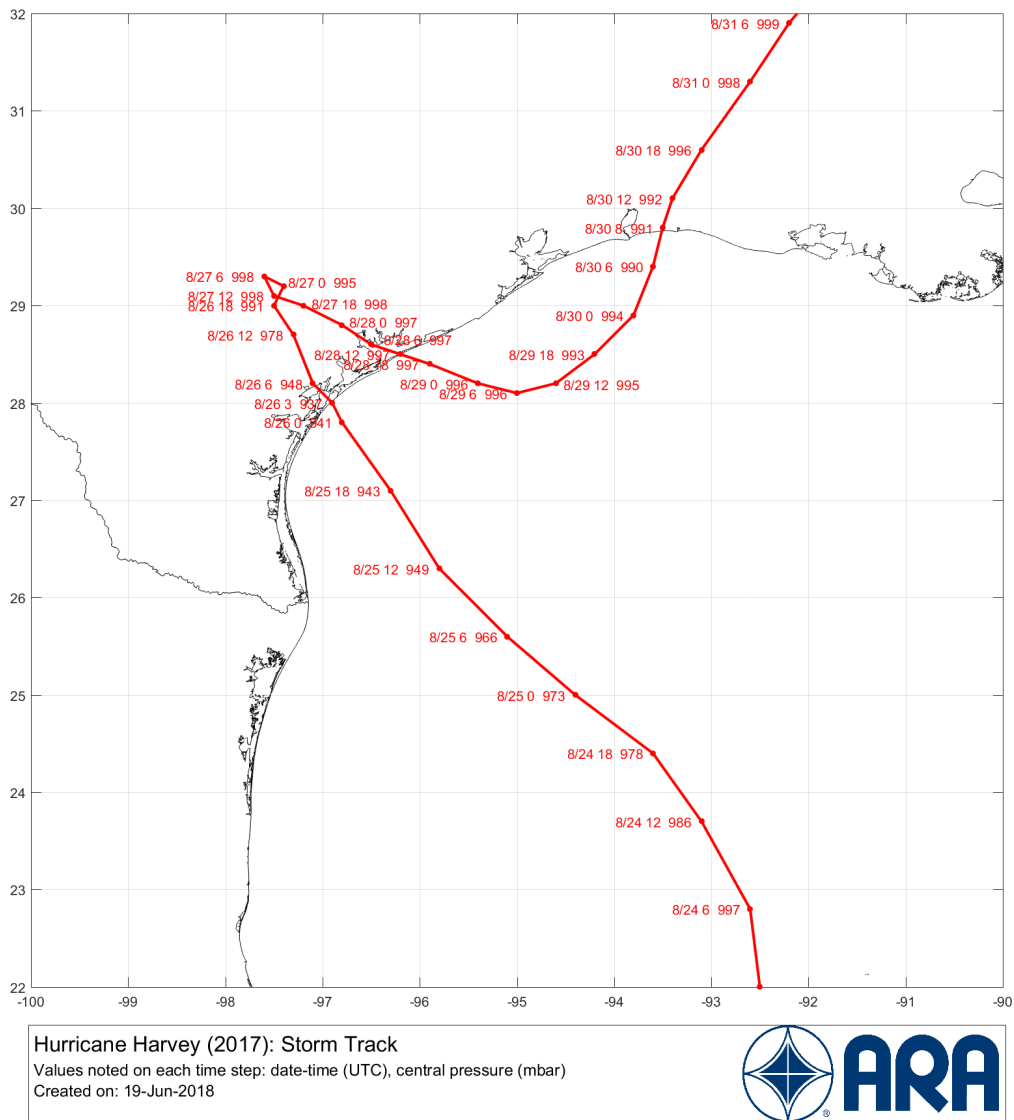


Figure 4-1. Best-track information of Hurricane Harvey (2017) collected from the NHC Atlantic Hurricane Database (HURDAT2).

4.2.2 Observations

Stations with observations during the lifespan of Hurricane Harvey and within 150 miles of a track point were used in the model validation and are shown in Figure 4-2. A table of station locations and anemometer heights is provided in Appendix A.

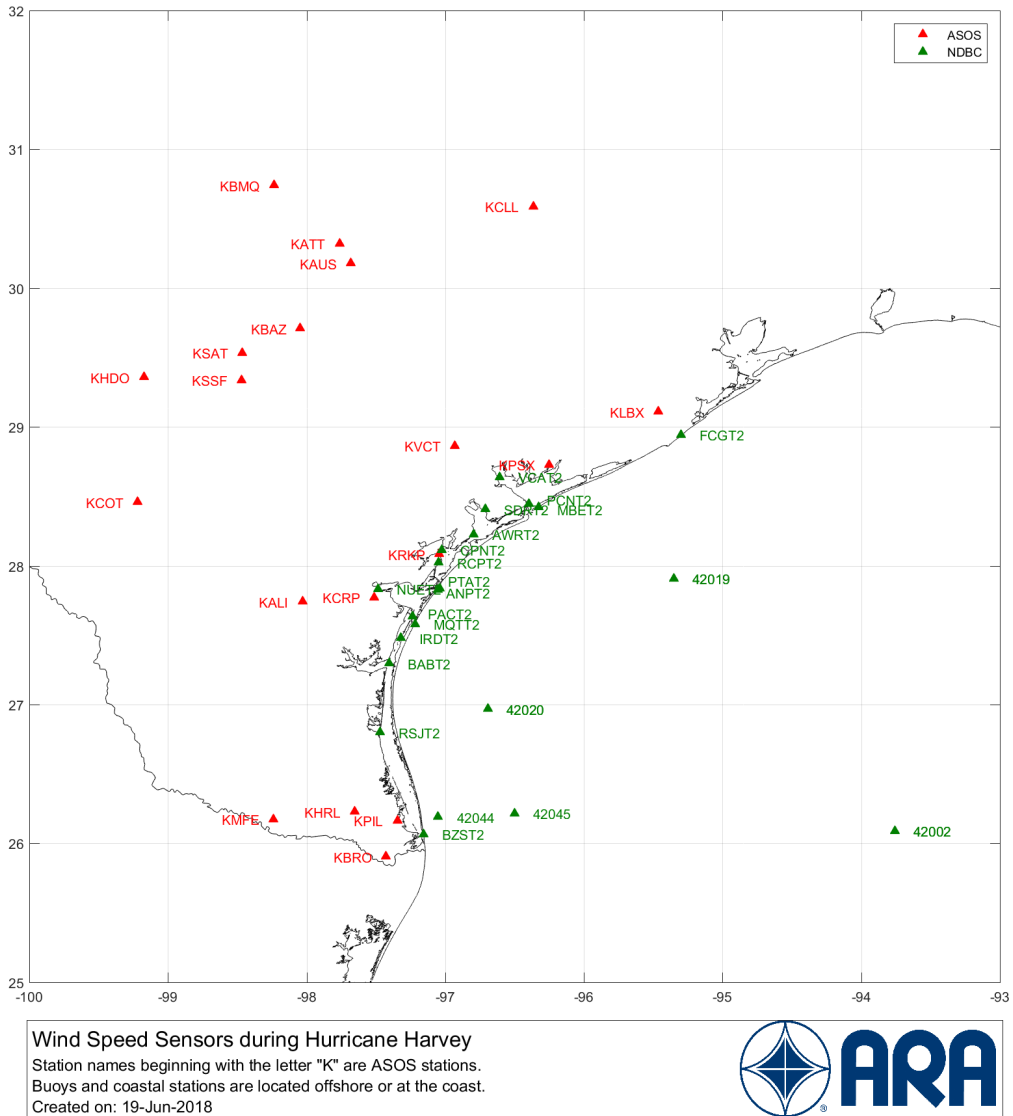


Figure 4-2. ASOS and NDBC stations with surface observations during the lifespan and within 150 miles of Hurricane Harvey.

A zoomed in view of NDBC stations located near landfall that captured some of the highest winds observed during Hurricane Harvey is shown in Figure 4-3. Most of the stations were located behind barrier islands or on the inland side of coastal bays where the land surrounding the station would act to reduce the strength of the winds.

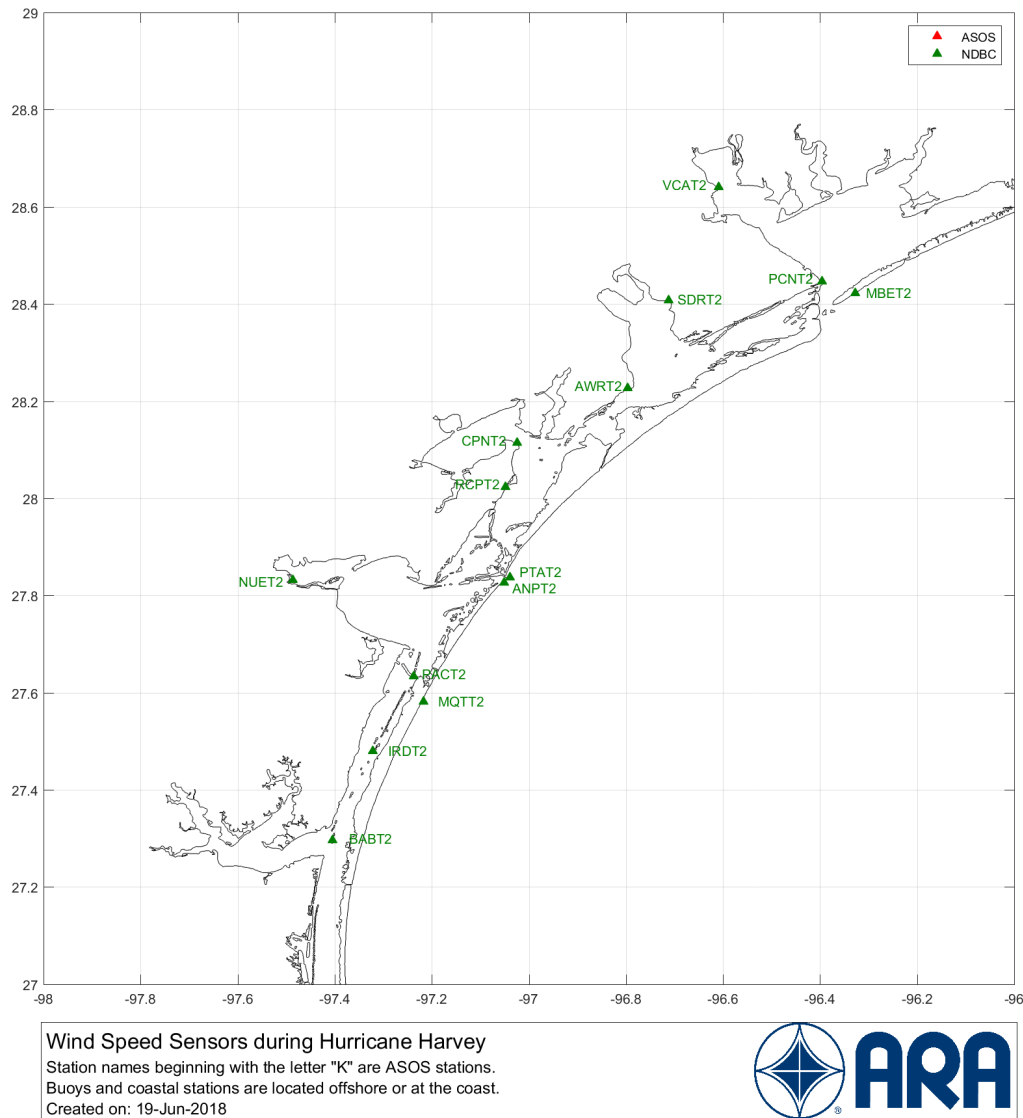


Figure 4-3. NDBC stations located near the period of high winds prior to and during landfall of Hurricane Harvey (2017).

4.3 DATA CORRECTIONS (DEVIATION FROM STANDARD PROCEDURES)

Wind speed observations at stations located very nearshore are often affected by the rougher terrain of nearby land and do not correspond to true marine terrain observations. In the case of Hurricane Harvey, several NDBC stations were located near the shore and often sheltered by barrier islands or coastal inlets as shown in Figure 4-3. As an example, NDBC station PTAT2, shown in Figure 4-4, has a beach park consisting of mostly grassland and dunes located to the north and a densely populated residential area to the east. Estimates of directional effective surface roughness have not been previously generated for NDBC locations. To account for terrain effects on these stations, a visual technique was used to estimate the directional surface roughness values from aerial imagery. Visually estimated values of z_0 served as input to the ESDU methodology.

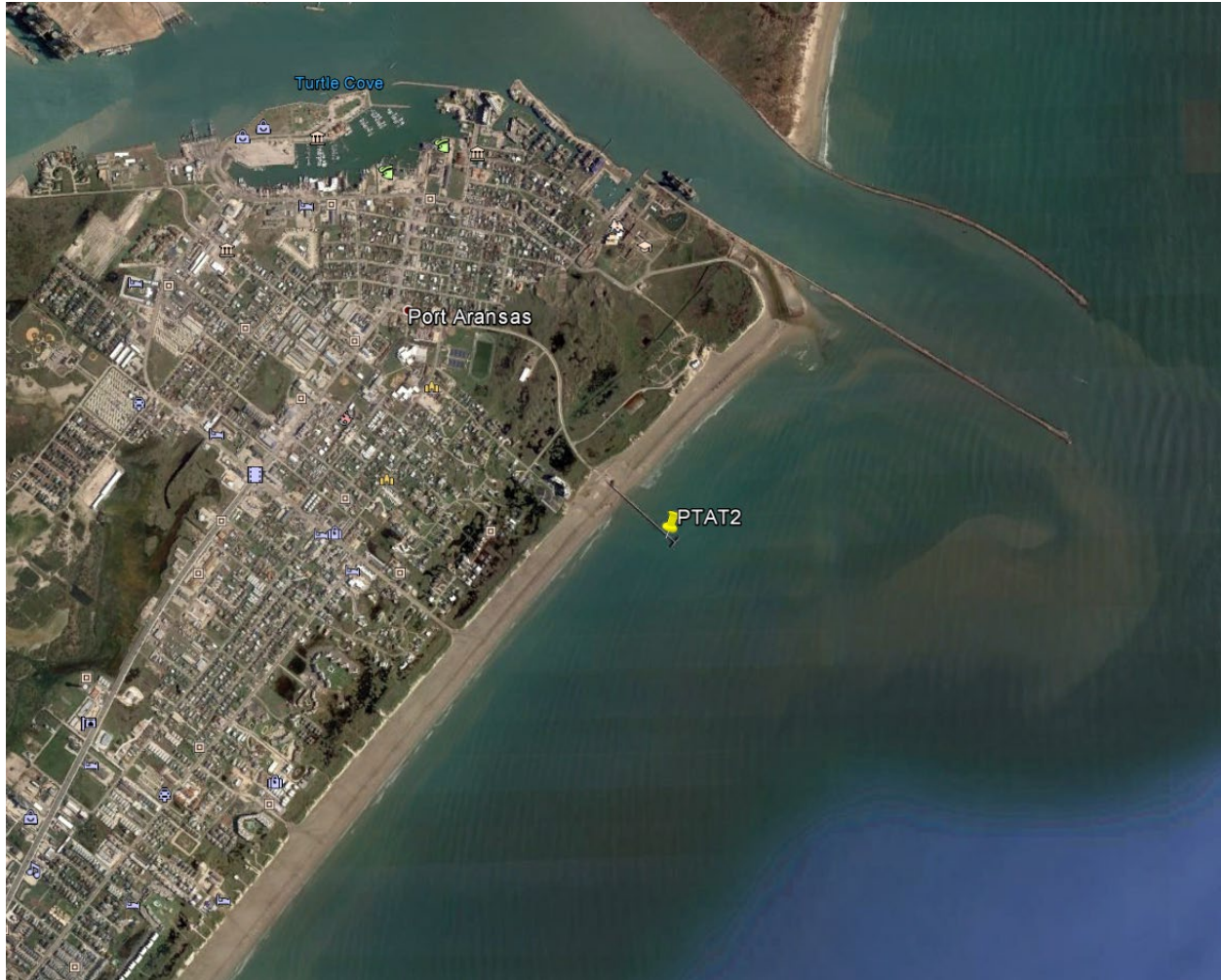


Figure 4-4. NDBC station PTAT2 located very nearshore with a beach park located to the north and residential structures located to the west.

4.4 DISCUSSION OF SELECT STATION TIME HISTORIES

The highest winds at NDBC station 42002 occurred around August 25 3:00 UTC, approximately 24 hours before Hurricane Harvey made landfall on the Texas coast. As shown in Figure 4-5, the model was able to accurately capture the peak winds experienced at 42002 when the storm was closest to the station. When the storm stalled over land, however, the far field winds decayed too quickly, resulting in an underprediction of winds at 42002 between August 26 0:00 UTC and August 28 12:00 UTC.

Nearer to the coast, though still over water, the peak winds modeled at NDBC stations 42045 and 42020 were overpredicted by approximately 10-15% as shown in Figure 4-6 and Figure 4-7. However, the agreement in the overall time series—notably after the storm had passed and was stalled over land—was better than that of station 42002.

Station IRDT2—located on the backside of a barrier island—was subjected to smaller wind speeds than station 42020 despite the intensification of Hurricane Harvey as it approached land. The peak modeled wind speeds, shown in Figure 4-8, were within 5% of the observed values, and the scatter index was

approximately 9%. The modeled wind directions, however, significantly deviated from the observed values following the passing of the storm.

Stations ANPT2 and KRKP (Aransas County Airport) captured the highest winds as Hurricane Harvey made landfall. At station ANPT2 located just off the coast of Port Aransas, the sustained winds were slightly underpredicted, while the peak gust wind speeds were approximately 5% higher than the observed value. In addition, the modeled wind direction lagged the observed values by approximately 45° over the entire time series. At KRKP, the official anemometer failed prior to the occurrence of the highest winds of Hurricane Harvey, though the peak gust wind speed data in Figure 4-10 was supplemented with observations captured by the University of Florida ultrasonic anemometer. The model captured the passage of the center of the storm directly over the station and was within 3% of the observed peak gust wind speed.

Station AWRT2 was located to the right of the storm center just outside the radius of maximum winds. Although the modeled and observed wind speeds showed high agreement, the sustained and peak gust wind speed were overpredicted by the model by 13% and 17%, respectively (see Figure 4-11). Because the anemometer was located on a tower near the coast of mainland Texas in the Aransas National Wildlife Refuge and behind the uninhabited Matagorda Island, the transition from smooth-rough-smooth-rough terrains likely reduced the wind speed experienced at the station.

Although Harvey passed almost directly over station VCAT2 around August 28 6:00 UTC as it moved from land back into the Gulf of Mexico, the peak winds experienced at the station occurred just after landfall on August 26. The modeled peak gust wind matched the observed value. As the storm re-entered the water, the modeled values were more peaked than the observed time history (see Figure 4-12).

The wind speed time history at station 42019, shown in Figure 4-13, was similar to that of station 42002, where winds were underpredicted by the model while the storm was stalled over land. Similar to station 42002, station 42019 was located offshore and to the right of the storm track as it approached landfall and intensified.

Finally, data from several inland stations are presented in Figure 4-14 through Figure 4-18. All of these stations experienced relatively low winds, with the maximum observed gust wind speed of 47 mph at stations KSAT and KLBX. All of the inland stations were located at airports where the uncertainty in the surrounding terrain roughness was less uncertain than the offshore and coastal stations. High agreement was seen between modeled and observed values of peak gust wind speed, sustained wind speed, and wind direction at all five stations.

Across all stations, agreement between modeled and observed central pressures was poor, and the scattered index values were much larger than those of the modeled wind speeds and wind directions. While some pressure time series compare more favorably than others, agreement of all meteorological parameters (e.g., wind speed, direction, central pressure) across all stations was not able to be achieved. Agreement between modeled and observed wind speeds and direction was prioritized over that of modeled and observed central pressures.

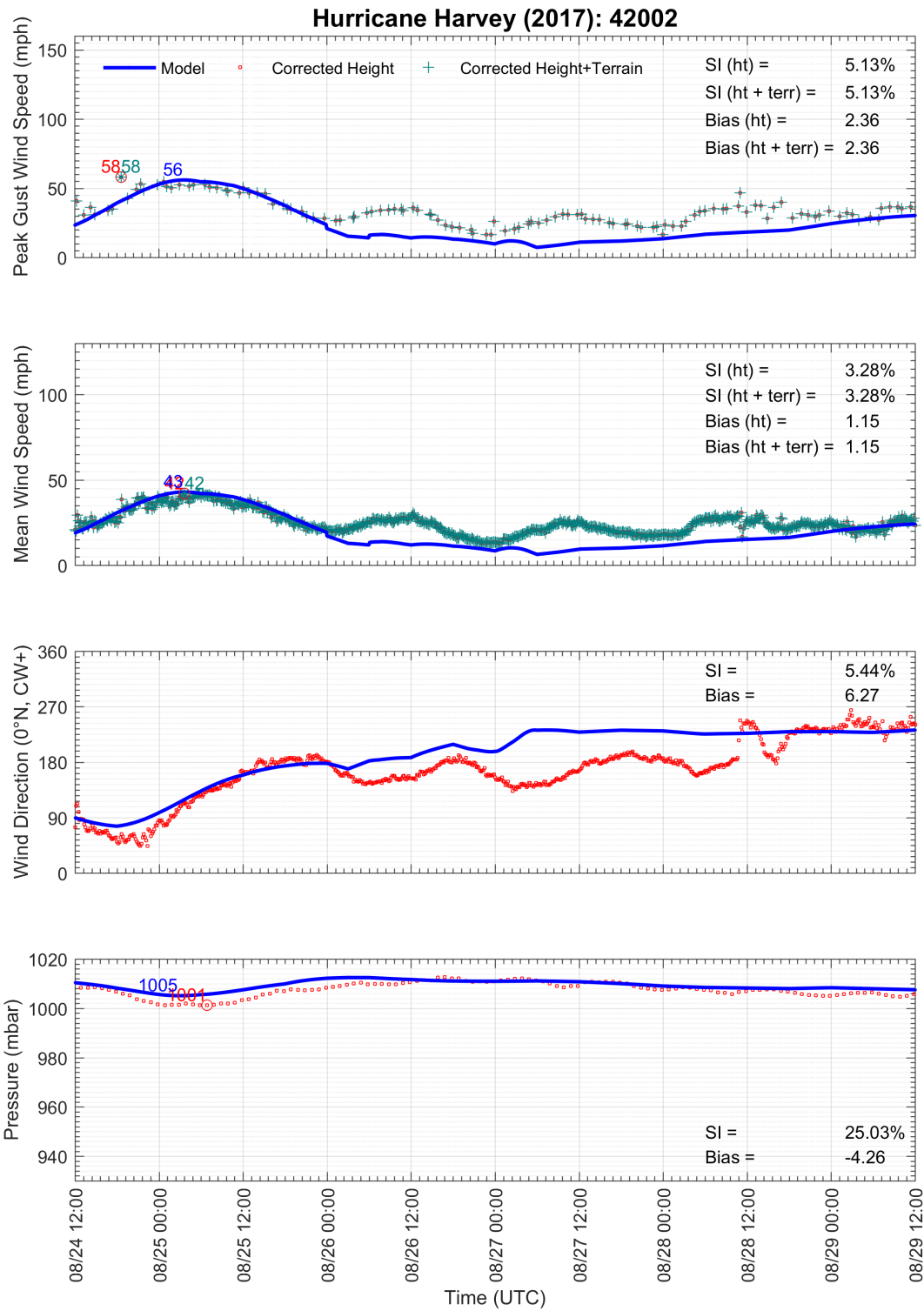


Figure 4-5. Modeled and observed meteorological time series at NDBC station 42002: 207 NM East of Brownsville, Texas.

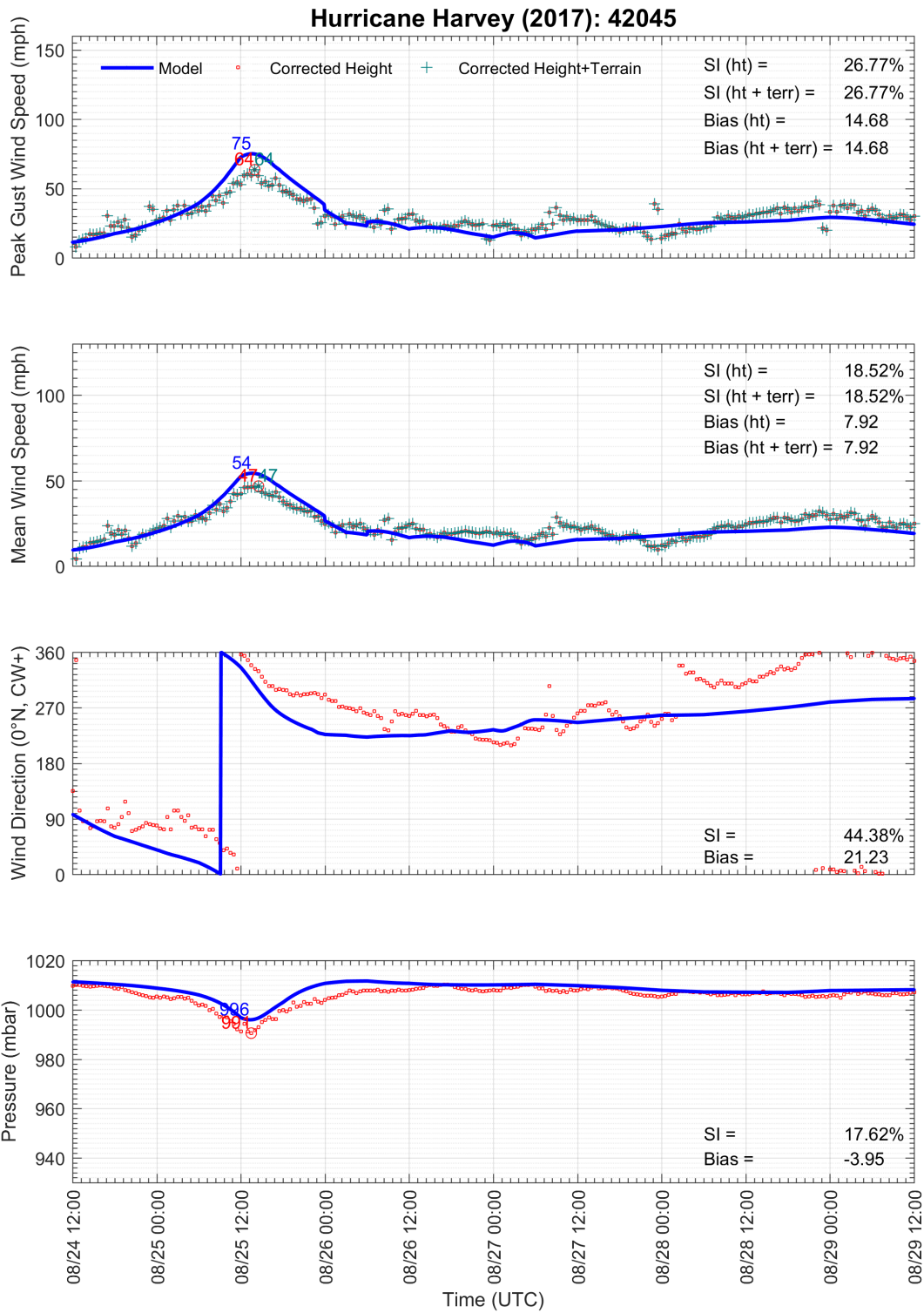


Figure 4-6. Modeled and observed meteorological time series at NDBC station 42045: TGLO TABS Buoy K.

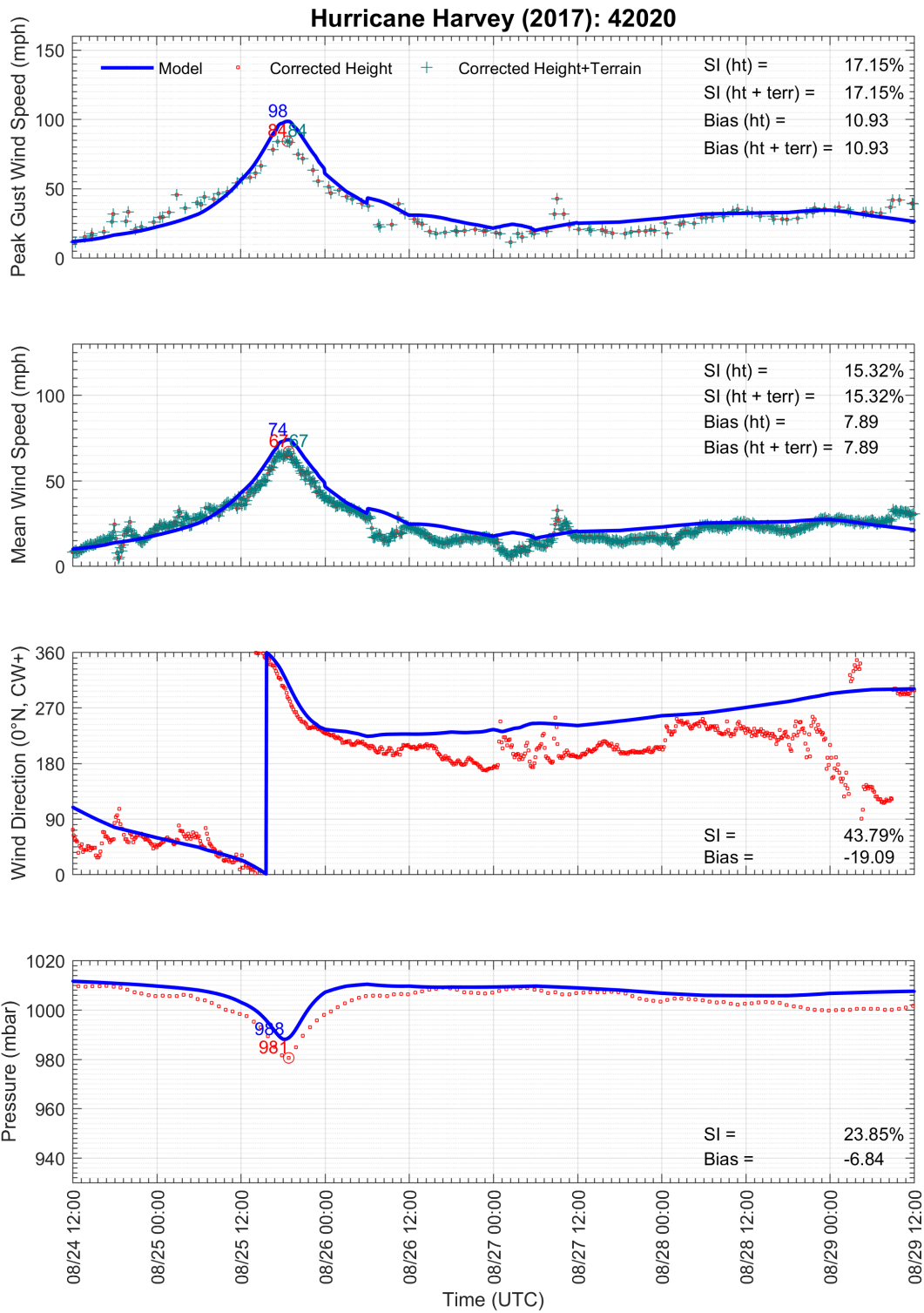


Figure 4-7. Modeled and observed meteorological time series at NDBC station 42020: 60NM SSE of Corpus Christi, Texas.

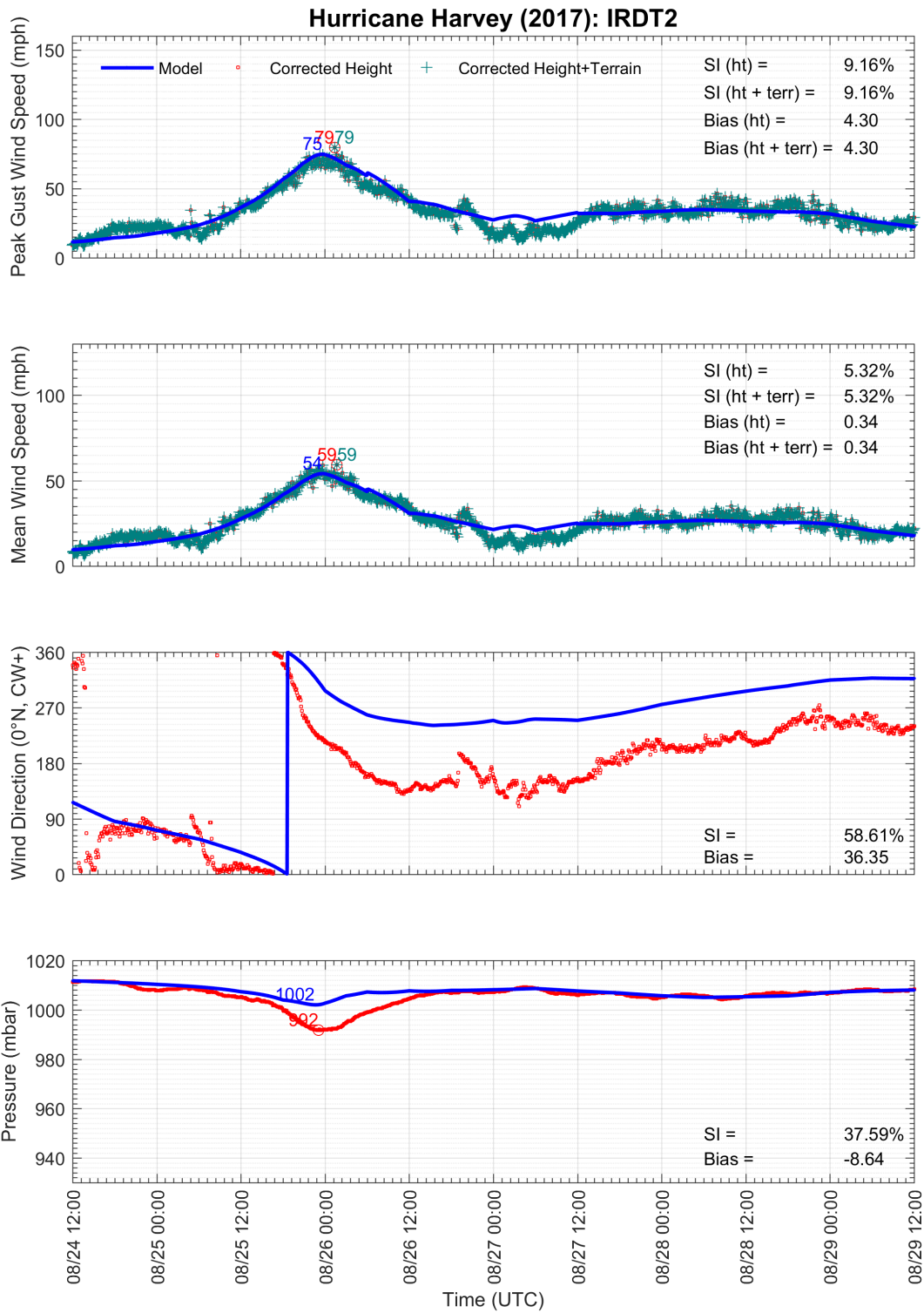


Figure 4-8. Modeled and observed meteorological time series at the Texas Coastal Observing Network's station IRDT2: South Bird Island, Texas.

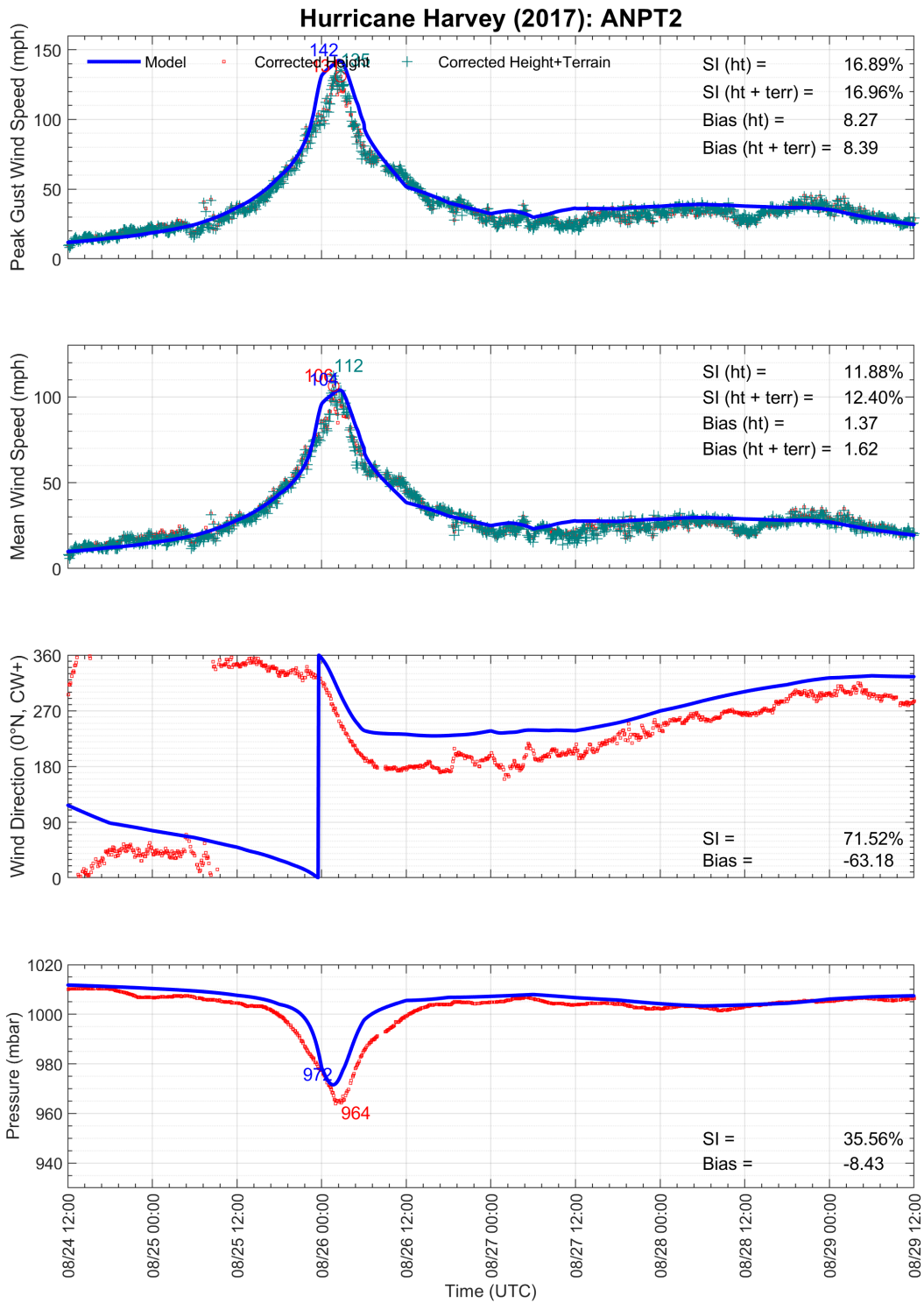


Figure 4-9. Modeled and observed meteorological time series at the Texas Coastal Observing Network's station ANPT2: Aransas Pass, Texas.

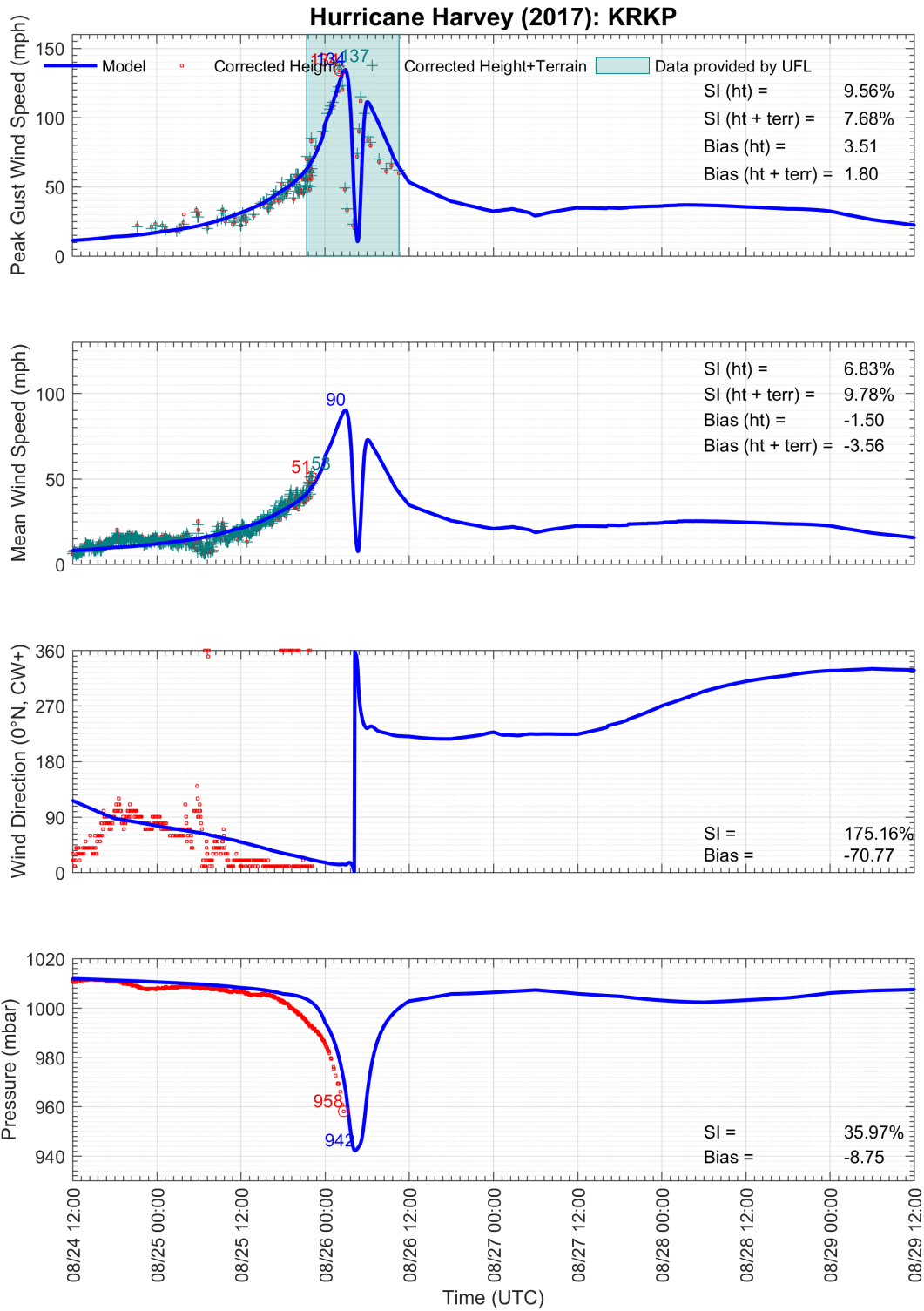


Figure 4-10. Modeled and observed meteorological time series at ASOS station KRKP: Aransas County Airport.

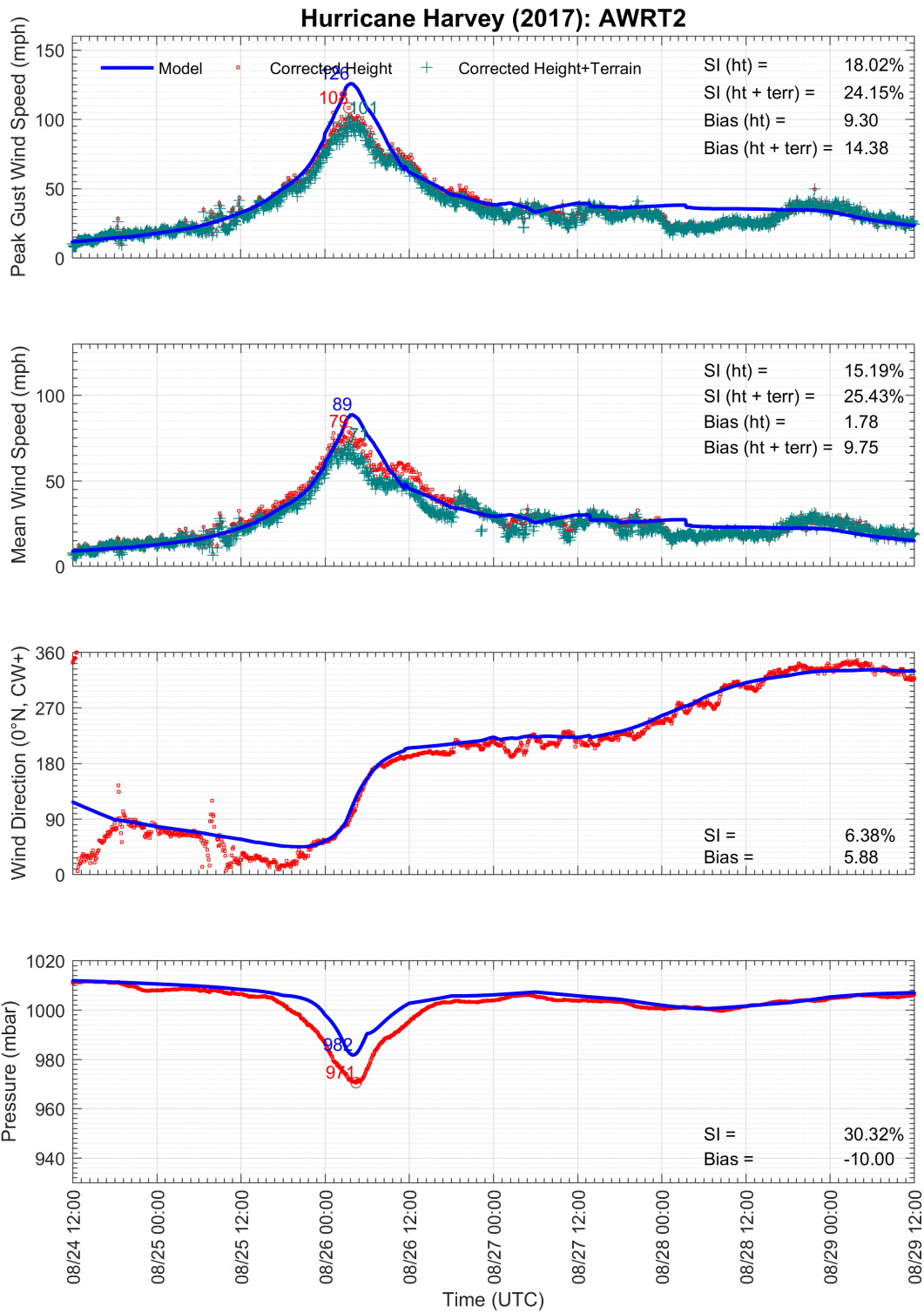


Figure 4-11. Modeled and observed meteorological time series at the Texas Coastal Observing Network's station AWRT2: Aransas Wildlife Refuge, Texas.

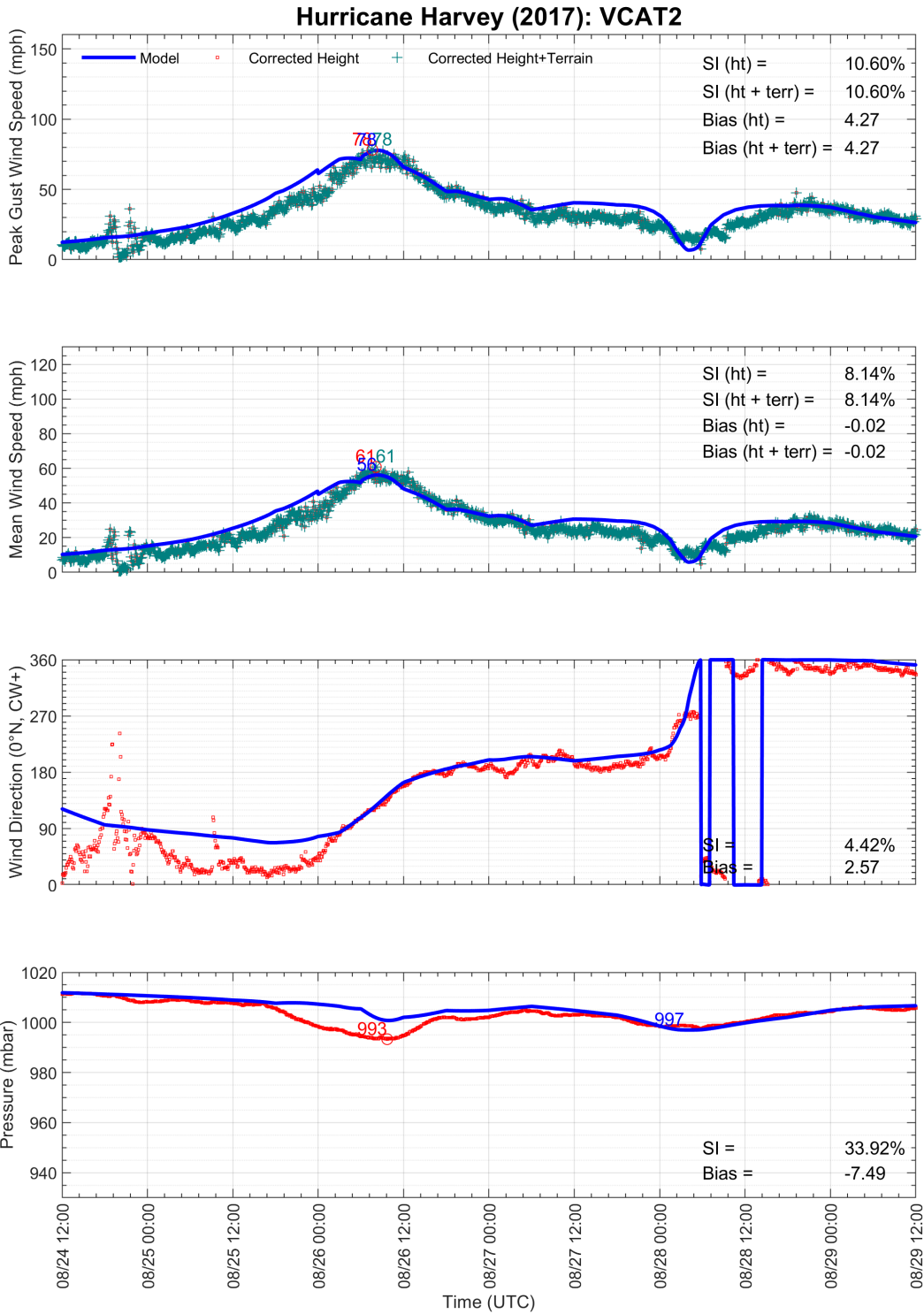


Figure 4-12. Modeled and observed meteorological time series at the Texas Coastal Observing Network's station VCAT2: Port Lavaca, Texas.

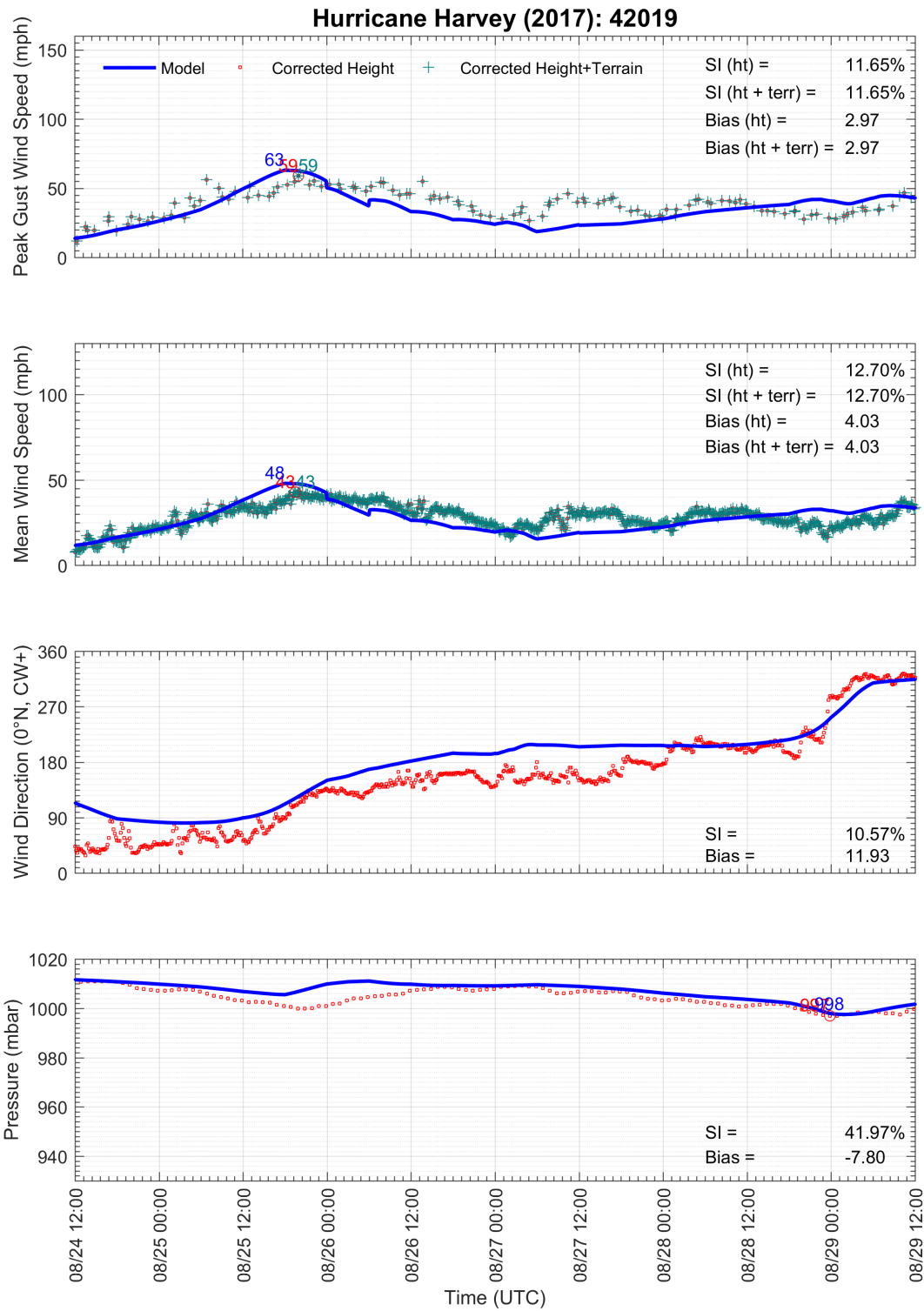


Figure 4-13. Modeled and observed meteorological time series at NDBC station 42019: 60 NM South of Freeport, Texas.

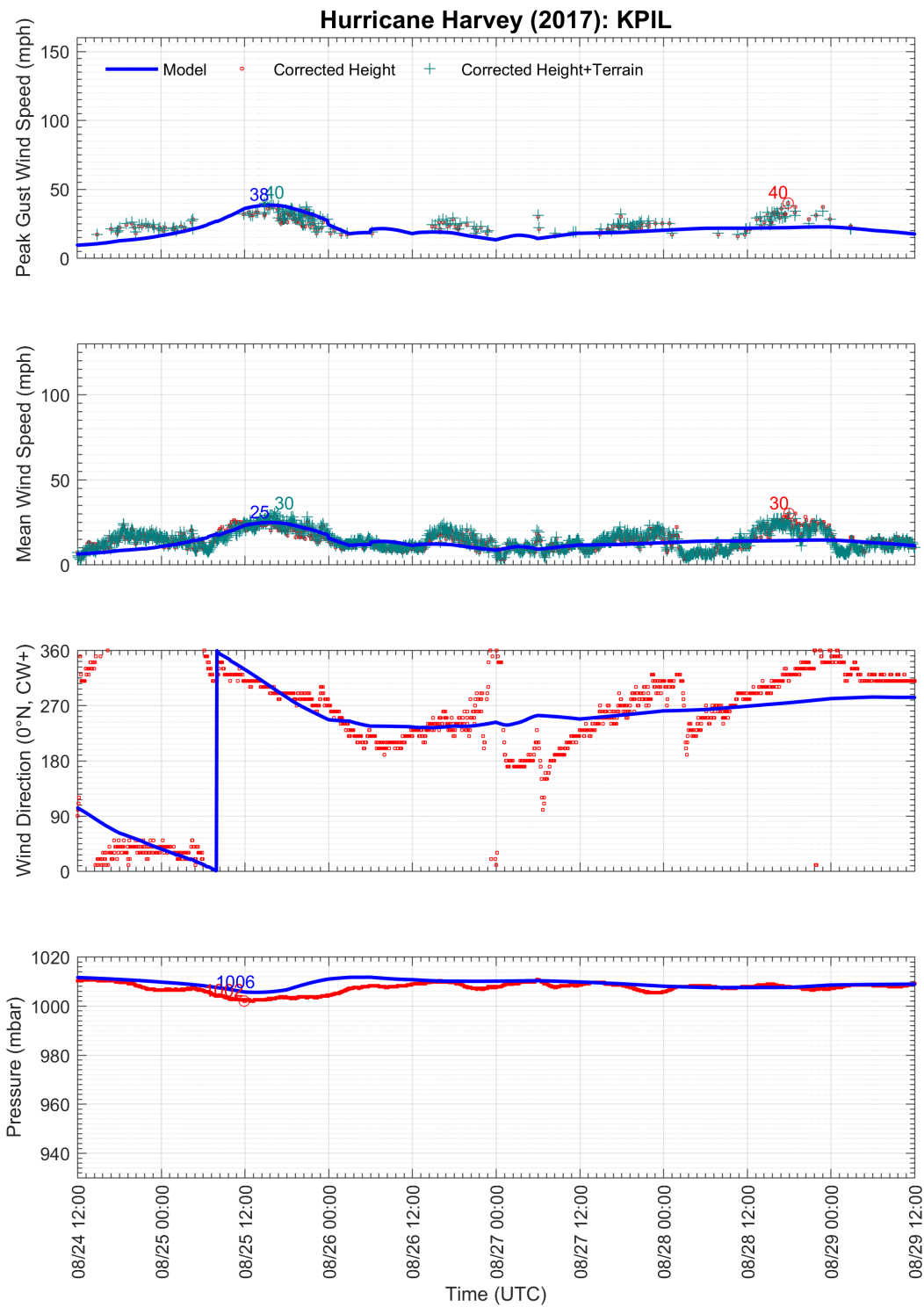


Figure 4-14. Modeled and observed meteorological time series at ASOS station KPIL: Port Isabel Cameron County Airport.

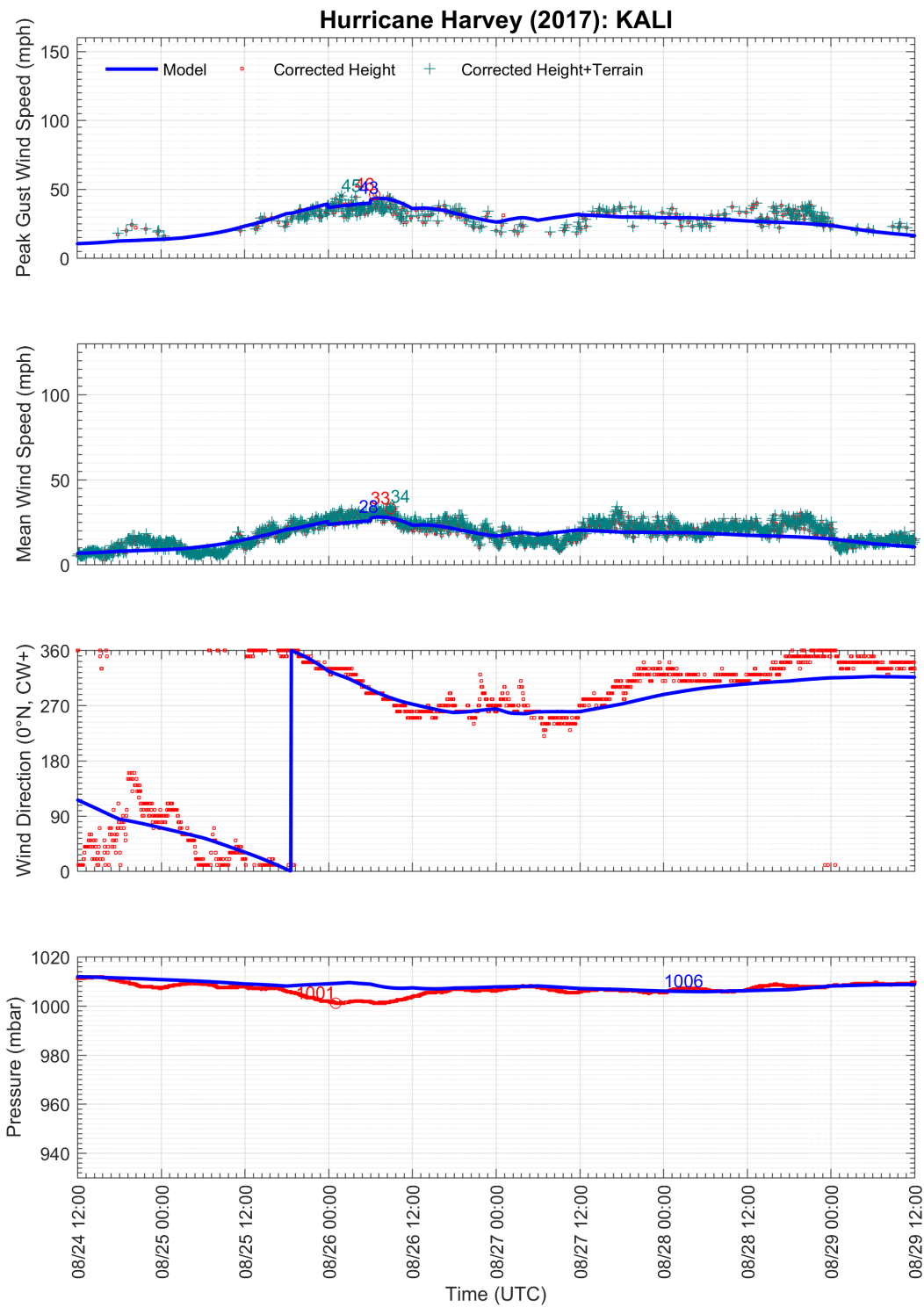


Figure 4-15. Modeled and observed meteorological time series at ASOS station KALI: Alice International Airport.

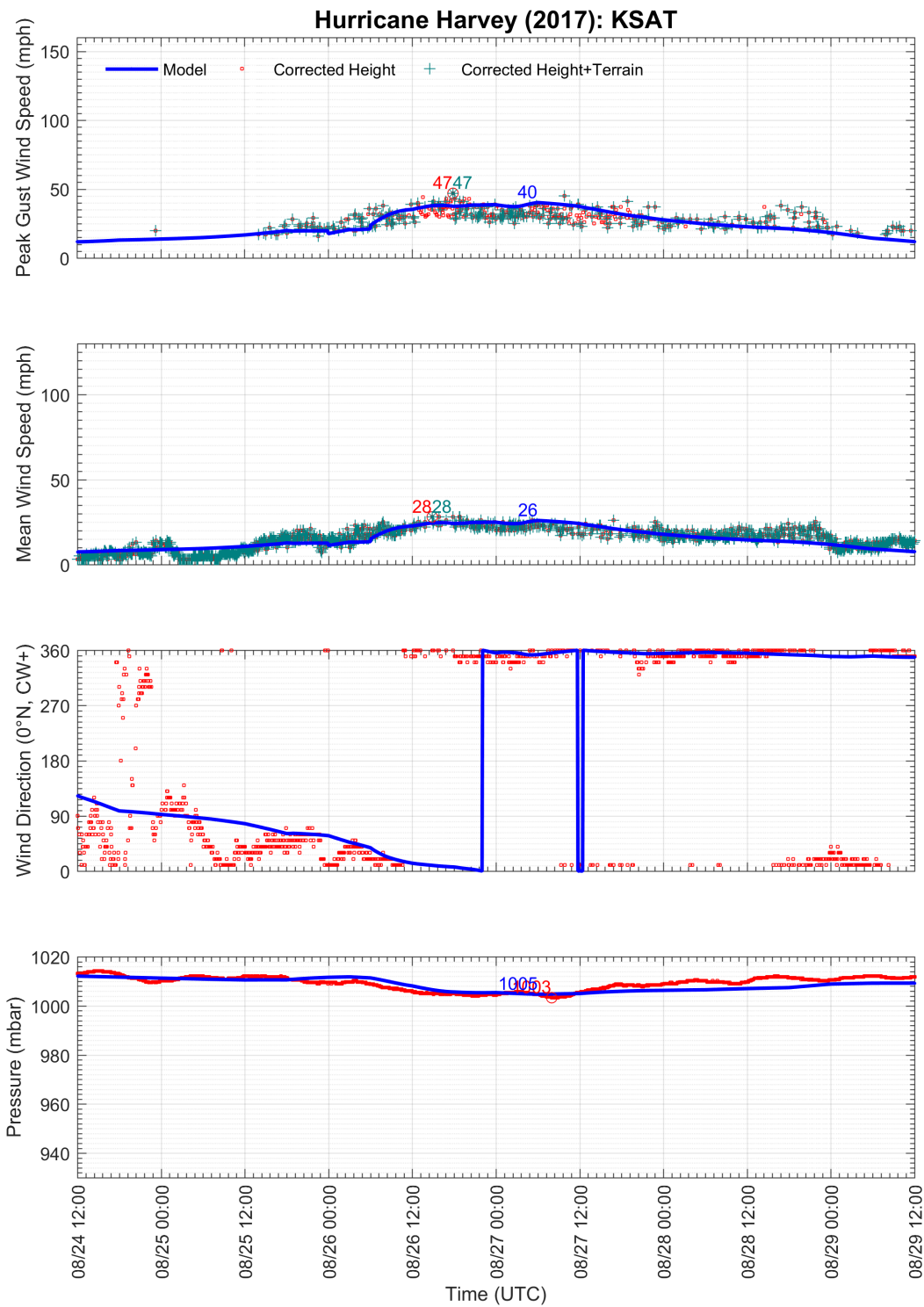


Figure 4-16. Modeled and observed meteorological time series at ASOS station KSAT: San Antonio International Airport.

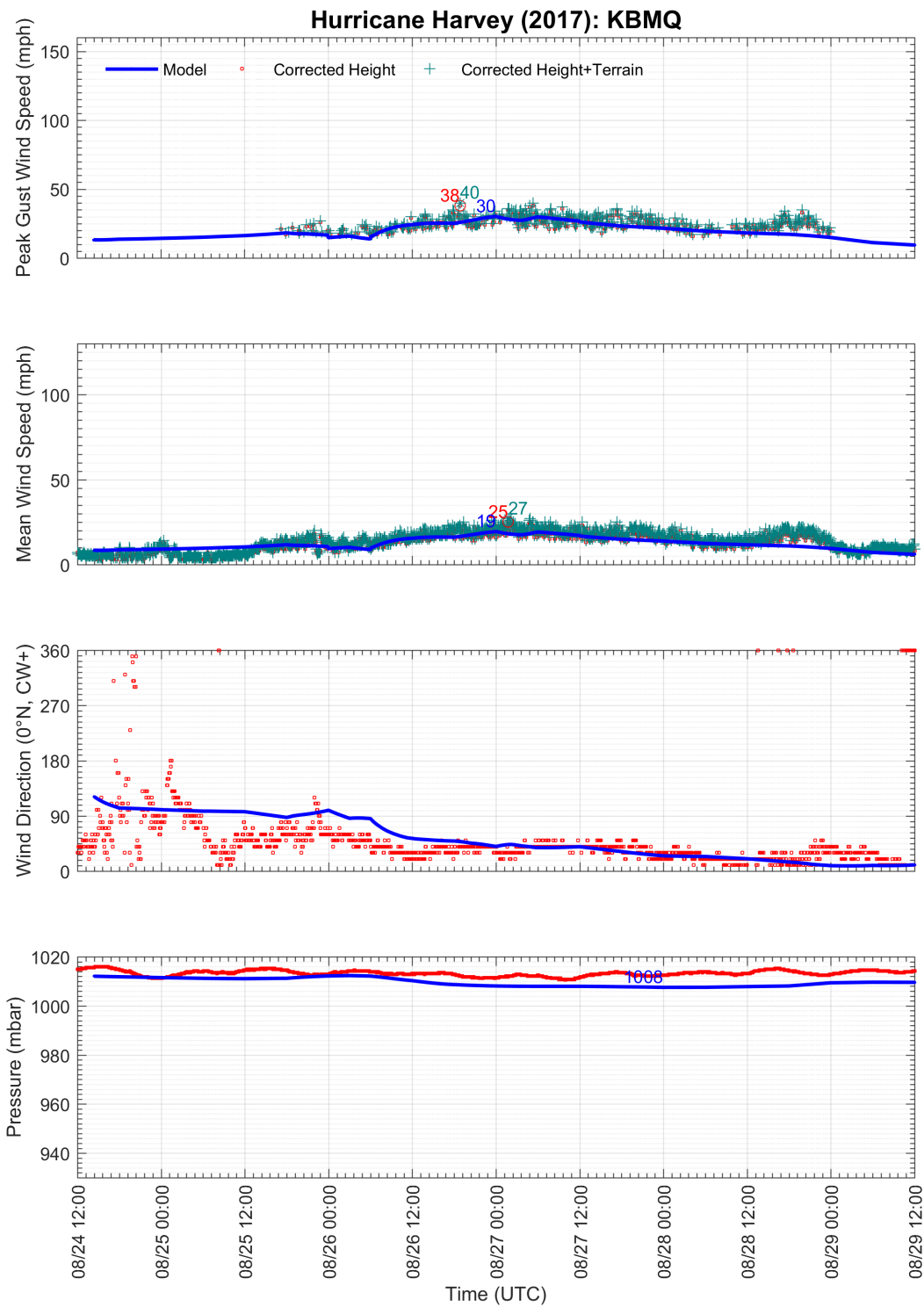


Figure 4-17. Modeled and observed meteorological time series at ASOS station KBMQ: Burnet Municipal Airport – Kate Craddock Field.

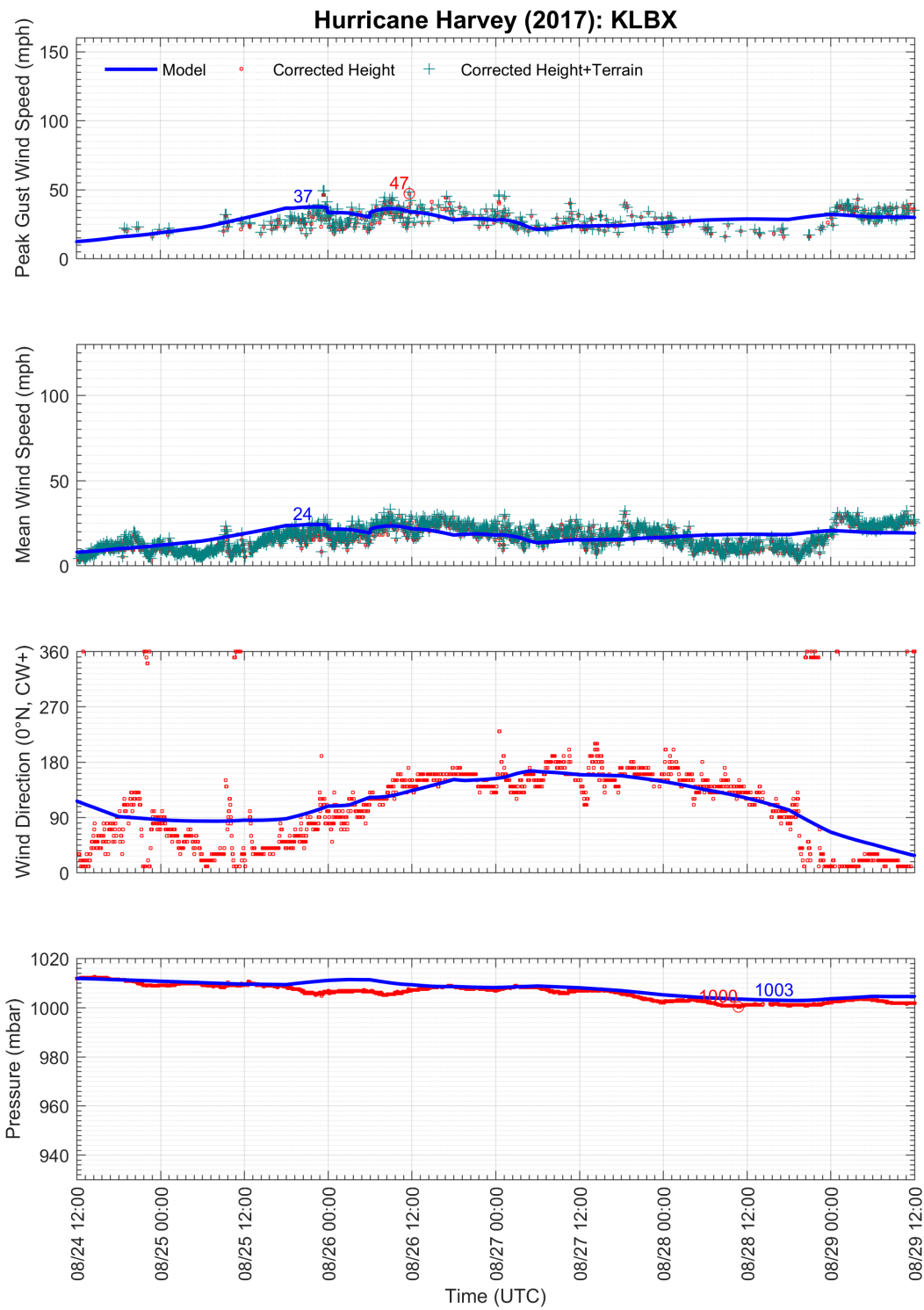


Figure 4-18. Modeled and observed meteorological time series at ASOS station KLBX: Texas Gulf Coast Regional Airport.

4.5 ERRORS AND UNCERTAINTY

Figure 4-19 and Figure 4-20 present comparisons of modeled and observed maximum gust wind speeds and minimum central pressures for the stations used in the model validation process. Stations that failed prior to the arrival of the highest winds were not included in the comparisons. The R^2 values for all parameters (e.g., peak gust wind speed, central pressure), with and without terrain corrections, were around 0.8.

Tabulated error values of peak gust wind speed are provided in Table 4-1 at the end of this section. No error data was provided for stations where the instrumentation failed prior to the occurrence of maximum winds.

The two outliers where the model largely overpredicted the maximum gust wind speed occurred at Texas Coastal Observing Network Stations CPNT2 and AWRT2. As shown in the aerial views of Figure 4-21 and Figure 4-22, both stations were subjected to complex wind interference. In the case of station CPNT2, the anemometer was located on an out-of-service bridge located approximately 100 feet to the northwest of its replacement. The replacement bridge was constructed at a higher elevation and would act to significantly reduce the winds experienced at the anemometer. This effect was not captured in the wind field model. Although station AWRT2 was located over water, it was surrounded by rough terrain of nearby uninhabited islands and Aransas National Wildlife Refuge on the mainland. Not shown in Figure 4-22, the strongest winds coming from offshore also had to pass over Matagorda Island, an uninhabited barrier island with rough terrain. Given that the strongest winds experienced at station AWRT2 occurred from the east, the winds would have transitioned from smooth to rough terrain several times before reaching the anemometer: from the open ocean, over Matagorda Island, into San Antonio Bay, over a small uninhabited island, and briefly back over open water. Such complex terrain interactions were not captured in the wind field model.

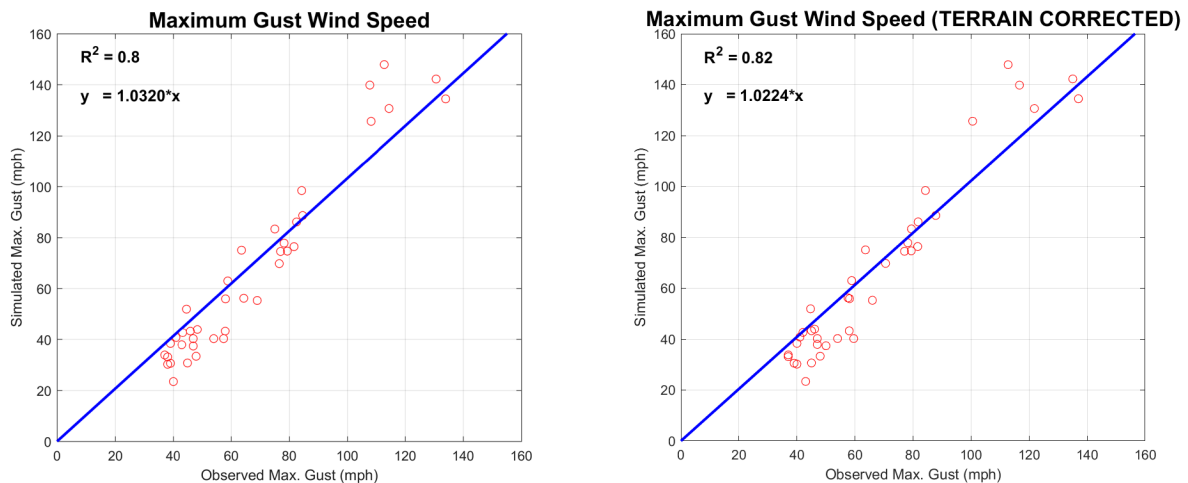


Figure 4-19. Modeled and observed maximum peak gust wind speed corrected only for height (left) and corrected for height and terrain (right).

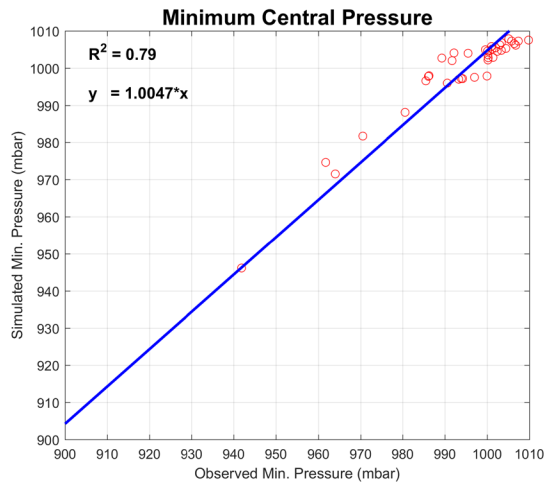


Figure 4-20. Modeled and observed minimum central pressure.

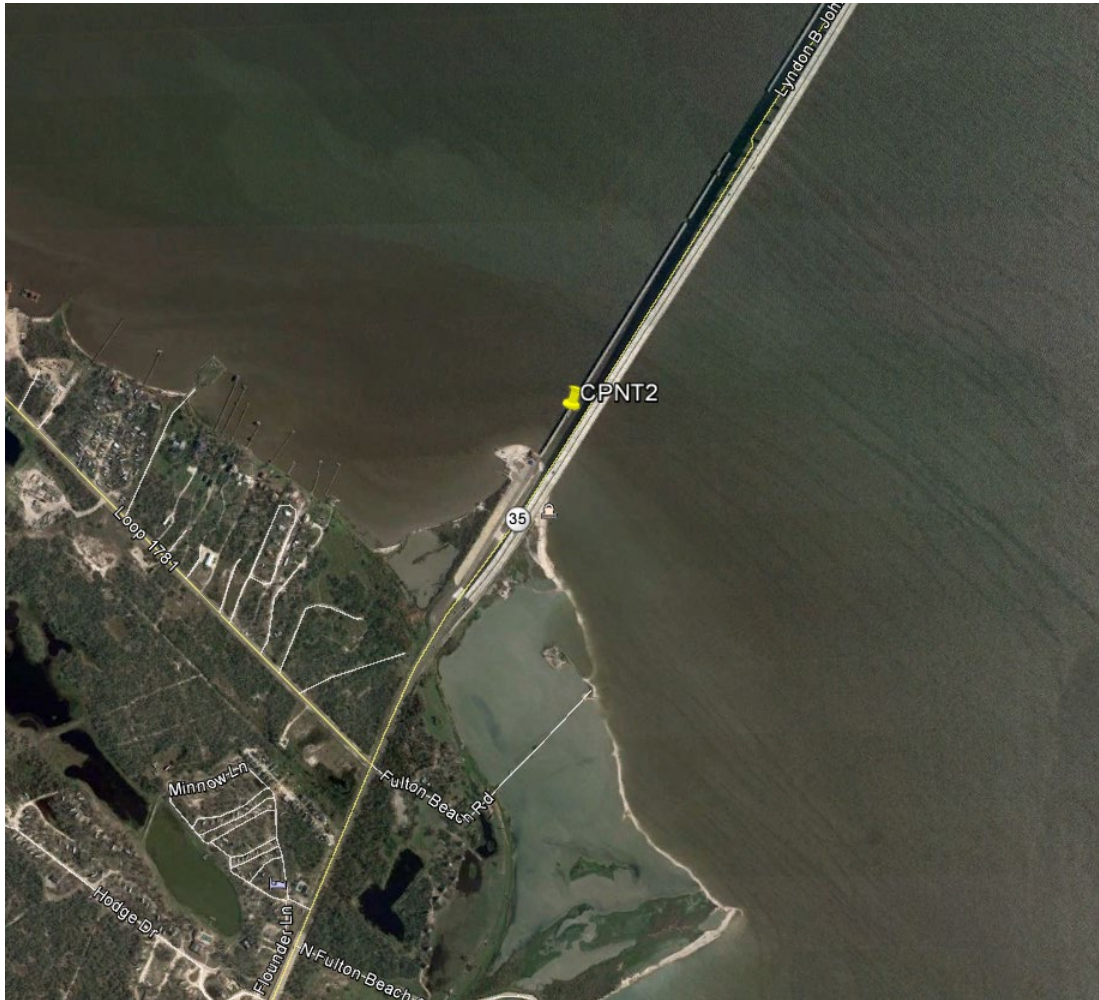


Figure 4-21. Aerial view of Texas Coastal Observing Network Station CPNT2.



Figure 4-22. Aerial view of Texas Coastal Observing Network Station AWRT2.

Table 4-1. Errors in modeled peak gust wind speed in Hurricane Harvey when observations are corrected for height only and for height and terrain. All wind speed values are presented at 10 m elevation in open terrain.

Station	Modeled Peak Gust Wind Speed (mph)	Observed Peak Gust Wind Speed (mph)		Error (mph)	
		Corrected for Height	Corrected for Height + Terrain	Corrected for Height	Corrected for Height + Terrain
KALI	43	46	45	-3	-2
KATT	38	43	47	-5	-9
KAUS	40	54	54	-14	-14
KBAZ	43	58	58	-15	-15
KBMQ	30	38	40	-8	-10
KBRO	34	37	37	-3	-3
KCLL	31	45	45	-14	-14
KCOT	31	39	39	-8	-8
KCRP	---	---	---	---	---

Station	Modeled Peak Gust Wind Speed (mph)	Observed Peak Gust Wind Speed (mph)		Error (mph)	
		Corrected for Height	Corrected for Height + Terrain	Corrected for Height	Corrected for Height + Terrain
KHDO	33	48	48	-15	-15
KHRL	33	37	37	-4	-4
KLBX	37	47	49	-10	-12
KMFE	23	40	43	-17	-20
KPIL	38	40	40	-2	-2
KPSX	---	---	---	---	---
KRKP	134	134	137	0	-3
KSAT	40	47	47	-7	-7
KSSF	41	41	41	0	0
KVCT	---	---	---	---	---
ANPT2	142	131	135	11	7
AWRT2	126	108	101	18	25
BABT2	56	64	58	-8	-2
BZST2	43	43	42	0	1
CPNT2	148	113	113	35	35
FCGT2	40	57	60	-17	-20
IRDT2	75	79	79	-4	-4
MBET2	75	77	77	-2	-2
MQTT2	83	75	79	8	4
NUET2	70	77	71	-7	-1
PACT2	86	82	82	4	4
PCNT2	76	82	82	-6	-6
PTAT2	140	108	117	32	23
RCPT2*	131	114	122	17	9
RSJT2	44	48	46	-4	-2
SDRT2	89	85	88	4	1
VCAT2	78	78	78	0	0
42002	56	58	58	-2	-2
42019	63	59	59	4	4
42020	98	84	84	14	14
42044	52	45	45	7	7
42045	75	64	64	11	11

* Note: Station RCPT2 failed very near the expected time of maximum winds and may not have captured the true maximum wind speed experienced.

4.6 WIND FIELD MAP

The final peak gust wind speed map of Hurricane Harvey is shown in Figure 4-23 with wind speed contours in increments of 10 mph. Peak gust wind speeds are defined as 3-second average at 10 m above ground over open terrain. The storm track is shown by the dashed blue line. All stations used in the wind field model validation are also shown: purple triangles indicate an ASOS station, and green triangles indicate a station in the NDBC database located over water or near the coast. The highest

winds are shown to have occurred near Holiday Beach, San Jose Island, and the western end of the Aransas National Wildlife Refuge.

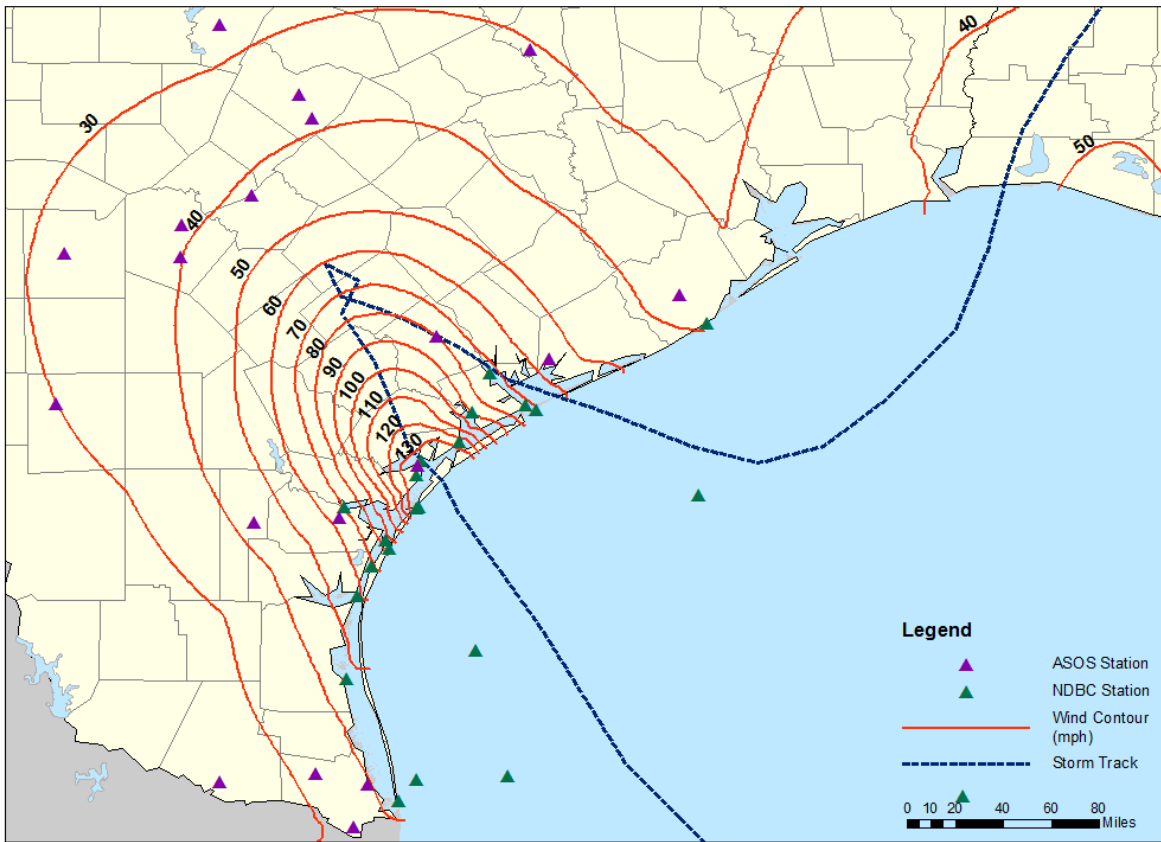


Figure 4-23. Peak gust wind speed contour map for Hurricane Harvey (2017) showing estimated 3-second peak gust wind speeds (mph) at 10 m above ground over open terrain. Model output obtained from ARA wind field model fit to surface level observations using NHC best track and central pressures.

5 HURRICANE IRMA (CONUS)

5.1 EVENT BACKGROUND

A brief background for Hurricane Irma (2017) and its impacts in the contiguous United States is presented in this section. For a full narrative of the storm, including synoptic history, meteorological statistics, casualty and damage statistics, and forecast and warning critique, see the National Hurricane Center's Tropical Cyclone Report on Hurricane Irma (Cangialosi et al., 2018) available at https://www.nhc.noaa.gov/data/tcr/AL112017_Irma.pdf.

Hurricane Irma was a Category 5 hurricane that made seven total landfalls, four of which occurred in the Caribbean Islands when Irma was a Category 5 event. The storm made initial landfall in the Florida Keys as a Category 4 on September 10 13:00 UTC, and made landfall on mainland Florida as a Category 3 on September 10 19:30 UTC. According to the NHC, Irma produced a maximum 1-minute sustained wind speed of 155 knots (178 mph) over water as the storm tracked westward near the Caribbean Islands of Barbuda and the U.S. Virgin Islands (USVI). The maximum sustained 1-minute wind speeds when Irma made landfall on the Florida Keys and the western Florida coastline are estimated to be 115 knots (132 mph) and 100 knots (115 mph), respectively. Minimum estimated central pressures for the Florida landfalls were 931 and 936 mbar. The highest observed gust wind speed over land in Florida was 123 knots (142 mph) at the Naples Municipal Airport (KAPF).

After making landfall in Florida, Irma weakened due to its interaction with land and the presence of a strong vertical wind shear. The storm tracked near Naples as a Category 2 hurricane on September 11 00:00 UTC, continued towards Tampa and Orlando as a Category 1 hurricane on September 11 6:00 UTC, and weakened to a tropical storm by September 11 12:00 UTC. The storm continued on a northwestern trajectory, transformed to a remnant low on September 12 6:00 UTC, and finally dissipated on September 13 12:00 UTC.

Maximum storm surge and tide inundation levels of 5 to 8 feet were estimated for portions of the Lower Florida Keys near and to the east of where Irma made landfall. In the Middle and Upper Florida Keys, maximum inundation levels of 4 to 6 feet were estimated. On mainland Florida, maximum inundation levels of 6 to 10 feet were estimated for the southwest coast, and 4 to 6 feet for the eastern Florida coast. Combined with rainfall totals of 10 to 15 inches across the Florida peninsula and Keys, several areas (such as Miami) saw extensive flooding during the event.

Hurricane Irma also produced 25 confirmed tornadoes, with the majority occurring along the east coast and central and northern Florida. Of the 25 tornadoes, 3 were given a maximum intensity of EF2, 15 EF1, and 7 EF0.

5.2 DATA COLLECTION

5.2.1 Track

A portion of the best track of Hurricane Irma is shown in Figure 5-1 as the storm is approached and made landfall along the Florida coastline.

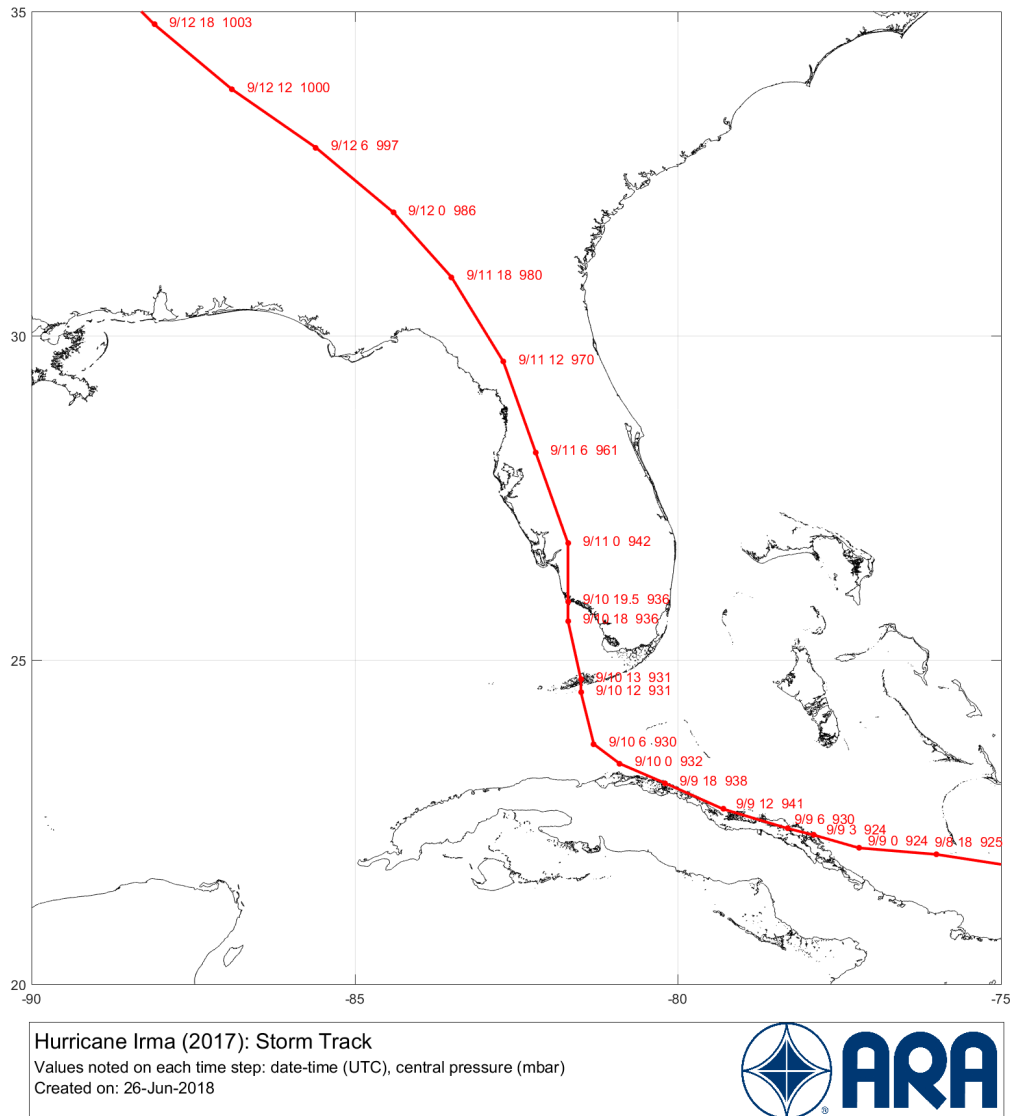


Figure 5-1. Best-track information of Hurricane Irma (2017) collected from the NHC Atlantic Hurricane Database (HURDAT2).

5.2.2 Observations

Stations with observations during the lifespan of Hurricane Irma and within 150 miles of a track point were used in the model validation and are shown in Figure 5-2. A table of station locations and anemometer heights is provided in Appendix B.

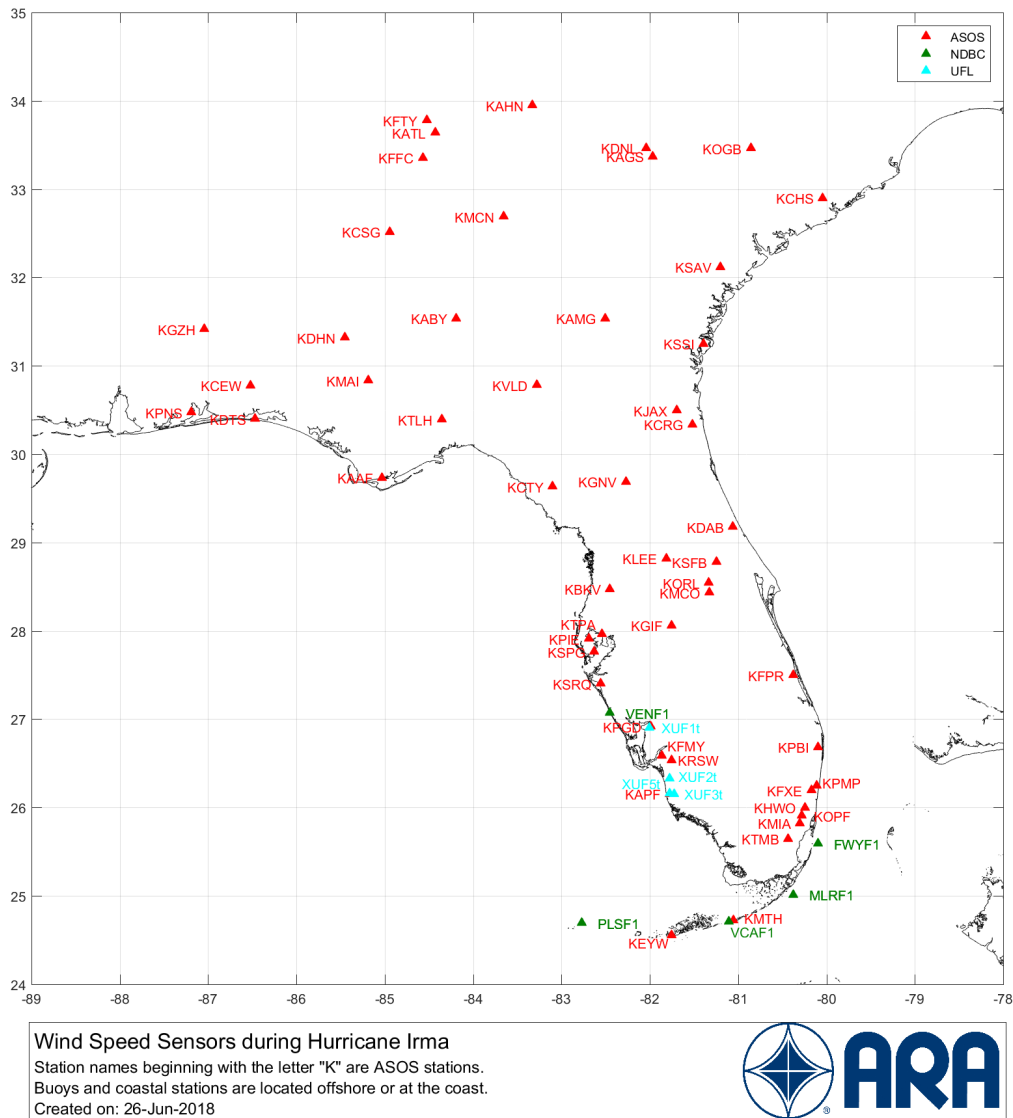


Figure 5-2. ASOS, NDBC and University of Florida mobile stations with surface observations in and near the Contiguous United States during the lifespan and within 150 miles of Hurricane Irma.

5.3 DATA CORRECTIONS (DEVIATION FROM STANDARD PROCEDURES)

Wind speed observations at stations located very nearshore are often affected by the rougher terrain of nearby land and do not correspond to true marine terrain observations. For example, Figure 5-3 shows the National Oceanic and Atmospheric Administration’s (NOAA) National Ocean Service station VCAF1 where a densely populated residential and condominium area lies to the east and south, and further to the south lies an uninhabited island consisting of mostly trees. Estimates of directional effective surface roughness have not been previously generated for very nearshore stations. To account for terrain effects on these stations, a visual technique was used to estimate the directional surface roughness values from aerial imagery. Visually estimated values of z_0 serve as input to the ESDU methodology.



Figure 5-3. NOAA National Ocean Service Station VCAF1 located very nearshore with condominiums, residential structures, and an uninhabited island located to the east and south.

5.4 DISCUSSION OF SELECT STATION TIME HISTORIES

The highest winds at three NDBC stations located in the Florida Keys—PLSF1, VCAF1, and FWYF1—were experienced just prior to landfall between September 10 6:00 UTC and 18:00 UTC. The time histories for each of these stations are shown in Figure 5-4 through Figure 5-6. Station PLSF1 was located on the left side of the storm track, while VCAF1 and FWYF1 were located on the right side of the storm and captured higher wind speeds. The time histories of sustained and gust wind speeds at station VCAF1 were consistently overpredicted, which is likely attributed to complex terrain interference as discussed in Section 5.5. The time histories for the modeled and observed values at PLSF1 and FWYF1 agreed well with low scatter index values of around 14% for gust wind speeds. The peak gust winds were underpredicted by 2% and 8% at Stations PLSF1 and FWYF1, respectively.

As Hurricane Irma moved inland, the eye passed directly over station KRSW where the peak winds occurred at the time of landfall (see Figure 5-7). The modeled peak sustained and gust wind speeds were about 3% and 11% overpredicted, respectively. The modeled wind direction agreed well through landfall, but significantly deviated from the observed values following the passing of the storm.

Further to the north, located on the west coast of Florida, station KSRQ captured wind speeds on the left side of the storm just outside the radius of maximum winds. As shown in Figure 5-8, the overall time series of modeled winds agreed well with observed values, displaying scatter indices of about 10% and 20% for gust and sustained with speeds, respectively. The peak gust wind speed was overpredicted by about 8%. Following the passing of the storm, similar patterns to those seen at station KRSW were shown in the deviation of modeled and observed wind directions.

Wind speed time histories to the right of the storm track were captured by stations KOPF, KPBI, and KFPR, located on Florida's east coast. At each station, the modeled gust wind speeds display scatter index values between about 10% and 20%, with a slightly high bias ranging from about 0 to 11 mph. (See Figure 5-9 through Figure 5-11.) The peak gust wind speed at each station was overpredicted between 4% and 7%. The central pressure time histories show a near zero bias at all three stations.

During the day of September 11, Hurricane Irma continued inland on a northwestern trajectory, passing by four stations: KGIF, KORL, KDAB, and KCRG. From south to north, as Irma continued to weaken, the bias of the modeled gust wind speed time series reduced from close to 24% at KGIF to -1% to -2% at KDAB and KCRG, respectively, as shown in Figure 5-12 through Figure 5-15. Nearer to the storm center at stations KGIF and KORL, the peak gust wind speed was overpredicted by 22% and 14%, respectively. At increasing distances from the storm center, the model first aligned with observed data (matching the observed gust wind speed at KDAB) and ultimately underpredicted the gust wind speed (by about 17% at KCRG).

Slightly to the right of the storm center at station KVLG, both the sustained and gust wind speed time histories agreed well (see Figure 5-16), though the instrumentation failed prior to the occurrence of the highest wind speeds.

Data from several inland stations are presented in Figure 5-17 through Figure 5-20. Maximum gust wind speeds at each station were relatively low, ranging from 30-40 mph on the left side of the track to 55-60 mph on the right side of the track. No values of scatter index or bias were calculated for these stations since there was no extended period of time with tropical storm force winds (≥ 40 mph sustained wind speed), though gust wind speeds were underpredicted at all stations. The modeled and observed pressure time histories differ by about 10 mbar prior to midday UTC on September 11, after which agreement significantly improved.

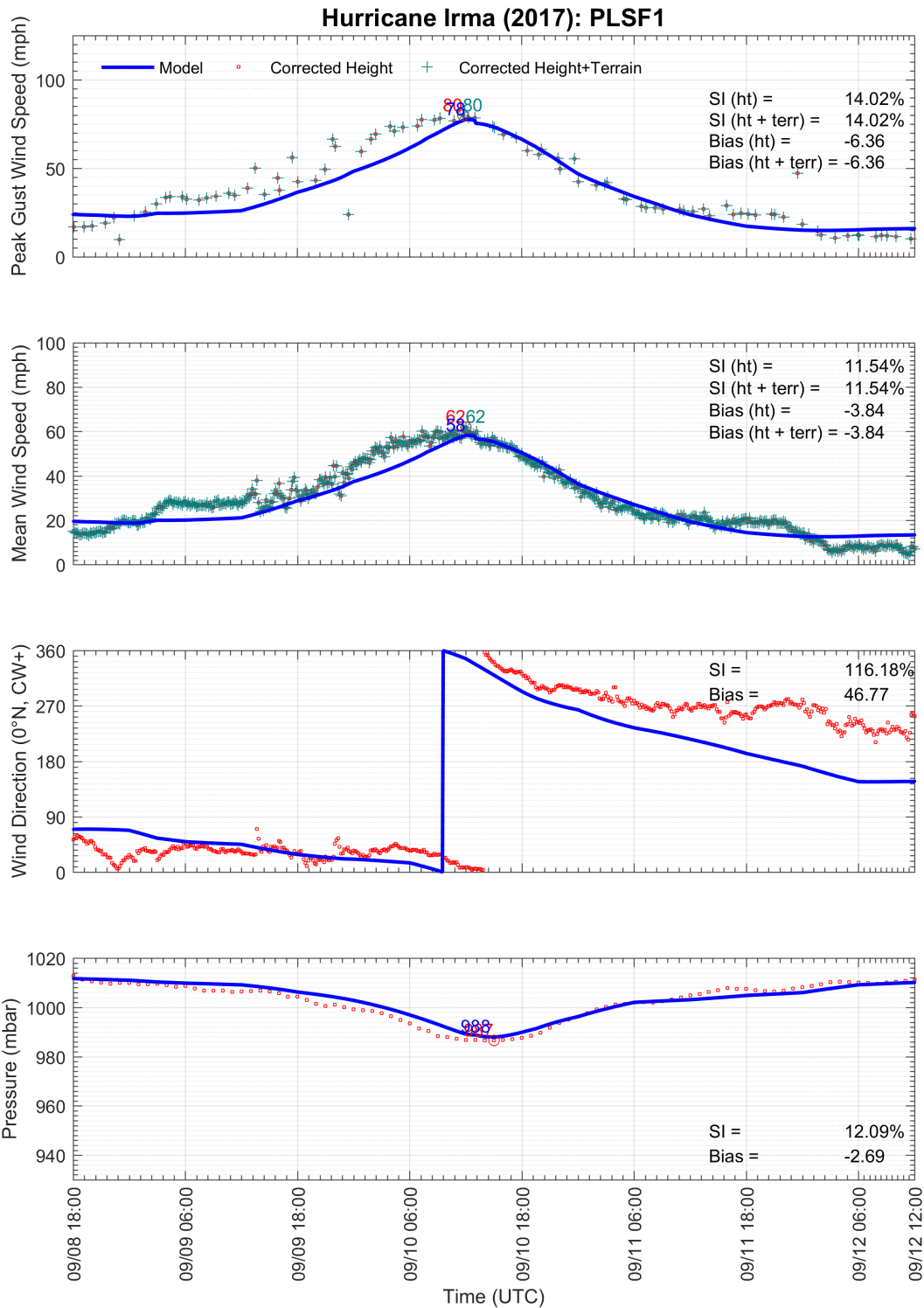


Figure 5-4. Modeled and observed meteorological time series at NDBC station PLSF1: Pulaski Shoals Light, Florida.

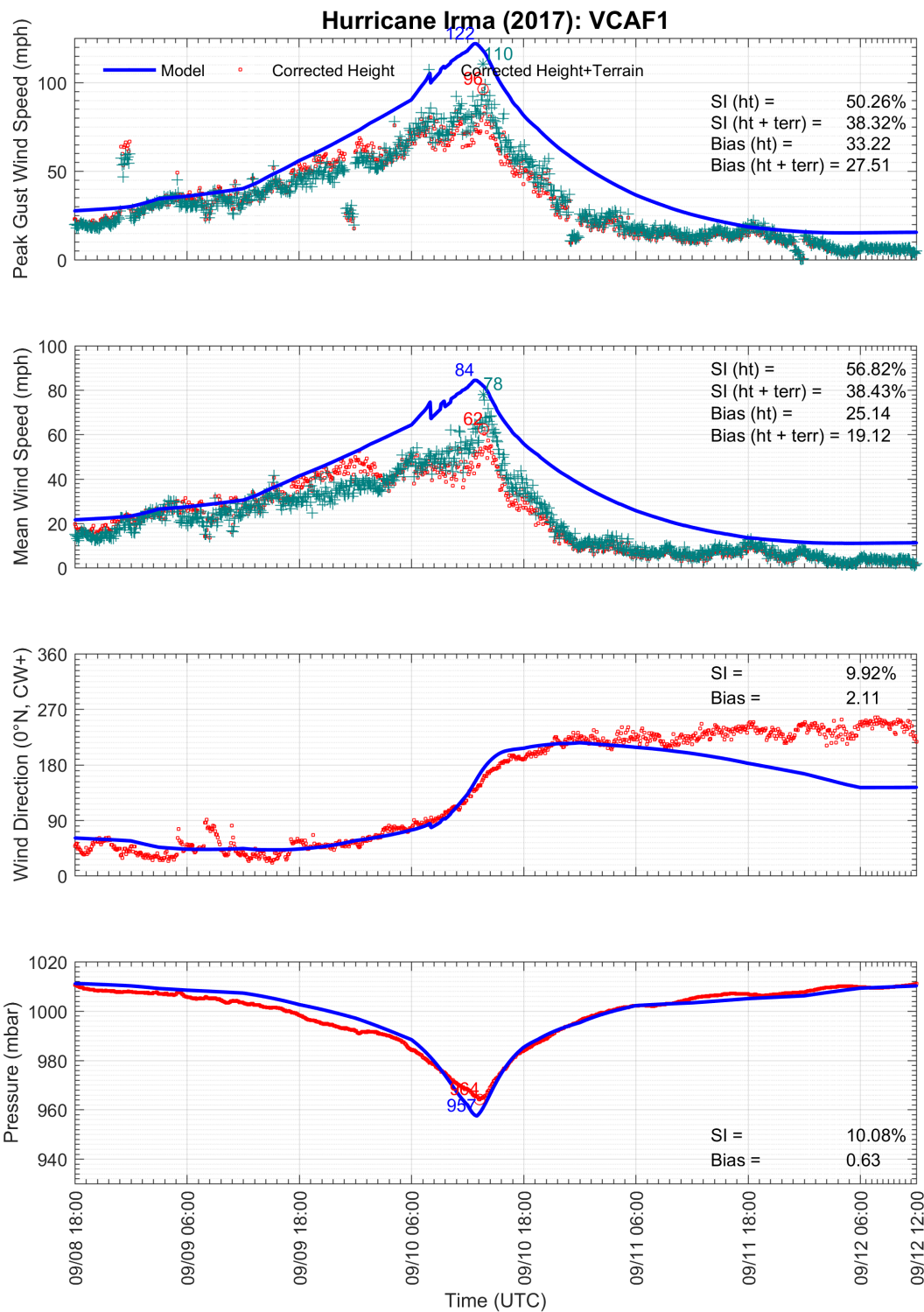


Figure 5-5. Modeled and observed meteorological time series at NDBC station VCAF1: Vaca Key, Florida.

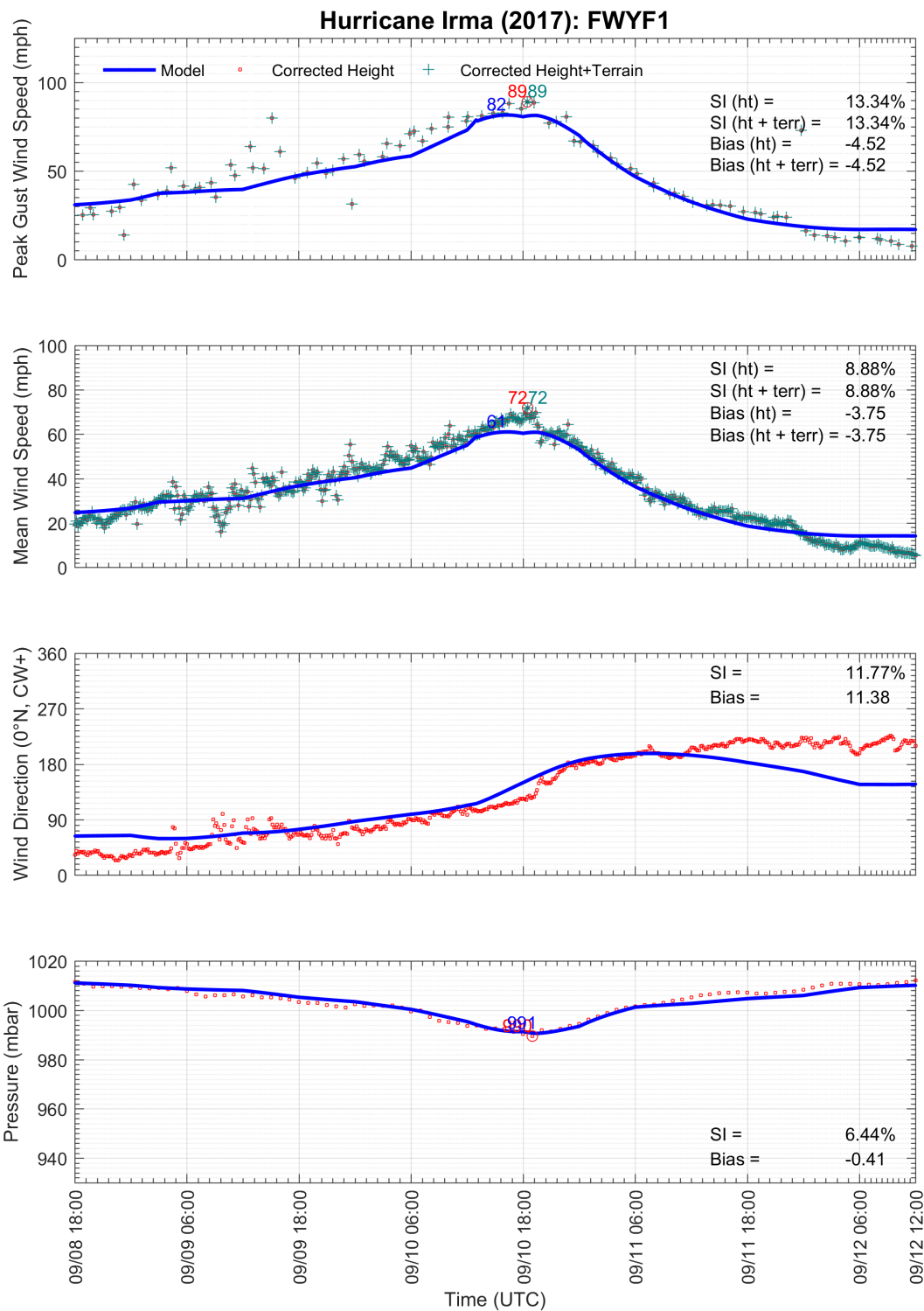


Figure 5-6. Modeled and observed meteorological time series at NDBC station FWYF1: Fowey Rock, Florida.

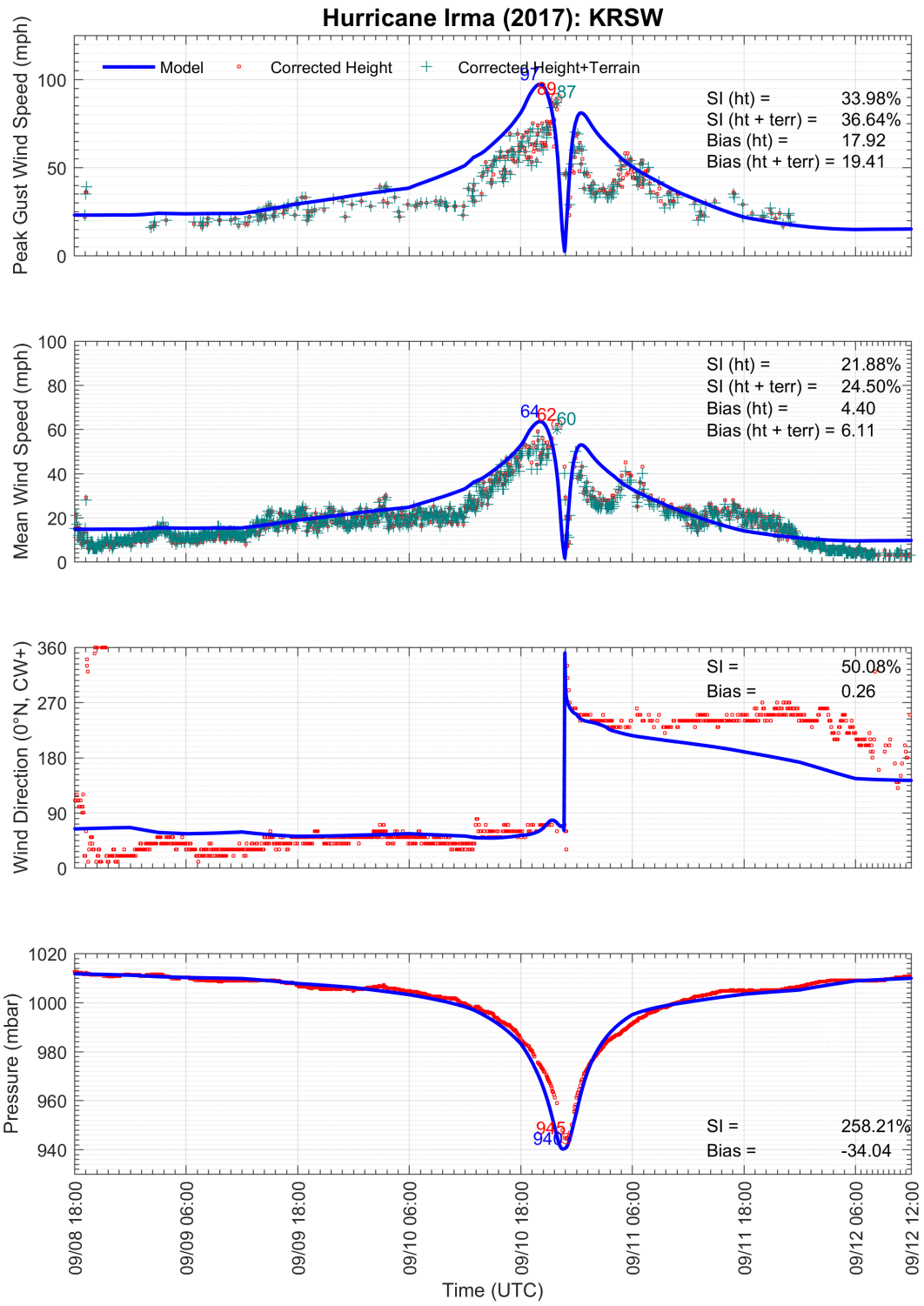


Figure 5-7. Modeled and observed meteorological time series at ASOS station KRSW: Southwest Florida International Airport.

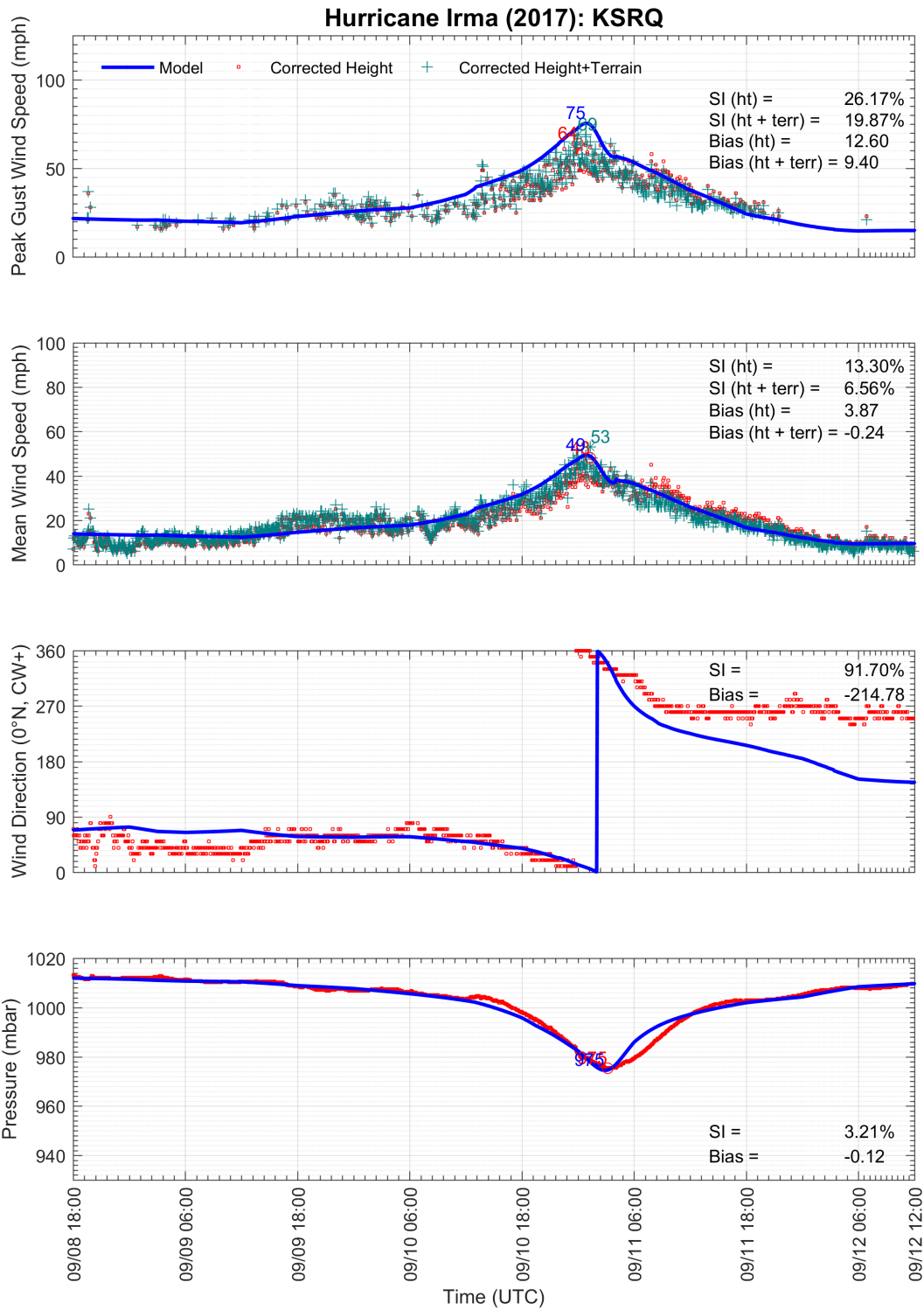


Figure 5-8. Modeled and observed meteorological time series at ASOS station KSRQ: Sarasota-Bradenton International Airport.

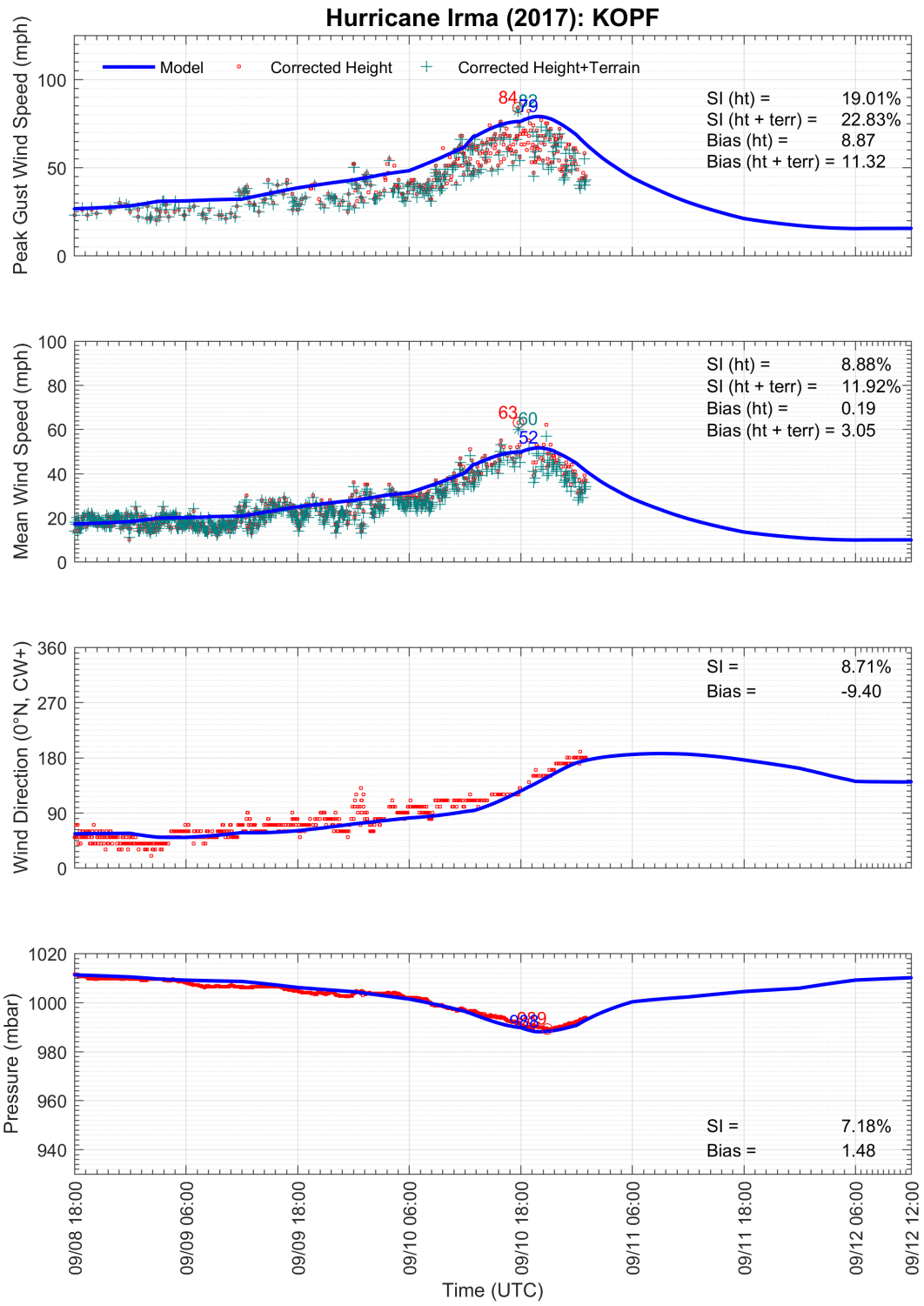


Figure 5-9. Modeled and observed meteorological time series at ASOS station KOPF: Miami-Opa Locka Executive Airport.

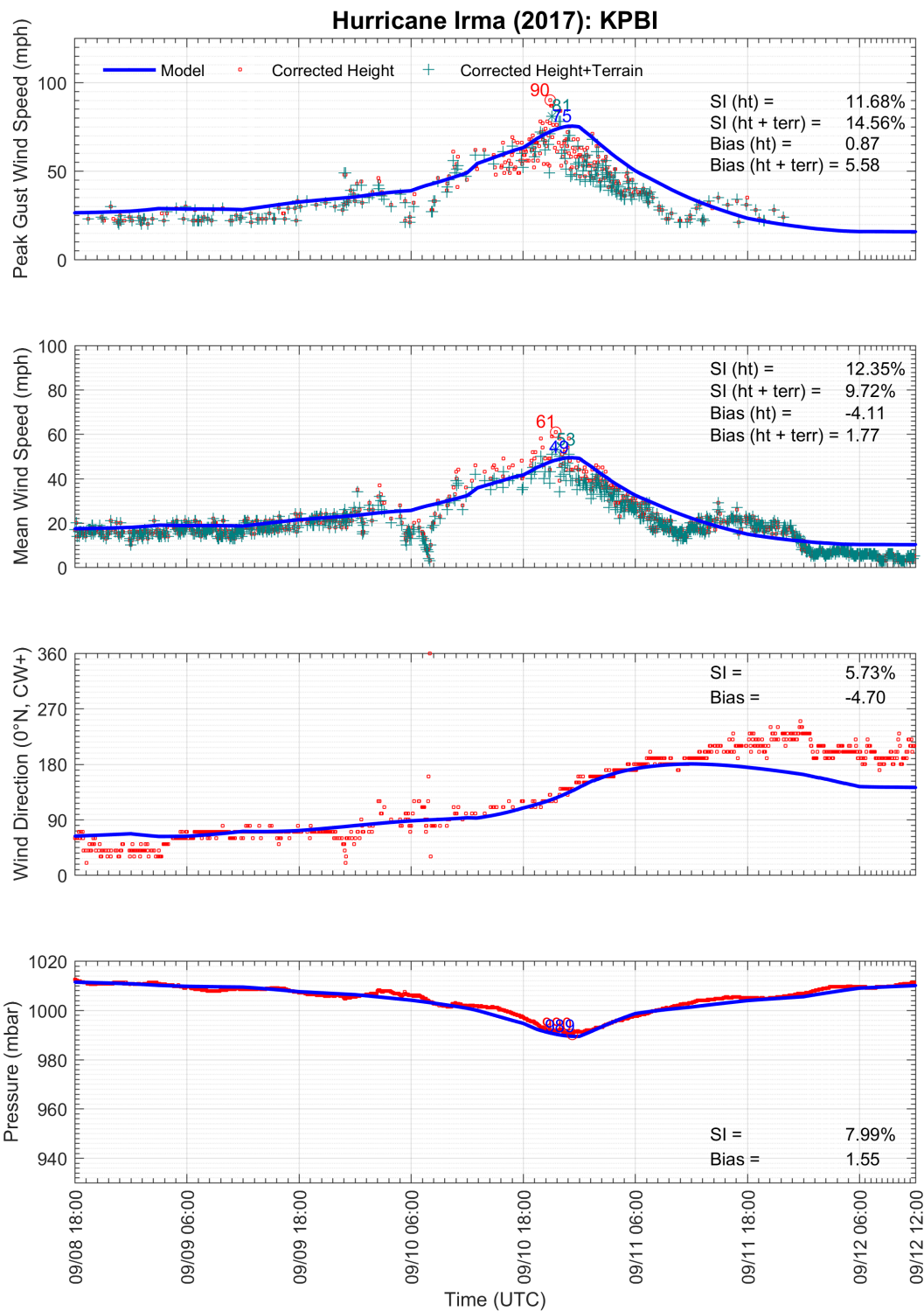


Figure 5-10. Modeled and observed meteorological time series at ASOS station KPBI: Palm Beach International Airport.

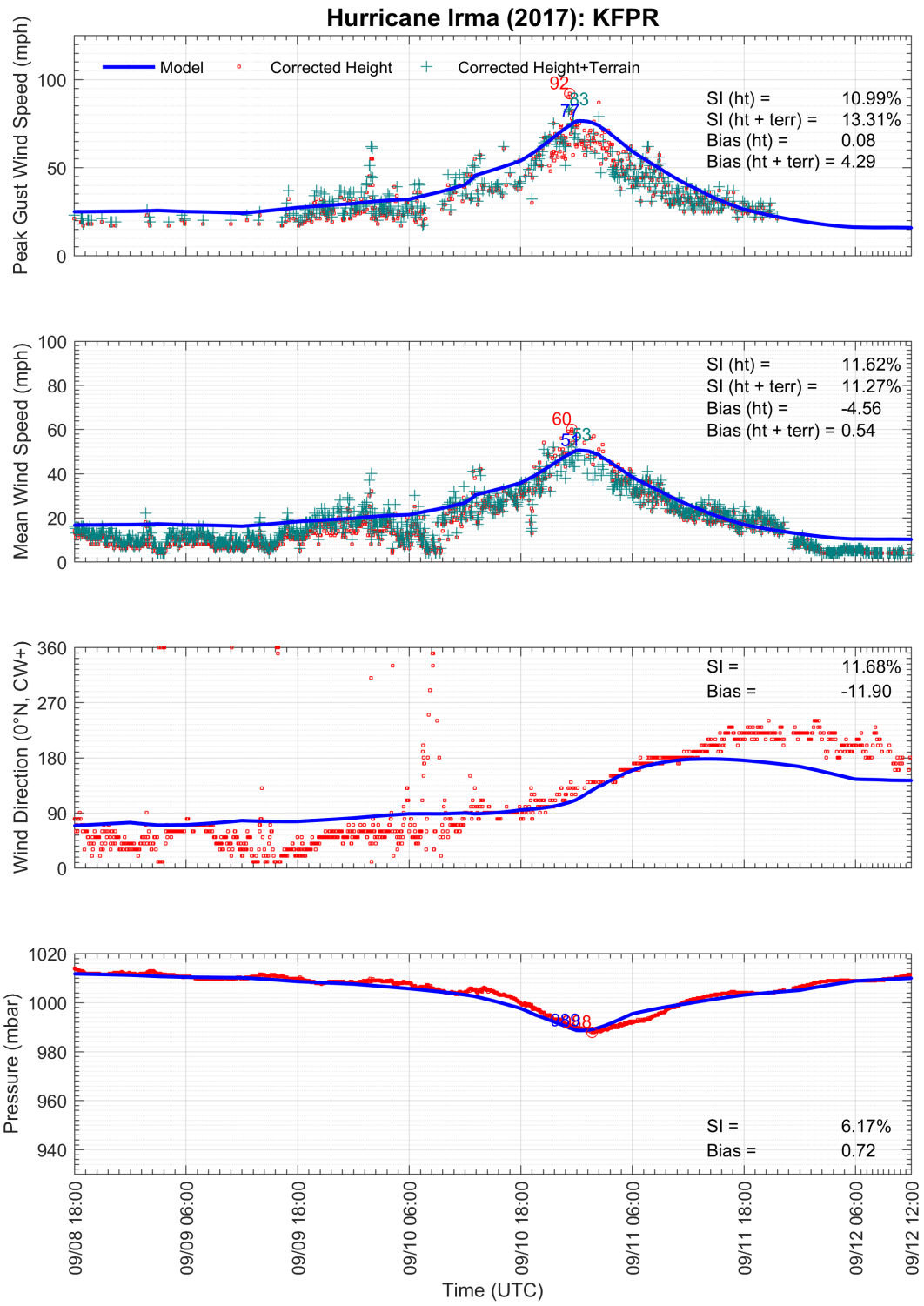


Figure 5-11. Modeled and observed meteorological time series at ASOS station KFPR: Treasure Coast International Airport and Business Park.

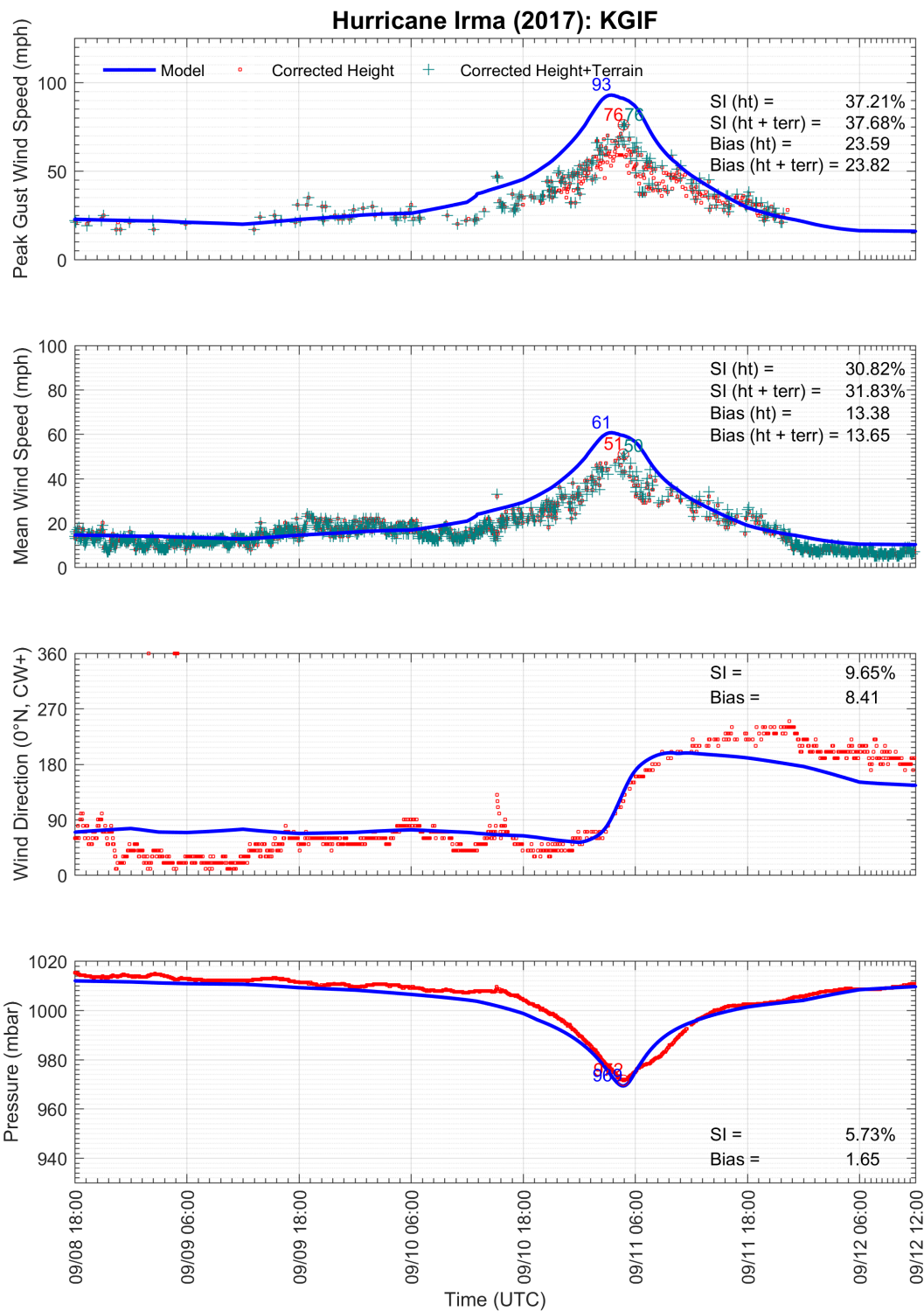


Figure 5-12. Modeled and observed meteorological time series at ASOS station KGIF: Winter Haven Regional Airport.

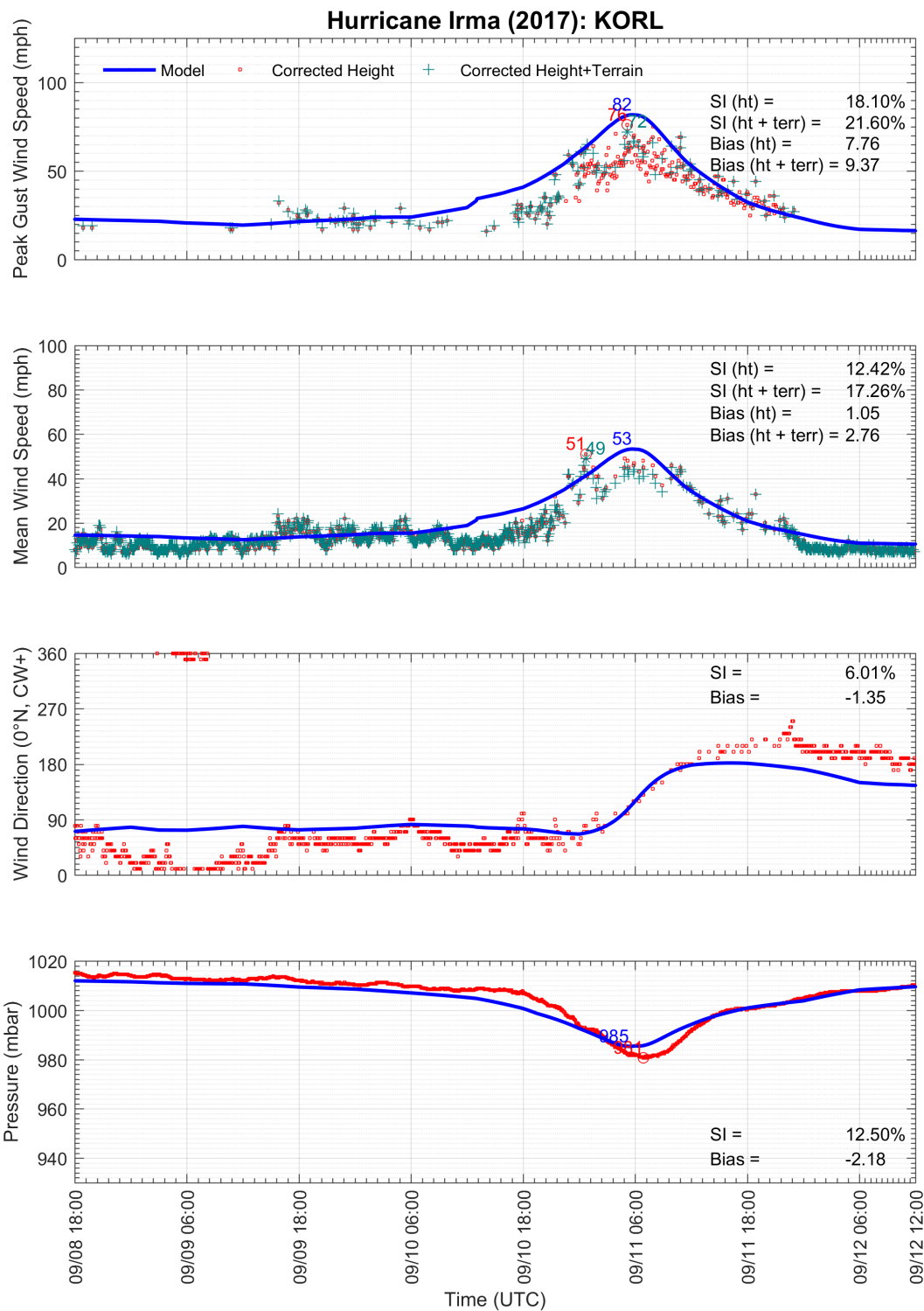


Figure 5-13. Modeled and observed meteorological time series at ASOS station KORL: Orlando Executive Airport.

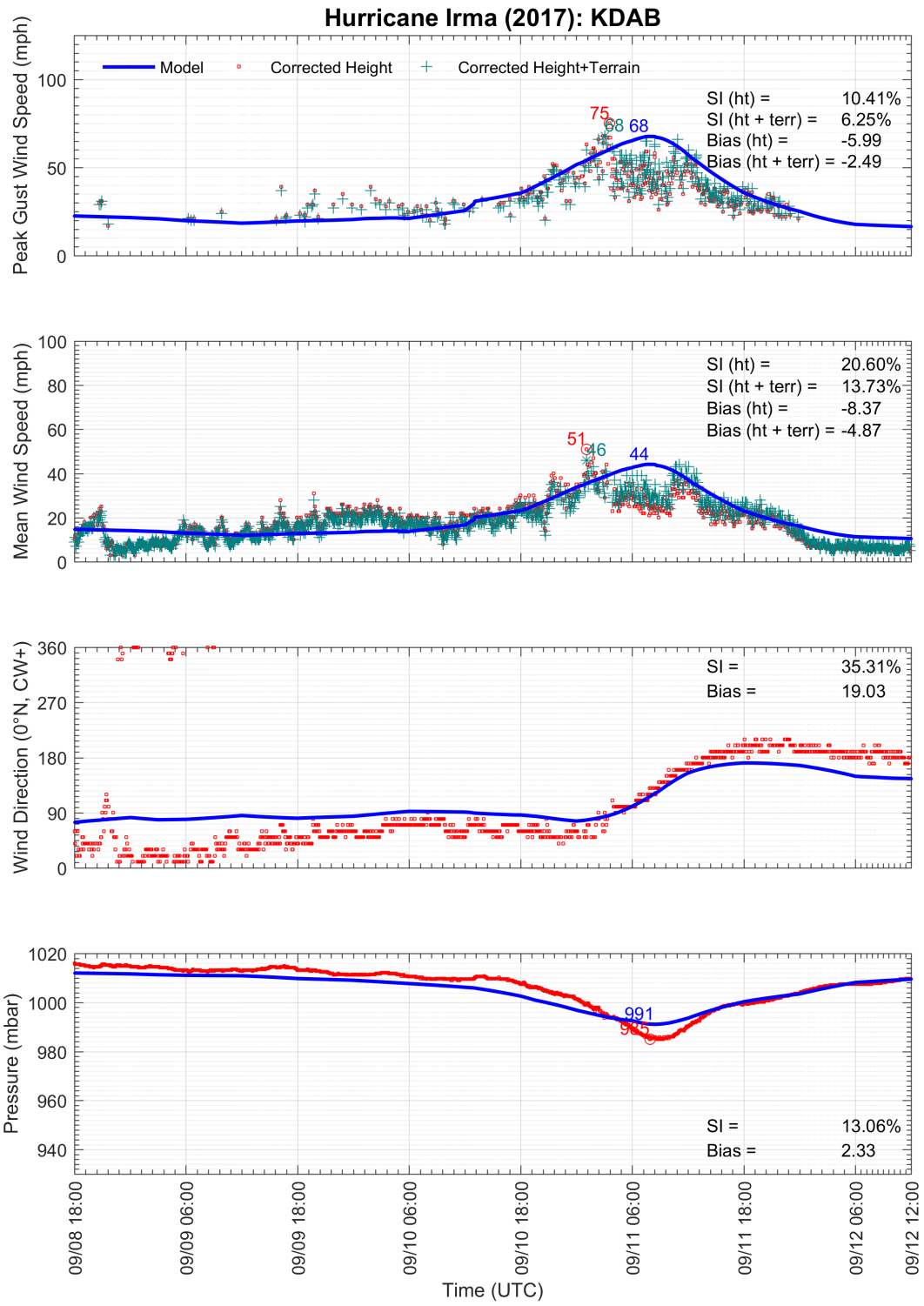


Figure 5-14. Modeled and observed meteorological time series at ASOS station KDAB: Daytona Beach International Airport.

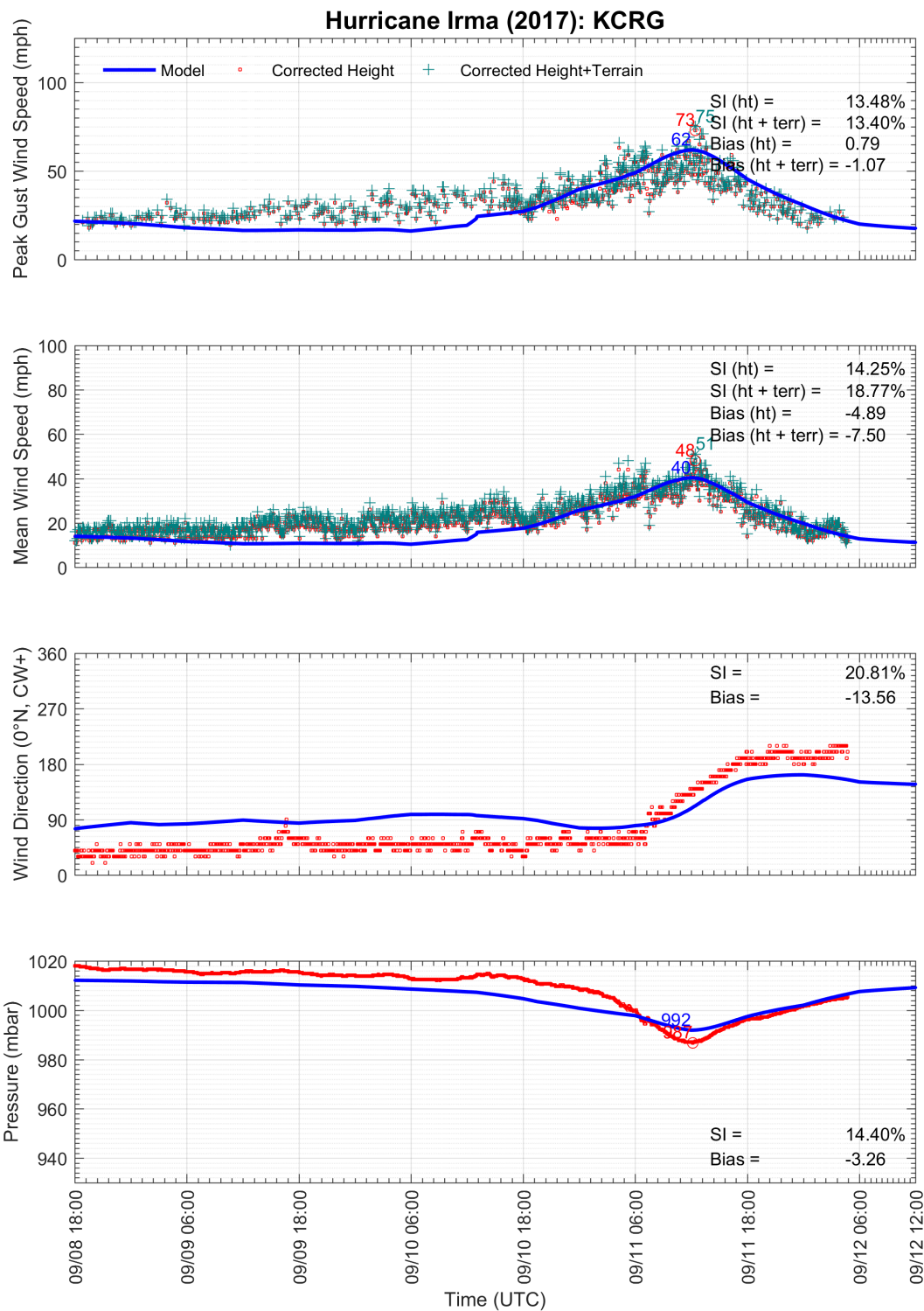


Figure 5-15. Modeled and observed meteorological time series at ASOS station KCRG: Jacksonville Executive at Craig Airport.

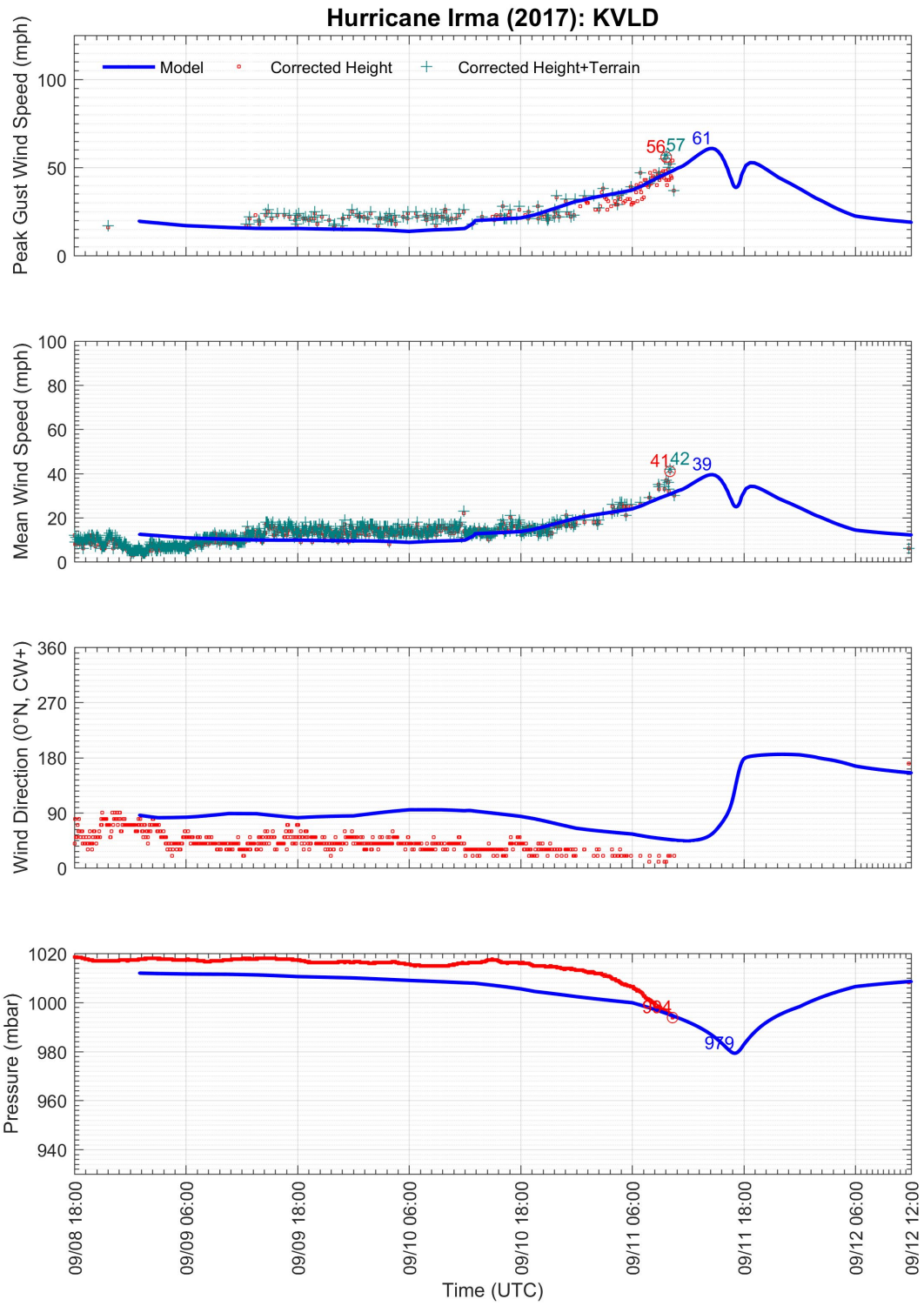


Figure 5-16. Modeled and observed meteorological time series at ASOS station KVLG: Valdosta Regional Airport.

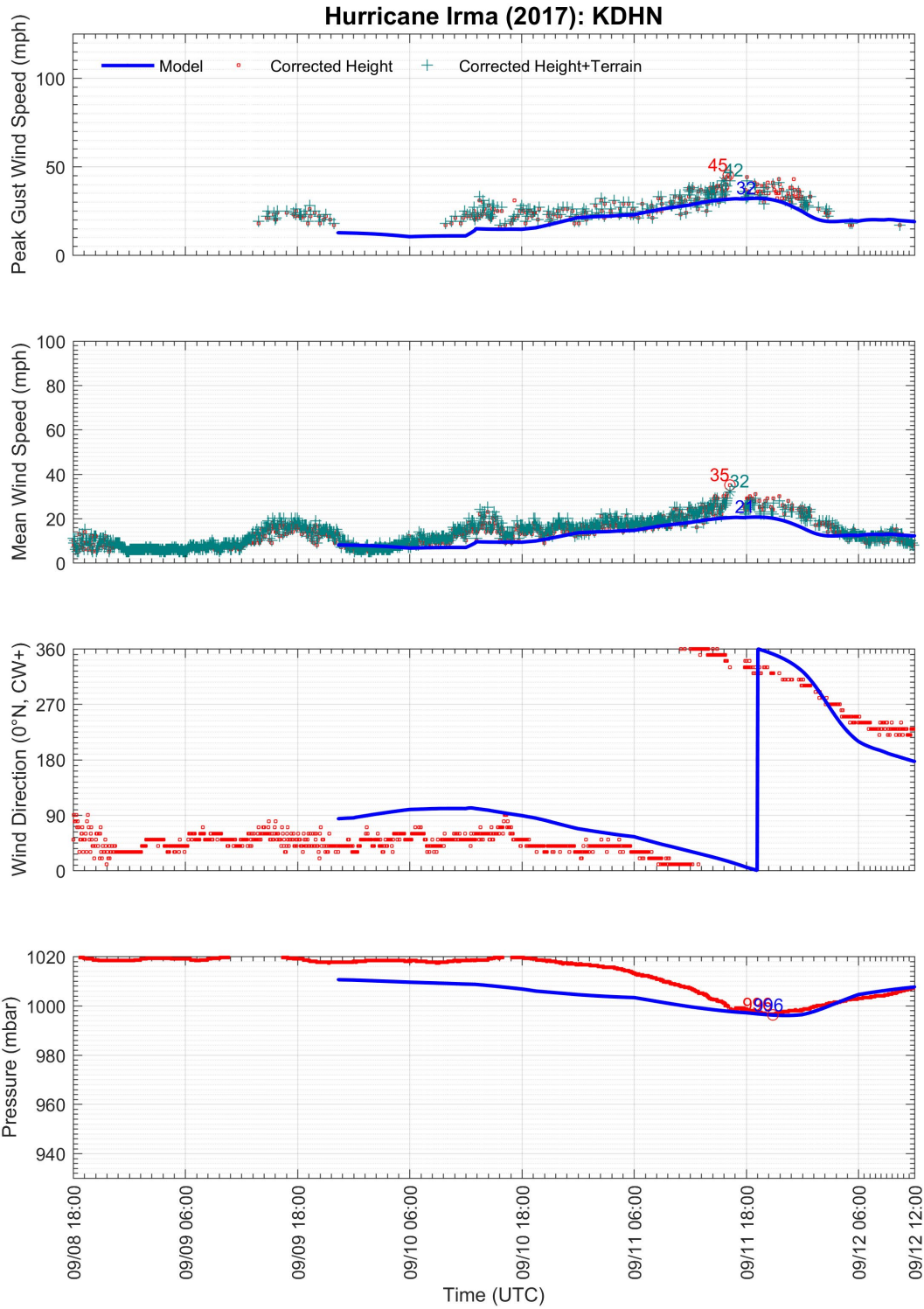


Figure 5-17. Modeled and observed meteorological time series at ASOS station KDHN: Dothan Regional Airport.

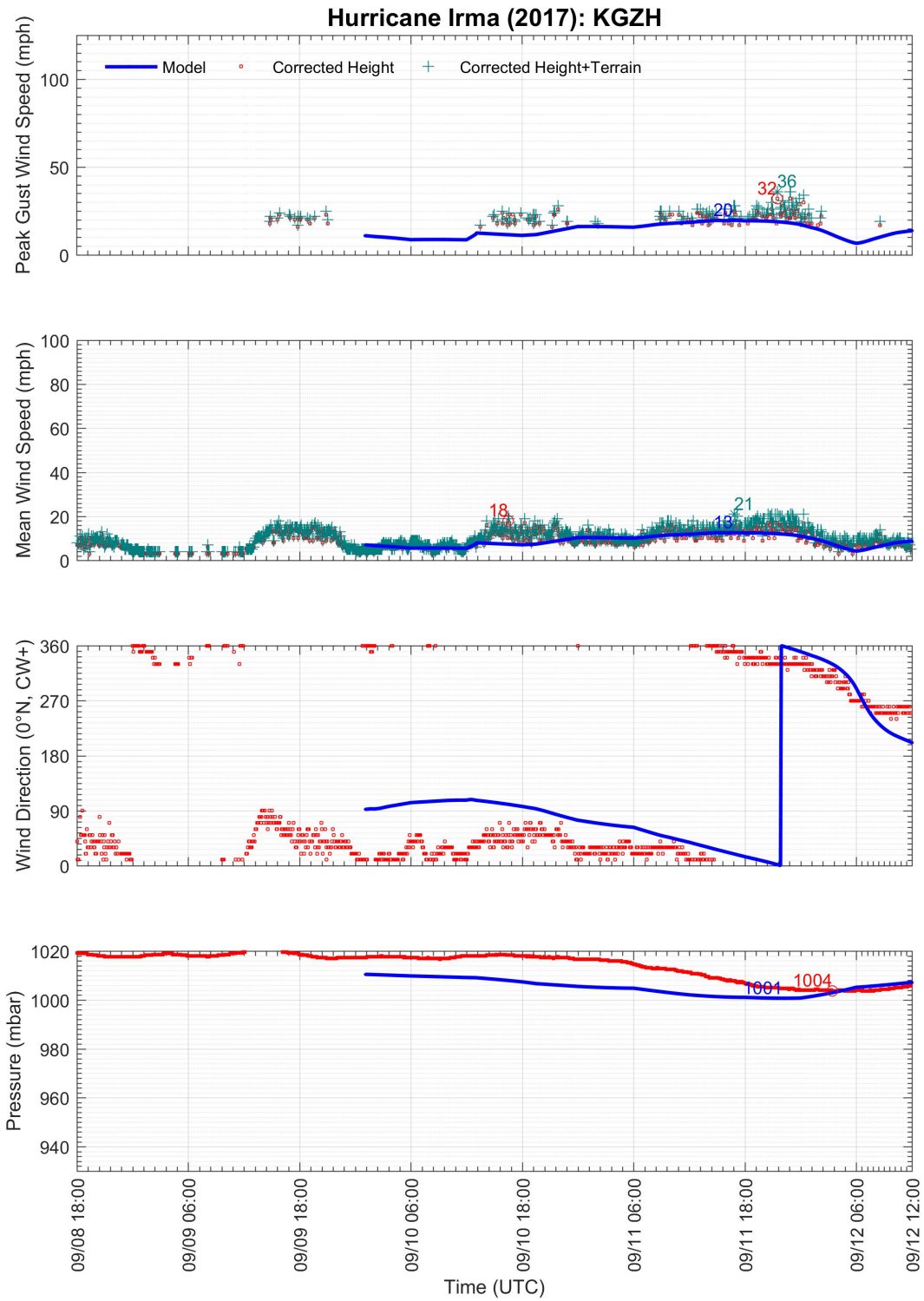


Figure 5-18. Modeled and observed meteorological time series at ASOS station KGZH: Middleton Field.

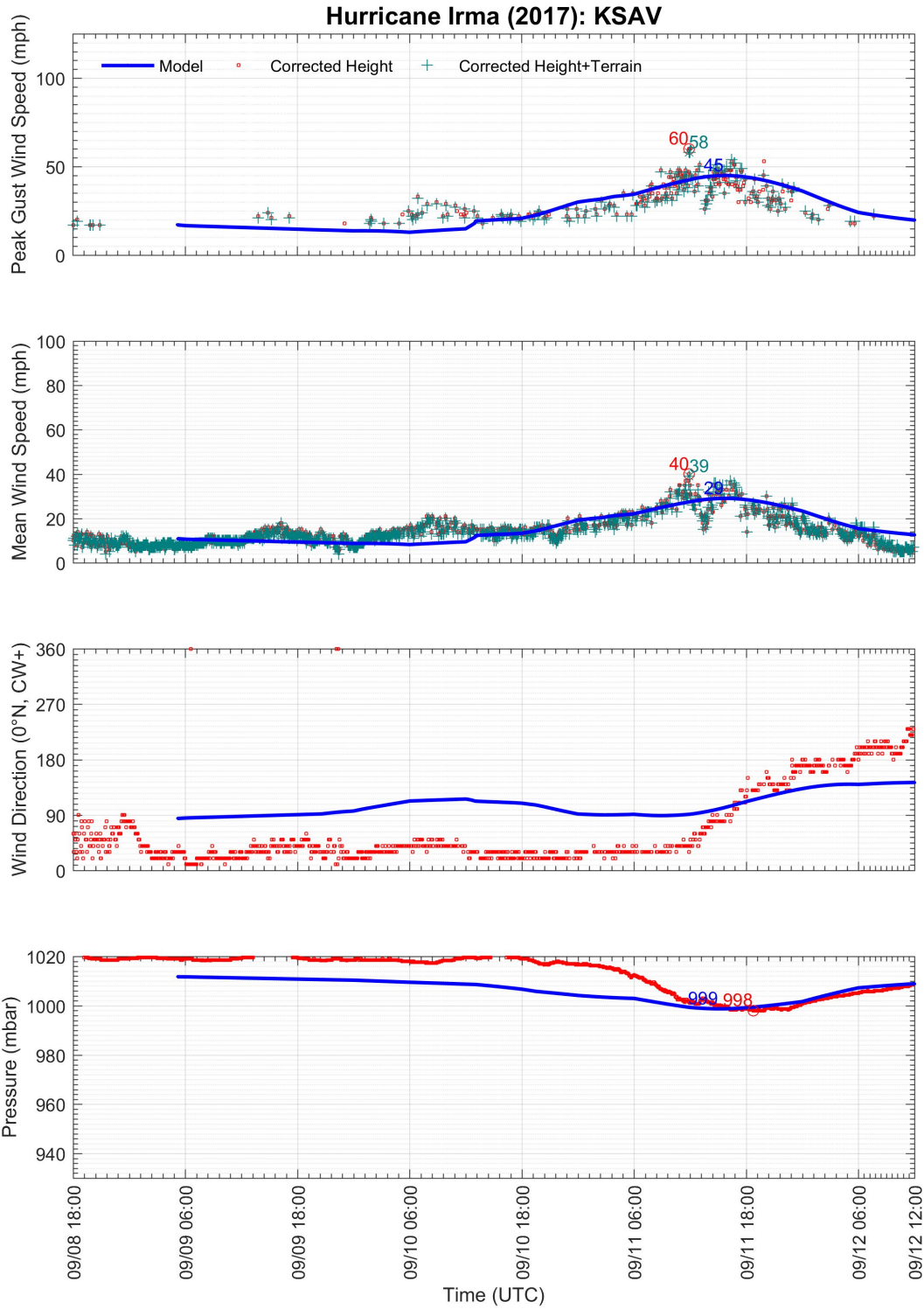


Figure 5-19. Modeled and observed meteorological time series at ASOS station KSAV: Savannah/Hilton Head International Airport.

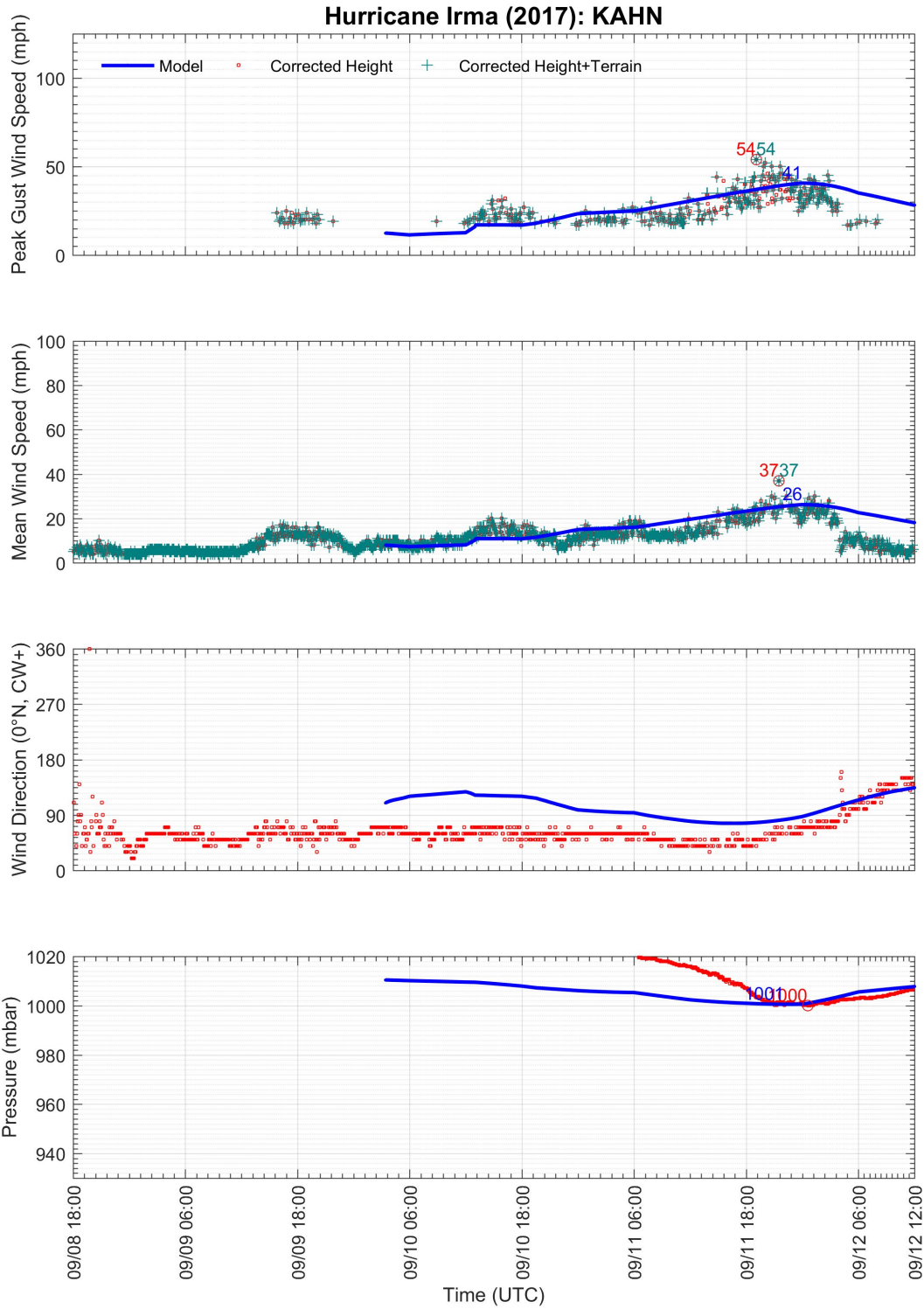


Figure 5-20. Modeled and observed meteorological time series at ASOS station KAHN: Athens-Ben Epps Airport.

5.5 ERRORS AND UNCERTAINTY

Figure 5-21 and Figure 5-22 present comparisons of modeled and observed maximum gust wind speeds and minimum central pressures for the stations used in the model validation process. Stations that failed prior to the arrival of the highest winds were not included in the comparisons. The R^2 values for peak gust wind speed with and without terrain corrections were around 0.45. The R^2 value for central pressure was 0.91.

Tabulated error values of peak gust wind speed are provided in Table 5-1 at the end of this section. No error data was provided for stations where the instrumentation failed prior to the occurrence of maximum winds.

One of the largest outliers where the model overpredicted the maximum gust wind speed occurred at NDBC station VCAF1 where the sustained wind speed was overpredicted by 35% when the observed data was corrected for height only and decreased to about 8% when the data was also corrected for terrain.

In the case of station VCAF1, the anemometer was located on a bridge that was surrounded by rough terrain of nearby buildings, trees, and boat docks as shown in Figure 5-23. While correcting the observed data for terrain using a visual technique to estimate the surface roughness reduced the model overprediction of peak sustained wind speed to about 8%, the overall time series was still consistently overpredicted. Winds that come from the north-northeast agreed well between the simulated and observed data; however, the strongest winds came from a direction between 90° and 180° where the winds had to pass over a greater distance of highly populated areas, as well as the uninhabited and rough terrain of Boot Key with smaller bays and inlets interspersed. Such complex terrain interactions were not captured in the wind field model.

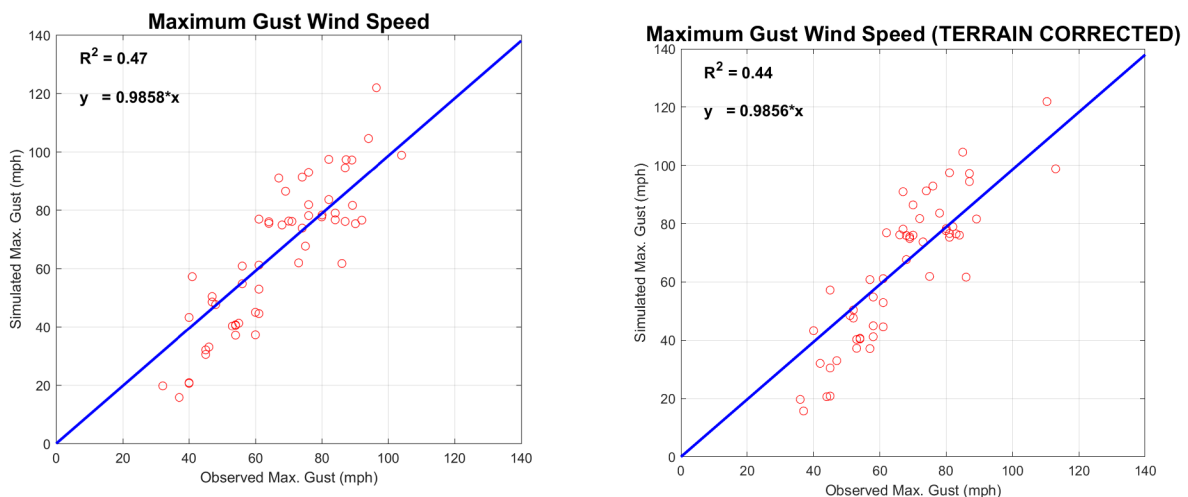


Figure 5-21. Modeled and observed maximum peak gust wind speed corrected only for height (left) and corrected for height and terrain (right).

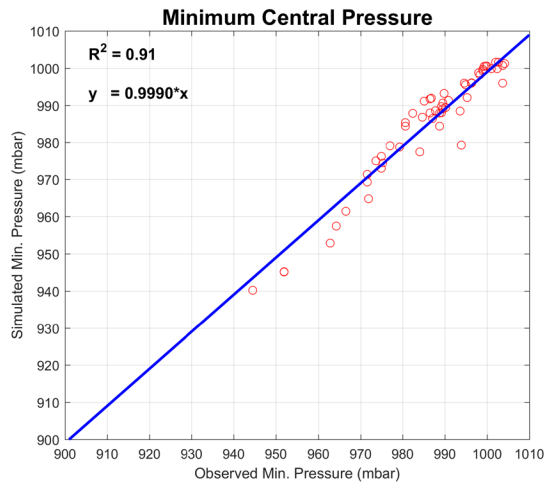


Figure 5-22. Modeled and observed minimum central pressure.



Figure 5-23. Aerial view of NDBC Station VCAF1.

Table 5-1. Errors in modeled peak gust wind speed in Hurricane Irma when observations are corrected for height only and for height and terrain. All wind speed values are presented at 10 m elevation in open terrain.

Station	Modeled Peak Gust Wind Speed (mph)	Observed Peak Gust Wind Speed (mph)		Error (mph)	
		Corrected for Height	Corrected for Height + Terrain	Corrected for Height	Corrected for Height + Terrain
KAAF	30	45	45	-15	-15
KABY	50	47	52	3	-2
KAGS	40	54	54	-14	-14
KAHN	41	54	54	-13	-13
KAMG	57	41	45	16	12
KAPF*	97	92	81	5	16
KATL	45	61	61	-16	-16
KBKV	76	64	68	12	8
KCEW	21	40	45	-19	-24
KCHS	37	60	53	-23	-16
KCRG	62	73	75	-11	-13
KCSG	49	47	51	2	-2
KCTY	61	61	61	0	0
KDAB	68	75	68	-7	0
KDHN	32	45	42	-13	-10
KDNL	40	53	53	-13	-13
KDTS	21	40	44	-19	-23
KEYW	---	---	---	---	---
KFFC	48	48	52	0	-4
KFMY	94	87	87	7	7
KFPR	77	92	83	-15	-6
KFTY	43	40	40	3	3
KFXE	77	84	81	-7	-4
KGIF	93	76	76	17	17
KGNV	77	61	62	16	15
KGZH	20	32	36	-12	-16
KHWO	---	---	---	---	---
KJAX	62	86	86	-24	-24
KLEE	86	62	70	24	16
KMAI	33	46	47	-13	-14
KMCN	53	61	61	-8	-8
KMCO	84	82	78	2	6
KMIA	---	---	---	---	---
KMTH	---	---	---	---	---
KOGB	37	54	57	-17	-20
KOPF	79	84	83	-5	-4
KORL	82	76	72	6	10
KPBI	75	90	81	-15	-6
KPGD	91	74	74	17	17

Station	Modeled Peak Gust Wind Speed (mph)	Observed Peak Gust Wind Speed (mph)		Error (mph)	
		Corrected for Height	Corrected for Height + Terrain	Corrected for Height	Corrected for Height + Terrain
KPIE	74	74	73	0	1
KPMP*	75	87	84	-12	-9
KPNS	15	37	37	-22	-22
KRSW	97	89	87	8	10
KSAV	45	60	58	-15	-13
KSFB*	76	70	66	6	10
KSPG	76	71	70	5	6
KSRQ	75	64	69	11	6
KSSI	---	---	---	---	---
KTLH	41	55	58	-14	-17
KTMB	---	---	---	---	---
KTPA	75	68	69	7	6
KVLD	---	---	---	---	---
FWYF1	82	89	89	-7	-7
MLRF1	97	87	87	10	10
PLSF1	78	80	80	-2	-2
VCAF1	122	96	110	26	12
VENF1	78	80	80	-2	-2
XUF1t	91	67	67	24	24
XUF2t	97	94	94	3	3
XUF3t	99	104	113	-5	-14
XUF5t	97	108	108	-11	-11

* Note: Stations KAPF, KPMP, KSFB failed very near the expected time of maximum winds and may not have captured the true maximum wind speed experienced.

5.6 WIND FIELD MAP

The final peak gust wind speed map of Hurricane Irma is shown in Figure 5-24 with wind speed contours in increments of 10 mph. Peak gust wind speeds are defined as 3-second average at 10 m above ground over open terrain. The storm track is shown by the dashed blue line. All stations used in the wind field model validation are also shown: purple triangles indicate an ASOS station, green triangles indicate a station in the NDBC database located over water or near the coast, and pink triangles indicate a mobile research observation tower operated by the University of Florida. The highest winds are shown to have occurred over the Florida Keys near the city of Marathon.

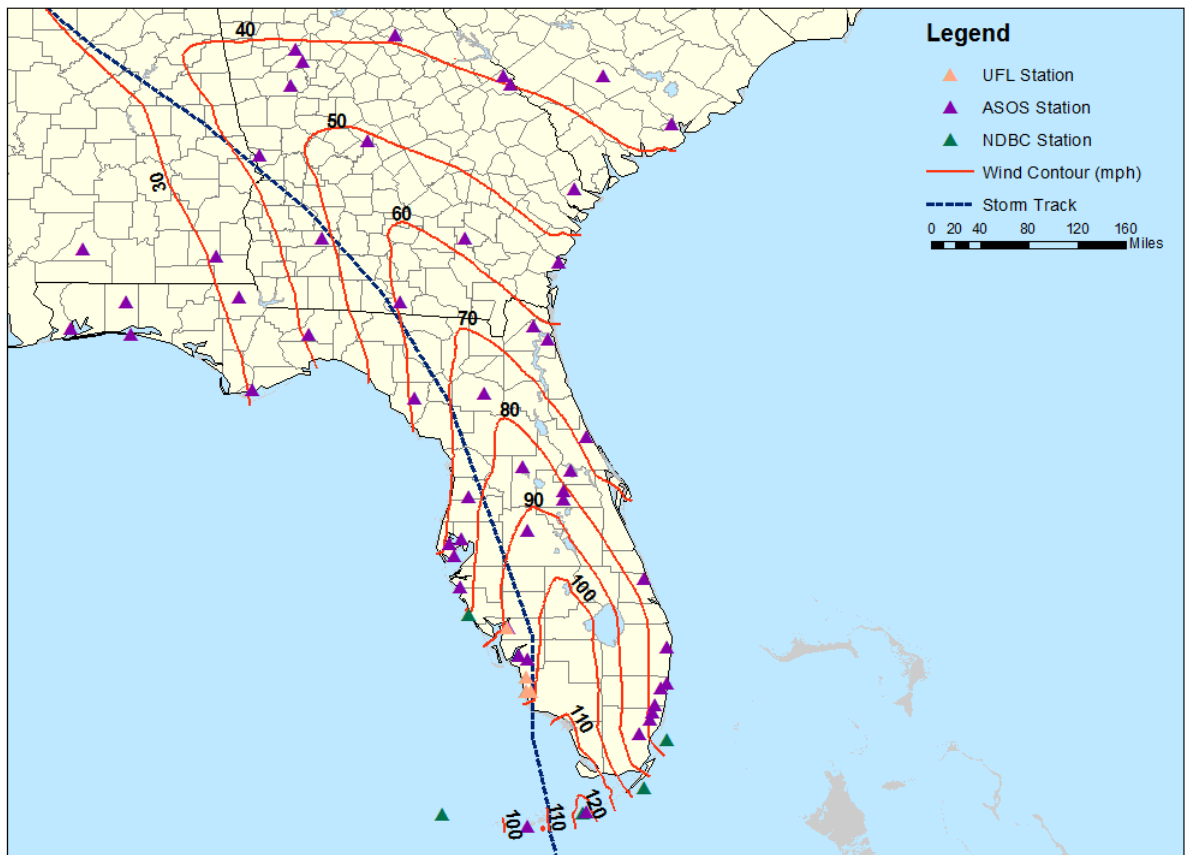


Figure 5-24. Peak gust wind speed contour map for Hurricane Irma (2017) showing estimated 3-second peak gust wind speeds (mph) at 10 m above ground over open terrain. Model output obtained from ARA wind field model fit to surface level observations using NHC best track and central pressures.

6 HURRICANE IRMA (OCONUS)

6.1 EVENT BACKGROUND

A brief background for Hurricane Irma (2017) and its impacts outside the contiguous United States is presented in this section. For a full narrative of the storm, including synoptic history, meteorological statistics, casualty and damage statistics, and forecast and warning critique, see the National Hurricane Center's Tropical Cyclone Report on Hurricane Irma (Cangialosi et al., 2018) available at https://www.nhc.noaa.gov/data/tcr/AL112017_Irma.pdf.

Hurricane Irma was a Category 5 hurricane that made seven total landfalls, four of which occurred in the Caribbean Islands when Irma was a Category 5 event. Irma first made landfall as a Category 5 hurricane on Barbuda at 5:45 UTC on September 6 with an estimated maximum wind speed of 155 knots (178 mph) and a minimum central pressure of 914 mbar. With no weakening of intensity, Irma made two additional landfalls that day at 11:15 UTC on the island of St. Martin and at 16:30 UTC in the British Virgin Islands.

Continuing on a northwestward trajectory, Irma weakened slightly but remained a Category 5 as it tracked approximately 50 nautical miles to the north of Puerto Rico and the Dominican Republic from September 6 18:00 UTC to September 7 18:00 UTC. Irma made its fourth landfall in the Caribbean at 5:00 UTC on September 8 as a strong Category 4 event with an estimated maximum wind speed of 135 knots (155 mph) and minimum central pressure of 924 mbar on Little Inagua Island in the Bahamas. Irma's trajectory turned slightly to the left towards the northern coast of Cuba where it re-intensified slightly before making its fifth and final landfall in the Caribbean on September 9 3:00 UTC near Cayo Romano, Cuba, with a maximum wind speed of 145 knots (167 mph).

The highest wind speeds caused by Hurricane Irma in the U.S. Virgin Islands occurred on Buck Island, with wind speeds of 92 knots (106 mph) and gusts of up to 119 knots (137 mph). The highest wind speed reported in Puerto Rico was 48 knots (55 mph) with gusts up to 64 knots (74 mph) at the National Ocean Service station SJNP4 at La Puntilla in San Juan Bay on September 6 22:30 UTC.

Maximum storm surge and tide inundation levels of 8 feet were estimated on the island of Barbuda. Significant storm surge was likely on the U.S. Virgin Islands of St. Thomas and St. John, but no tide gauge data is available to confirm the highest inundation levels on the islands. Maximum inundation levels of 1 to 2 feet were estimated to have occurred along the coast of Puerto Rico. Rainfall totals between 10 and 15 inches occurred over high elevations in the central portion of Puerto Rico.

6.2 DATA COLLECTION

6.2.1 Track

A portion of the best track of Hurricane Irma is shown in Figure 6-1 as the storm approached the Virgin Islands and Puerto Rico.

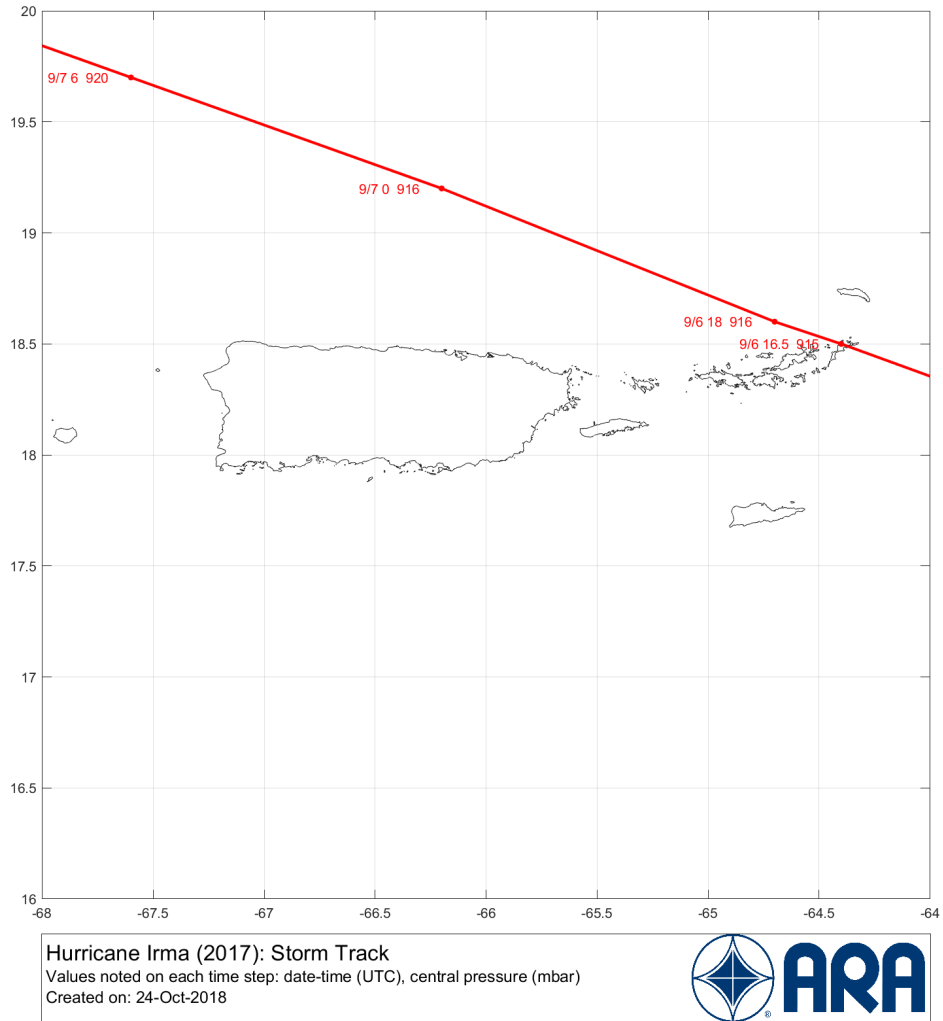


Figure 6-1. Best-track information of Hurricane Irma (2017) collected from the NHC Atlantic Hurricane Database (HURDAT2).

6.2.2 Observations

Stations with observations during the lifespan of Hurricane Irma and within 150 miles of a track point were used in the model validation and are shown in Figure 6-2. A table of station locations and anemometer heights is provided in Appendix C.

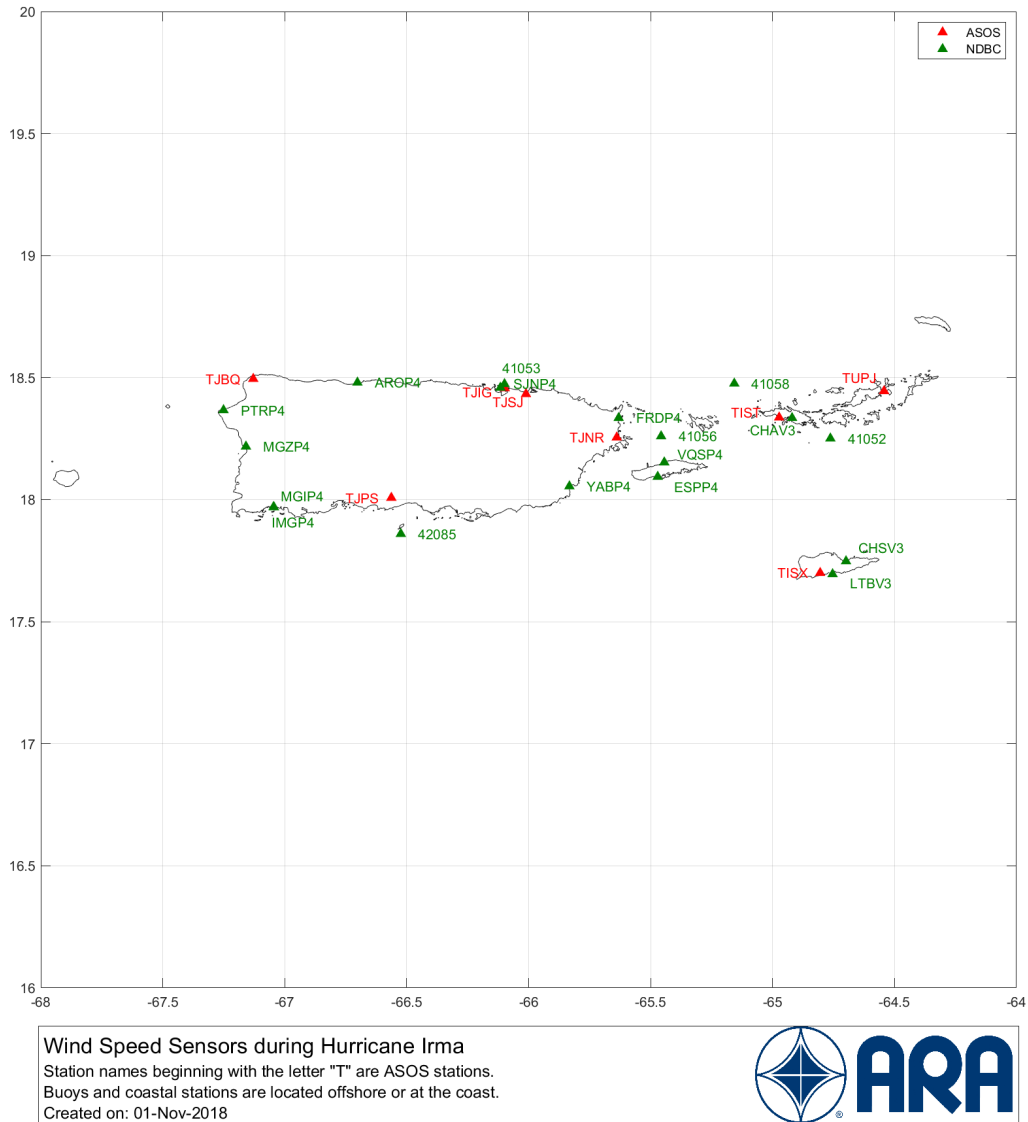


Figure 6-2. ASOS and NDBC stations in and near the Virgin Islands and Puerto Rico with surface observations during the lifespan and within 150 miles of Hurricane Irma.

6.3 DATA CORRECTIONS (DEVIATION FROM STANDARD PROCEDURES)

Estimates of directional effective surface roughness have not been previously generated for any stations (ASOS or NDBC) outside the contiguous United States. Wind speed observations at NDBC stations located very nearshore are often affected by the rougher terrain of nearby land and may not correspond to true marine terrain observations. NOAA National Ocean Service station LTBV3—shown in Figure 6-3—is located on the dock of a shipping port with an oil and gas refinery and highly populated communities to the north. To account for terrain effects on these stations, a visual technique was used to estimate the directional surface roughness values from aerial imagery; both the values and aerial imagery used are provided in Appendix C. Visually estimated values of z_0 serve as input to the ESDU terrain correction methodology.



Figure 6-3. NOAA National Ocean Service Station LTBV3 located very nearshore with a refinery, shipping port, and populated communities located to the north.

Under separate Federal Emergency Management Agency (FEMA) task orders, topographic wind speed-up factors were created for the U.S. Virgin Islands and Puerto Rico. Wind speed-ups were computed for 16 different wind directions at increments of 22.5 degrees. The speed-up factor increases with increasing slope in front of the point of interest. If the slope to the immediate left or right of the site (90 degrees or 270 degrees) is positive (i.e., downhill) the wind speed is decreased as the wind is able to go around the location. Conversely, if the slope is negative (e.g., the walls of a valley) the wind speed is increased due to the effects of channeling. For very steep negative slopes, the speed-up becomes less than 1 since the flow separates and locations on the hill are in a wake region having a recirculated flow. The same applies on the leeward side of steep hills. For points located at or near a ridge or hill top, the positive slope behind the point increases the speed-up such that, all else being equal, a ridge produces a

maximum speed-up. Maximum topographic speed-up factors for the U.S. Virgin Islands and Puerto Rico are shown in Figure 6-4 and Figure 6-5, respectively. A detailed derivation of the topographic speed-up factors is provided in Vickery et al. (2018).

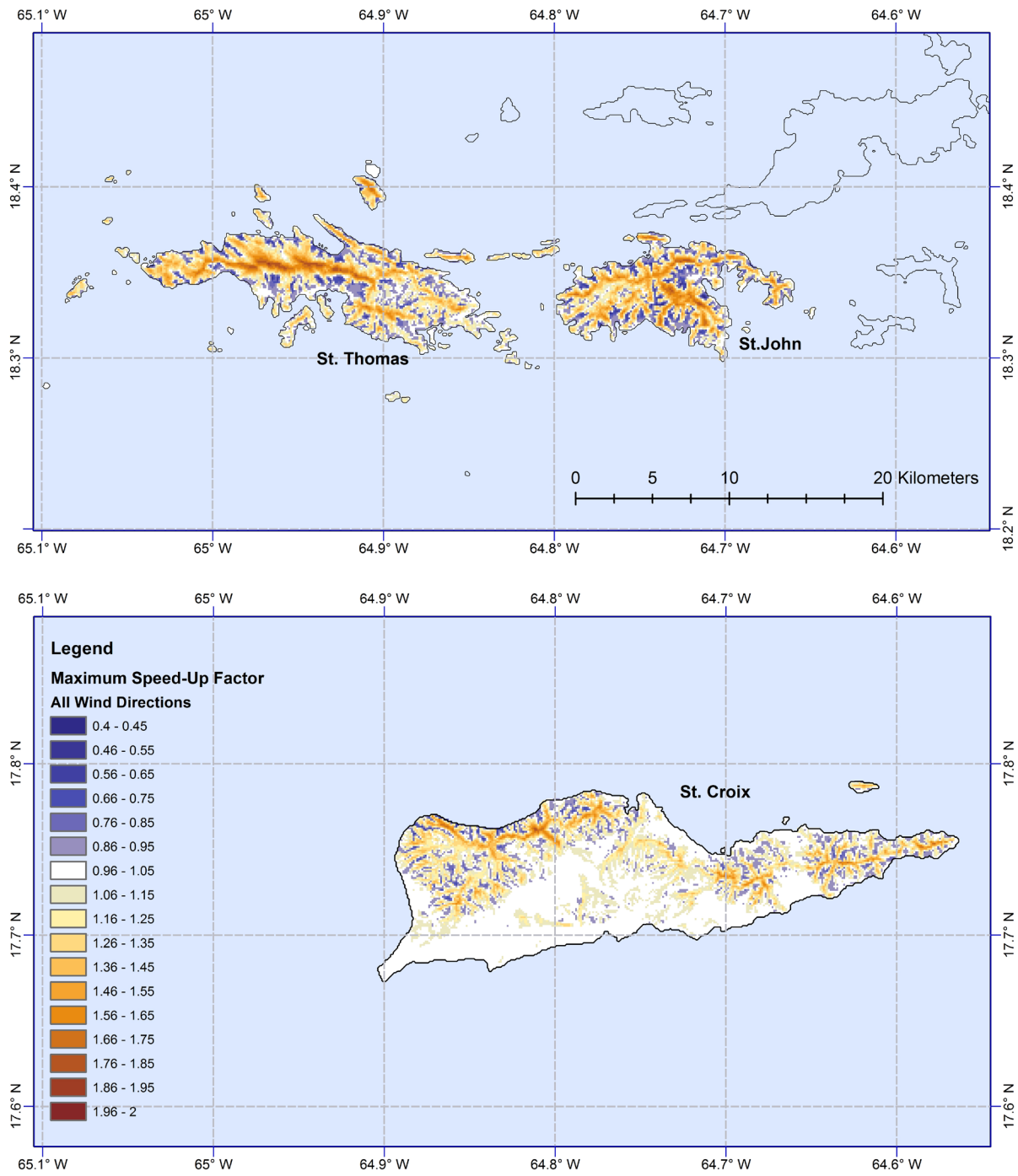


Figure 6-4. Maximum topographic speed-up factors for the U.S. Virgin Islands.

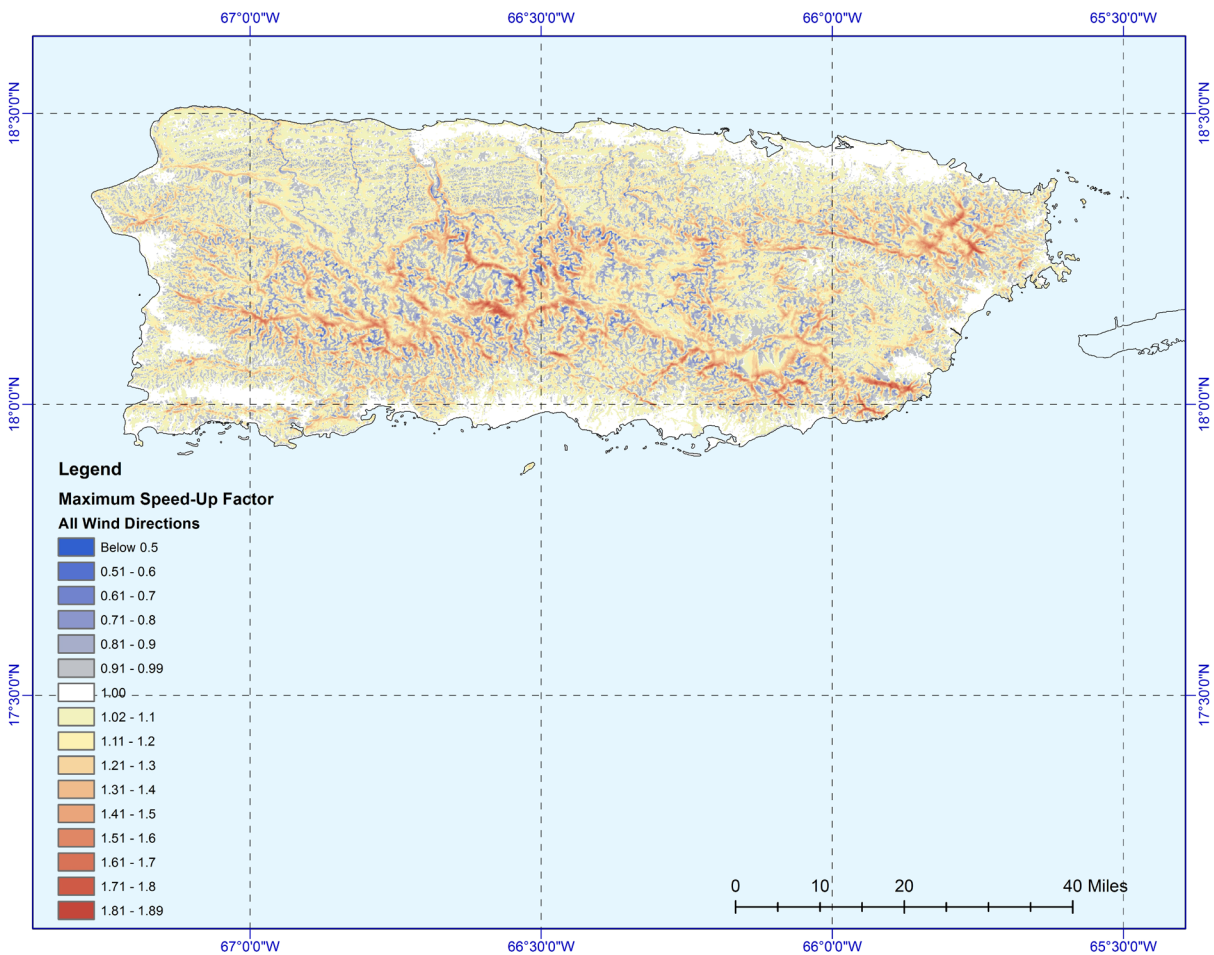


Figure 6-5. Maximum topographic speed-up factors for Puerto Rico.

The speed-up factors were used in the track fitting process by adjusting the observations to an equivalent wind speed at 10 m height over open terrain and *flat* topography. The final wind field maps presented in Section 6.6 have been adjusted back to the local topography (e.g., 3-second gust wind speed at 10 m height over open terrain and the *native* topography).

6.4 DISCUSSION OF SELECT STATION TIME HISTORIES

The highest winds at NDBC station CHSV3 located on the U.S. Virgin Island of St. Croix were experienced around September 6 at 17:00 UTC. (The time history is shown in Figure 6-6.) St. Croix was positioned to the south of Hurricane Irma's track and just outside the likely double eyewall that had developed around the time of the peak winds on the island. The maximum peak gust wind speed was within 5% of the observed values with and without corrections for terrain.

On and near the islands of St. Thomas and St. John, closer to the center of the storm, NDBC stations 41052, CHAV3, and 41058, along with ASOS station TIST, experienced much higher wind speeds than observed in St. Croix. The maximum peak gust winds at these stations occurred between 18:00 – 19:00 UTC on September 6, as shown in Figure 6-7 through Figure 6-10. Station 41052 was the only one of the four stations with a nearly complete central pressure time trace where the modeled and observed wind

speeds agreed well with a low scatter index of about 15%. The observed wind speeds at station 41052 were an anomaly among the four nearby stations; with a maximum observed peak gust wind speed of only 88 mph, the model overpredicted by 55 mph. Given that the wind direction time series shows no incongruities, it is unlikely that the buoy drifted away during the passage of the hurricane. One possible explanation for this inconsistency is that the anemometer was sheltered by large waves. The largest wave height recorded at station 41053 was 6 m (20 ft). Anemometers at the other three stations likely failed prior to capturing the true maximum wind speed experienced. The last and maximum peak gust wind speed observations at the three stations that failed ranged from 81 mph at NDBC station 41058 to 152 mph at NDBC station CHAV3. The anemometers at NDBC stations 41058 and CHAV3 failed several hours before and very near to the time of occurrence of the modeled maximum wind speeds, respectively. Scatter indices at stations CHAV3, TIST, and 41058 were around 20-25%, and the modeled wind directions agreed well with the observed.

Further from the eye of the storm to the west, NDBC station ESPP4 captured wind speeds on the Puerto Rican island of Vieques (see Figure 6-11). The modeled and observed time series parameters agreed well with 4-10% scatter indices for wind speeds, 8% for wind direction, and 18% for central pressure. The maximum peak gust wind speed was overestimated by approximately 8%, and the minimum central pressure difference was underestimated by 4 mbar.

On the eastern side of mainland Puerto Rico, NDBC stations FRDP4 and 41056 and ASOS station TJNR captured maximum peak gust wind speeds ranging from 57 to 71 mph, as shown in Figure 6-12 through Figure 6-14. Similar to station 41053, the anemometer at station 41056 was also likely sheltered by large waves. The largest waves recorded at station 41056 were 4.5 m (15 ft). The wind directions agreed well at all three locations with scatter indices between 4-6%. Wind directions at station FRDP4 between September 6 19:00 to 22:00 UTC were an exception as this station likely experienced interference from a nearby ferry during this time (see Section 6.5).

NDBC stations SJNP4 and AROP4 captured wind speeds on the northern coast of Puerto Rico (shown in Figure 6-15 and Figure 6-16). At station SJNP4, where the highest over land wind speeds in Puerto Rico were observed, the modeled peak gust wind speed time series showed a high bias of around 15 mph with the wind speeds overpredicted prior to and following the occurrence of the maximum peak gust wind speed. The maximum peak gust wind speed was overpredicted by 6 percent at station SJNP4, and was underpredicted by 3 percent at station AROP4. The wind directions at both stations showed low scatter index values around 7-9%.

From east to west on the southern and western coast of Puerto Rico, NDBC stations YABP4, 42085, IMG4, and MGZP4 captured maximum peak gust wind speeds ranging from 40 to 48 mph as shown in Figure 6-17 through Figure 6-20. No scatter indices or bias calculations were performed since there was no extended period of tropical cyclone winds experienced at these stations. Overall agreement between the modeled and observed time histories was high, with the exception of winds blowing from about 270° to 360° at station YABP4. As discussed in Section 6.5, this station likely experienced interference from a nearby ship or dock from these directions.

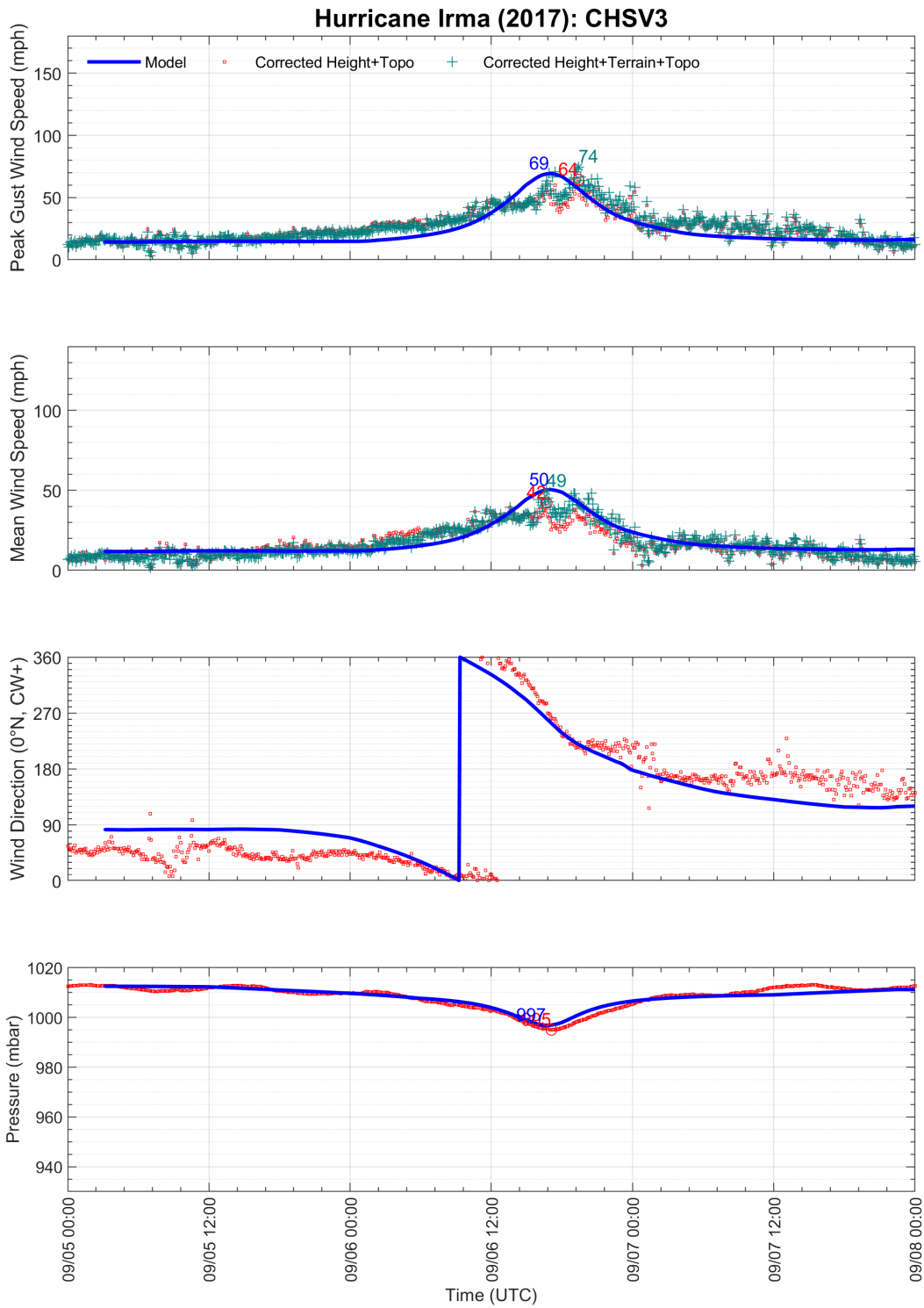


Figure 6-6. Modeled and observed meteorological time series at NDBC station CHSV3: Christiansted Harbor, St. Croix, USVI.

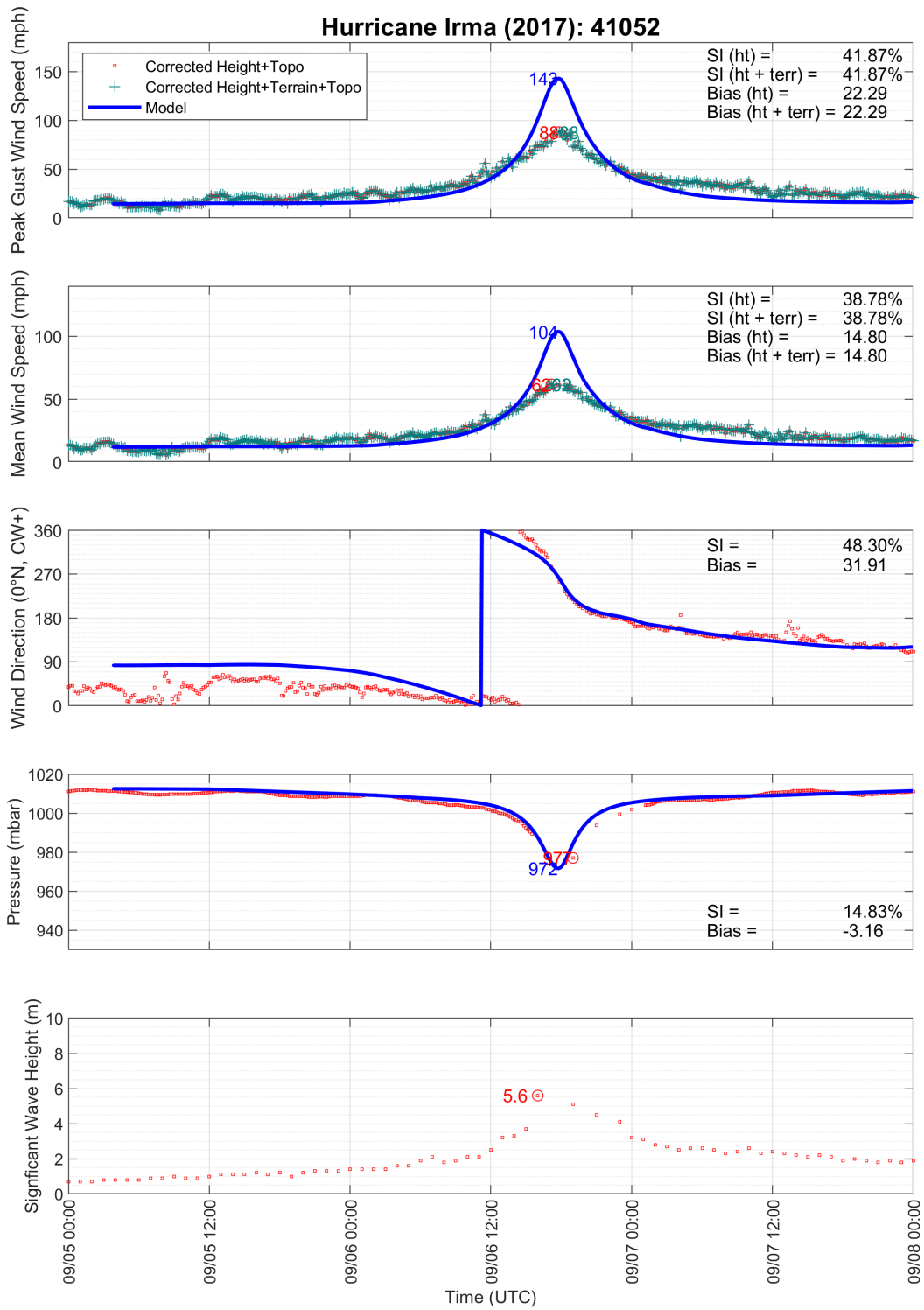


Figure 6-7. Modeled and observed meteorological time series at NDBC station 41052: South of St. John, USVI.

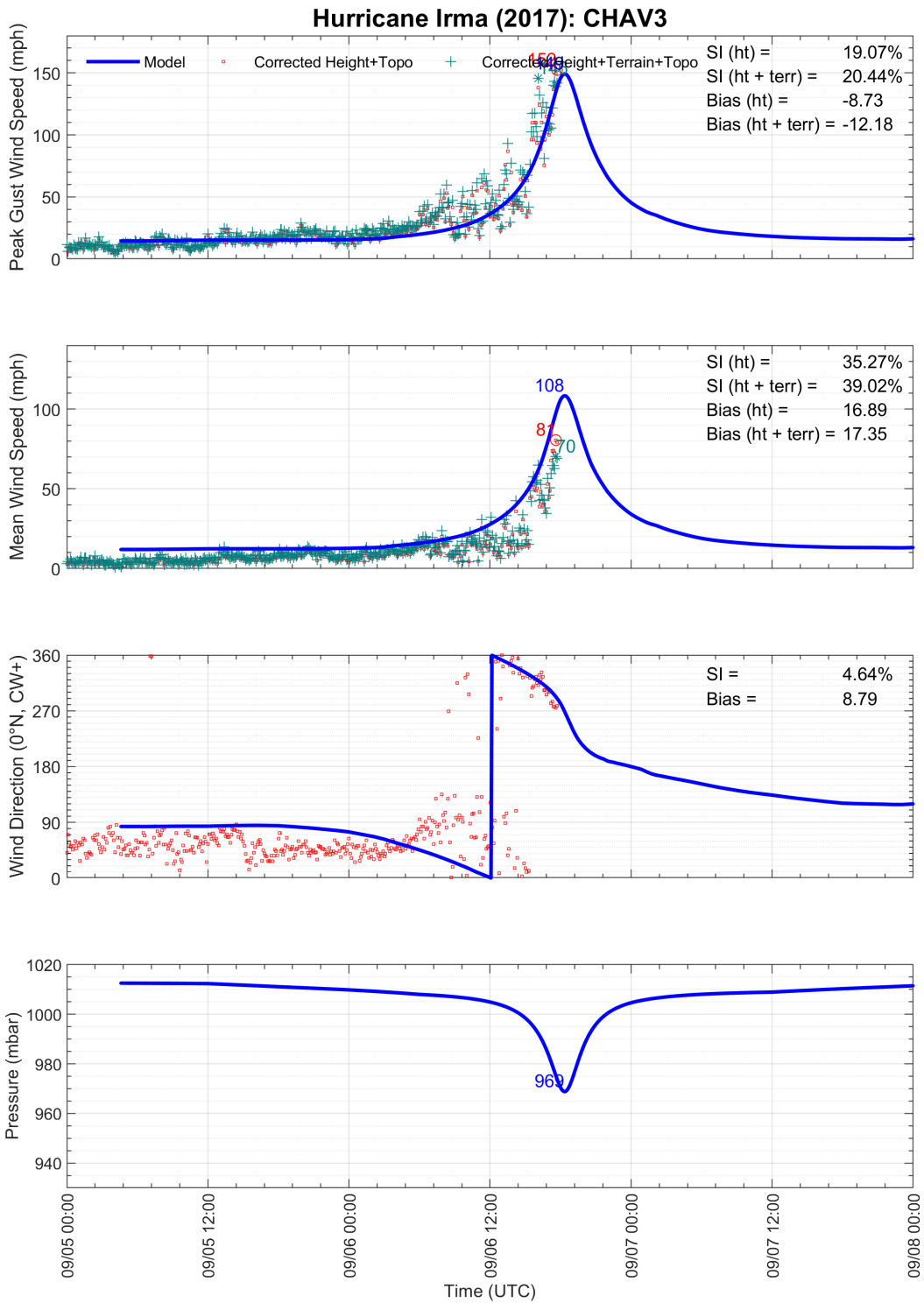


Figure 6-8. Modeled and observed meteorological time series at NDBC station CHAV3: Charlotte Amalie, USVI.

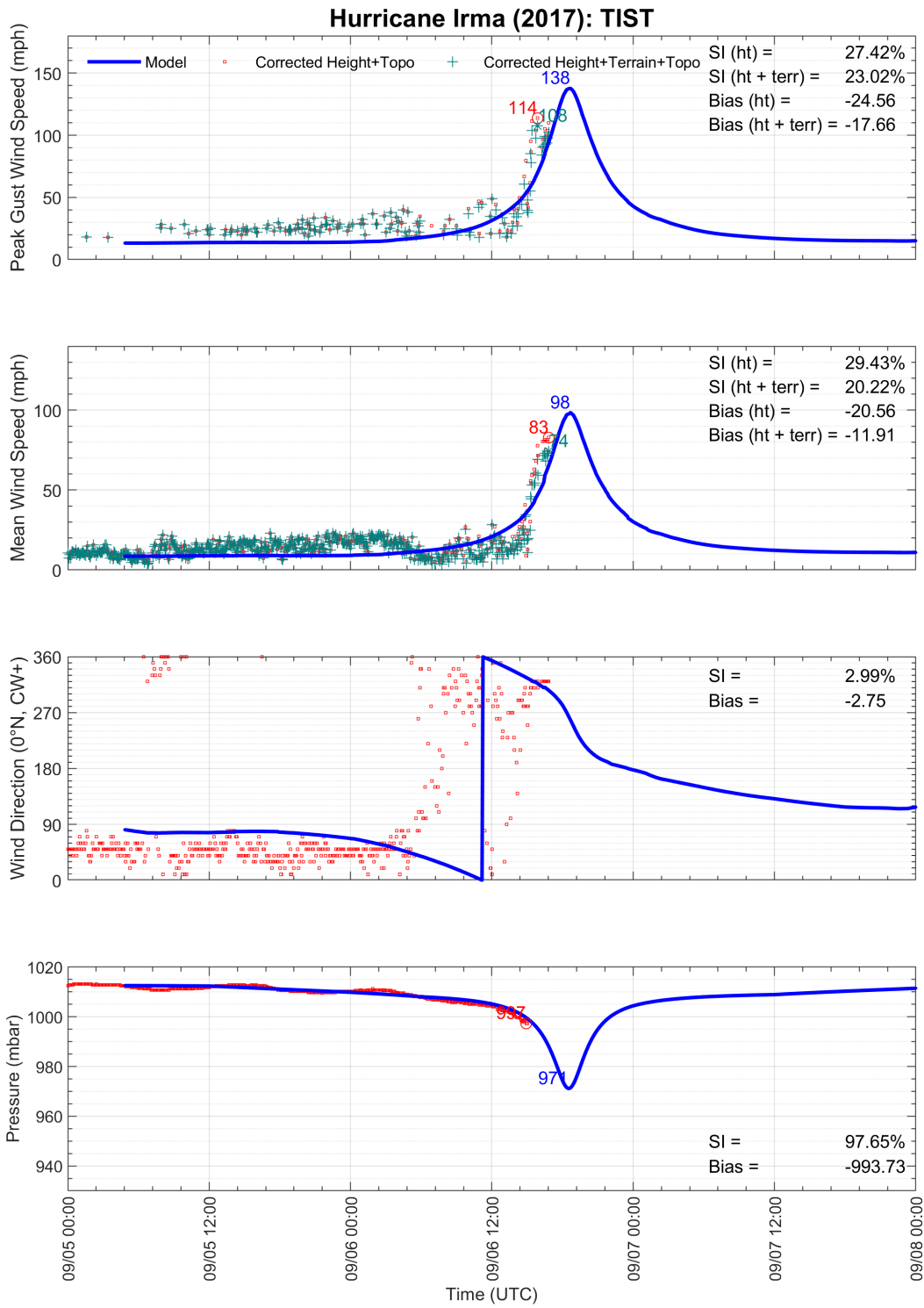


Figure 6-9. Modeled and observed meteorological time series at ASOS station TIST: Cyril E King Airport, St. Thomas, USVI.

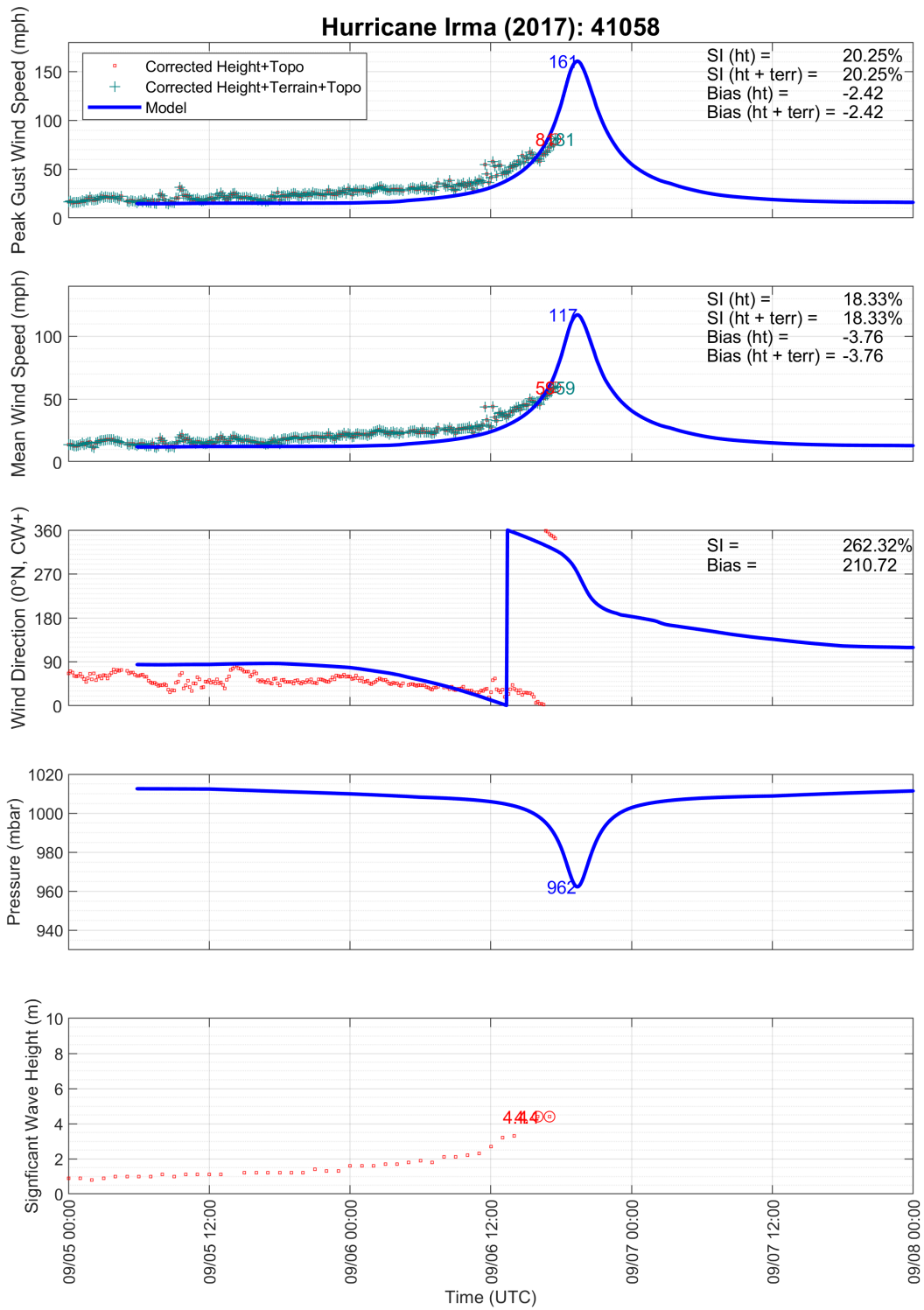


Figure 6-10. Modeled and observed meteorological time series at NDBC station 41058: North of St. Thomas, USVI.

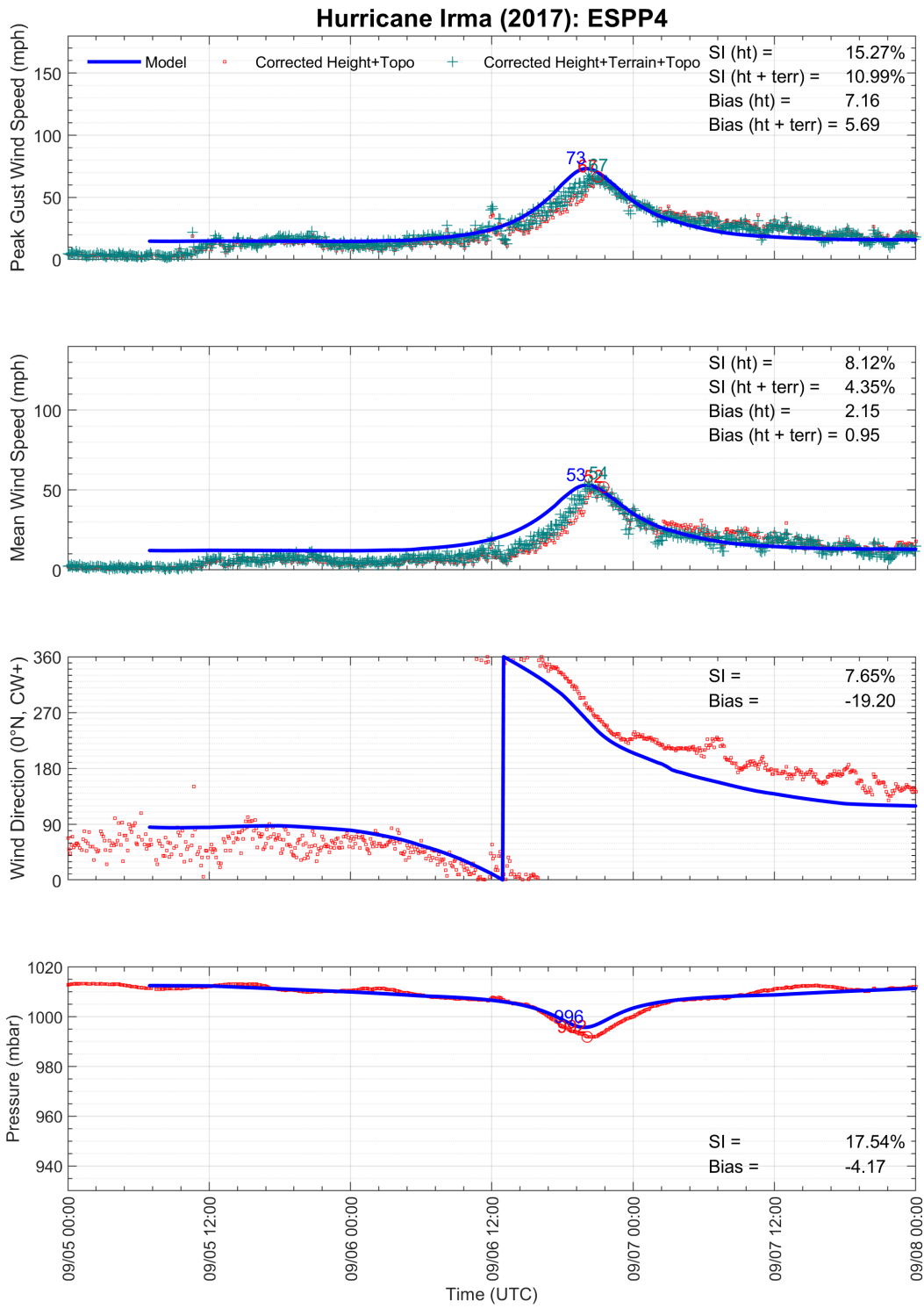


Figure 6-11. Modeled and observed meteorological time series at NDBC station ESPP4: Esperanza, Vieques Island, Puerto Rico.

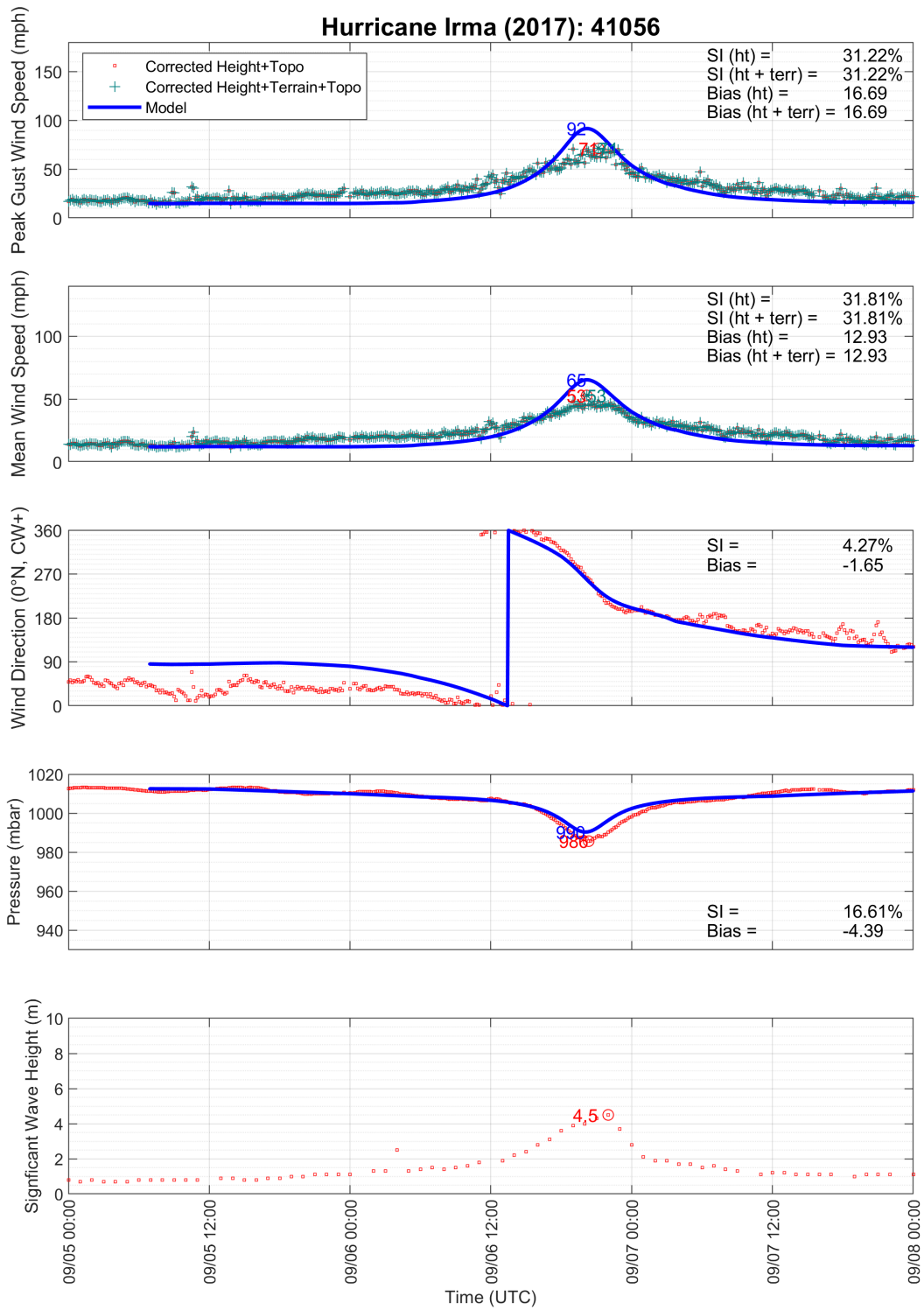


Figure 6-12. Modeled and observed meteorological time series at NDBC station 41056: Vieques Island, Puerto Rico.

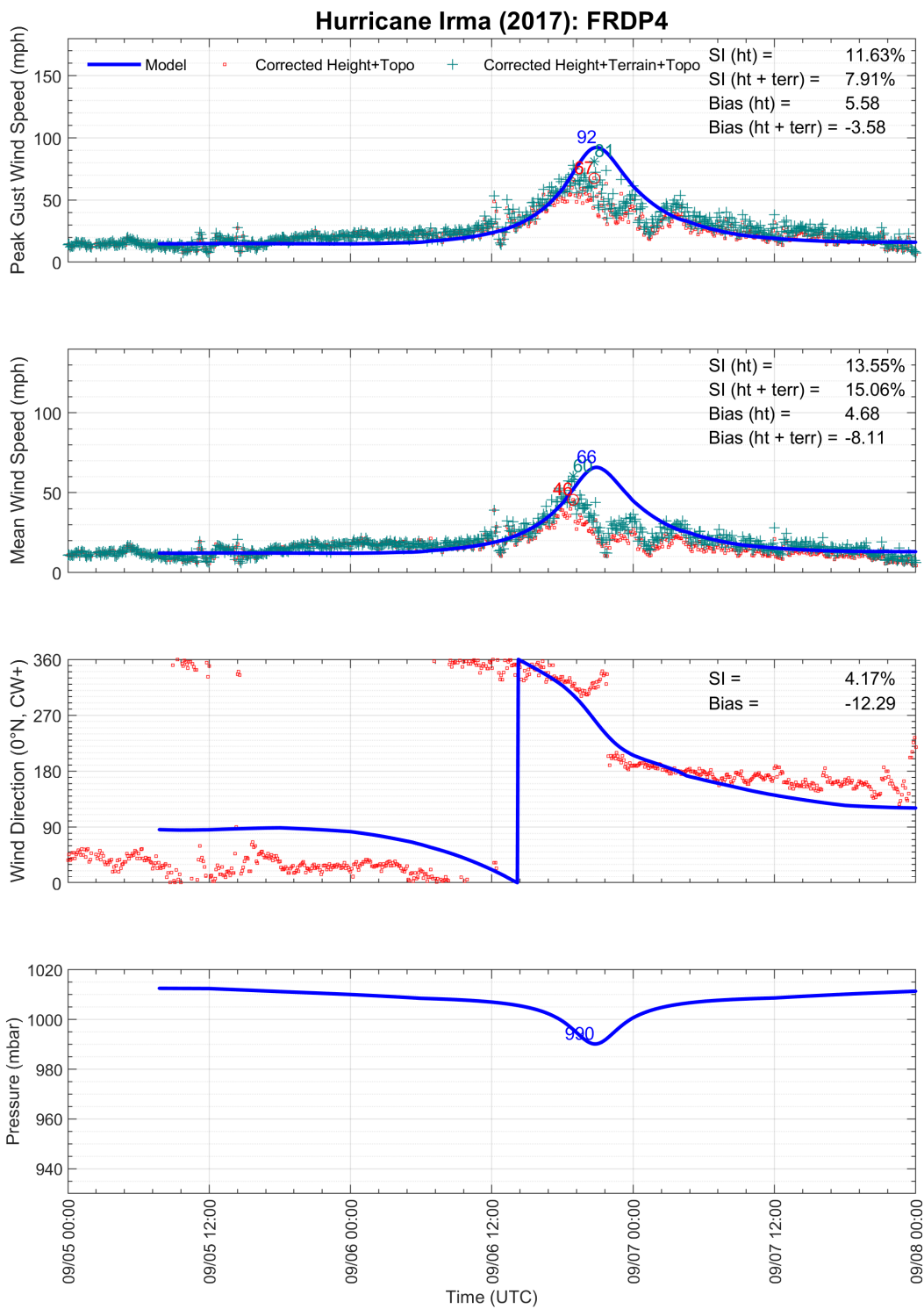


Figure 6-13. Modeled and observed meteorological time series at NDBC station FRDP4: Fajardo, Puerto Rico.

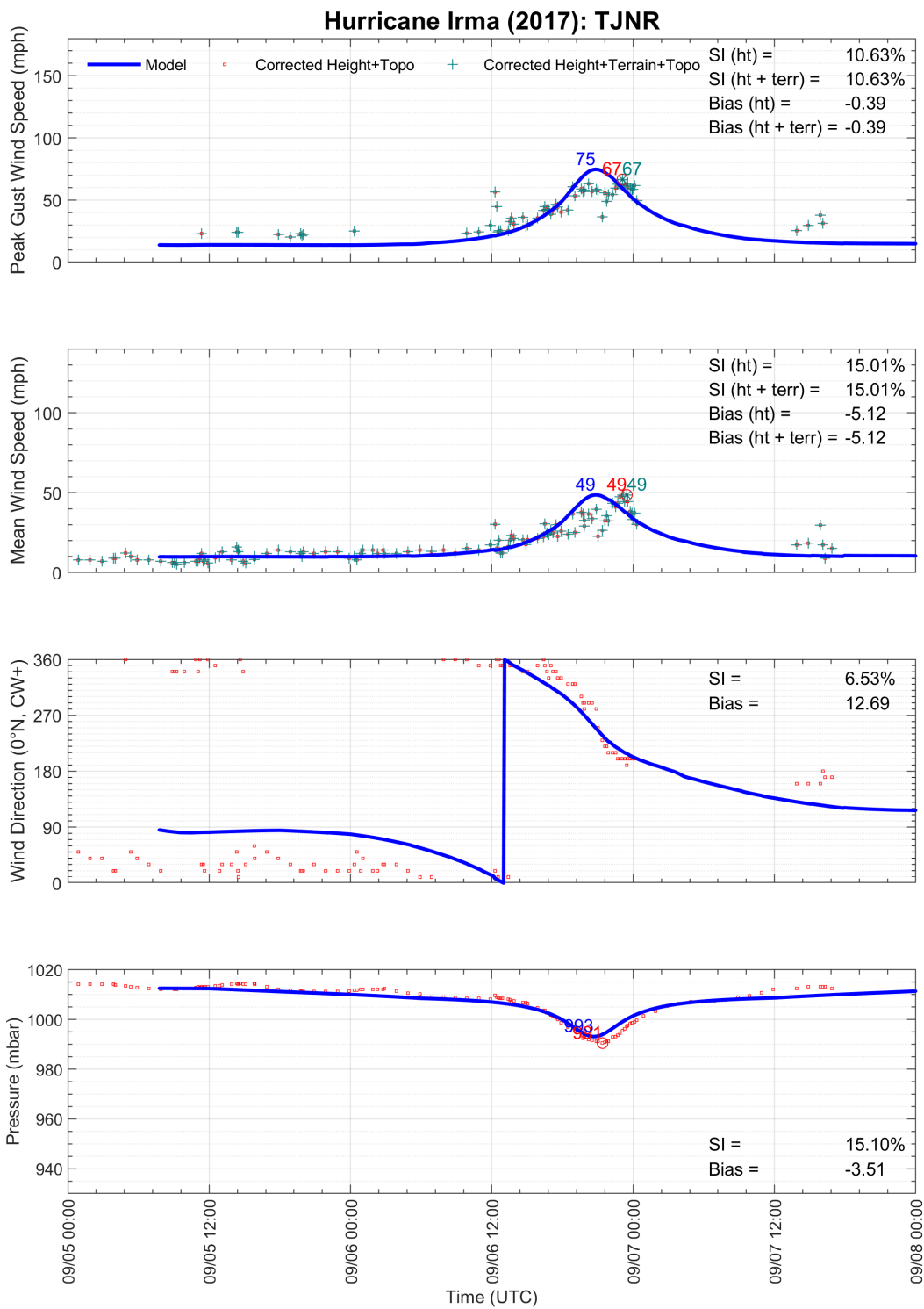


Figure 6-14. Modeled and observed meteorological time series at ASOS station TJNR: Roosevelt Roads Naval Station, Puerto Rico.

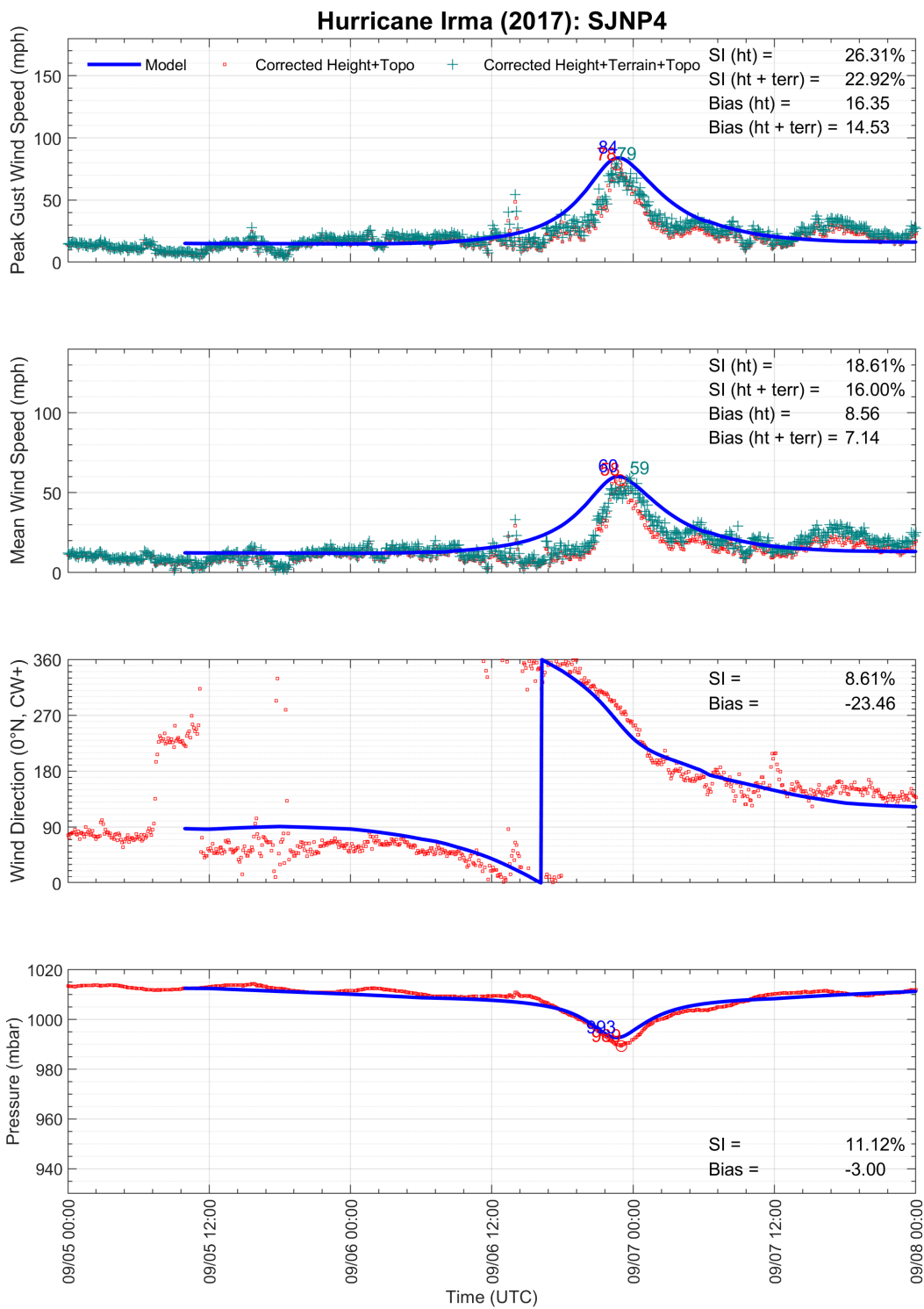


Figure 6-15. Modeled and observed meteorological time series at NDBC station SJNP4: San Juan, La Puntilla, San Juan Bay, Puerto Rico

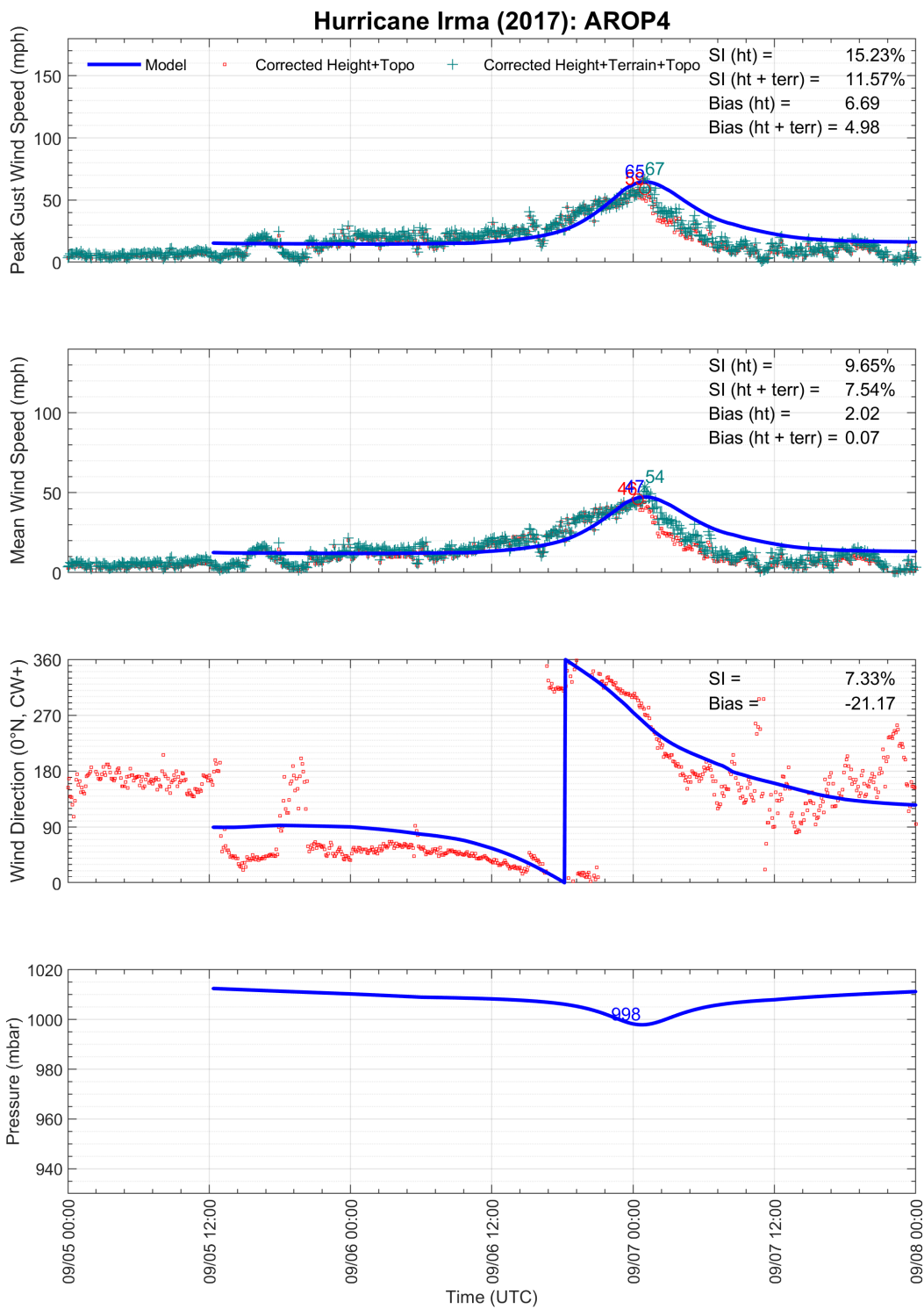


Figure 6-16. Modeled and observed meteorological time series at NDBC station AROP4: Arcibo, Puerto Rico.

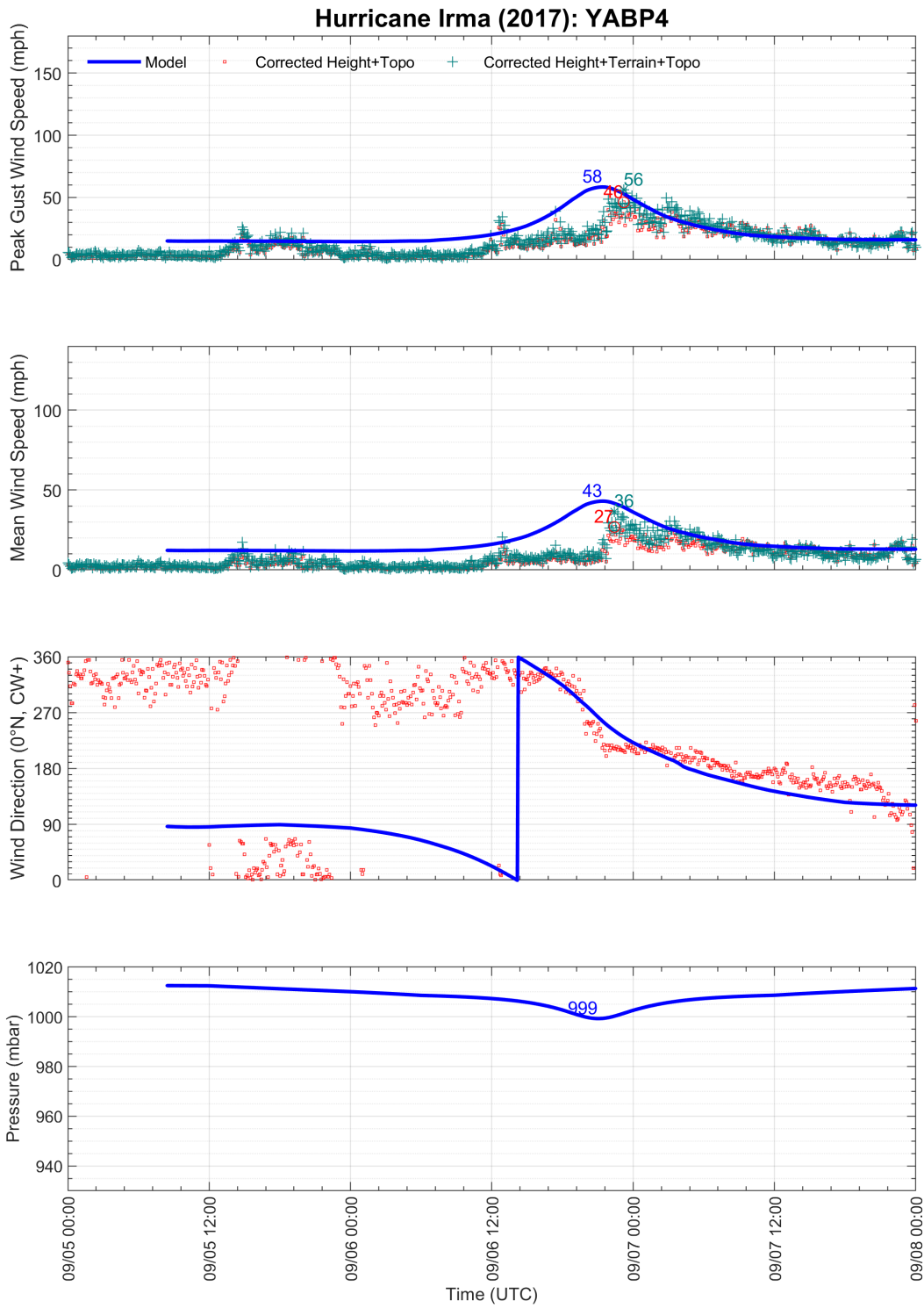


Figure 6-17. Modeled and observed meteorological time series at NDBC station YABP4: Yabucoa Harbor, Puerto Rico.

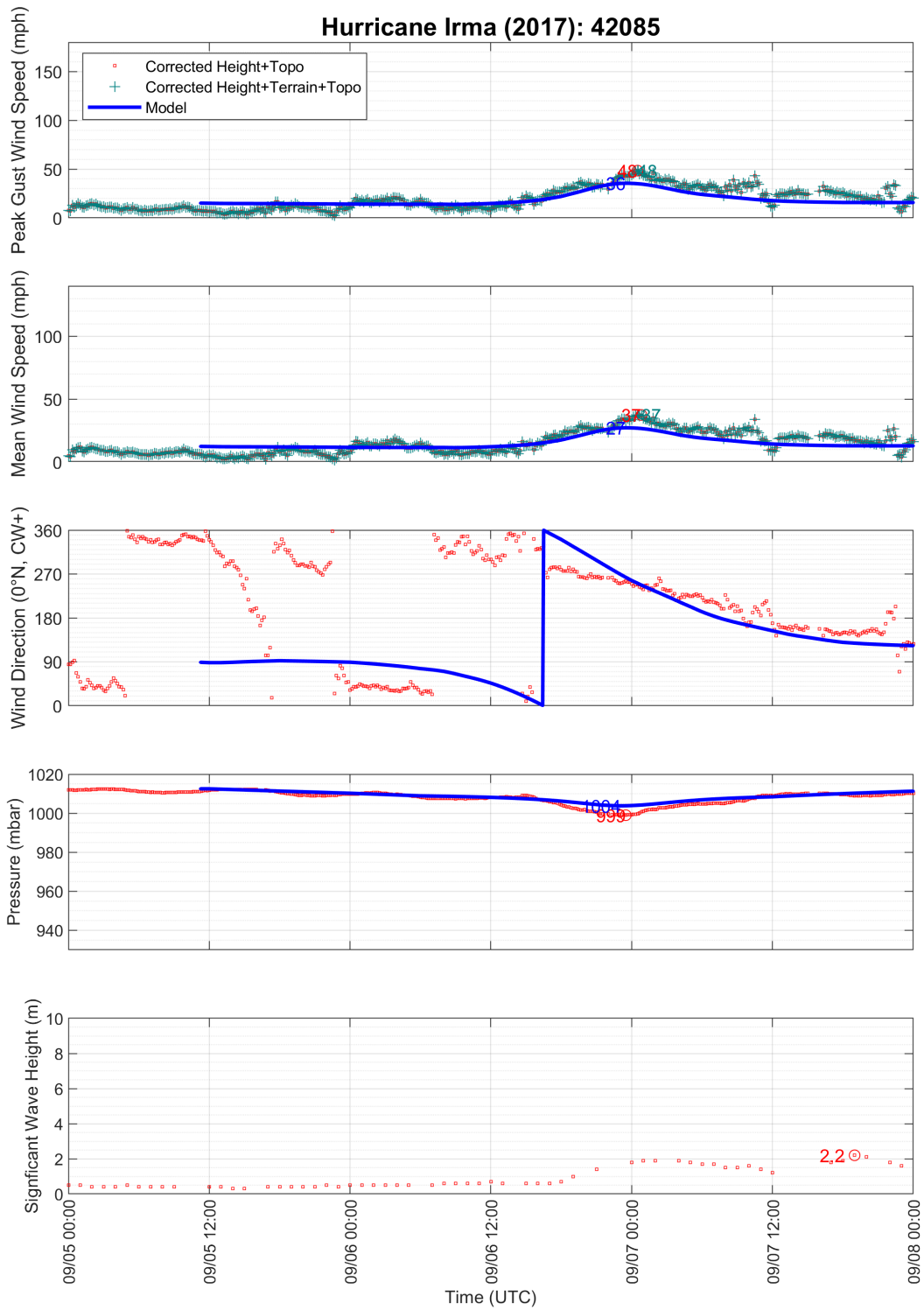


Figure 6-18. Modeled and observed meteorological time series at NDBC station 42085: Southeast of Ponce, Puerto Rico.

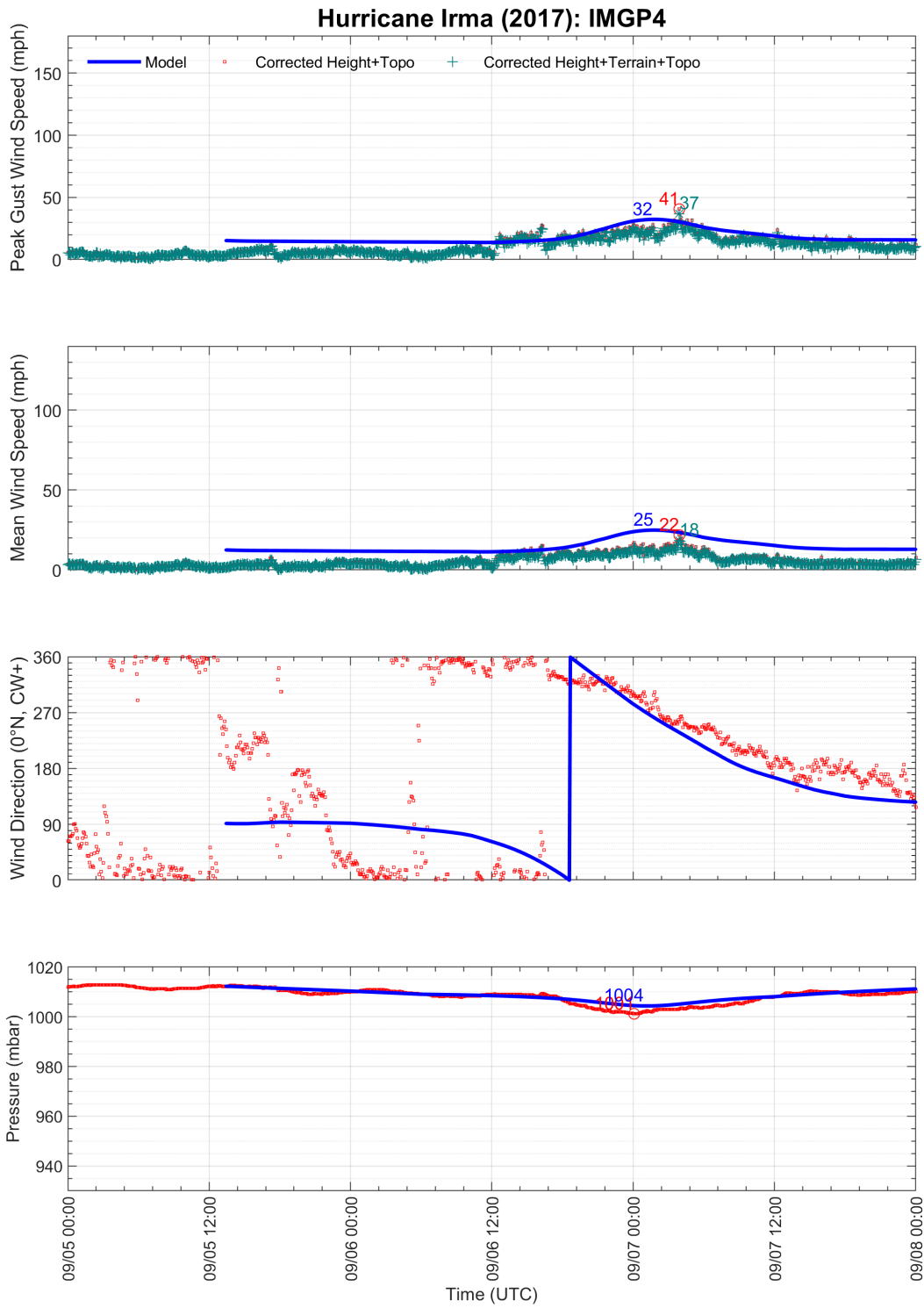


Figure 6-19. Modeled and observed meteorological time series at NDBC station IMG4: Isla Magueyes, Puerto Rico.

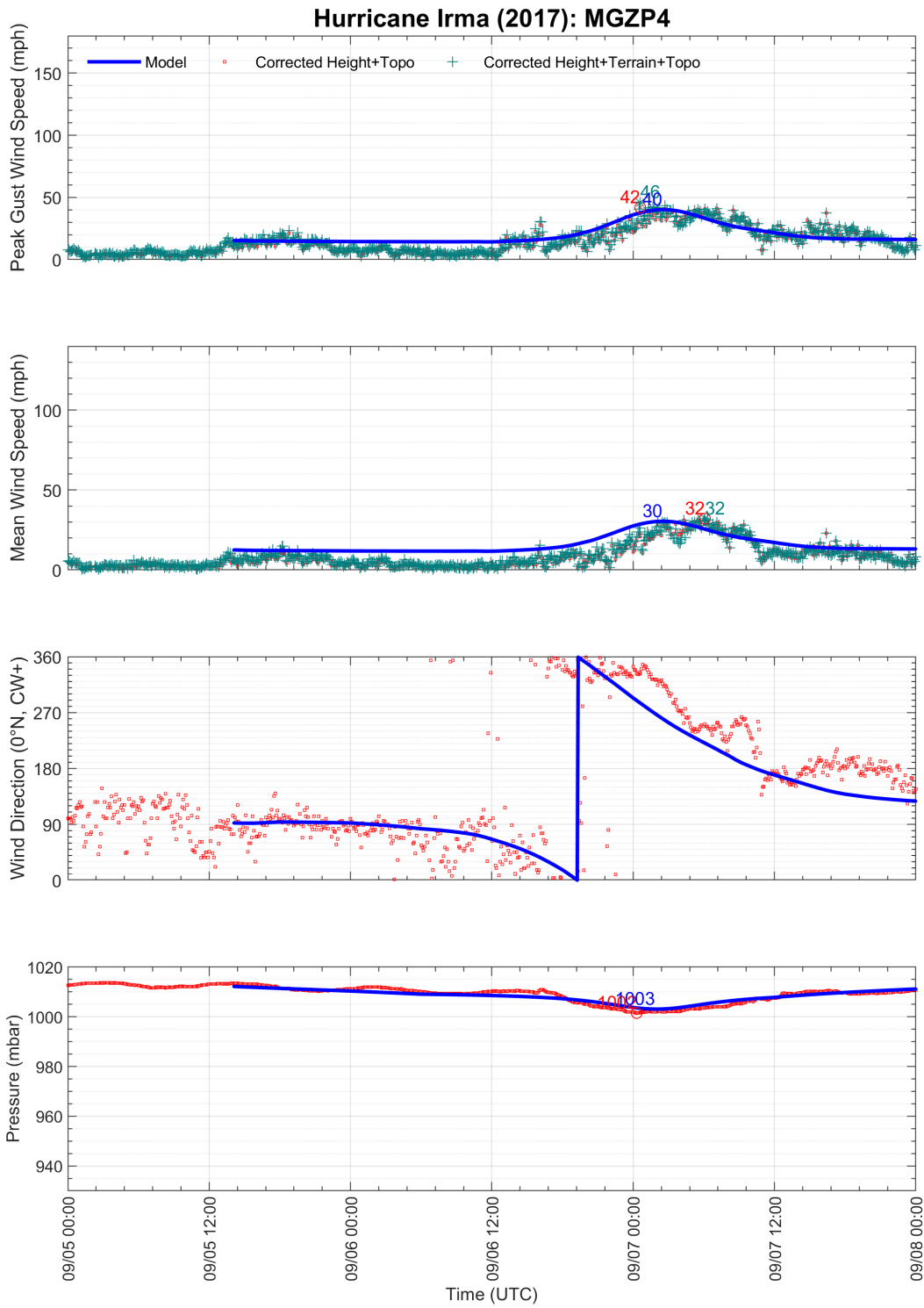


Figure 6-20. Modeled and observed meteorological time series at NDBC station MGZP4: 9759394 - Mayaguez, Puerto Rico.

6.5 ERRORS AND UNCERTAINTY

Figure 6-21 and Figure 6-22 present comparisons of modeled and observed maximum gust wind speeds and minimum central pressures for the stations used in the model validation process. Stations that failed prior to the arrival of the highest winds were not included in the comparisons. The R^2 values for peak gust wind speed with and without terrain corrections were 0.76 and 0.77, respectively. The R^2 value for central pressure was 0.92.

Tabulated error values of peak gust wind speed are provided in Table 6-1 at the end of this section. No error data was provided for stations where the instrumentation failed prior to the occurrence of maximum winds.

The largest outliers where the model overpredicted the maximum gust wind speed occurred south of the U.S. Virgin Islands of St. Thomas and St. John and eastward to Puerto Rico, notably NDBC station 41052. As discussed in Section 6.4, this was likely due to sheltering effects of large waves experienced at offshore buoys.

Modeled wind speeds at NDBC station FRDP4 between September 6 19:00 to 22:00 UTC ranged from approximately 300° to 210° . This station was located on the dock of a ferry terminal where large commercial ferries can be docked on either side of the anemometer and the ferry terminal itself is located to the south of the anemometer (see Figure 6-23 and Figure 6-24). If a ferry was parked on the west and/or northwestern side of the dock, winds from between 300° to 210° could have been blocked, and the true maximum wind speeds may not have been captured.

NDBC station YABP4 is located in the port of an oil refinery and has a dock located to the west and northwest where heavy machinery, shipping containers, and large ships have the opportunity to block winds between approximately 270° to 360° (see Figure 6-25). Similar to station FRDP4, it is likely that the true maximum wind speeds from these directions were not captured.

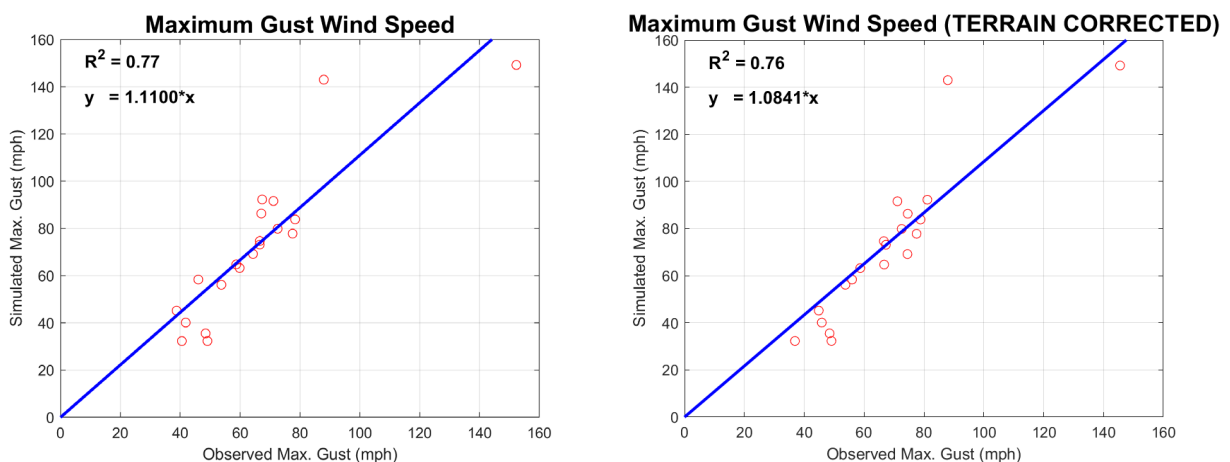


Figure 6-21. Modeled and observed maximum peak gust wind speed corrected only for height (left) and corrected for height and terrain (right).

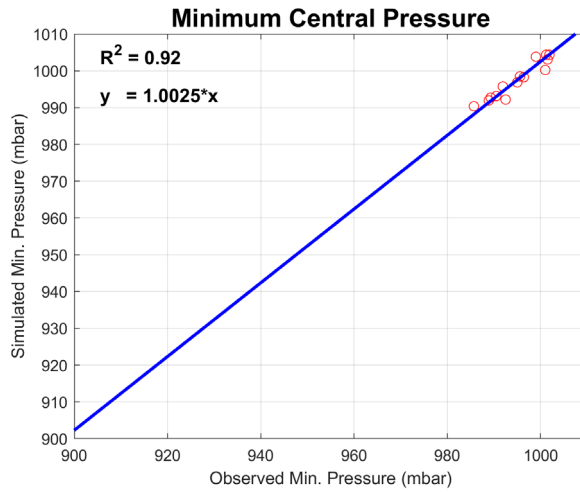


Figure 6-22. Modeled and observed minimum central pressure.



Figure 6-23. Aerial view of NDBC Station FRDP4.



Figure 6-24. NDBC Station FRDP4: view from dock towards anemometer.



Figure 6-25. Aerial view of NDBC Station YABP4.

Table 6-1. Errors in modeled peak gust wind speed in Hurricane Irma OCONUS when observations are corrected for height only and for height and terrain. All wind speed values are presented at 10 m elevation in open terrain.

Station	Modeled Peak Gust Wind Speed (mph)	Observed Peak Gust Wind Speed (mph)		Error (mph)	
		Corrected for Height	Corrected for Height + Terrain	Corrected for Height	Corrected for Height + Terrain
TIST	---	---	---	---	---
TISX	56	54	54	2	2
TJBQ	---	---	---	---	---
TJIG	---	---	---	---	---
TJNR	75	67	67	8	8
TJPS	---	---	---	---	---
TJSJ*	78	78	78	0	0
AROP4	65	59	67	6	-2
CHAV3*	149	152	146	-3	3
CHSV3	69	64	74	5	-5
ESPP4	73	67	67	6	6
FRDP4	92	67	81	25	11
IMGP4	32	41	37	-9	-5
LTBV3	63	60	59	3	4
MGIP4	32	49	49	-17	-17
MGZP4	40	42	46	-2	-6
PTRP4	45	39	45	6	0
SJNP4	84	78	79	6	5
VQSP4	80	73	73	7	7
YABP4	58	46	56	12	2
41052	143	88	88	55	55
41053	86	67	75	19	11
41056	92	71	71	21	21
41058	---	---	---	---	---
42085	36	48	48	-12	-12

* Note: Stations TJSJ and CHAV3 failed very near the expected time of maximum winds and may not have captured the true wind speed experienced.

6.6 WIND FIELD MAPS

The final peak gust wind speed maps of Hurricane Irma in Puerto Rico and the Virgin Islands are shown in Figure 6-26 through Figure 6-28 with wind speed bands in increments of 10 mph. Peak gust wind speeds are defined as 3-second average at 10 m above ground over open terrain. Peak gust wind speeds are presented in the *native* topography (i.e., topography speed-up factors have been applied to the wind field). The storm track is shown by the dashed blue line. All stations used in the wind field model validation are also shown: purple triangles indicate an ASOS station, and green triangles indicate a station in the NDBC database located over water or near the coast. The highest winds are shown to have occurred over the U.S. Virgin Islands of St. John and St. Thomas in mountainous terrain.

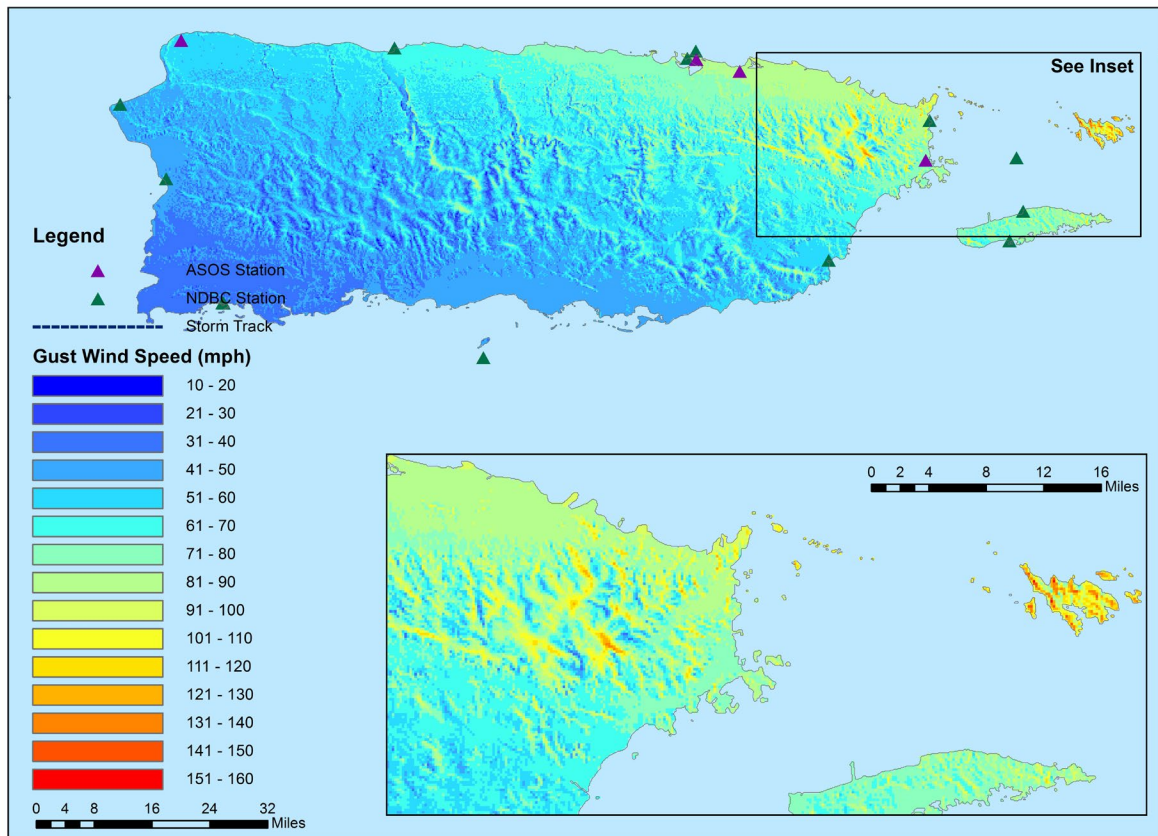


Figure 6-26. Peak gust wind speed map for Hurricane Irma (2017) showing estimated 3-second peak gust wind speeds (mph) at 10 m above ground over open terrain. Model output obtained from ARA wind field model fit to surface level observations using NHC best track and central pressures. Modeled gust wind speeds include the effects of topography.

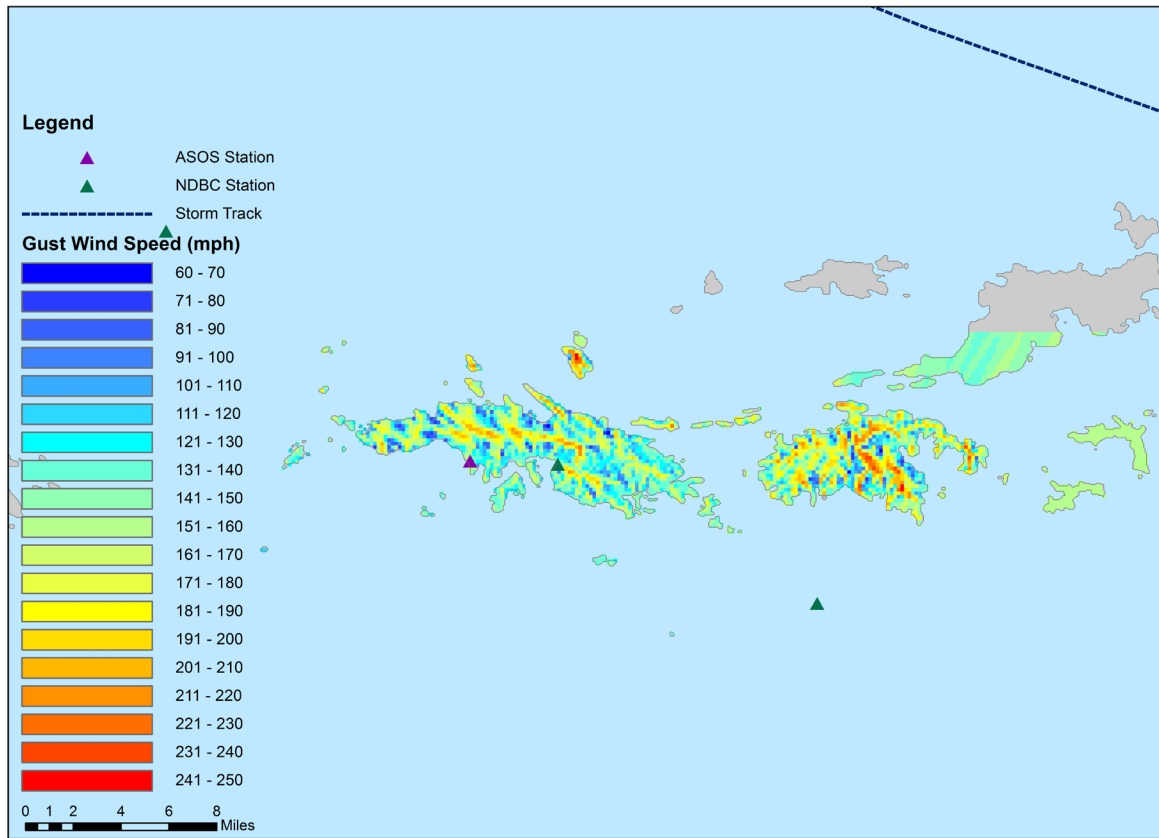


Figure 6-27. Peak gust wind speed map for Hurricane Irma (2017) in St. Thomas and St. John, USVI, showing estimated 3-second peak gust wind speeds (mph) at 10 m above ground over open terrain. Model output obtained from ARA wind field model fit to surface level observations using NHC best track and central pressures. Modeled gust wind speeds include the effects of topography.

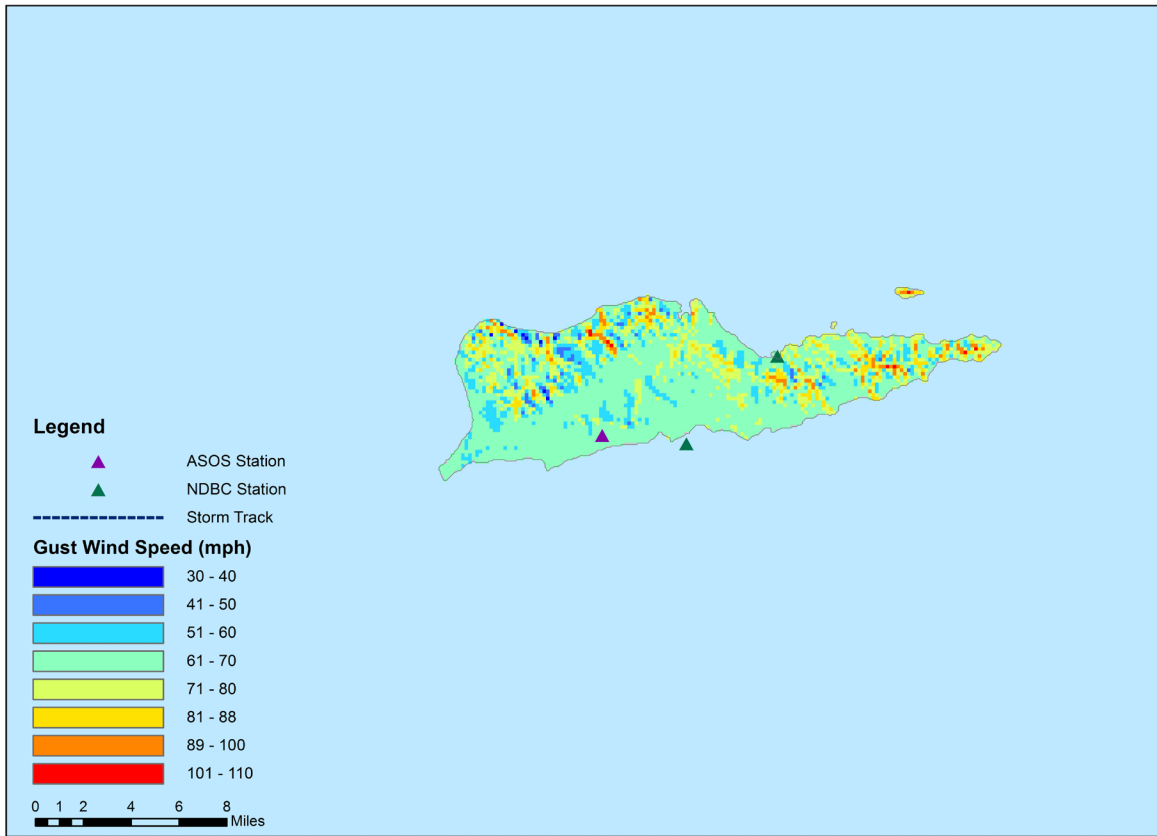


Figure 6-28. Peak gust wind speed map for Hurricane Irma (2017) in St. Croix, USVI, showing estimated 3-second peak gust wind speeds (mph) at 10 m above ground over open terrain. Model output obtained from ARA wind field model fit to surface level observations using NHC best track and central pressures. Modeled gust wind speeds include the effects of topography.

7 HURRICANE MARIA

7.1 EVENT BACKGROUND

A brief background for Hurricane Maria (2017) is presented in this section. For a full narrative of the storm, including synoptic history, meteorological statistics, casualty and damage statistics, and forecast and warning critique, see the National Hurricane Center's Tropical Cyclone Report on Hurricane Maria (Pasch et al., 2018) available at https://www.nhc.noaa.gov/data/tcr/AL152017_Maria.pdf.

Hurricane Maria made landfall in Dominica as a Category 5 hurricane and in Puerto Rico as a Category 4 hurricane. The storm became a major hurricane by 12:00 UTC on September 18 and had strengthened to a category 5 event 12 hours later. Maria made landfall in Dominica with maximum winds of 145 knots (167 mph) and an estimated central pressure of 922 mbar around 1:15 UTC on September 19.

After making landfall in Dominica, Hurricane Maria continued on a west-northwestward trajectory into the Caribbean Sea where it strengthened to its peak intensity of 150 knots (173 mph) with a minimum central pressure of 908 mbar at 3:00 UTC on September 20 while centered approximately 25 nm south of St. Croix in the U.S. Virgin Islands. Maria weakened slightly and grew in size before making landfall on the southeast coast of Puerto Rico near Yabucoa around 10:15 UTC on September 20 with maximum wind speeds around 135 knots (155 mph). Over the next several hours, Maria crossed from the southeast coast of the island to the northeast, finally emerging into the Atlantic Ocean around 18:00 UTC on September 20. While crossing Puerto Rico, the maximum wind speeds of the storm weakened to 95 knots (109 mph).

As Maria turned towards the north, it traveled through the Bahamas and the Turks and Caicos Islands before passing about 130 nm east of Cape Hatteras, North Carolina, at 6:00 UTC on September 27. By this time, the storm had weakened to a Category 1 hurricane with maximum wind speeds of 65 knots (75 mph). Maria moved rapidly on an east-northeastward trajectory and became an extratropical cyclone by 18:00 UTC on September 30, before ultimately dissipating 400 nm southwest of Ireland by 18:00 UTC on October 2.

Maximum storm surge and tide inundation levels of 6 to 9 feet were estimated to the north of Maria's landfall along the coasts of Humacao, Naguabo, and Ceiba municipalities in Puerto Rico. On the northeast coast of Puerto Rico maximum inundation levels were 3 to 5 feet above ground level, and on the north coast inundation levels ranged from 2 to 4 feet. On the islands of Vieques in Puerto Rico, and St. Croix, in the U.S. Virgin Islands, maximum storm surge inundation levels of 3 to 5 feet above ground level were estimated. On the U.S. Virgin Islands of St. Thomas and St. John and along the coast of North Carolina, maximum storm surge inundation levels of 1 to 3 feet were estimated.

Hurricane Maria also caused significant rainfall on the islands that it passed over. Maximum rainfall totals of 22.8 inches were observed in Dominica, and up to 38 inches in Puerto Rico. Rainfall totals of 10 to 13 inches also occurred in Guadeloupe and portions of the Dominican Republic.

7.2 DATA COLLECTION

7.2.1 Track

A portion of the best track of Hurricane Maria is shown in Figure 4-1, as the storm approached and made landfall in Puerto Rico.

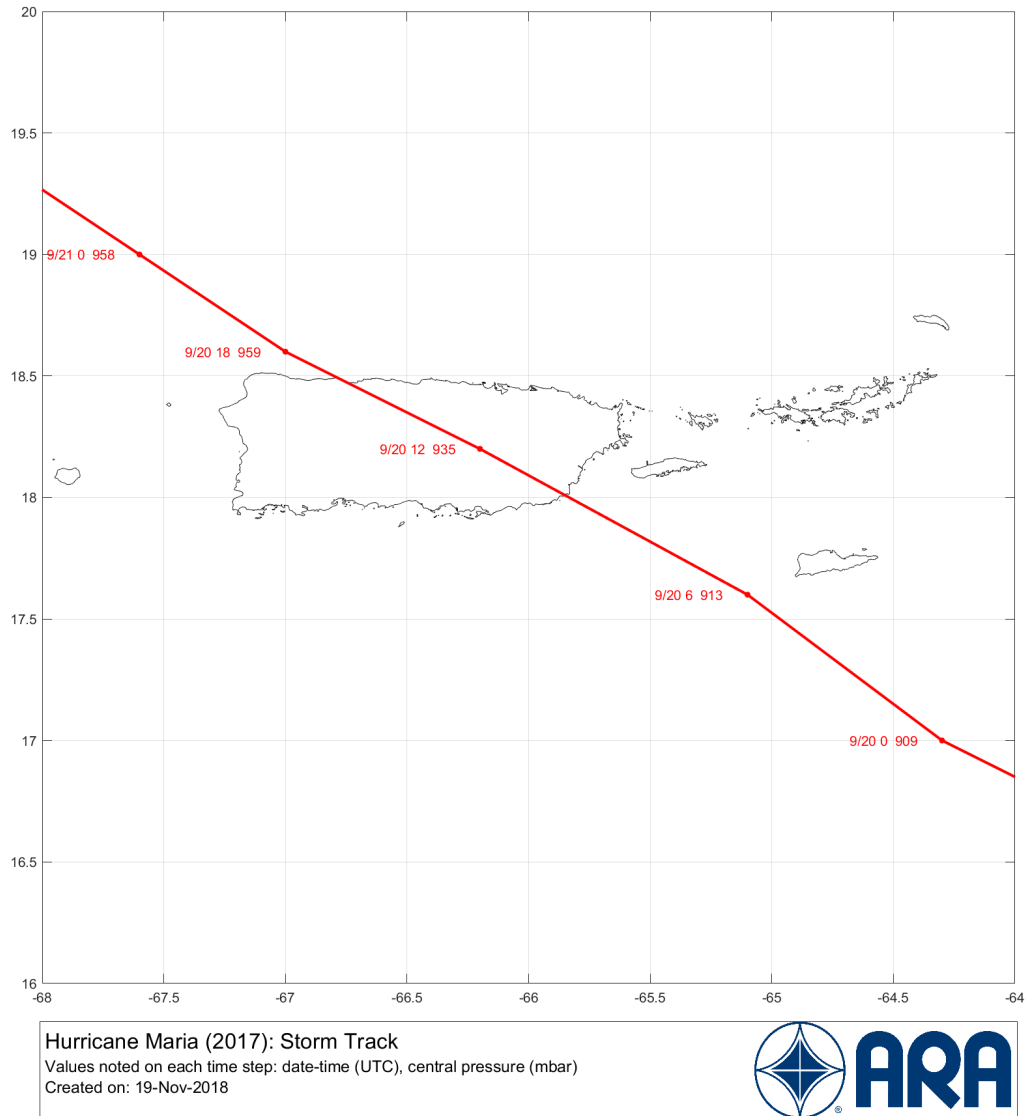


Figure 7-1. Best-track information of Hurricane Maria (2017) collected from the NHC Atlantic Hurricane Database (HURDAT2).

7.2.2 Observations

Stations with observations during the lifespan of Hurricane Maria and within 150 miles of a track point were used in the model validation and are shown in Figure 5-2. A table of station locations, anemometer heights, and values local surface roughness are provided in Appendix D.

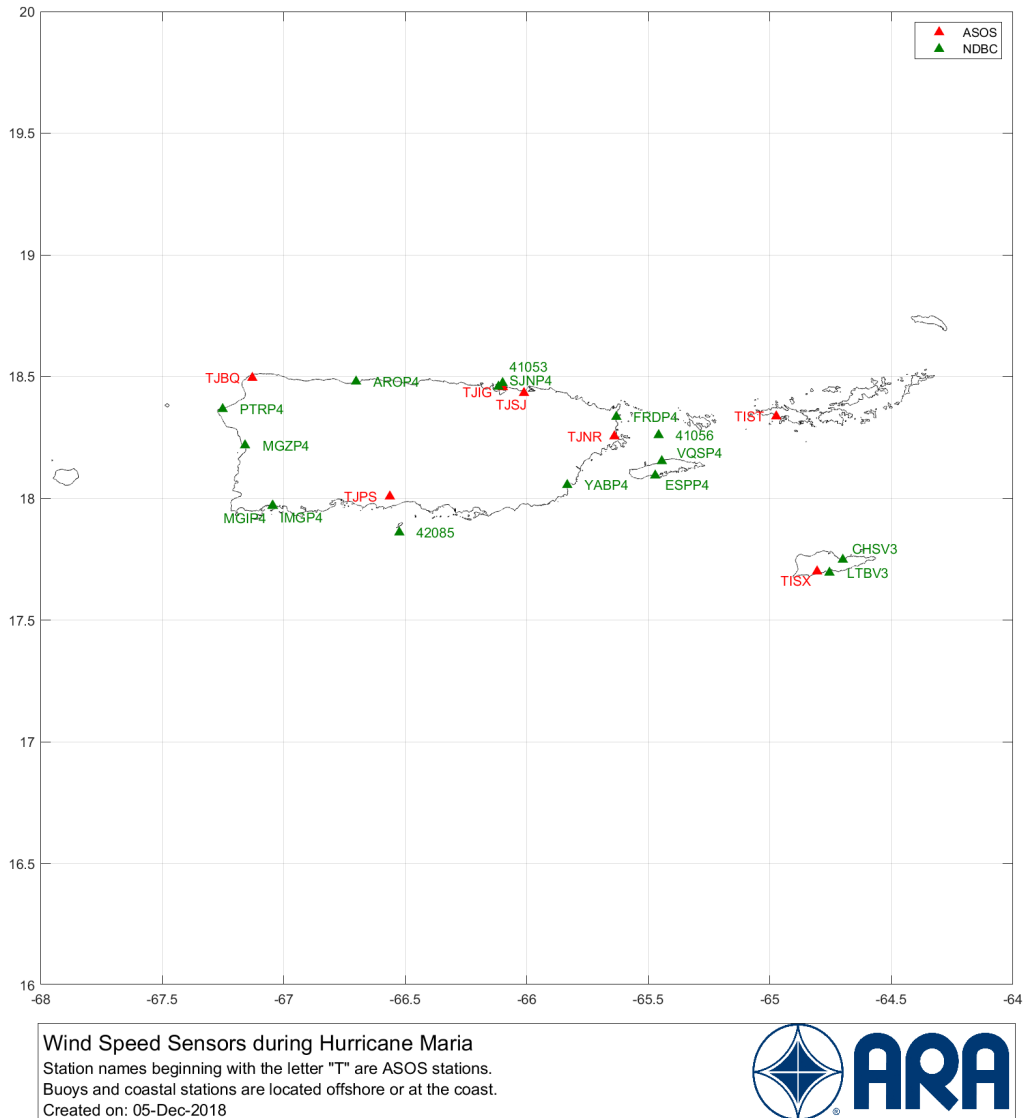


Figure 7-2. ASOS and NDBC stations with surface observations during the lifespan and within 150 miles of Hurricane Maria.

7.3 DATA CORRECTIONS (DEVIATION FROM STANDARD PROCEDURES)

Estimates of directional effective surface roughness have not been previously generated for any stations (ASOS or NDBC) outside the contiguous United States. Wind speed observations at NDBC stations located very nearshore are often affected by the rougher terrain of nearby land and may not correspond to true marine terrain observations. NOAA National Ocean Service station LTBV3—shown in Figure 6-3—is located on the dock of a shipping port with an oil and gas refinery and highly populated communities to the north. To account for terrain effects on these stations, a visual technique was used to estimate the directional surface roughness values from aerial imagery; both the values and aerial imagery used are provided in Appendix D. Visually estimated values of z_0 serve as input to the ESDU (1982, 1983) terrain correction methodology.



Figure 7-3. NOAA National Ocean Service Station LTBV3 located very-near shore with a refinery, shipping port, and populated communities located to the north.

Under separate FEMA task orders, topographic wind speed-up factors were created for the U.S. Virgin Islands and Puerto Rico. Wind speed-ups were computed for 16 different wind directions at increments of 22.5 degrees. The speed-up factor generally increases with increasing slope in front of the point of interest. If the slope to the immediate left or right of the site (90 degrees or 270 degrees) is positive (i.e., downhill) the wind speed is decreased as the wind is able to go around the location. Conversely, if the slope is negative (e.g., the walls of a valley) the wind speed is increased due to the effects of channeling. For very steep negative slopes, the speed-up becomes less than 1 since the flow separates and locations on the hill are in a wake region having a recirculated flow. The same applies on the leeward side of steep hills. For points located at or near a ridge or hill top, the positive slope behind the point increases the speed-up such that, all else being equal, a ridge produces a maximum speed-up. Maximum topographic

speed-up factors for the U.S. Virgin Islands and Puerto Rico are shown in Figure 6-4 and Figure 6-5, respectively. A detailed derivation of the topographic speed-up factors is provided in Vickery et al. (2018).

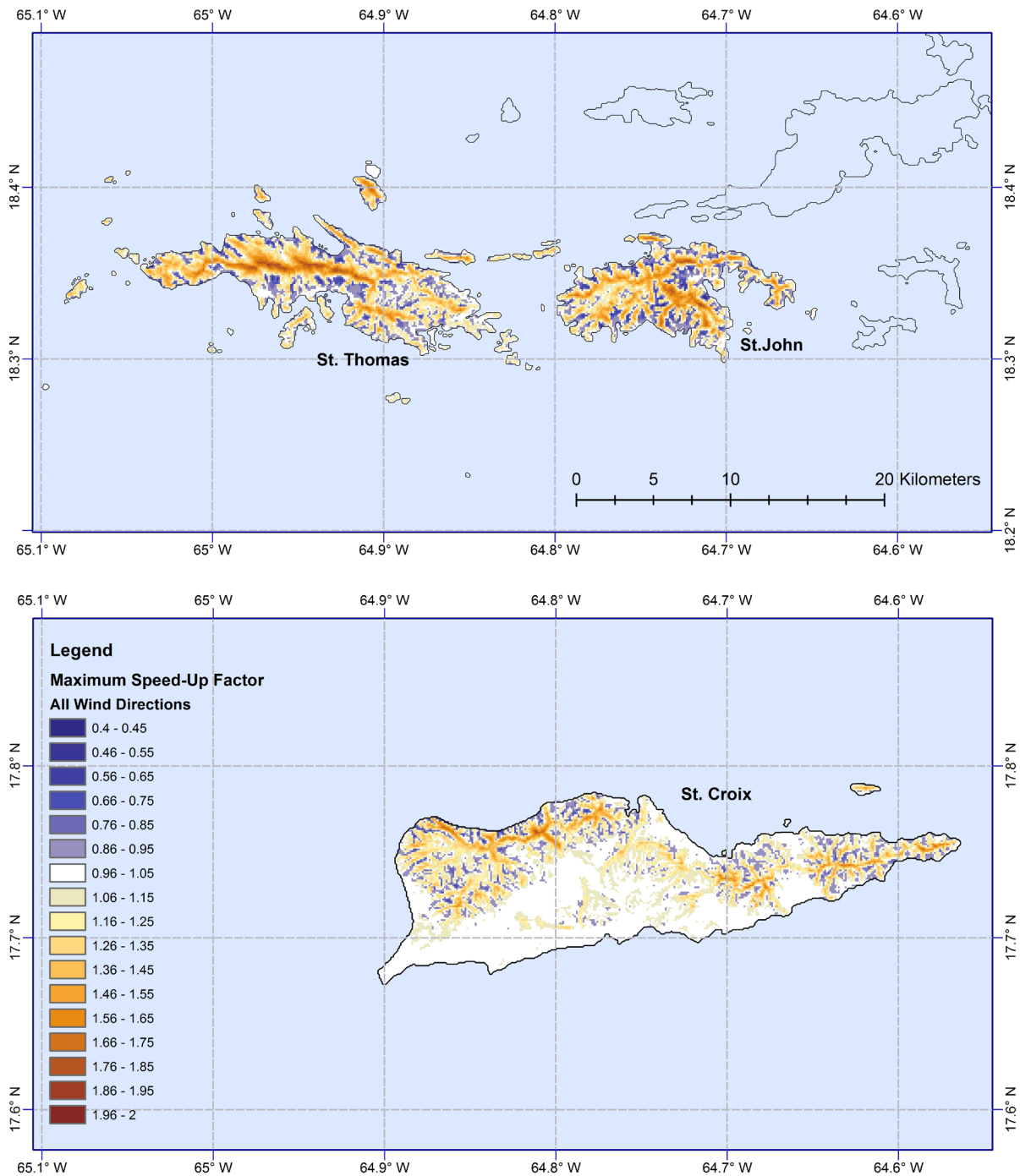


Figure 7-4. Maximum topographic speed-up factors for the U.S. Virgin Islands.

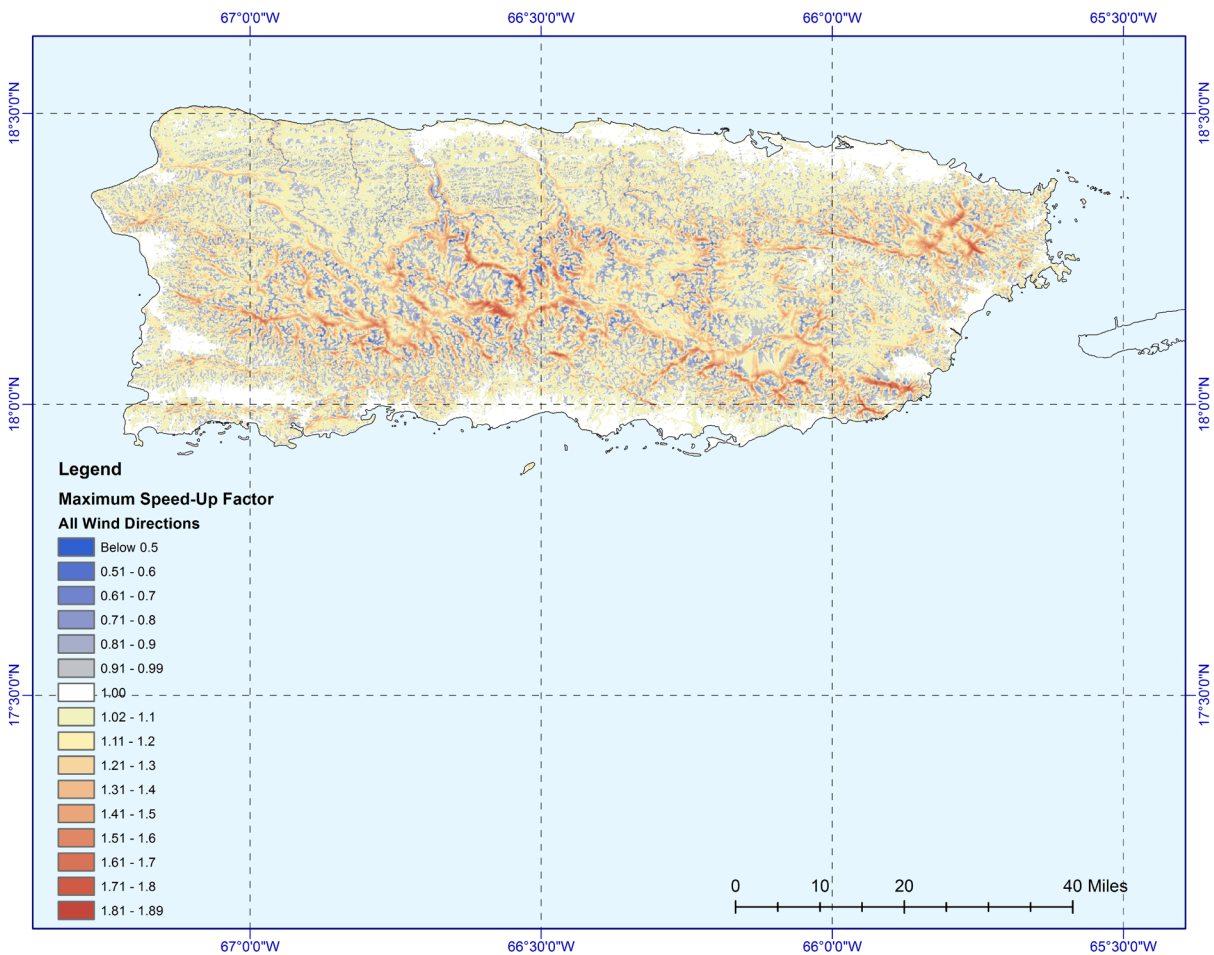


Figure 7-5. Maximum topographic speed-up factors for Puerto Rico.

The speed-up factors were used in the track fitting process by adjusting the observations to an equivalent wind speed at 10 m height over open terrain and *flat* topography. The final wind field maps presented in Section 7.6 have been adjusted back to the local topography (e.g., 3-second gust wind speed at 10 meter height over open terrain and the *native* topography).

7.4 DISCUSSION OF SELECT STATION TIME HISTORIES

The anemometers at many stations located in and near Puerto Rico and the U.S. Virgin Islands failed prior to the occurrence of maximum gust wind speeds. At stations where the complete, observed wind speed time history was not captured during the passage of Hurricane Maria, priority was placed on modeling the observed pressure time series, if it existed.

The highest winds at NDBC station CHSV3 located on the U.S. Virgin Island of St. Croix occurred around September 20 at 5:00 UTC. (The time history is shown in Figure 7-6.) St. Croix was positioned to the north of Hurricane Maria's track, just outside the eyewall. The maximum observed peak gust wind speed was not captured before failure of the anemometer, though the time series leading up to failure shows a high bias in modeled wind speeds. The modeled and observed central pressure time histories showed

good agreement during the entire time series with a low scatter index of about 3% and a nearly negligible bias of -0.16 mbar.

On the island of St. Thomas, which was further from the center of the storm, ASOS station TIST experienced lower wind speeds than observed in St. Croix. The maximum peak gust winds occurred around 7:00 UTC on September 20, as shown in Figure 7-7. The anemometer at the station failed, but winds were observed at the time of the modeled peak gust wind speeds. The model underestimated the maximum peak gust wind speed by about 3%. The central pressure and wind direction time series prior to failure of the anemometer showed high agreement between the modeled and observed data.

To the west, closer to the eye of the storm, NDBC station VQSP4 captured wind speed observations on the Puerto Rican island of Vieques (see Figure 7-8). The anemometer failed very close to the occurrence of the maximum peak gust wind speed experienced at the station and may not have captured the true maximum value. The peak gust wind speed was overestimated by only 2%, though the sustained wind speed time trace showed a consistent high bias up to 30 mph. No central pressure data was observed at this station.

On the eastern side of mainland Puerto Rico, NDBC stations 41056, FDRP4, and YABP4 captured maximum peak gust wind speeds of 82, 111, and 146 mph, respectively, as shown in Figure 7-9 through Figure 7-11. The modeled values of maximum peak gust wind speed at stations 41056 and FDRP4 were 117 and 119 mph, respectively, which was an overestimation of 43% and 7%, respectively. To the right of the storm's track, the modeled maximum peak gust wind speed at station YABP4 was 134 mph, or an underestimation of 8%. The wind direction time series at station 41056 shows no incongruities, indicating it is unlikely that the buoy drifted away during the passage of the hurricane. Given that significantly higher winds were observed at nearby station FDRP4, it is likely that the anemometer at station 41056 was sheltered by large waves. The largest significant wave heights recorded at station 41056 were 6.4 meters (21 feet), and the anemometer is only 4 m above sea level. The effect of the waves on the measured wind speed is a function of both the wave height and the buoy type; however, the magnitude of the reduction is difficult to quantify. The modeled and observed time histories of central pressure at stations 41056 and YABP4 agreed well, with low scatter indices of about 10% and low biases around 1.5 mbar. No central pressure observations existed at station FRDP4.

ASOS station TJSJ and NDBC stations 41053 and AROP4 captured wind speeds on the northern coast of Puerto Rico as shown in Figure 7-12 through Figure 7-14. The anemometer at station TJSJ failed just prior to the occurrence of the peak gust wind speeds. The time series of modeled and observed peak gust winds agreed well with one another having a scatter index around 13% and an average underestimation of about 3.5 mph. The modeled peak gust wind speed at station TJSJ was 118 mph.

At station 41053, the anemometer failed during the occurrence of the maximum gust wind speeds experienced at the station, but resumed taking measurements a short time later. The overall time series at 41053 had a scatter index around 38% and a high bias of about 22 mph. However, the measured wind speeds would be expected to have a low bias due to the effects of the waves. The modeled maximum peak gust wind speed at the station was 129 mph. The time series of central pressures at both stations showed high agreement with scatter indices ranging from 4 to 11 percent and low biases of only 0.16 to 1.22 mbar.

Further to the west of the island, station AROP4 experienced a direct hit of the hurricane eye. The model underestimated the maximum peak gust wind speed by about 7%. The overall modeled and observed wind speed time series agreed well prior to the arrival of the hurricane eye. After passage of the eye, the model overestimated the peak gust wind speeds.

From east to west on the southern and western coast of Puerto Rico, NDBC stations 42085, MGIP4, and MGZP4 captured maximum peak gust wind speeds ranging from 68 to 108 mph as shown in Figure 7-15 through Figure 7-17. The model overpredicted the maximum peak gust wind speed at station 42085 by about 9%. However, prior to the occurrence of the maximum winds, the temporal density of observations decreased, suggesting the true maximum wind speed may not have been recorded. At station MGIP4, the anemometer failed prior to the occurrence of the maximum peak gust wind speed. Prior to the failure, the modeled time series of peak gust wind speed agreed well with the observed with a small over-bias around 5 to 7 mph.

The anemometer at station MGZP4 also failed, but after the maximum wind speed occurred (see Figure 7-17). The maximum modeled peak gust wind speed was 94 mph, while the maximum observed peak gust wind speed was 95 mph correcting for height of the anemometer only, and 108 mph when correcting for anemometer height and surrounding terrain using the visual estimation of surface roughness technique. The modeled and observed wind directions at all three locations had low scatter indices ranging from 3 to 8%, and the modeled and observed central pressures had scatter indices ranging from 5 to 10%.

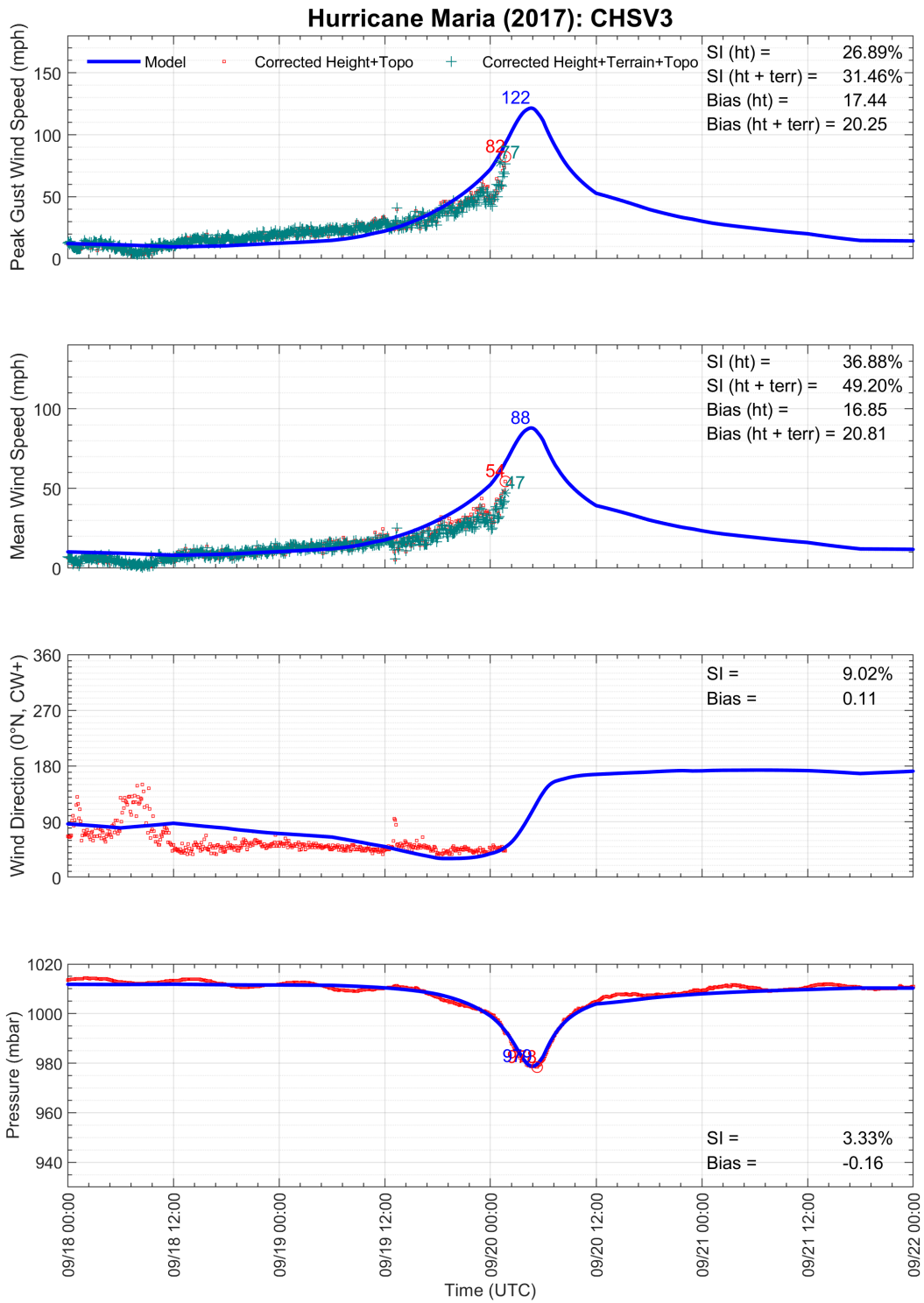


Figure 7-6. Modeled and observed meteorological time series at NDBC station CHSV3: Christiansted Harbor, St. Croix, USVI.

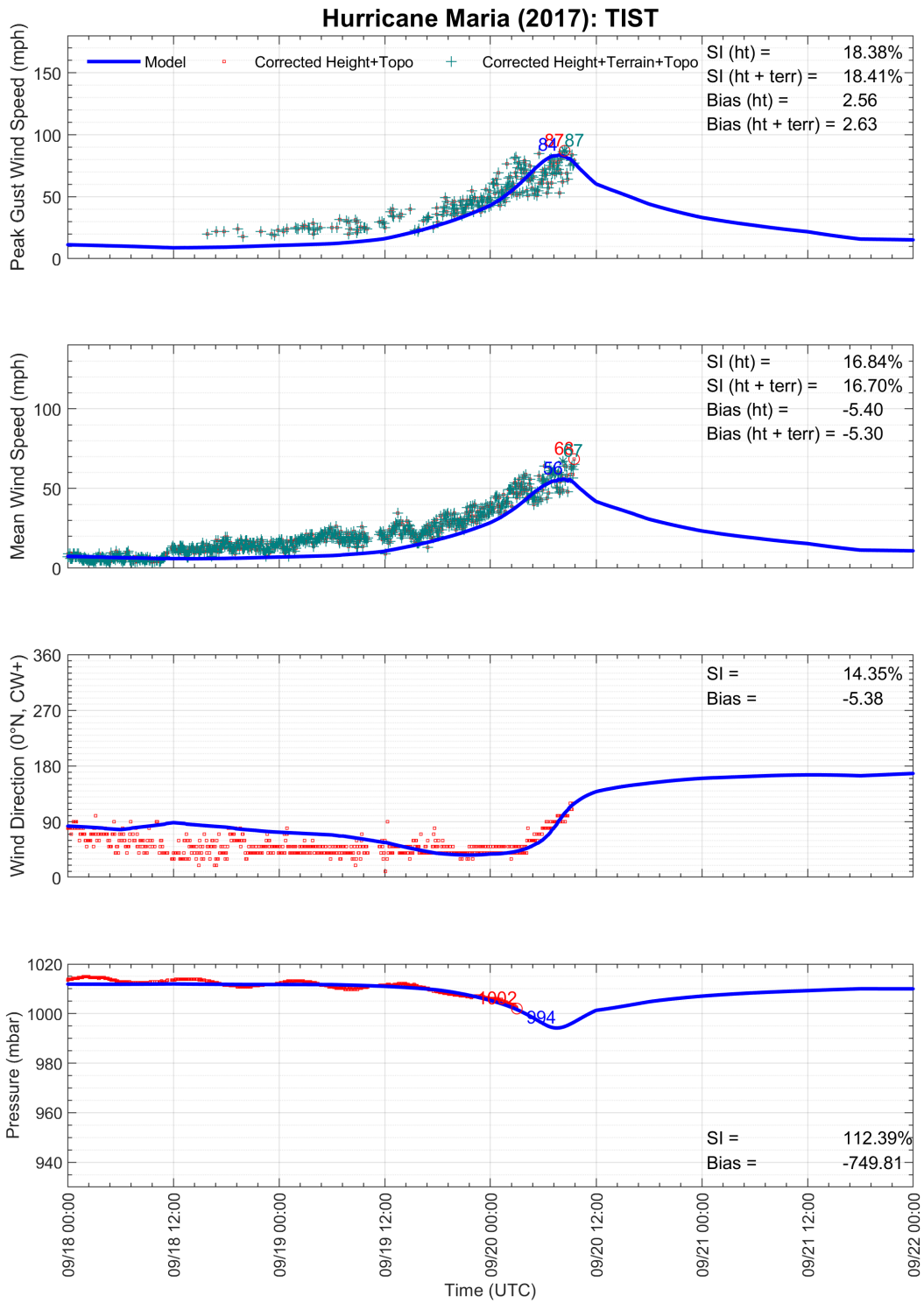


Figure 7-7. Modeled and observed meteorological time series at ASOS station TIST: Cyril E King Airport, St. Thomas, USVI.

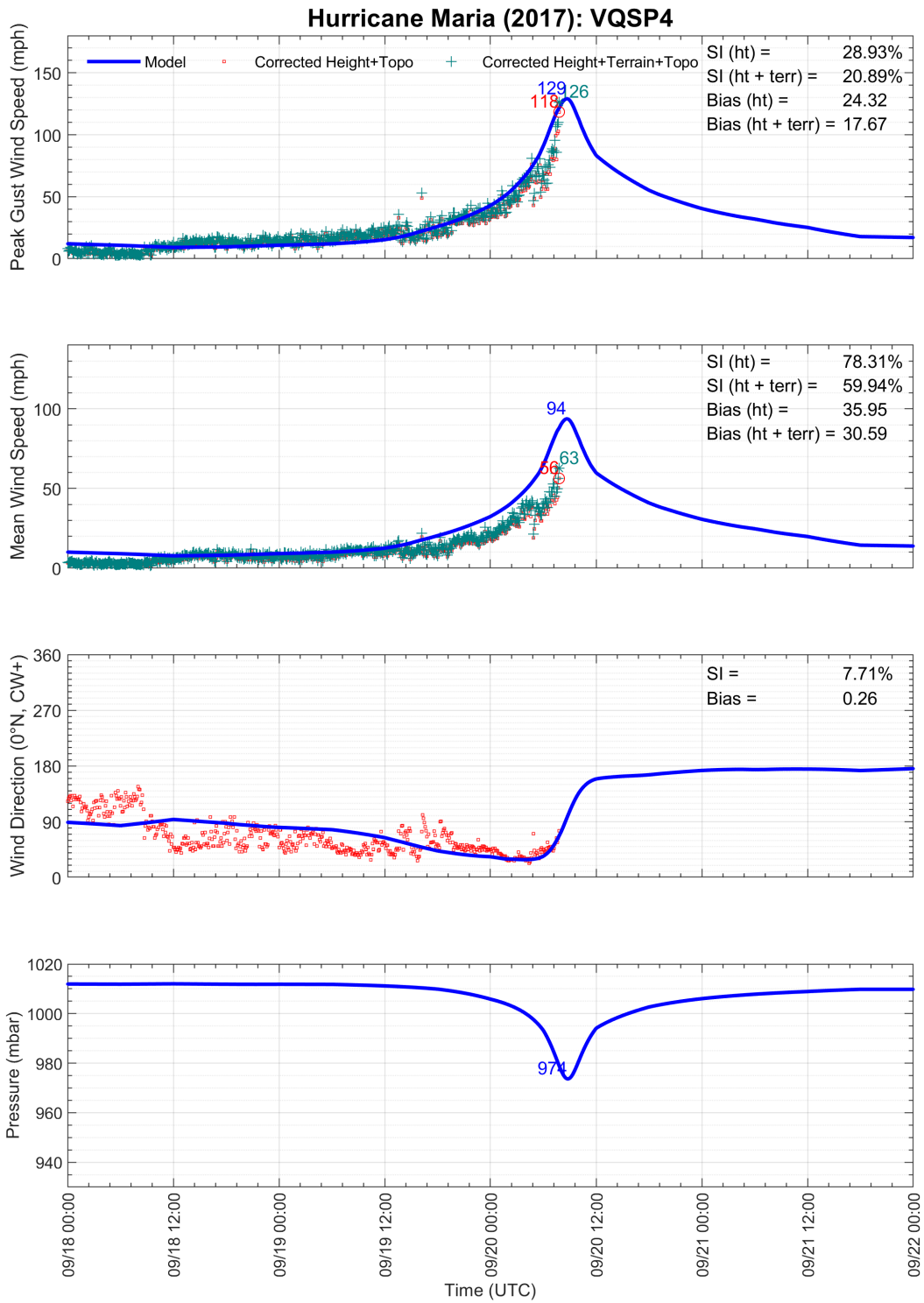


Figure 7-8. Modeled and observed meteorological time series at NDBC station VQSP4: Isabel Segunda, Vieques Island, Puerto Rico.

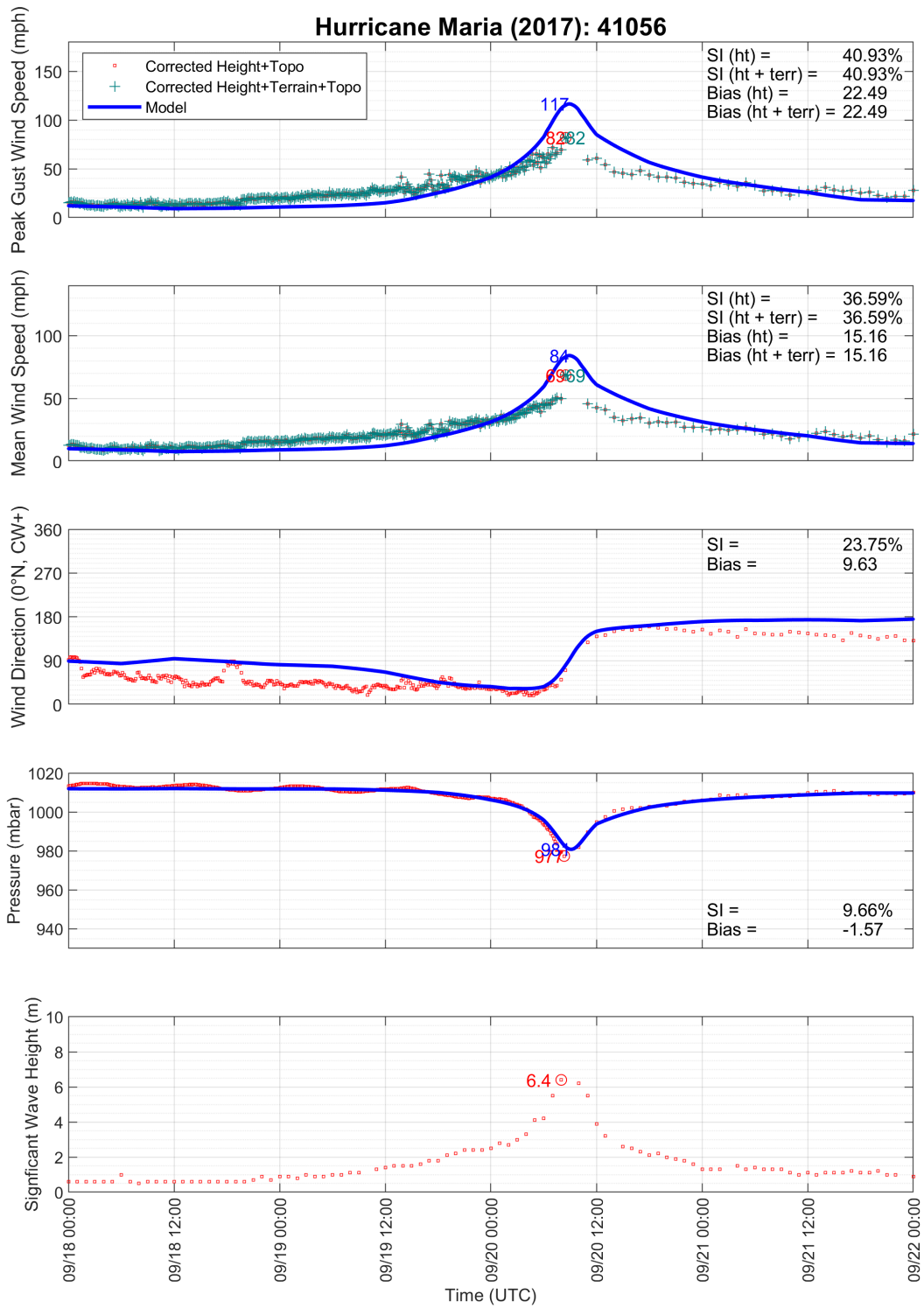


Figure 7-9. Modeled and observed meteorological time series at NDBC station 41056: Vieques Island, Puerto Rico.

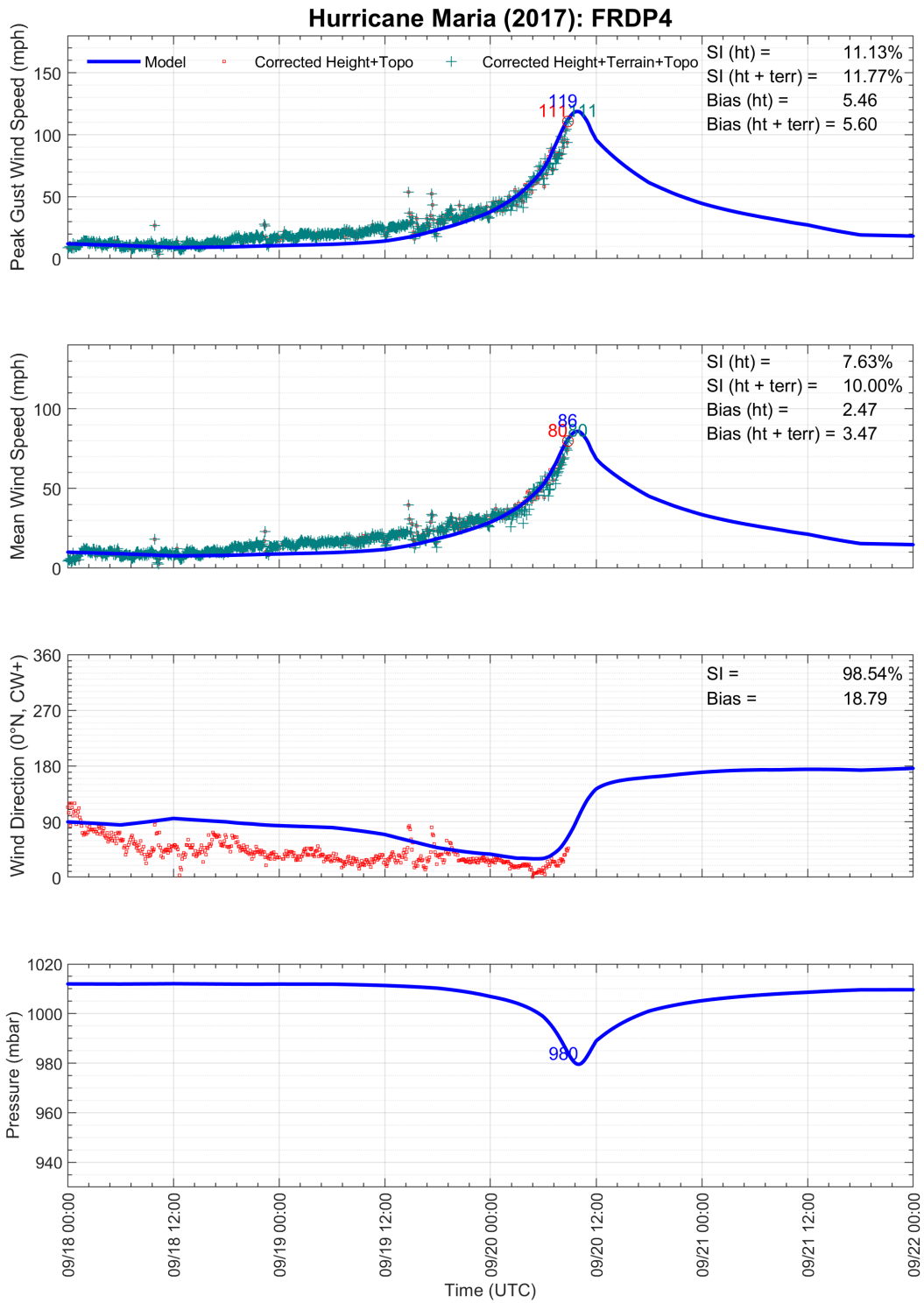


Figure 7-10. Modeled and observed meteorological time series at NDBC station FRDP4: Fajardo, Puerto Rico.

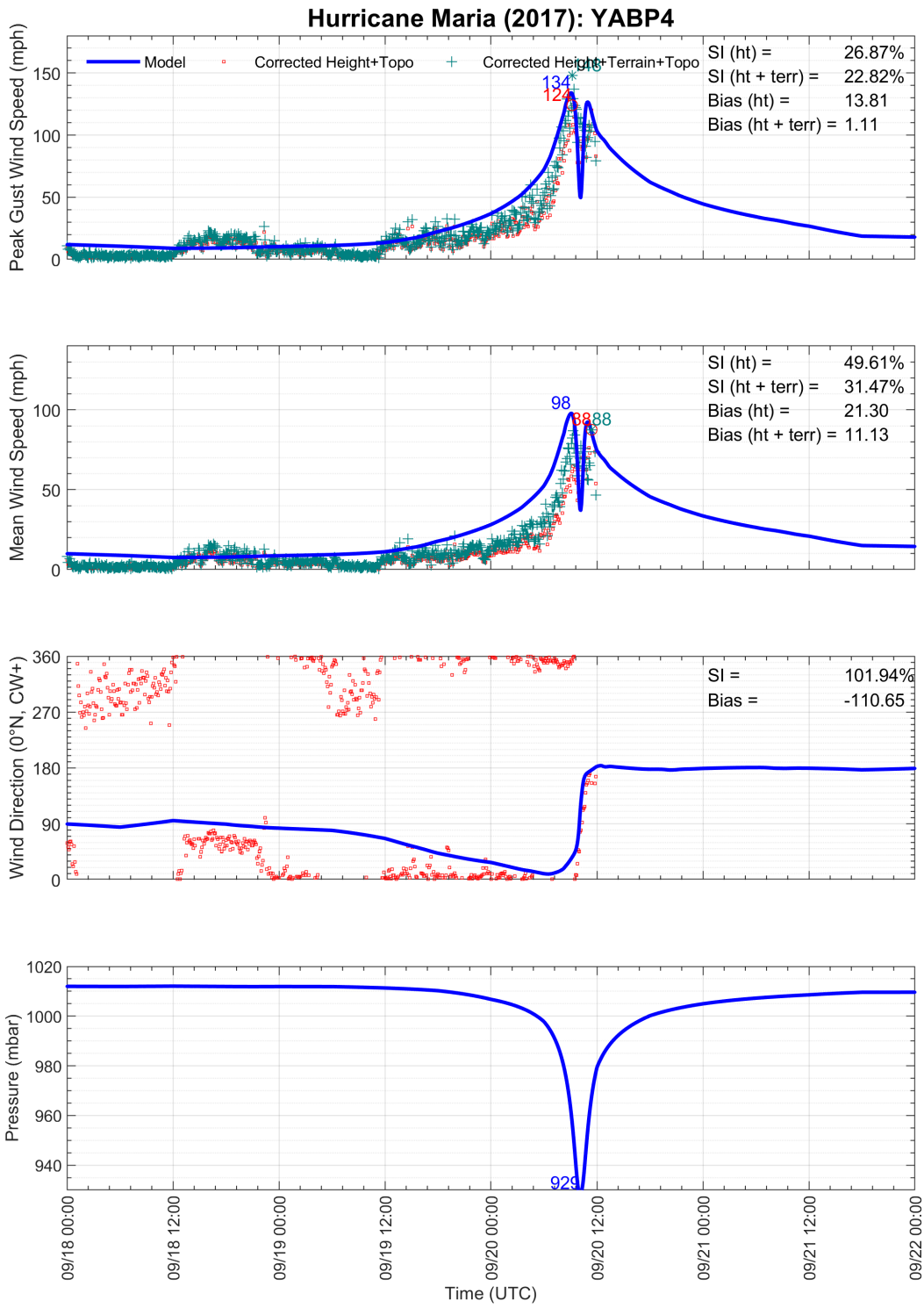


Figure 7-11. Modeled and observed meteorological time series at NDBC station YABP4: Yabucoa Harbor, Puerto Rico.

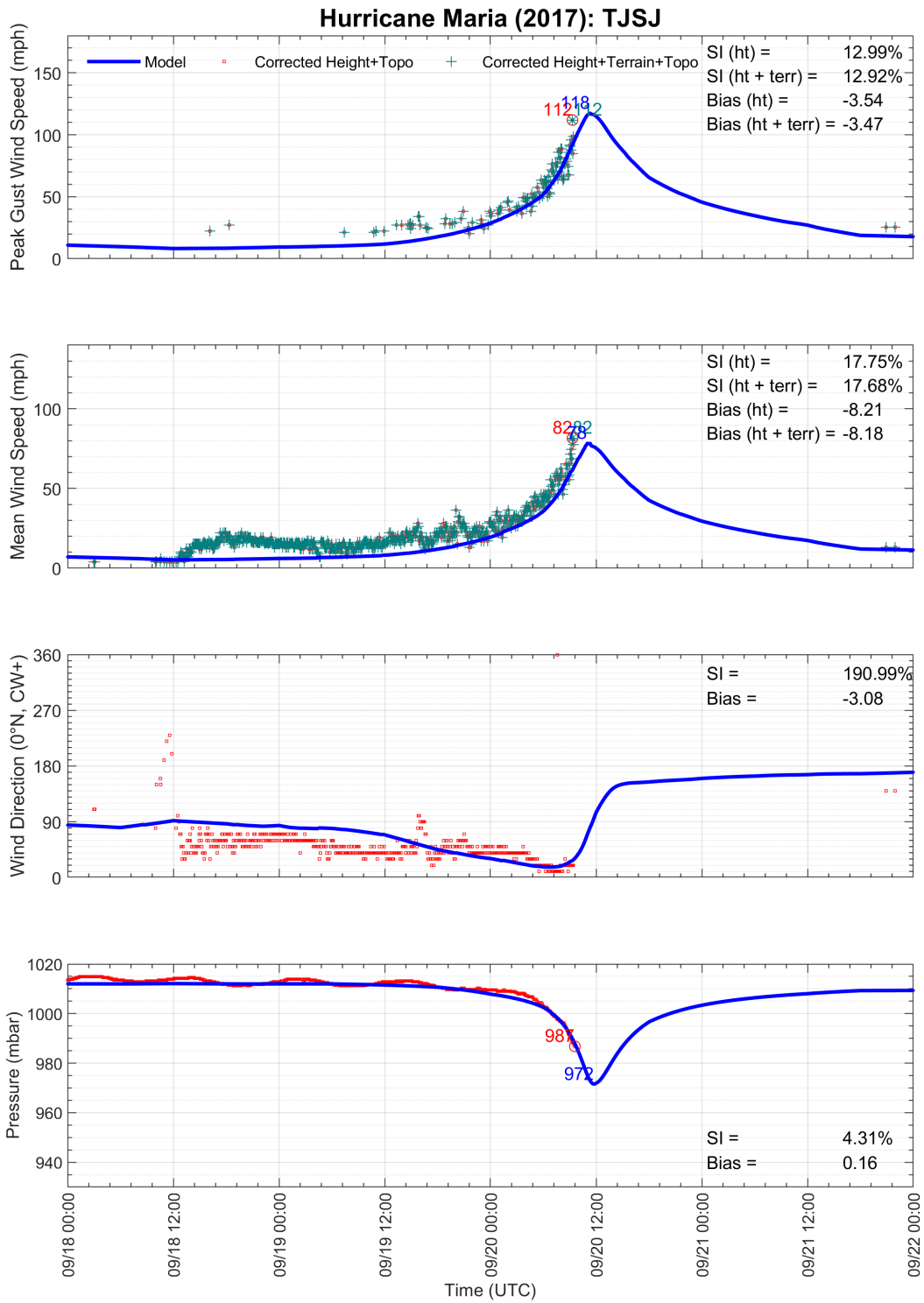


Figure 7-12. Modeled and observed meteorological time series at ASOS station TJSJ: Luis Muñoz Marín International Airport, Puerto Rico.

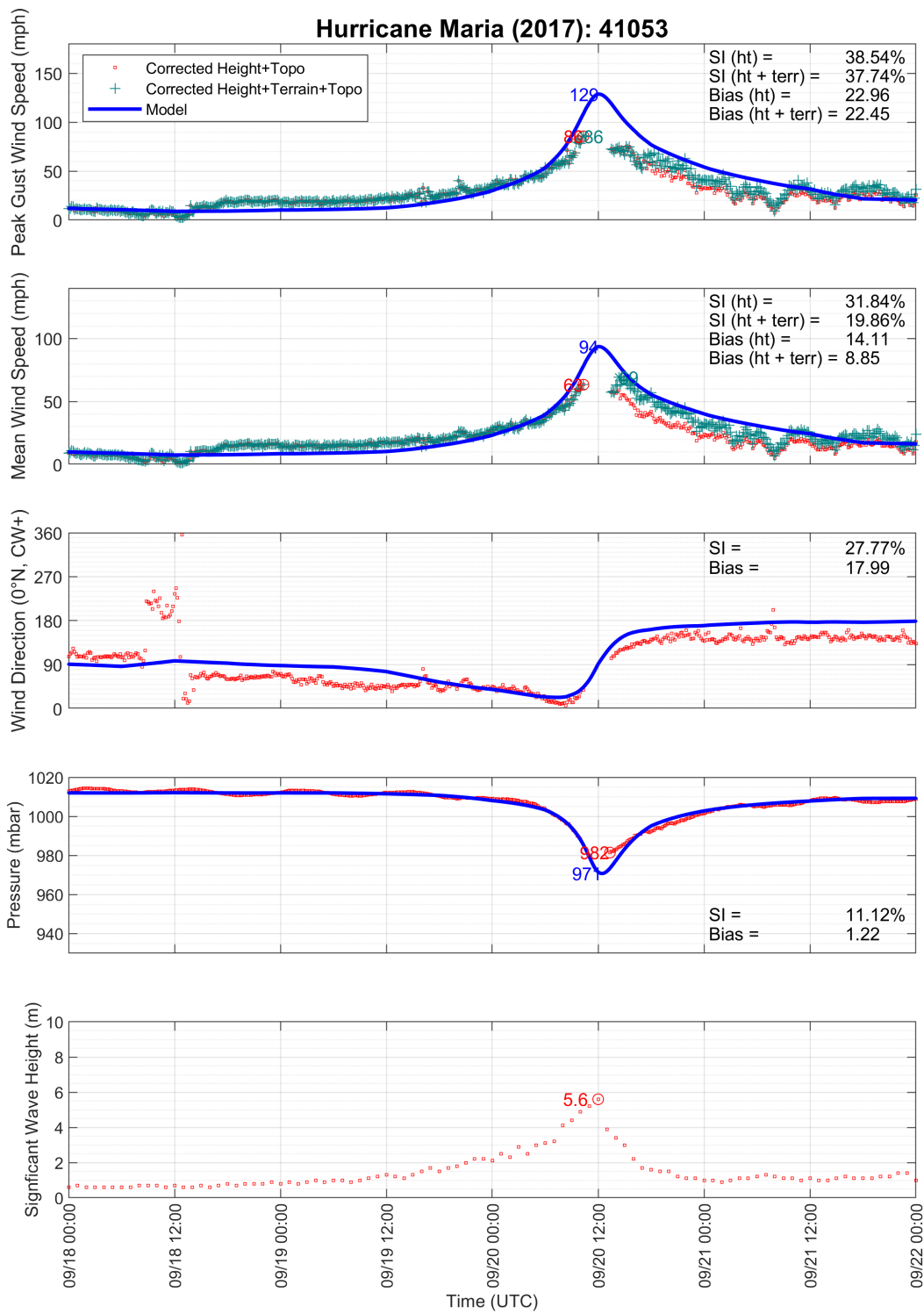


Figure 7-13. Modeled and observed meteorological time series at NDBC station 41053: San Juan, Puerto Rico.

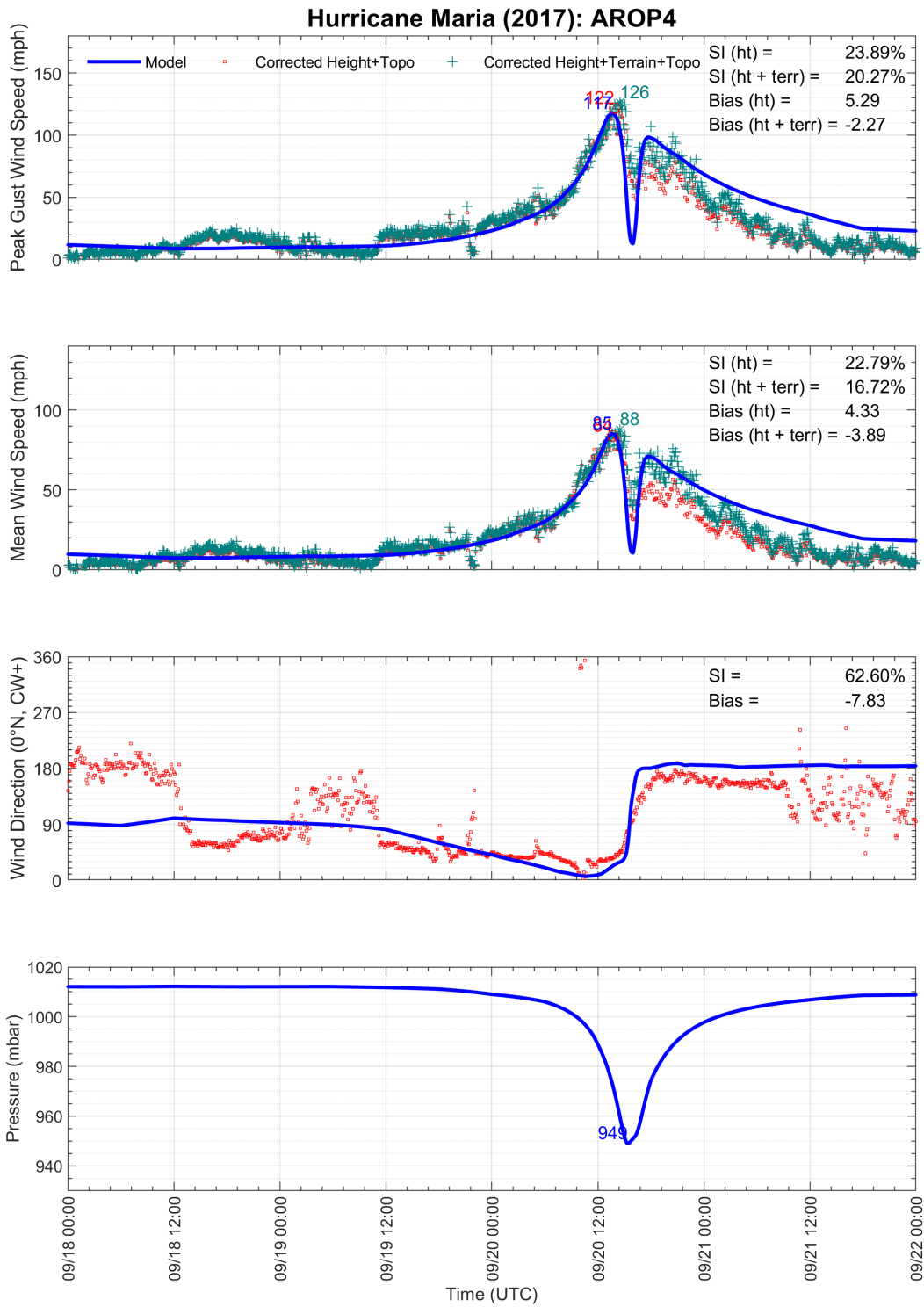


Figure 7-14. Modeled and observed meteorological time series at NDBC station AROP4: Arcibo, Puerto Rico.

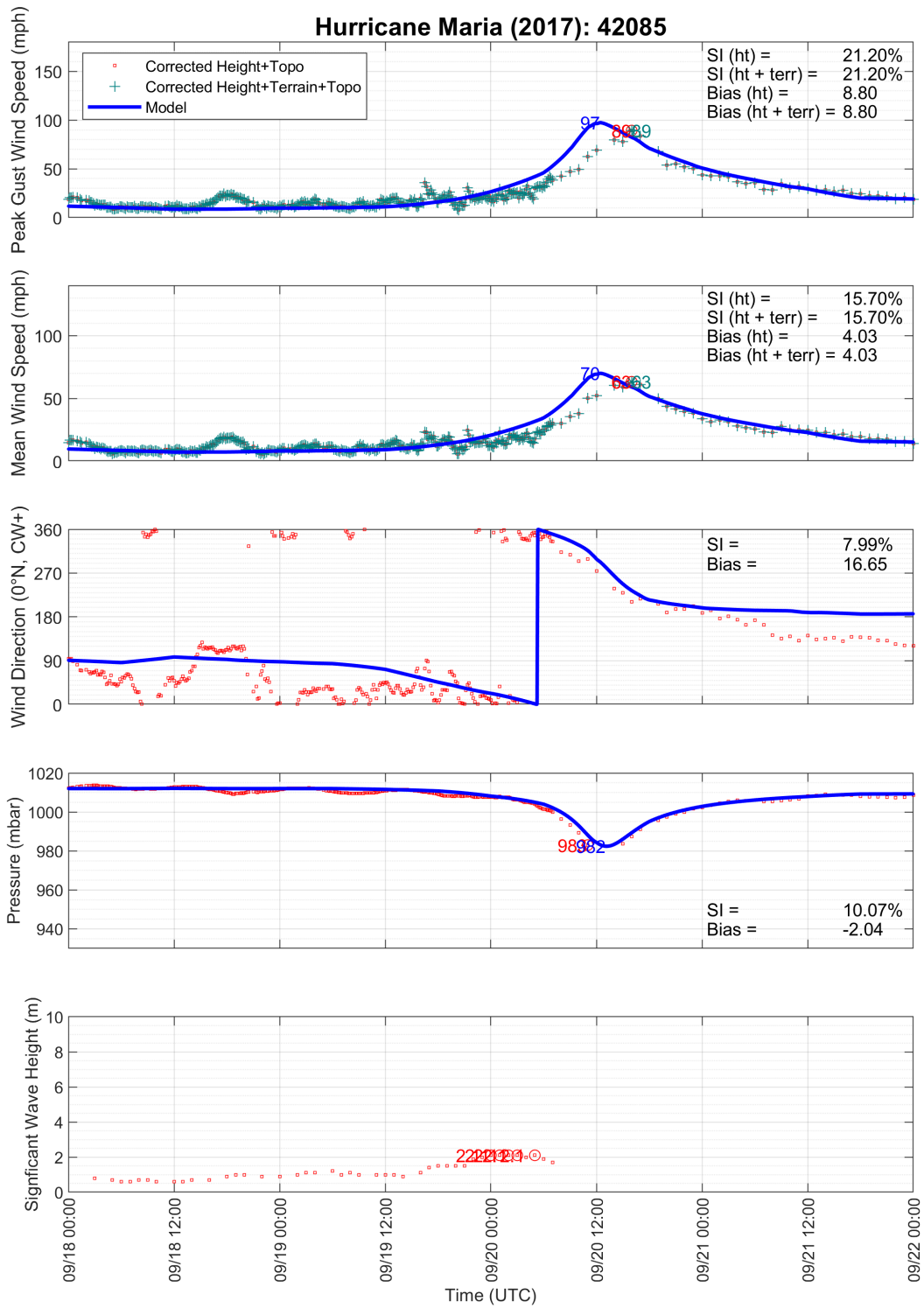


Figure 7-15. Modeled and observed meteorological time series at NDBC station 42085: Southeast of Ponce, Puerto Rico.

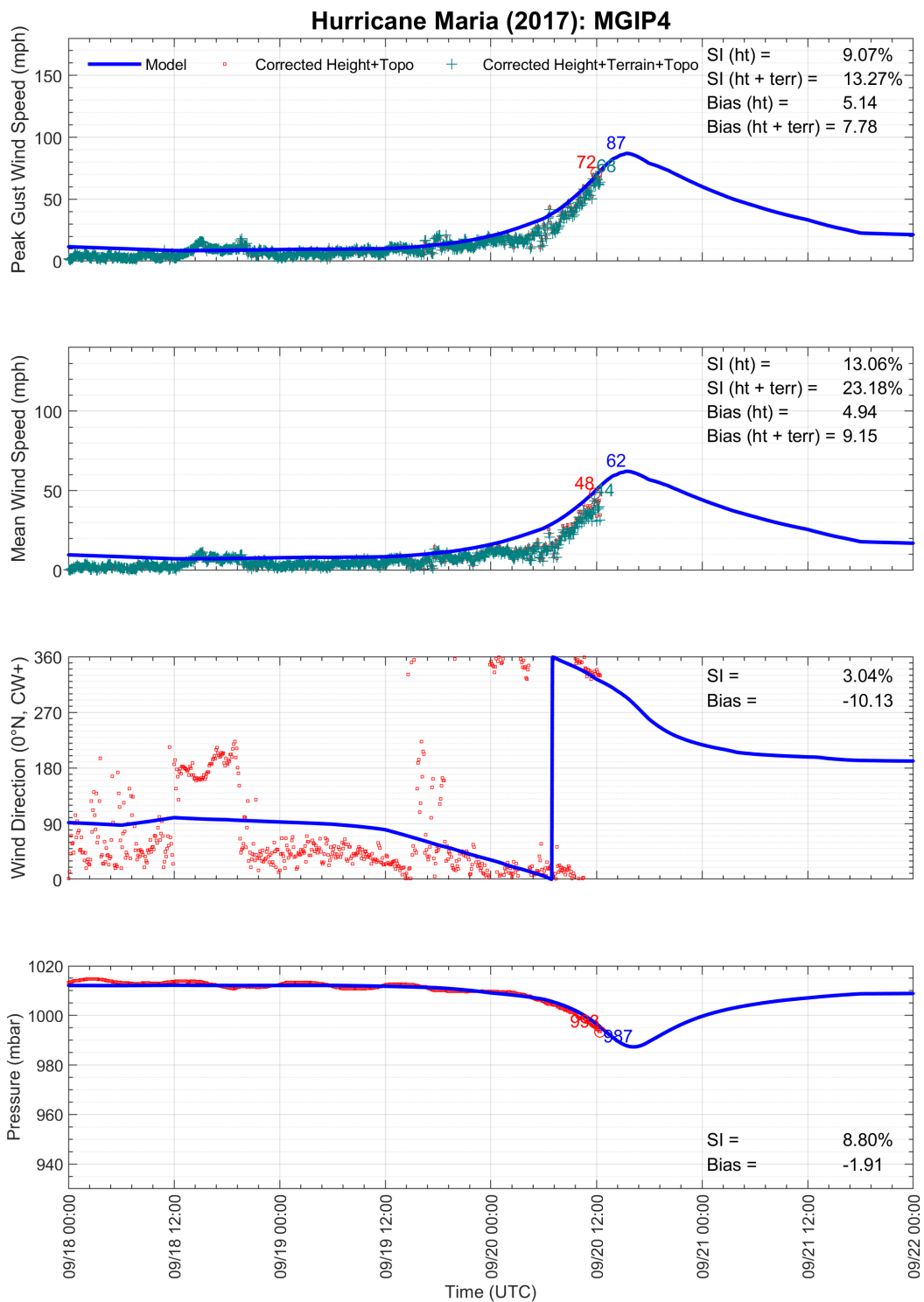


Figure 7-16. Modeled and observed meteorological time series at NDBC station MGIP4: Magueyes Islands, Puerto Rico.

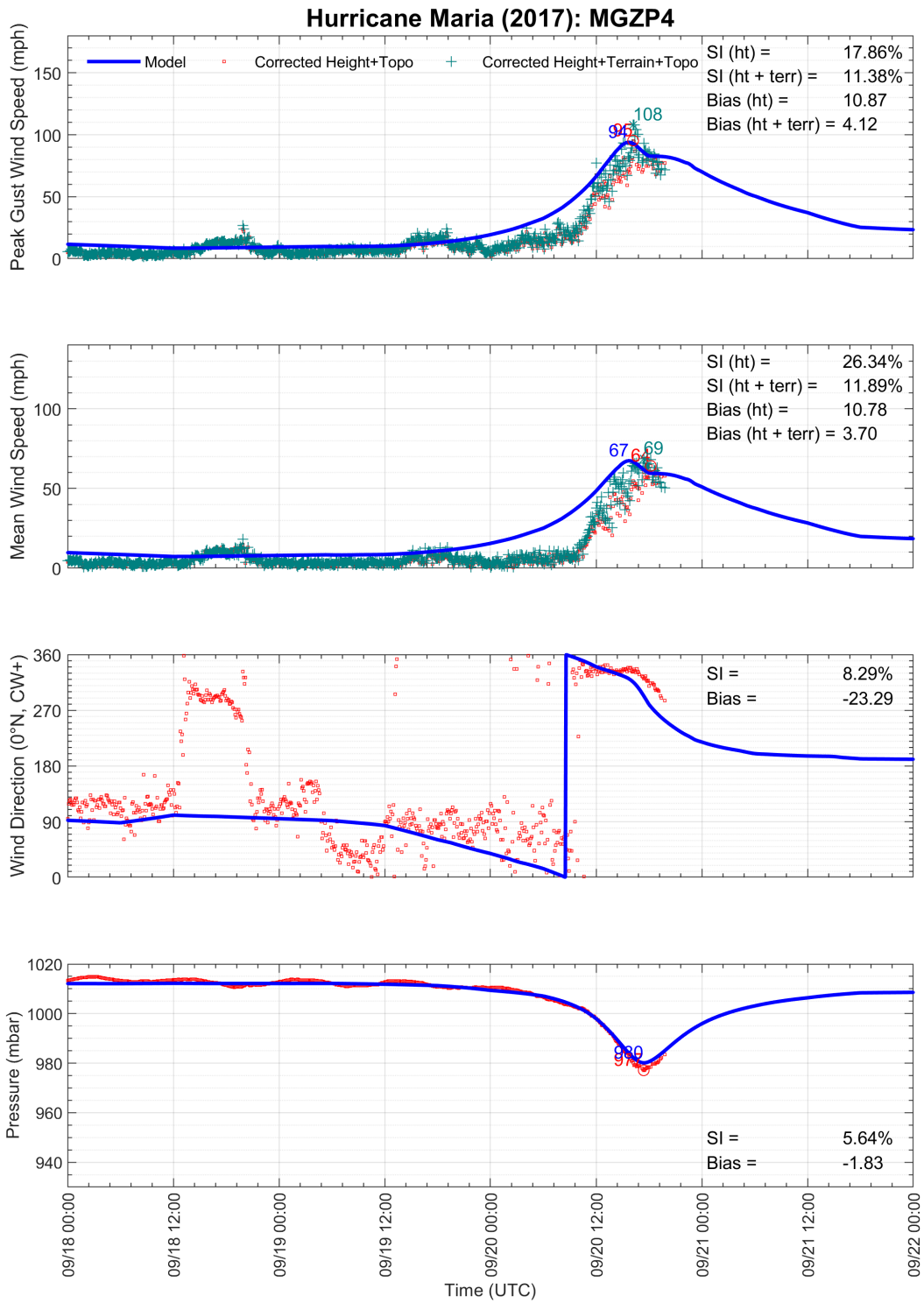


Figure 7-17. Modeled and observed meteorological time series at NDBC station MGZP4: 9759394 - Mayaguez, Puerto Rico.

7.5 ERRORS AND UNCERTAINTY

Figure 7-18 through Figure 7-20 present comparisons of modeled and observed maximum gust wind speeds and minimum central pressures for the stations used in the model validation process. Figure 7-18 and Figure 7-19 both show gust wind speed comparisons, but NDBC station 41056, where large waves may have affected the observed wind speed record, has been removed in Figure 7-19. Stations that failed prior to the arrival of the highest winds were not included in the comparisons. The R^2 values for peak gust wind speed with and without terrain corrections was 0.67 when station 41056 is included, and 0.87 and 0.82, respectively, when station 41056 is removed. The R^2 value for central pressure was 0.83. Because most anemometers failed prior to the occurrence of the maximum peak gust wind speed, only 9 stations were included in the R^2 calculations.

Tabulated error values of peak gust wind speed are provided in Table 6-1 at the end of this section. No error data was provided for stations where the instrumentation failed prior to the occurrence of maximum winds. The largest outliers where the model overpredicted the maximum gust wind speed occurred at NDBC buoy locations, notably NDBC station 41056. As discussed in Section 6.4, this is likely due to the effects of large waves at offshore buoys.

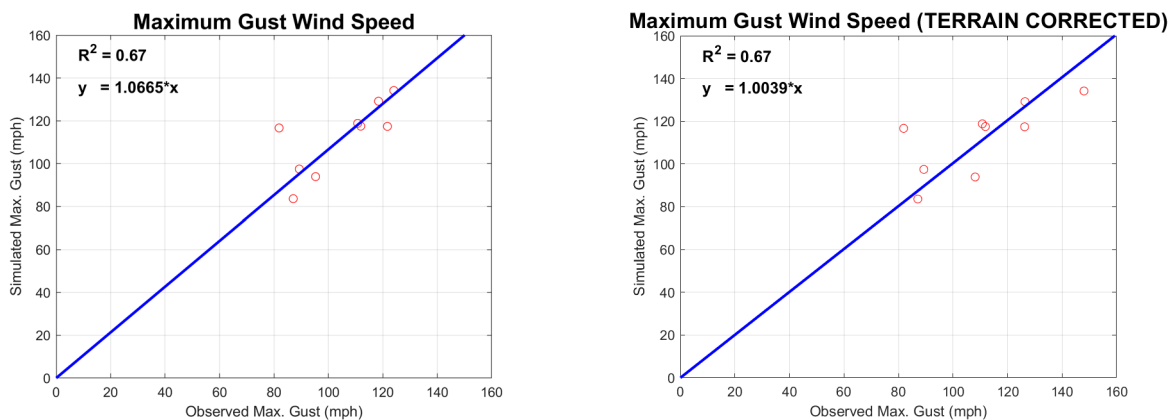


Figure 7-18. Modeled and observed maximum peak gust wind speed corrected only for height (left) and corrected for height and terrain (right).

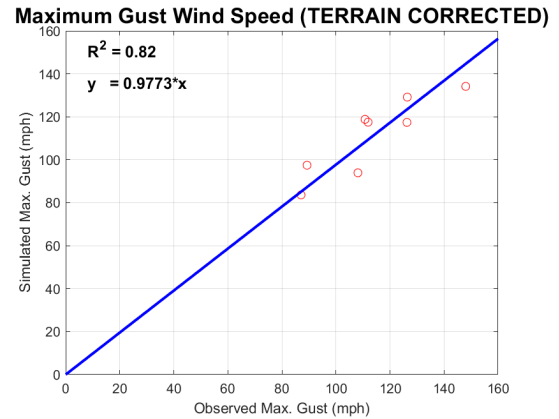
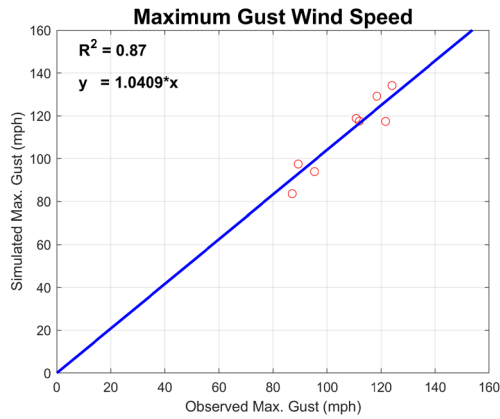


Figure 7-19. Modeled and observed maximum peak gust wind speed corrected only for height (left) and corrected for height and terrain (right) excluding NDBC station 41056.

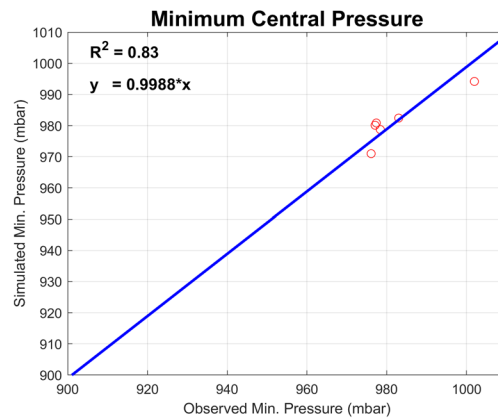


Figure 7-20. Modeled and observed minimum central pressure.

Table 7-1. Errors in modeled peak gust wind speed in Hurricane Maria when observations are corrected for height only and for height and terrain. All wind speed values are presented at 10 m elevation in open terrain.

Station	Modeled Peak Gust Wind Speed (mph)	Observed Peak Gust Wind Speed (mph)		Error (mph)	
		Corrected for Height	Corrected for Height + Terrain	Corrected for Height	Corrected for Height + Terrain
TIST	84	87	87	-3	-3
TISX	---	---	---	---	---
TJNR	---	---	---	---	---
TJSJ*	118	112	112	6	6
AROP4	117	122	126	-5	-9
CHSV3	---	---	---	---	---
ESPP4	---	---	---	---	---
FRDP4*	119	111	111	8	8
IMGP4	---	---	---	---	---
LTBV3	---	---	---	---	---

Station	Modeled Peak Gust Wind Speed (mph)	Observed Peak Gust Wind Speed (mph)		Error (mph)	
		Corrected for Height	Corrected for Height + Terrain	Corrected for Height	Corrected for Height + Terrain
MGIP4	---	---	---	---	---
MGZP4	94	95	108	-1	-14
PTRP4	---	---	---	---	---
SJNP4	---	---	---	---	---
VQSP4*	129	118	126	11	3
YABP4	134	124	146	10	-12
41053	---	---	---	---	---
41056*	117	82	82	35	35
42085*	97	89	89	8	8

* Stations TJSJ, FRDP4, and VQSP4 failed very near the expected time of maximum winds and may not have captured the true wind speed experienced. The resolution of observations at buoy stations 41056 and 42085 decreased prior to the time of maximum winds, thus the true wind speed experienced may not have been captured.

7.6 WIND FIELD MAPS

The final peak gust wind speed maps of Hurricane Maria in Puerto Rico and the Virgin Islands are shown in Figure 7-21 through Figure 7-23 with wind speed bands in increments of 10 mph. Peak gust wind speeds are defined as 3-second average at 10 m above ground over open terrain. Peak gust wind speeds are presented in the *native* topography (i.e., topography speed-up factors have been applied to the wind field). The storm track is shown by the dashed blue line. All stations used in the wind field model validation are also shown: purple triangles indicate an ASOS station, and green triangles indicate a station in the NDBC database located over water or near the coast. The highest winds are shown to have occurred to the right of the storm track over mountainous topography in Puerto Rico.

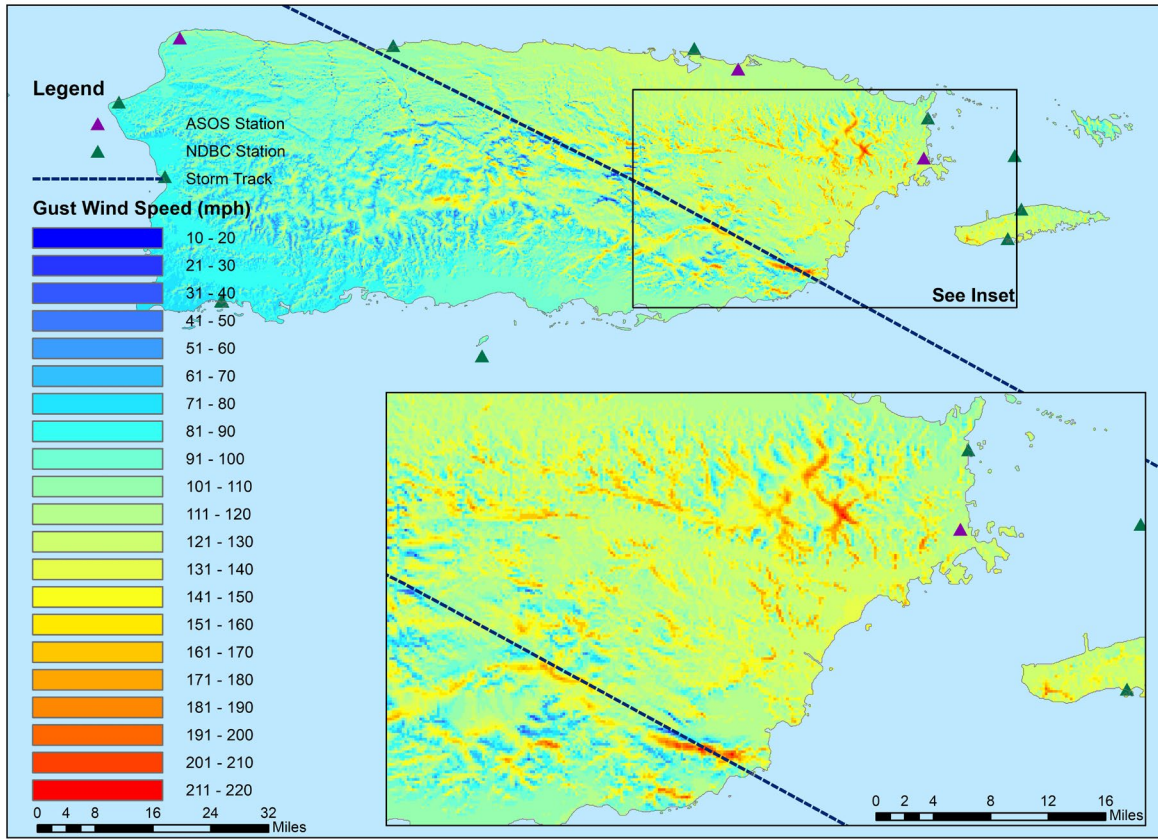


Figure 7-21. Peak gust wind speed map for Hurricane Maria (2017) in Puerto Rico showing estimated 3-second peak gust wind speeds (mph) at 10 m above ground over open terrain. Model output obtained from ARA wind field model fit to surface level observations using NHC best track and central pressures. Modeled gust wind speeds include the effects of topography.

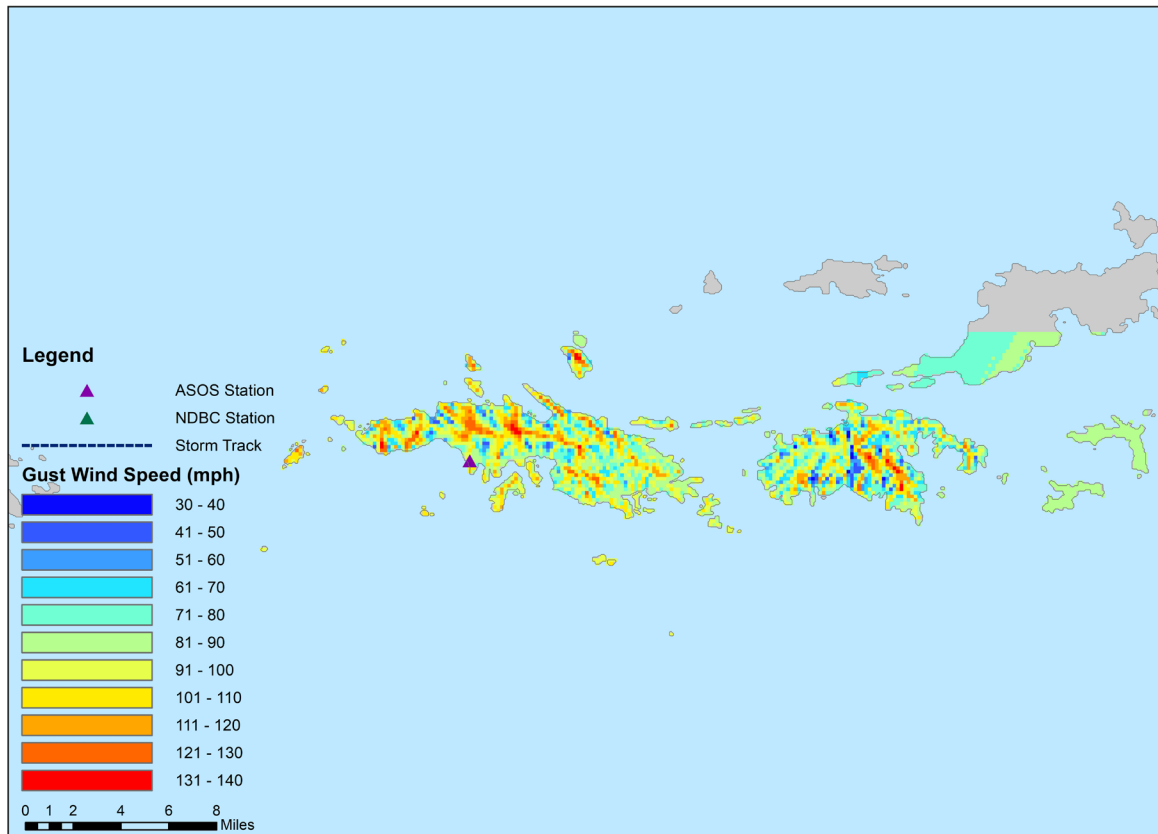


Figure 7-22. Peak gust wind speed map for Hurricane Maria (2017) in St. Thomas and St. John, USVI, showing estimated 3-second peak gust wind speeds (mph) at 10 m above ground over open terrain. Model output obtained from ARA wind field model fit to surface level observations using NHC best track and central pressures. Modeled gust wind speeds include the effects of topography.

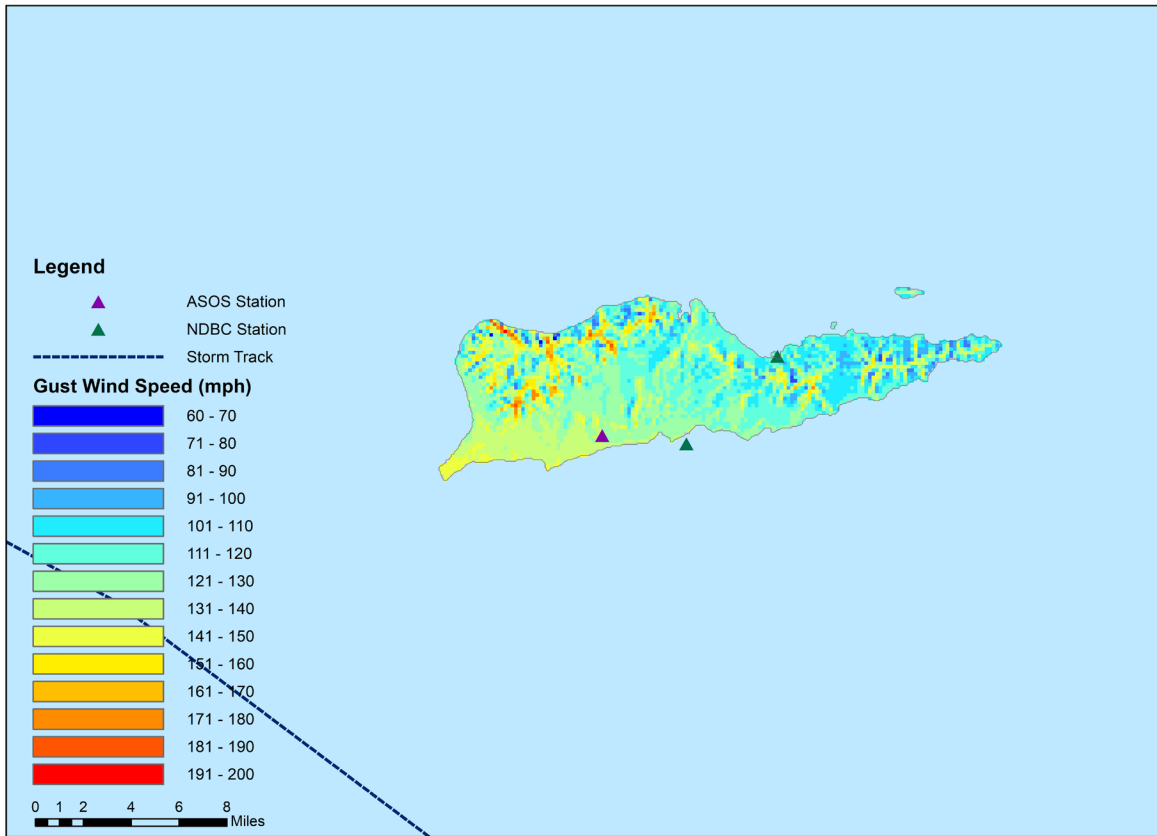


Figure 7-23. Peak gust wind speed map for Hurricane Maria (2017) in St. Croix, USVI, showing estimated 3-second peak gust wind speeds (mph) at 10 m above ground over open terrain. Model output obtained from ARA wind field model fit to surface level observations using NHC best track and central pressures. Modeled gust wind speeds include the effects of topography.

8 HURRICANE NATE

8.1 EVENT BACKGROUND

A brief background for Hurricane Nate (2017) is presented in this section. For a full narrative of the storm, including synoptic history, meteorological statistics, casualty and damage statistics, and forecast and warning critique, see the National Hurricane Center's Tropical Cyclone Report on Hurricane Nate (Beven and Berg, 2018) available at https://www.nhc.noaa.gov/data/tcr/AL162017_Nate.pdf.

Hurricane Nate was a Category 1 hurricane that made two landfalls along the Louisiana / Mississippi coastline during the 2017 hurricane season. According to the NHC, Nate produced a maximum 1-minute sustained wind speed of 80 knots (92 mph), which occurred over water as it moved across the Gulf on October 7 12:00 UTC. (The NHC best track wind speed data is reported to the nearest 5 knots.) With a forward translation speed of 25 knots (28 mph) in the Gulf of Mexico, Hurricane Nate is the fastest-moving tropical cyclone on record in the Gulf.

Hurricane Nate first made landfall in the U.S. on October 8 00:00 UTC near the Pass a Loutre State Wildlife Management Area in Louisiana with maximum sustained winds around 75 knots (86 mph). The second landfall was near Biloxi, Mississippi, on October 8 5:20 UTC with maximum sustained winds of around 65 knots (75 mph). The estimated central pressure at landfall was 981 mbar. Though aircraft reconnaissance observations suggest Nate caused hurricane conditions over land near the southeastern tip of Louisiana, no surface observations of sustained hurricane-force winds were captured. The highest gust wind speed over land observed from the surface was 71 knots (82 mph) at the Ingalls Shipbuilding facility in Pascagoula on October 8 5:05 UTC at 19.5 m elevation. A storm chaser reported a gust wind speed of 66 knots (76 mph) and central pressure of 984.6 mbar near Biloxi Bay on October 8 4:27 UTC.

Nate continued inland on a northeastern trajectory moving across western and northern Alabama and into central Tennessee by October 9 00:00 UTC where it had decayed to a remnant low. As the storm moved into the Ohio Valley, it further decayed into an extratropical system. Nate continued as an extratropical low through New England and across the Canadian Maritime Provinces on October 10 before dissipating on October 11.

Maximum storm surge and tide inundation levels of 6 to 9 feet were estimated near and to the east of Nate's Mississippi landfall. The highest water levels measured by National Ocean Service tide gauges were 6.2 and 6.15 feet above mean higher high water at the Pascagoula NOAA Lab and Dock E at the Port of Pascagoula in Mississippi, respectively. In Alabama, the highest water level measured by a National Ocean Service tide gauge was 5.9 feet above mean higher high water at the Bayou La Batre Bridge. Elsewhere, maximum inundation levels of 4 to 7 feet above ground level occurred in Mobile Bay, 3 to 5 feet on the barrier islands east of the entrance to the bay, 2 to 4 feet along the Florida panhandle, and 3 to 5 feet in southeastern Louisiana.

As it moved inland, hurricane Nate produced 3-7 inches of rain from the central Gulf Coast to the southern Appalachian Mountains, and 1-3 inches of rainfall further inland. The rainfall from Hurricane Nate resulted in localized freshwater flooding.

Nate produced 16 known tornadoes from Mississippi to North Carolina on October 8, all of which were rated EF0 or EF1 in magnitude.

8.2 DATA COLLECTION

8.2.1 Track

A portion of the best track of Hurricane Nate is shown in Figure 8-1 as the storm approached and made landfall along the Gulf of Mexico coastline near Louisiana and Mississippi.

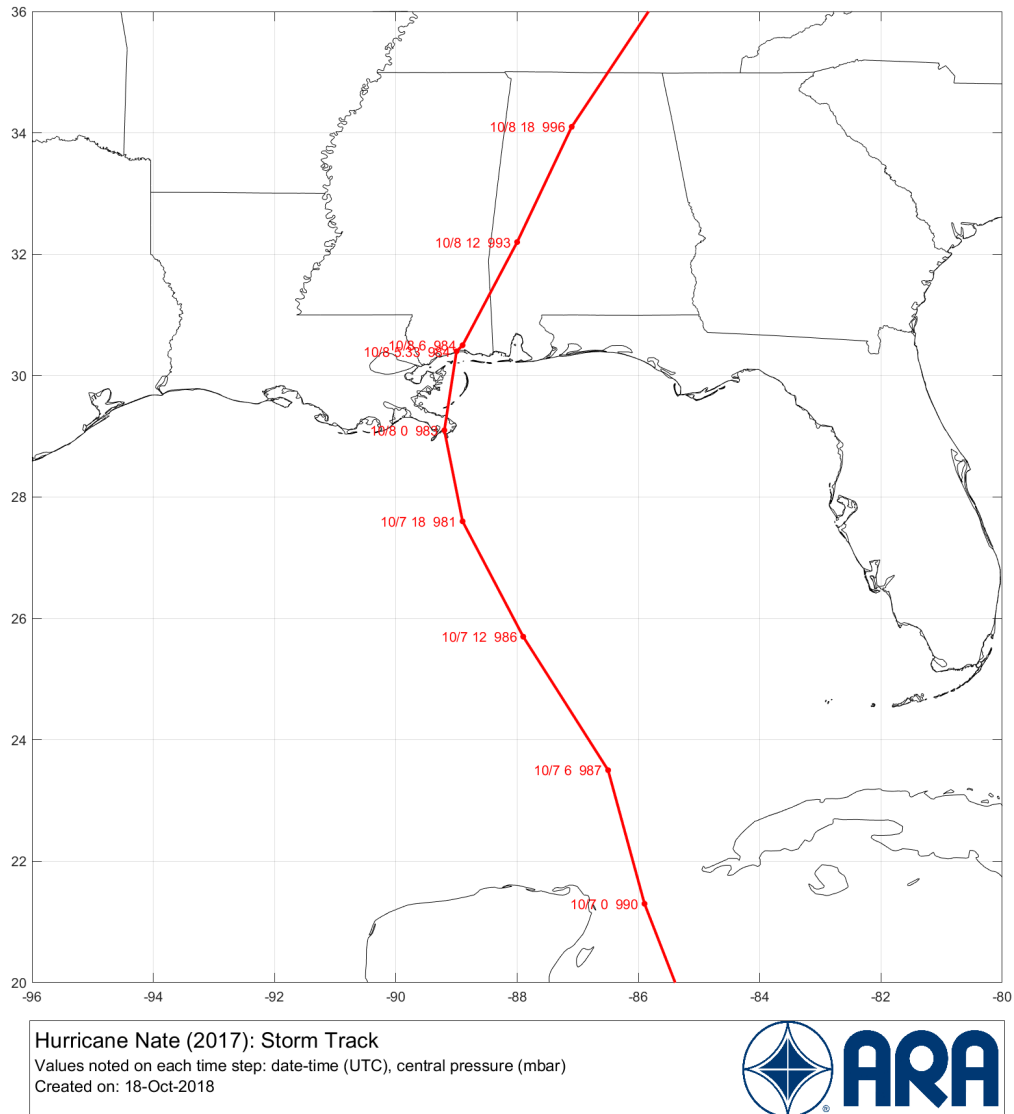


Figure 8-1. Best-track information of Hurricane Nate (2017) collected from the NHC Atlantic Hurricane Database (HURDAT2).

8.2.2 Observations

Stations with observations during the lifespan of Hurricane Nate and within 150 miles of a track point were used in the model validation and are shown in Figure 8-2. A table of station locations and anemometer heights is provided in Appendix E.

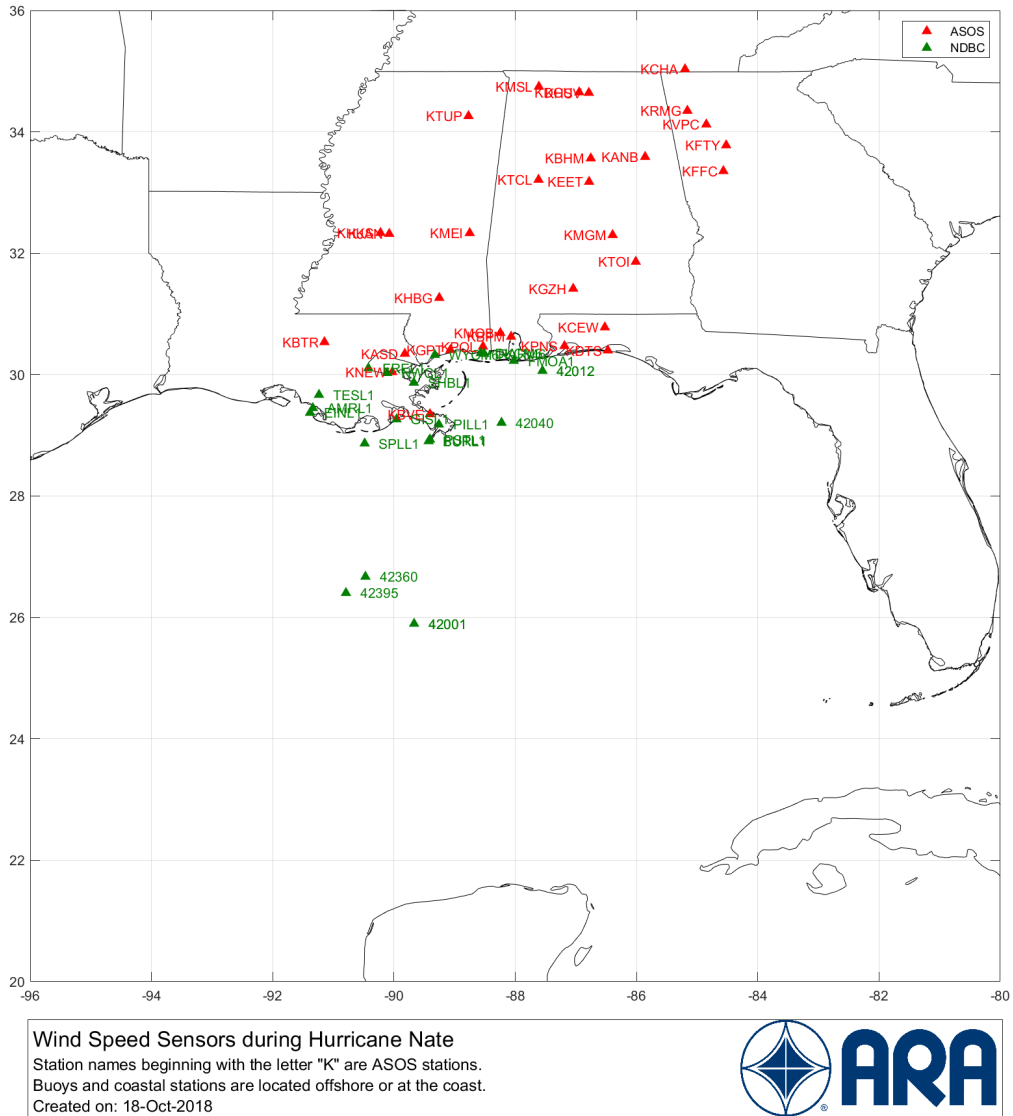


Figure 8-2. ASOS and NDBC stations with surface observations during the lifespan and within 150 miles of Hurricane Nate.

8.3 DISCUSSION OF SELECT STATION TIME HISTORIES

Several stations captured wind speed traces on the left side of the storm track as Hurricane Nate approached and made landfall along the Louisiana and Mississippi coastline. NDBC stations 42001 and SPLL1 captured peak gust wind speeds around 45 mph prior to landfall (see Figure 8-3 and Figure 8-4). Following the first and second landfalls, stations KNEW and KHBG captured sparse measurements of peak gust wind speeds of 38 and 31 mph, respectively (see Figure 8-5 and Figure 8-6). At all four stations, the model predicted peak gust wind speeds between 32 and 34 mph. Values of scatter index and bias were not calculated at any of the four stations as none of the stations had tropical storm strength or higher sustained wind speeds.

Stations BURL1 and KGPT were located near the center of the storm track prior to and just after Hurricane Nate made landfall in Mississippi. The observed peak gust wind speeds were 54 mph, while

modeled values were 54 and 47 mph at BURL1 and KGPT, respectively, as shown in Figure 8-7 and Figure 8-8. Though the peak values agreed well, the modeled time history suggests the eye wall made a direct pass over both stations; however, the data does not show the short decay of winds typically experienced in the eye of the storm. The modeled central pressure time traces showed almost no bias at both stations.

The strongest observed winds—shown in Figure 8-9 through Figure 8-12—were captured on the right side of the storm track near landfall at stations 42040, DKCM6, FMOA1, and KMOB. Modeled time histories of winds at station 42040 had very low values of scatter index between 5-10%, though the peak gust and sustained wind speeds were both underpredicted on the order of 15%. The highest recorded wind speeds during Hurricane Nate were at station DKCM6 with a peak gust of 73 mph and a peak sustained wind speed of 56 mph. The modeled peak sustained wind speed matched the observed value, and the peak gust wind speed was slightly overpredicted by the model at 77 mph. Modeled wind speeds at DKCM6 had scatter indices ranging from 12-15%, with a high bias on the order of 3 mph and 6 mph for sustained and gust wind speeds, respectively. Stations FMOA1 and KMOB, which were further from the storm track, observed slightly lower peak gust wind speeds between 60-66 mph. The modeled time history of winds at both stations agreed well with the observed traces, with a slight low bias as shown in Figure 8-11 and Figure 8-12.

As Hurricane Nate continued to move inland, the observed wind speeds decayed quickly to non-tropical storm force winds as captured by stations KGZH, KTCL, KMSL, and KDCU, and displayed in Figure 8-13 through Figure 8-16. Though peak gust wind speed observations were sparse at inland locations, complete time traces of sustained wind speed can be seen at each of the stations. Scatter indices and biases were not calculated for these stations due to the low wind speeds, but a small upward model bias can be seen in the sustained wind speed traces. Similarly, all four stations show a small downward model bias in central pressure at time steps prior to and following the occurrence of the minimum central pressure.

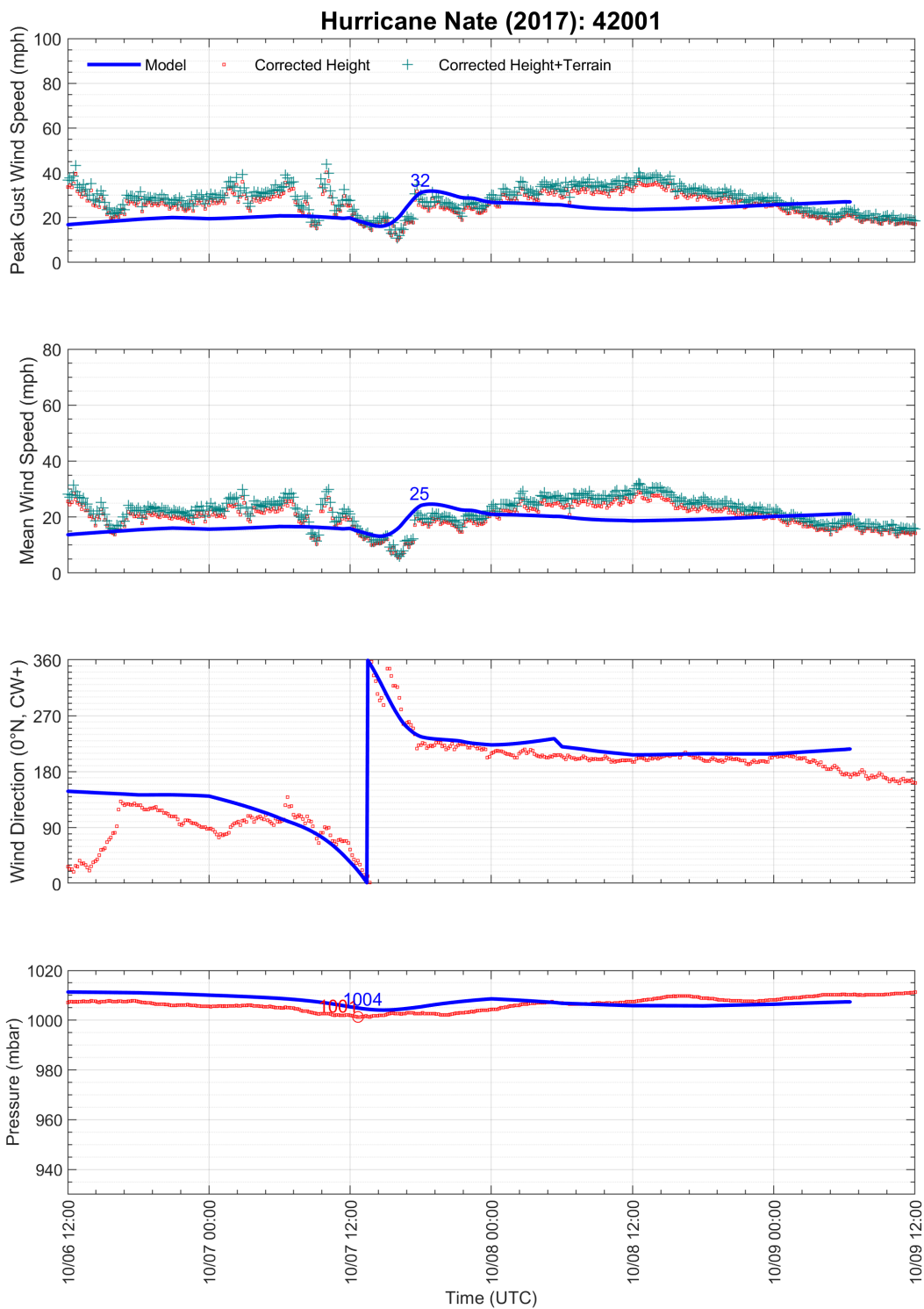


Figure 8-3. Modeled and observed meteorological time series at NDBC station 42001: Mid Gulf located 180NM south of Southwest Pass, Louisiana.

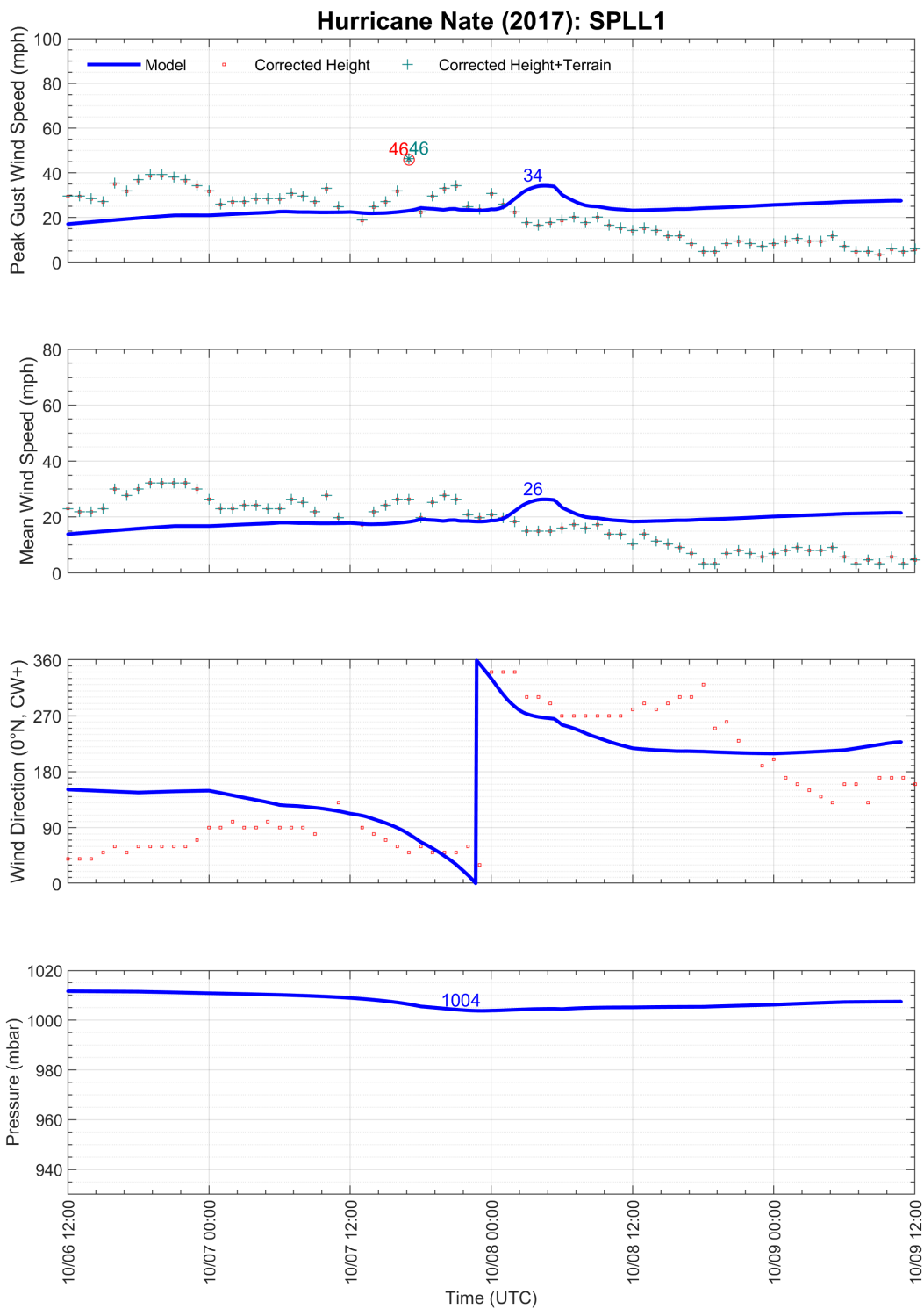


Figure 8-4. Modeled and observed meteorological time series at NDBC station SPLL1: South Timbalier Block 52, Louisiana.

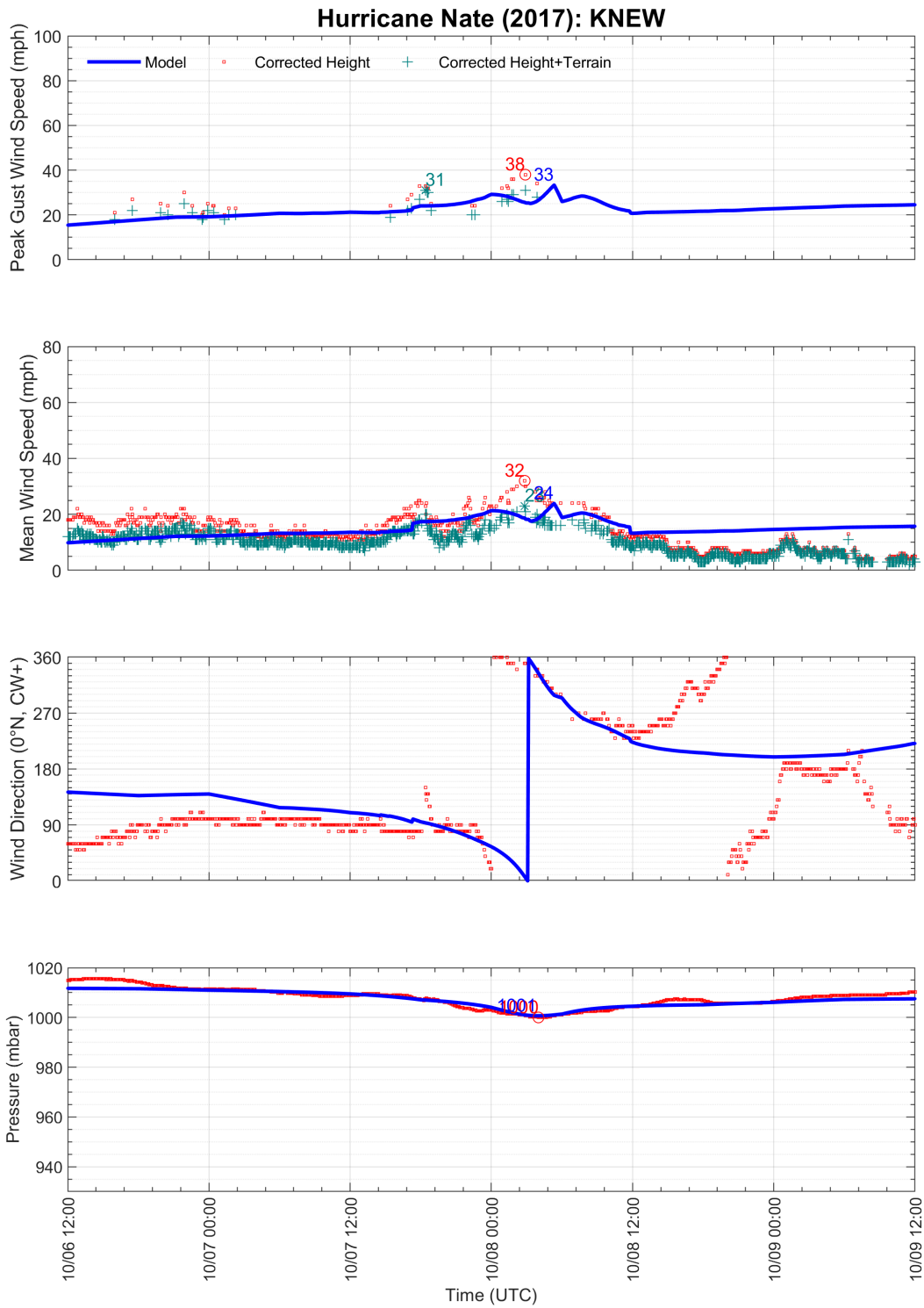


Figure 8-5. Modeled and observed meteorological time series at ASOS station KNEW: New Orleans Lakefront Airport.

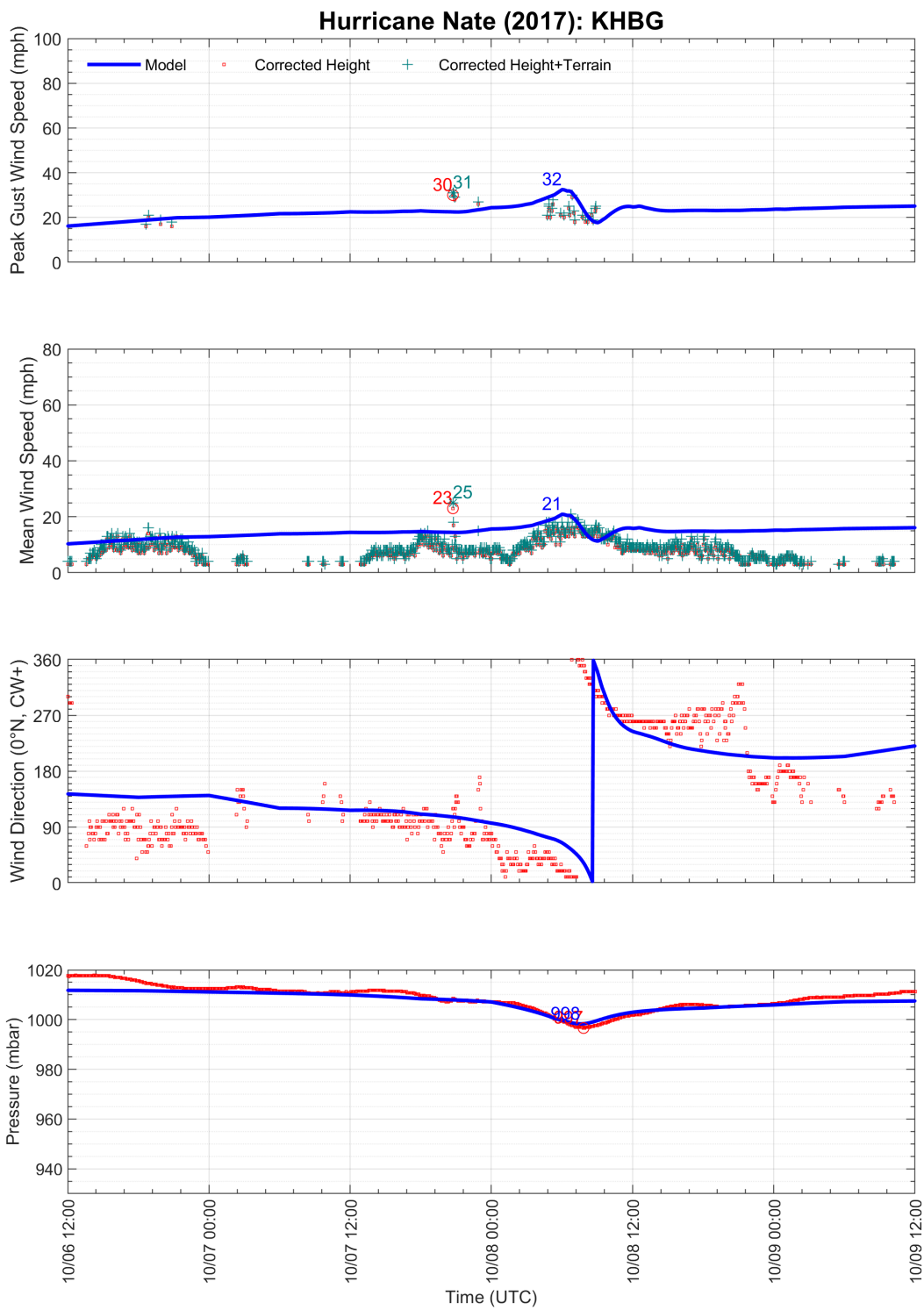


Figure 8-6. Modeled and observed meteorological time series at ASOS station KHBG: Hattiesburg Bobby L. Chain Municipal Airport.

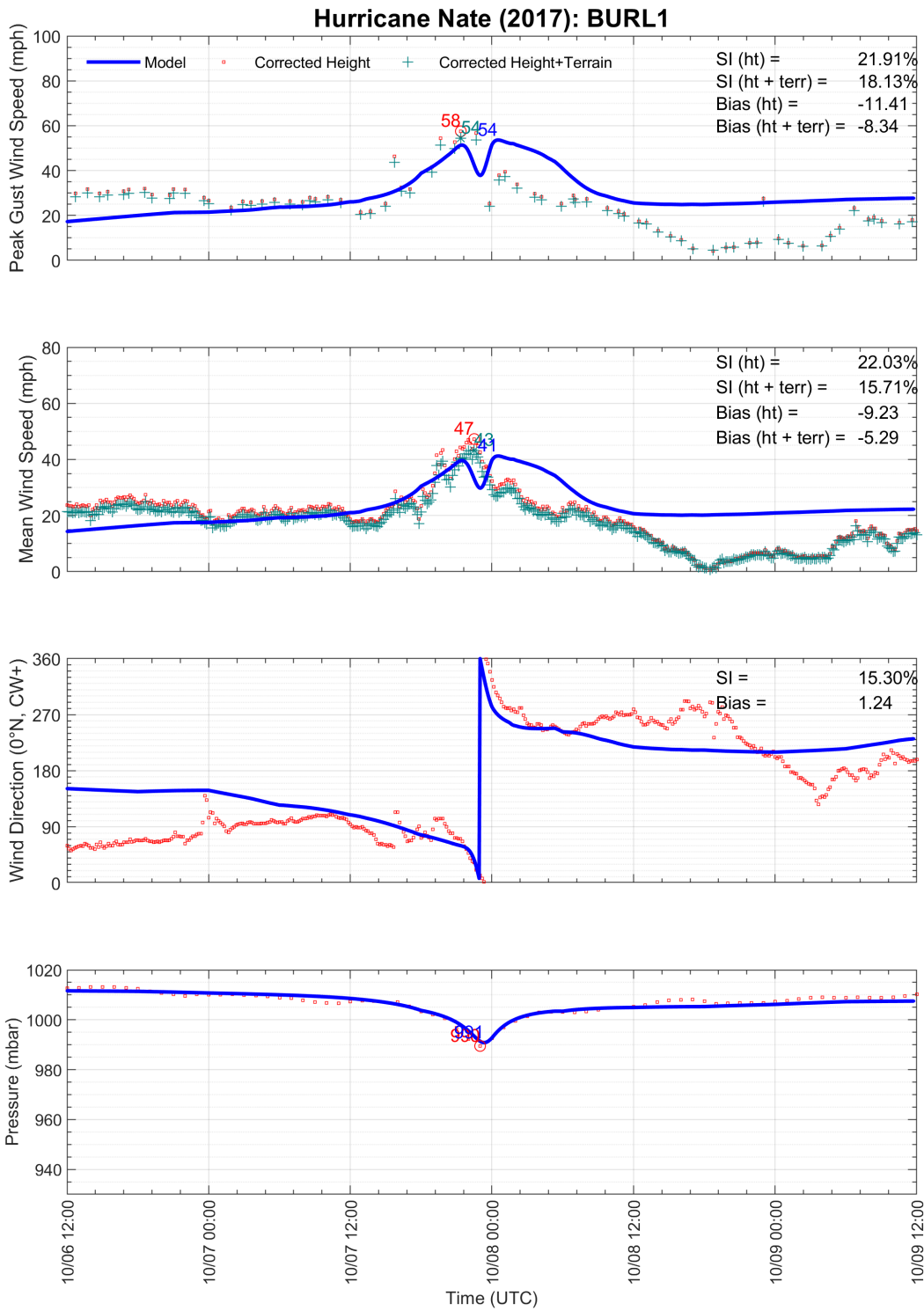


Figure 8-7. Modeled and observed meteorological time series at NDBC station BURL1: Southwest Pass, Louisiana.

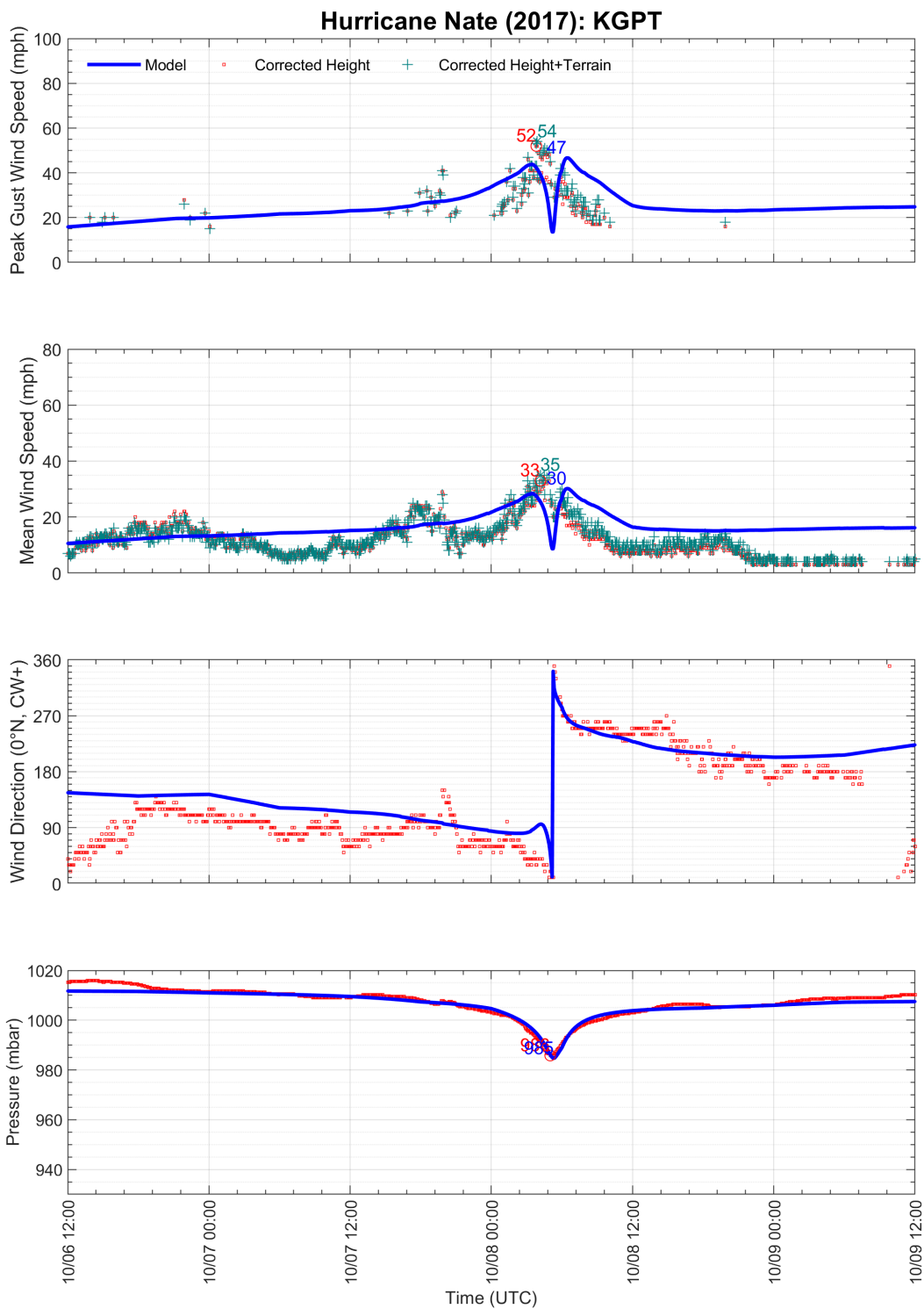


Figure 8-8. Modeled and observed meteorological time series at ASOS station KGPT: Gulfport-Biloxi International Airport.

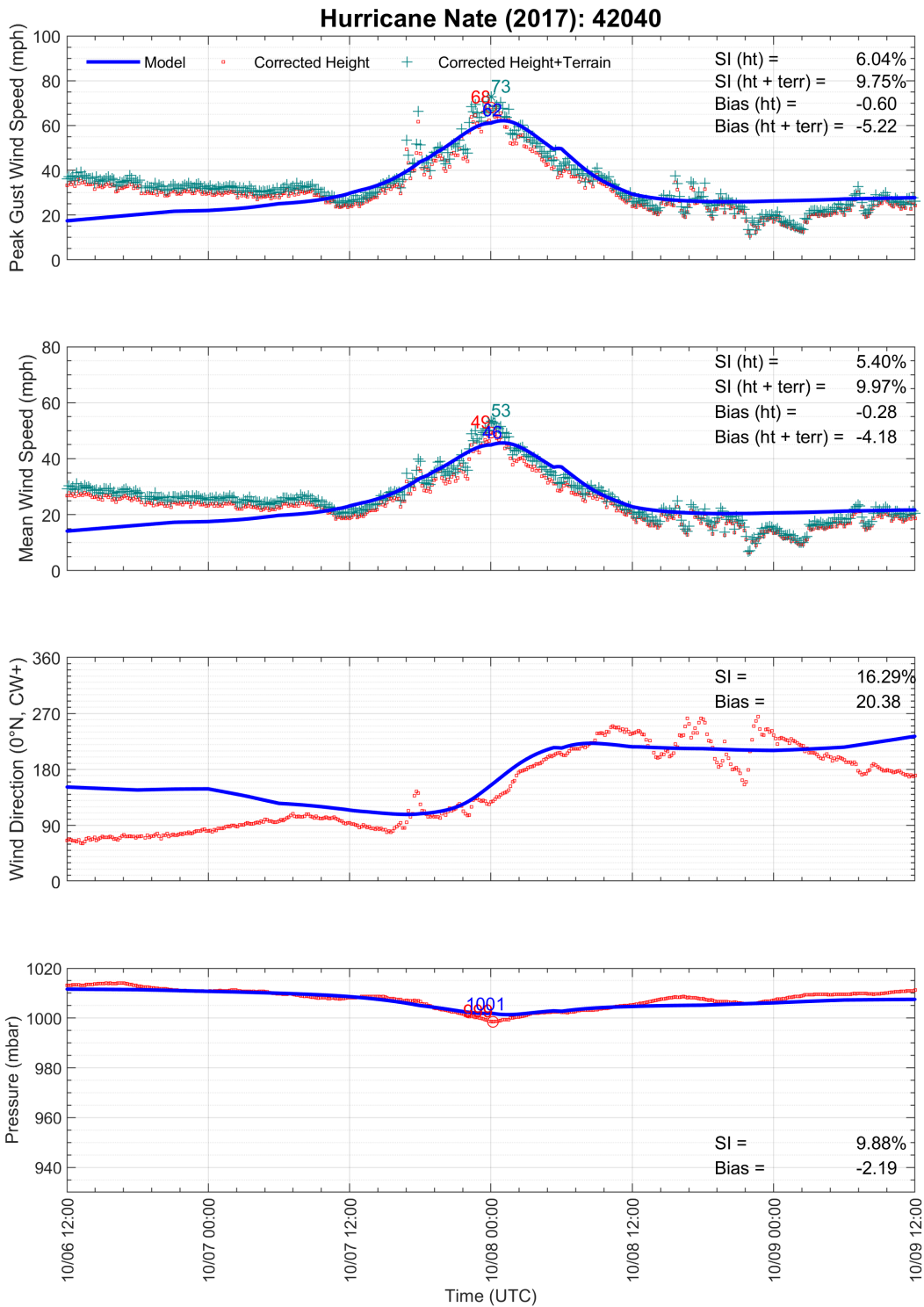


Figure 8-9. Modeled and observed meteorological time series at NDBC station 42040: Luke Offshore Test Platform 63NM south of Dauphin Island, Alabama.

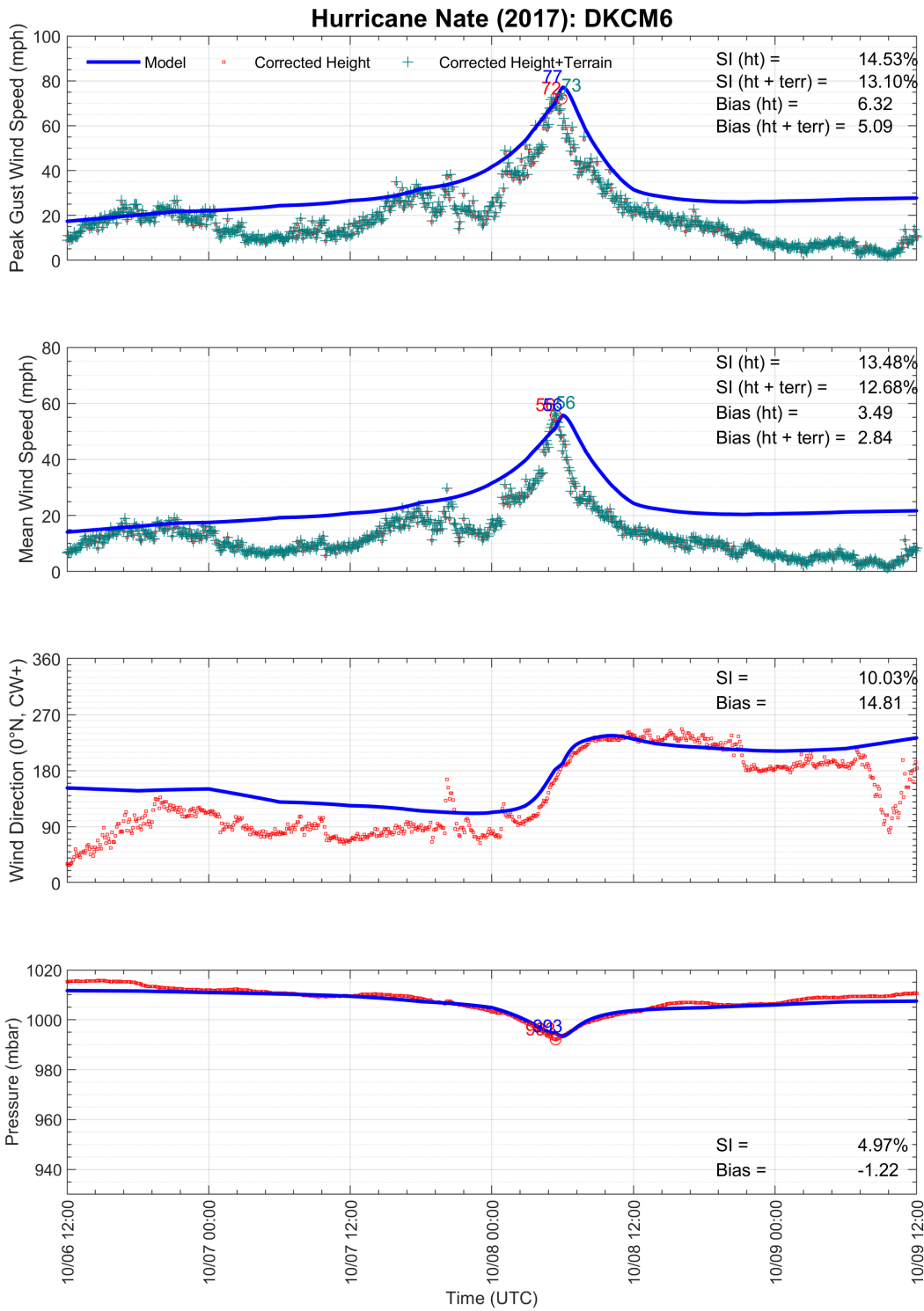


Figure 8-10. Modeled and observed meteorological time series at NDBC station DKCM6: Dock C, Port of Pascagoula, Mississippi.

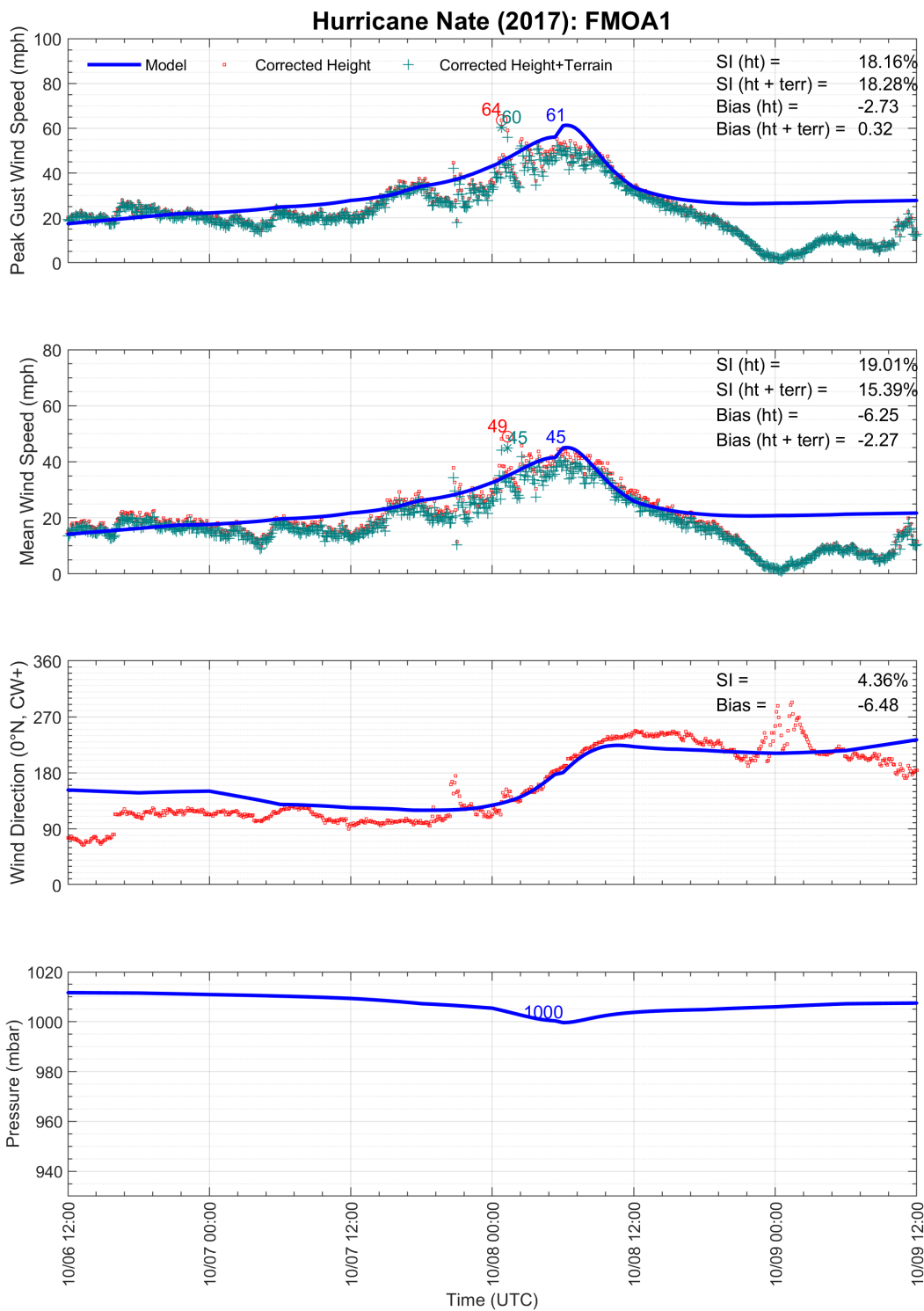


Figure 8-11. Modeled and observed meteorological time series at NDBC station FMOA1: Fort Morgan, Alabama.

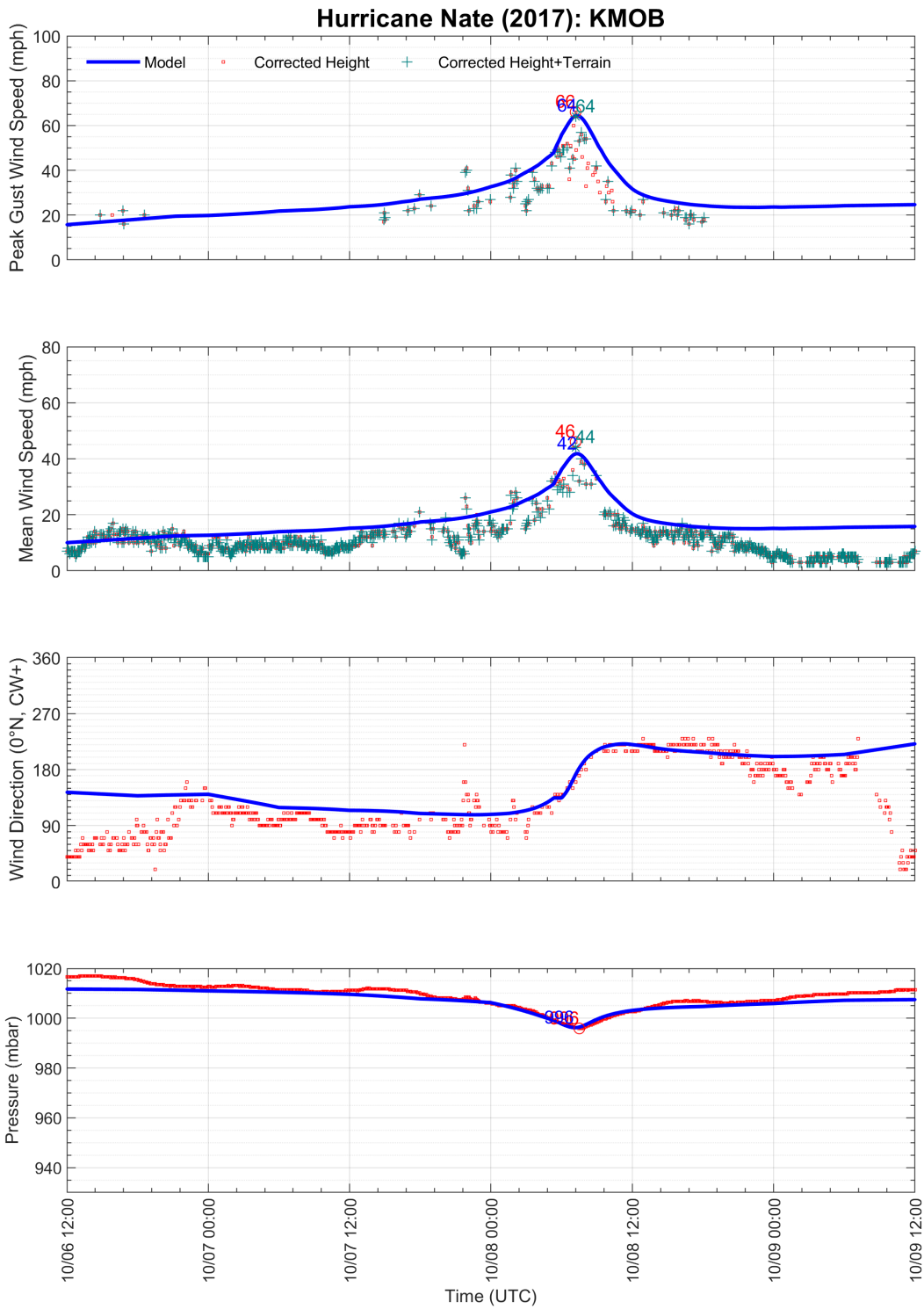


Figure 8-12. Modeled and observed meteorological time series at ASOS station KMOB: Mobile Regional Airport.

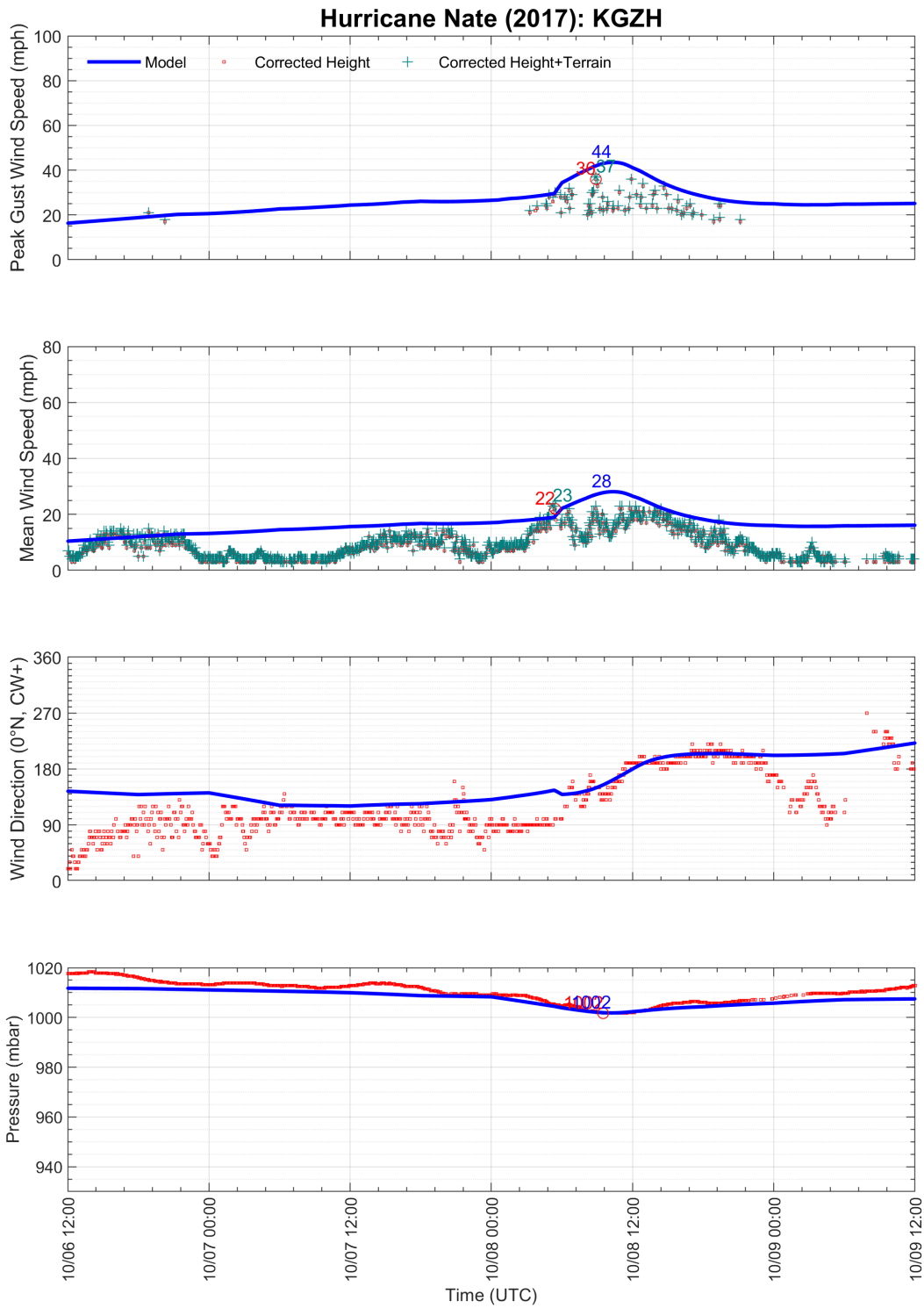


Figure 8-13. Modeled and observed meteorological time series at ASOS station KGZH: Middleton Field.

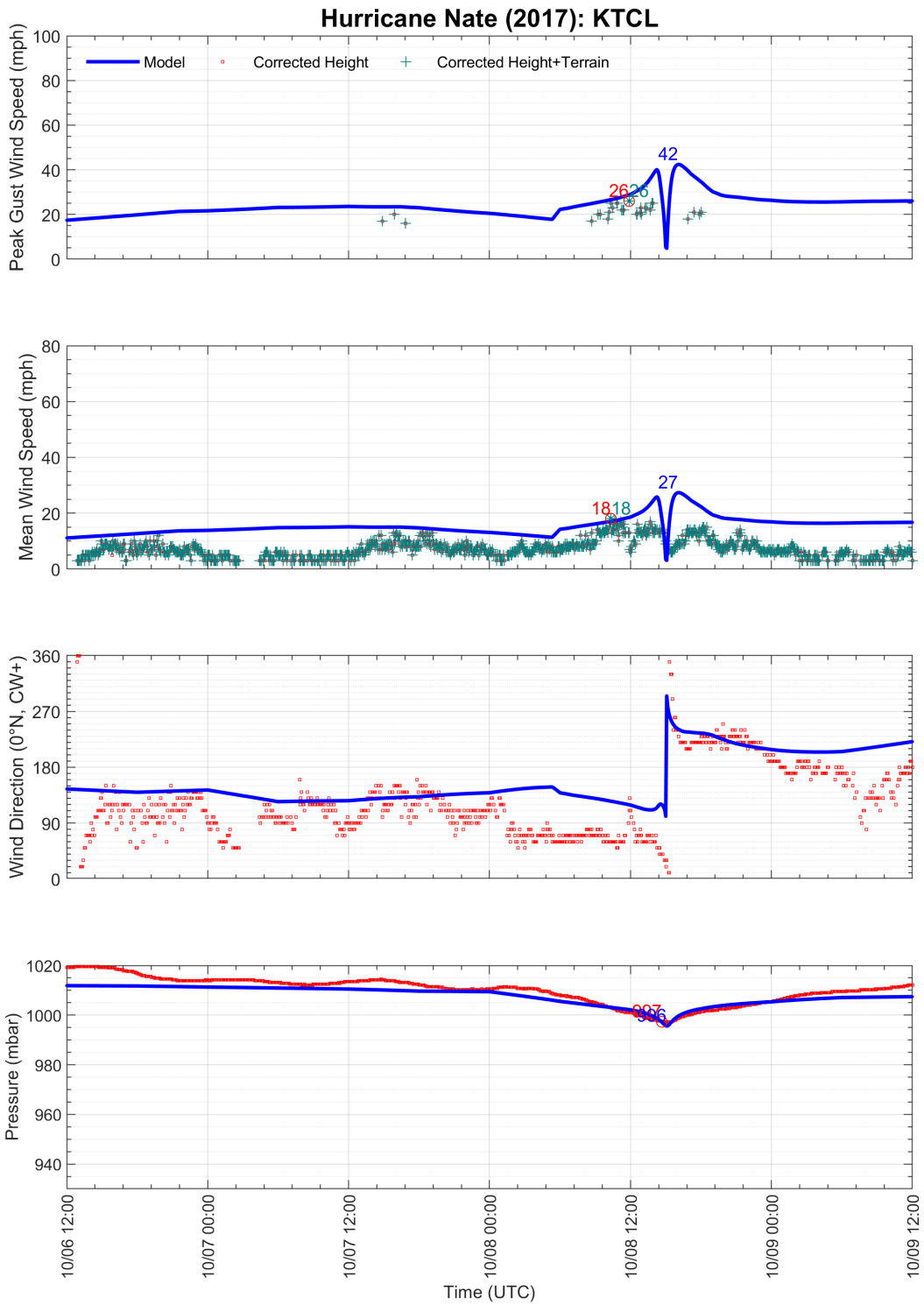


Figure 8-14. Modeled and observed meteorological time series at ASOS station KTCL: Tuscaloosa Regional Airport.

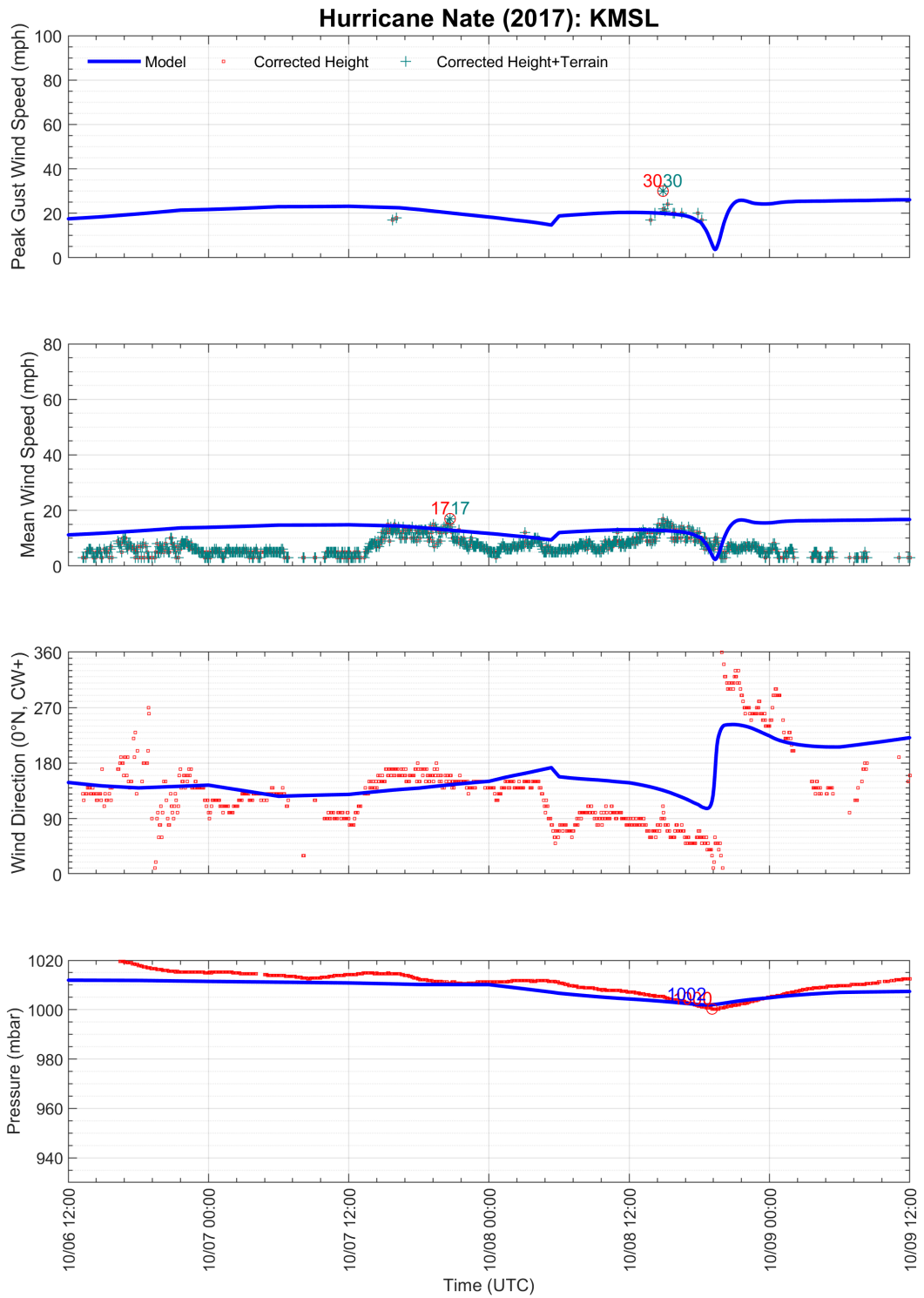


Figure 8-15. Modeled and observed meteorological time series at ASOS station KMSL: Northwest Alabama Regional Airport.

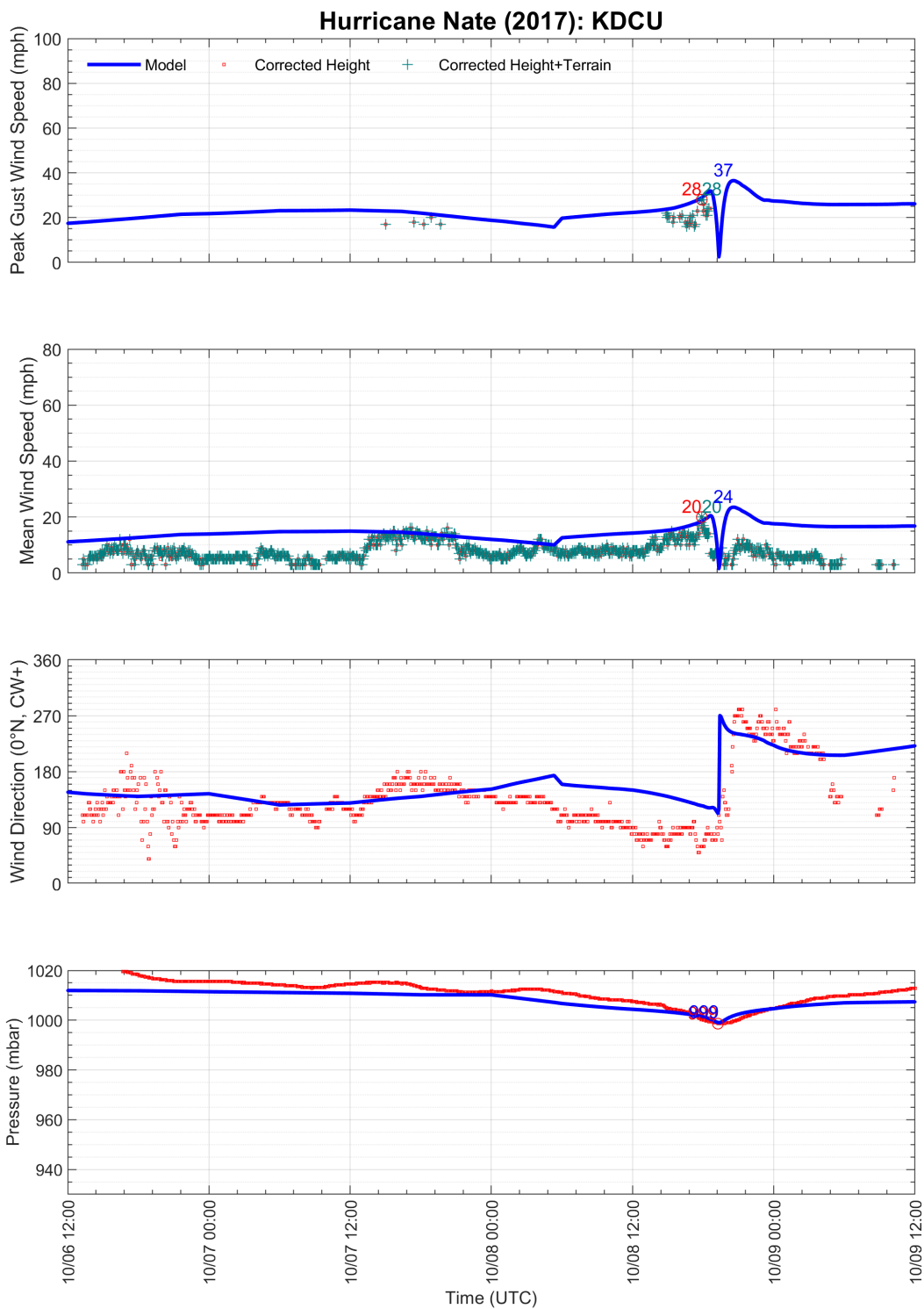


Figure 8-16. Modeled and observed meteorological time series at ASOS station KDCU: Pryor Field Airport.

8.4 ERRORS AND UNCERTAINTY

Figure 8-17 and Figure 8-18 present comparisons of modeled and observed maximum gust wind speeds and minimum central pressures for the stations used in the model validation process. Stations that failed prior to the arrival of the highest winds were not included in the comparisons. The R^2 values for peak gust wind speed with and without terrain corrections ranged from 0.58 to 0.66. The R^2 value for central pressure was 0.9. Tabulated error values of peak gust wind speed are provided in Table 8-1 at the end of this section.

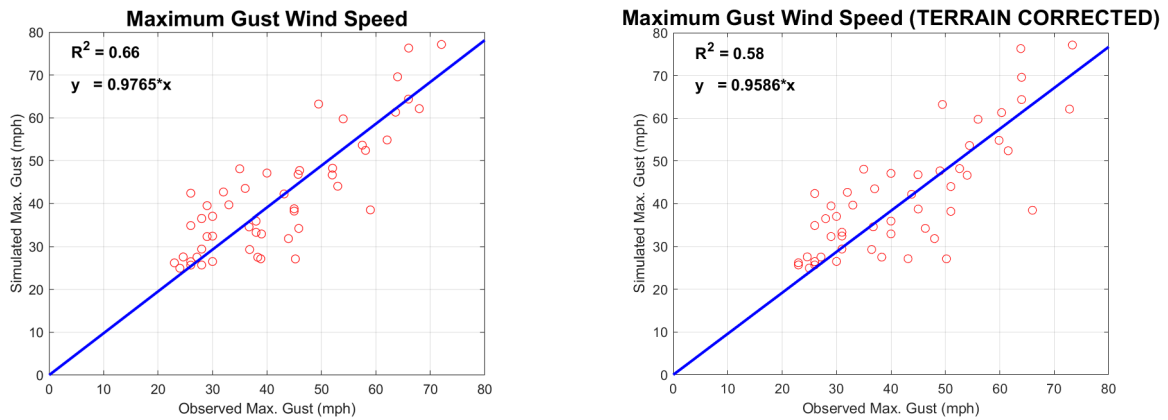


Figure 8-17. Modeled and observed maximum peak gust wind speed corrected only for height (left) and corrected for height and terrain (right).

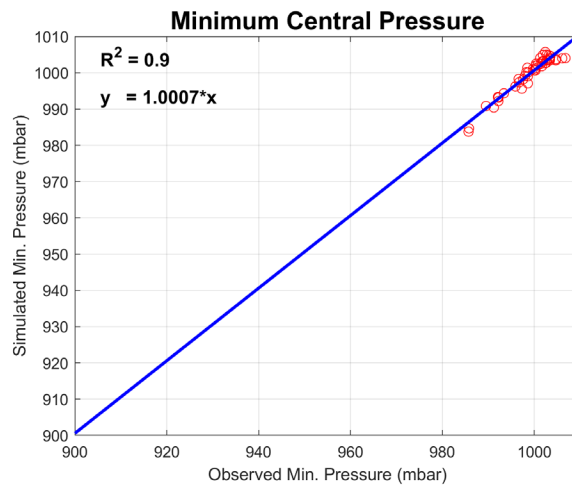


Figure 8-18. Modeled and observed minimum central pressure.

Table 8-1. Errors in modeled peak gust wind speed in Hurricane Nate when observations are corrected for height only and for height and terrain. All wind speed values are presented at 10 m elevation in open terrain.

Station	Modeled Peak Gust Wind Speed (mph)	Observed Peak Gust Wind Speed (mph)		Error (mph)	
		Corrected for Height	Corrected for Height + Terrain	Corrected for Height	Corrected for Height + Terrain
KANB	39	45	45	-6	-6
KASD	29	28	31	1	-2
KBFM	60	54	56	6	4
KBHM	48	35	35	13	13
KBTR	25	24	25	1	0
KBVE	48	46	49	2	-1
KCEW	38	45	51	-7	-13
KCHA	39	29	29	10	10
KDCU	37	28	28	9	9
KDTS	38	59	66	-21	-28
KEET	47	40	40	7	7
KFFC	32	29	29	3	3
KFTY	33	39	40	-6	-7
KGPT	47	52	54	-5	-7
KGZH	44	36	37	8	7
KHBG	32	30	31	2	1
KHKS	26	26	26	0	0
KHSV	43	32	32	11	11
KJAN	26	28	23	-2	3
KMEI	26	26	26	0	0
KMGM	40	33	33	7	7
KMOB	64	66	64	-2	0
KMSL	27	30	30	-3	-3
KNEW	33	38	31	-5	2
KPNS	44	53	51	-9	-7
KPQL	70	64	64	6	6
KRMG	37	30	30	7	7
KTCL	42	26	26	16	16
KTOI	36	38	40	-2	-4
KTUP	26	23	23	3	3
KVPC	35	26	26	9	9
AMRL1	28	27	27	1	1
BURL1	54	58	54	-4	0
DKCM6	77	72	73	5	4
EINL1	28	38	38	-10	-10
FMOA1	61	64	60	-3	1
FREL1	29	37	36	-8	-7
GISL1	42	43	44	-1	-2
NWCL1	35	37	37	-2	-2

Station	Modeled Peak Gust Wind Speed (mph)	Observed Peak Gust Wind Speed (mph)		Error (mph)	
		Corrected for Height	Corrected for Height + Terrain	Corrected for Height	Corrected for Height + Terrain
PILL1	63	49	49	14	14
PSTL1	55	62	60	-7	-5
RARM6	76	66	64	10	12
SHBL1	47	46	45	1	2
SPLL1	34	46	46	-12	-12
TESL1	28	25	25	3	3
WYCM6	48	52	53	-4	-5
42001	32	44	48	-12	-16
42012	52	58	62	-6	-10
42040	62	68	73	-6	-11
42360	27	39	43	-12	-16
42395	27	45	50	-18	-23

8.5 WIND FIELD MAP

The final peak gust wind speed map of Hurricane Nate is shown in Figure 8-19 with wind speed contours in increments of 10 mph. Peak gust wind speeds are defined as 3-second average at 10 m above ground over open terrain. The storm track is shown by the dashed blue line. All stations used in the wind field model validation are also shown: purple triangles indicate an ASOS station, and green triangles indicate a station in the NDBC database located over water or near the coast. The highest winds are shown to have occurred over southeast Louisiana and Mississippi near the city of Biloxi.

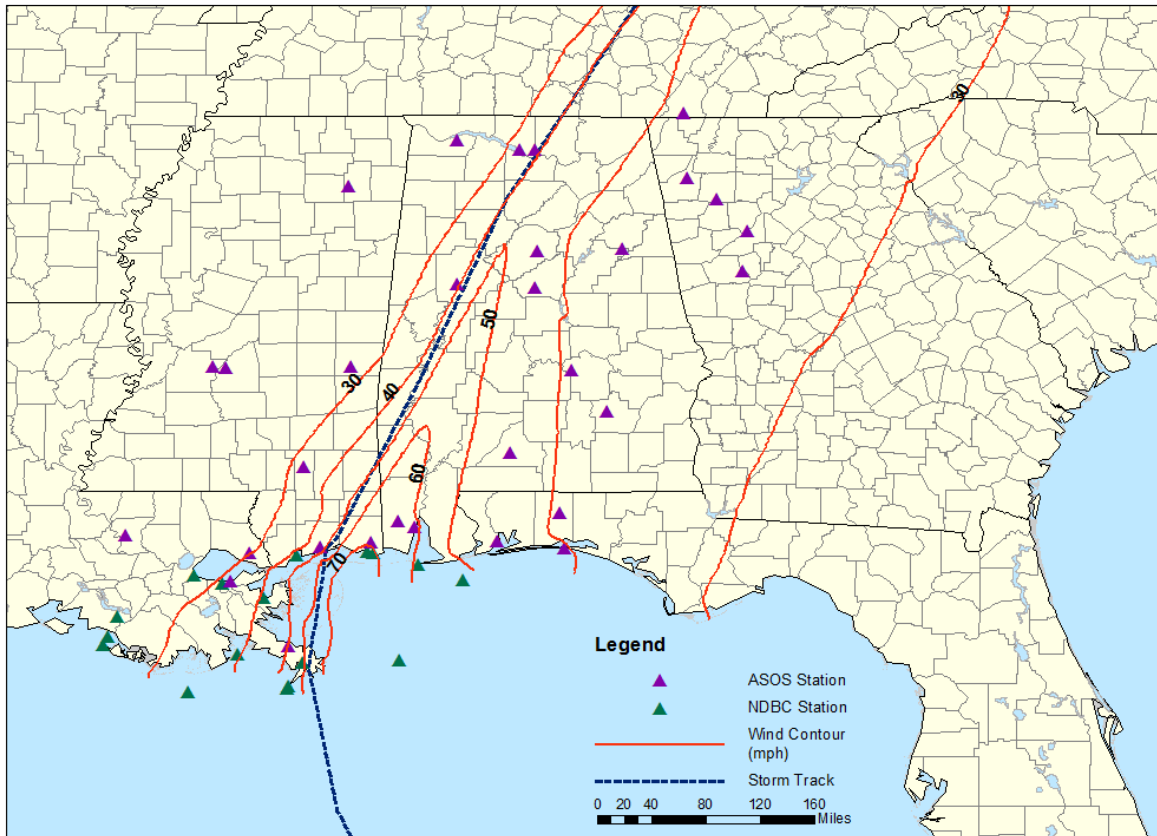


Figure 8-19. Peak gust wind speed contour map for Hurricane Nate (2017) showing estimated 3-second peak gust wind speeds (mph) at 10 m above ground over open terrain. Model output obtained from ARA wind field model fit to surface level observations using NHC best track and central pressures.

9 SUMMARY

Under this project, five wind field maps were created for Hurricane Harvey (Texas only), Hurricane Irma (CONUS and OCONUS), Hurricane Maria, and Hurricane Nate. The hurricane wind field modeling used ARA's hurricane simulation code described in Vickery et al. (2009b), which forms the basis for the design wind speeds in the United States as specified in ASCE 7-10 and ASCE 7-16. The wind field model has been extensively validated for surface level winds at both coastal and inland stations as described in Vickery et al. (2009a).

Historical track information was obtained from the NHC Atlantic hurricane database (HURDAT2) and surface level meteorological observations were obtained from land based stations in the ASOS system, marine stations in the NDBC database, and mobile data towers deployed by the University of Florida.

This report outlines the general methodology including 1) data collection and standardization, and 2) wind field modeling, errors, and uncertainties associated with both. Storm-specific information is presented for each modeled hurricane, including event background, data, and model results.

10 REFERENCES

- Beven II, J.L., and Berg, R. (2018). *Tropical Cyclone Report: Hurricane Nate (AL162017)*. National Hurricane Center Report. https://www.nhc.noaa.gov/data/tcr/AL162017_Nate.pdf.
- Blake, E. S. and Zelinsky, D. A. (2018). *Tropical Cyclone Report: Hurricane Harvey (AL092017)*. National Hurricane Center Report. https://www.nhc.noaa.gov/data/tcr/AL092017_Harvey.pdf.
- Bryant, M. A., Hesser, T. J., and Jensen, R. E. (2016). *Evaluation Statistics Computed for the Wave Information Studies (WIS)*. US Army Engineer Research and Development Center Vicksburg United States.
- Cangialosi, J.P., Latto, A.S., and Berg, R. (2018). *Tropical Cyclone Report: Hurricane Irma (AL112017)*. National Hurricane Center Report. https://www.nhc.noaa.gov/data/tcr/AL112017_Irma.pdf.
- ESDU. (1982). Strong Winds in the Atmospheric Boundary Layer, Part 1: Mean Hourly Wind Speed, Engineering Sciences Data Unit Item No. 82026, London, England.
- ESDU. (1983). Strong Winds in the Atmospheric Boundary Layer, Part 2: Discrete Gust Speeds, Engineering Sciences Data Unit Item No. 83045, London, England.
- Masters, F. J., Vickery, P. J., Bacon, P., and Rappaport, E. N. (2010). Toward objective, standardized intensity estimates from surface wind speed observations. *Bulletin of the American Meteorological Society*, **91**(12), 1665-1681.
- Pasch, R.J., Penny, A.B., and Berg, R. (2018). *Tropical Cyclone Report: Hurricane Maria (AL152017)*. National Hurricane Center Report. https://www.nhc.noaa.gov/data/tcr/AL152017_Maria.pdf.
- Powell, M.D., Houston, S., and Reinhold, T.A. (1996). Hurricane Andrew's landfall in South Florida. Part I: Standardizing measurements for documentation of surface wind fields. *Weather Forecasting*, **11**, 304–328.

Powell, M.D., Soukup, G., Cocke, S., Gulati, S., Morisseau-Leroy, N., Hamid, S., Dorst, N., and Axe, L. (2005). State of Florida hurricane loss projection model: atmospheric science component, *Journal of Industrial Aerodynamics*, **93**, 651-674.

Simiu, E., and Scanlan, R.H. (1996). *Wind Effects on Structures: An Introduction to Wind Engineering*, 3rd Ed., John Wiley Sons, New York.

Vickery, P.J., Skerlj, P.F., Steckley, A.C., and Twisdale Jr., L.A. (2000). Hurricane wind field model for use in hurricane simulations. *Journal of Structural Engineering*, **126**, 1203-1221.

Vickery, P.J., and Skerlj, P.F. (2005): Gust factors revisited. *Journal of Structural Engineering*, **131**, 825–832.

Vickery, P.J., and Wadhera, D. (2008). Statistical Models of Holland Pressure Profile Parameter and Radius to Maximum Winds of Hurricanes from Flight Level Pressure and H*Wind Data. *Journal of Applied Meteorology and Climatology*, **47**, 2497-2517.

Vickery, P.J., Wadhera, D., Powell, M.D., and Chen, Y. (2009a). A Hurricane Boundary Layer and Wind Field Model for Use in Engineering Applications. *Journal of Applied Meteorology and Climatology*, **48**, 381-405.

Vickery, P.J., Wadhera, D., Twisdale, L.A. and Lavelle, F.M. (2009b). United States Hurricane Wind Speed Risk and Uncertainty. *Journal of Structural Engineering*, **135**, 301-320.

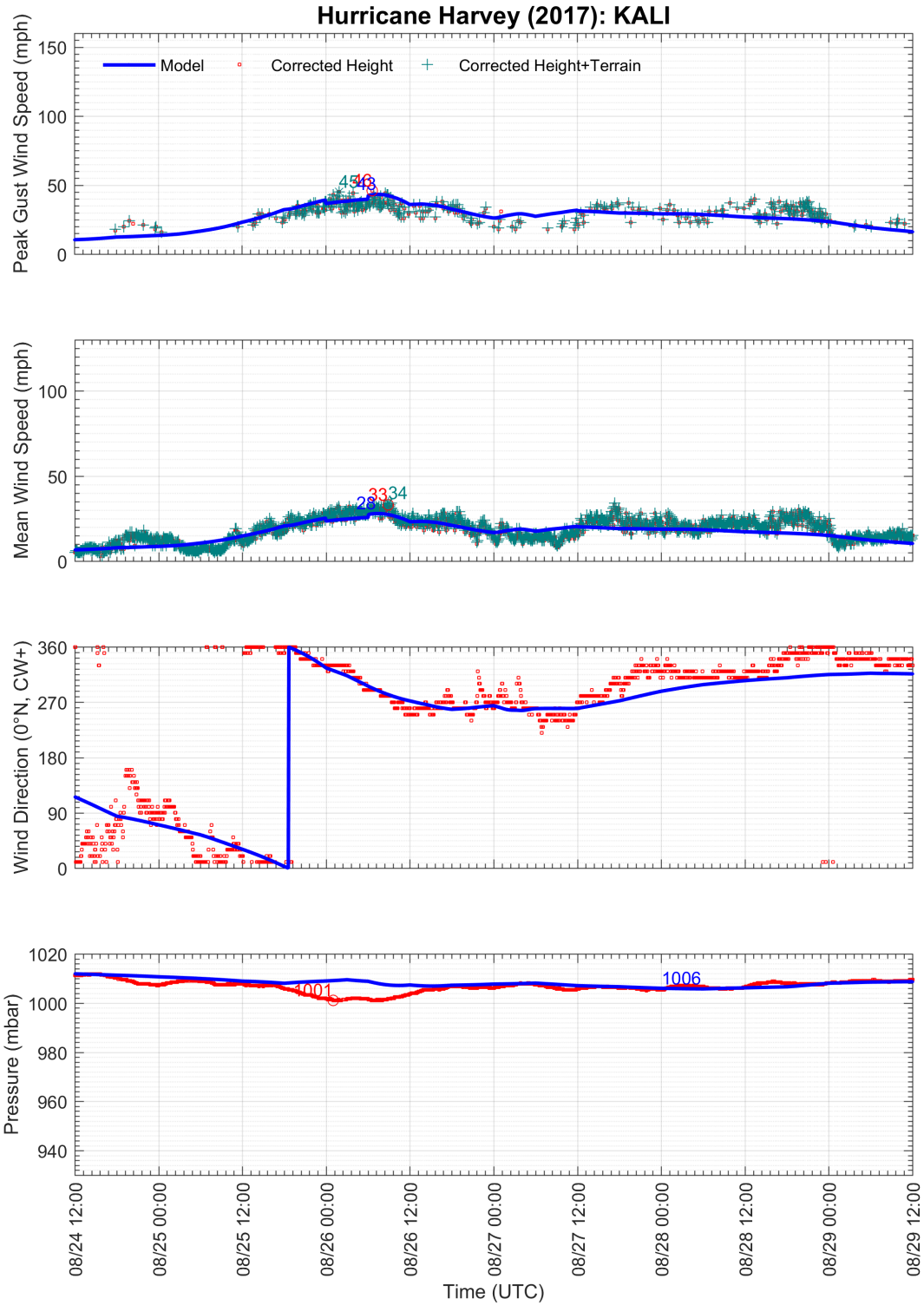
Vickery, P.J., Wadhera, D., Galsworthy, J., Peterka, J.A., Irwin, P., and Griffis, L. (2010). Ultimate Wind Load Design Gust Wind Speeds in the United States for Use in ASCE7. *Journal of Structural Engineering*, **136**(5), 613-625.

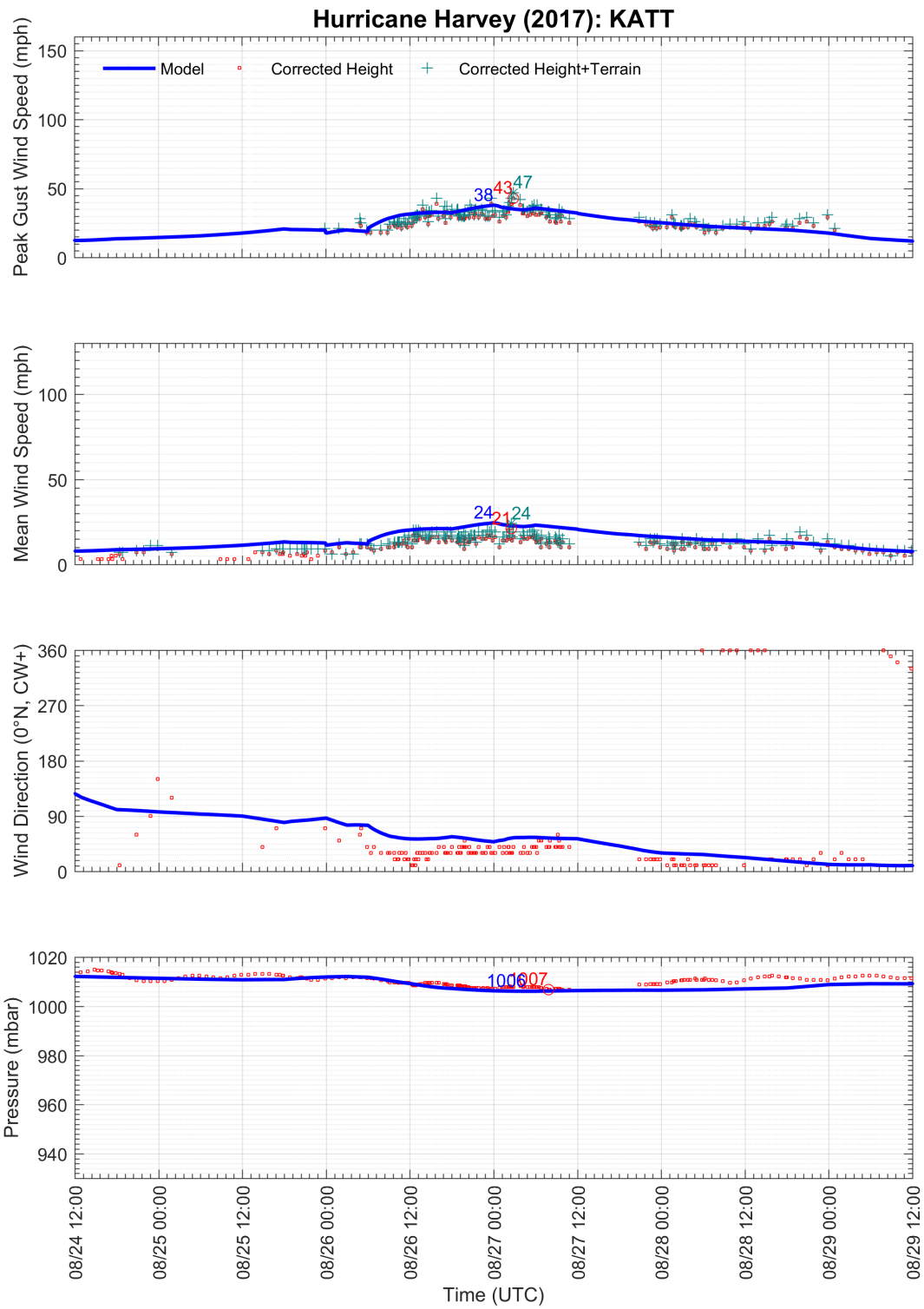
Vickery, P.J., Liu, F., Lavelle, F.M., and Mizzen, D. (2018). Development of Wind Speed-ups and Hurricane Hazard Maps for the United States Virgin Islands. Applied Research Associates report for FEMA Task Order Number 70FBR2-18-F-00000012.

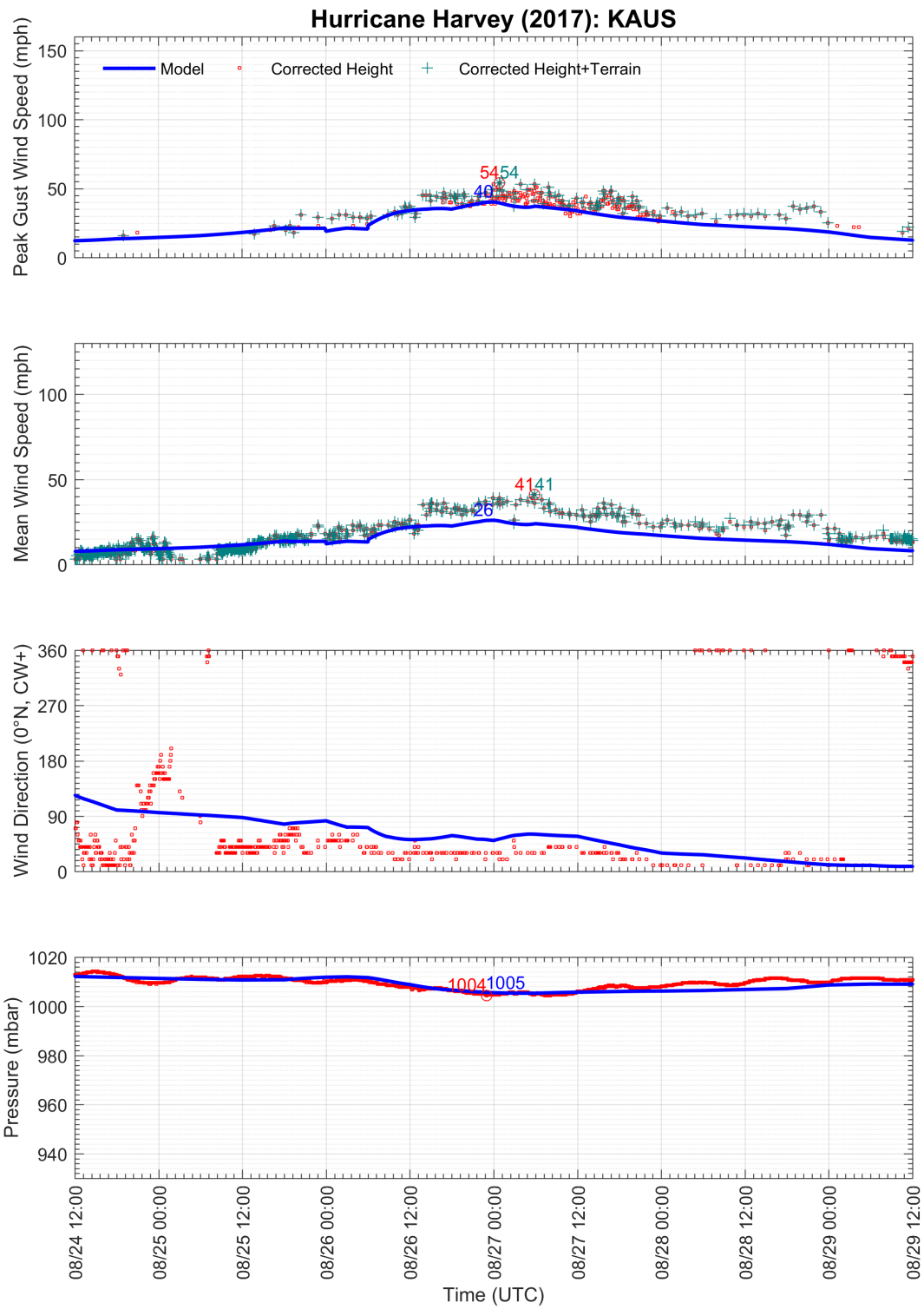
Appendix A. HURRICANE HARVEY

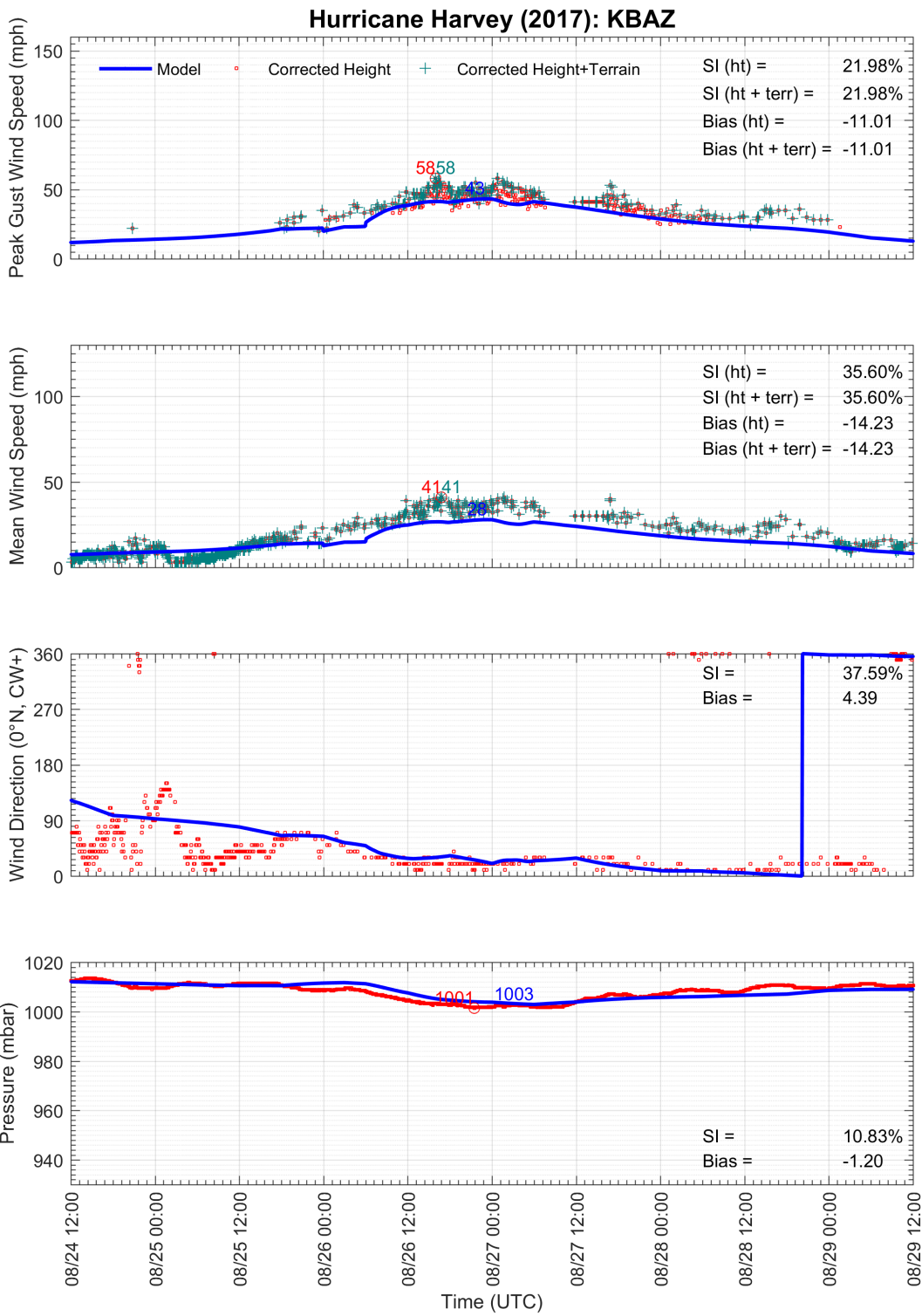
Appendix A.1 SURFACE OBSERVATION STATION DETAILS

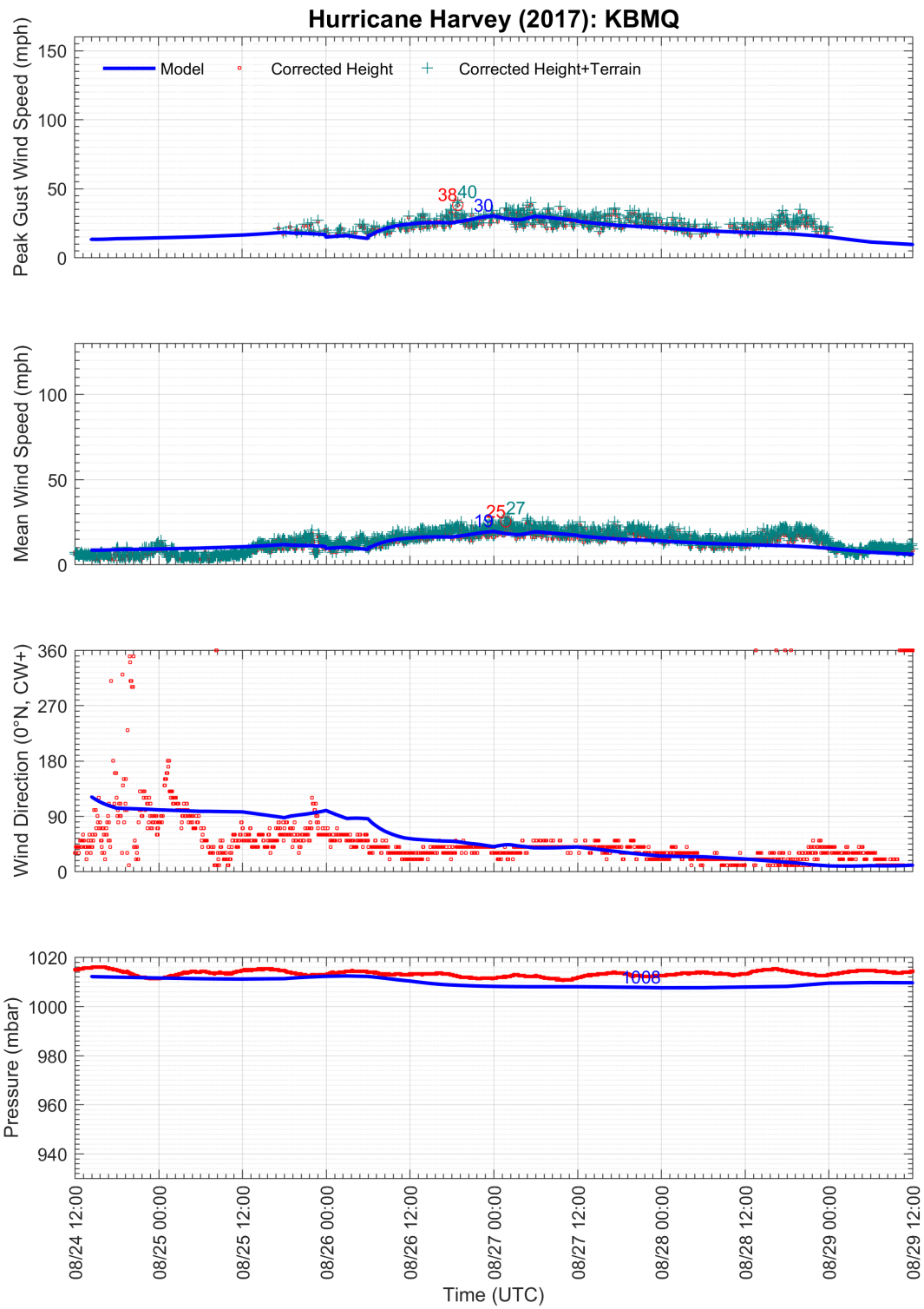
Station	Latitude (°N)	Longitude (°W)	Anemometer Height (m)
KALI	27.741	98.027	10.00
KATT	30.321	97.760	10.00
KAUS	30.179	97.681	10.00
KBAZ	29.709	98.045	10.00
KBMQ	30.741	98.235	10.00
KBRO	25.906	97.426	10.00
KCLL	30.588	96.364	8.00
KCOT	28.458	99.220	10.00
KCRP	27.773	97.513	10.00
KHDO	29.359	99.174	10.00
KHRL	26.228	97.654	10.00
KLBX	29.110	95.462	10.00
KMFE	26.175	98.238	10.00
KPIL	26.166	97.346	10.00
KPSX	28.727	96.251	10.00
KRKP	28.084	97.046	10.00
KSAT	29.533	98.464	10.00
KSSF	29.337	98.471	10.00
KVCT	28.863	96.930	10.00
ANPT2	27.837	97.039	14.22
AWRT2	28.227	96.796	10.00
BABT2	27.297	97.405	10.00
BZST2	26.067	97.155	14.51
CPNT2	28.114	97.024	10.00
FCGT2	28.943	95.302	11.20
IRDT2	27.480	97.322	4.30
MBET2	28.422	96.327	12.00
MQTT2	27.581	97.217	12.70
NUET2	27.832	97.486	10.00
PACT2	27.634	97.237	10.70
PCNT2	28.446	96.396	9.00
PTAT2	27.826	97.051	14.90
RCPT2	28.024	97.048	7.50
RSJT2	26.801	97.471	10.00
SDRT2	28.407	96.712	10.10
VCAT2	28.640	96.609	10.00
42002	26.091	93.758	5.00
42019	27.907	95.352	5.00
42020	26.968	96.694	5.00
42044	26.191	97.051	5.00
42045	26.217	96.500	4.00

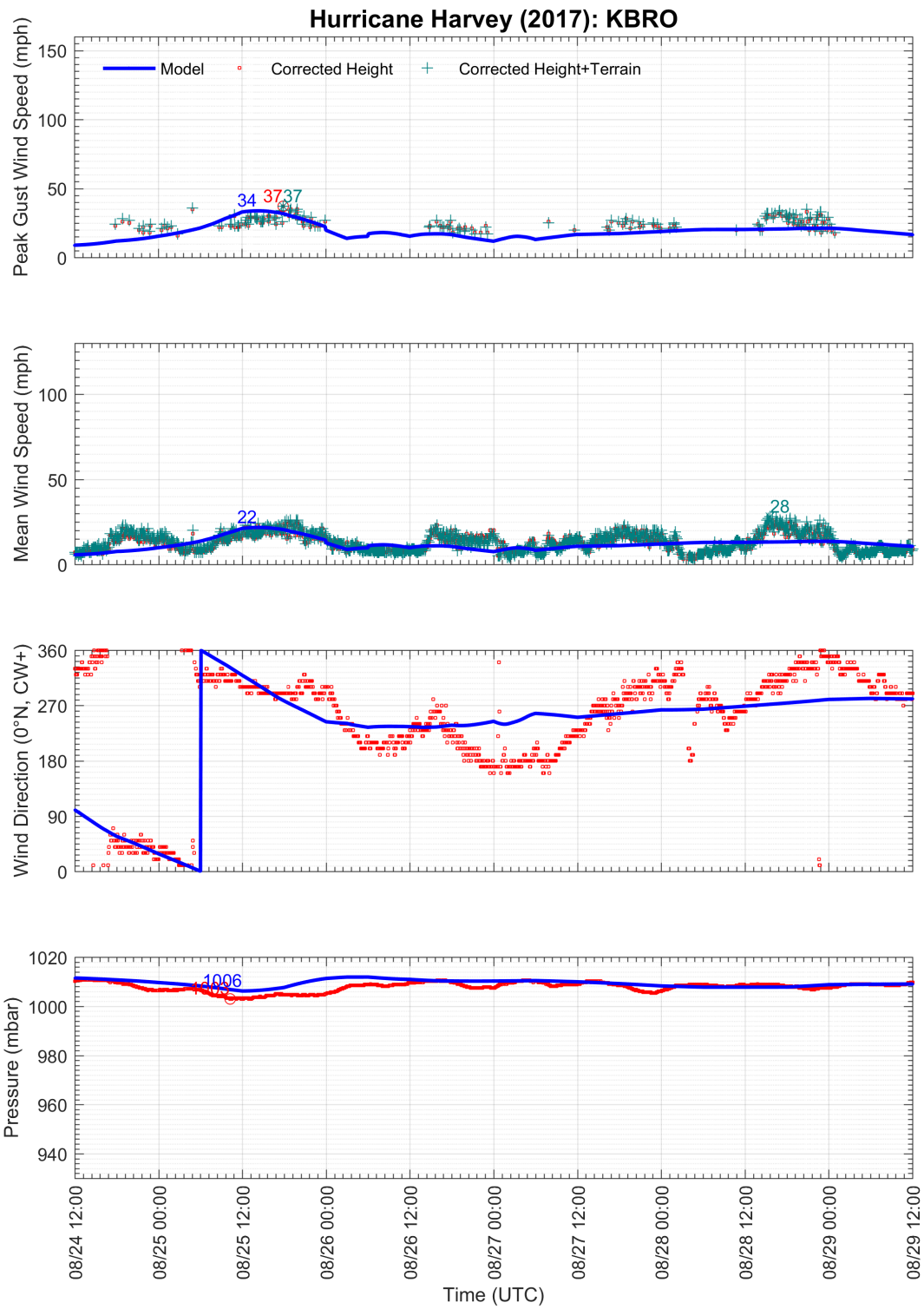


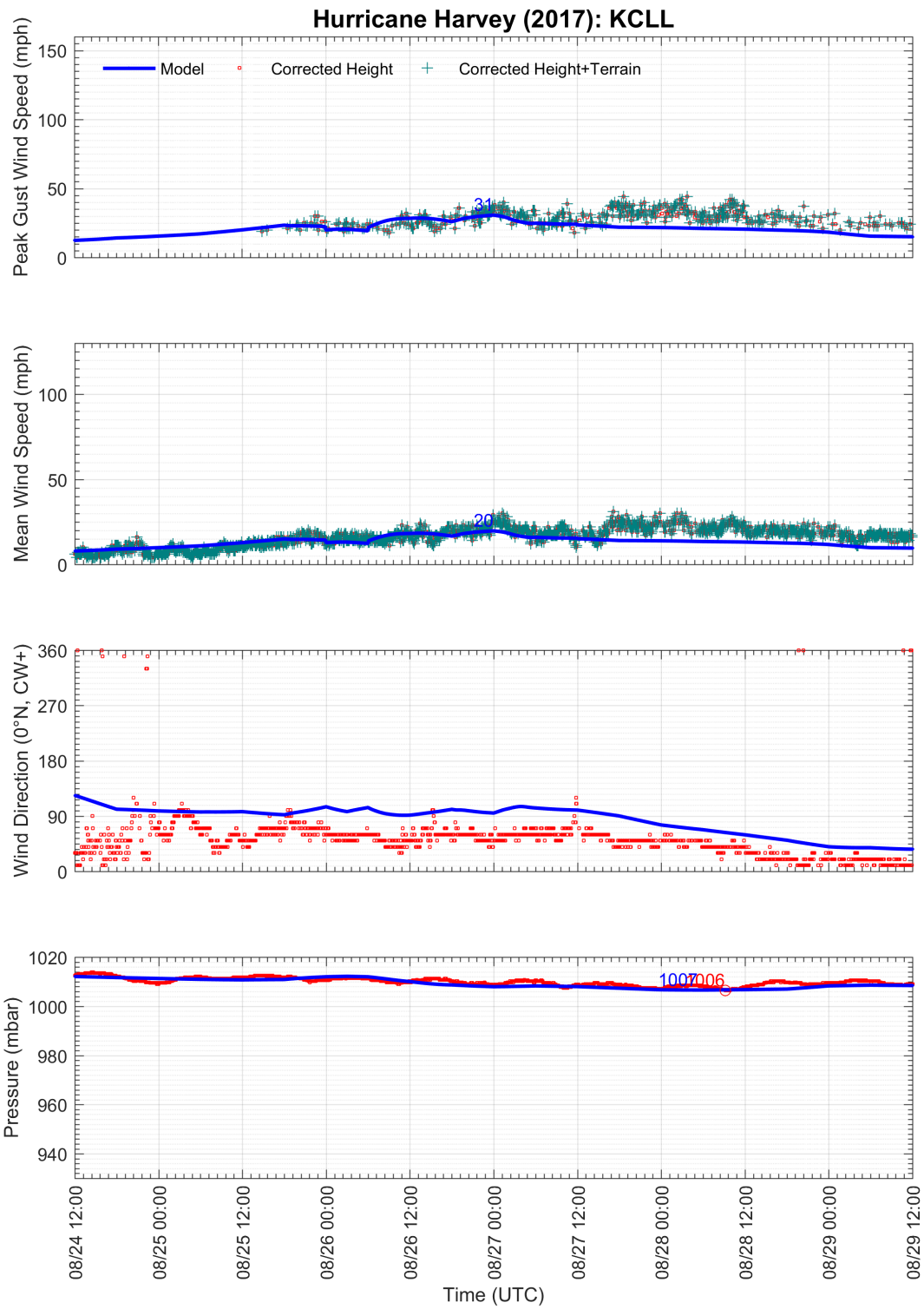


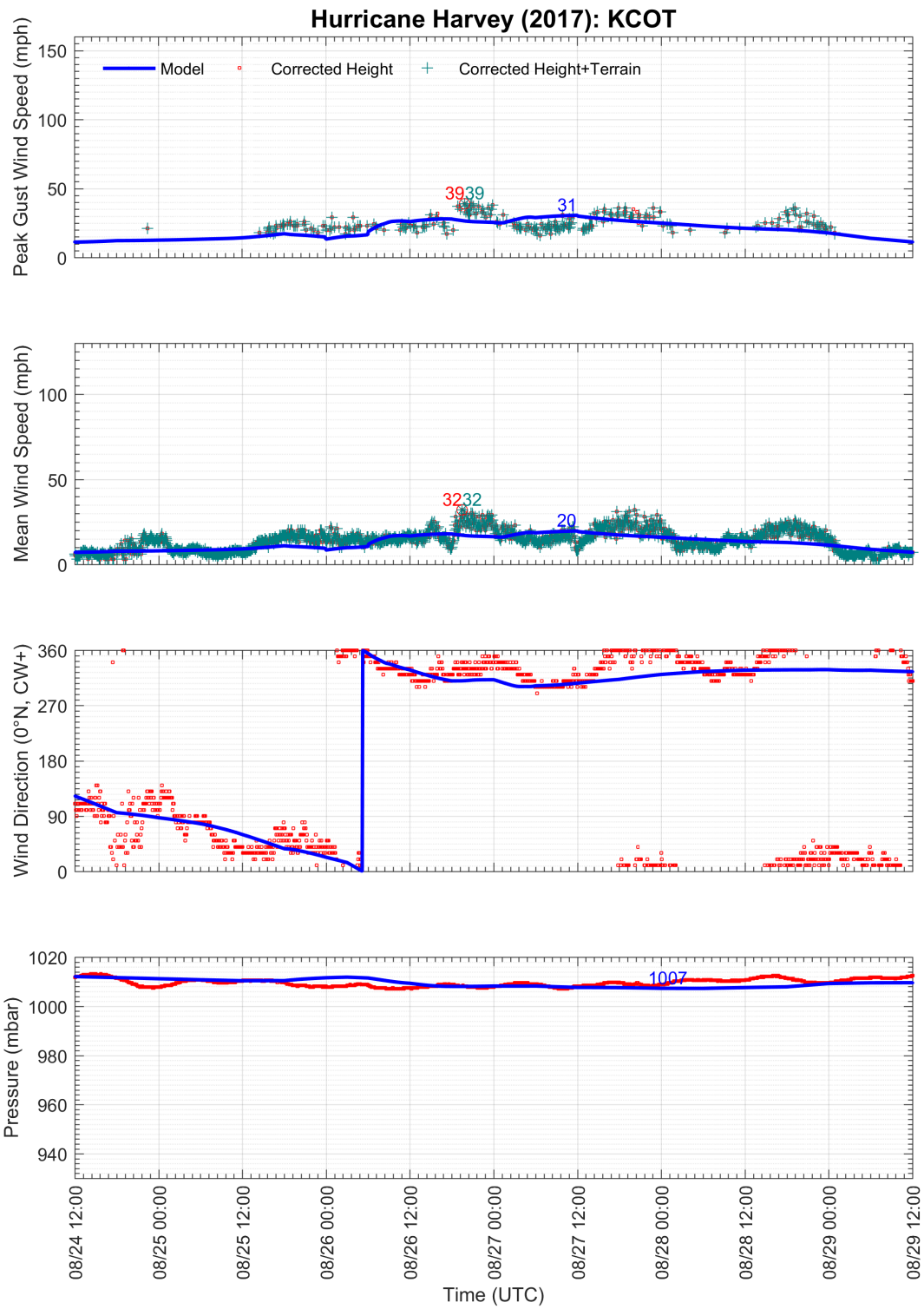


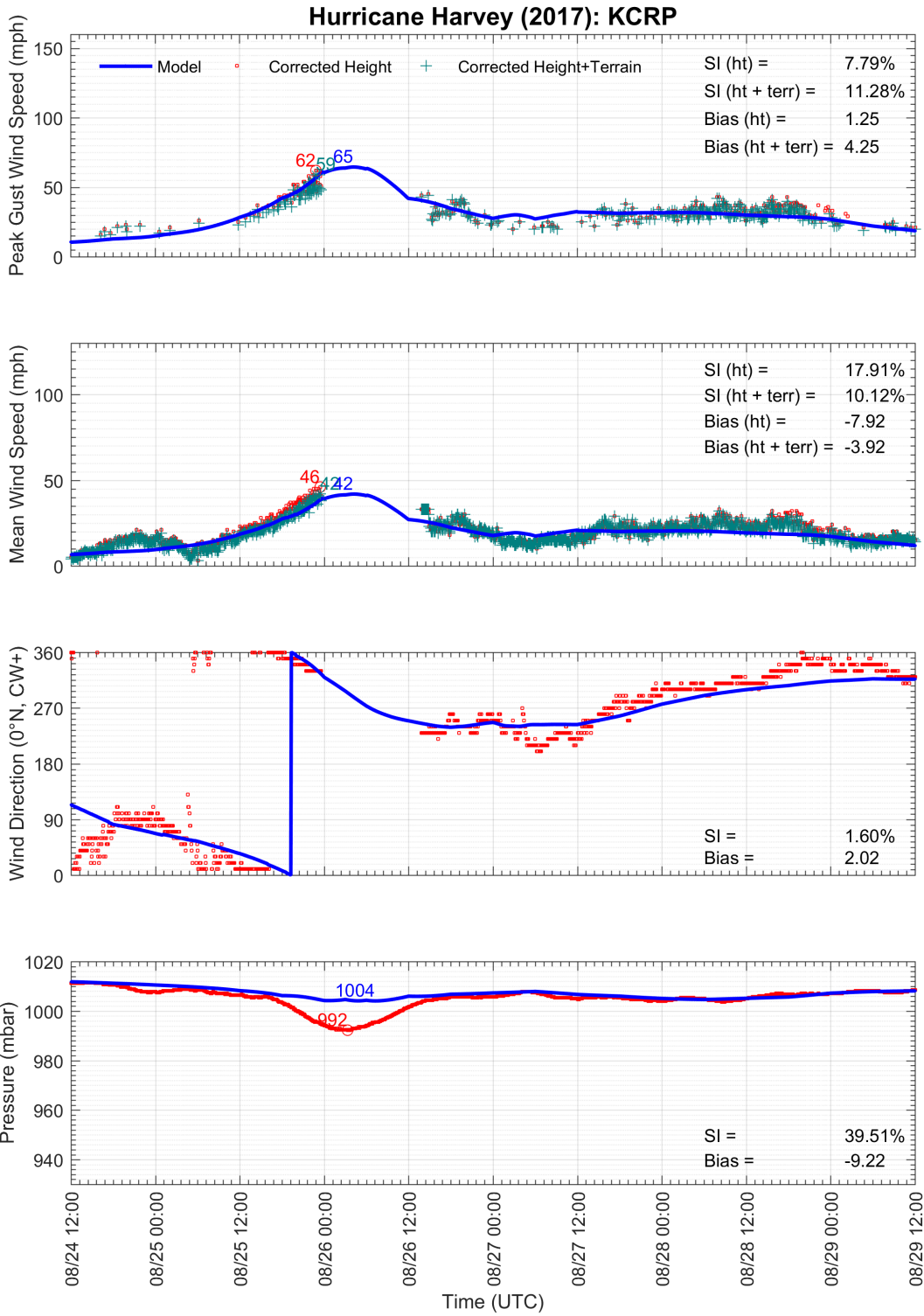


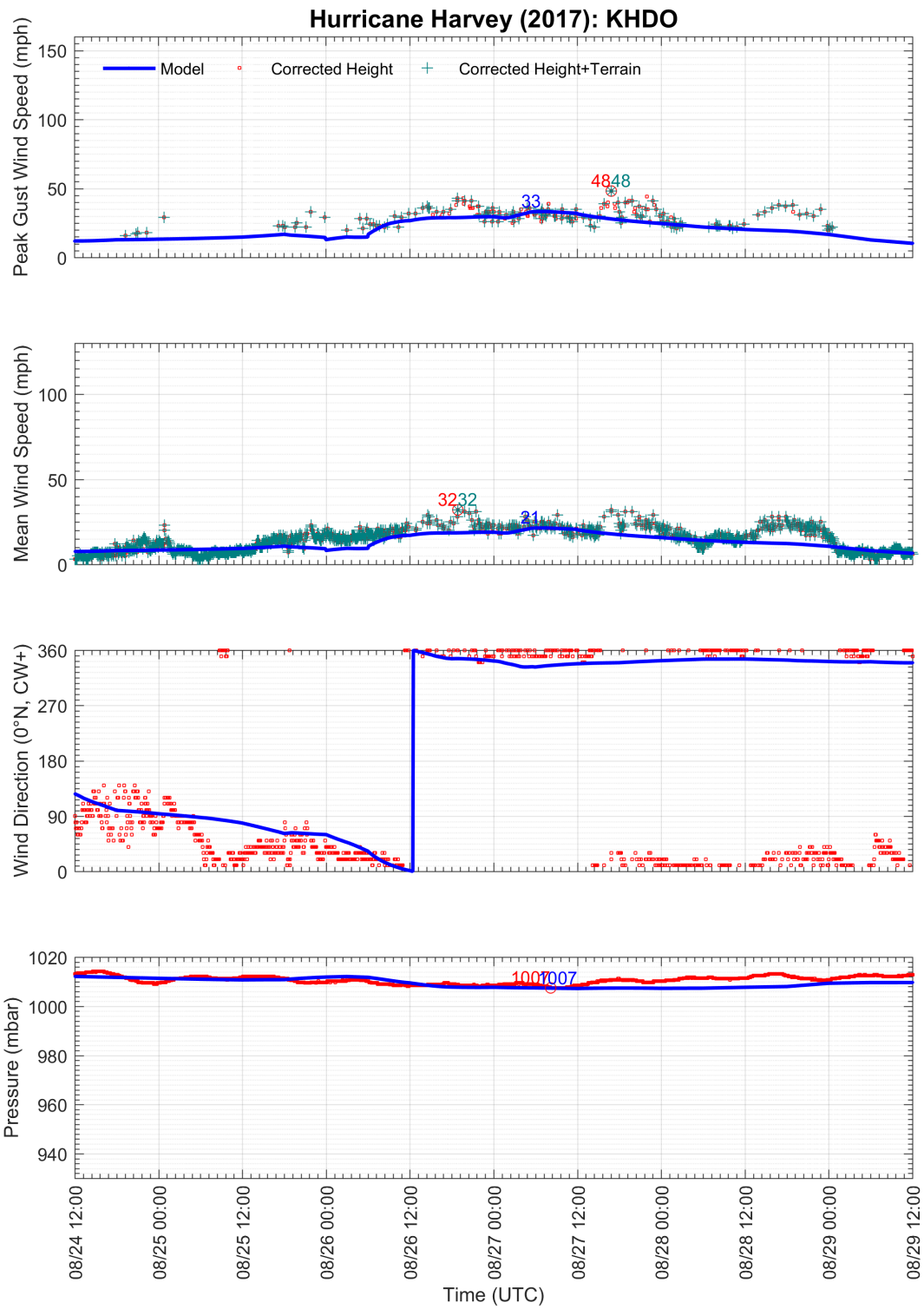


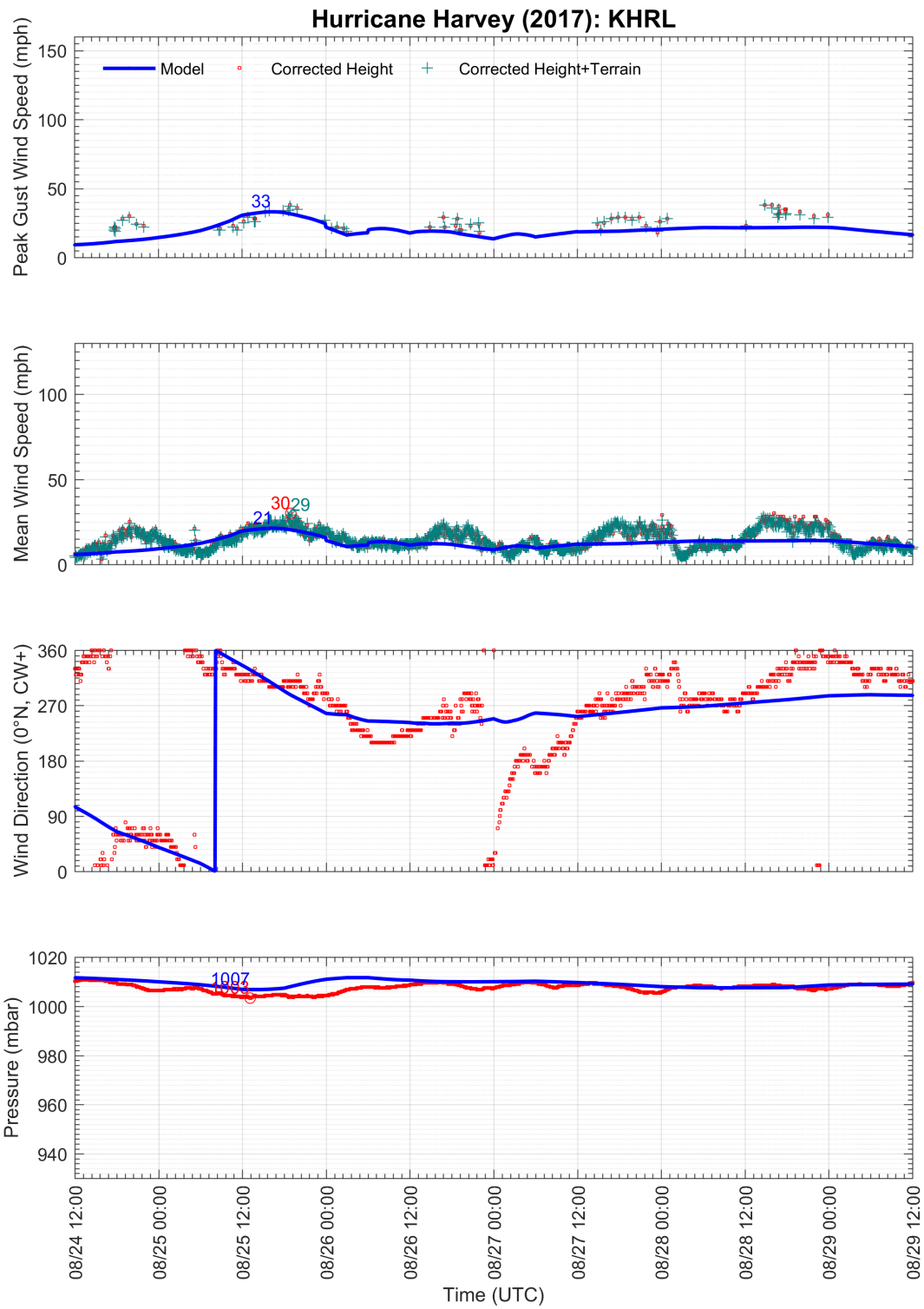


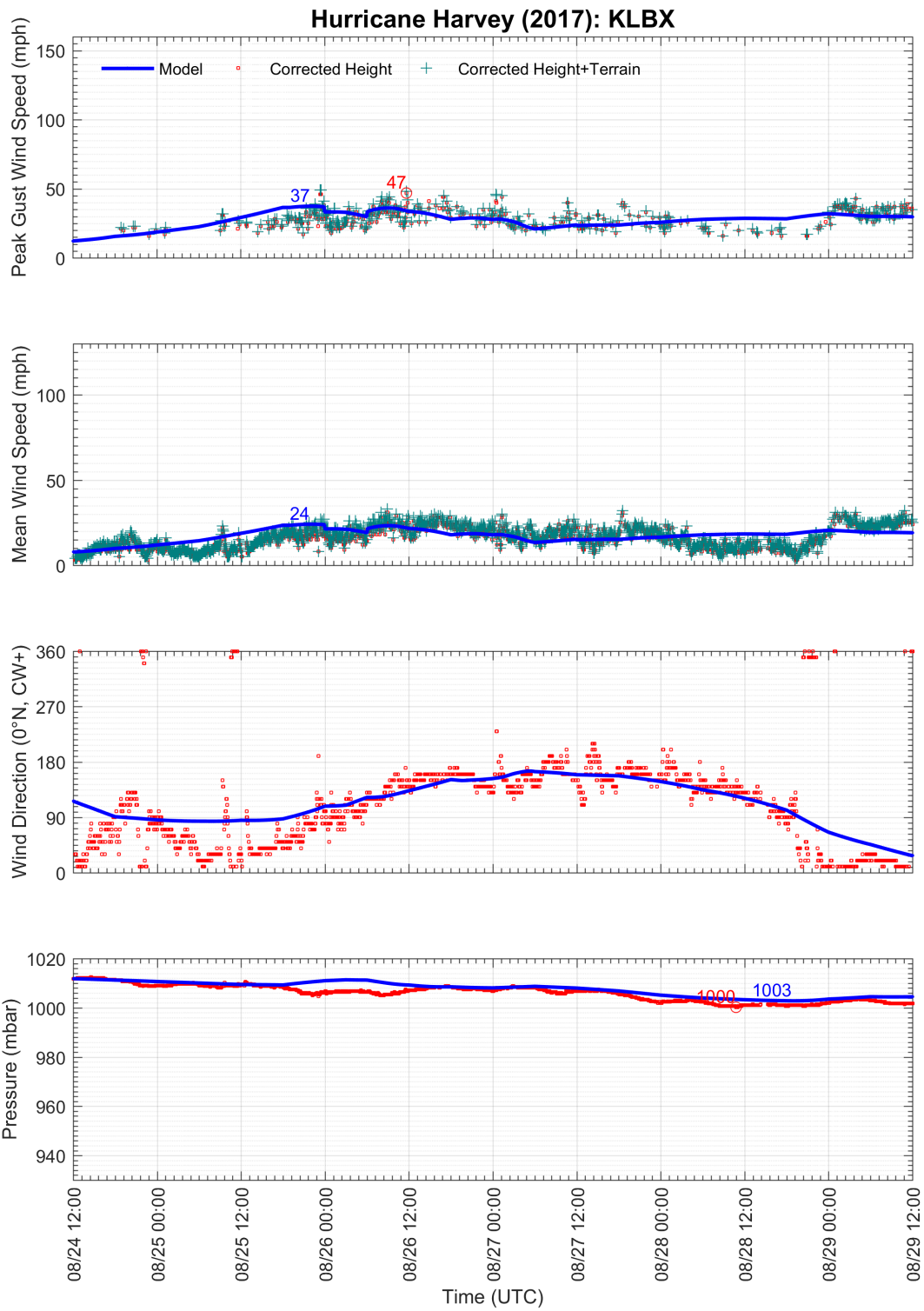


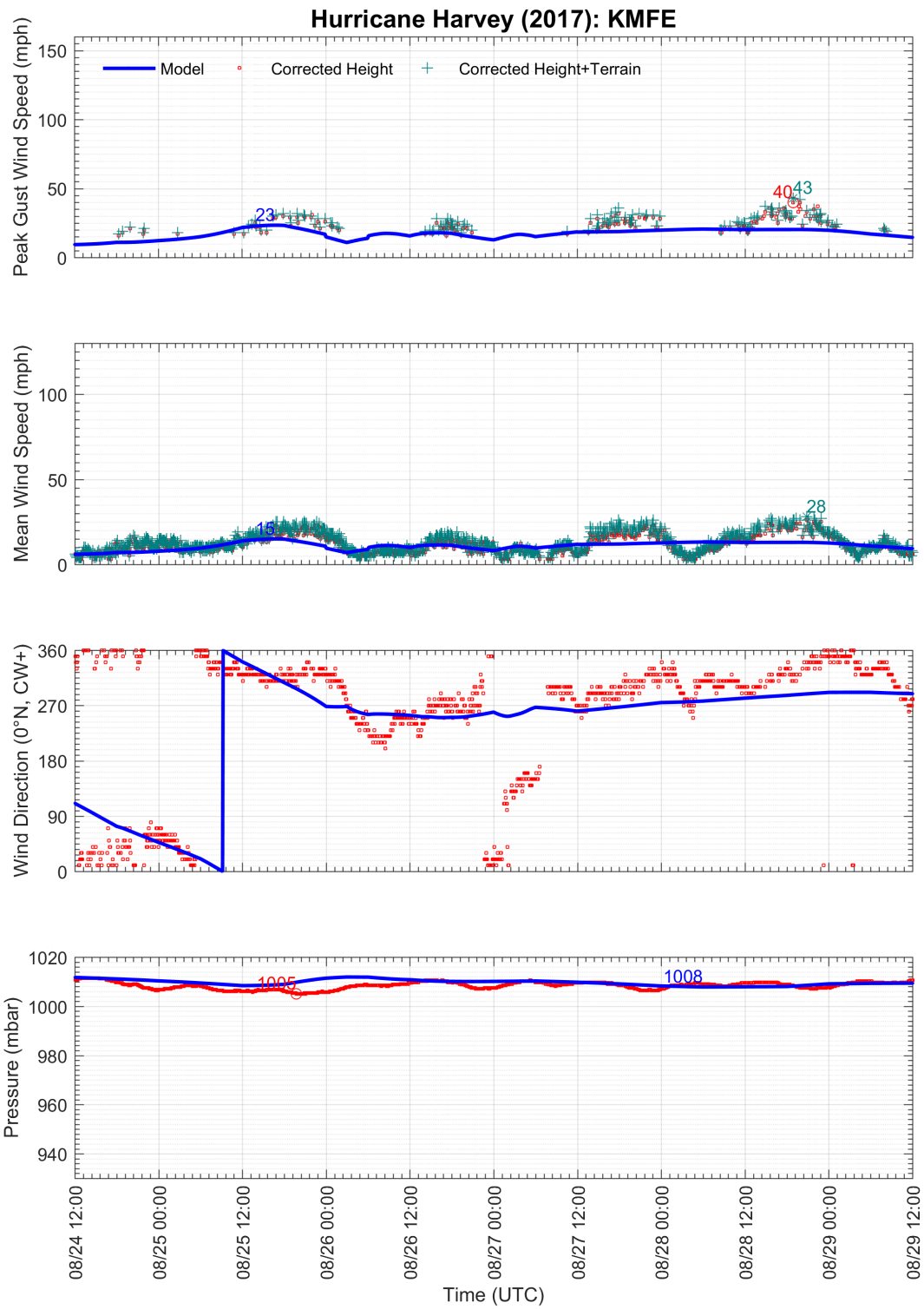


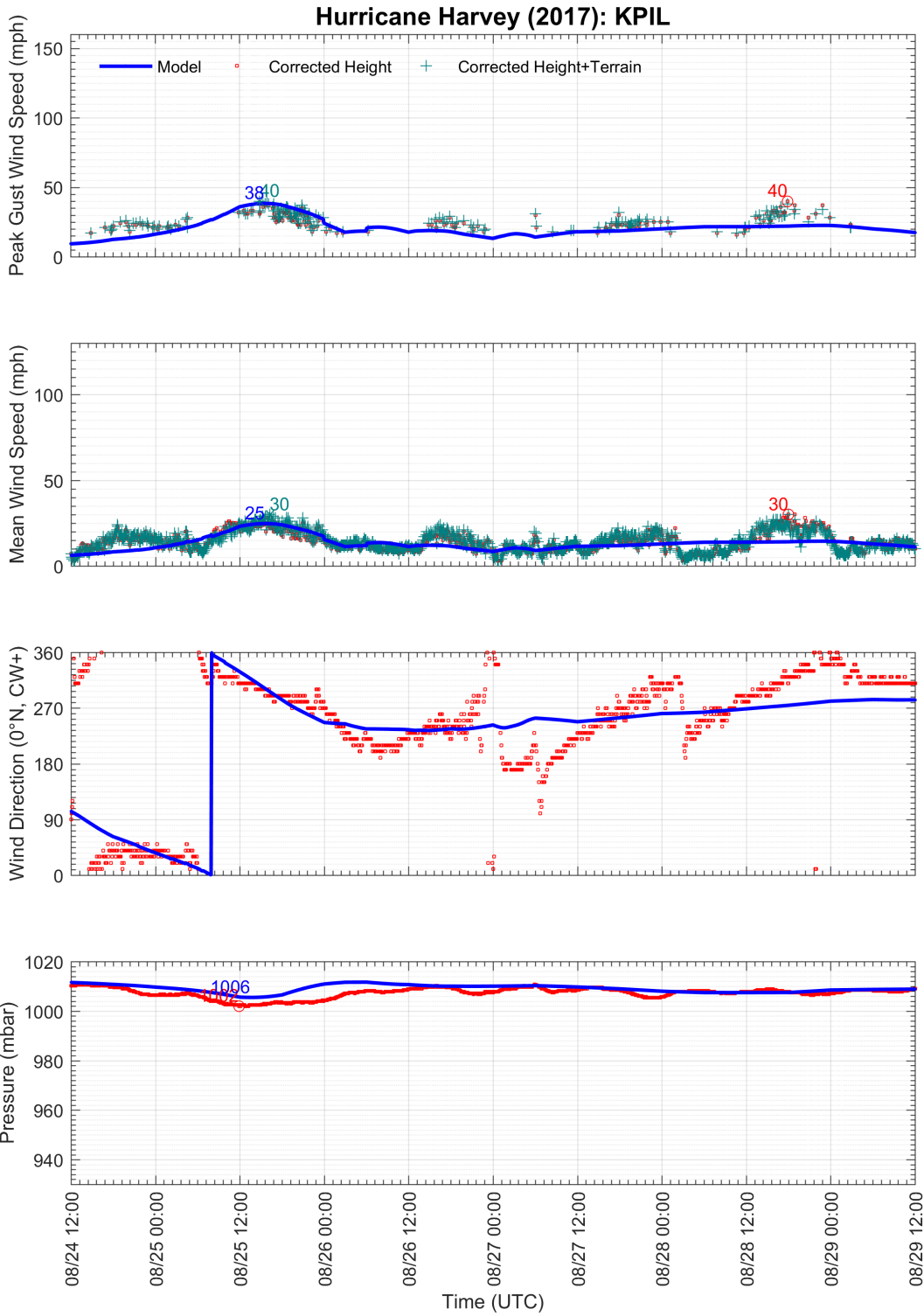


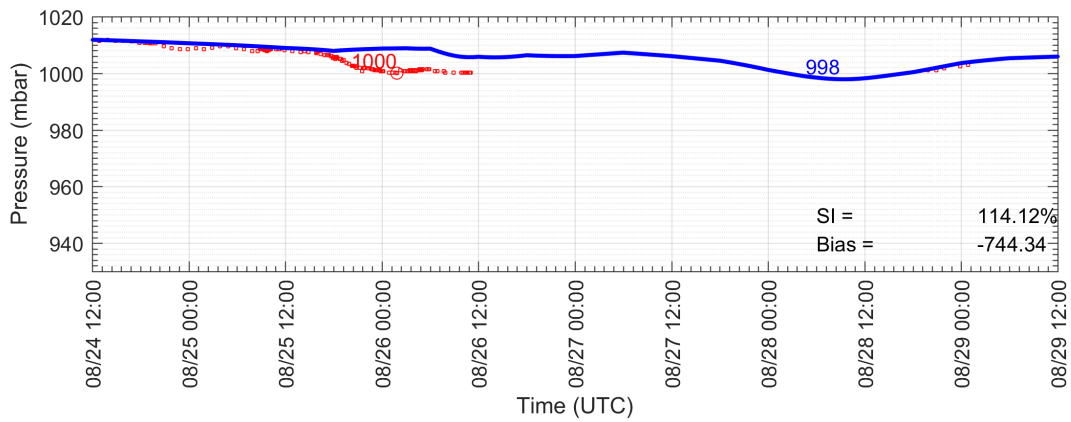
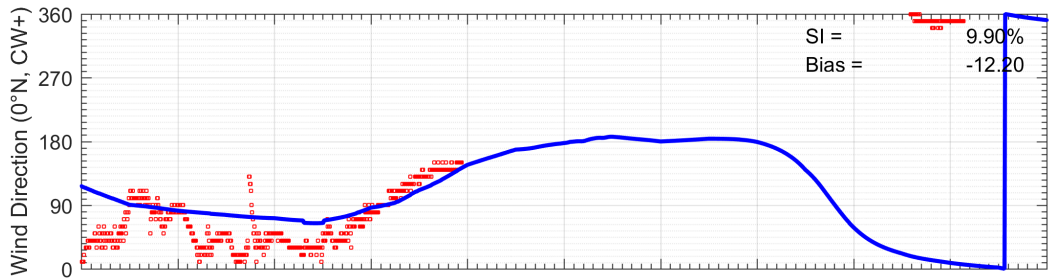
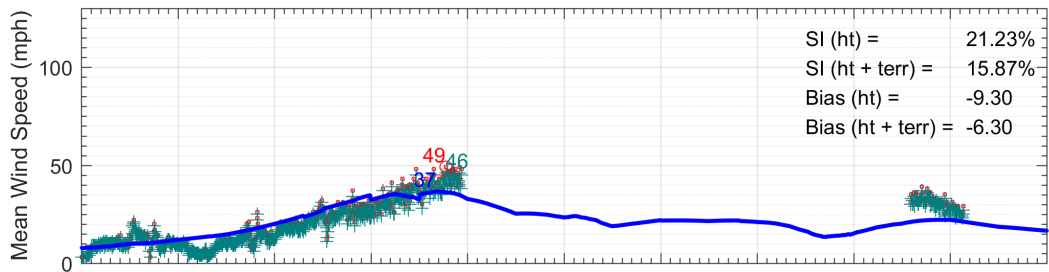
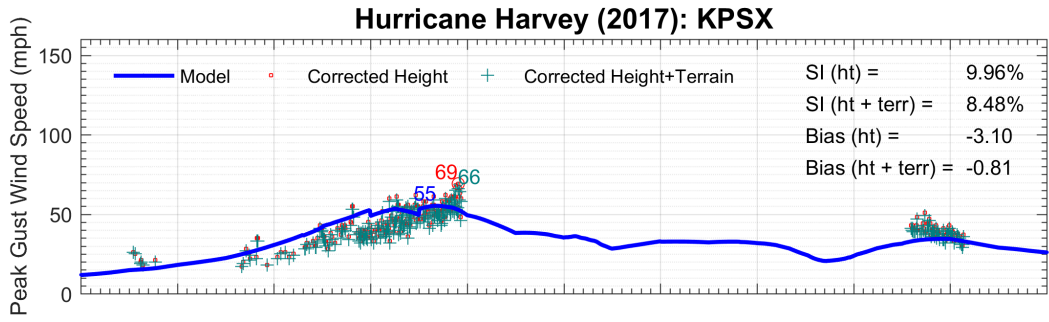


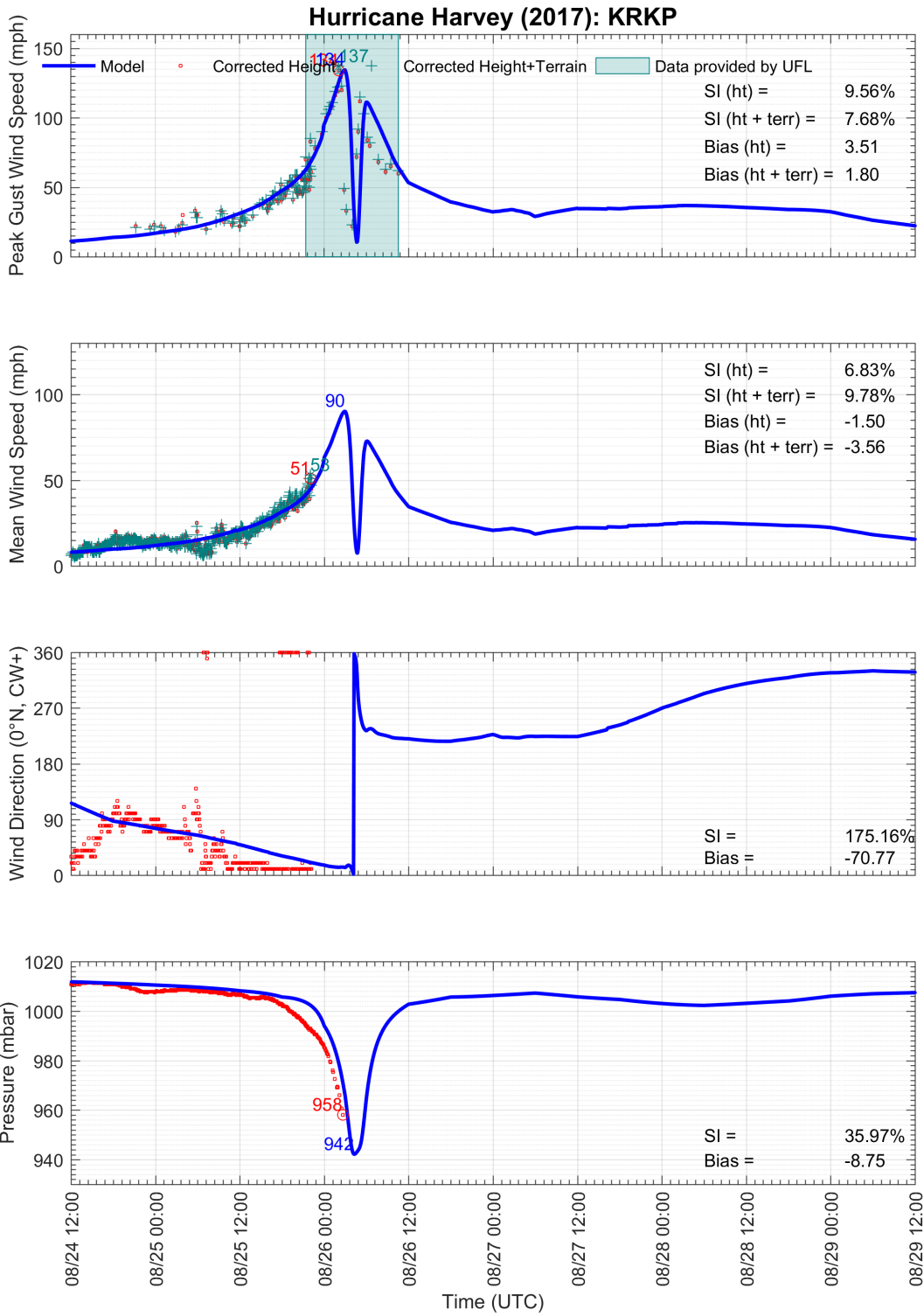


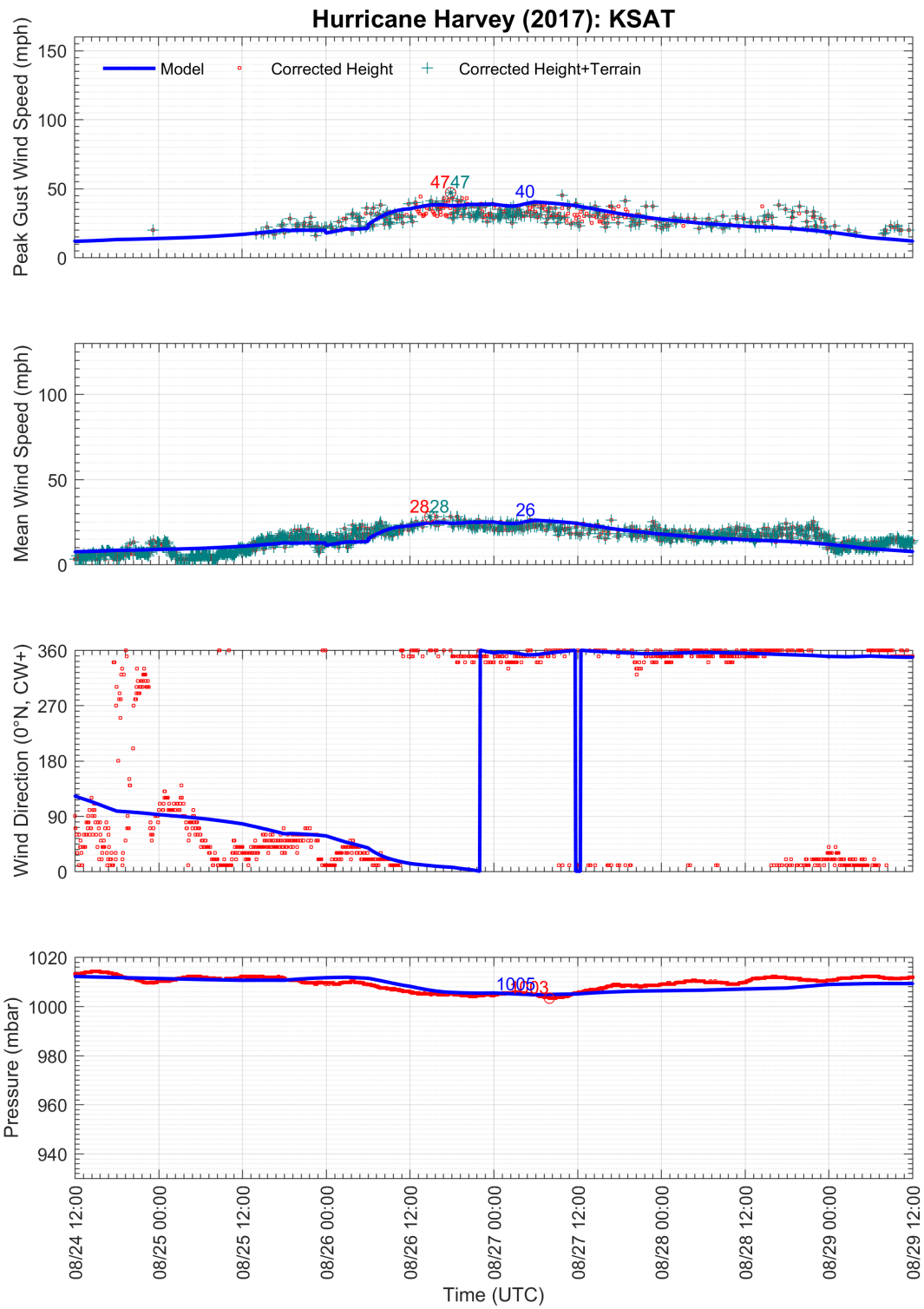


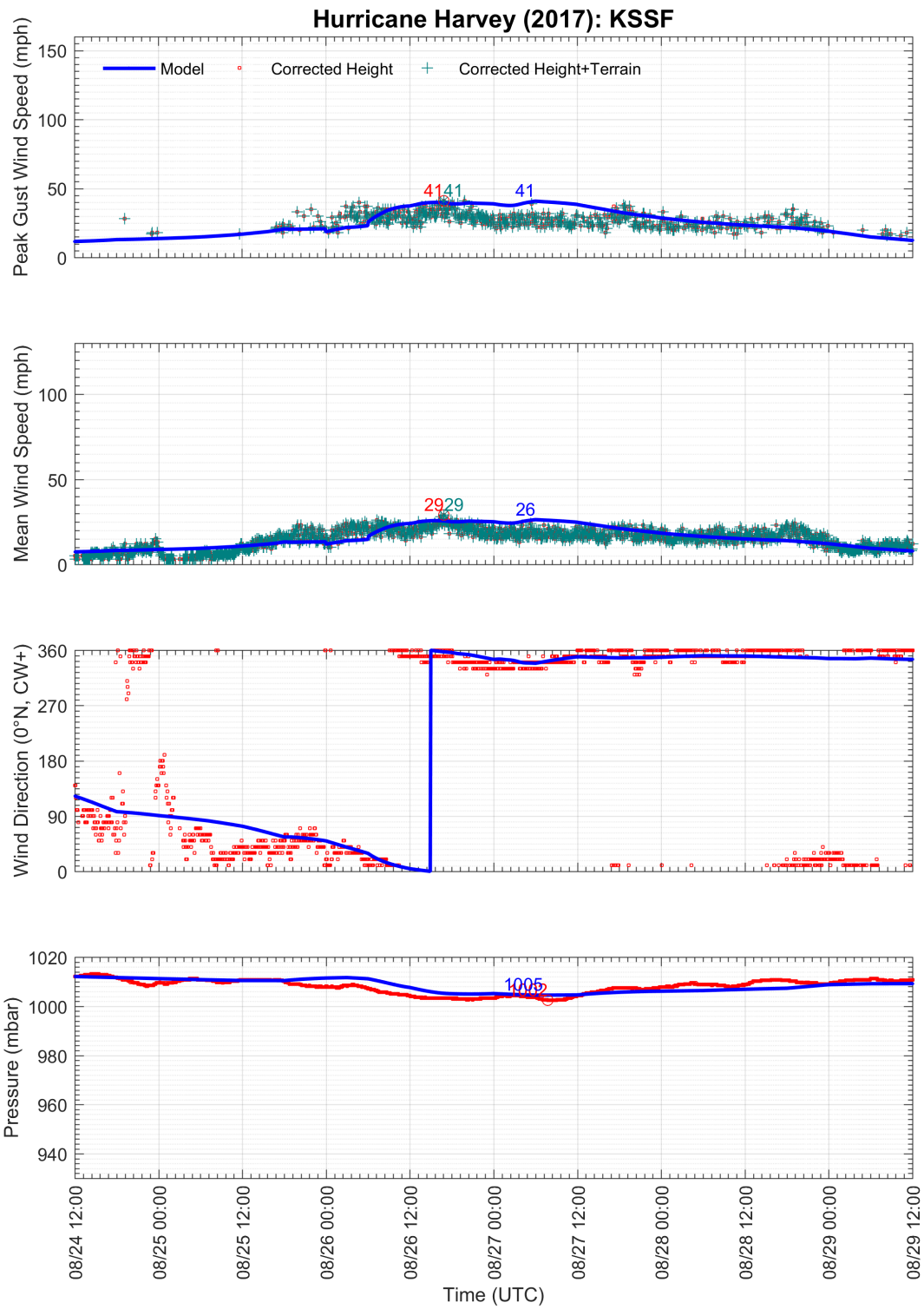


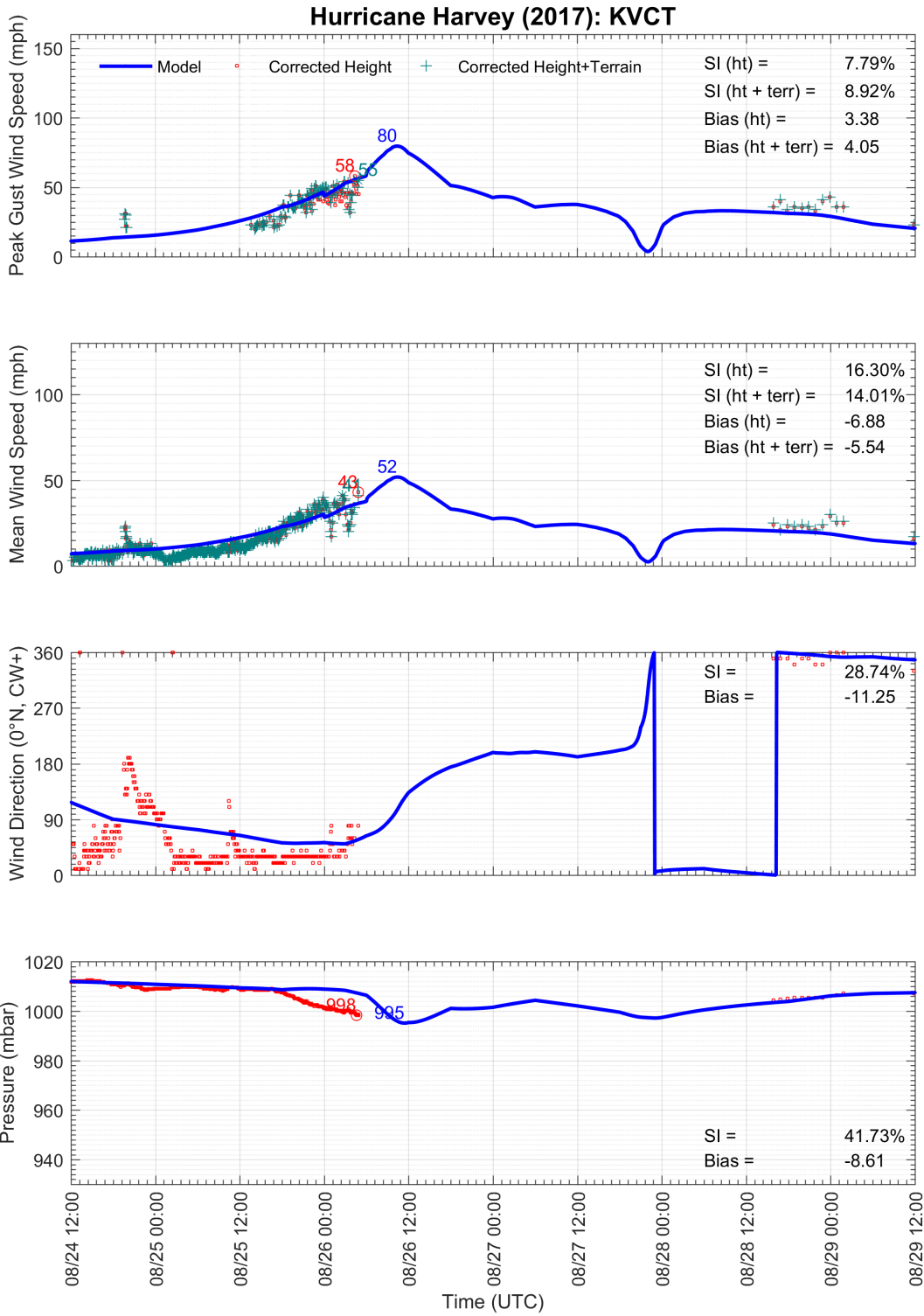


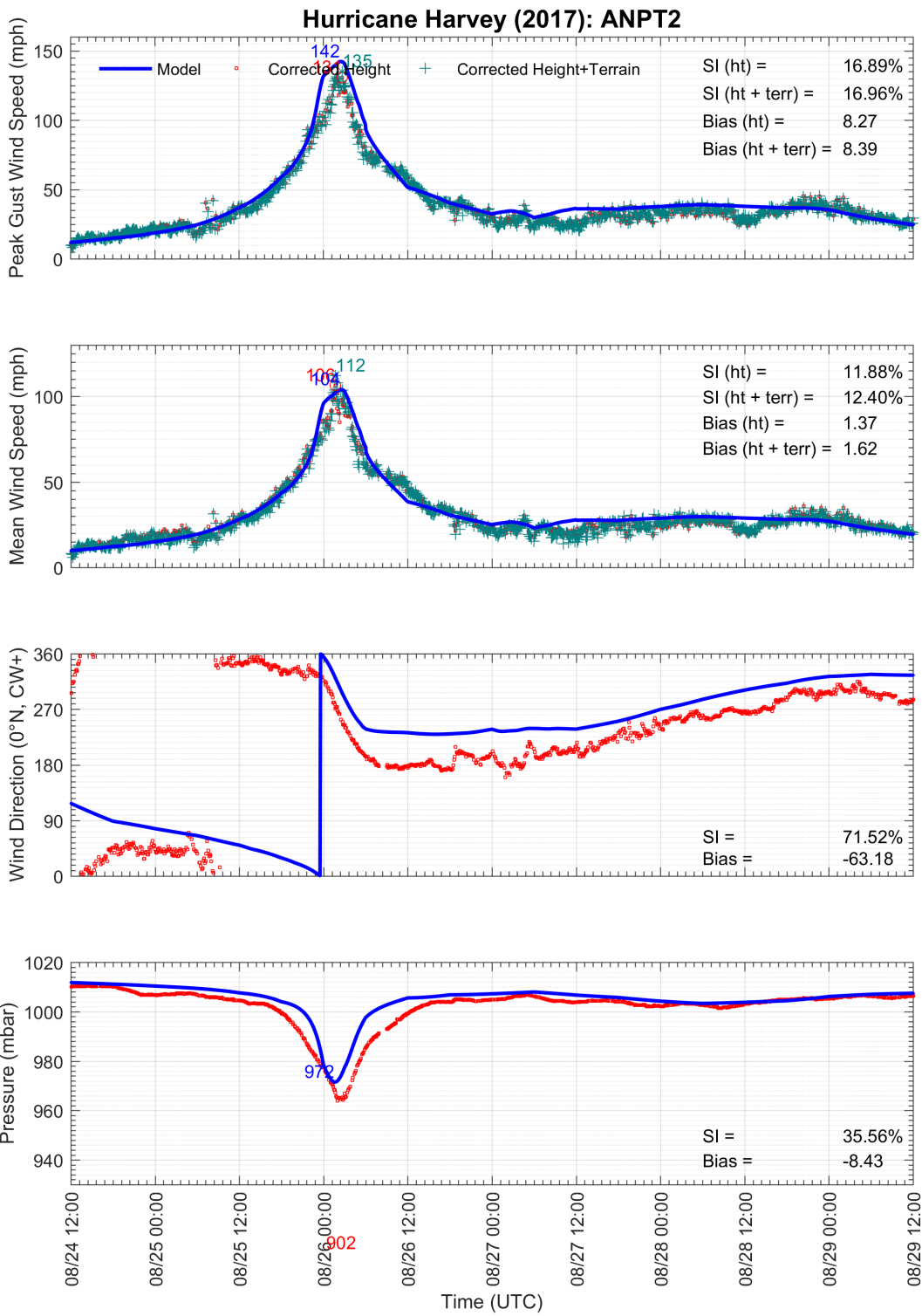


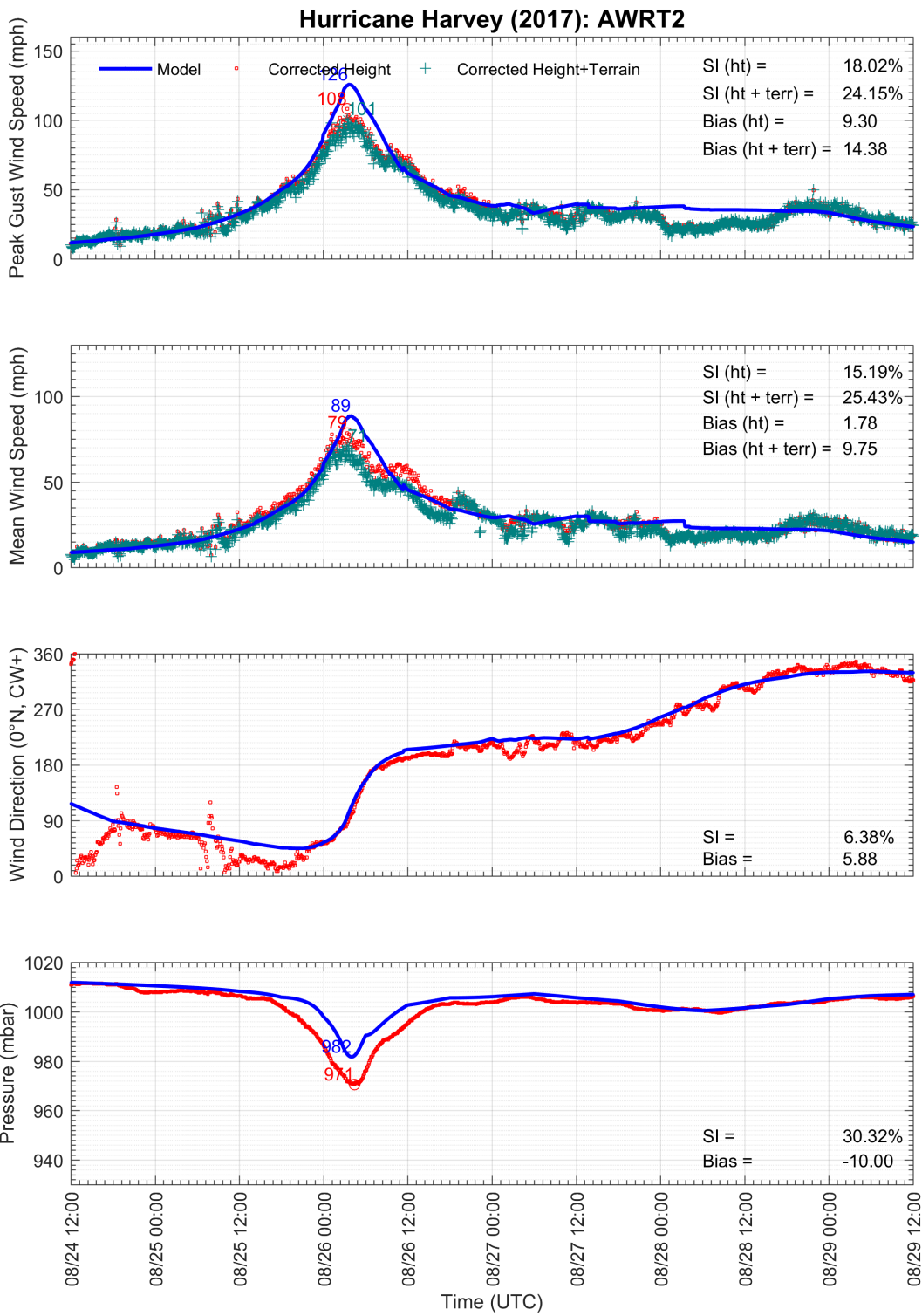


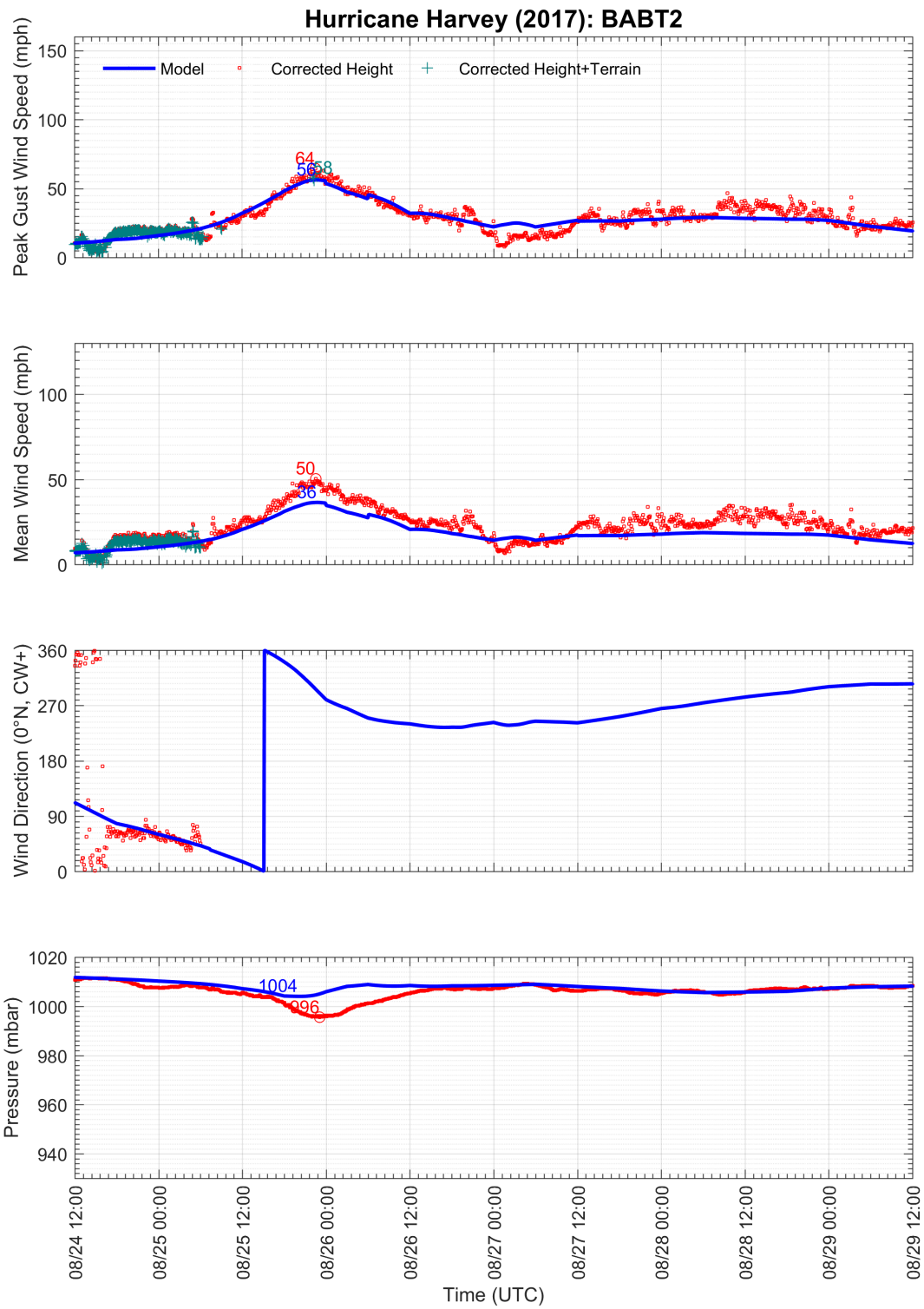


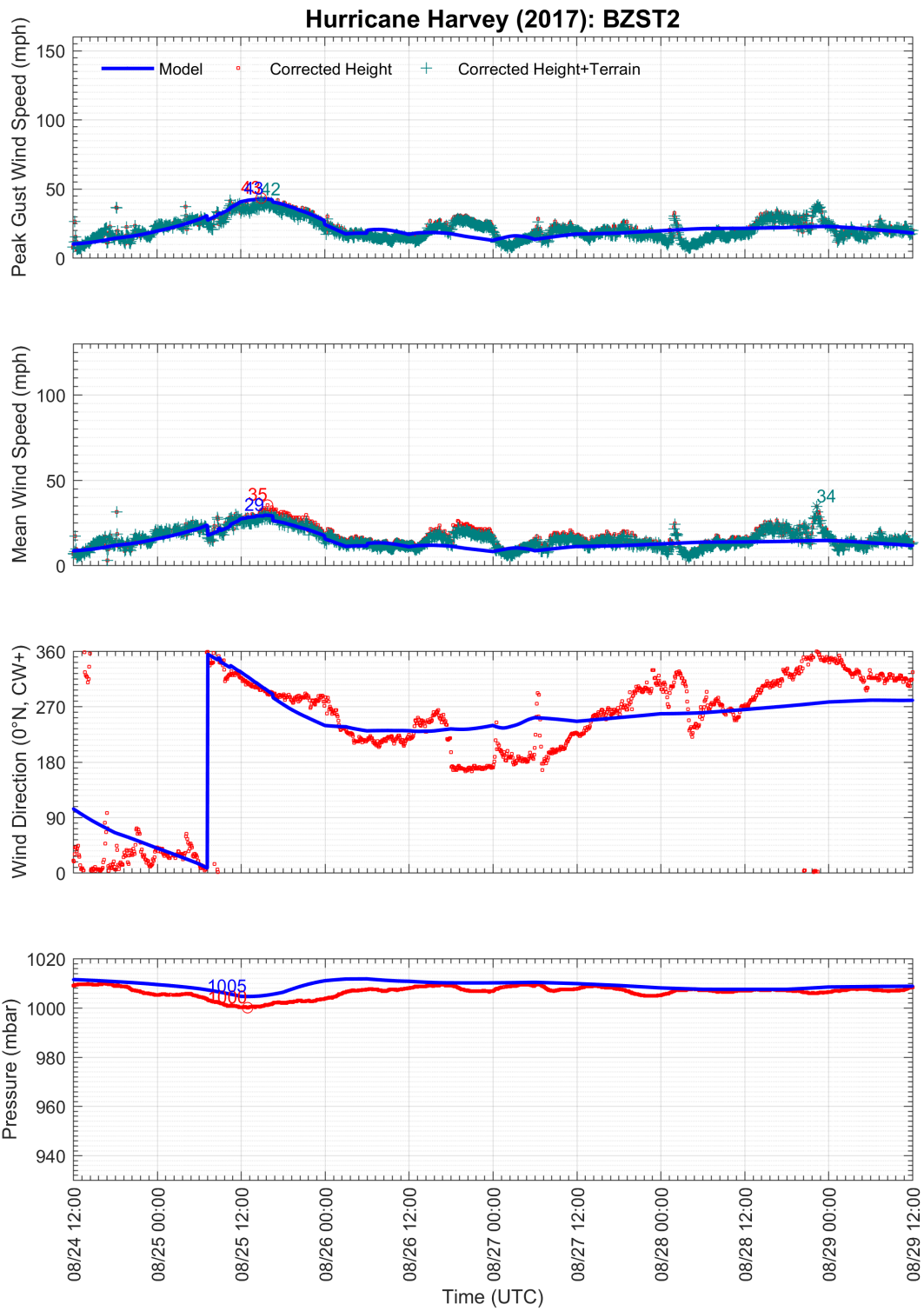


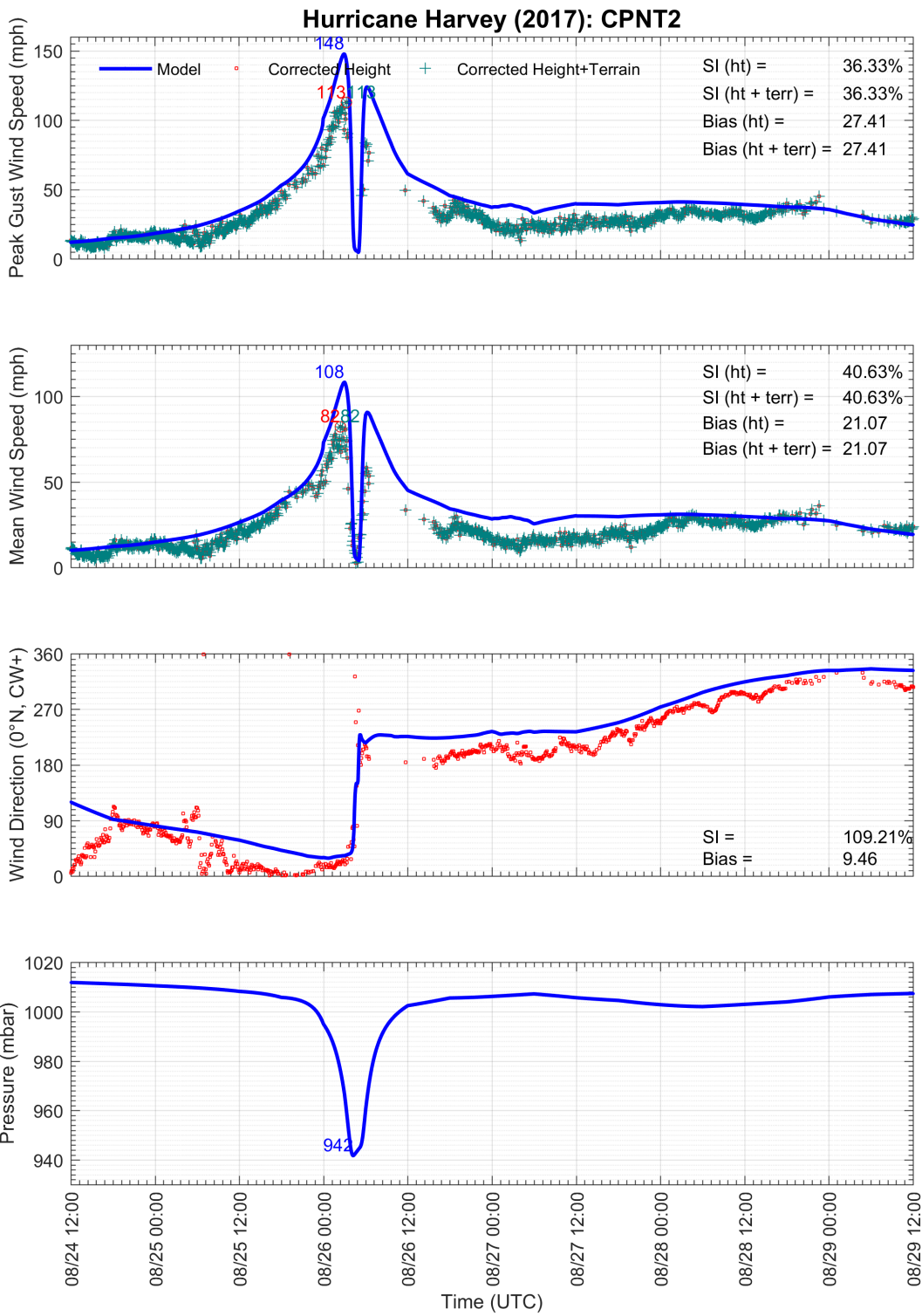


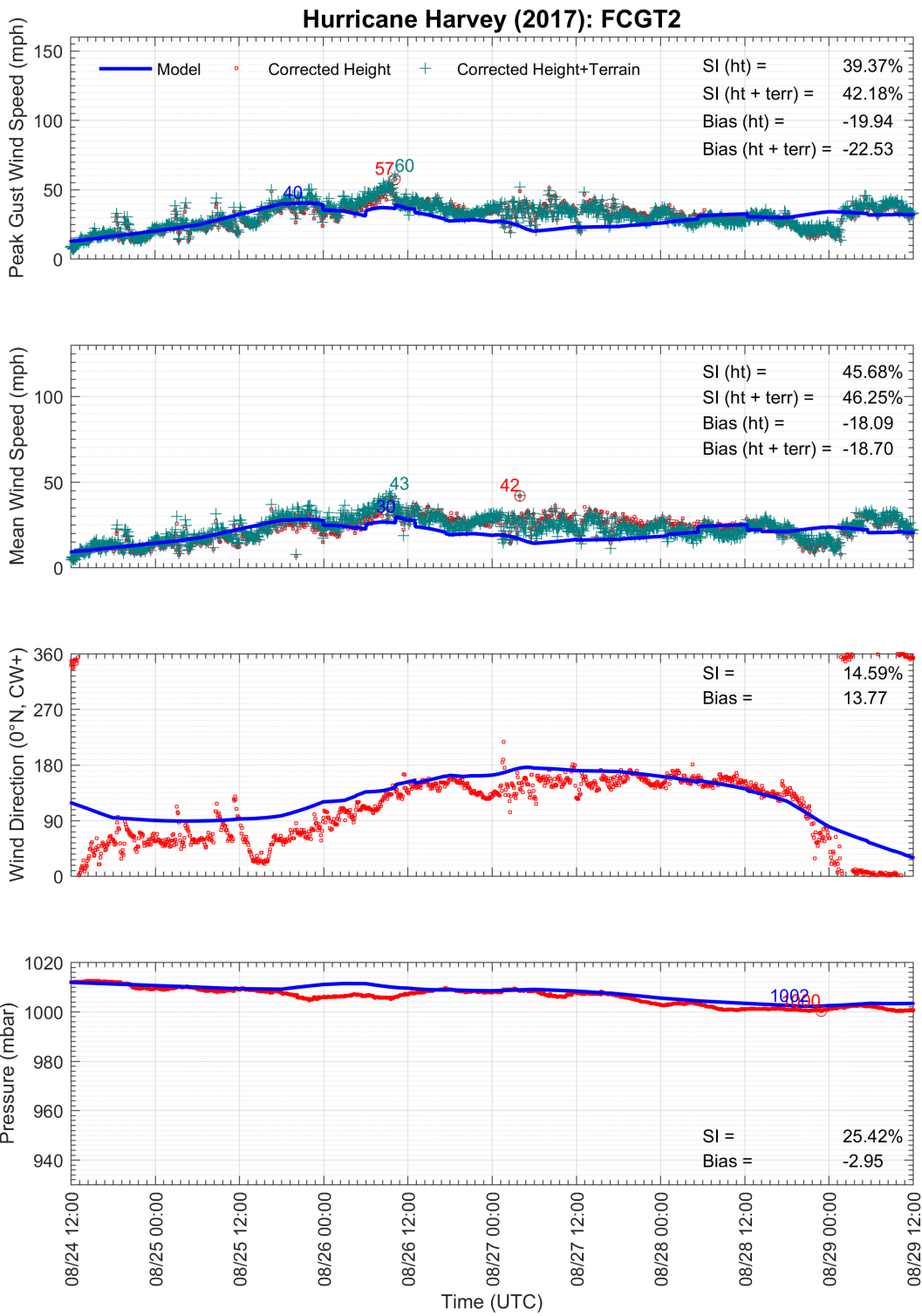


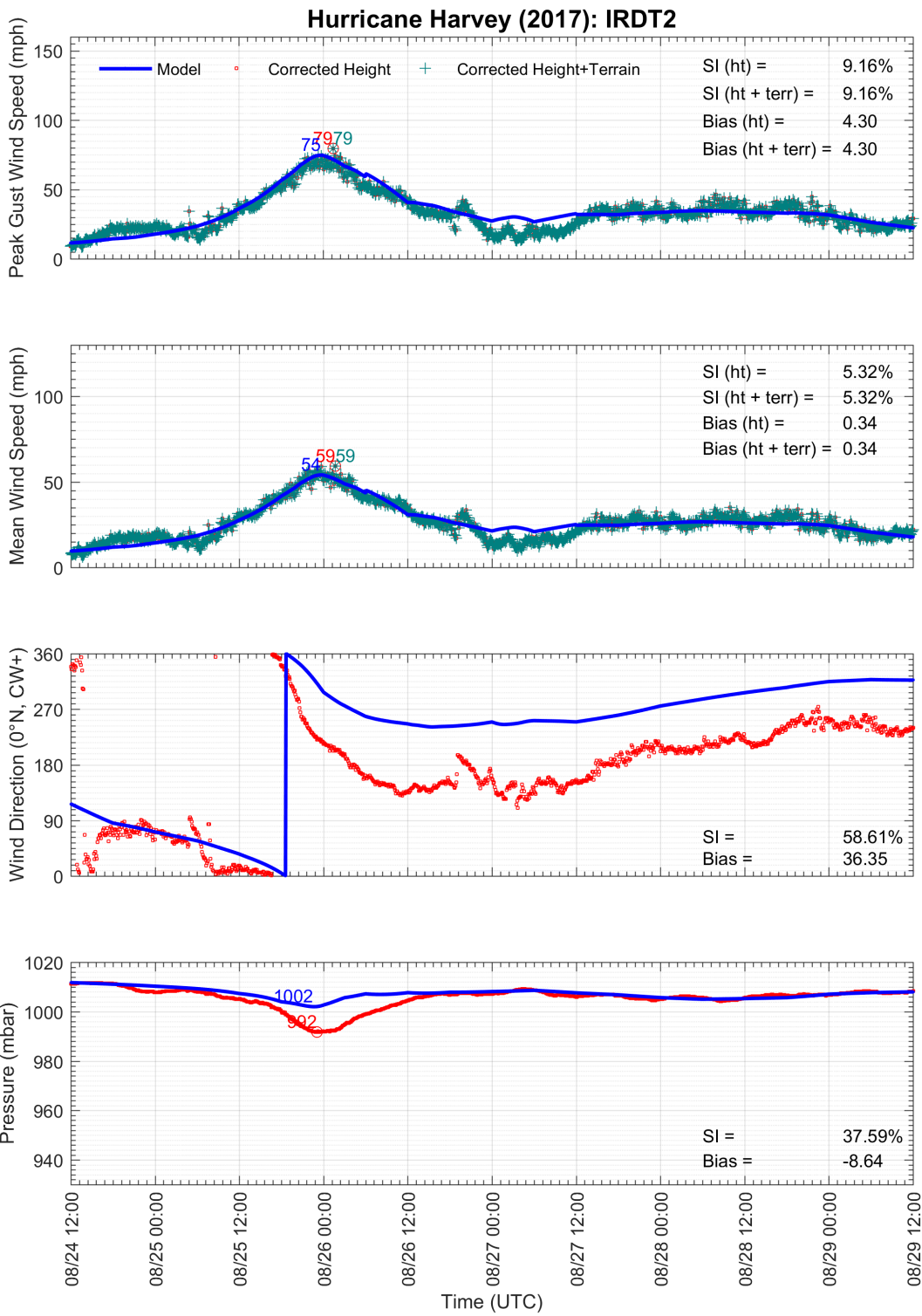


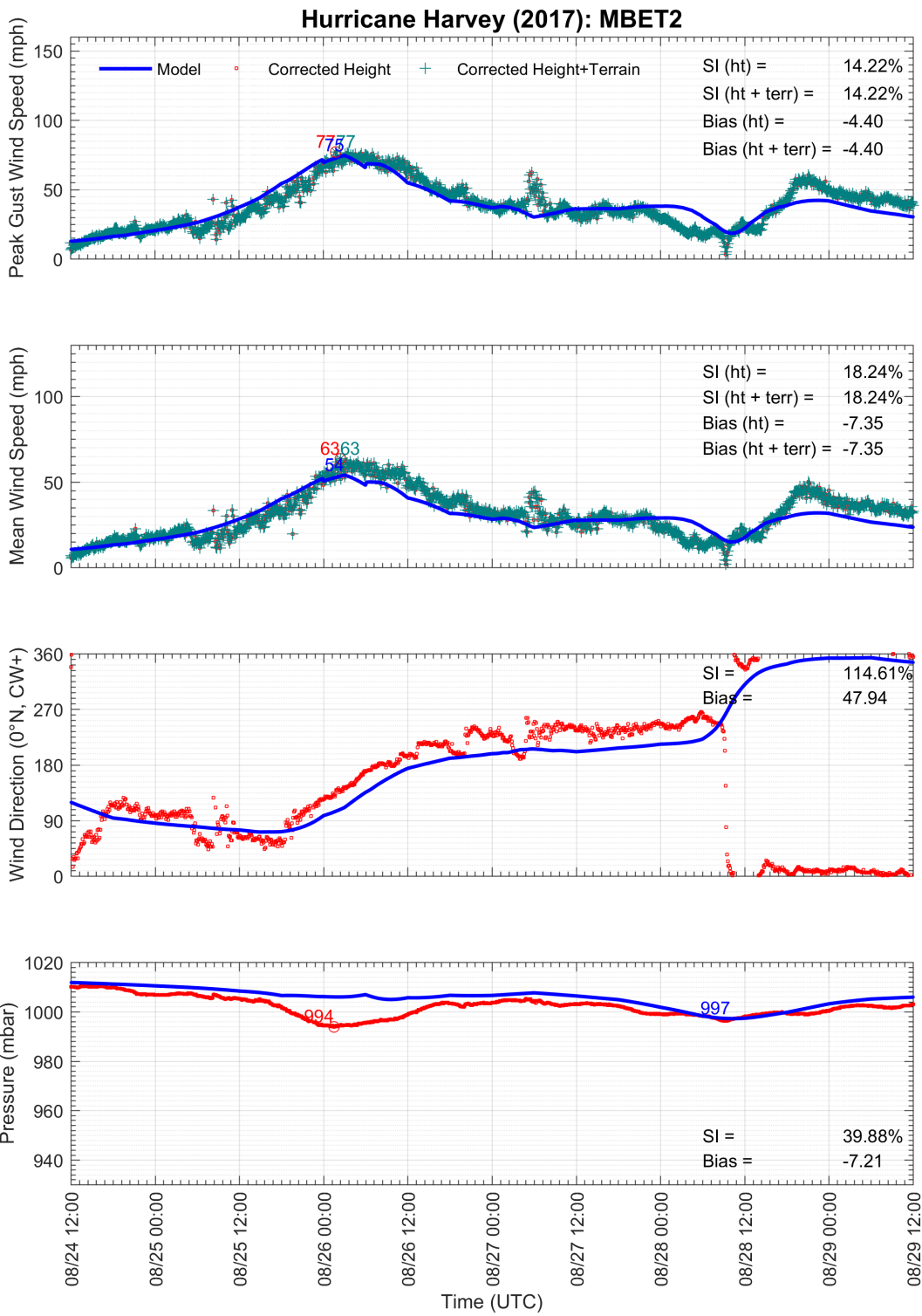


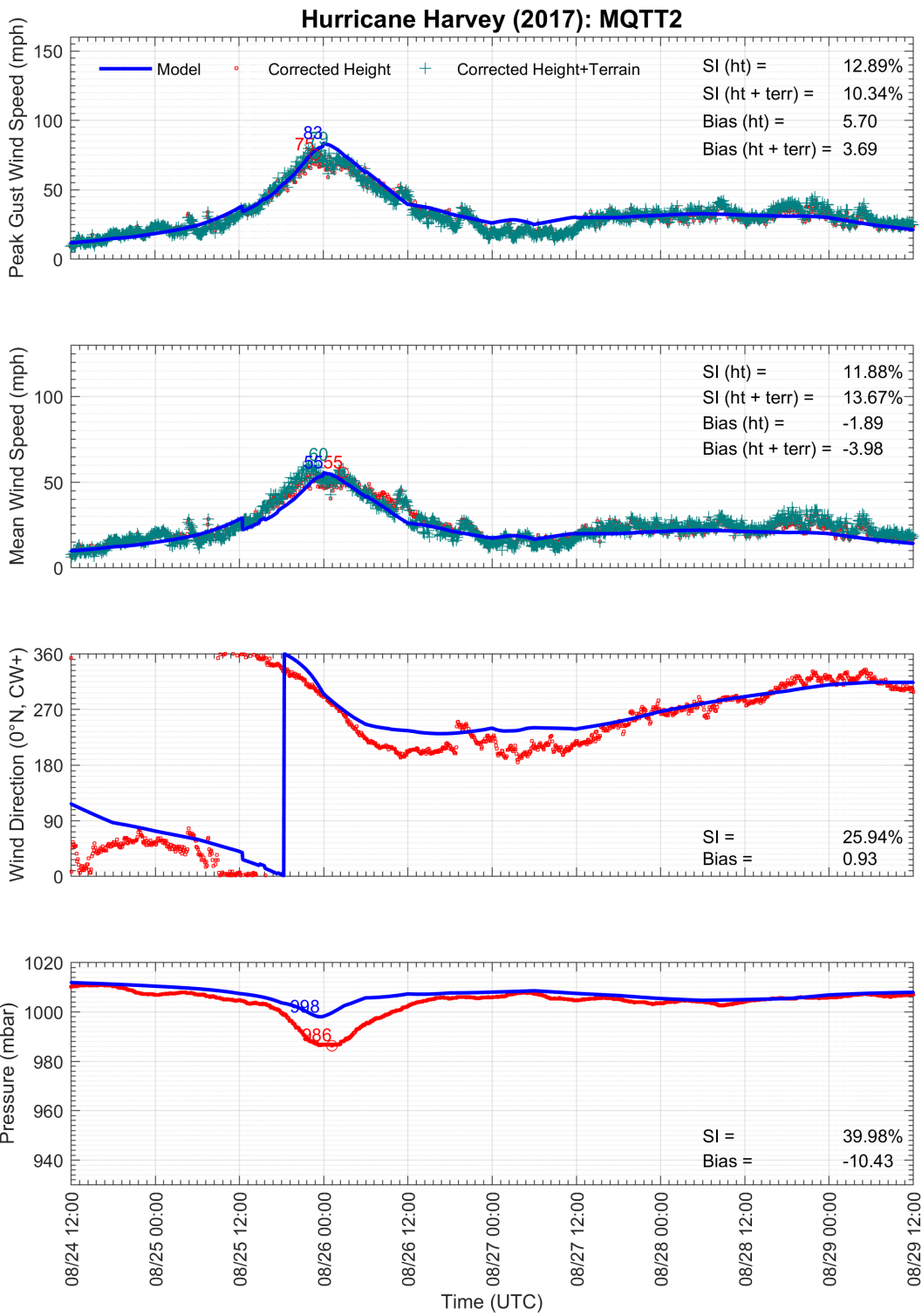


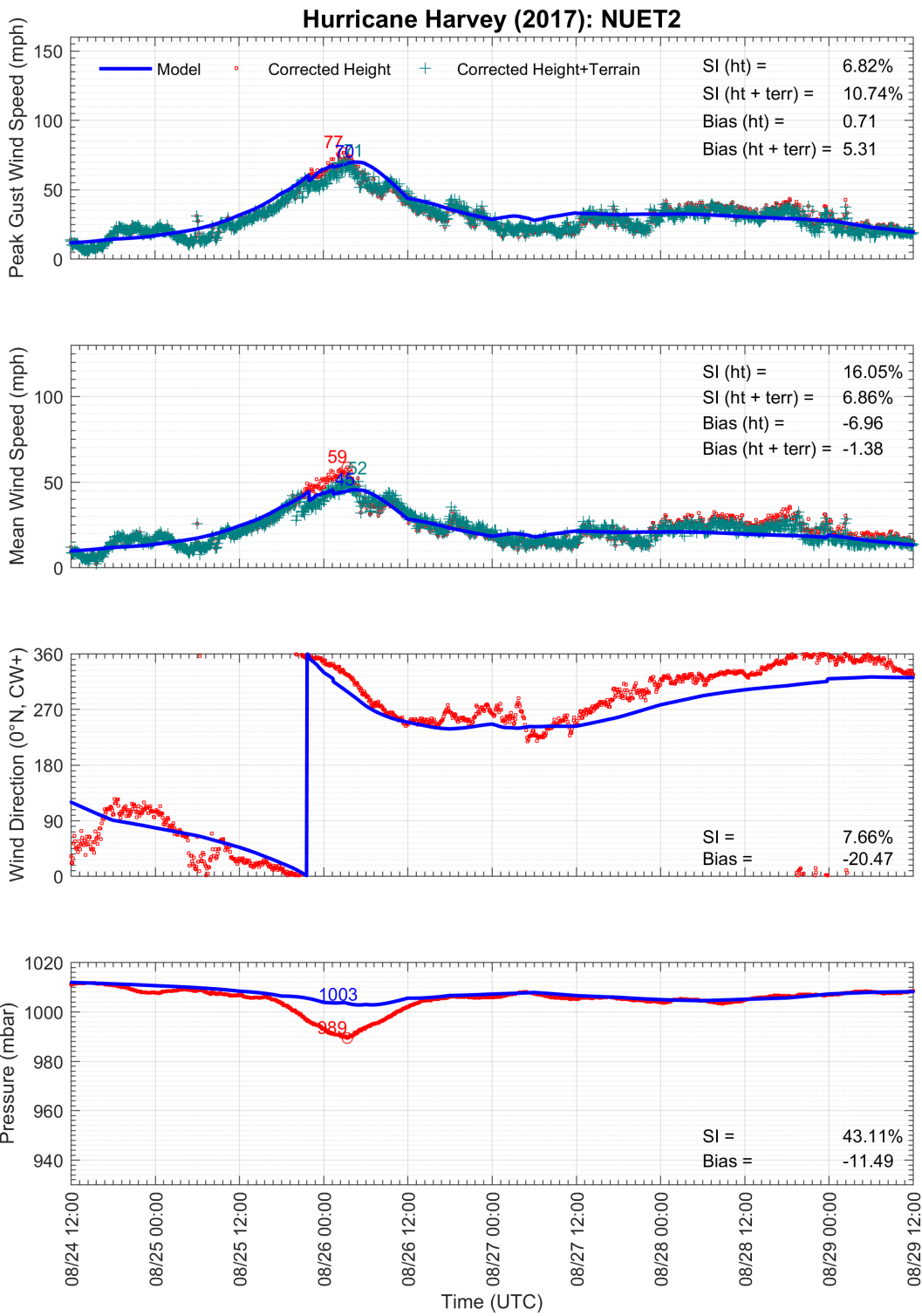


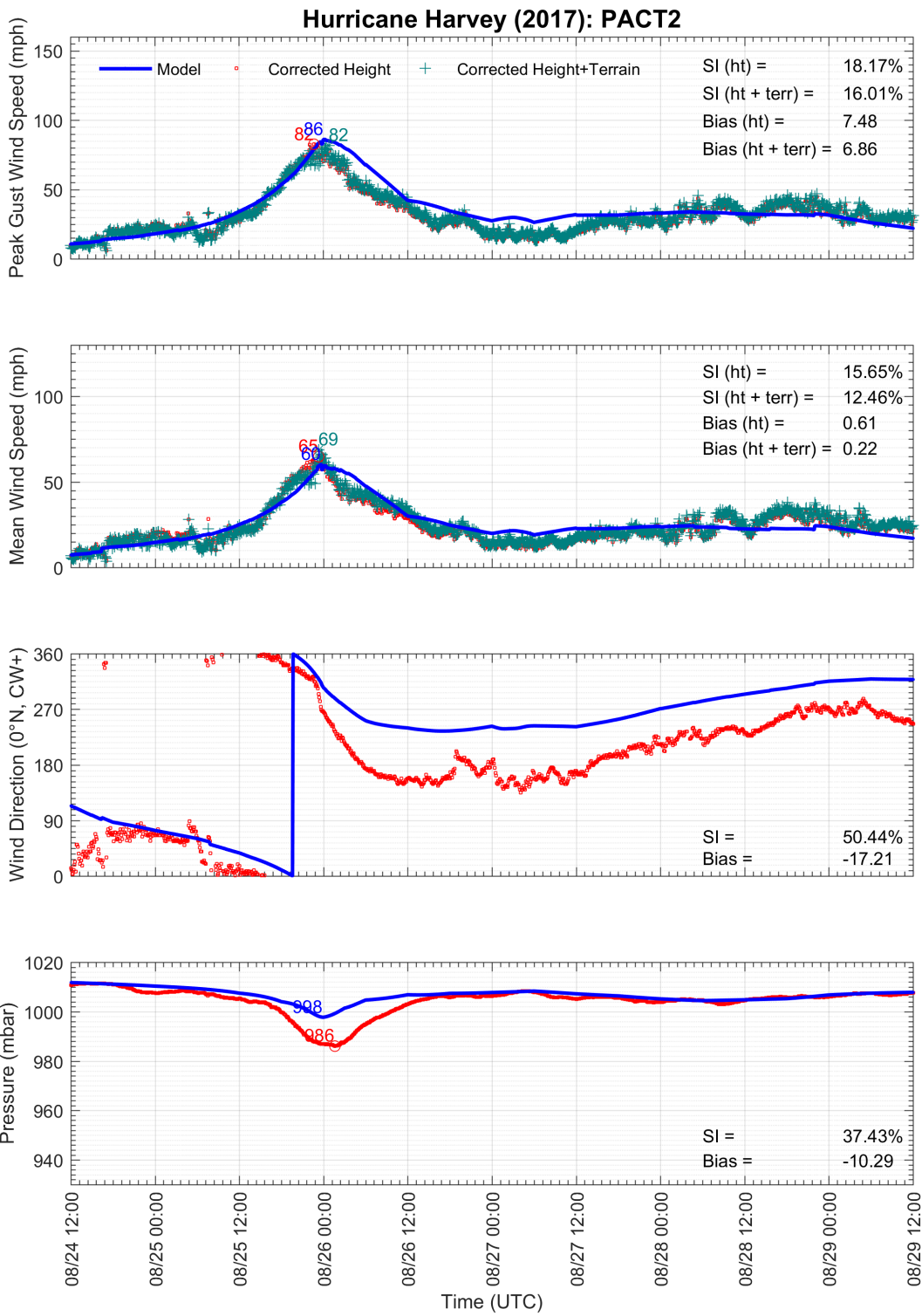


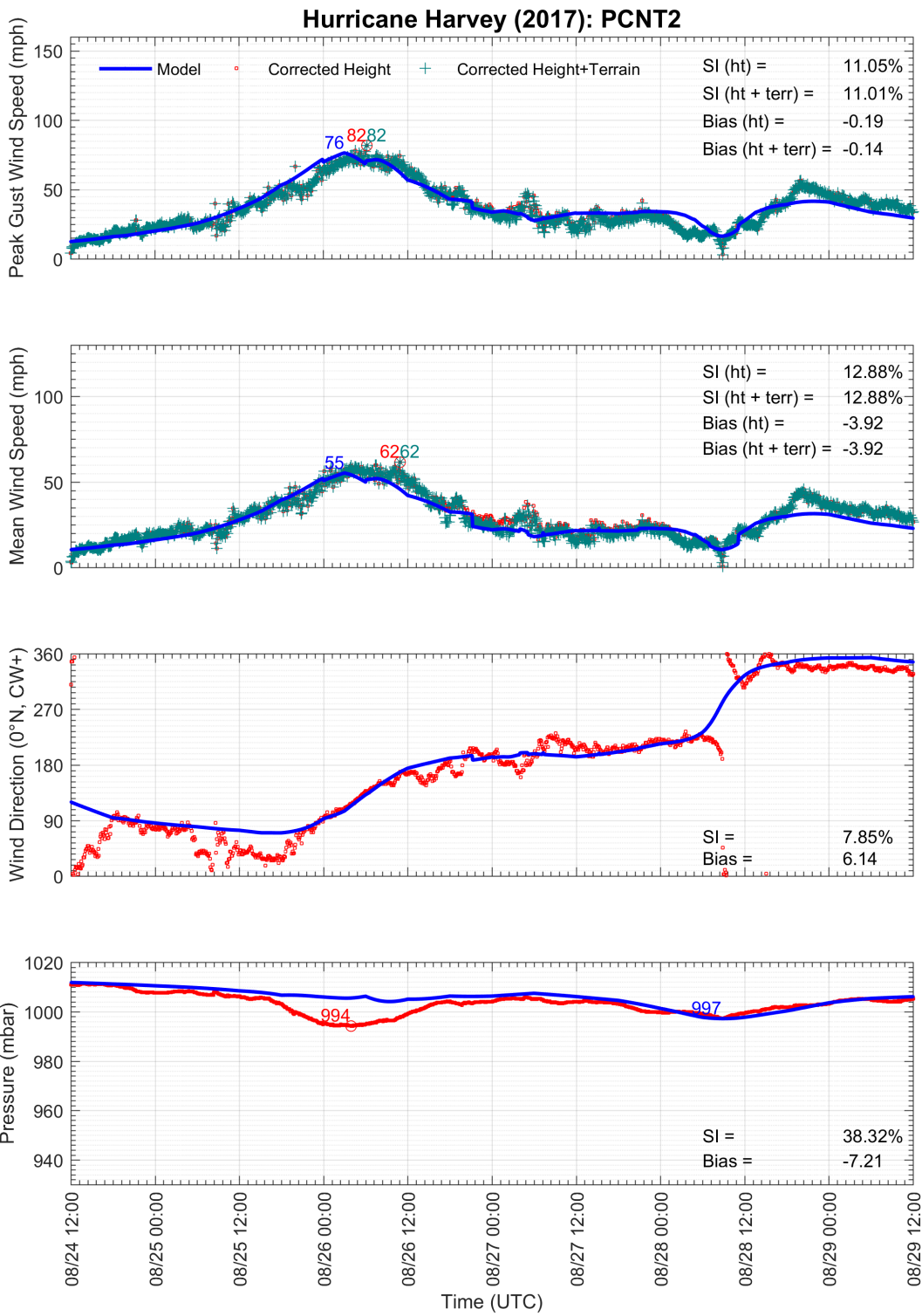


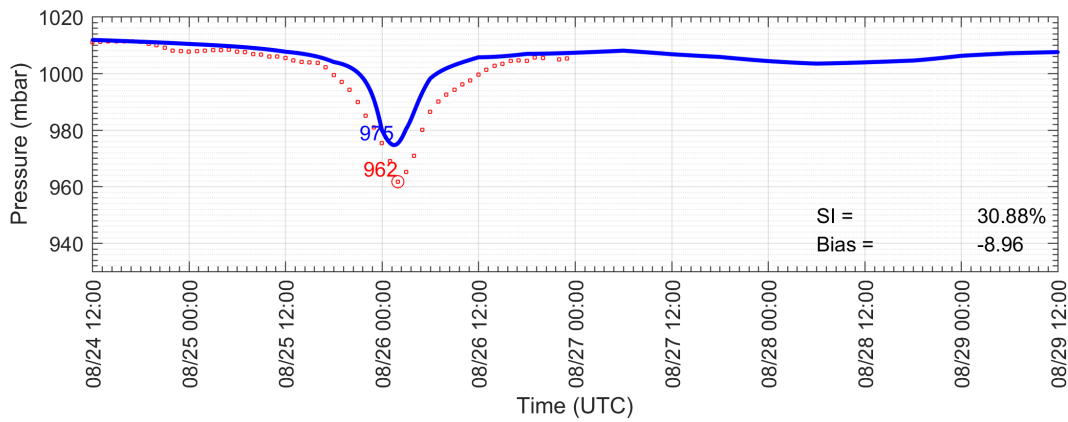
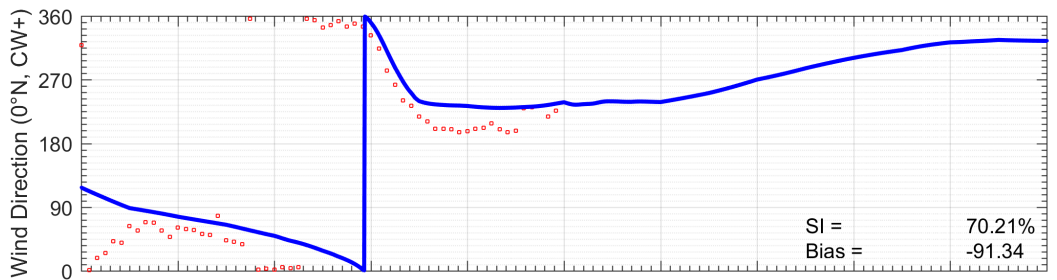
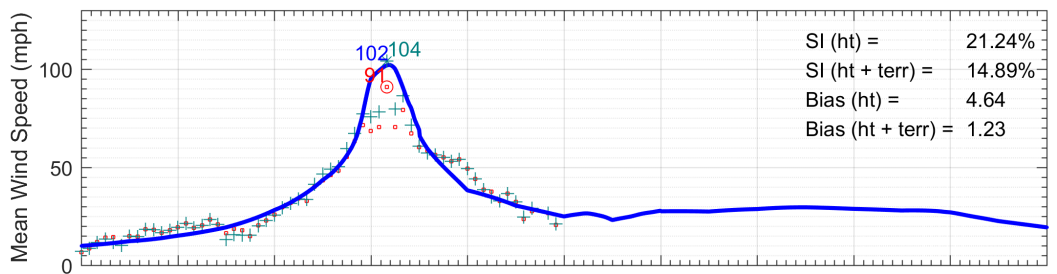
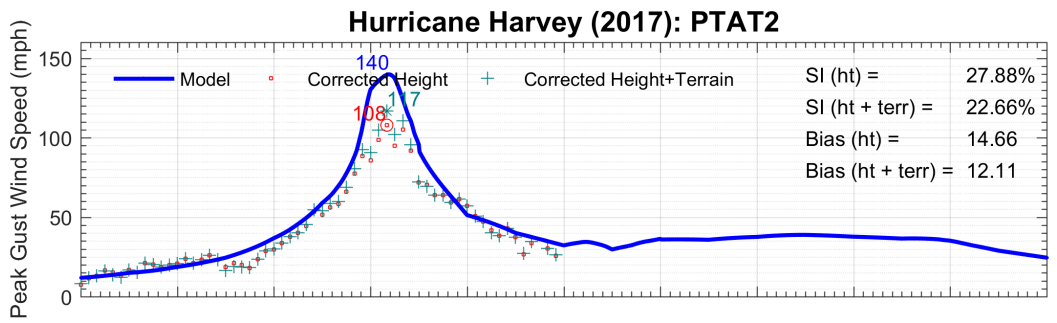


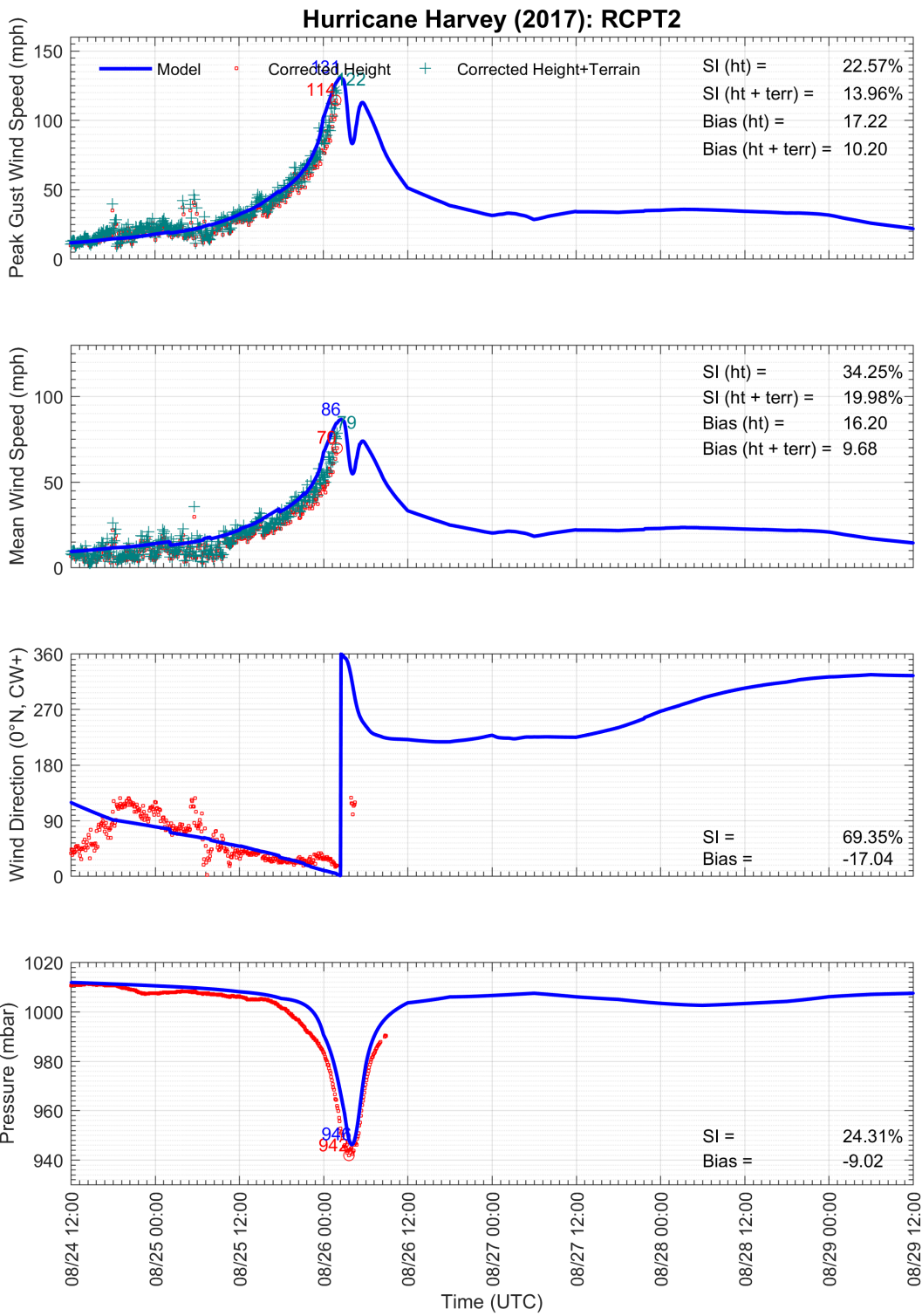


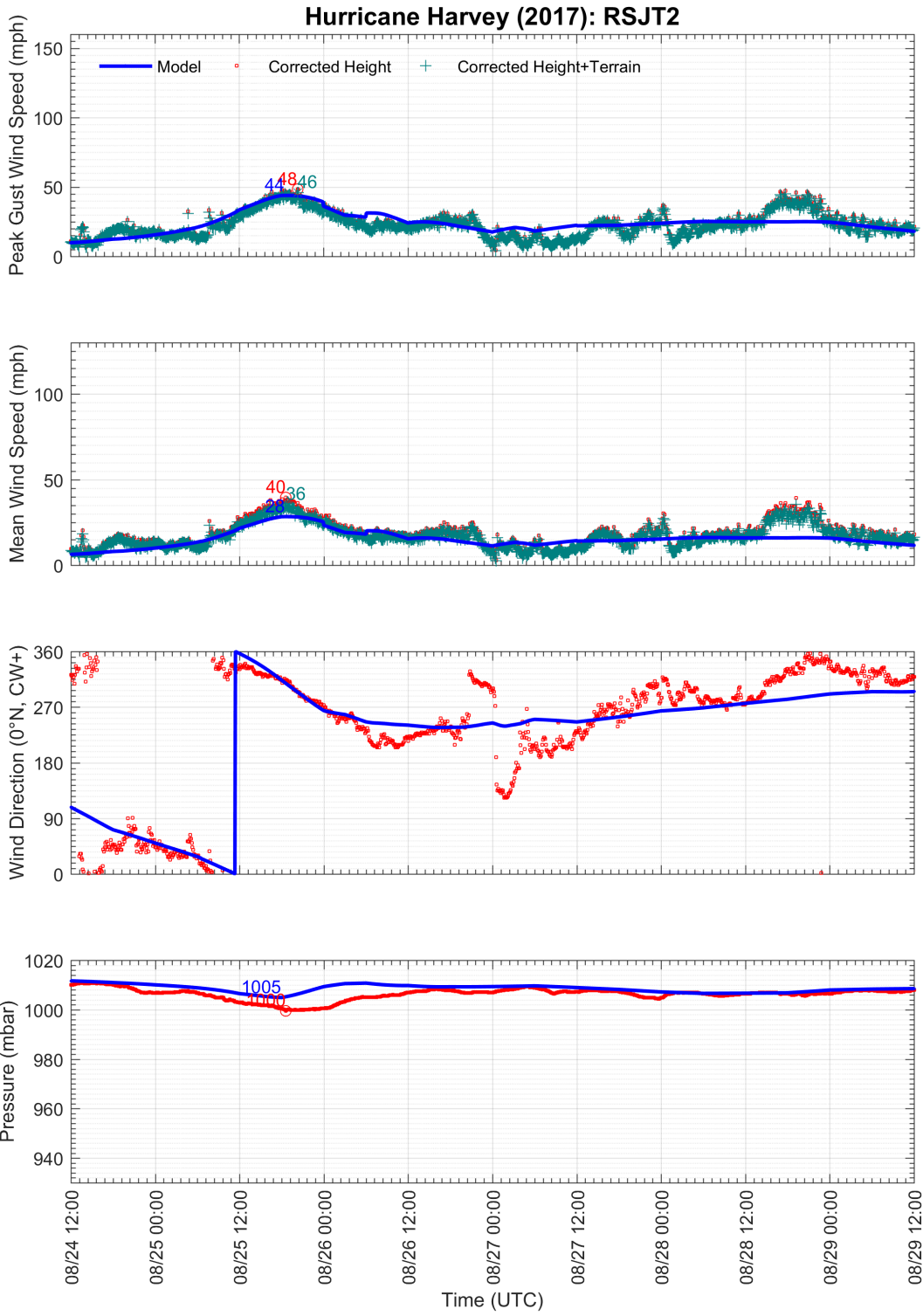


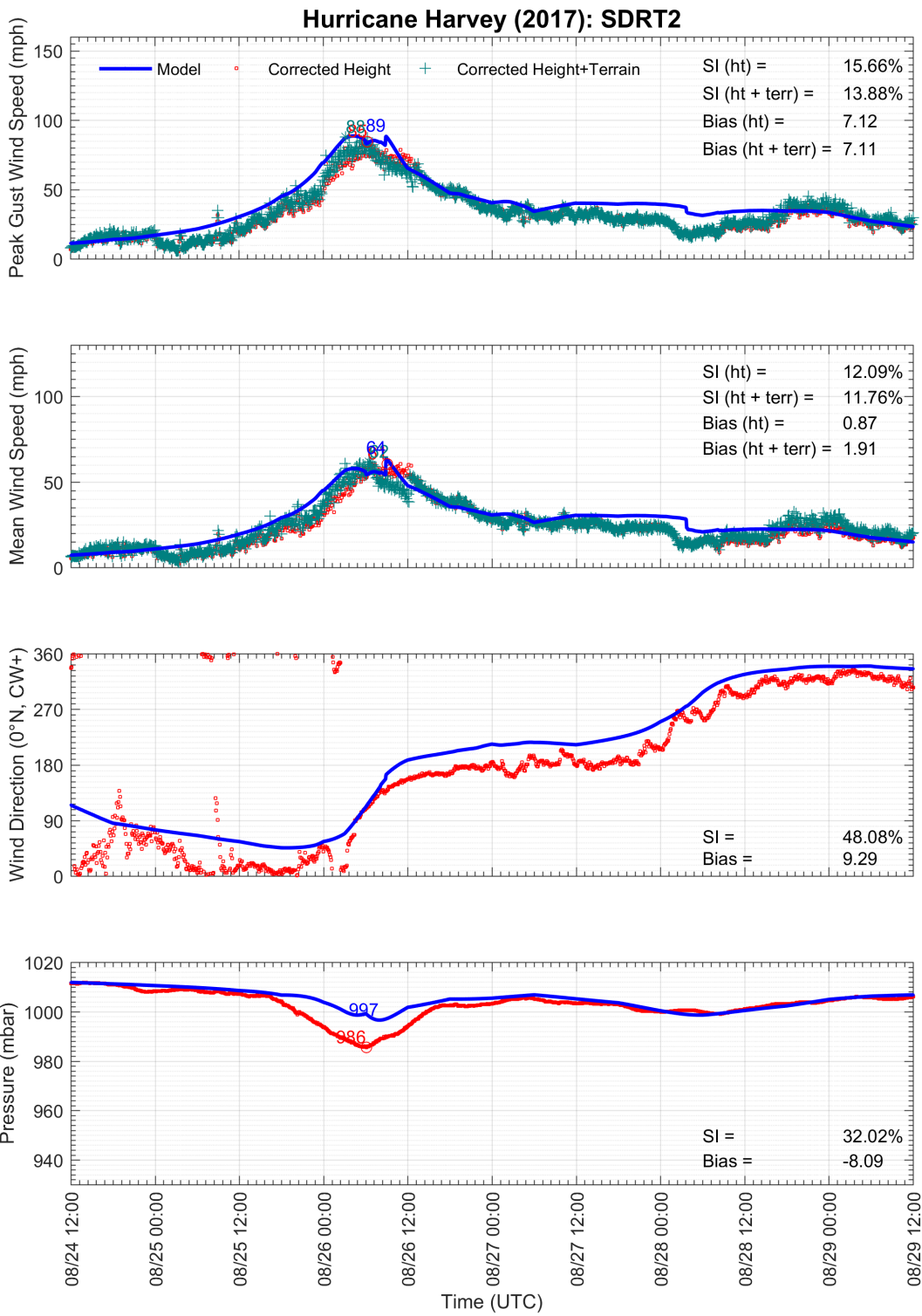


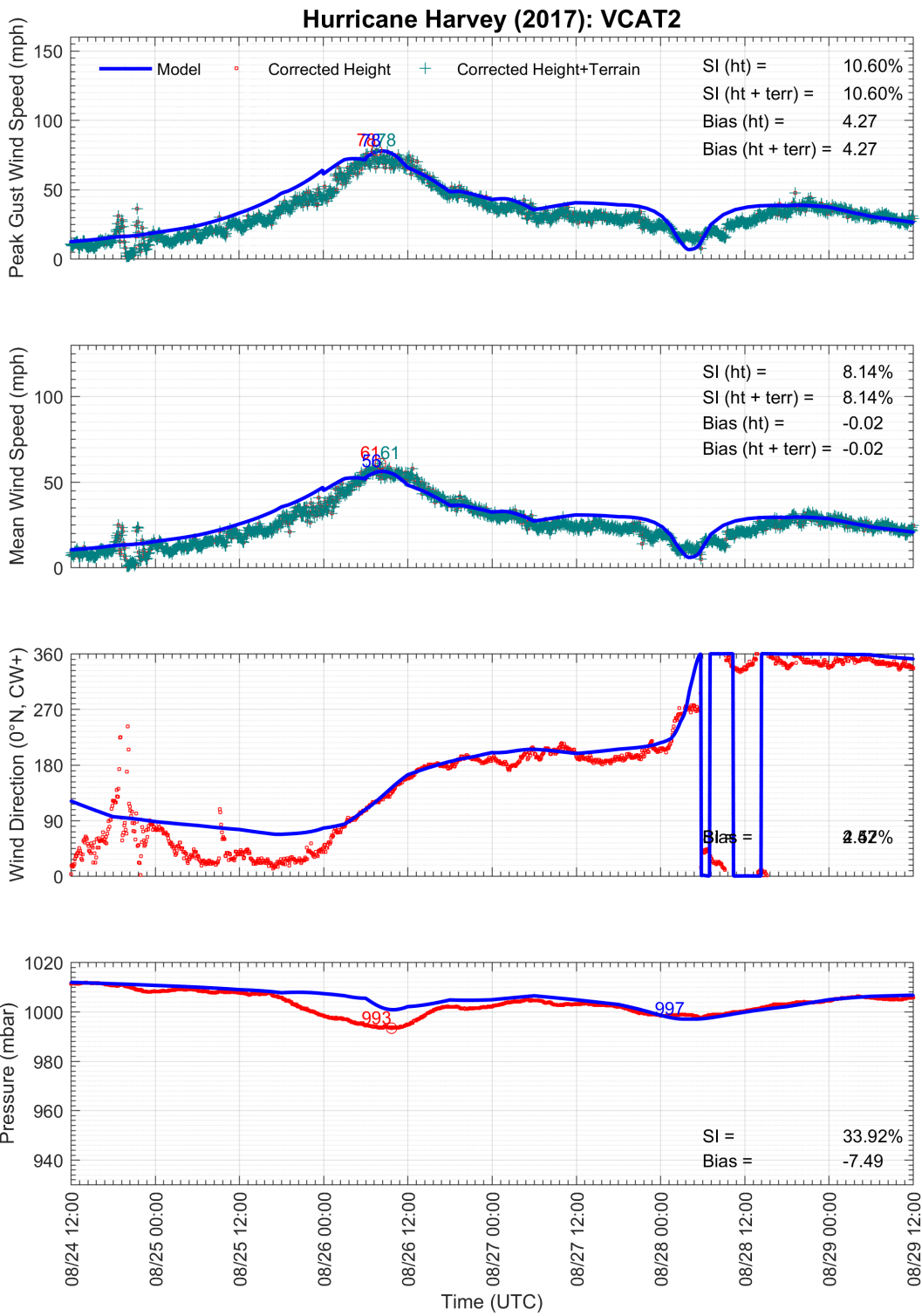


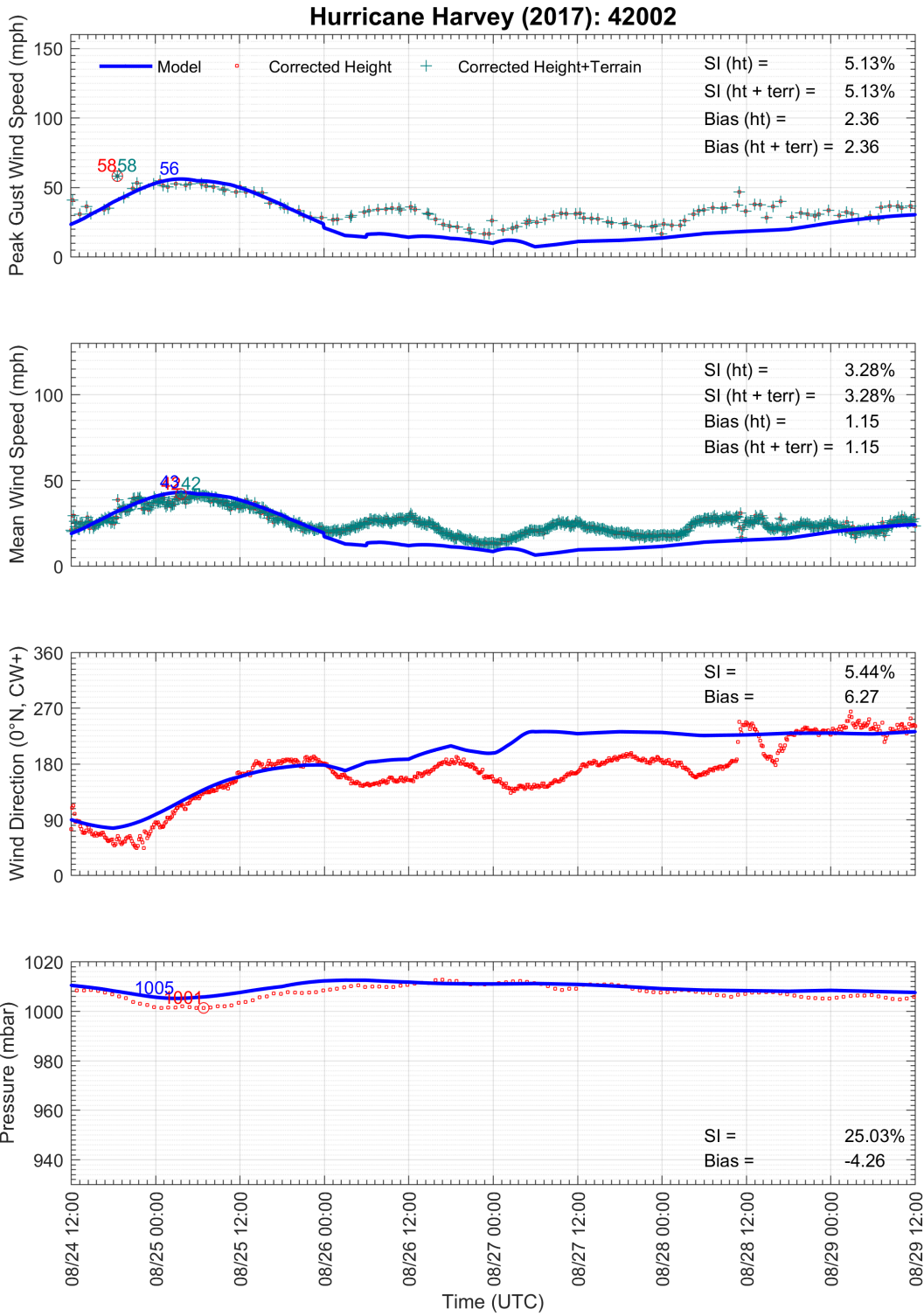


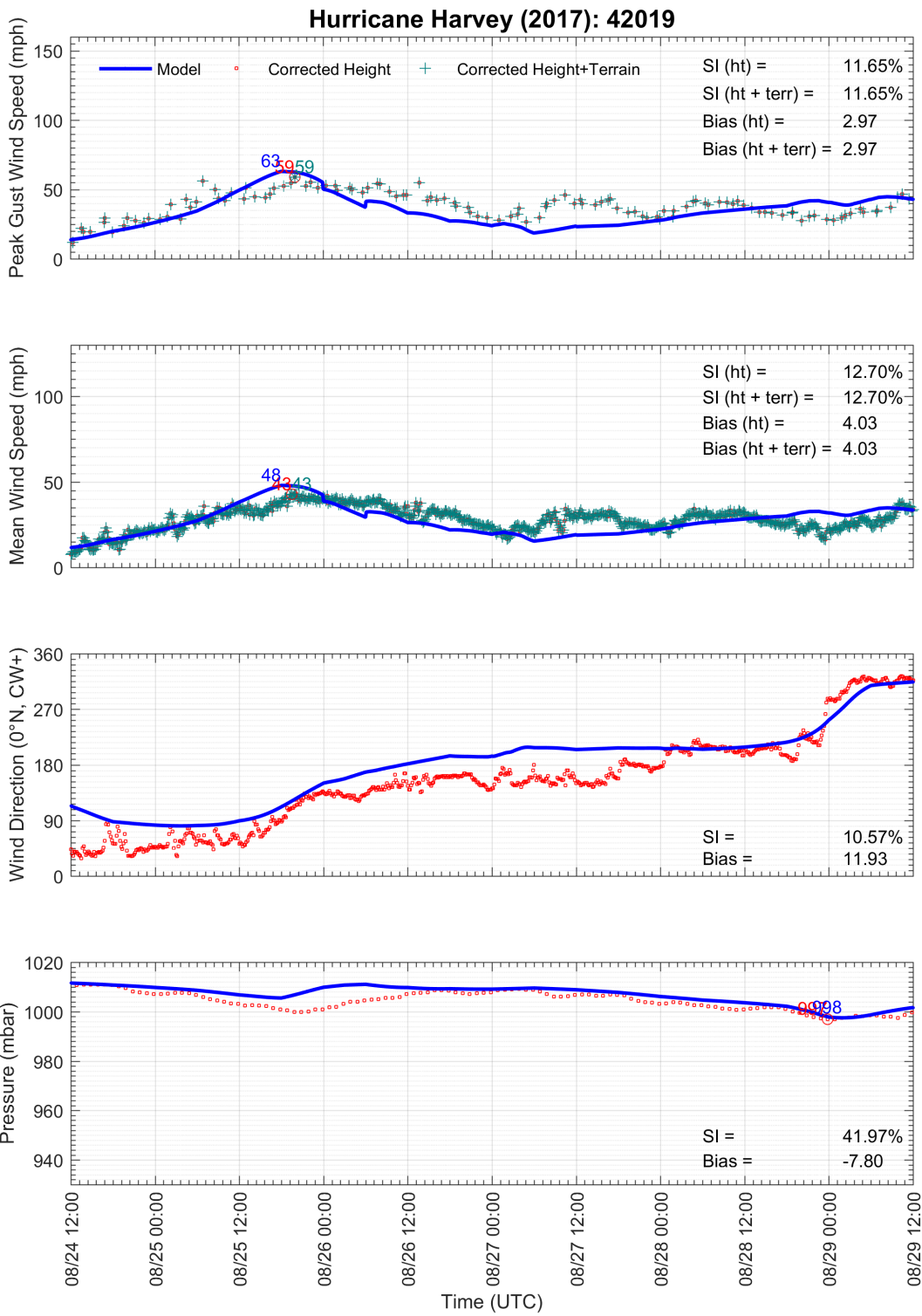


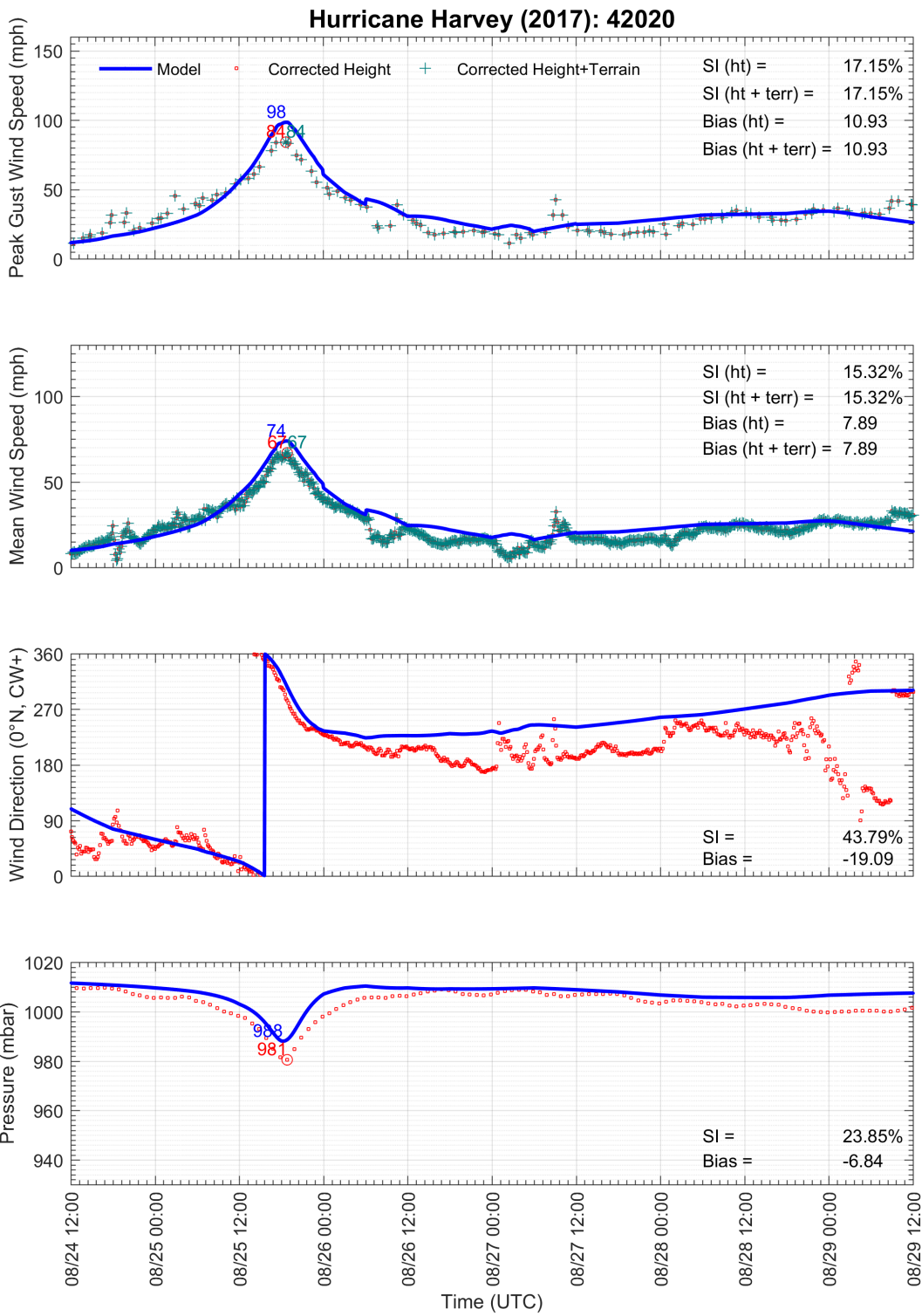


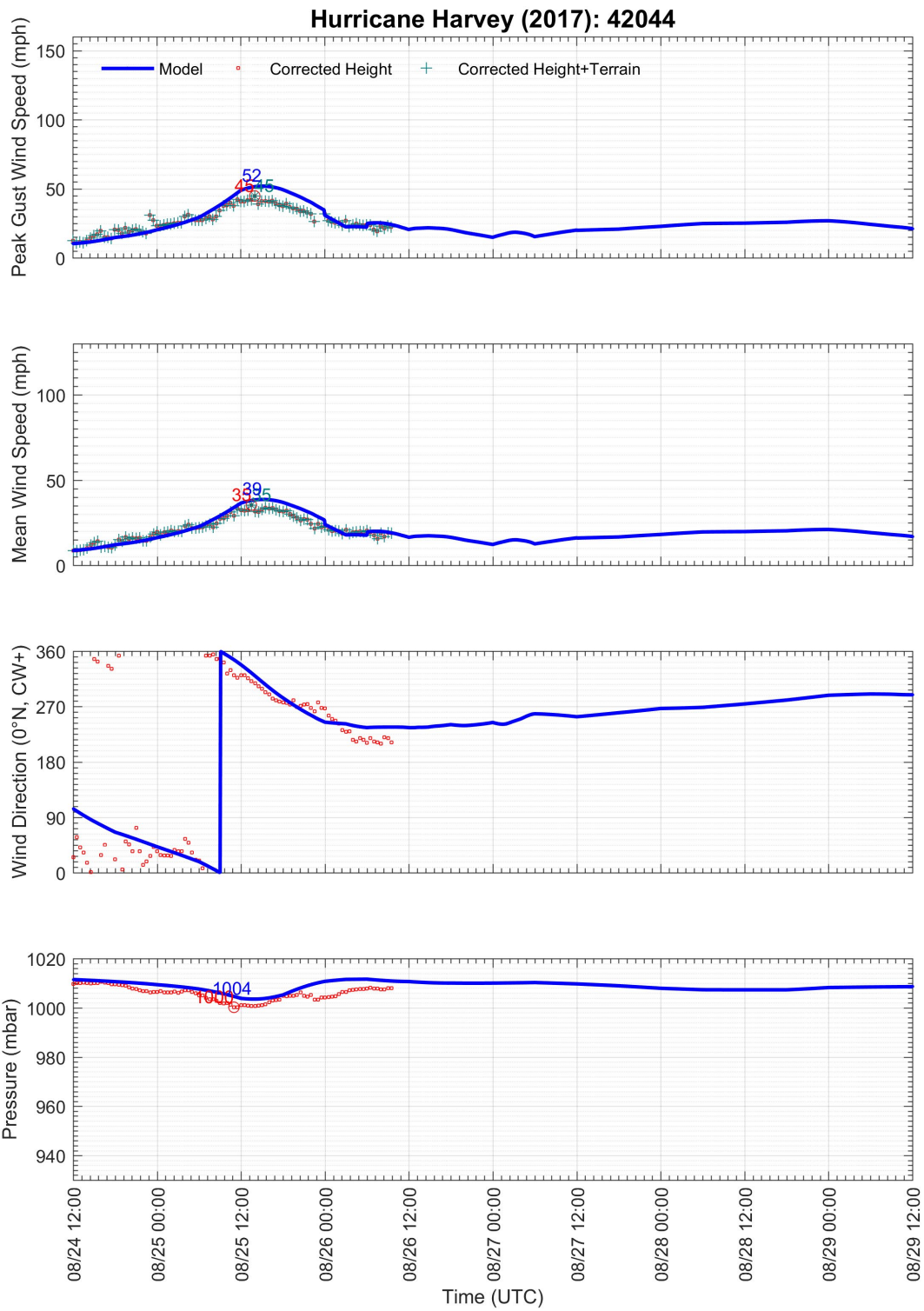


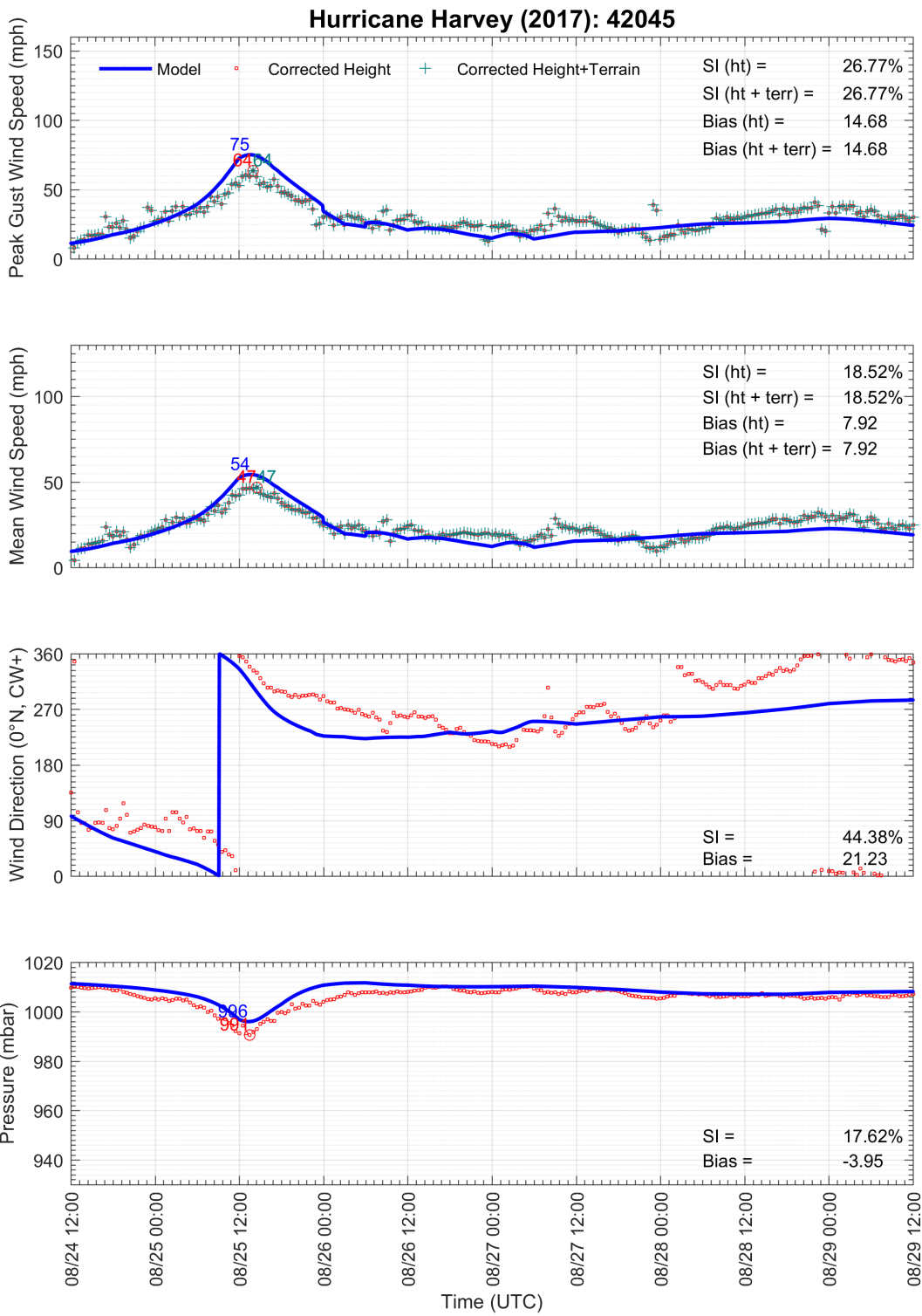












Appendix A.3 STATION DIRECTIONAL SURFACE ROUGHNESS VALUES

Station	Direction (0°N, CW+)															
	0	22.5	45	67.5	90	112.5	135	157.5	180	202.5	225	247.5	270	292.5	315	337.5
KALI	0.0449	0.0345	0.0344	0.0486	0.0489	0.0403	0.0346	0.0530	0.0741	0.0665	0.1004	0.1100	0.0456	0.0535	0.0315	0.0363
KATT	0.3000	0.3000	0.3000	0.3000	0.3000	0.3000	0.3000	0.3000	0.3000	0.3000	0.3000	0.3000	0.3000	0.3000	0.3000	0.3000
KAUS	0.0300	0.0300	0.0300	0.0300	0.0300	0.0300	0.0300	0.0300	0.0300	0.1000	0.1000	0.1000	0.1000	0.1000	0.1000	0.1000
KBAZ	0.0300	0.0300	0.0300	0.0300	0.0300	0.0300	0.0300	0.0300	0.0300	0.0300	0.0300	0.0300	0.0300	0.0300	0.0300	0.0300
KBMQ	0.3000	0.1000	0.1000	0.0500	0.1000	0.1000	0.1000	0.1000	0.0500	0.1000	0.0300	0.0500	0.0500	0.1000	0.1000	0.2000
KBRO	0.1910	0.1967	0.1066	0.0521	0.0456	0.0291	0.0203	0.0130	0.0093	0.0128	0.0357	0.0599	0.0431	0.0440	0.1055	0.0911
KCLL	0.0300	0.0300	0.0300	0.0300	0.0300	0.0300	0.0300	0.0300	0.0300	0.0300	0.0300	0.0300	0.0300	0.0300	0.0300	0.0300
KCOT	0.0300	0.0300	0.0300	0.0300	0.0300	0.0300	0.0300	0.0300	0.0300	0.0300	0.0300	0.0300	0.0300	0.0300	0.0300	0.0300
KCRP	0.0063	0.0057	0.0040	0.0071	0.0105	0.0114	0.0128	0.0127	0.0134	0.0120	0.0216	0.0371	0.0393	0.0235	0.0186	0.0076
KHDO	0.0300	0.0300	0.0300	0.0300	0.0300	0.0300	0.0300	0.0300	0.0300	0.0300	0.0300	0.0300	0.0300	0.0300	0.0300	0.0300
KHRL	0.0134	0.0169	0.0263	0.0202	0.0200	0.0145	0.0095	0.0122	0.0168	0.0144	0.0180	0.0404	0.0647	0.0544	0.0110	0.0085
KLBX	0.0508	0.0424	0.0734	0.1580	0.2118	0.1790	0.0890	0.0577	0.0225	0.0484	0.3007	0.6871	0.9999	0.9999	0.8585	0.5007
KMFE	0.0552	0.0755	0.1415	0.1271	0.0603	0.0341	0.0171	0.0319	0.0728	0.2972	0.3500	0.3000	0.3000	0.3896	0.1422	0.0836
KPIL	0.0330	0.0449	0.0619	0.0492	0.0235	0.0090	0.0104	0.0203	0.0535	0.1069	0.1085	0.0723	0.1899	0.1192	0.0090	0.0044
KPSX	0.0184	0.0173	0.0156	0.0147	0.0212	0.0179	0.0143	0.0153	0.0366	0.0378	0.0770	0.1219	0.1385	0.0855	0.0459	0.0192
KRKP	0.0652	0.0661	0.0355	0.0133	0.0123	0.0112	0.0177	0.1672	0.6075	0.9983	0.9999	1.0000	0.6472	0.7571	0.1180	0.0272
KSAT	0.0300	0.0300	0.0300	0.0300	0.0300	0.0300	0.0300	0.0300	0.0300	0.0300	0.0300	0.0300	0.0300	0.0300	0.0300	0.0300
KSSF	0.0300	0.0300	0.0300	0.0300	0.0300	0.0300	0.0300	0.0300	0.0300	0.0300	0.0300	0.0300	0.0300	0.0300	0.0300	0.0300
KVCT	0.0534	0.0449	0.0240	0.0199	0.0210	0.0341	0.0245	0.0125	0.0151	0.0239	0.0263	0.0453	0.0385	0.0423	0.0352	0.0558
ANPT2	0.0300	0.0300	0.0000	0.0000	0.0000	0.0000	0.0000	0.0000	0.0000	0.0000	0.0500	0.1000	0.1000	0.0300	0.0300	0.0300
AWRT2	0.0100	0.0050	0.0100	0.0100	0.0100	0.0050	0.0050	0.0050	0.0050	0.0000	0.0000	0.0100	0.0300	0.0300	0.0300	0.0300
BABT2	0.0100	0.0050	0.0030	0.0030	0.0030	0.0030	0.0030	0.0030	0.0010	0.0030	0.0030	0.0010	0.0010	0.0030	0.0050	0.0050
BZST2	0.0000	0.0000	0.0000	0.0000	0.0000	0.0000	0.0000	0.0050	0.0080	0.0080	0.0080	0.0080	0.0100	0.0100	0.0300	0.0600
CPNT2	0.0000	0.0000	0.0000	0.0000	0.0000	0.0000	0.0000	0.0000	0.0000	0.0000	0.0000	0.0000	0.0000	0.0000	0.0000	0.0000
FCGT2	0.0800	0.0500	0.0500	0.3000	0.3000	0.3000	0.0500	0.0010	0.0100	0.0100	0.0800	0.0300	0.0800	0.1000	0.1000	0.1000
IRDT2	0.0000	0.0000	0.0000	0.0000	0.0000	0.0000	0.0000	0.0000	0.0000	0.0000	0.0000	0.0000	0.0000	0.0000	0.0000	0.0000
MBET2	0.0000	0.0000	0.0000	0.0000	0.0000	0.0000	0.0000	0.0000	0.0000	0.0000	0.0000	0.0000	0.0000	0.0000	0.0000	0.0000
MQTT2	0.0300	0.0300	0.0000	0.0000	0.0000	0.0000	0.0000	0.0000	0.0000	0.0000	0.0300	0.0300	0.1000	0.1000	0.2000	0.1000
NUET2	0.0000	0.0000	0.0000	0.0000	0.0000	0.0000	0.3000	0.3000	0.1000	0.0800	0.0800	0.0800	0.1000	0.0500	0.0100	0.0050
PACT2	0.0300	0.0300	0.0100	0.0000	0.0000	0.0100	0.2000	0.2000	0.1000	0.0500	0.1000	0.1000	0.1000	0.1000	0.0000	0.0300

Station	Direction (0°N, CW+)															
	0	22.5	45	67.5	90	112.5	135	157.5	180	202.5	225	247.5	270	292.5	315	337.5
PCNT2	0.0000	0.0000	0.0000	0.0000	0.0000	0.0000	0.0000	0.0000	0.0000	0.0100	0.0100	0.3000	0.3000	0.3000	0.0000	0.0000
PTAT2	0.0500	0.0300	0.0000	0.0000	0.0000	0.0000	0.0000	0.0000	0.0000	0.0000	0.0800	0.2000	0.3000	0.3000	0.2000	0.2000
RCPT2	0.3000	0.1000	0.3000	0.3000	0.3000	0.3000	0.0300	0.0000	0.0000	0.0300	0.3000	0.3000	0.3000	0.3000	0.3000	0.3000
RSJT2	0.0100	0.0100	0.0100	0.0100	0.0100	0.0100	0.0100	0.0050	0.0050	0.0100	0.0100	0.0100	0.0100	0.0100	0.0100	0.0100
SDRT2	0.3000	0.3000	0.3000	0.1000	0.1000	0.0500	0.0100	0.0000	0.0000	0.0000	0.0000	0.0000	0.0000	0.3000	0.3000	0.3000
VCAT2	0.0000	0.0000	0.0000	0.0000	0.0000	0.0000	0.0000	0.0000	0.0000	0.0000	0.0000	0.0000	0.0000	0.0000	0.0000	0.0000
42002	0.0000	0.0000	0.0000	0.0000	0.0000	0.0000	0.0000	0.0000	0.0000	0.0000	0.0000	0.0000	0.0000	0.0000	0.0000	0.0000
42019	0.0000	0.0000	0.0000	0.0000	0.0000	0.0000	0.0000	0.0000	0.0000	0.0000	0.0000	0.0000	0.0000	0.0000	0.0000	0.0000
42020	0.0000	0.0000	0.0000	0.0000	0.0000	0.0000	0.0000	0.0000	0.0000	0.0000	0.0000	0.0000	0.0000	0.0000	0.0000	0.0000
42044	0.0000	0.0000	0.0000	0.0000	0.0000	0.0000	0.0000	0.0000	0.0000	0.0000	0.0000	0.0000	0.0000	0.0000	0.0000	0.0000
42045	0.0000	0.0000	0.0000	0.0000	0.0000	0.0000	0.0000	0.0000	0.0000	0.0000	0.0000	0.0000	0.0000	0.0000	0.0000	0.0000

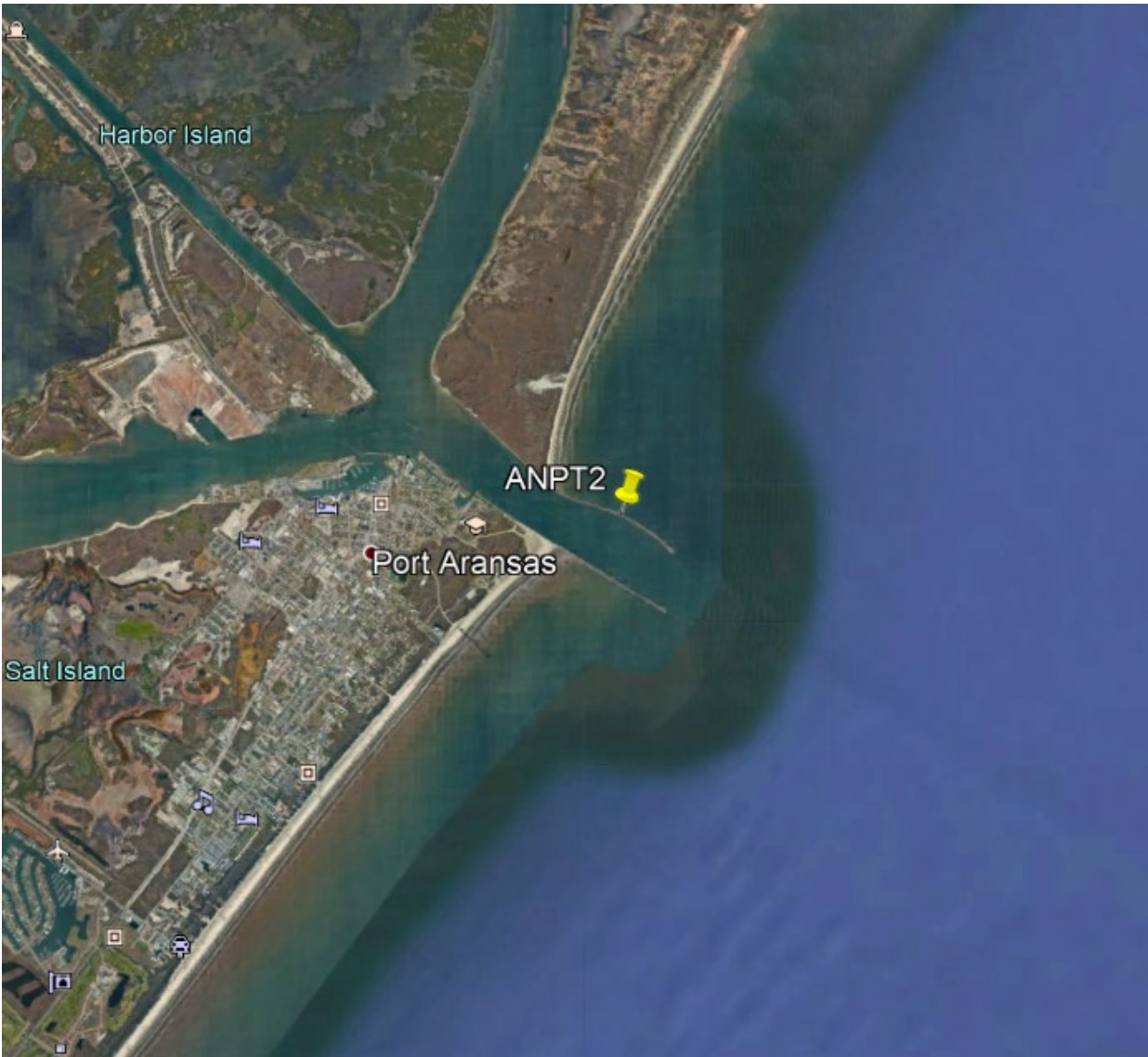


Figure A-1. Aerial image of NDBC station ANPT2: Aransas, Aransas Pass, TX.

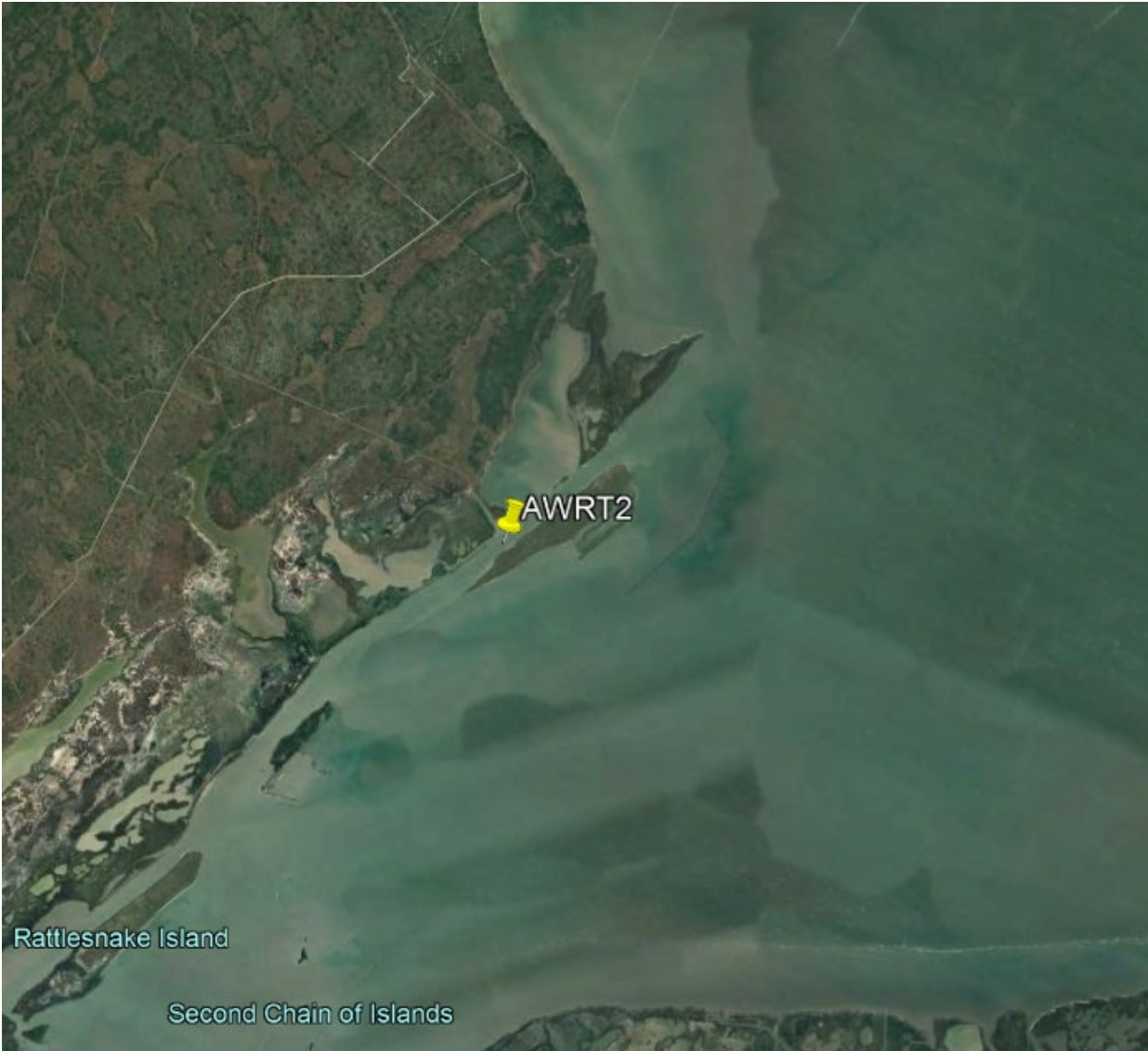


Figure A-2. Aerial image of NDBC station AWRT2: Aransas Wildlife Refuge, TX.



Figure A-3. Aerial image of NDBC station BAPT2: Baffin Bay, TX.

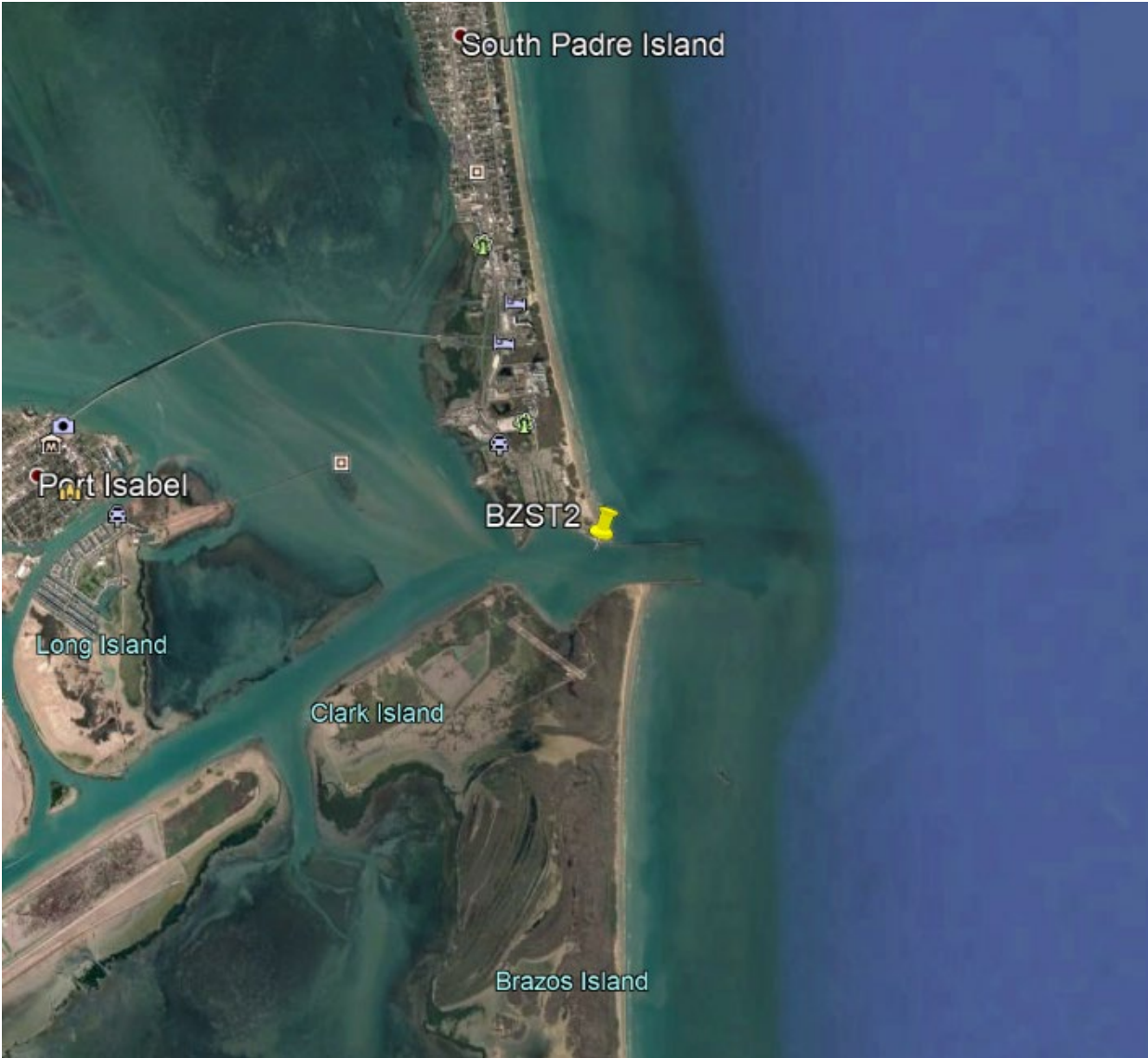


Figure A-4. Aerial image of NDBC station BZST2: SPI Brazos Santiago, TX.

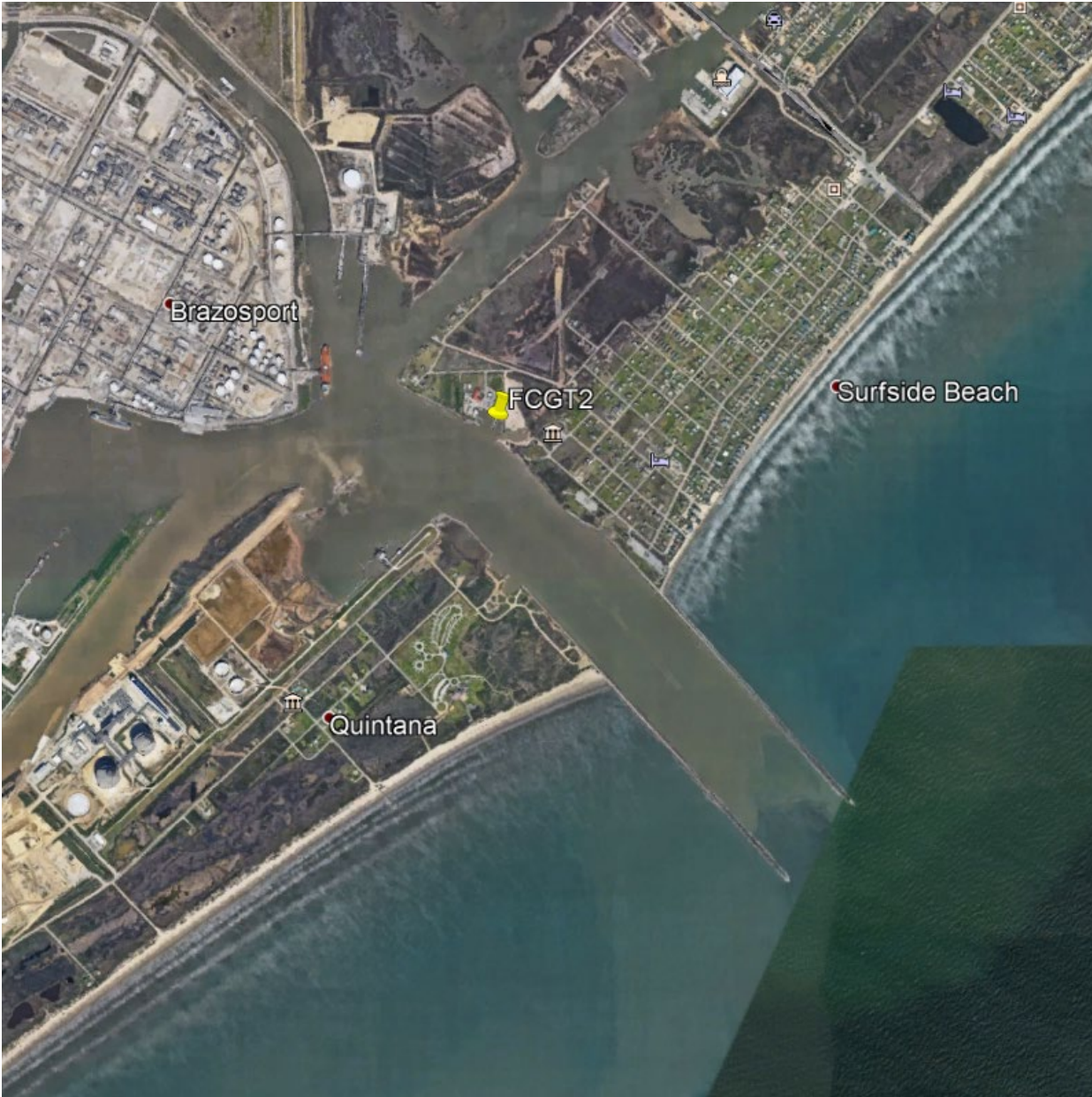


Figure A-5. Aerial image of NDBC station FCGT2: USCG Freeport, TX.

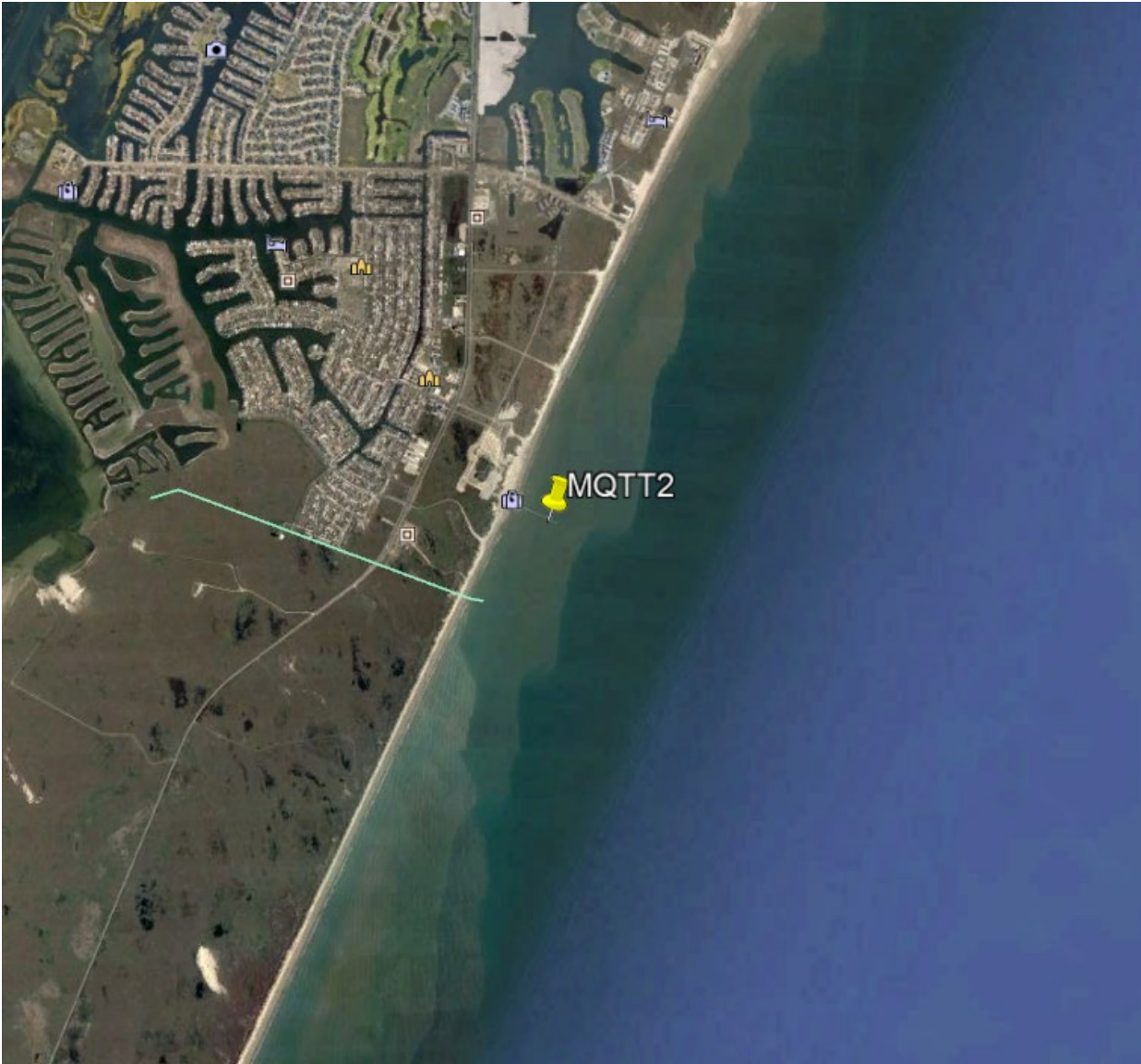


Figure A-6. Aerial image of NDBC station MQTT2: Bob Hall Pier, Corpus Christi, TX.

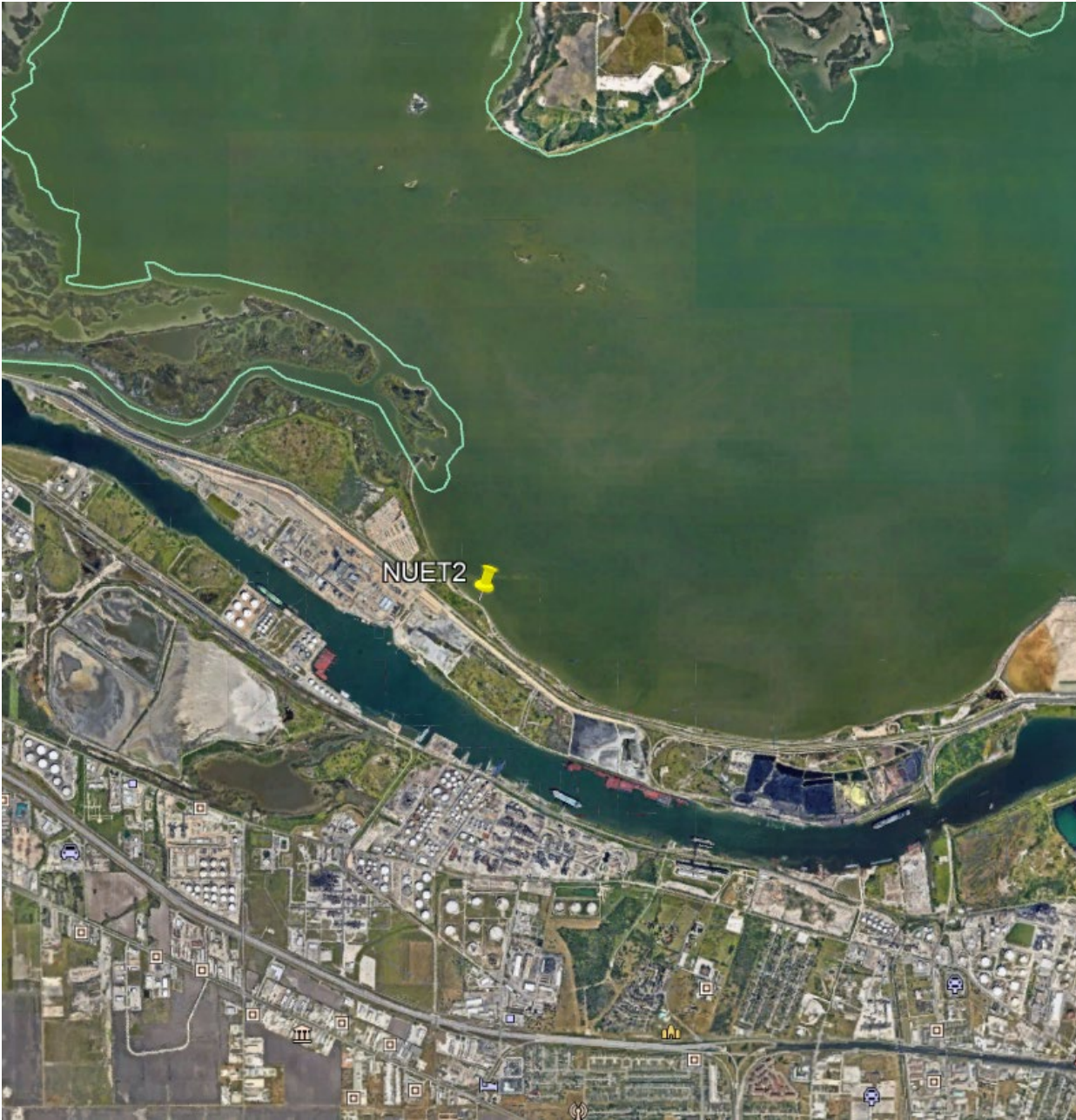


Figure A-7. Aerial image of NDBC station NUET2: Nueces Bay, TX.



Figure A-8. Aerial image of NDBC station PACT2: Packery Channel, TX.



Figure A-9. Aerial image of NDBC station PCNT2: Port O'Connor, Matagorda Bay, TX.

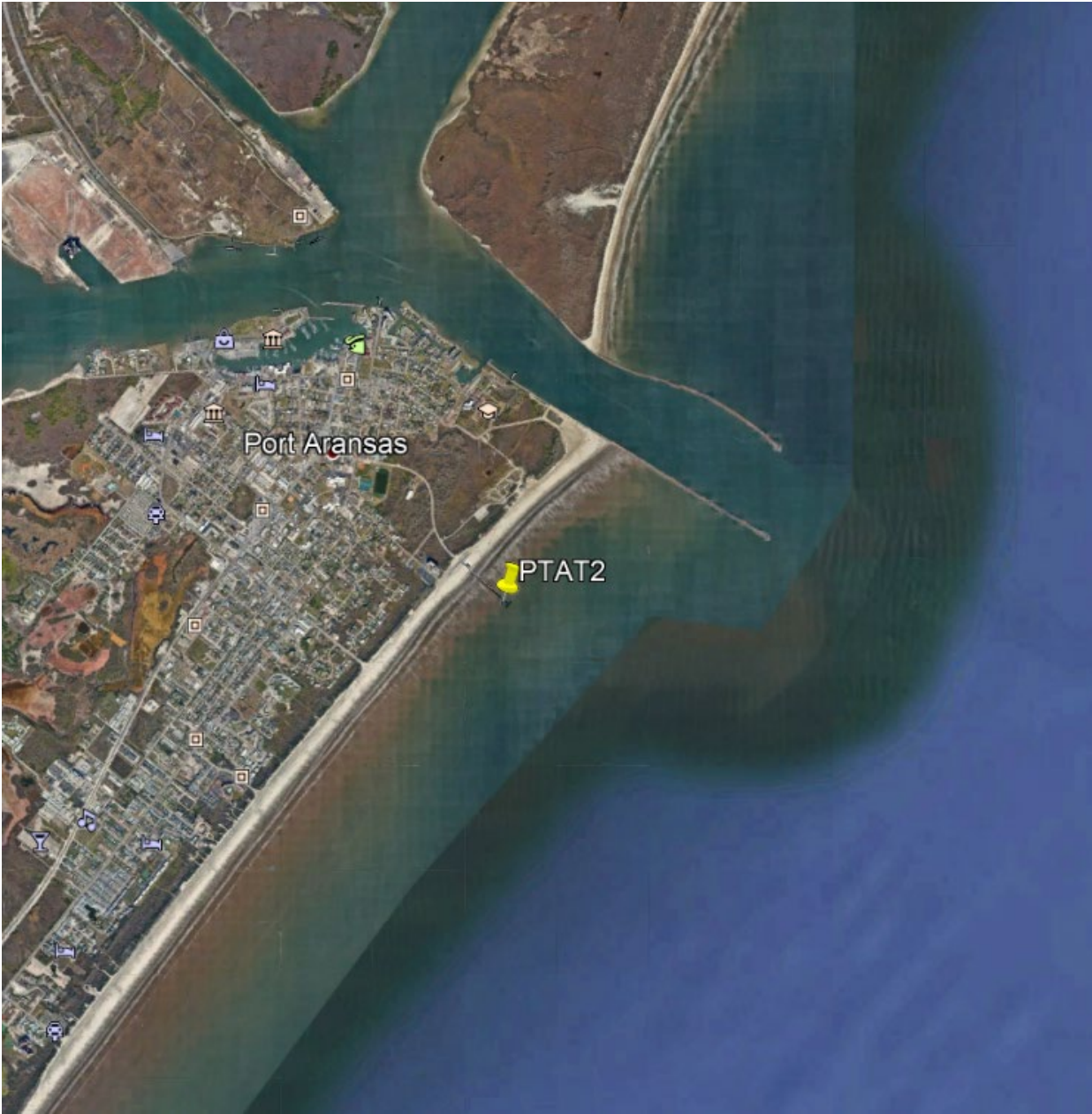


Figure A-10. Aerial image of NDBC station PTAT2: Port Aransas, TX.



Figure A-11. Aerial image of NDBC station RCPT2: Rockport, TX.



Figure A-12. Aerial image of NDBC station RSJT2: Rincon del San Jose, TX.

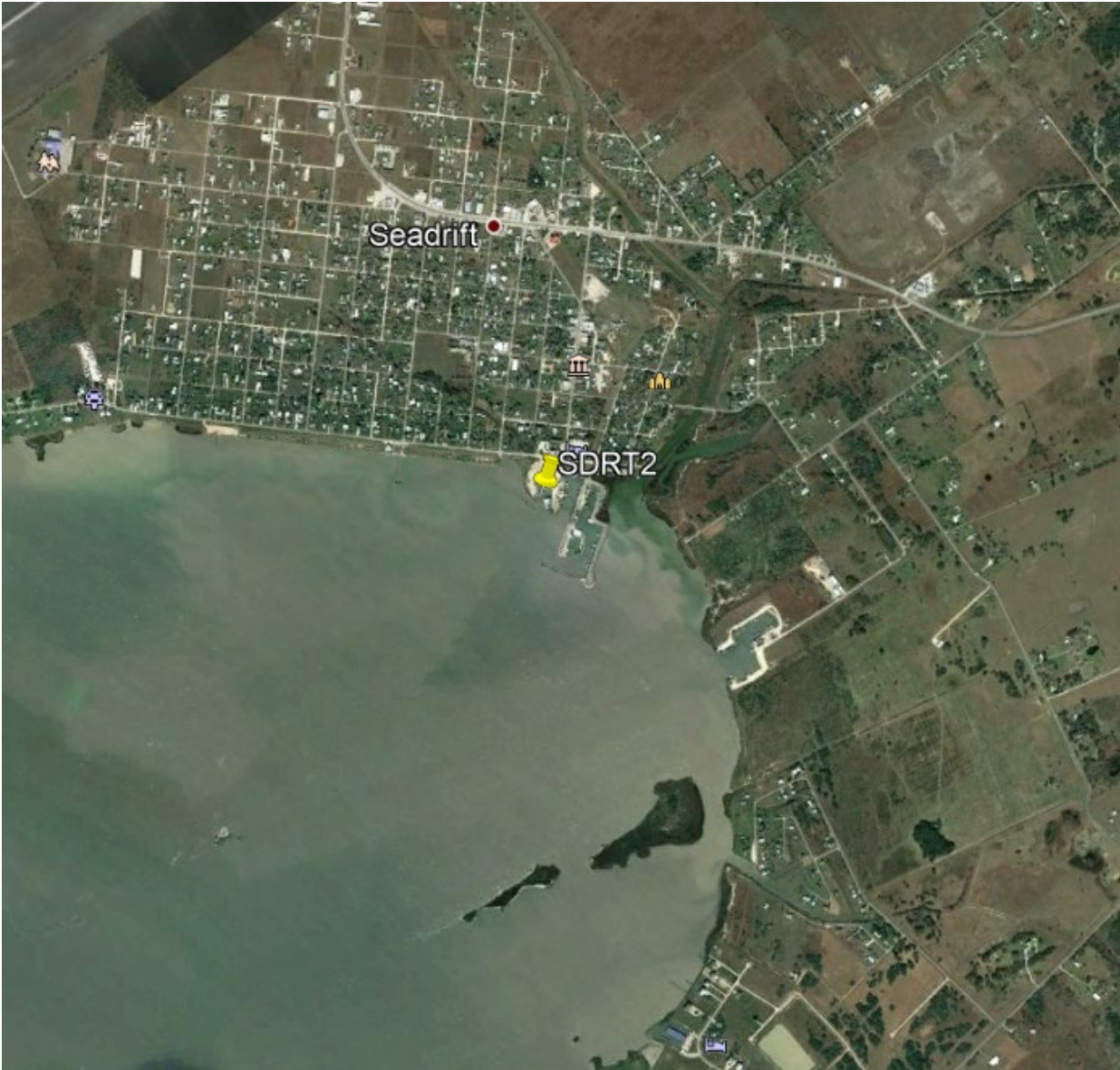


Figure A-13. Aerial image of NDBC station SDRT2: Seadrift, TX.

Appendix B. HURRICANE IRMA (CONUS)

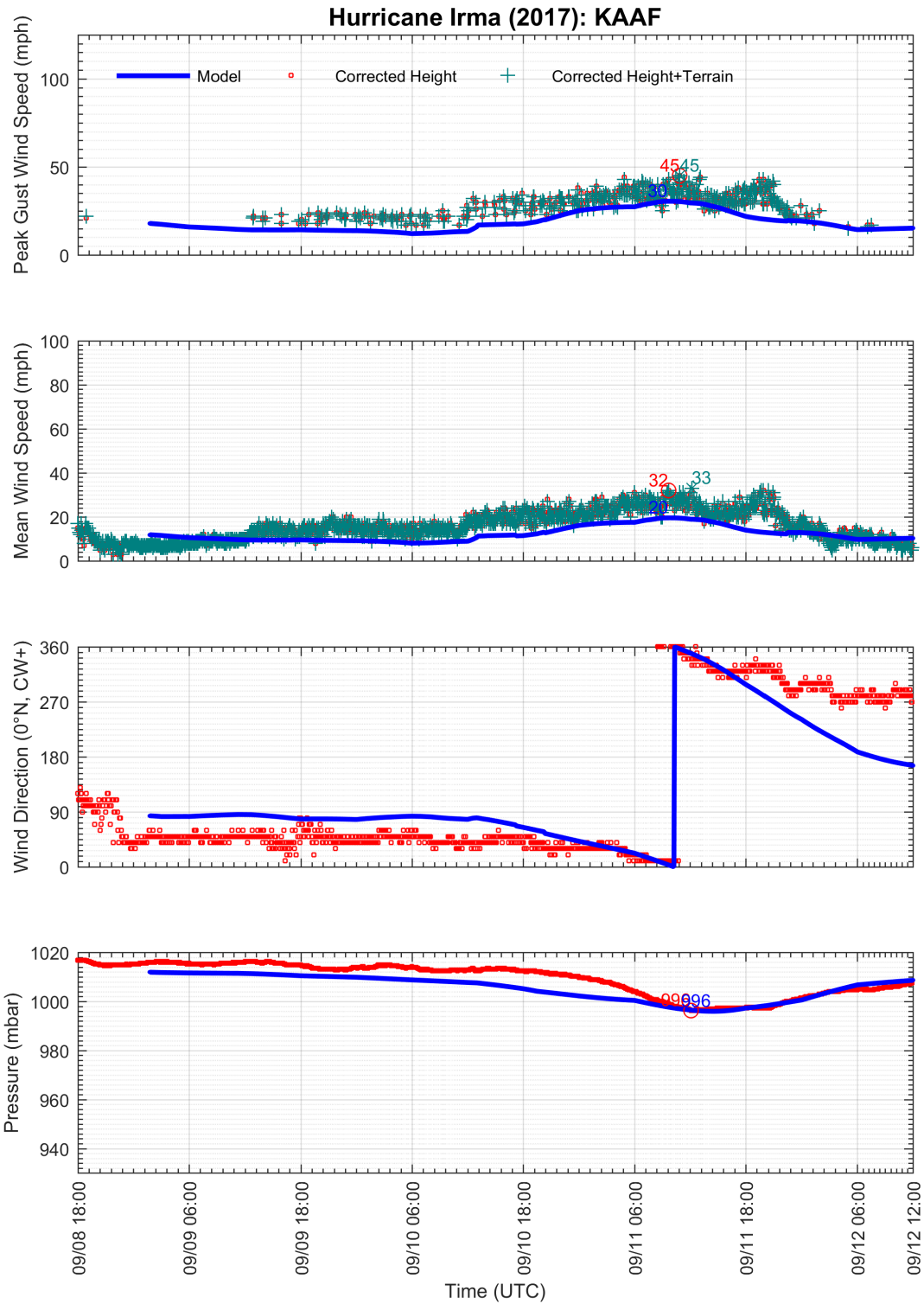
Appendix B.1 SURFACE OBSERVATION STATION DETAILS

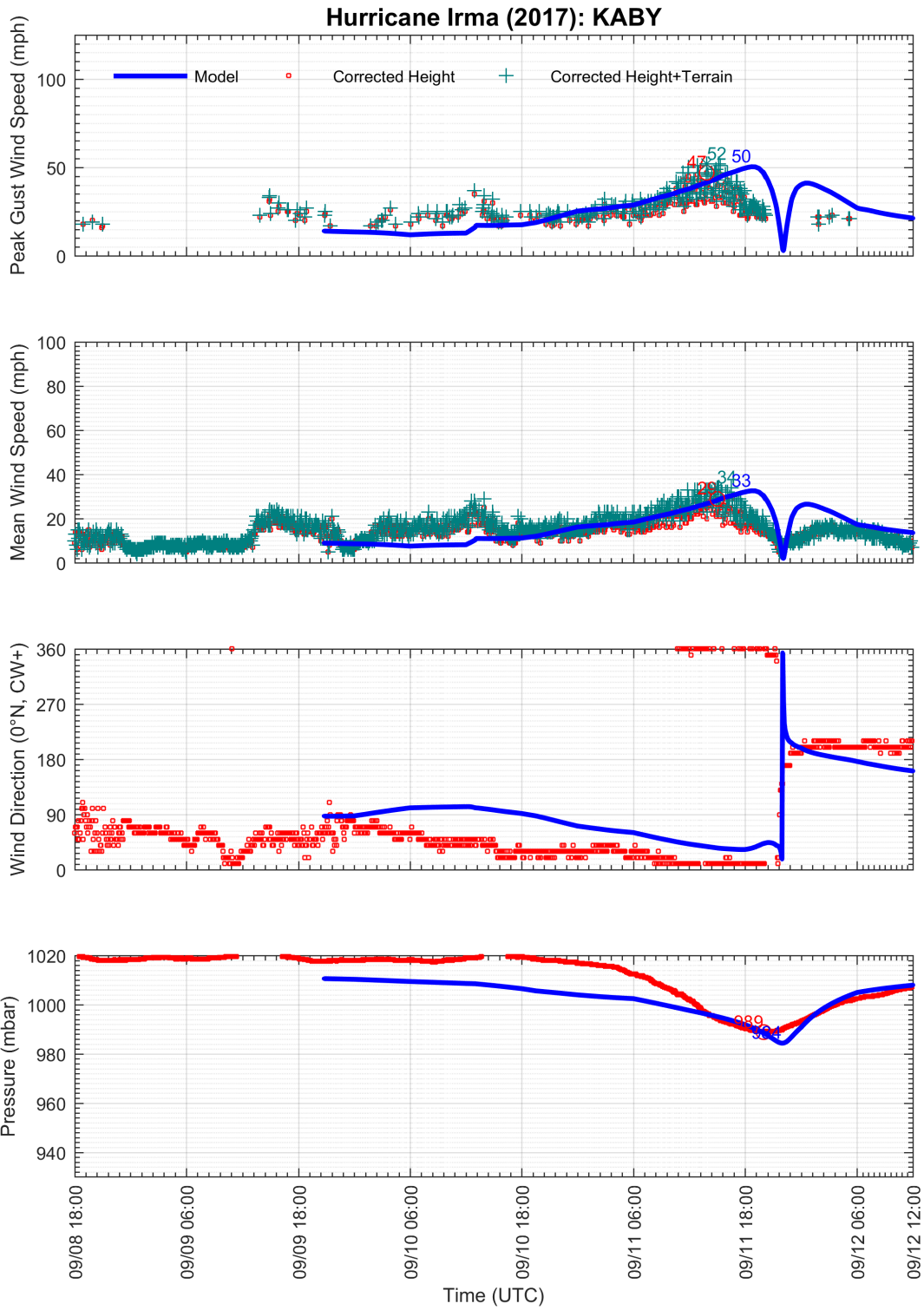
Station	Latitude (°N)	Longitude (°W)	Anemometer Height (m)
KAAF	29.733	85.033	10.00
KABY	31.536	84.194	10.00
KAGS	33.370	81.965	10.00
KAHN	33.948	83.327	8.00
KAMG	31.536	82.507	10.00
KAPF	26.153	81.775	10.00
KATL	33.640	84.427	10.00
KBKV	28.474	82.454	10.00
KCEW	30.780	86.522	10.00
KCHS	32.899	80.041	10.00
KCRG	30.336	81.515	8.00
KCSG	32.516	84.942	10.00
KCTY	29.633	83.105	10.00
KDAB	29.177	81.060	10.00
KDHN	31.321	85.450	10.00
KDNL	33.467	82.039	10.00
KDTS	30.400	86.472	8.00
KEYW	24.553	81.754	10.00
KFFC	33.355	84.567	10.00
KFMY	26.586	81.864	8.00
KFPR	27.498	80.377	8.00
KFTY	33.779	84.521	8.00
KFXE	26.197	80.171	10.00
KGIF	28.062	81.754	10.00
KGNV	29.690	82.272	10.00
KGZH	31.416	87.044	10.00
KHWO	25.999	80.241	10.00
KJAX	30.494	81.693	10.00
KLEE	28.821	81.810	10.00
KMAI	30.836	85.184	10.00
KMCN	32.688	83.654	10.00
KMCO	28.434	81.325	8.00
KMIA	25.824	80.300	10.00
KMTH	24.726	81.052	8.00
KOGB	33.462	80.858	10.00
KOPF	25.907	80.280	10.00
KORL	28.545	81.333	10.00
KPBI	26.685	80.099	10.00
KPGD	26.917	81.991	10.00
KPIE	27.911	82.688	10.00
KPMP	26.250	80.108	10.00

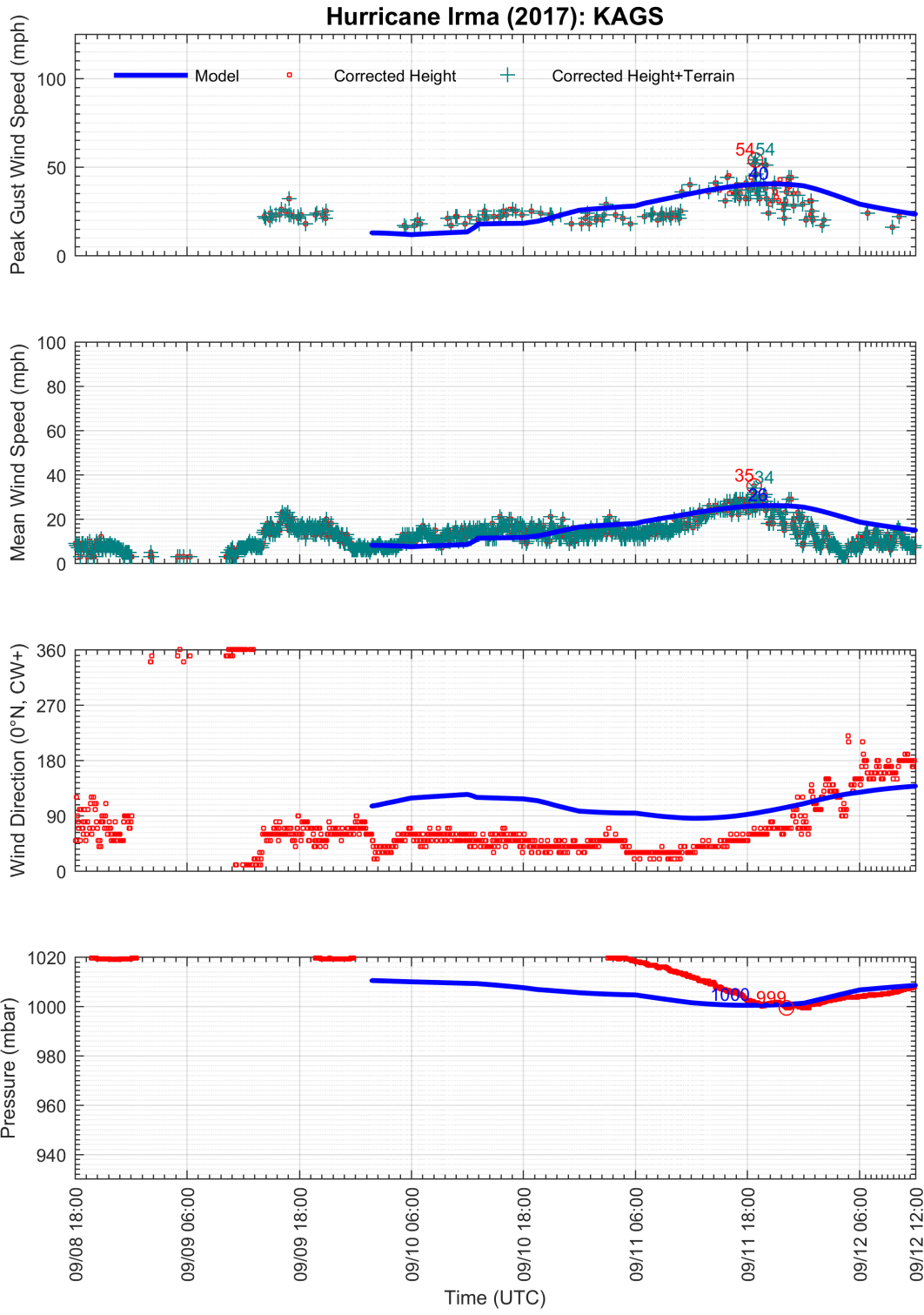
Station	Latitude (°N)	Longitude (°W)	Anemometer Height (m)
KPNS	30.473	87.188	10.00
KRSW	26.536	81.755	10.00
KSAV	32.119	81.202	10.00
KSFB	28.780	81.244	10.00
KSPG	27.765	82.627	8.00
KSRQ	27.401	82.559	10.00
KSSI	31.252	81.391	10.00
KTLH	30.393	84.353	10.00
KTMB	25.648	80.433	10.00
KTPA	27.961	82.540	8.00
KVLD	30.782	83.277	10.00
FWYF1	25.591	80.097	43.90
MLRF1	25.012	80.376	15.80
PLSF1	24.693	82.773	17.70
VCAF1	24.711	81.107	9.60
VENF1	27.073	82.453	11.60
XUF1t	26.907	82.006	10.00
XUF2t	26.330	81.779	10.00
XUF3t	26.156	81.721	10.00
XUF5t	26.159	81.776	10.00

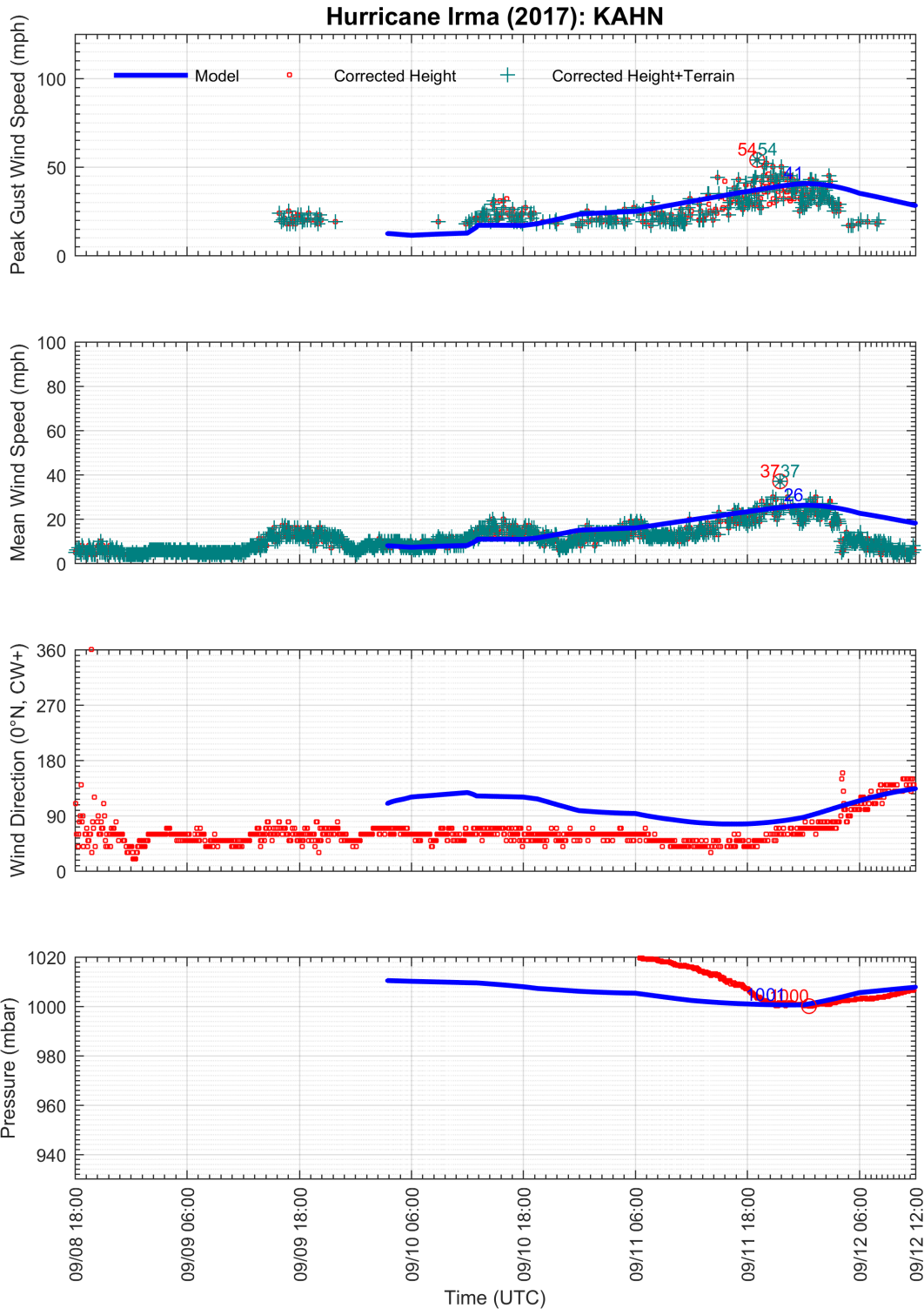
Appendix B.2

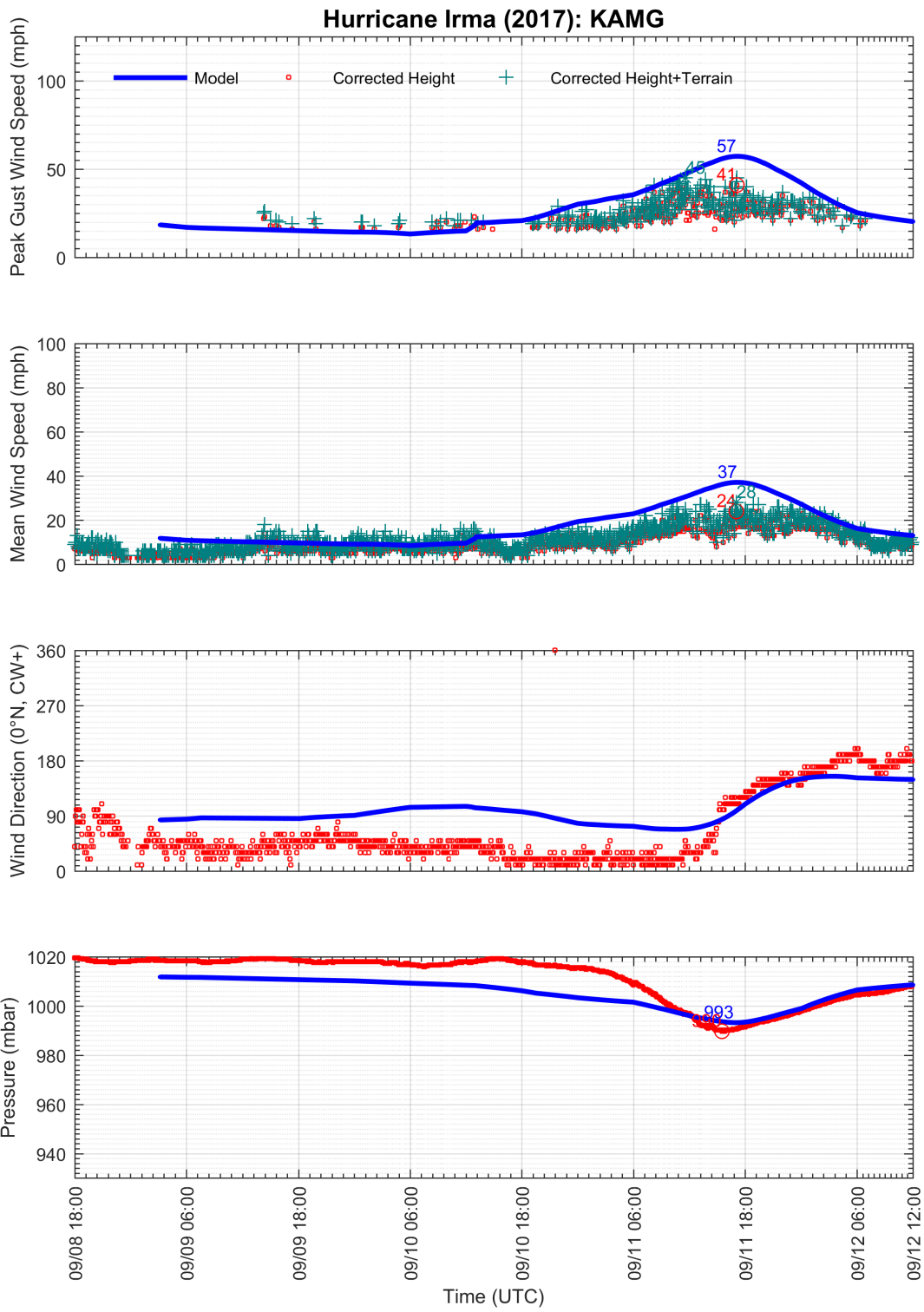
MODELED AND OBSERVED STATION TIME HISTORIES

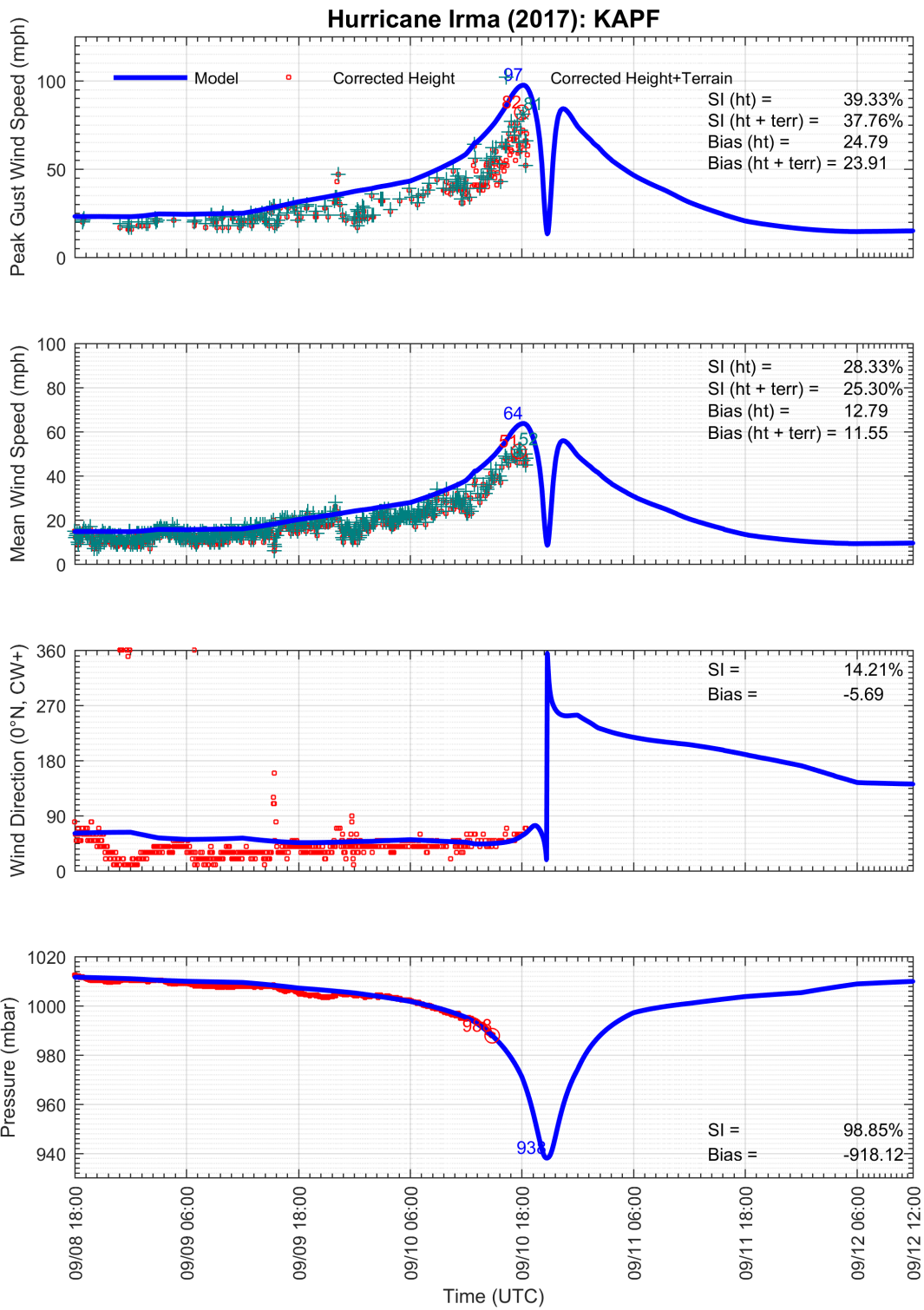


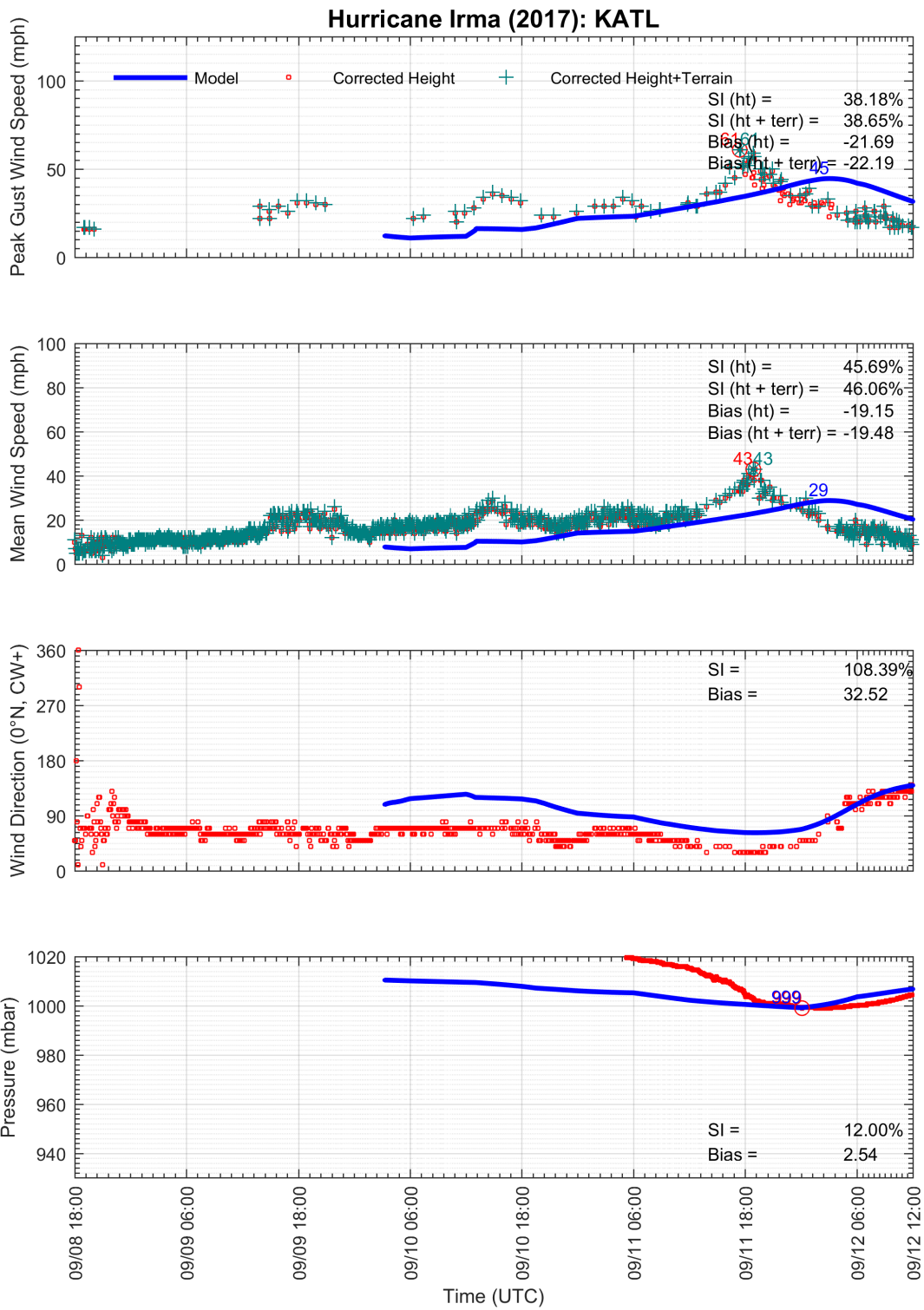


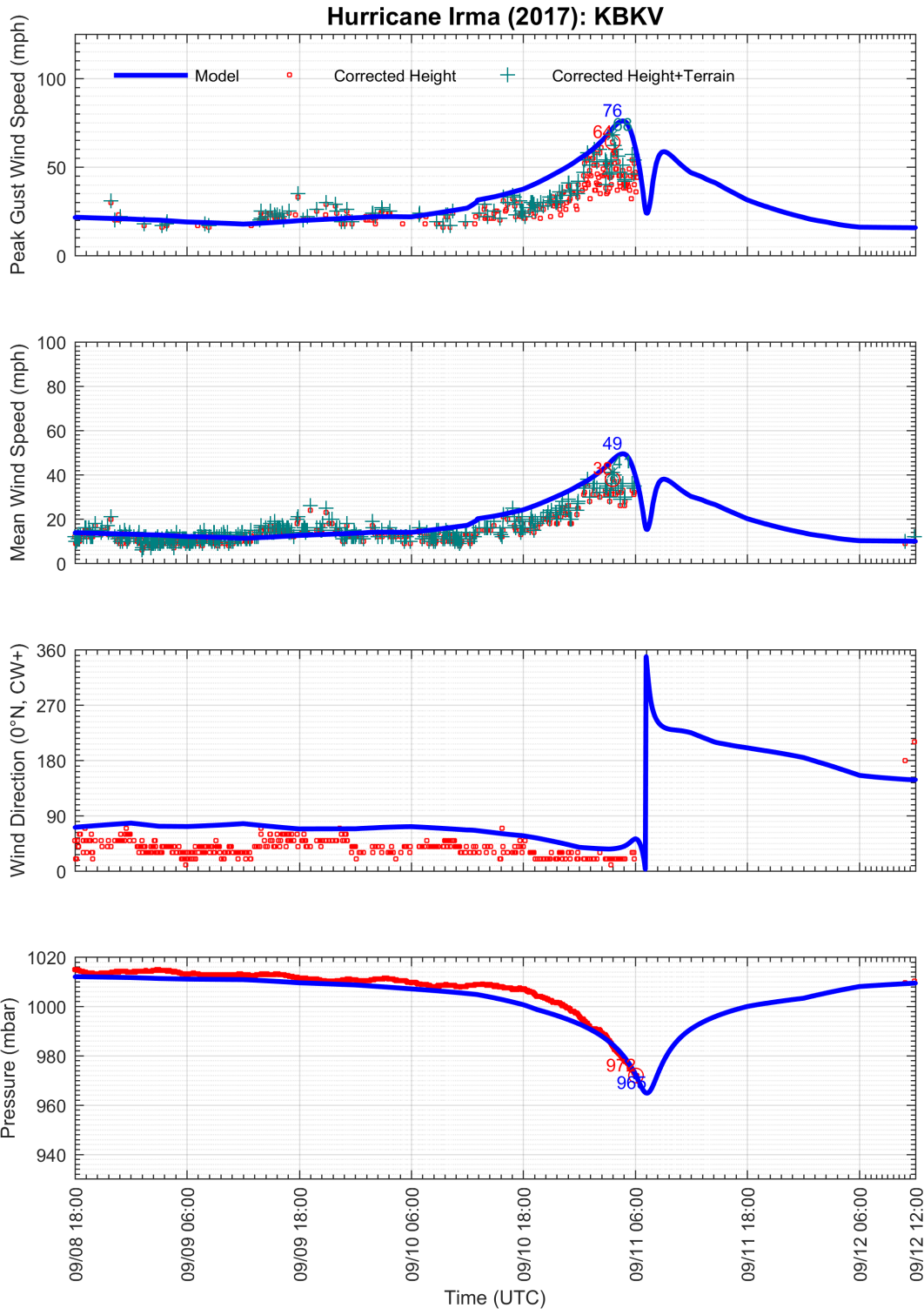


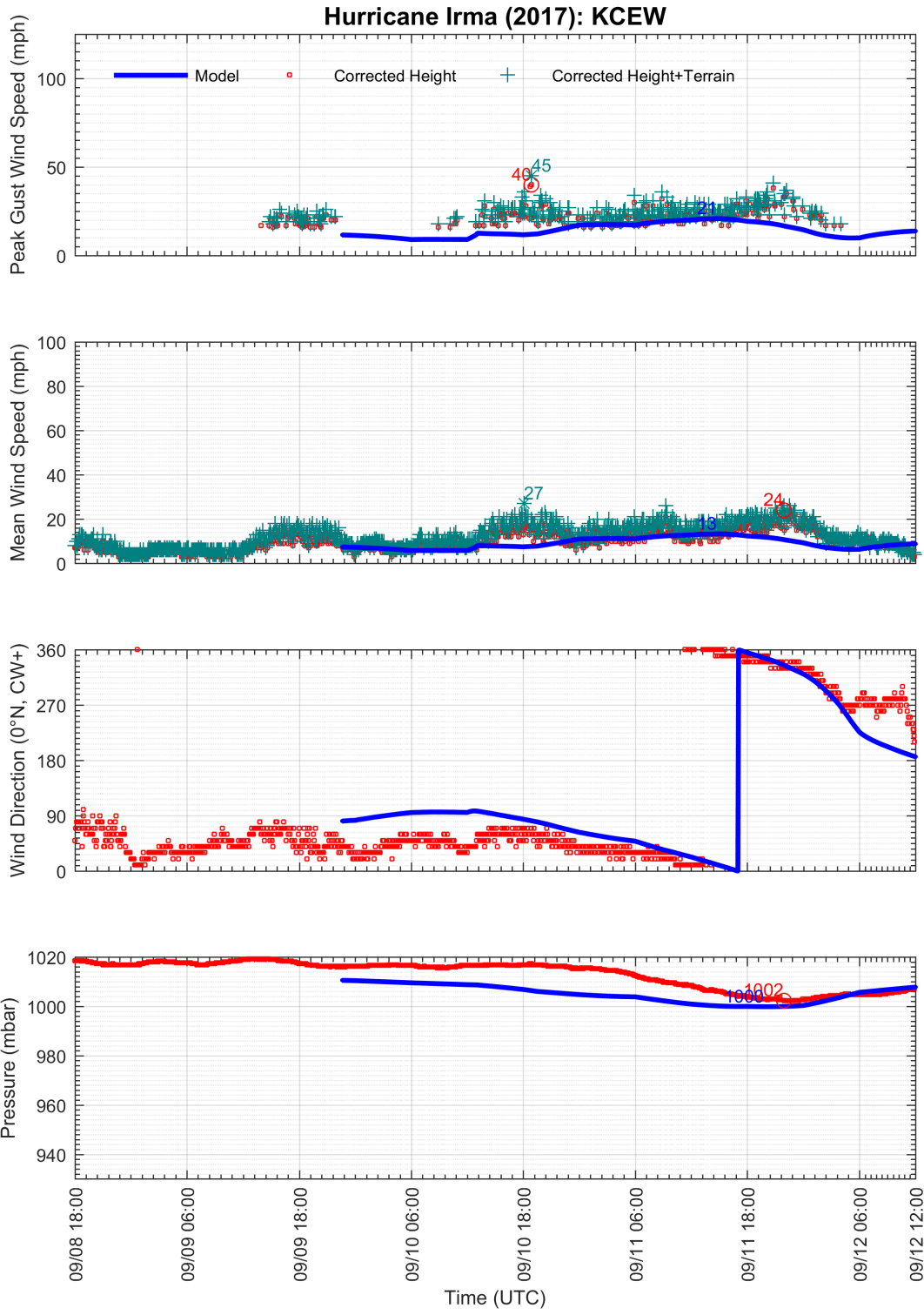


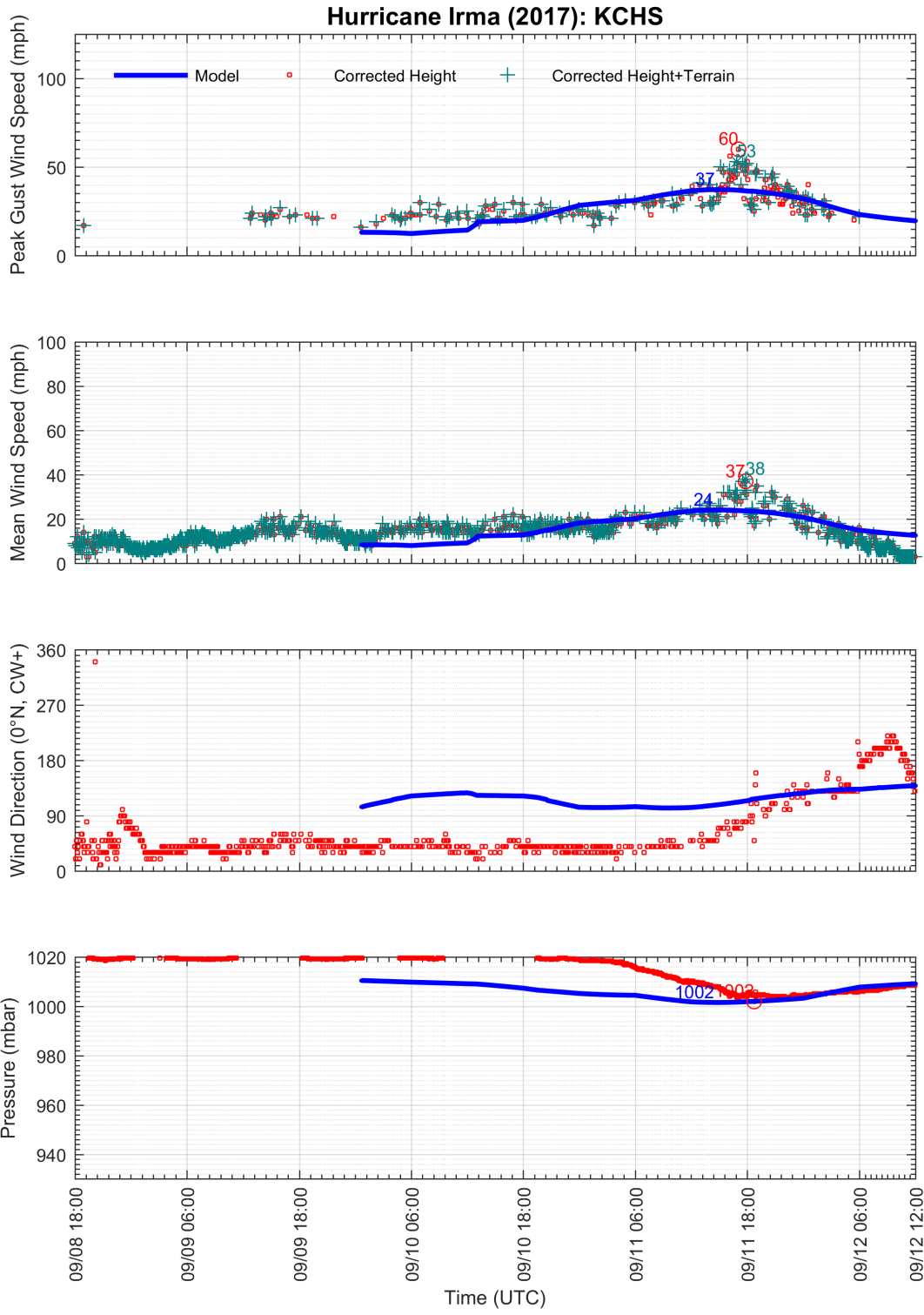


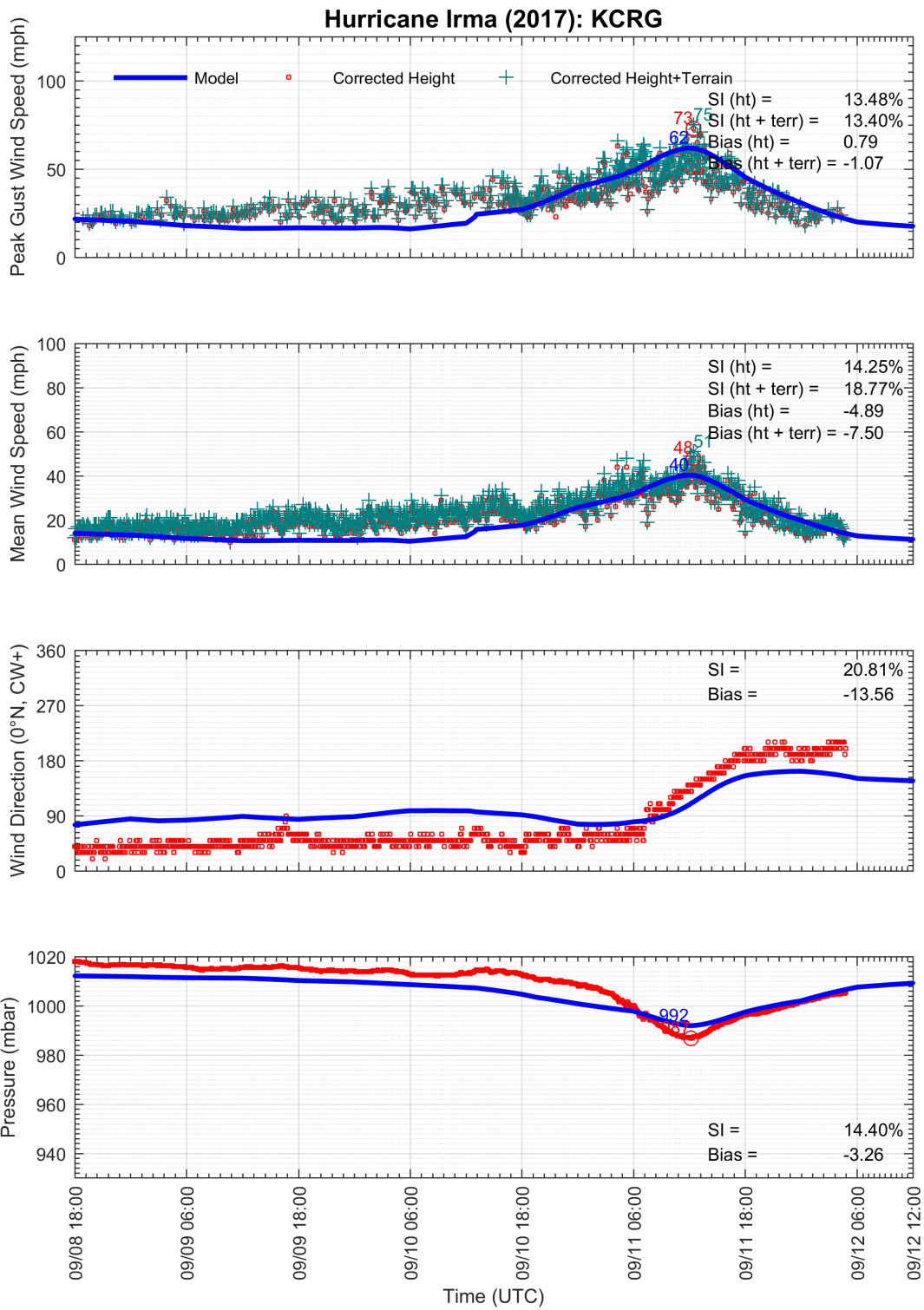


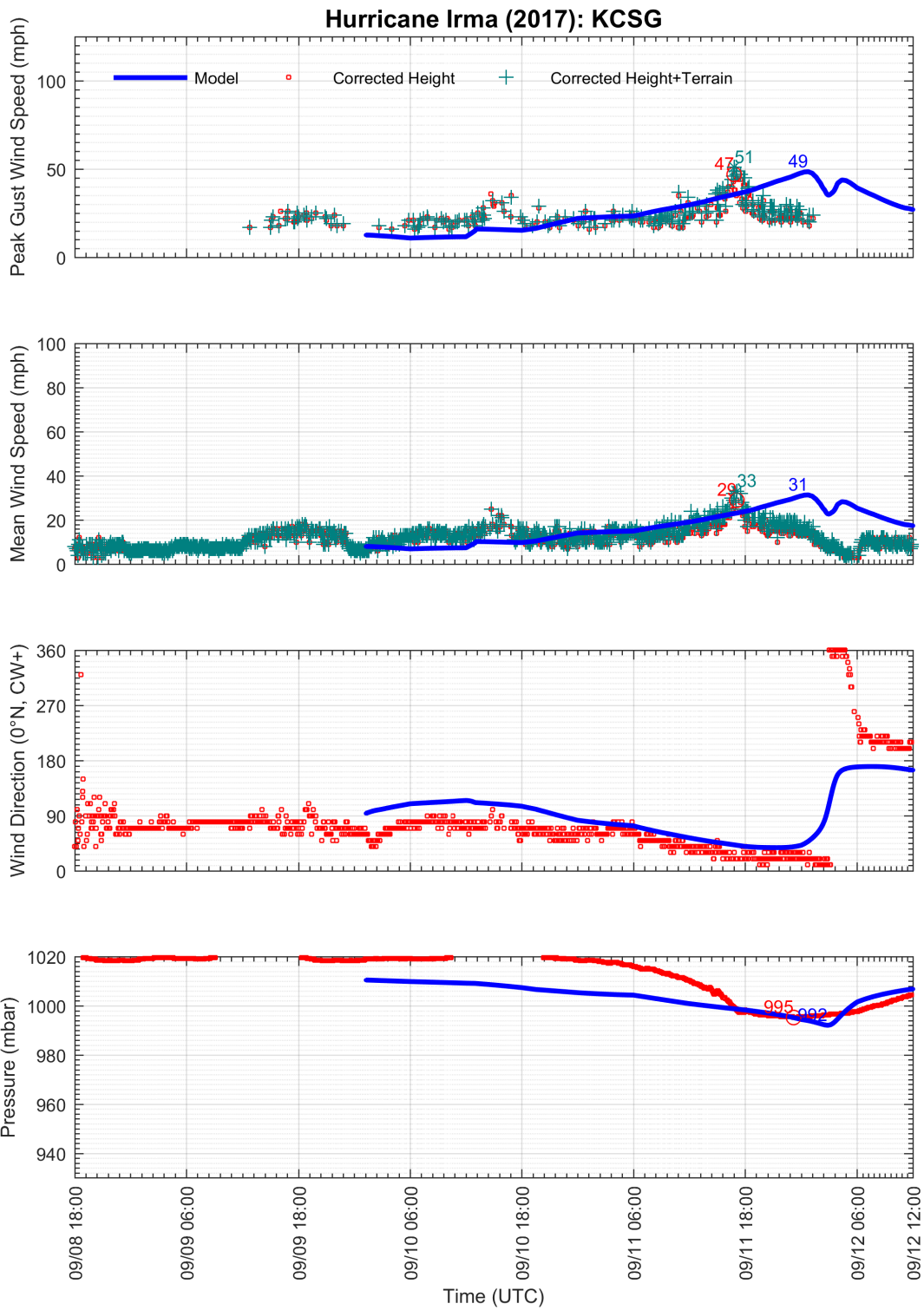


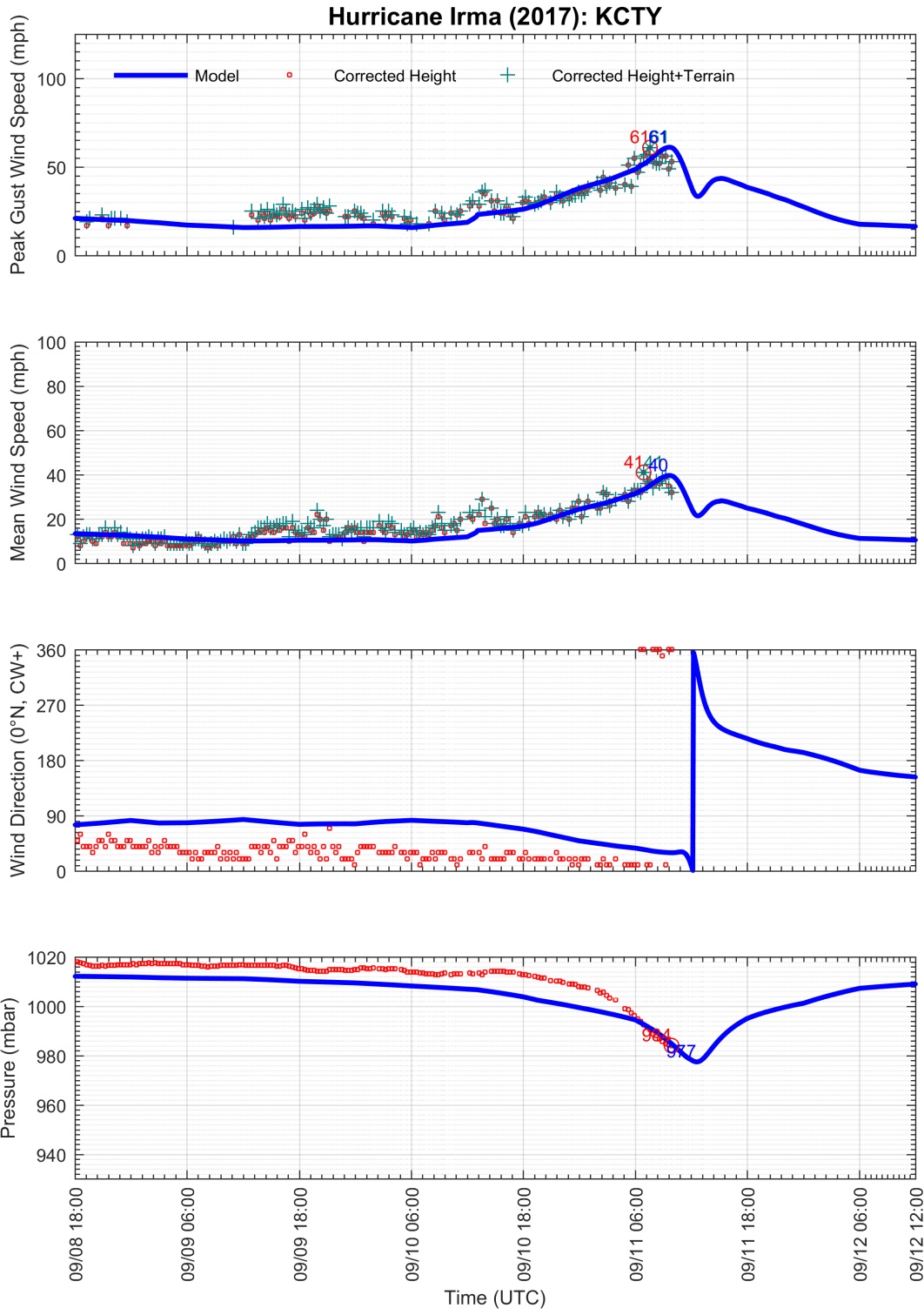


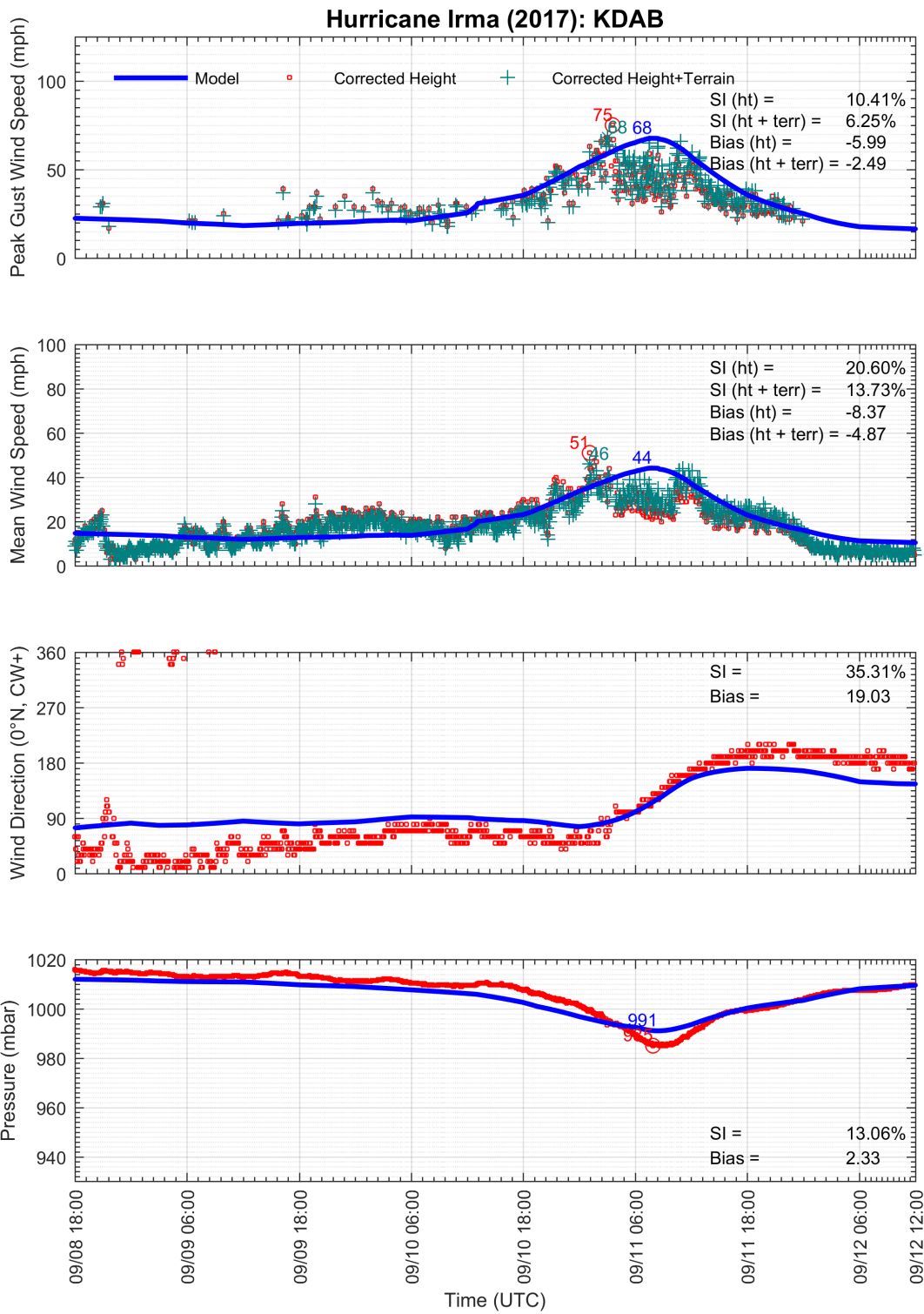


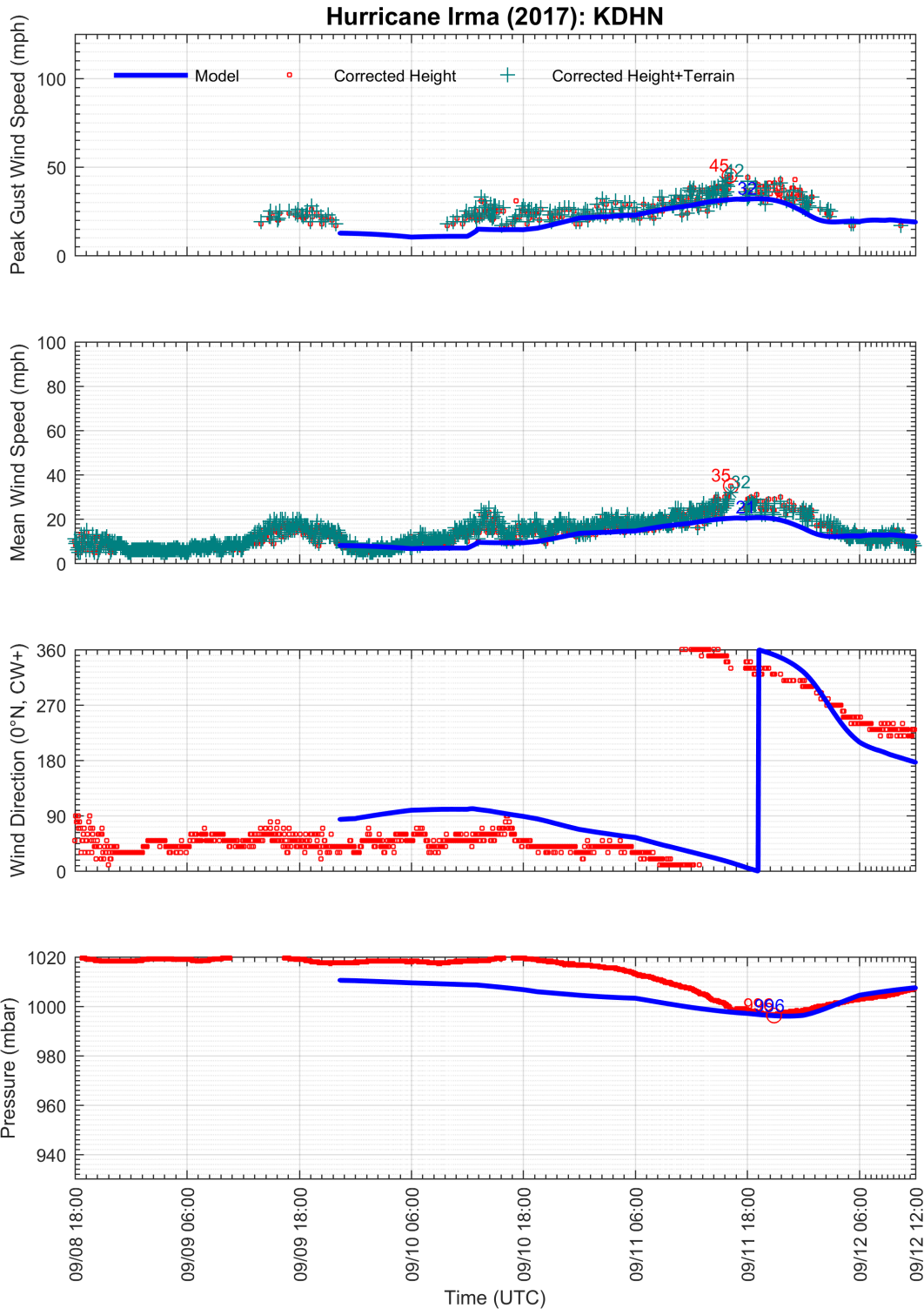


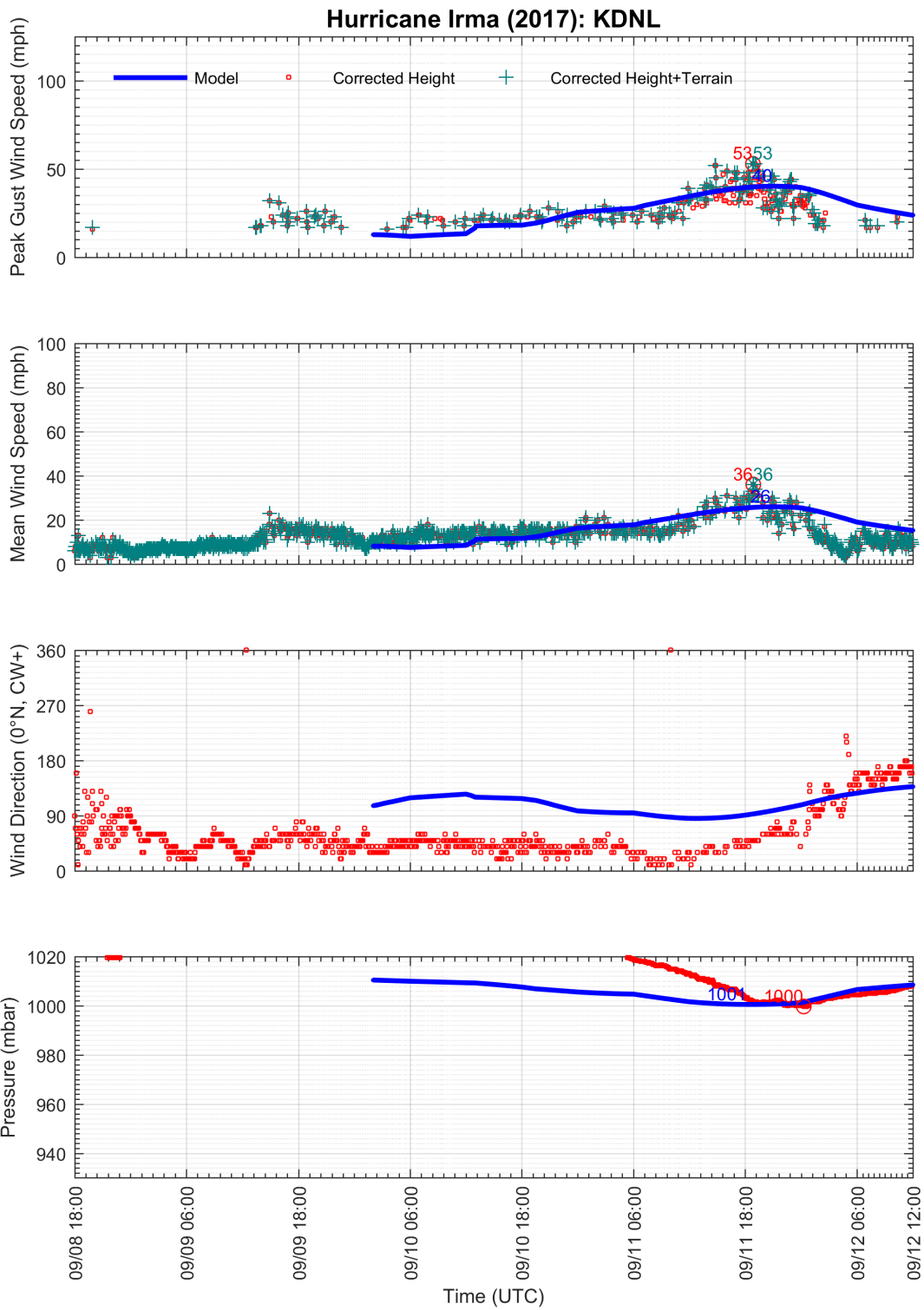


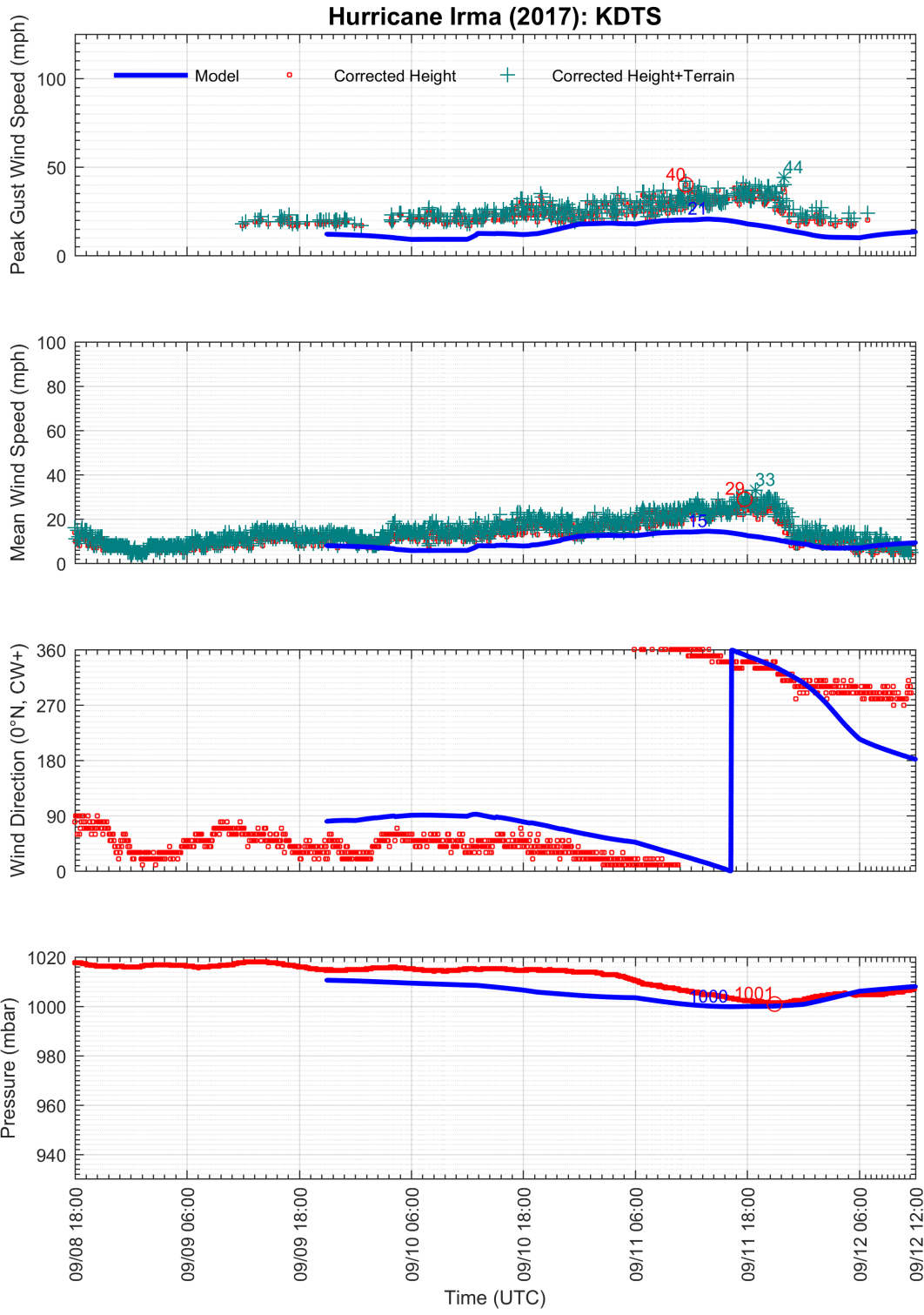


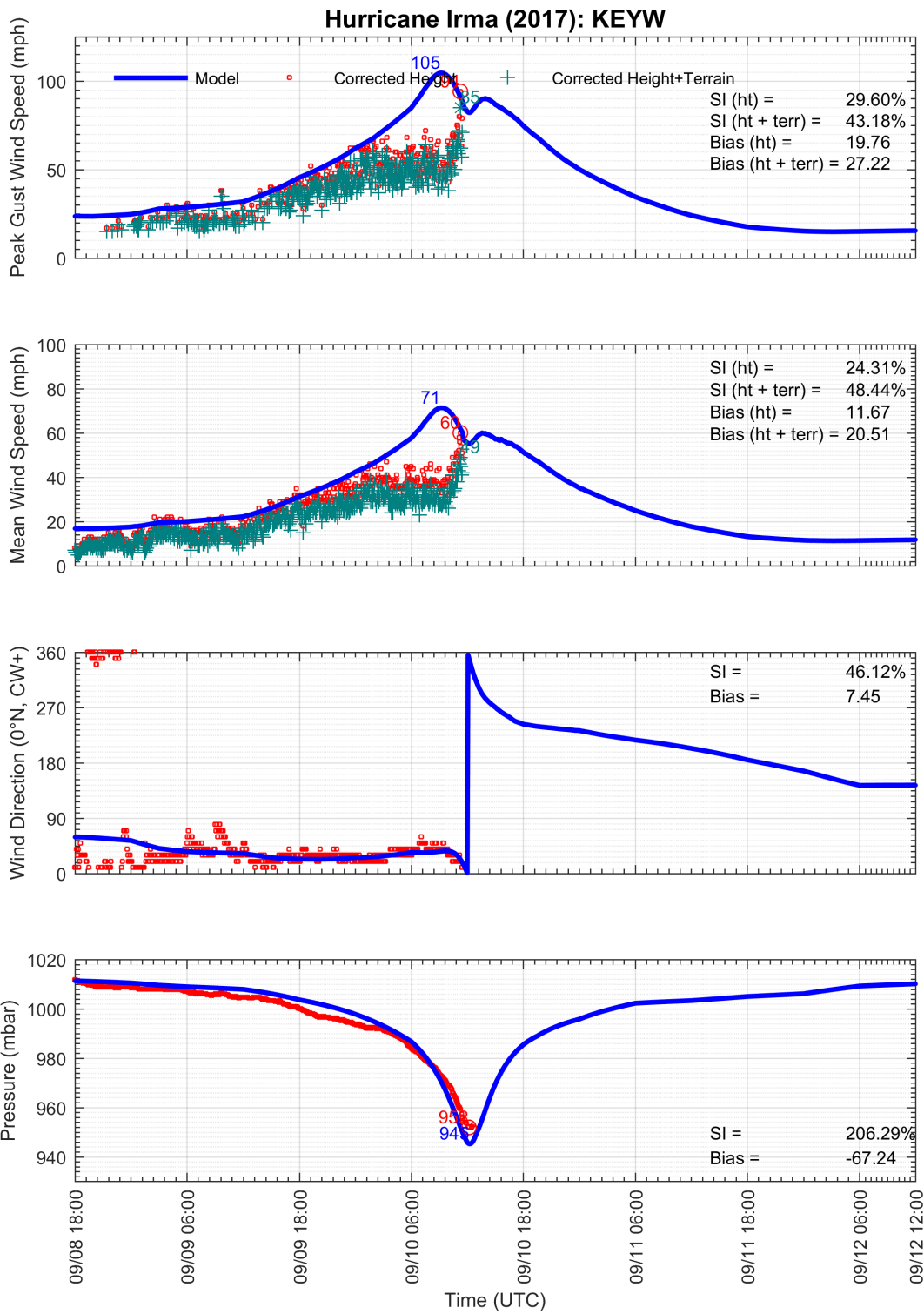


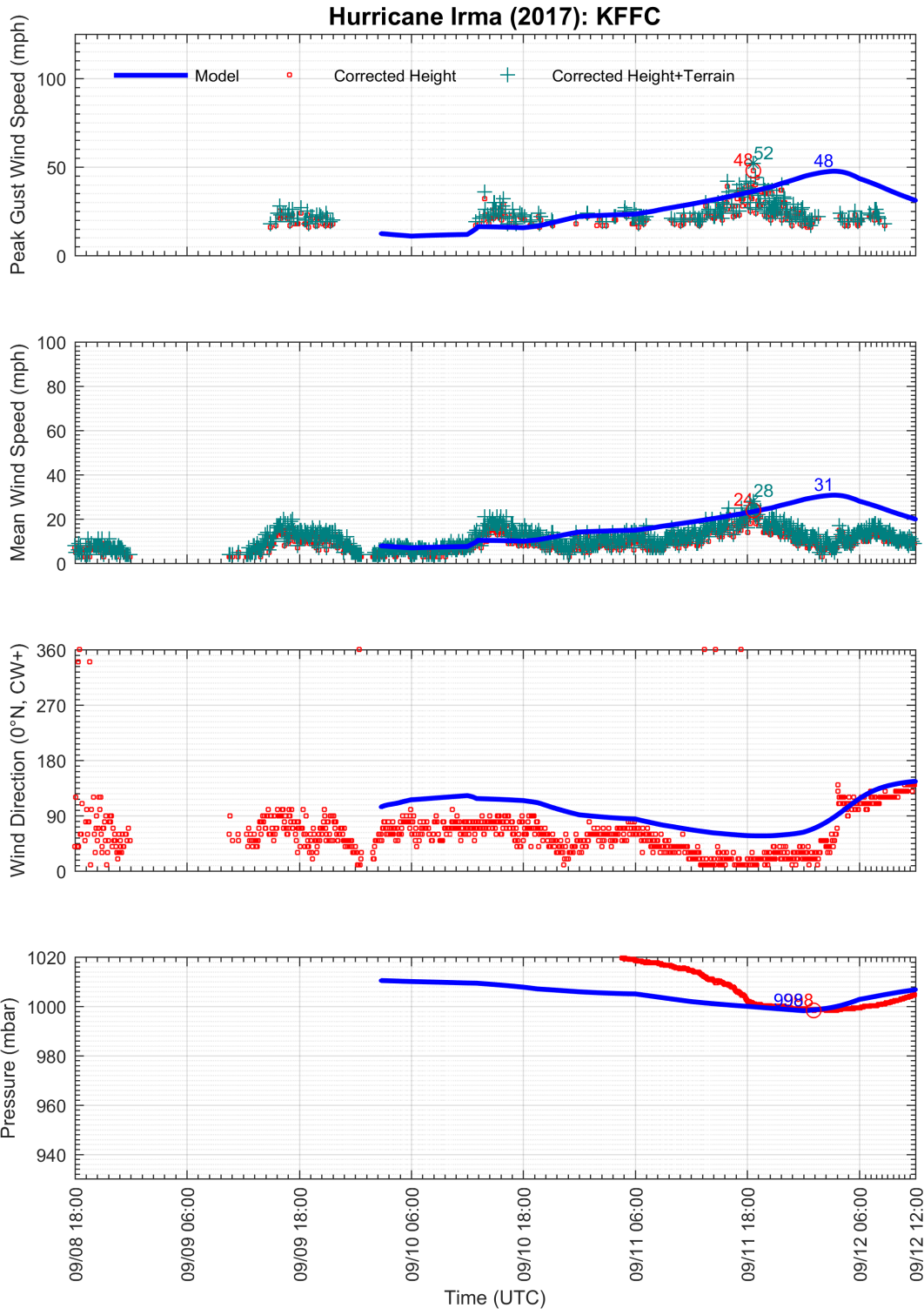


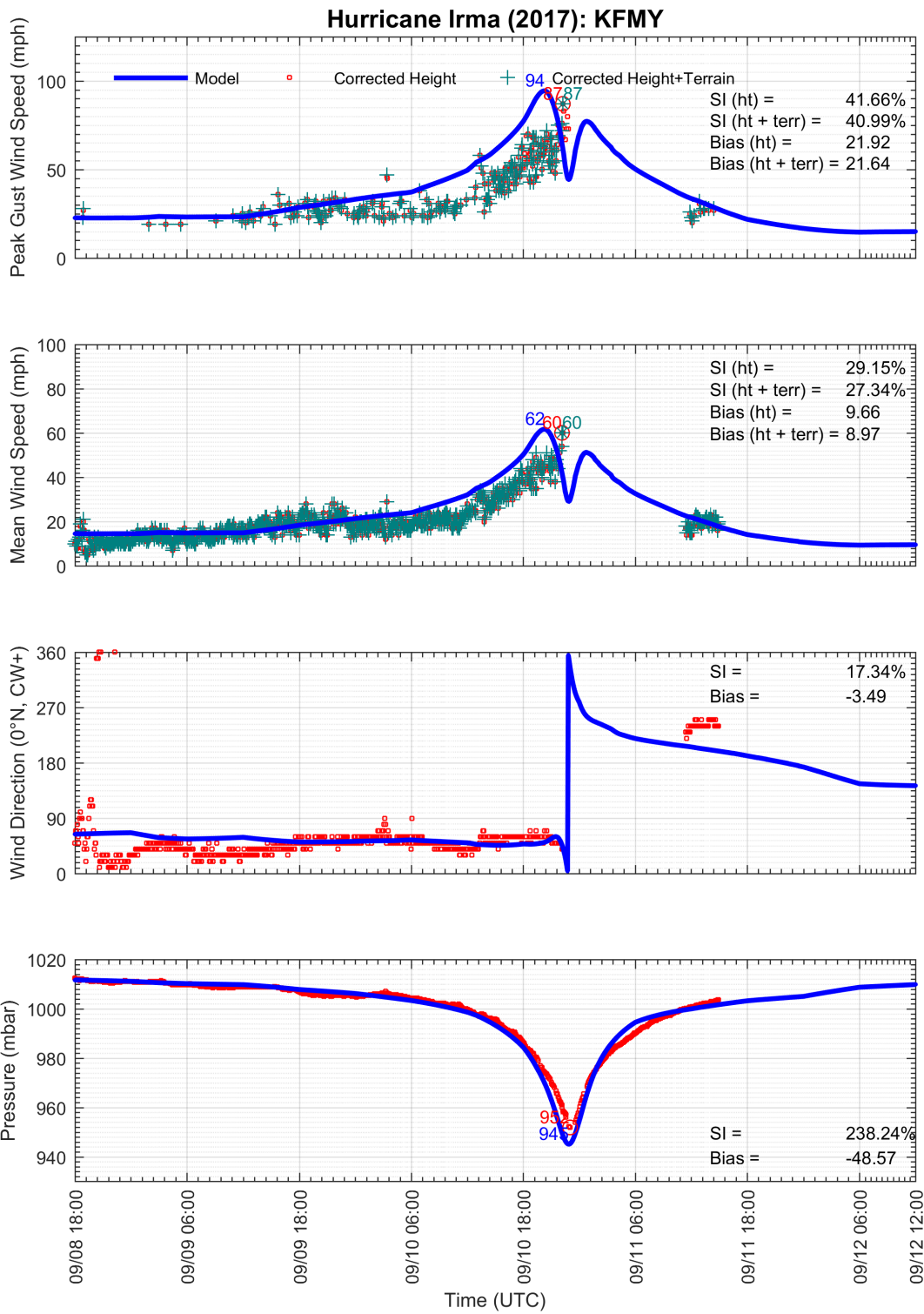


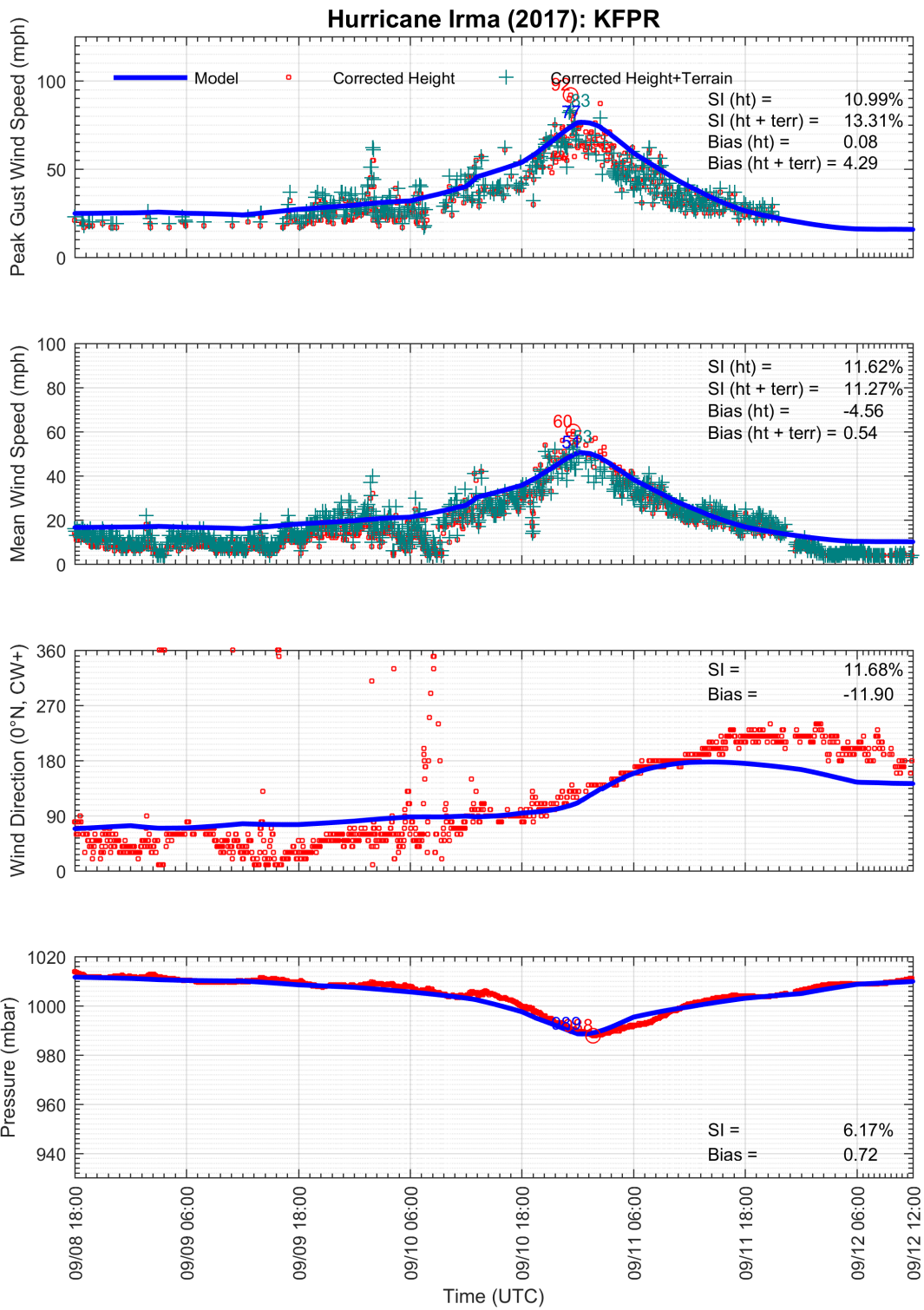


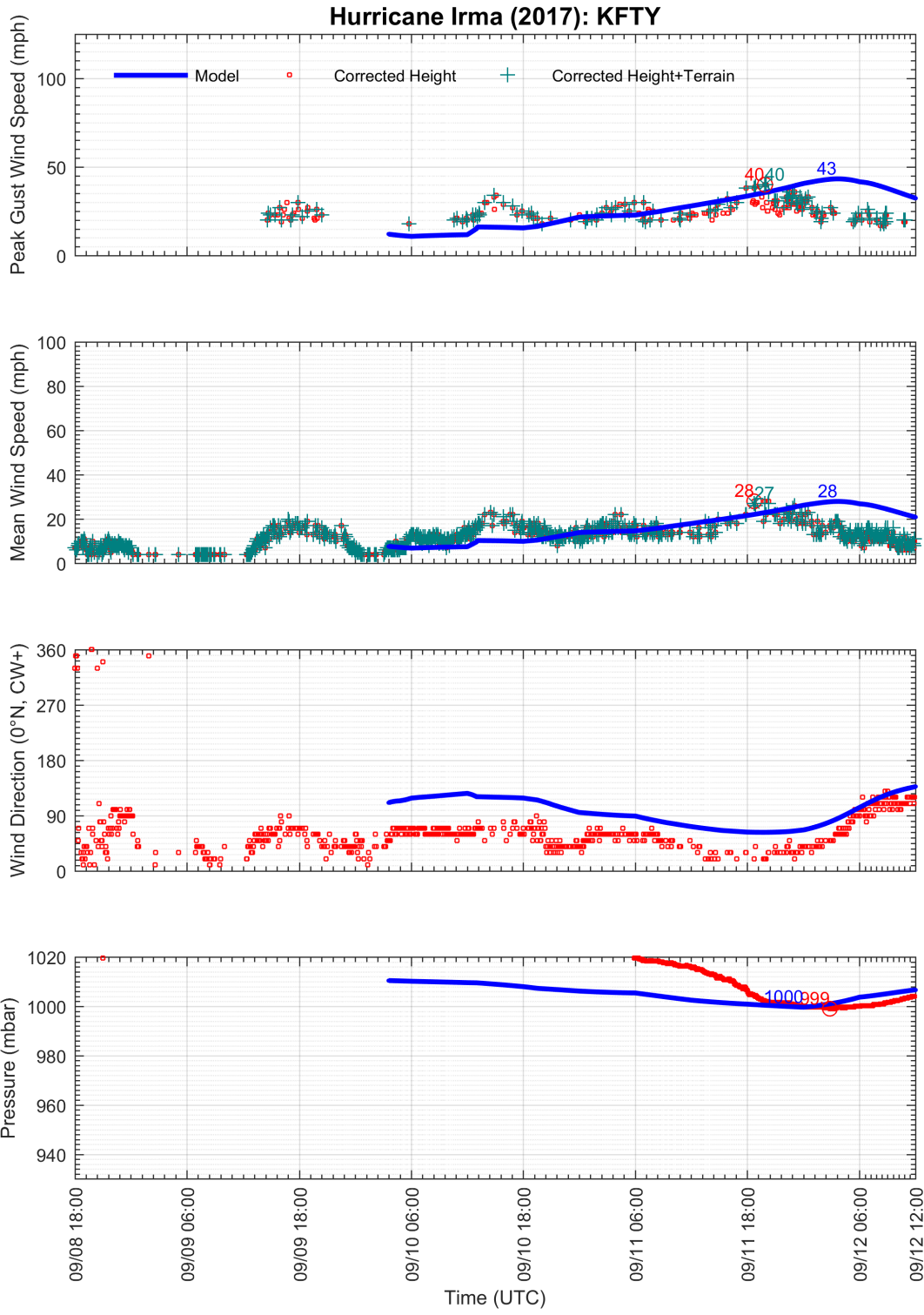


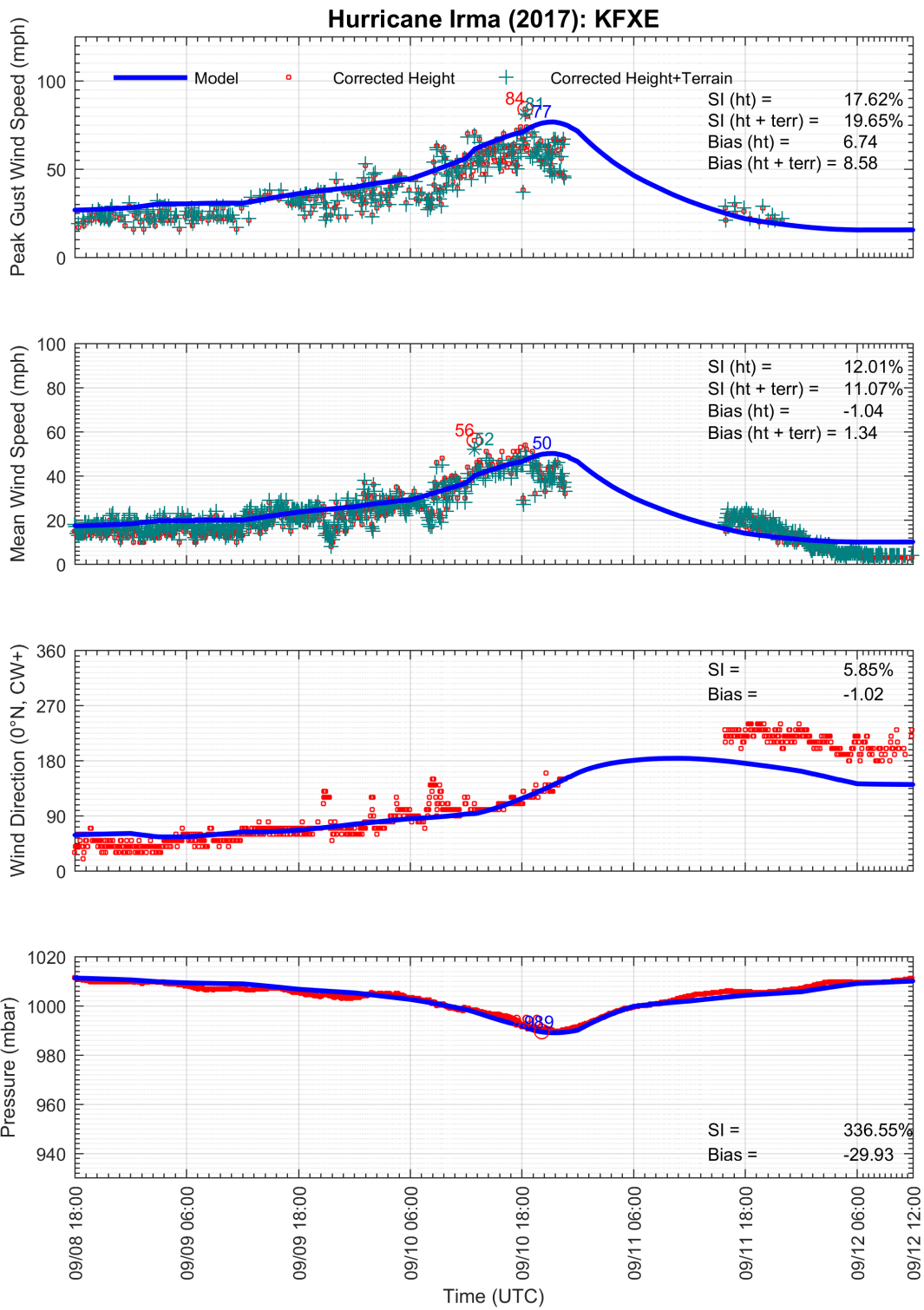


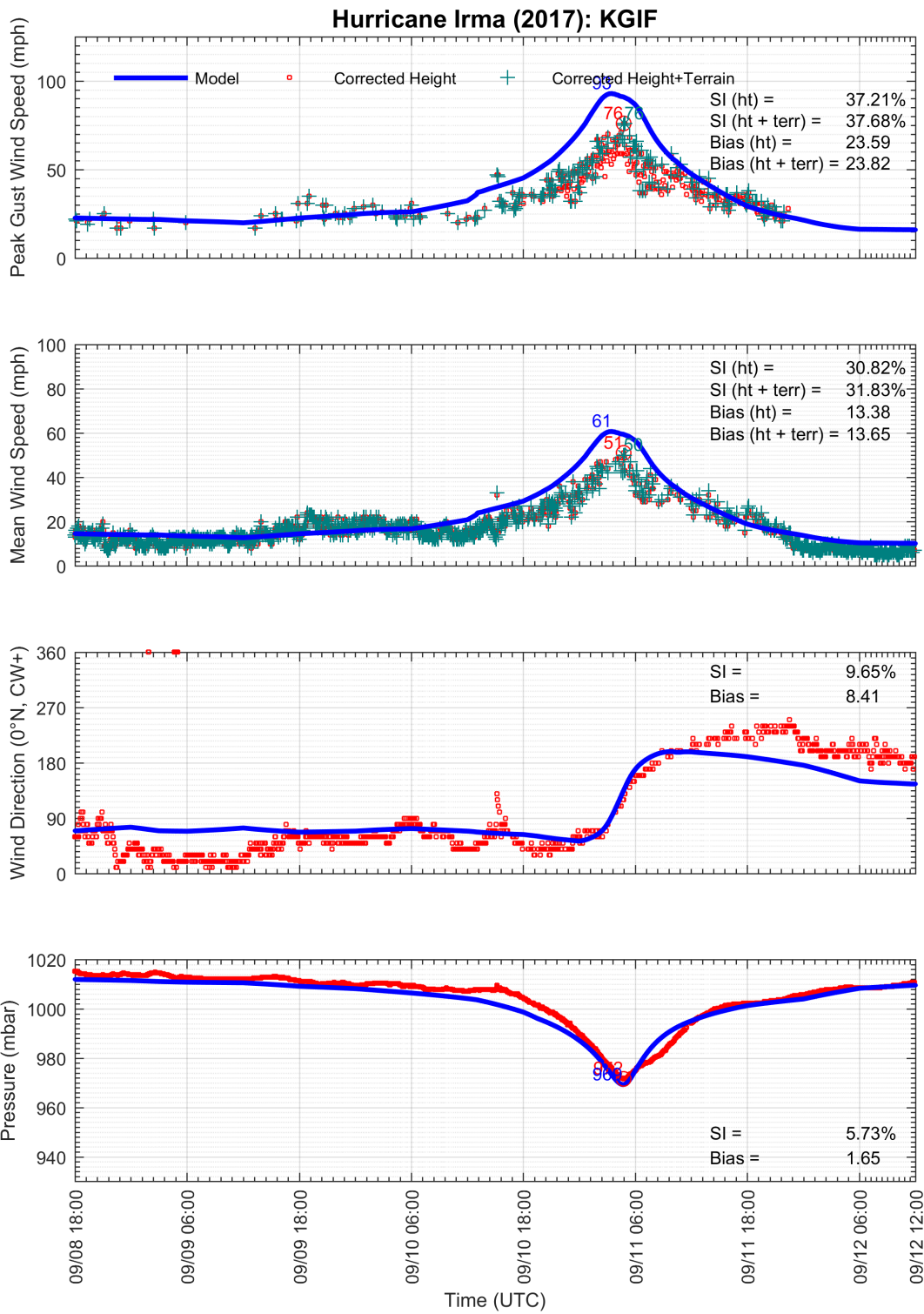


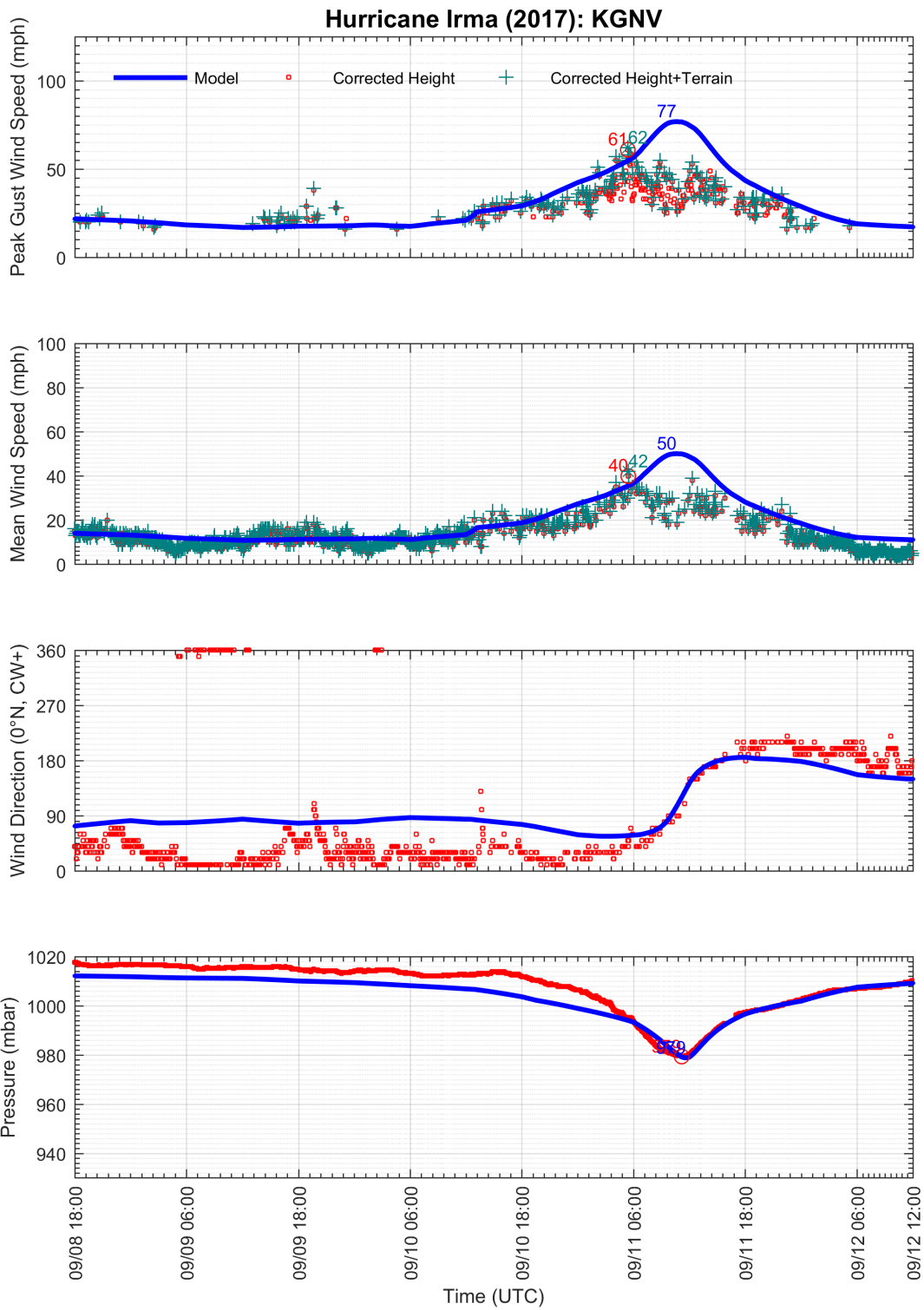


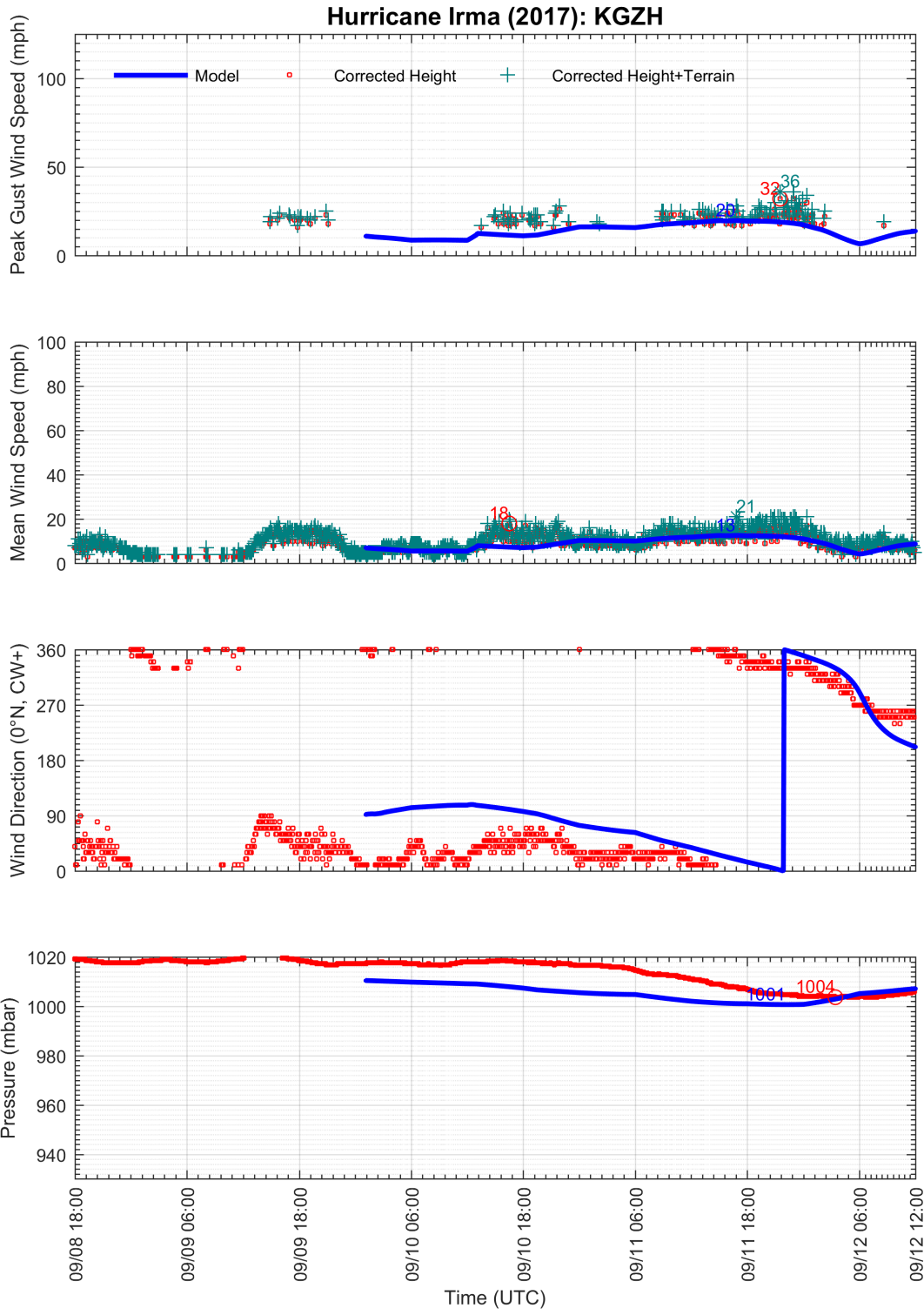


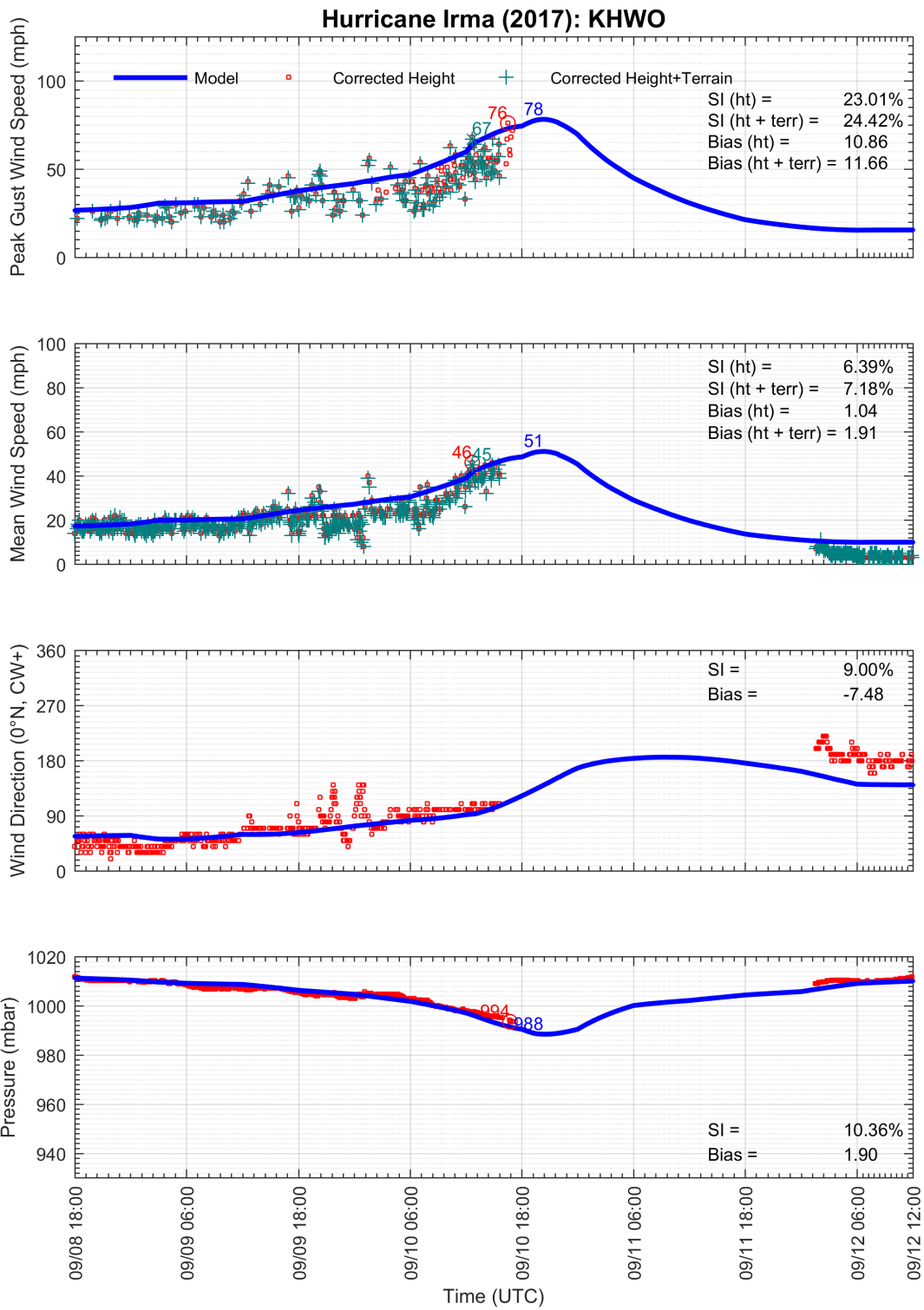


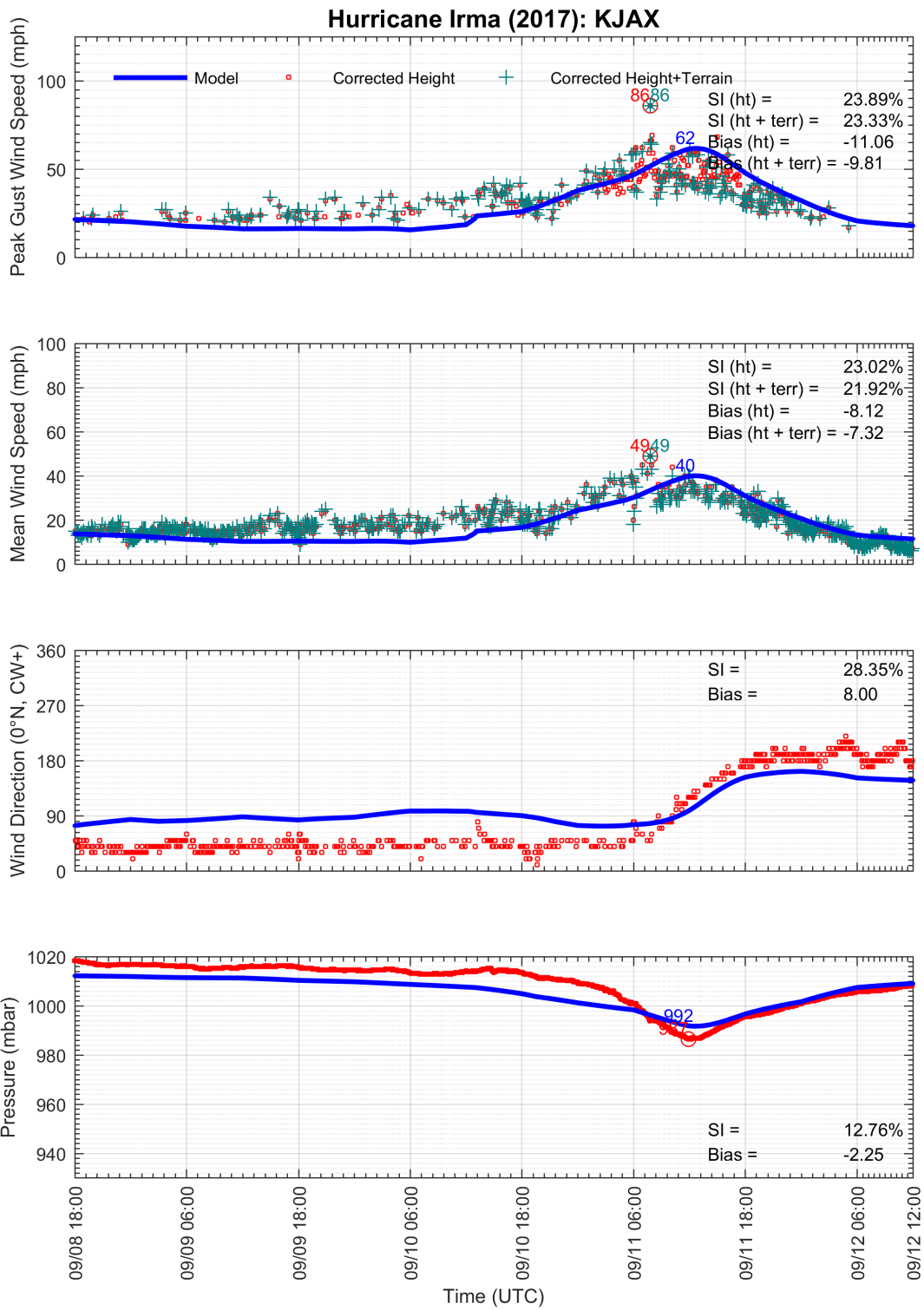


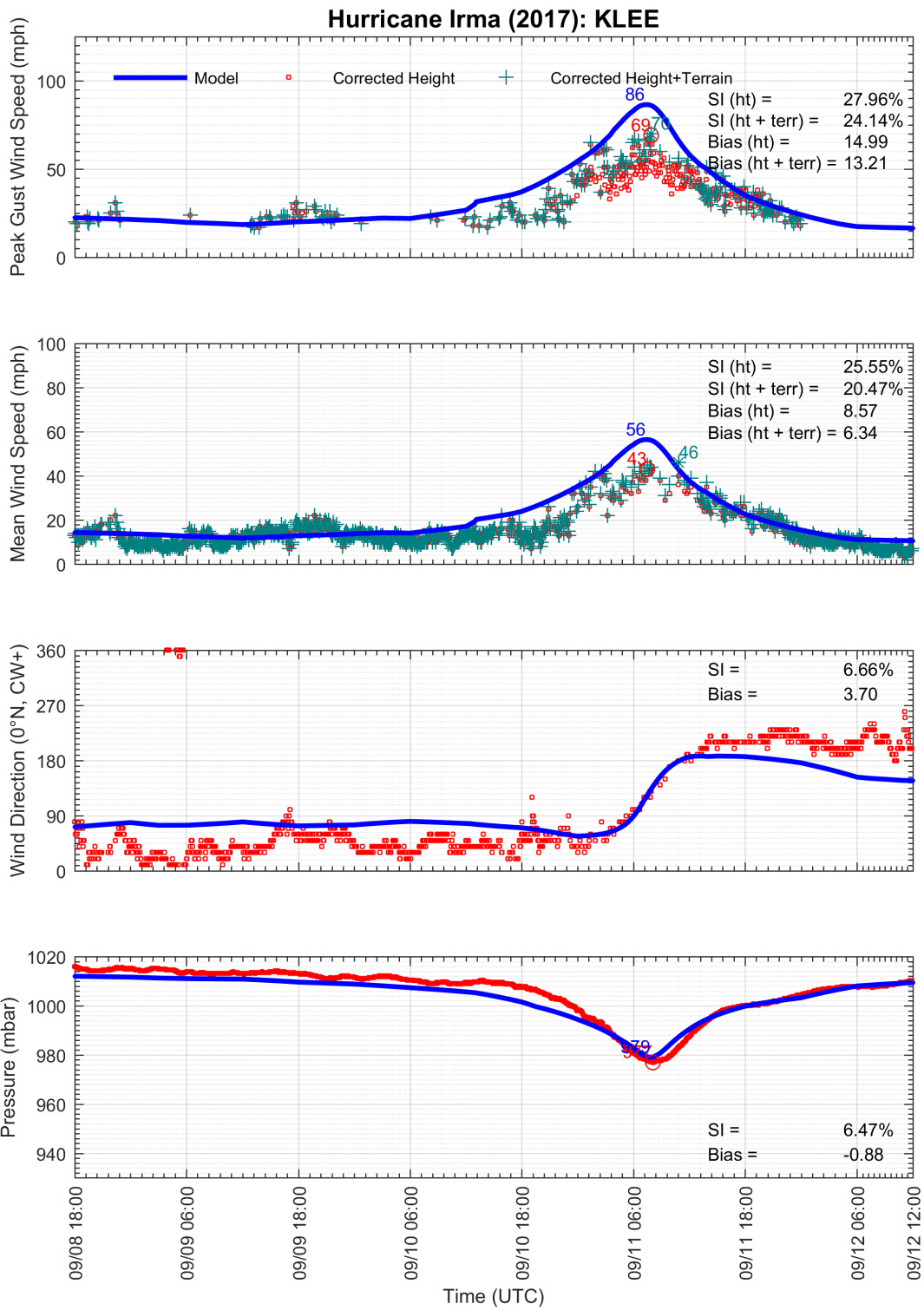


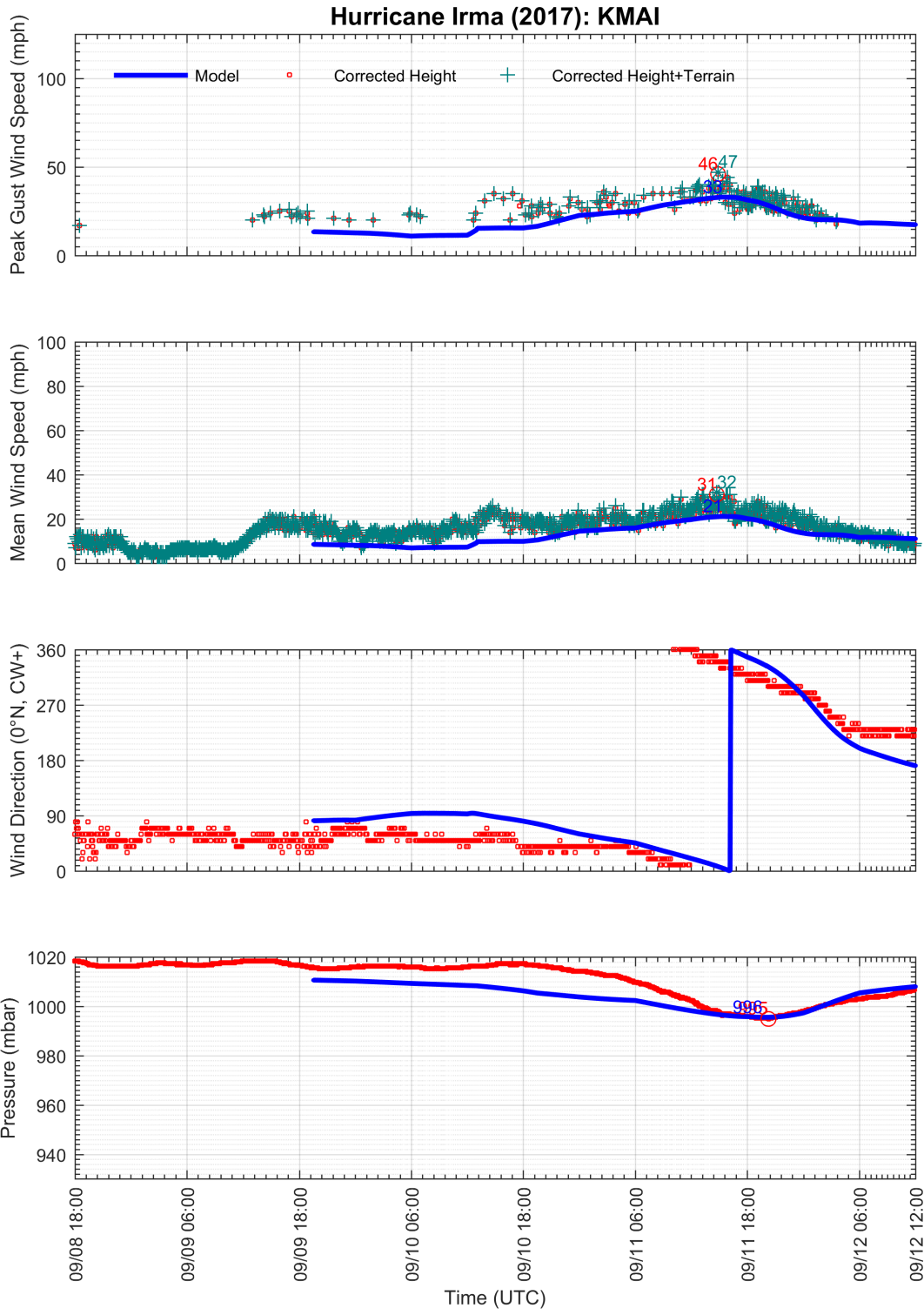


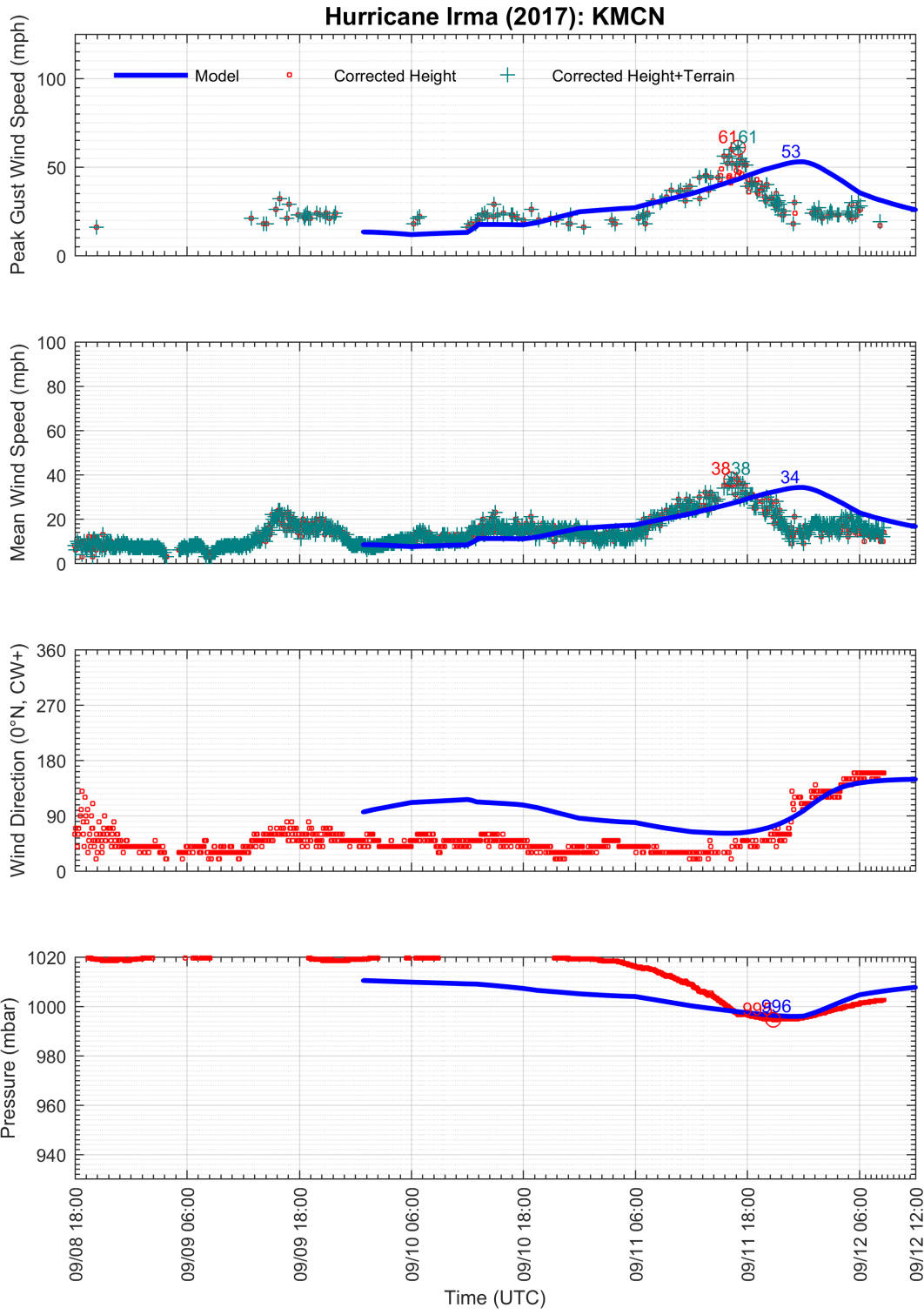


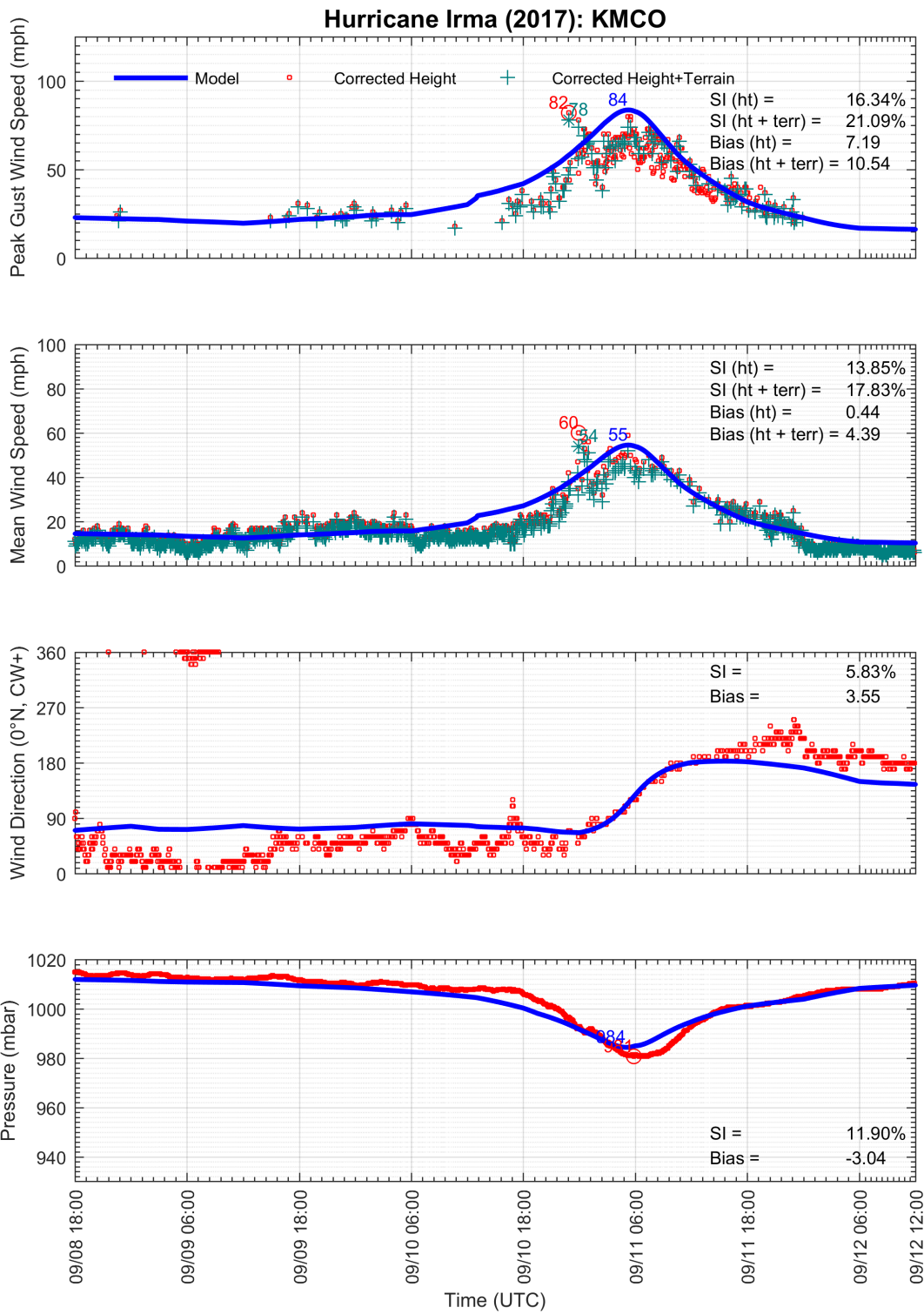


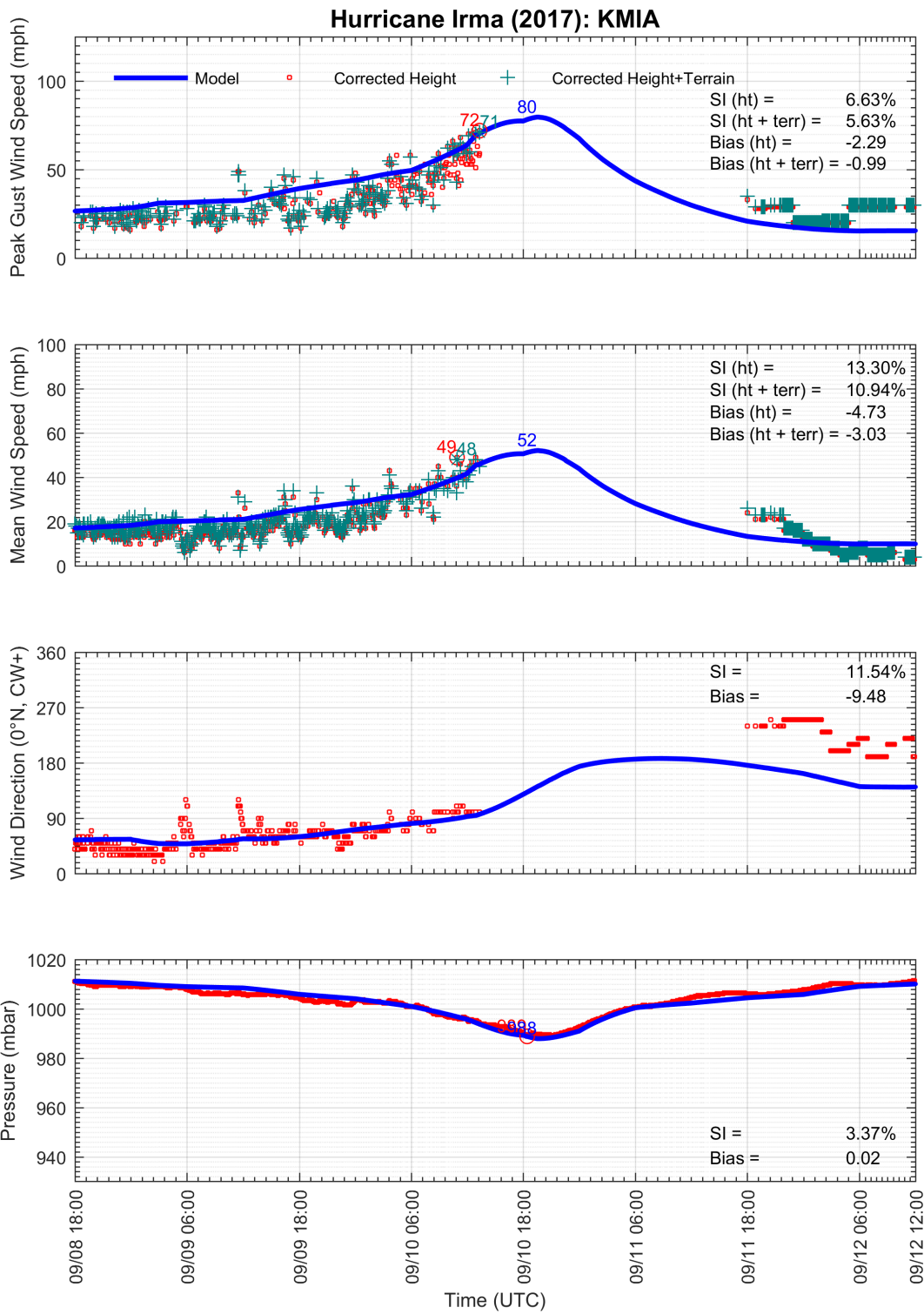


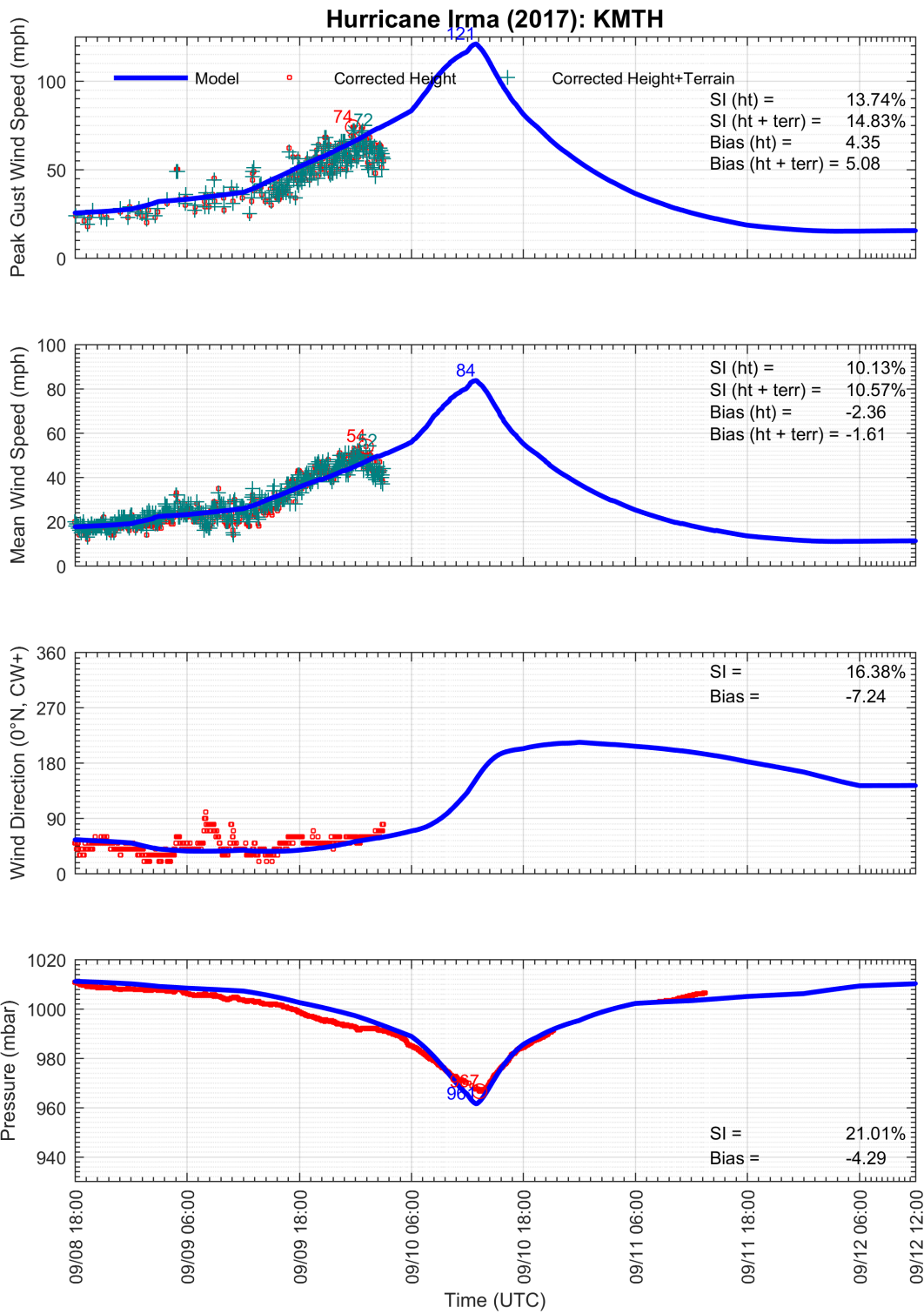


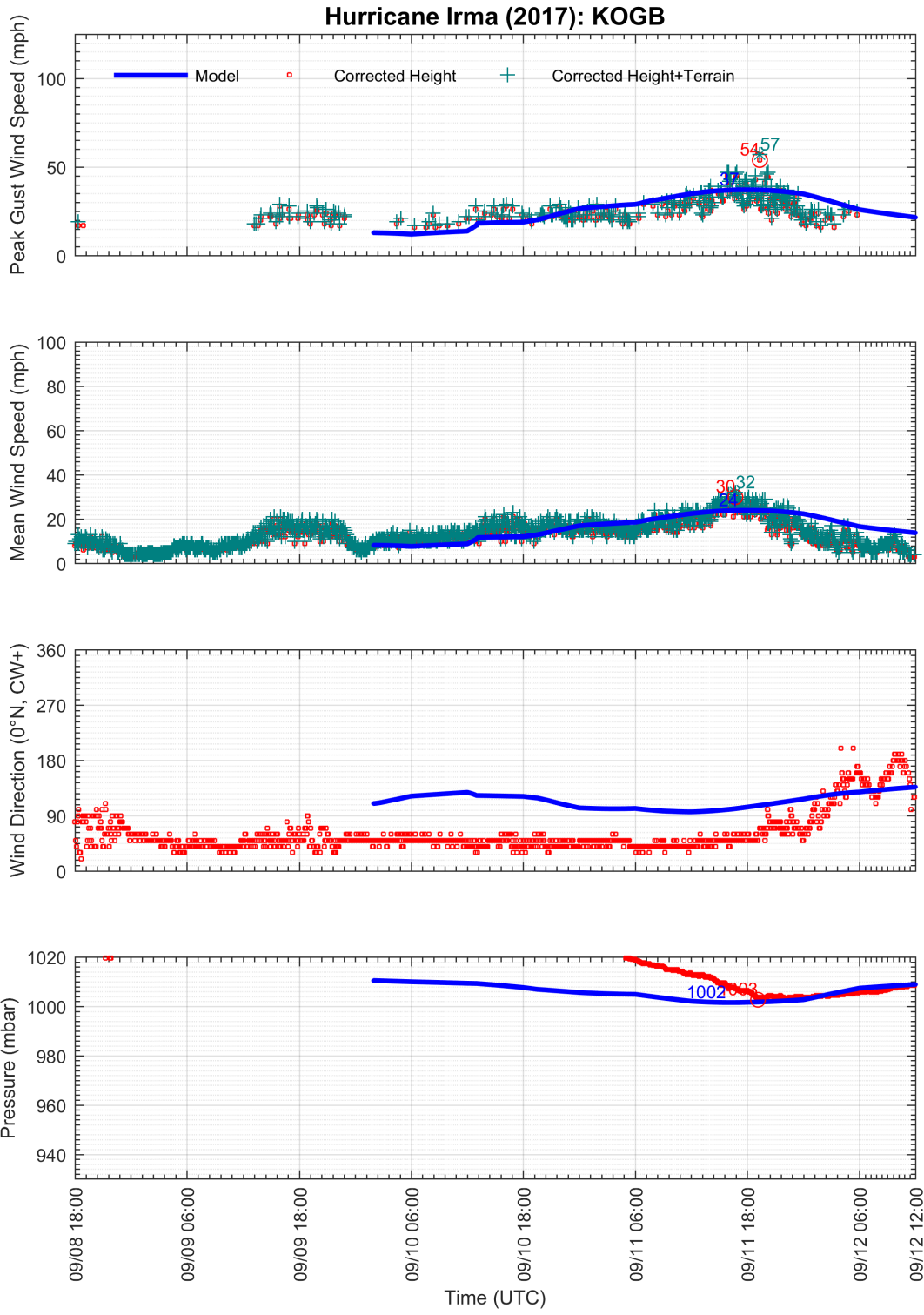


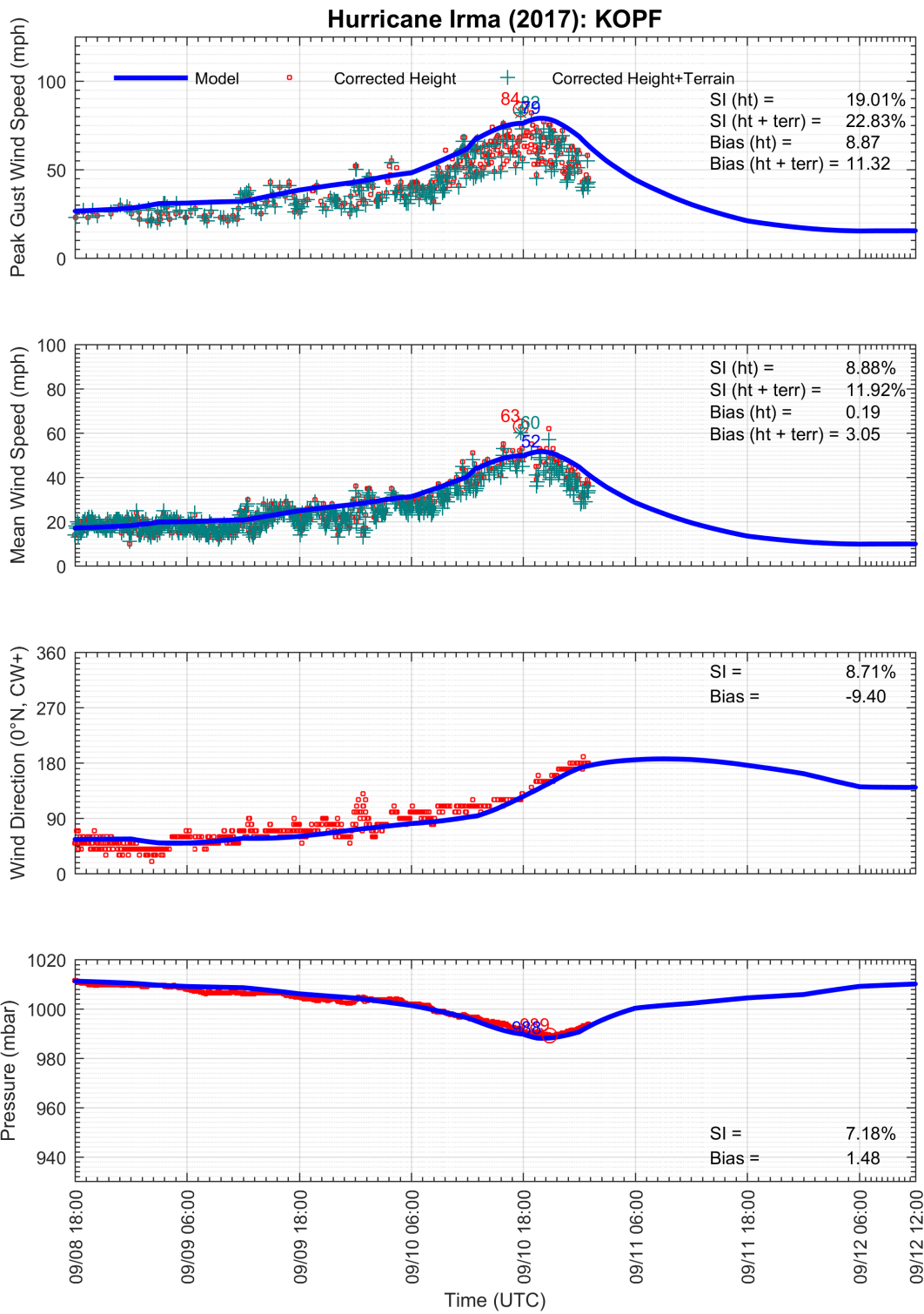


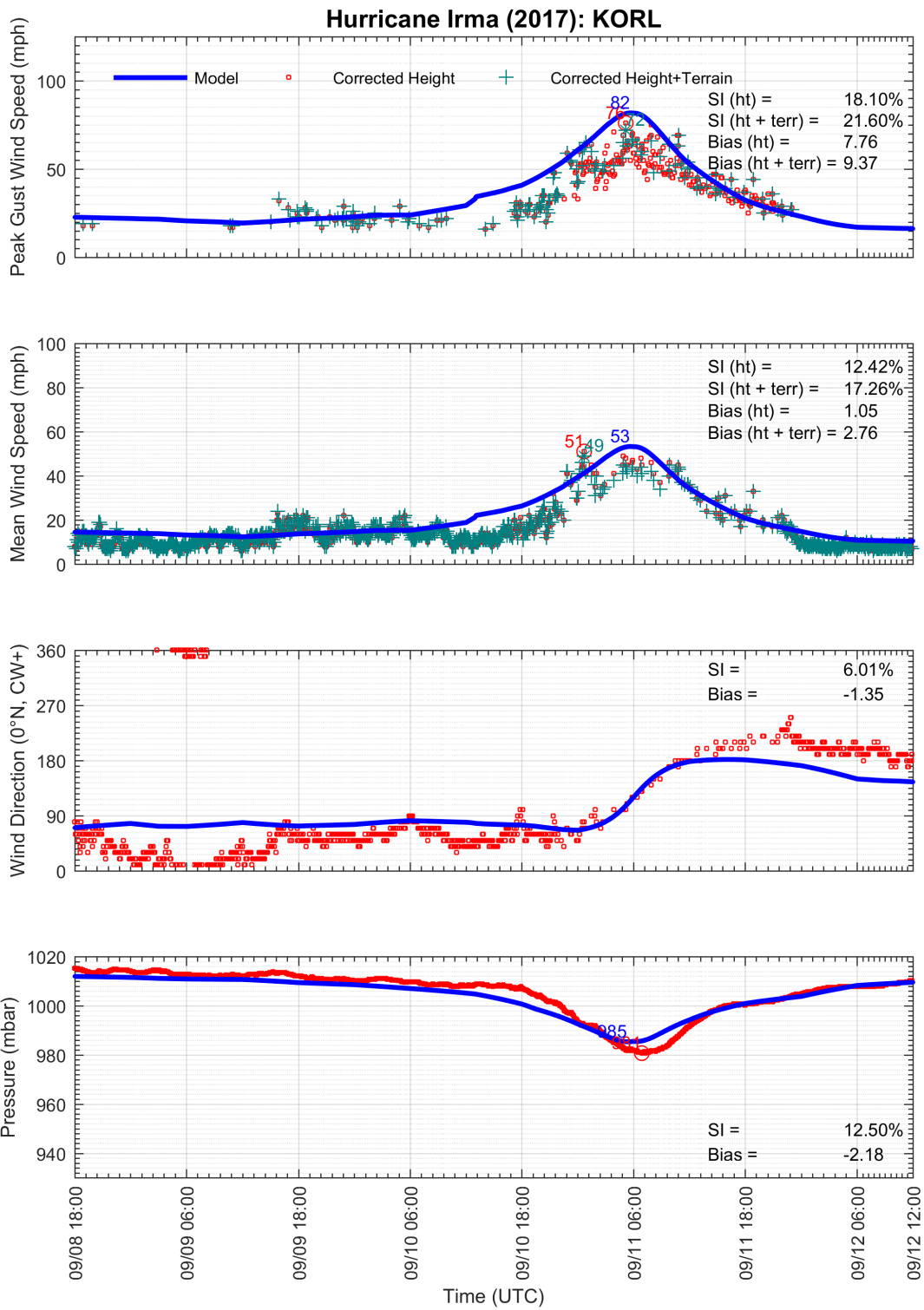


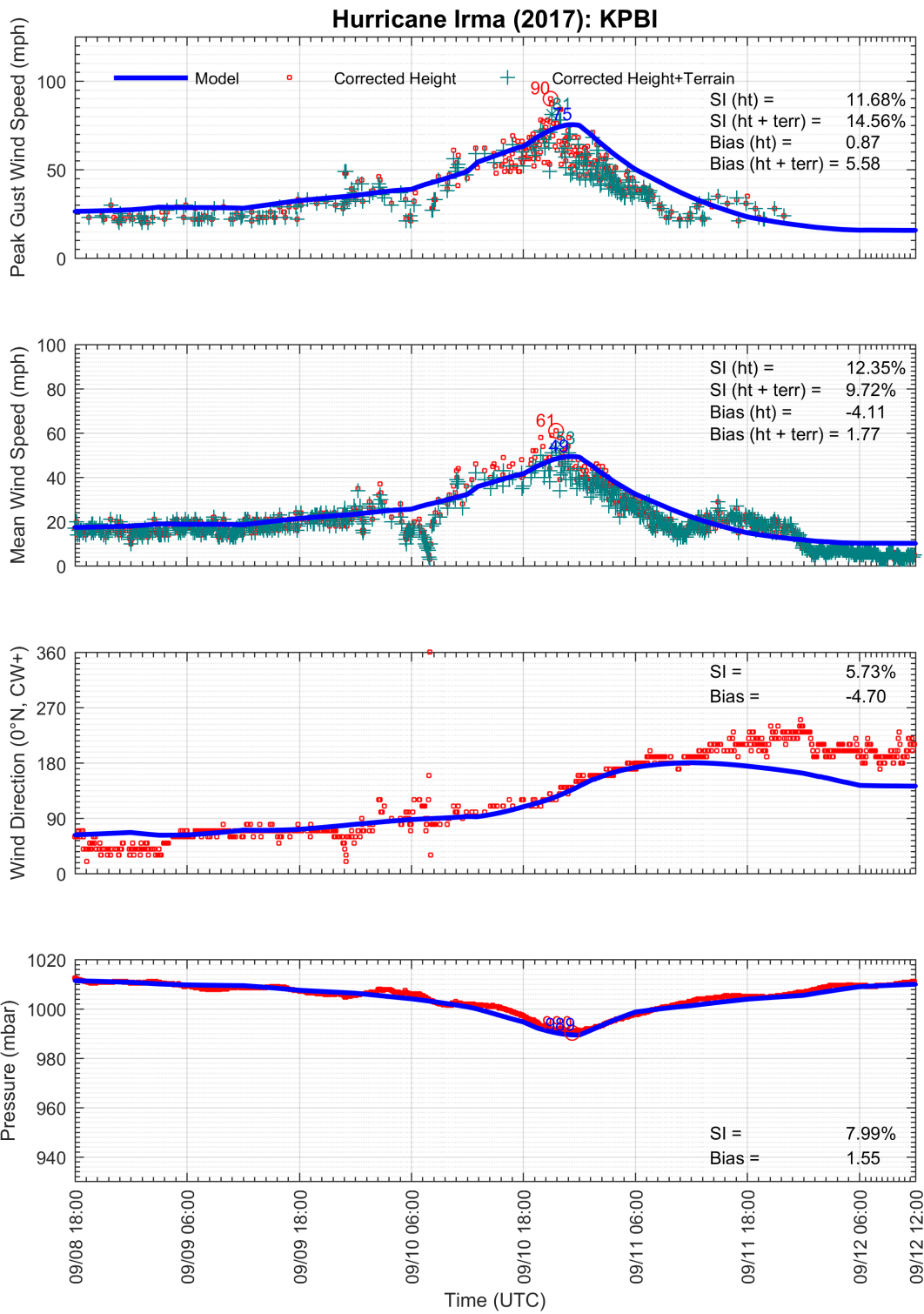


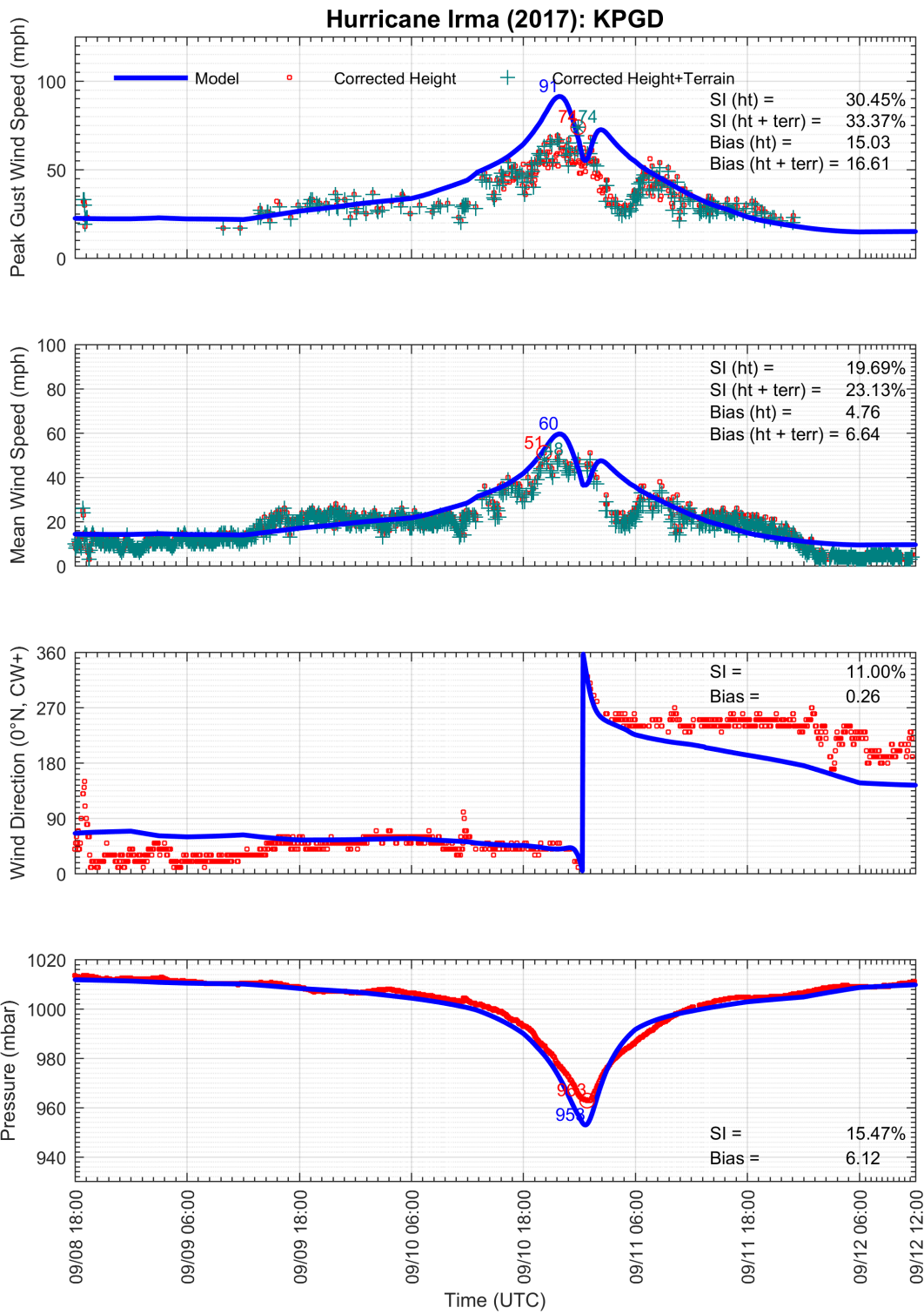


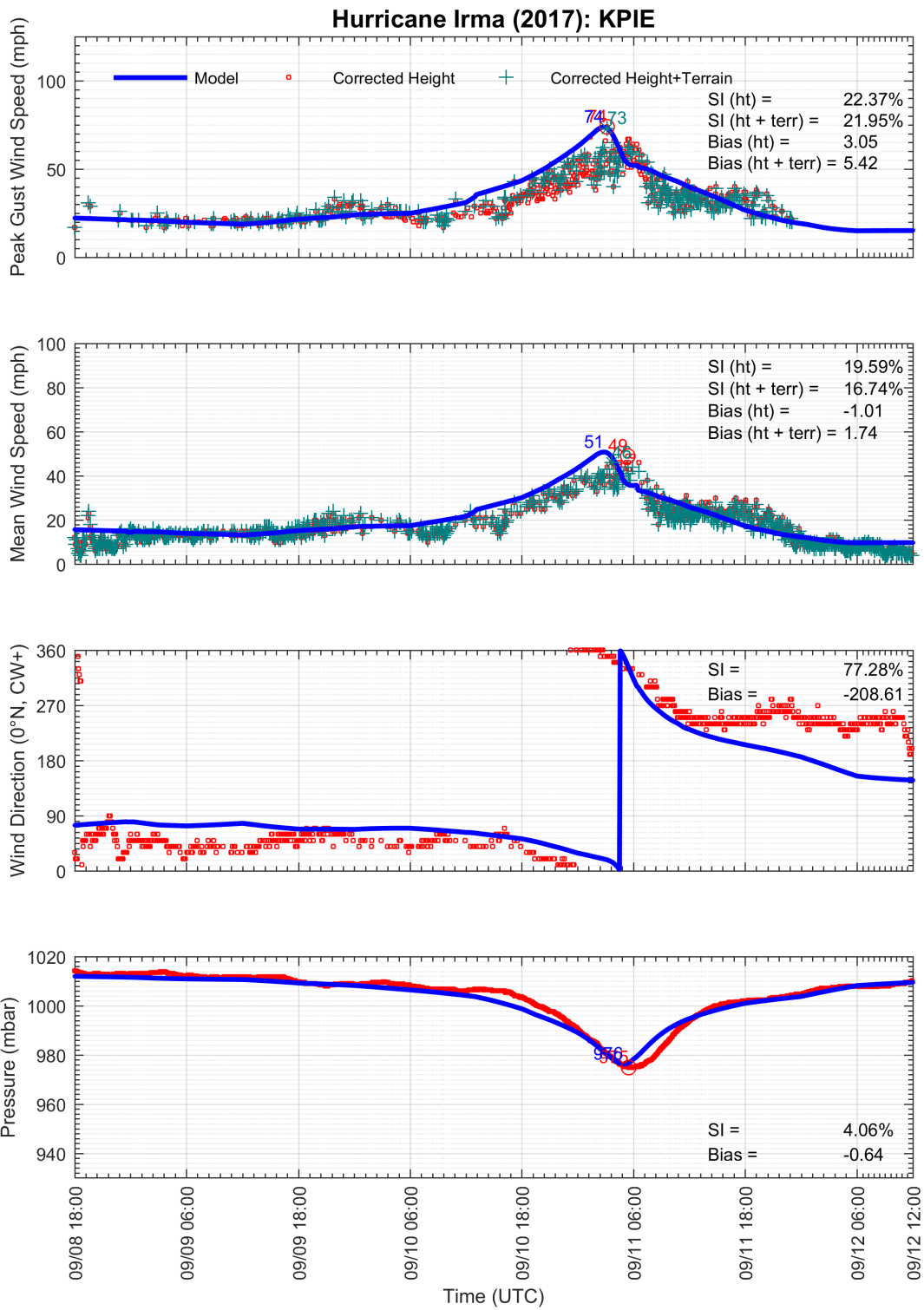


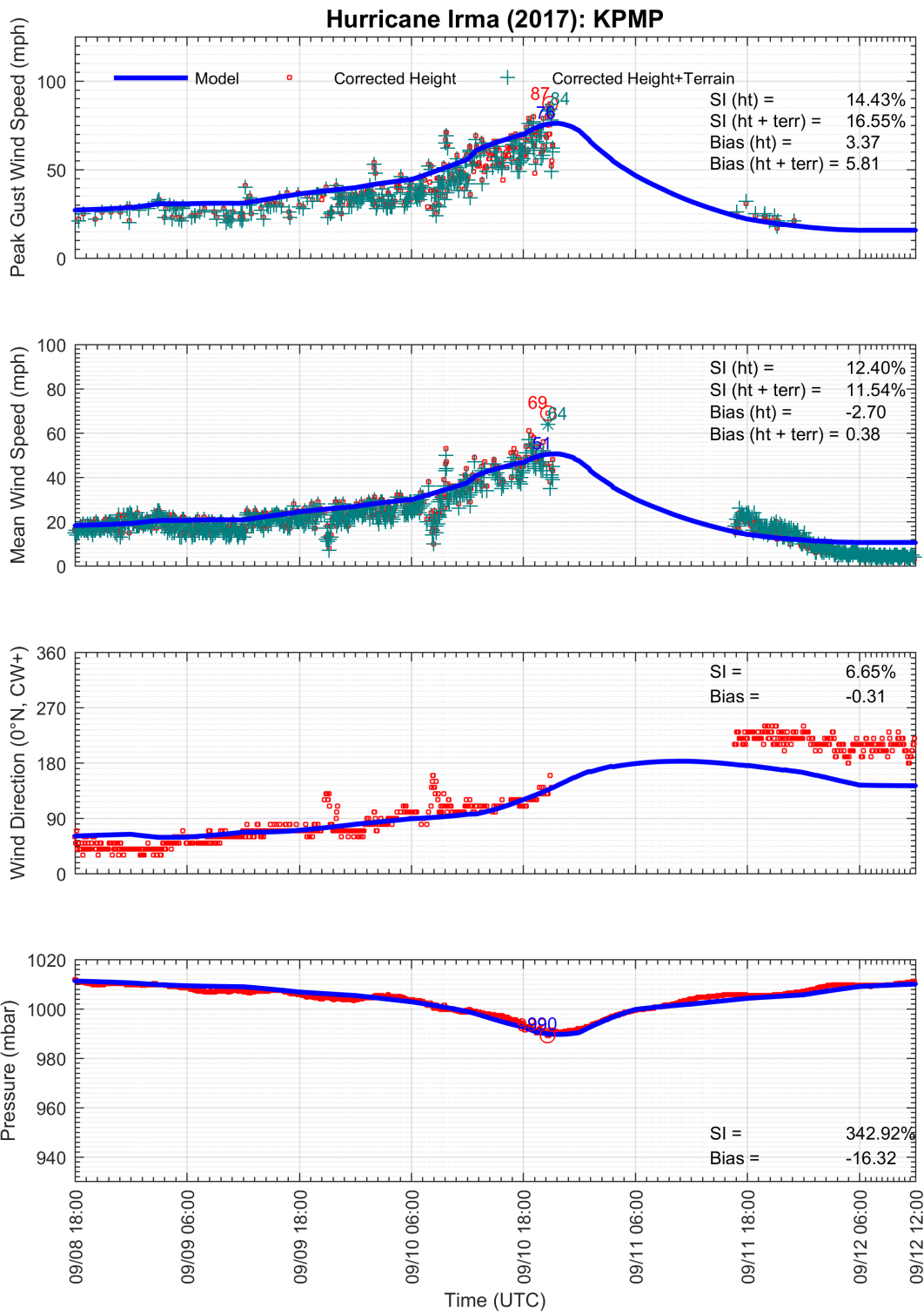


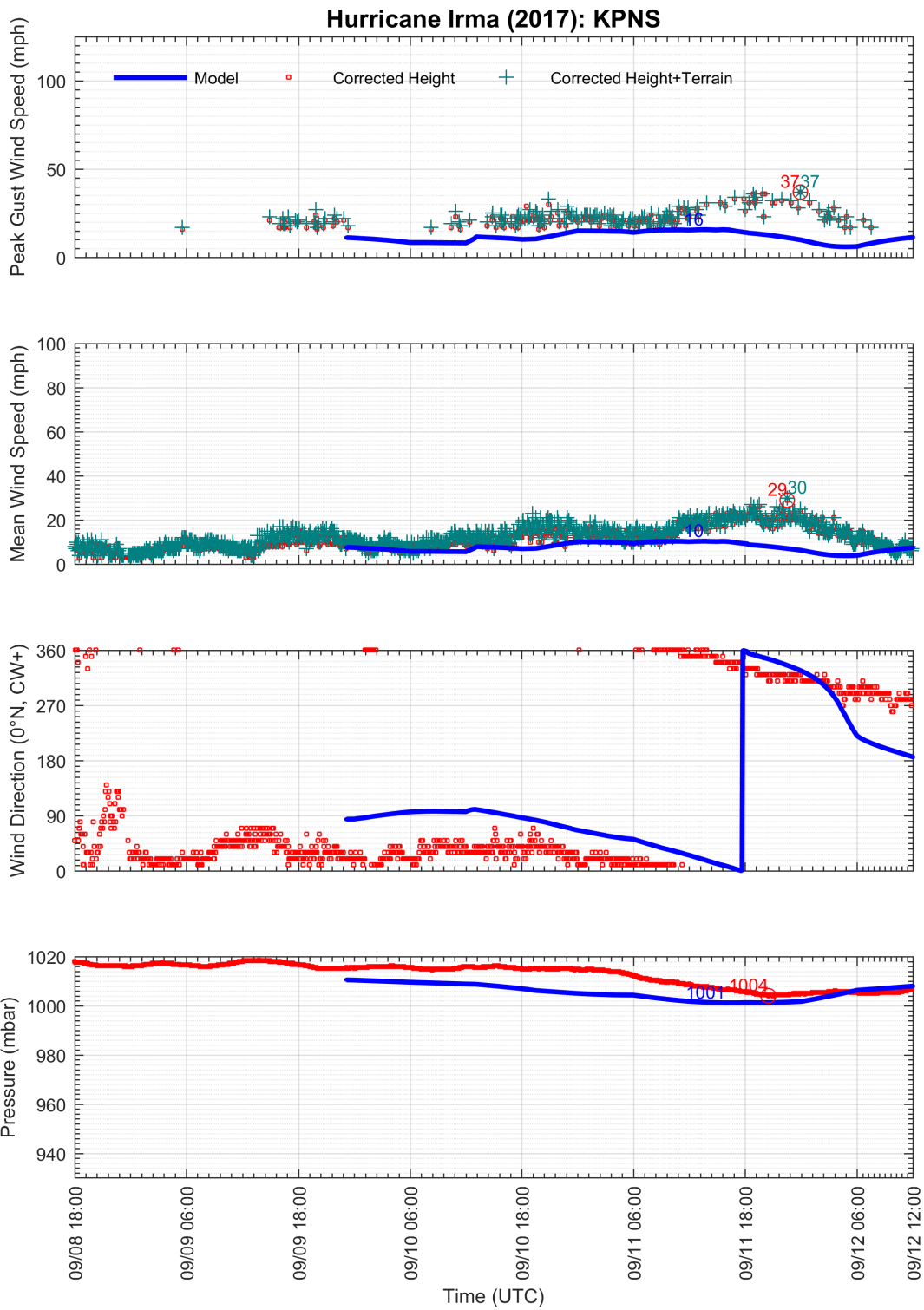


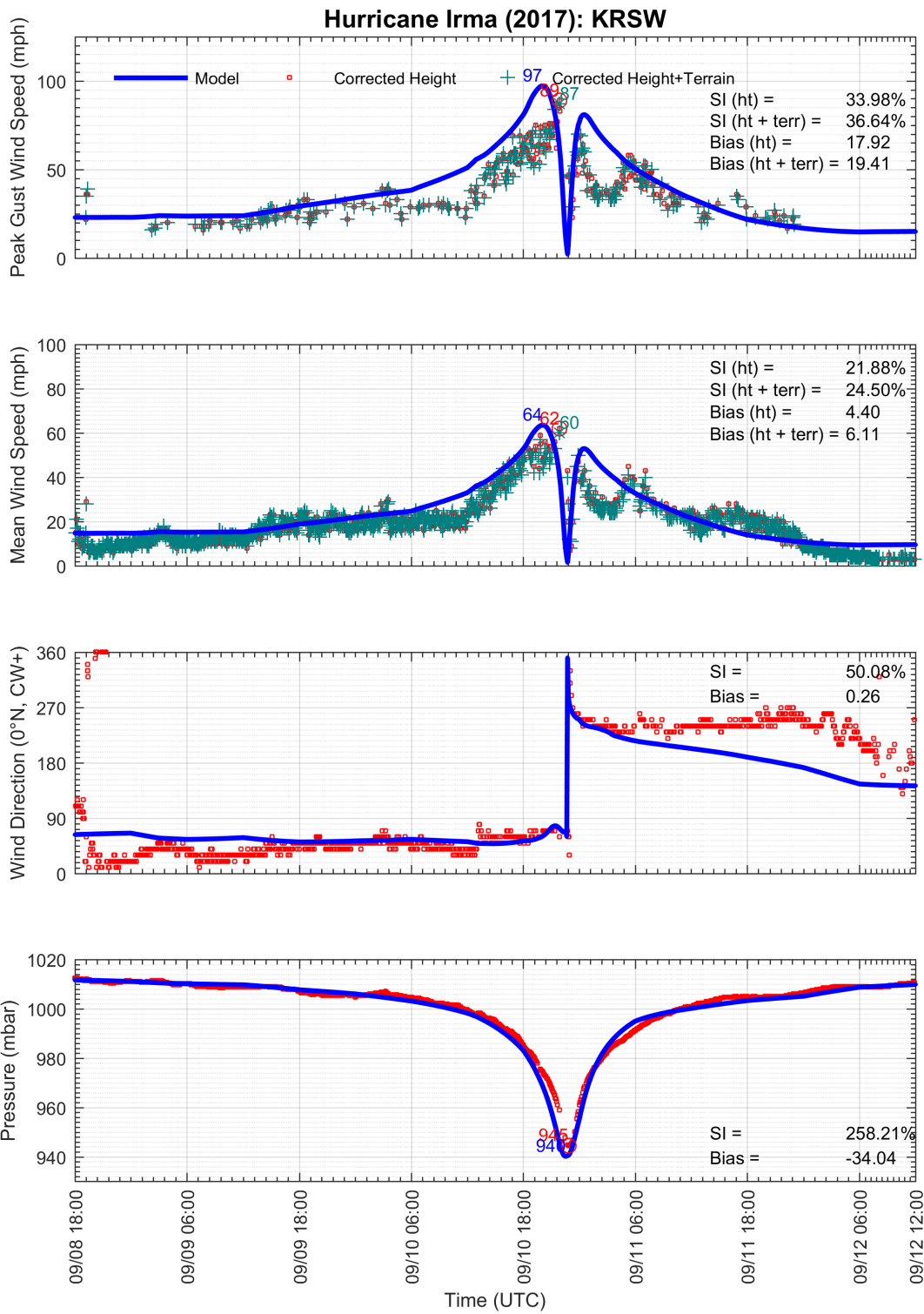


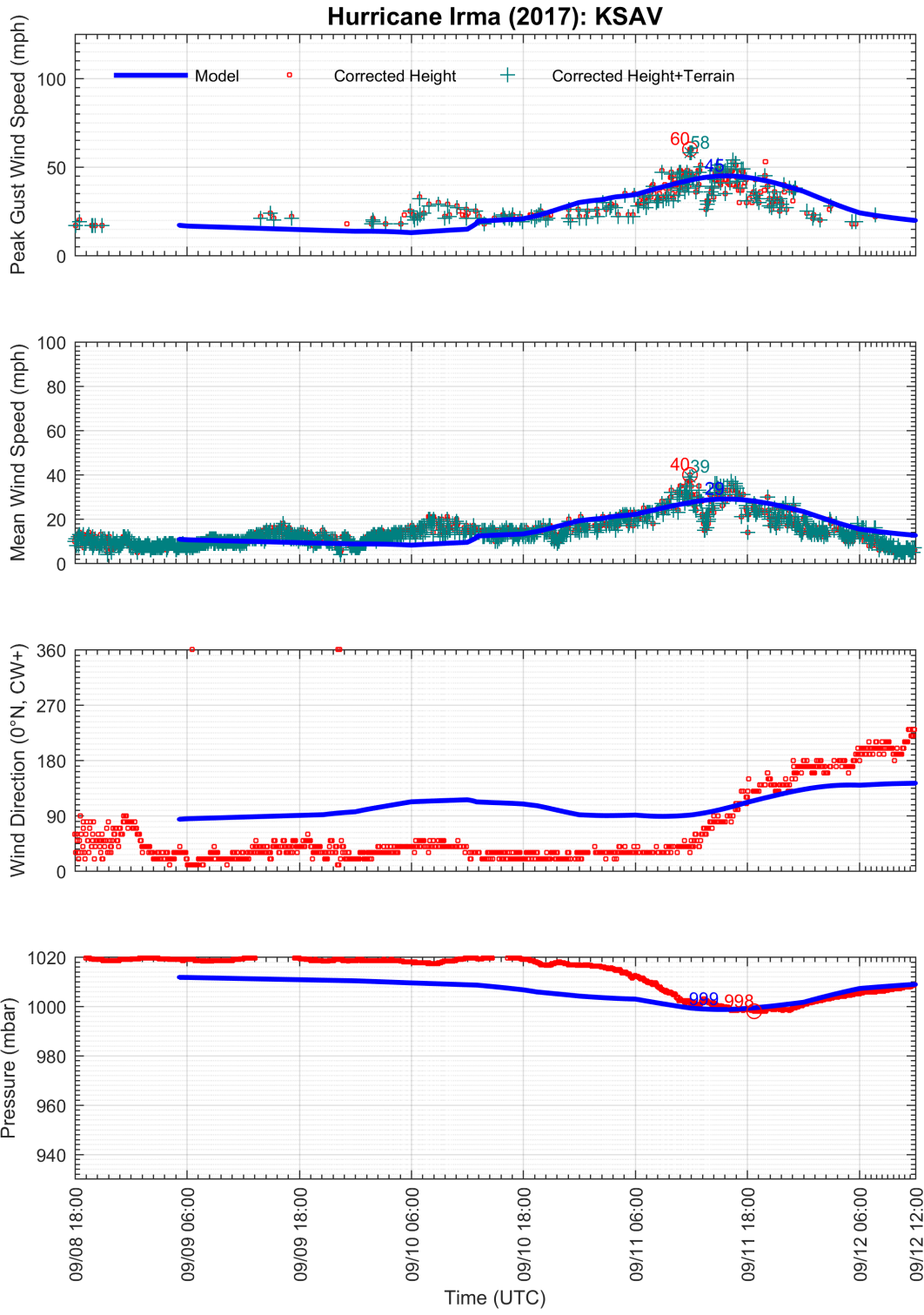


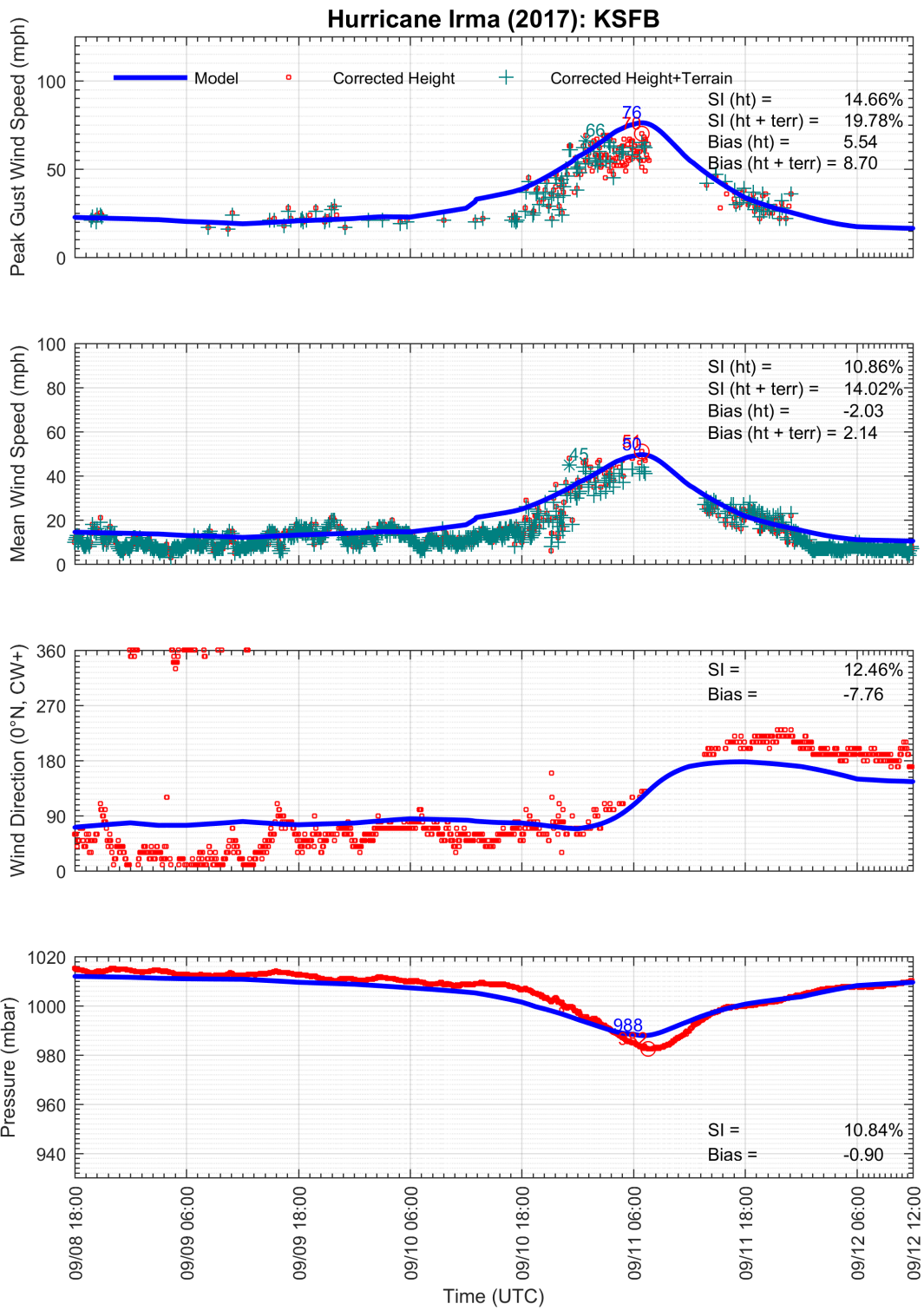


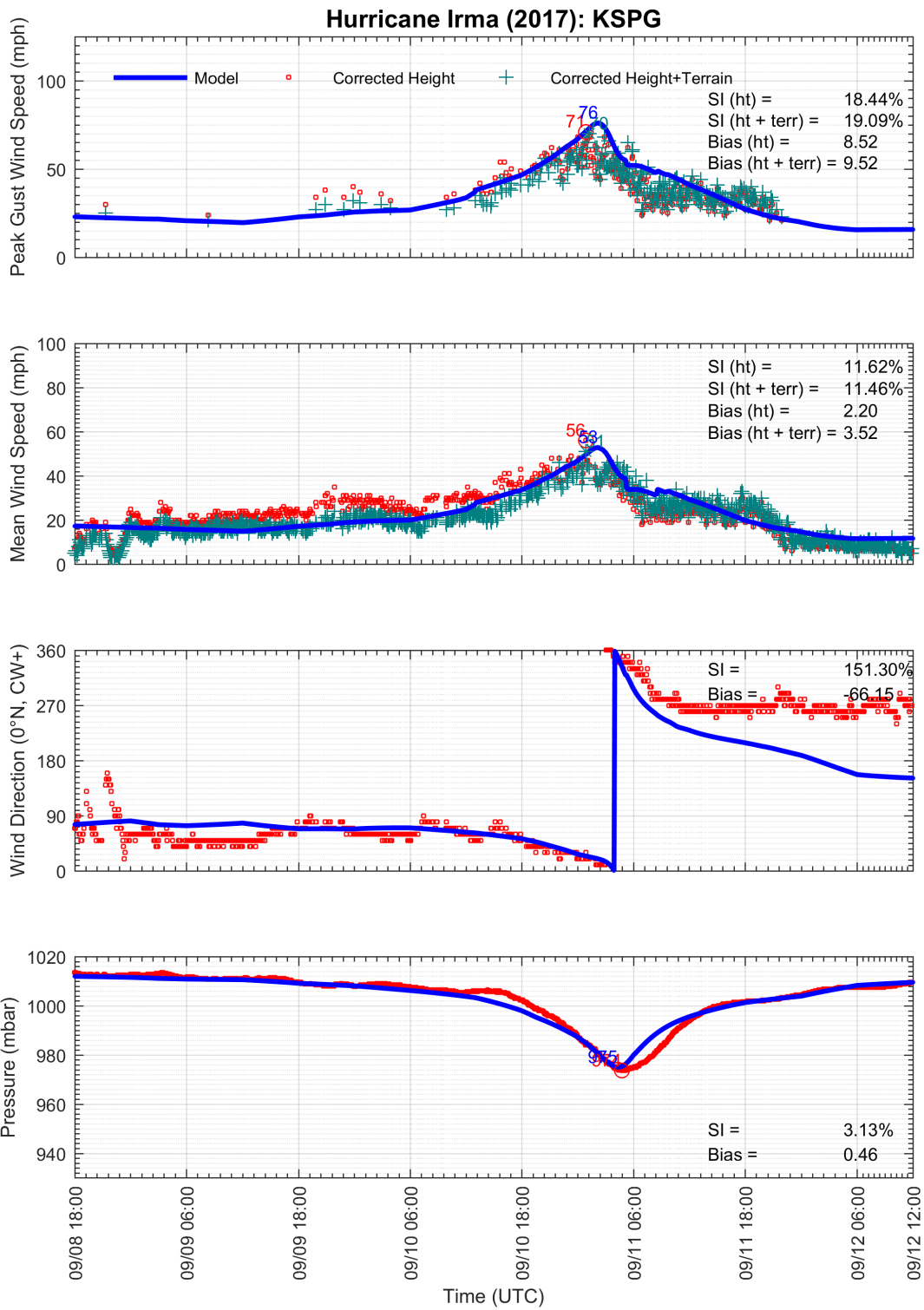


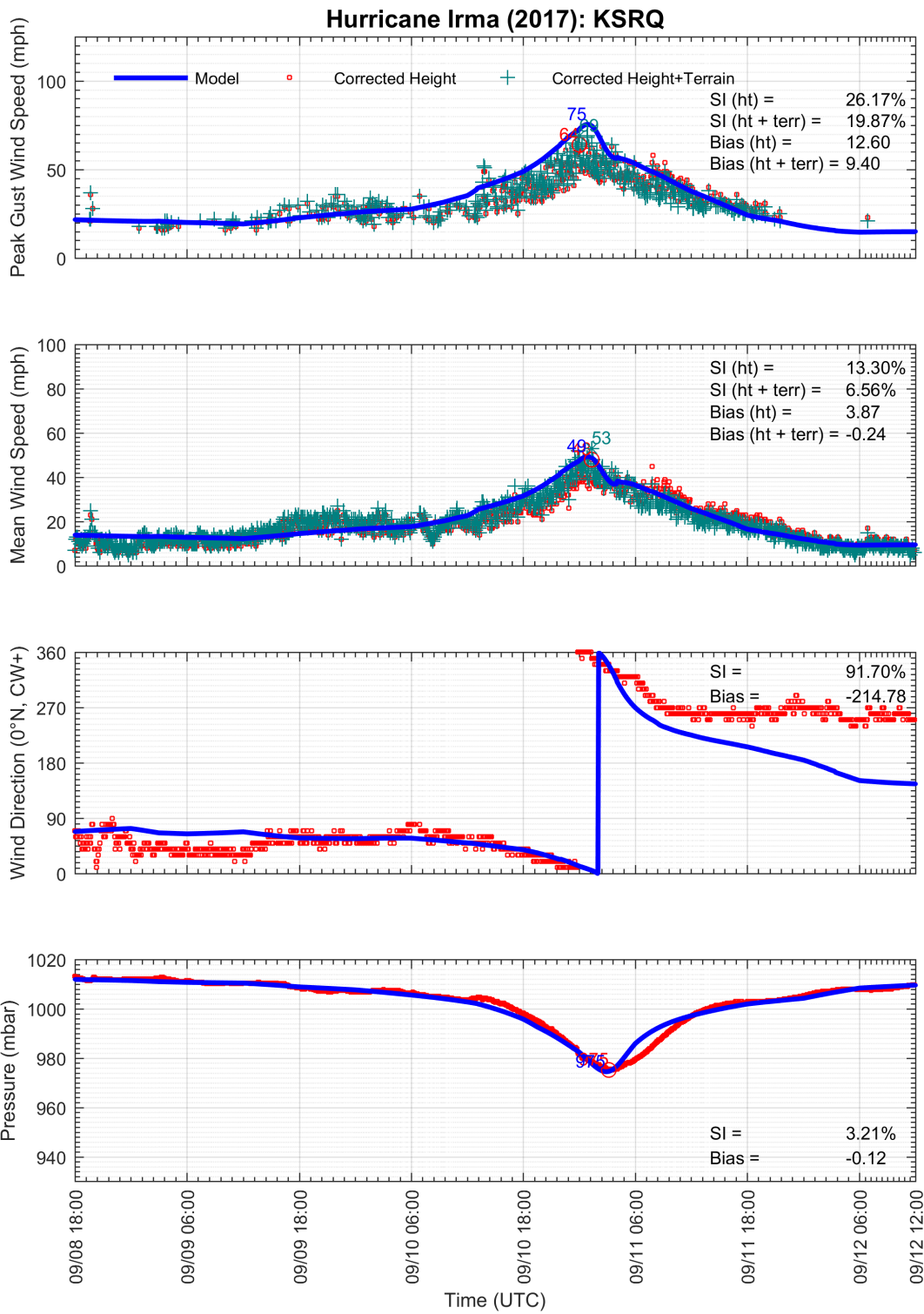


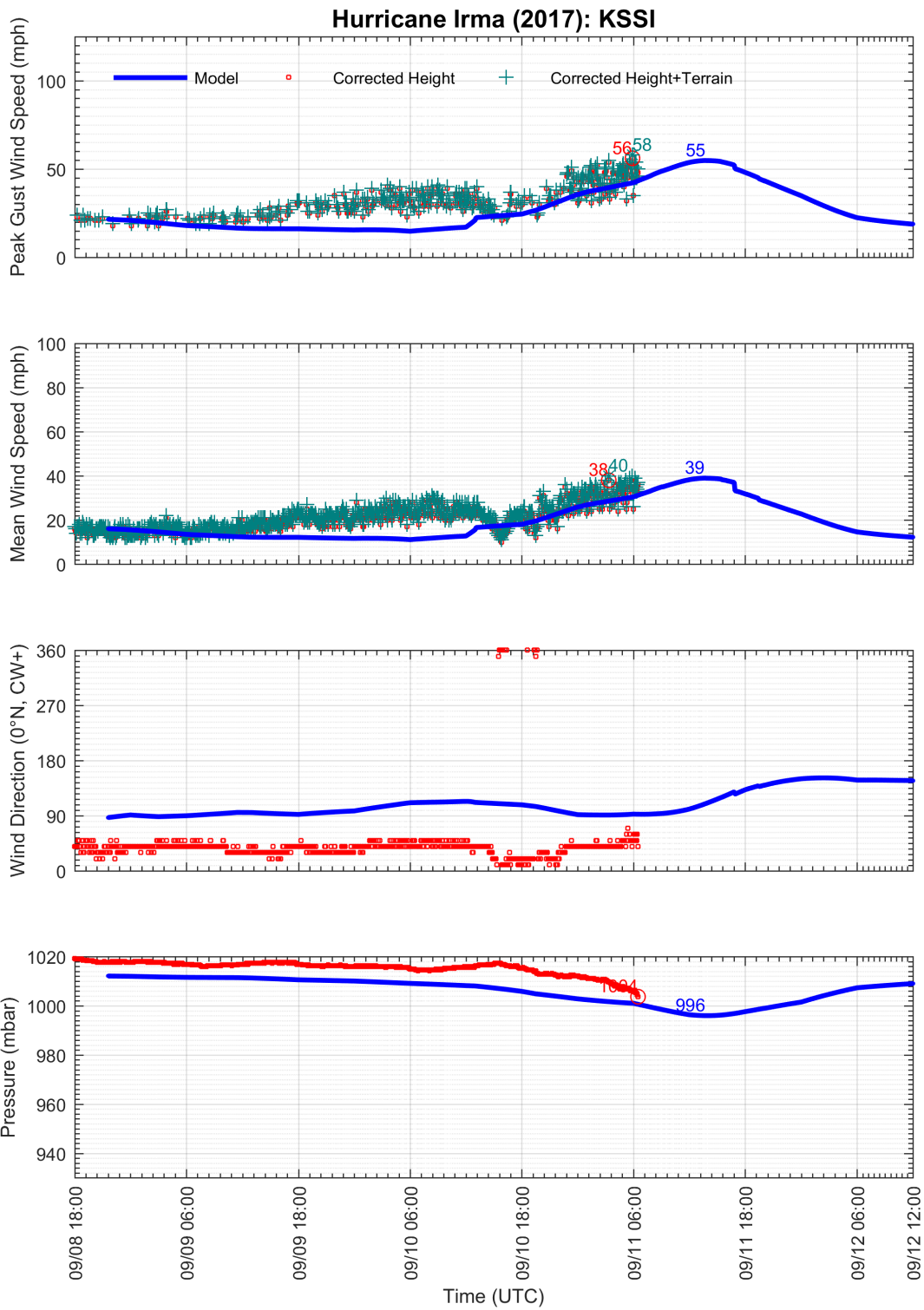


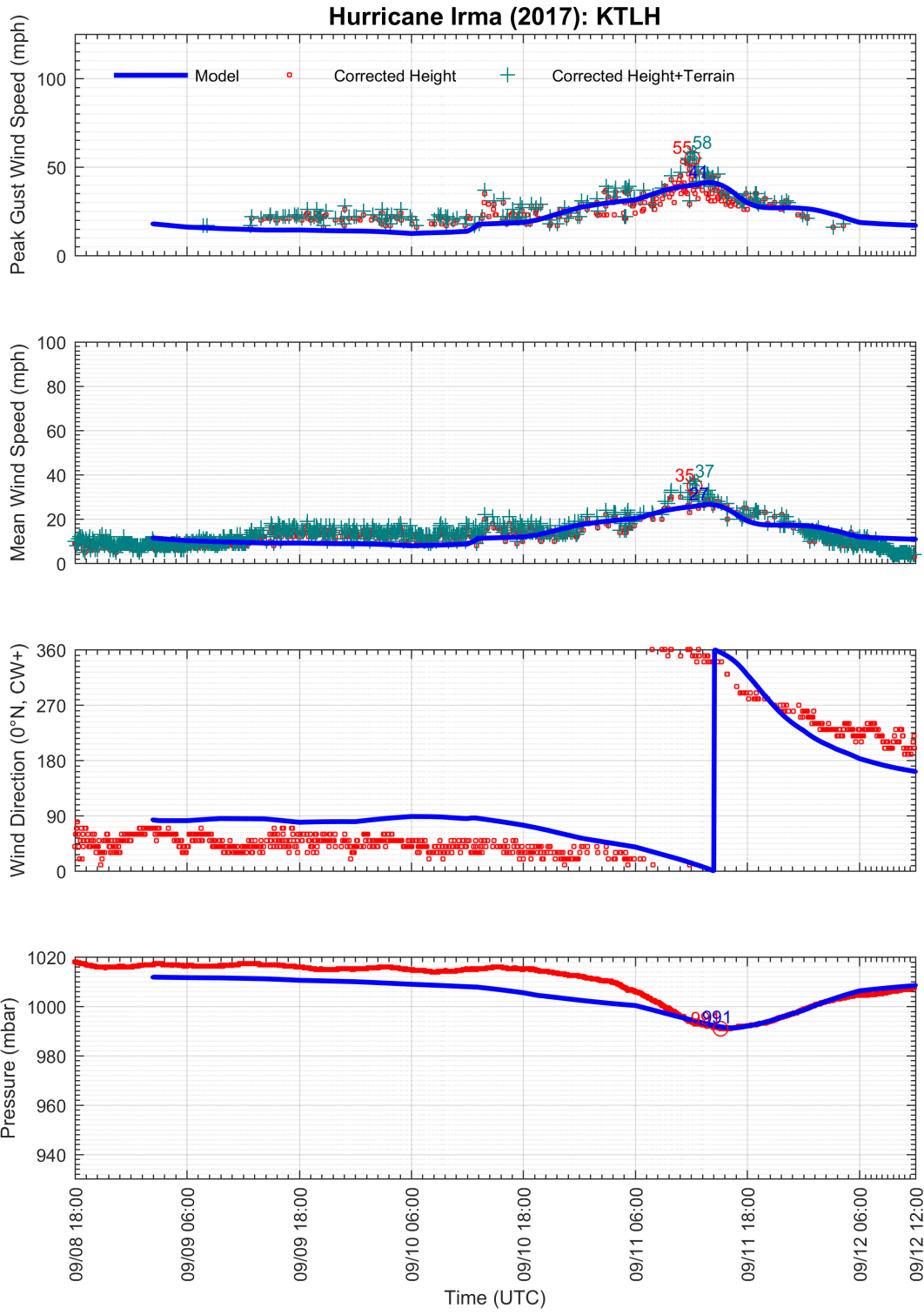


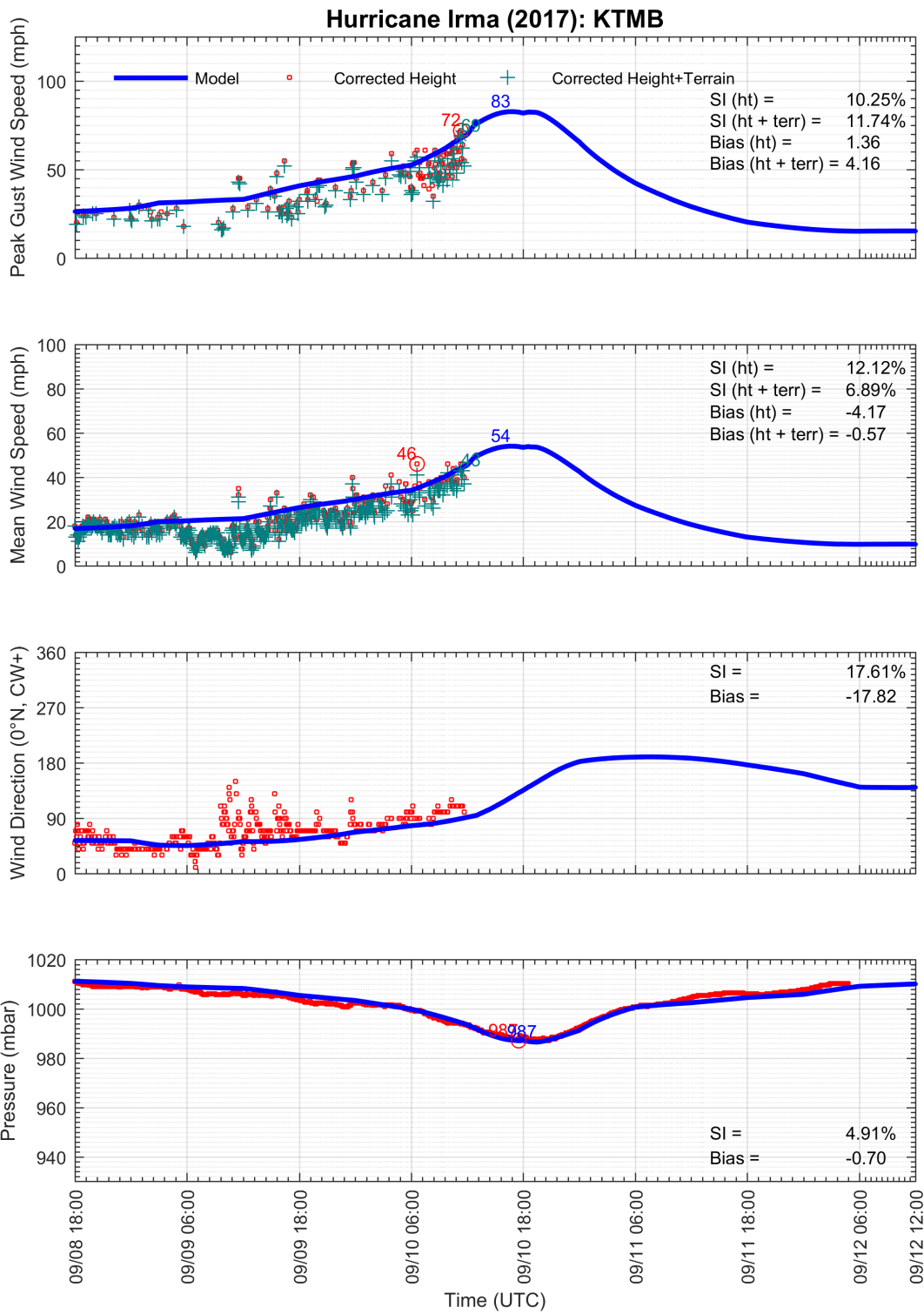


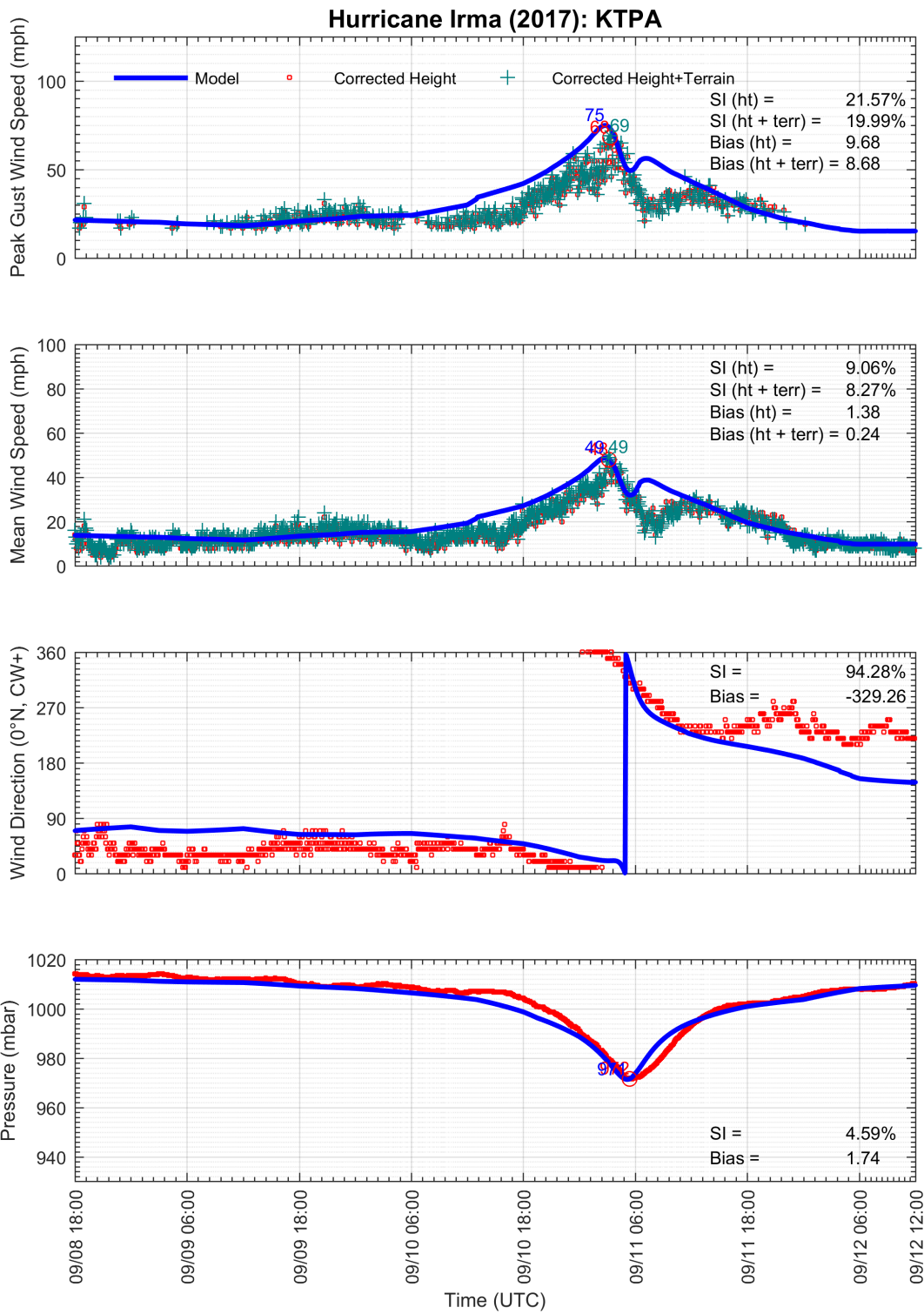


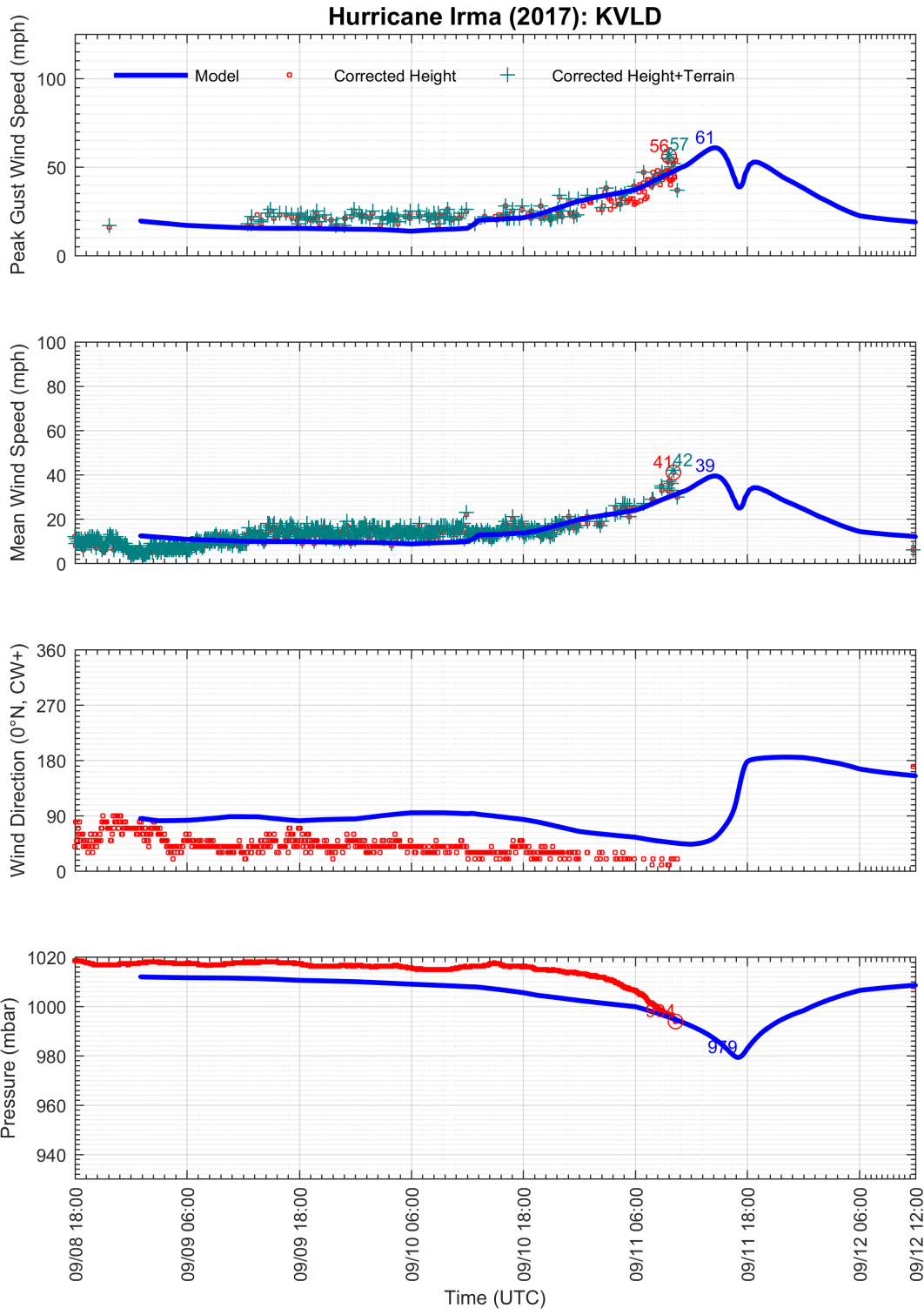


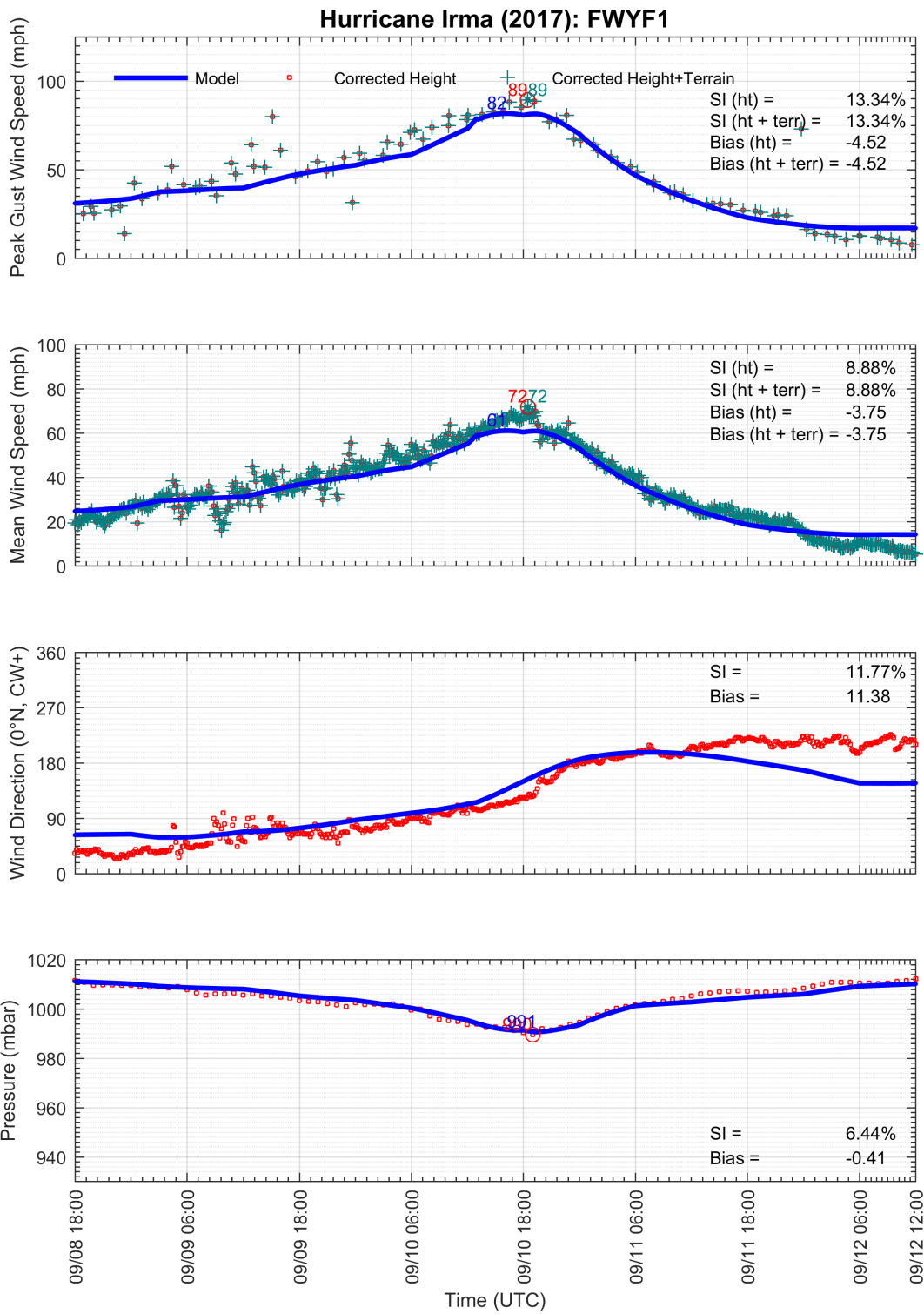


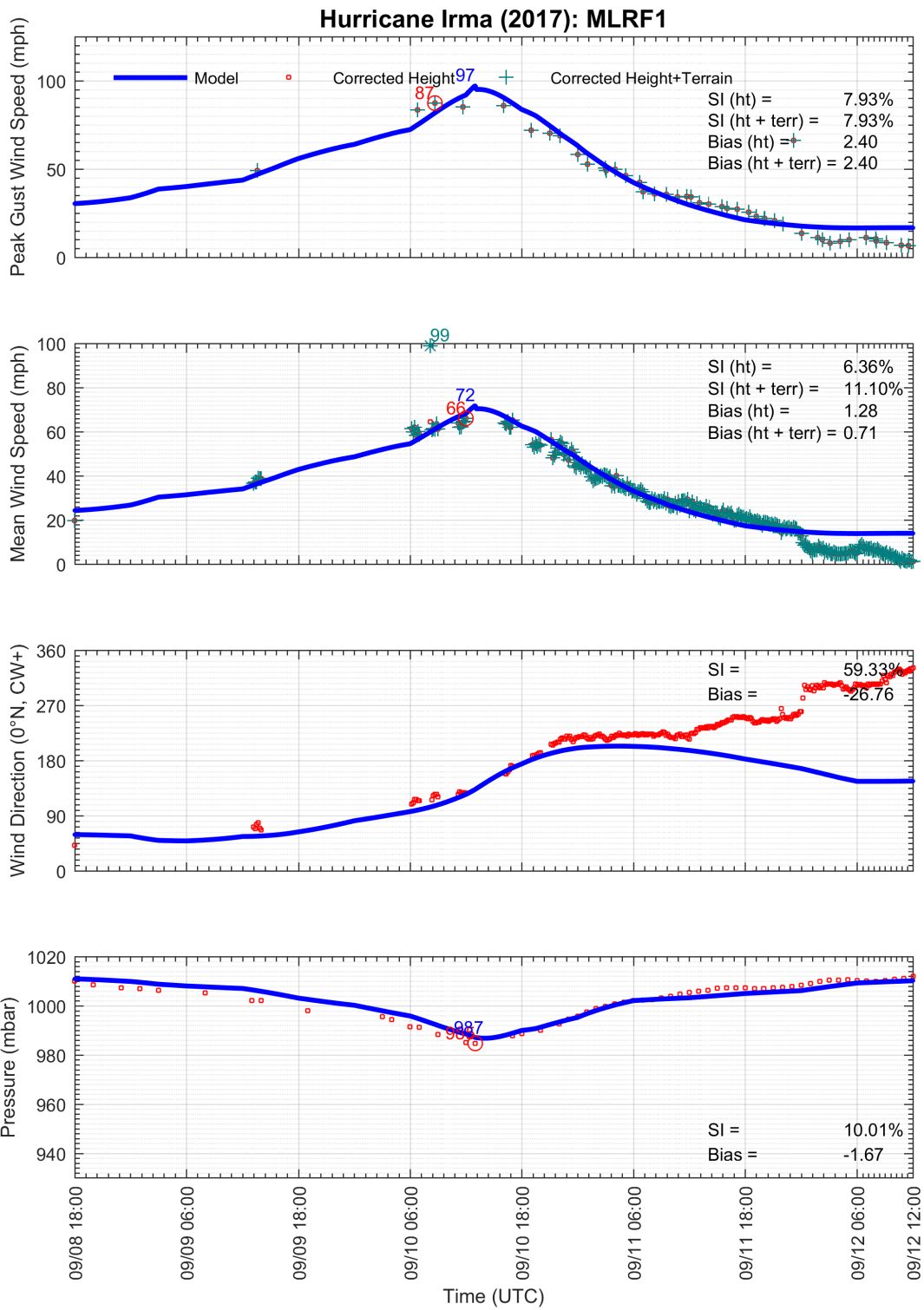




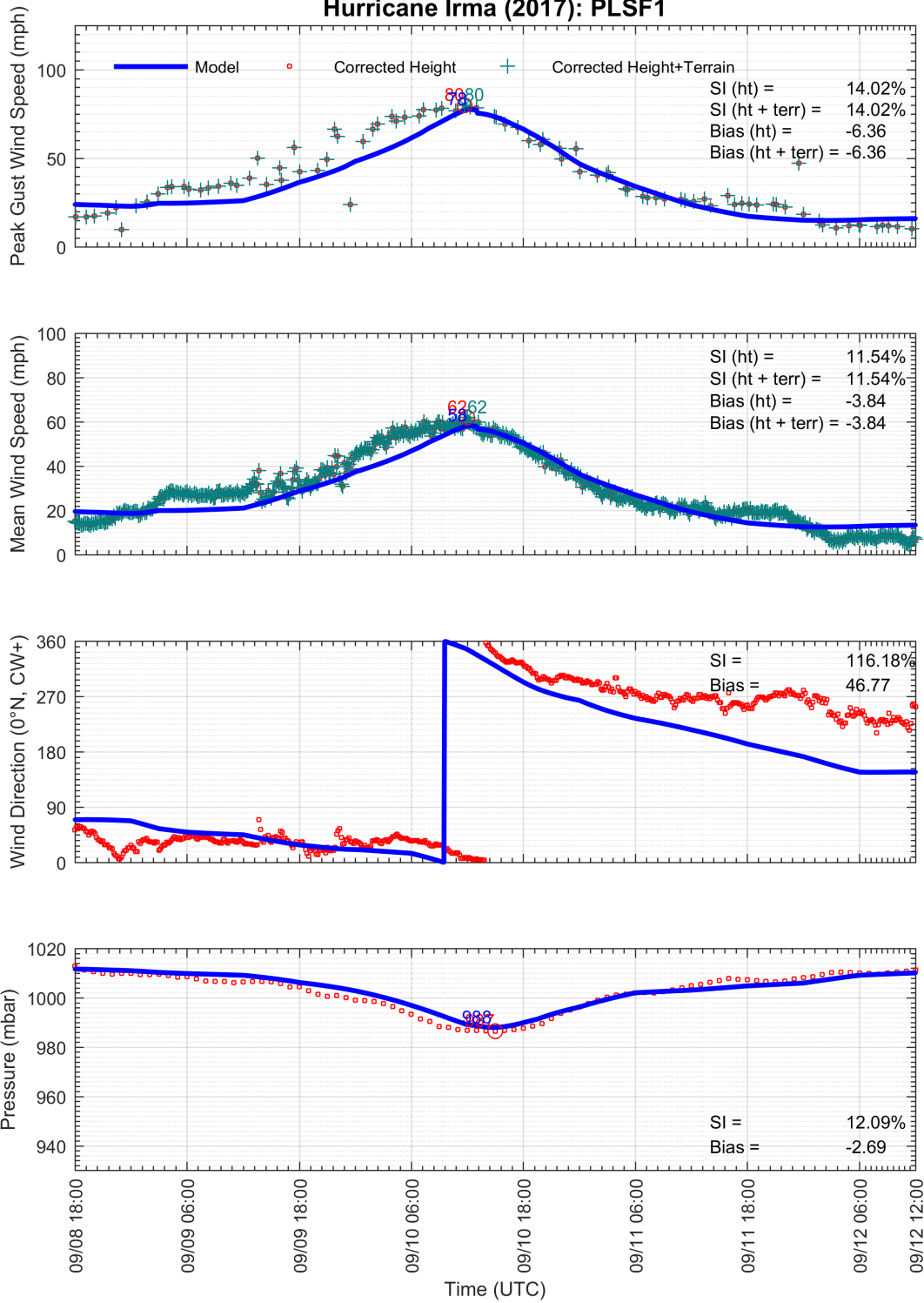


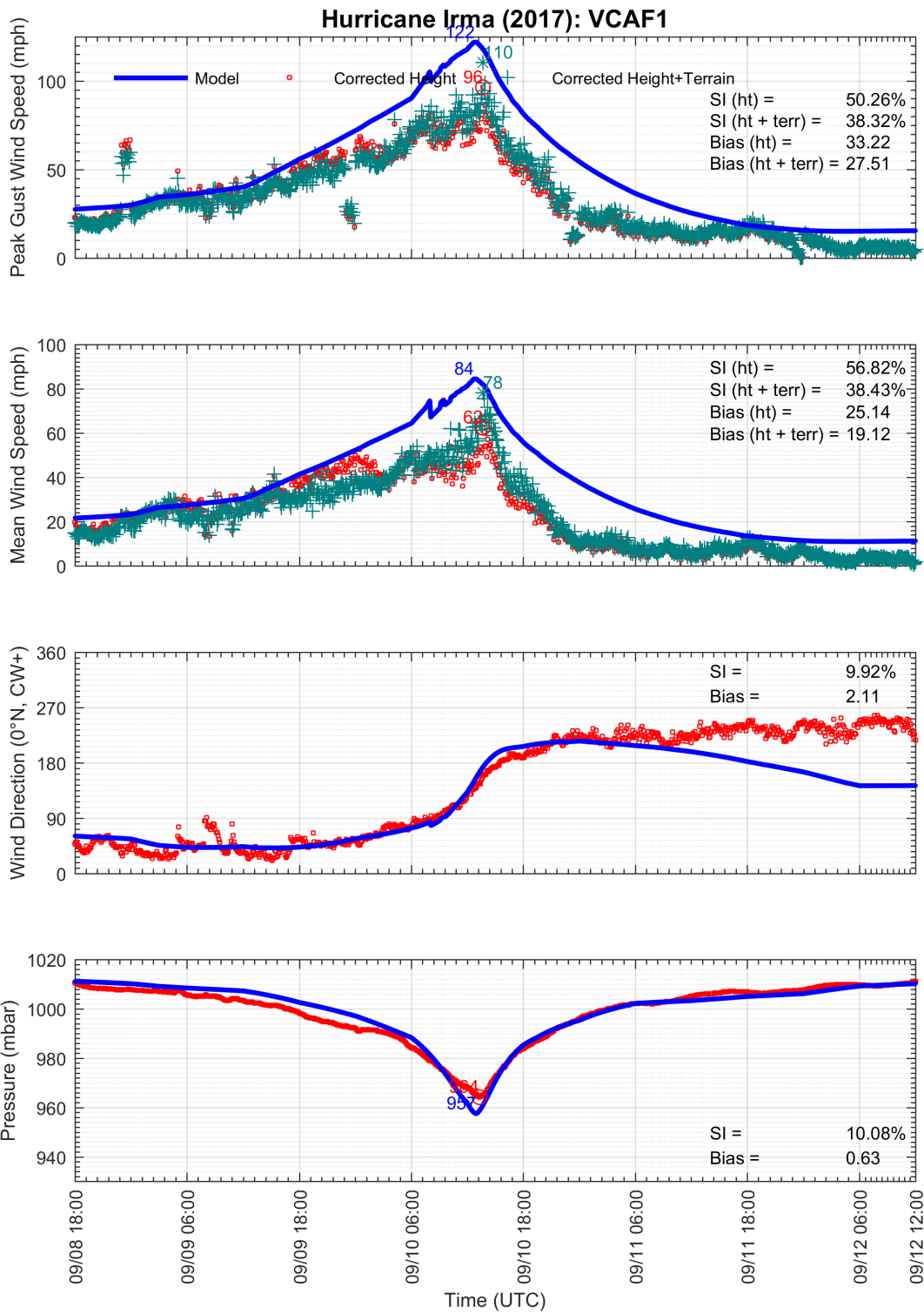


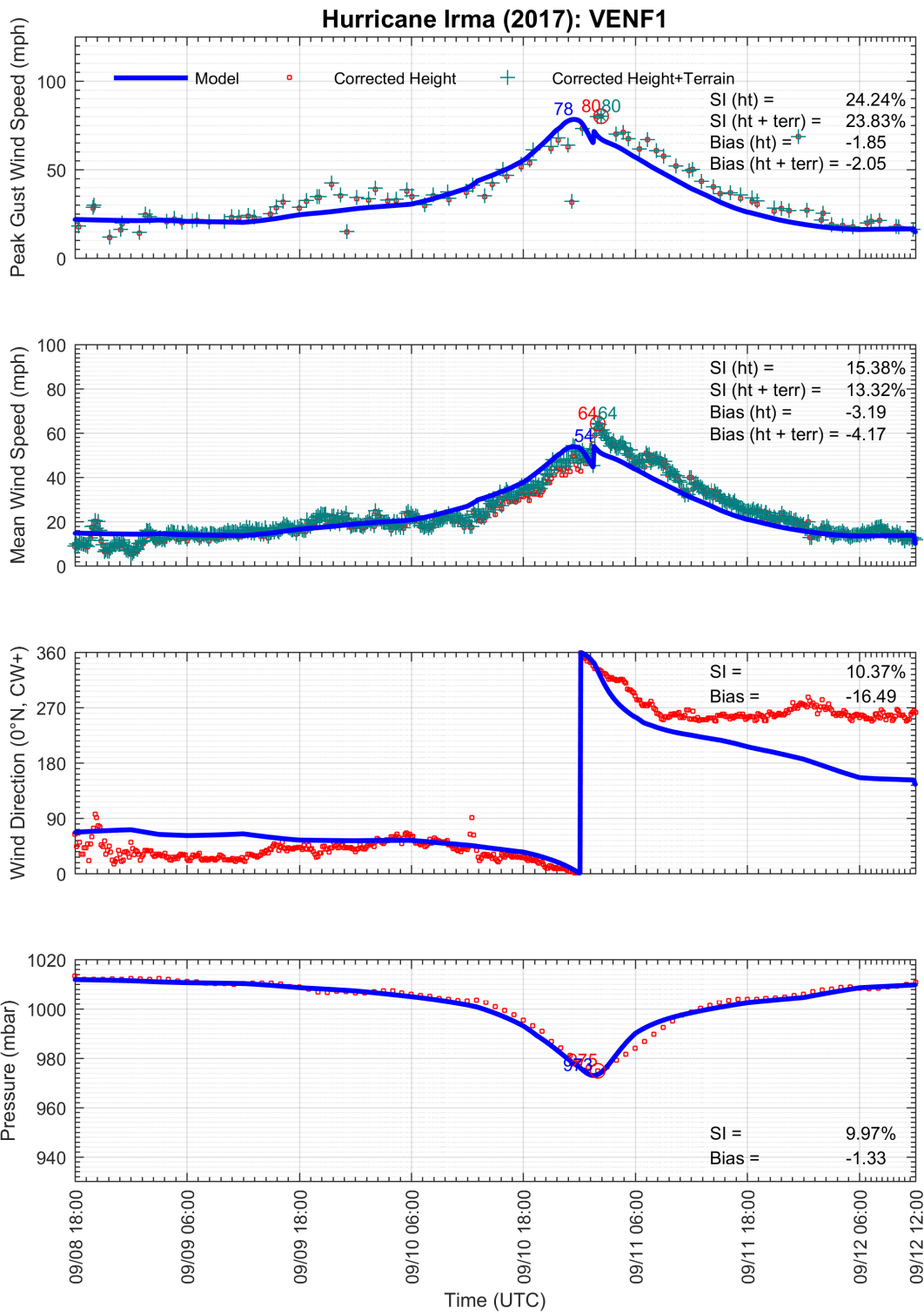


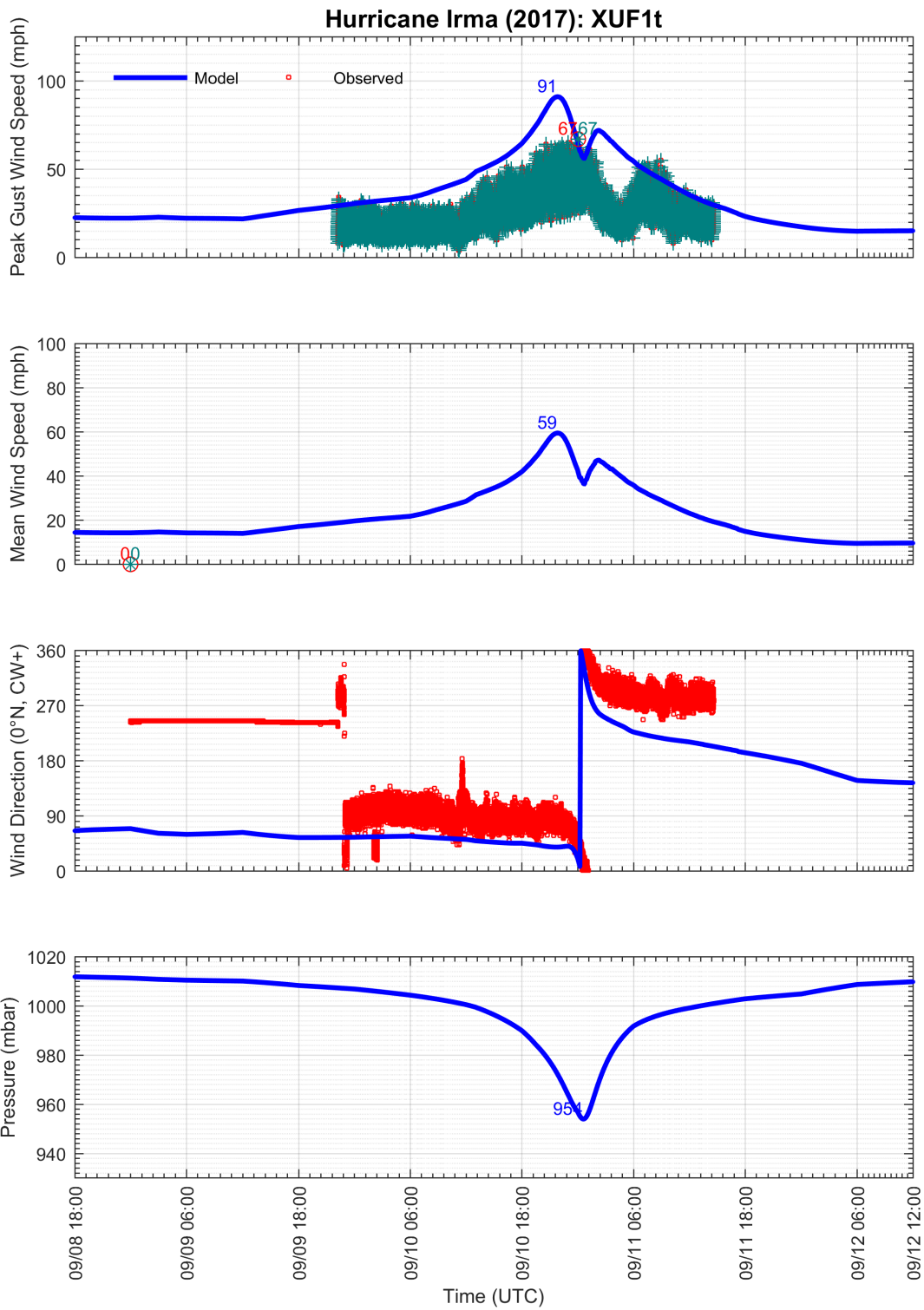


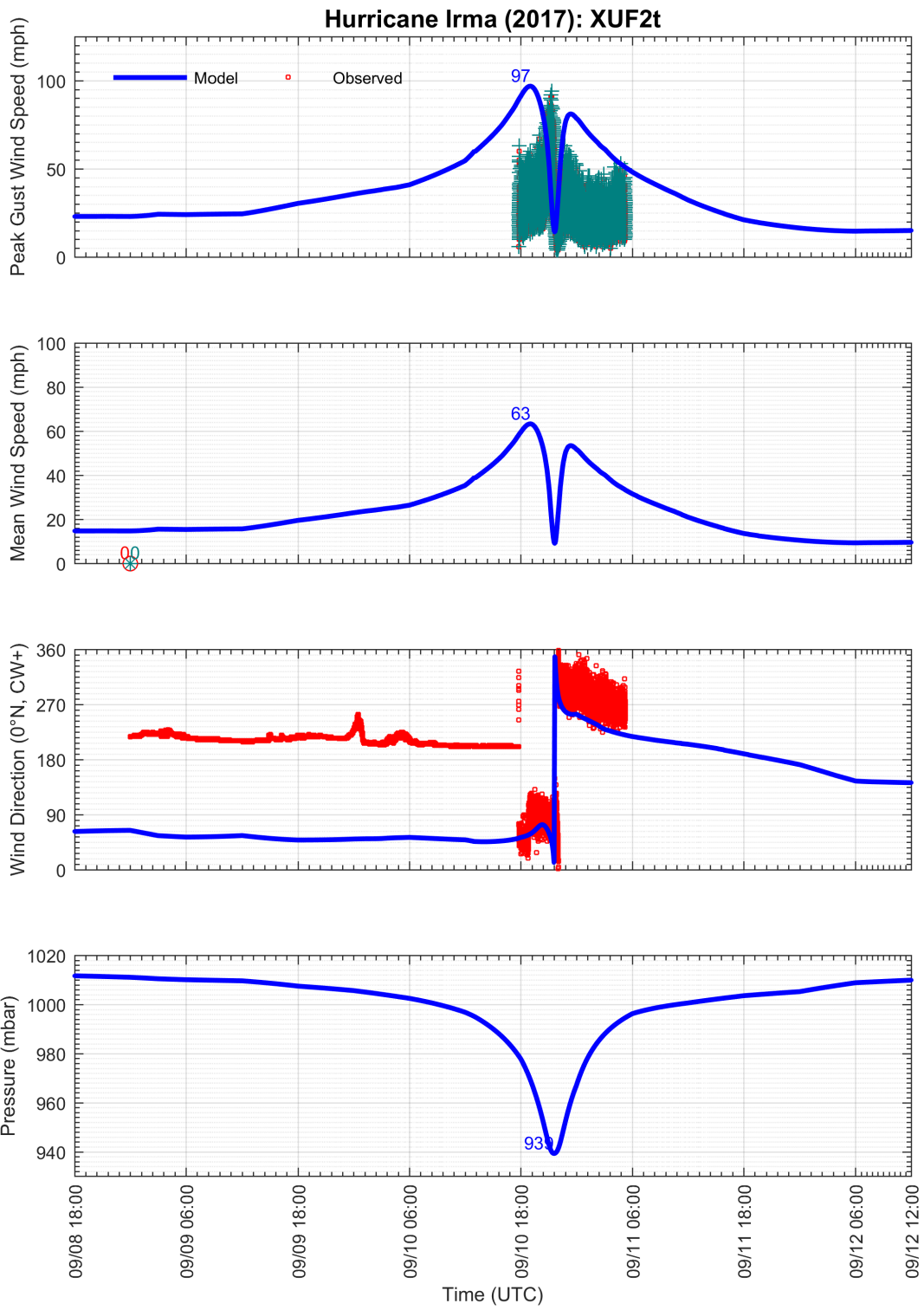
Hurricane Irma (2017): PLSF1

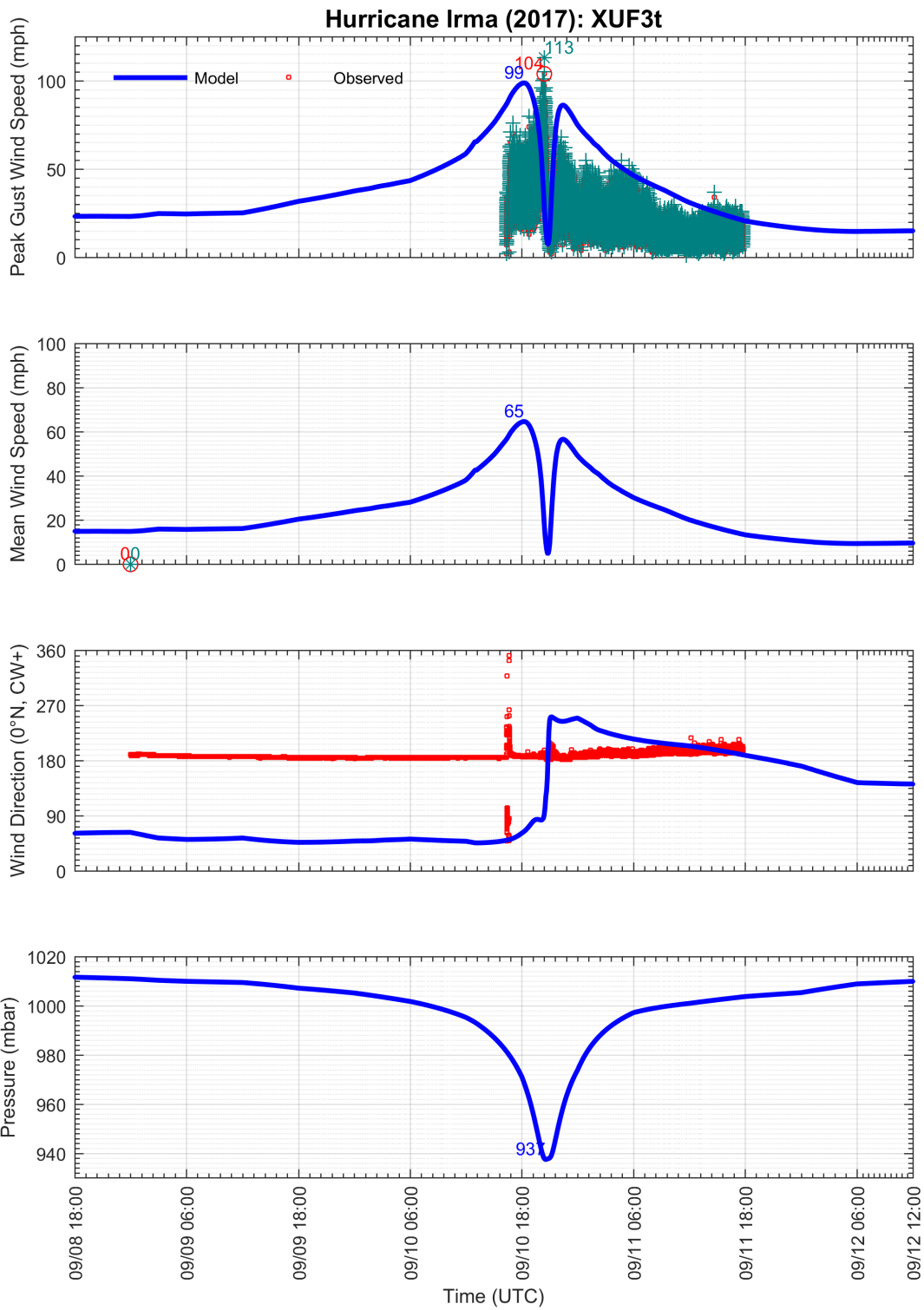


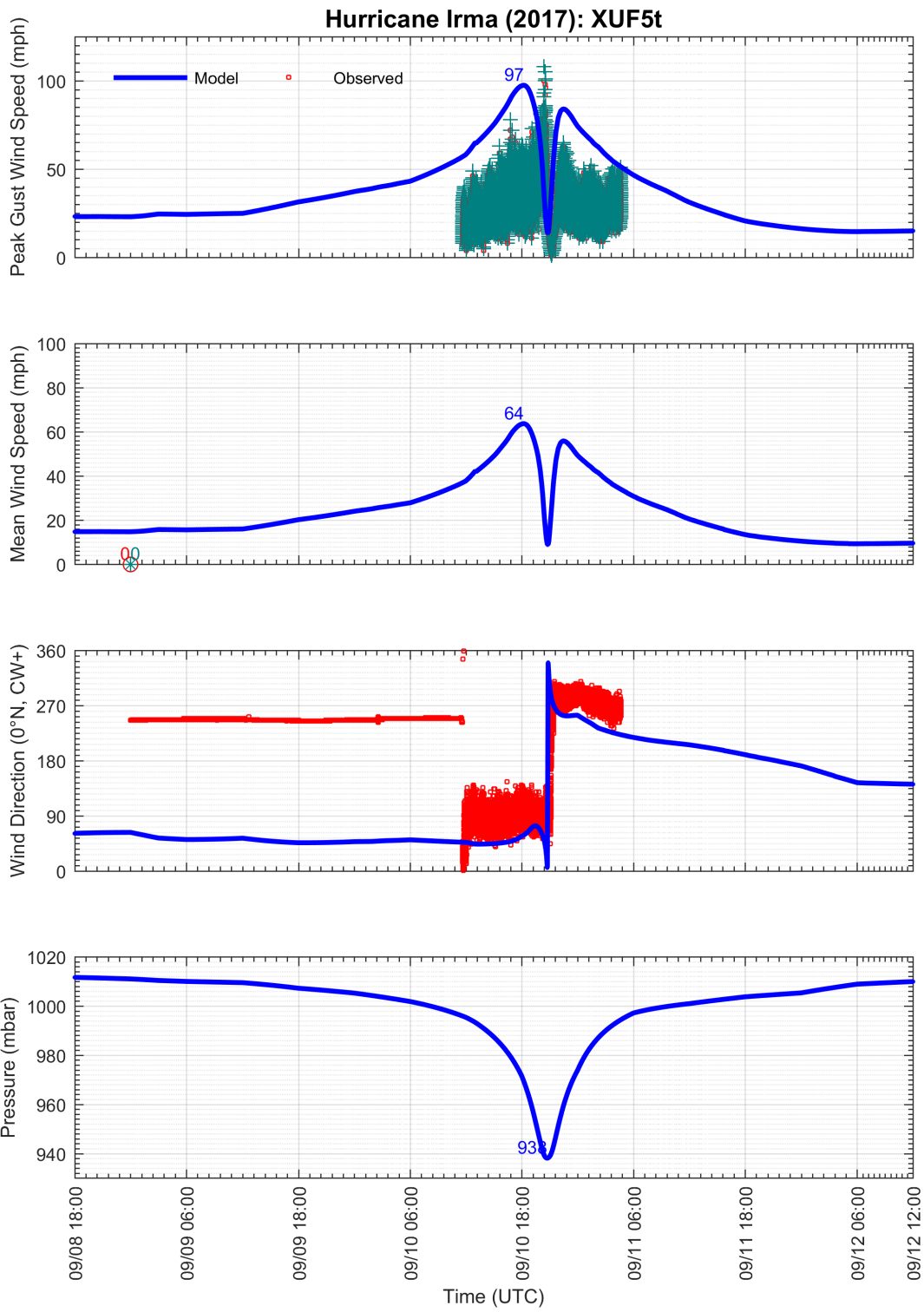












Appendix B.3 STATION DIRECTIONAL SURFACE ROUGHNESS VALUES

Station	Direction (0°N, CW+)															
	0	22.5	45	67.5	90	112.5	135	157.5	180	202.5	225	247.5	270	292.5	315	337.5
KAFF	0.0439	0.0247	0.0245	0.0393	0.1423	0.1780	0.0966	0.0311	0.0071	0.0091	0.0188	0.0128	0.0051	0.0357	0.0316	0.0468
KABY	0.4049	0.4049	0.2095	0.0227	0.0290	0.0441	0.0472	0.0349	0.0250	0.0283	0.0329	0.1488	0.1018	0.1093	0.1416	0.0631
KAGS	0.0300	0.0300	0.0300	0.0300	0.0300	0.0300	0.0300	0.0300	0.0300	0.0300	0.0300	0.0300	0.0300	0.0300	0.0300	0.0300
KAHN	0.0500	0.0500	0.0300	0.0300	0.0300	0.0700	0.1000	0.1000	0.0300	0.0500	0.1000	0.0700	0.0300	0.0500	0.0700	0.0700
KAMG	0.2530	0.3696	0.6994	0.8603	0.4573	0.2407	0.2315	0.1381	0.1118	0.0865	0.1124	0.1634	0.2428	0.1384	0.0969	0.0641
KAPF	0.2753	0.1660	0.0545	0.0377	0.0432	0.0651	0.0407	0.0329	0.0352	0.0097	0.0150	0.0363	0.0206	0.0311	0.1743	0.3631
KATL	0.1000	0.0300	0.0500	0.0700	0.0300	0.0300	0.0300	0.0300	0.0300	0.0300	0.0300	0.0300	0.0300	0.0300	0.0500	0.0700
KBKV	0.0747	0.1275	0.1016	0.0753	0.0598	0.1613	0.0775	0.1094	0.1664	0.2235	0.2806	0.0730	0.0255	0.0226	0.0381	0.0462
KCEW	0.6042	0.5590	0.5138	0.4686	0.4234	0.4635	0.5036	0.5437	0.4809	0.0774	0.0843	0.0735	0.1048	0.1433	0.0819	0.1263
KCHS	0.0684	0.0615	0.0397	0.0530	0.0627	0.0306	0.0231	0.0179	0.0146	0.0125	0.0309	0.0685	0.0856	0.1210	0.0865	0.0392
KCRG	0.1217	0.1188	0.1347	0.0780	0.0770	0.0951	0.0943	0.0426	0.1152	0.0672	0.0352	0.0774	0.1258	0.1203	0.0516	0.0287
KCSG	0.3000	0.2500	0.2500	0.0300	0.0300	0.0300	0.0300	0.0300	0.0300	0.0300	0.0500	0.0700	0.0500	0.0300	0.0500	0.2000
KCTY	0.0300	0.0300	0.3000	0.3000	0.3000	0.3000	0.3000	0.0700	0.0300	0.0300	0.0300	0.0300	0.0300	0.0300	0.0300	0.0300
KDAB	0.0505	0.0226	0.0108	0.0085	0.0408	0.3695	0.3211	0.2726	0.2171	0.1624	0.0625	0.0475	0.0475	0.0838	0.0774	0.0600
KDHN	0.0331	0.0659	0.1010	0.1301	0.0881	0.1853	0.0571	0.0305	0.0197	0.0270	0.0300	0.0638	0.0696	0.0315	0.0127	0.0153
KDNL	0.0800	0.0300	0.0300	0.0300	0.0500	0.0800	0.0800	0.0800	0.0700	0.0600	0.3000	0.3500	0.3500	0.4000	0.0600	0.0700
KDTS	0.0755	0.1020	0.1955	0.2230	0.1583	0.1111	0.0246	0.0318	0.4051	0.5141	0.4197	0.3253	0.9999	0.9999	0.7167	0.0507
KEYW	0.0030	0.0030	0.0017	0.0036	0.0132	0.0077	0.0005	0.0020	0.0010	0.0155	0.0017	0.0132	0.0713	0.0134	0.0051	0.0011
KFFC	0.2000	0.2500	0.3000	0.5000	0.4000	0.2000	0.0500	0.0300	0.1000	0.1500	0.1500	0.0800	0.0800	0.0300	0.0300	0.1500
KFMY	0.0617	0.0406	0.0256	0.0504	0.0968	0.0757	0.0593	0.0785	0.1257	0.1437	0.0797	0.0432	0.0202	0.0207	0.0208	0.0242
KFPR	0.5716	0.6042	0.6369	0.4465	0.0543	0.0114	0.0023	0.0107	0.0902	0.1145	0.0959	0.1038	0.0649	0.1066	0.5063	0.5390
KFTY	0.0300	0.0300	0.0300	0.0300	0.1500	0.1500	0.1500	0.0300	0.2000	0.2500	0.2000	0.2000	0.0500	0.0300	0.0300	0.0300
KFXE	0.4116	0.3956	0.1700	0.0733	0.0197	0.0130	0.0255	0.0435	0.1076	0.0992	0.0869	0.0531	0.0465	0.0814	0.2490	0.4672
KGIF	0.0246	0.0430	0.0396	0.0208	0.0192	0.0161	0.0415	0.0889	0.0813	0.0691	0.0863	0.0650	0.0736	0.0854	0.0767	0.1178
KGNV	0.1854	0.0947	0.0543	0.0413	0.0813	0.0509	0.0286	0.0525	0.0871	0.1376	0.1566	0.0851	0.0503	0.0580	0.1303	0.1278
KGZH	0.3109	0.2081	0.1139	0.1249	0.1359	0.0317	0.0400	0.0754	0.0452	0.0721	0.1161	0.2052	0.6000	0.5516	0.5033	0.4549
KHWO	0.0299	0.0294	0.0332	0.0210	0.0207	0.0248	0.0221	0.0310	0.0373	0.0654	0.0466	0.0409	0.0431	0.0642	0.0364	0.0222
KJAX	0.1052	0.0776	0.0328	0.0120	0.0111	0.0270	0.0265	0.0173	0.0436	0.0771	0.0586	0.0412	0.0237	0.0495	0.0868	0.1016
KLEE	0.0217	0.0272	0.0316	0.0495	0.1179	0.1129	0.0351	0.1132	0.2082	0.0790	0.0345	0.0345	0.0404	0.1135	0.2820	0.1780
KMAI	0.0551	0.0689	0.0388	0.0282	0.0693	0.3000	0.4000	0.4955	0.1677	0.0211	0.0397	0.0452	0.0582	0.0715	0.0457	0.0483

Station	Direction (0°N, CW+)															
	0	22.5	45	67.5	90	112.5	135	157.5	180	202.5	225	247.5	270	292.5	315	337.5
KMCN	0.0300	0.0300	0.0300	0.0300	0.0300	0.0300	0.0700	0.2500	0.3000	0.3000	0.2500	0.0700	0.0500	0.0800	0.0500	0.0500
KMCO	0.0049	0.0065	0.0109	0.0108	0.0110	0.0076	0.0134	0.0209	0.0201	0.0187	0.0168	0.0203	0.0240	0.0291	0.0278	0.0139
KMIA	0.4752	0.6981	0.2023	0.1167	0.0277	0.0128	0.0451	0.1280	0.1556	0.1288	0.1367	0.1114	0.1272	0.2470	0.2511	0.2981
KMTH	0.6111	0.2798	0.0402	0.0109	0.0817	0.2251	0.3270	0.3924	0.2272	0.7371	0.5298	0.9010	0.1033	0.1156	0.1865	0.5520
KOGB	0.2769	0.1547	0.1058	0.1572	0.2228	0.4418	0.1944	0.1475	0.2075	0.2221	0.0810	0.0659	0.0833	0.1140	0.2595	0.3845
KOPF	0.0400	0.0415	0.0493	0.0231	0.0148	0.0211	0.0142	0.0118	0.0116	0.0231	0.0280	0.0338	0.0398	0.0302	0.0279	0.0285
KORL	0.0677	0.0564	0.0607	0.0443	0.0074	0.0154	0.0115	0.0146	0.0358	0.0298	0.0276	0.0344	0.0399	0.0267	0.0266	0.1172
KPBI	0.0347	0.0320	0.0405	0.0303	0.0156	0.0056	0.0070	0.0096	0.0222	0.0431	0.0437	0.0438	0.0388	0.0357	0.0239	0.0086
KPGD	0.0394	0.0226	0.0185	0.0230	0.0419	0.0497	0.0579	0.0363	0.0181	0.0133	0.0189	0.0089	0.0124	0.0108	0.0207	0.0277
KPIE	0.0476	0.0460	0.0494	0.0641	0.0645	0.0553	0.0264	0.0465	0.0244	0.0089	0.0106	0.0158	0.0217	0.0342	0.0139	0.0042
KPMP	0.0534	0.0537	0.0169	0.0199	0.0233	0.0159	0.0134	0.0120	0.0232	0.0781	0.0797	0.0556	0.0338	0.0376	0.0280	0.0171
KPNS	0.1012	0.1155	0.5000	0.5000	0.5429	0.1356	0.0167	0.0138	0.0088	0.0140	0.0310	0.0248	0.0473	0.0321	0.0598	0.0276
KRSW	0.1036	0.0792	0.0329	0.0157	0.0231	0.0479	0.0737	0.0306	0.0243	0.0206	0.0065	0.0231	0.1129	0.2749	0.2628	0.2256
KSAV	0.0290	0.0220	0.0178	0.0357	0.0729	0.0546	0.0337	0.0301	0.0553	0.2267	0.4087	0.3988	0.4216	0.3188	0.1612	0.0534
KSFB	0.0318	0.0289	0.0350	0.0148	0.0109	0.0122	0.0048	0.0066	0.0370	0.0781	0.0653	0.0212	0.0272	0.0167	0.0293	0.0517
KSPG	0.0614	0.0156	0.0016	0.0001	0.0001	0.0002	0.0003	0.0002	0.0007	0.0180	0.0205	0.0668	0.1565	0.2283	0.3031	0.2054
KSRQ	0.1807	0.1941	0.1334	0.0685	0.0347	0.0236	0.0180	0.0168	0.0175	0.0139	0.0095	0.0116	0.0039	0.0029	0.0197	0.0714
KSSI	0.1160	0.0797	0.0614	0.0475	0.0335	0.0308	0.0109	0.0324	0.1896	0.3116	0.0538	0.0405	0.1309	0.3957	0.4613	0.4497
KTLH	0.1492	0.1714	0.1901	0.1458	0.0381	0.0120	0.0399	0.0941	0.1038	0.1260	0.0555	0.0346	0.0357	0.0296	0.0318	0.0384
KTMB	0.0145	0.0176	0.0213	0.0127	0.0088	0.0143	0.0401	0.0880	0.1298	0.1301	0.1118	0.0707	0.0291	0.0376	0.0169	0.0181
KTPA	0.0512	0.0874	0.1616	0.2922	0.5253	0.4552	0.4563	0.2739	0.2487	0.0842	0.0650	0.0177	0.0101	0.0198	0.0705	0.0509
KVLD	0.0439	0.0351	0.0792	0.1605	0.2402	0.3203	0.2500	0.0577	0.0366	0.3142	0.4000	0.5000	0.5000	0.4000	0.3000	0.0500
FWYF1	0.0000	0.0000	0.0000	0.0000	0.0000	0.0000	0.0000	0.0000	0.0000	0.0000	0.0000	0.0000	0.0000	0.0000	0.0000	0.0000
MLRF1	0.0000	0.0000	0.0000	0.0000	0.0000	0.0000	0.0000	0.0000	0.0000	0.0000	0.0000	0.0000	0.0000	0.0000	0.0000	0.0000
PLSF1	0.0000	0.0000	0.0000	0.0000	0.0000	0.0000	0.0000	0.0000	0.0000	0.0000	0.0000	0.0000	0.0000	0.0000	0.0000	0.0000
VCAF1	0.1000	0.0500	0.0000	0.0050	0.1000	0.3000	0.5000	0.6000	0.6000	0.5000	0.3000	0.2000	0.0000	0.0000	0.0000	0.1000
VENF1	0.1500	0.1500	0.0500	0.0500	0.0500	0.0500	0.1000	0.0000	0.0000	0.0000	0.0000	0.0000	0.0000	0.0000	0.0000	0.0000
XUF1t	0.0300	0.0300	0.0300	0.0300	0.0300	0.0300	0.0300	0.0300	0.0300	0.0300	0.0300	0.0300	0.0300	0.0300	0.0300	0.0300
XUF2t	0.2000	0.3000	0.1000	0.0300	0.0800	0.0800	0.0500	0.0500	0.0800	0.0800	0.1500	0.2000	0.3000	0.2000	0.2000	0.2000
XUF3t	0.4000	0.3200	0.2500	0.2500	0.2500	0.2500	0.2500	0.2500	0.2500	0.2500	0.2500	0.2500	0.4000	0.2500	0.2500	0.2500
XUF5t	0.3000	0.3000	0.3000	0.3000	0.0700	0.1000	0.1000	0.1000	0.1000	0.1000	0.2000	0.1500	0.0800	0.0800	0.0800	0.1500



Figure B-1. Aerial image of NDBC station VCAF1: Vaca Key, FL.

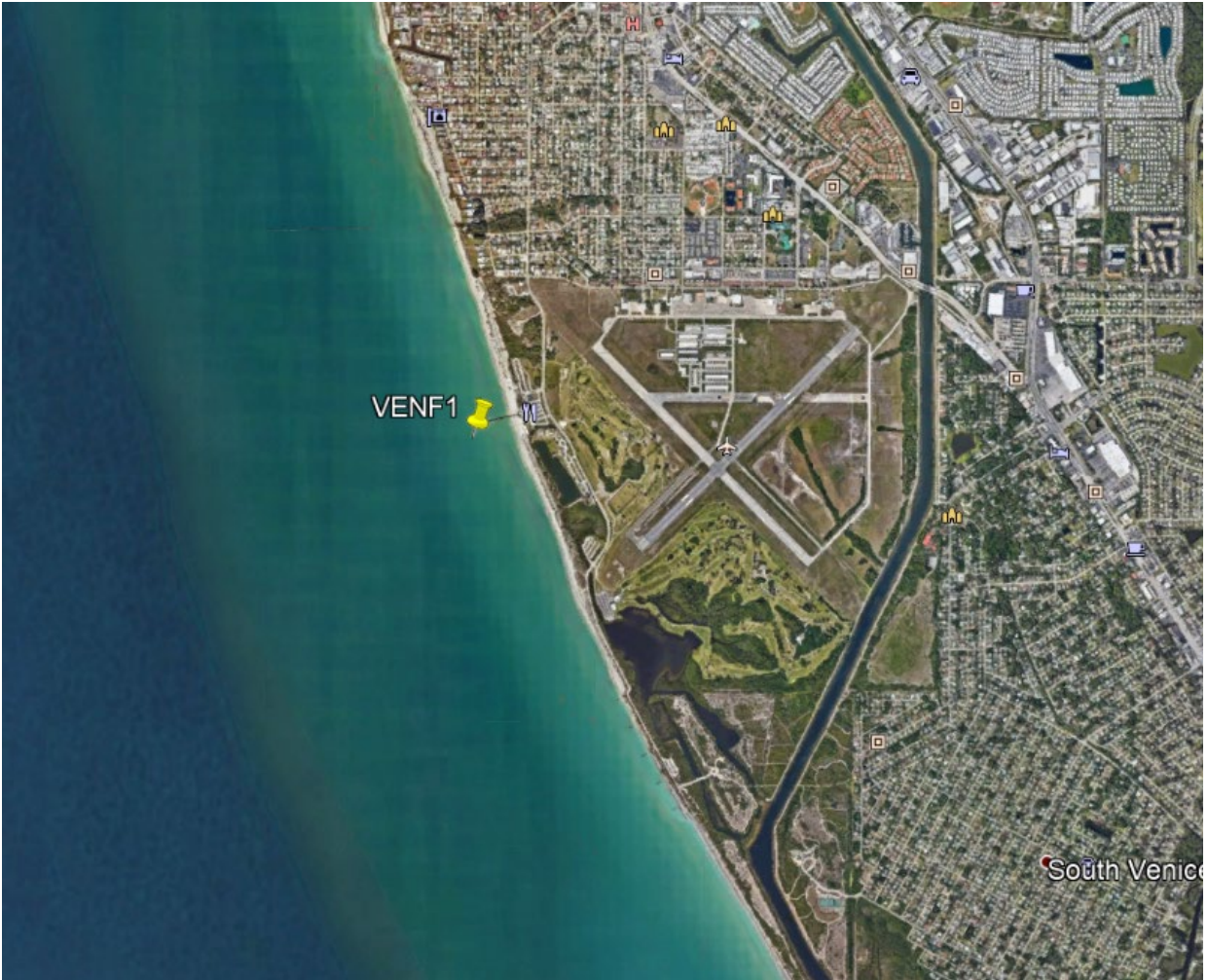


Figure B-2. Aerial image of NDBC station VENF1 Vaca Key, FL.

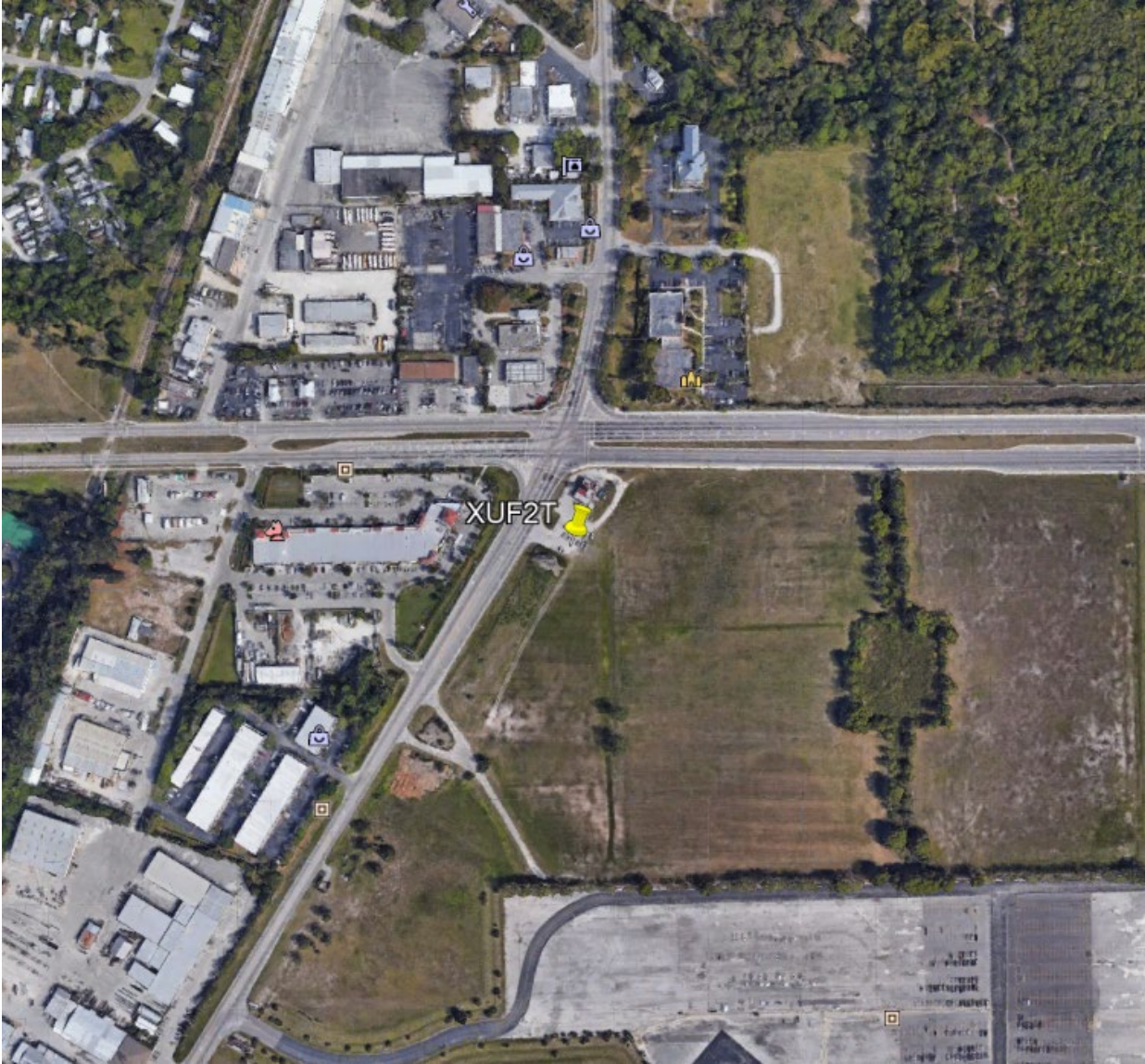


Figure B-3. Aerial image of University of Florida station XUF2T.

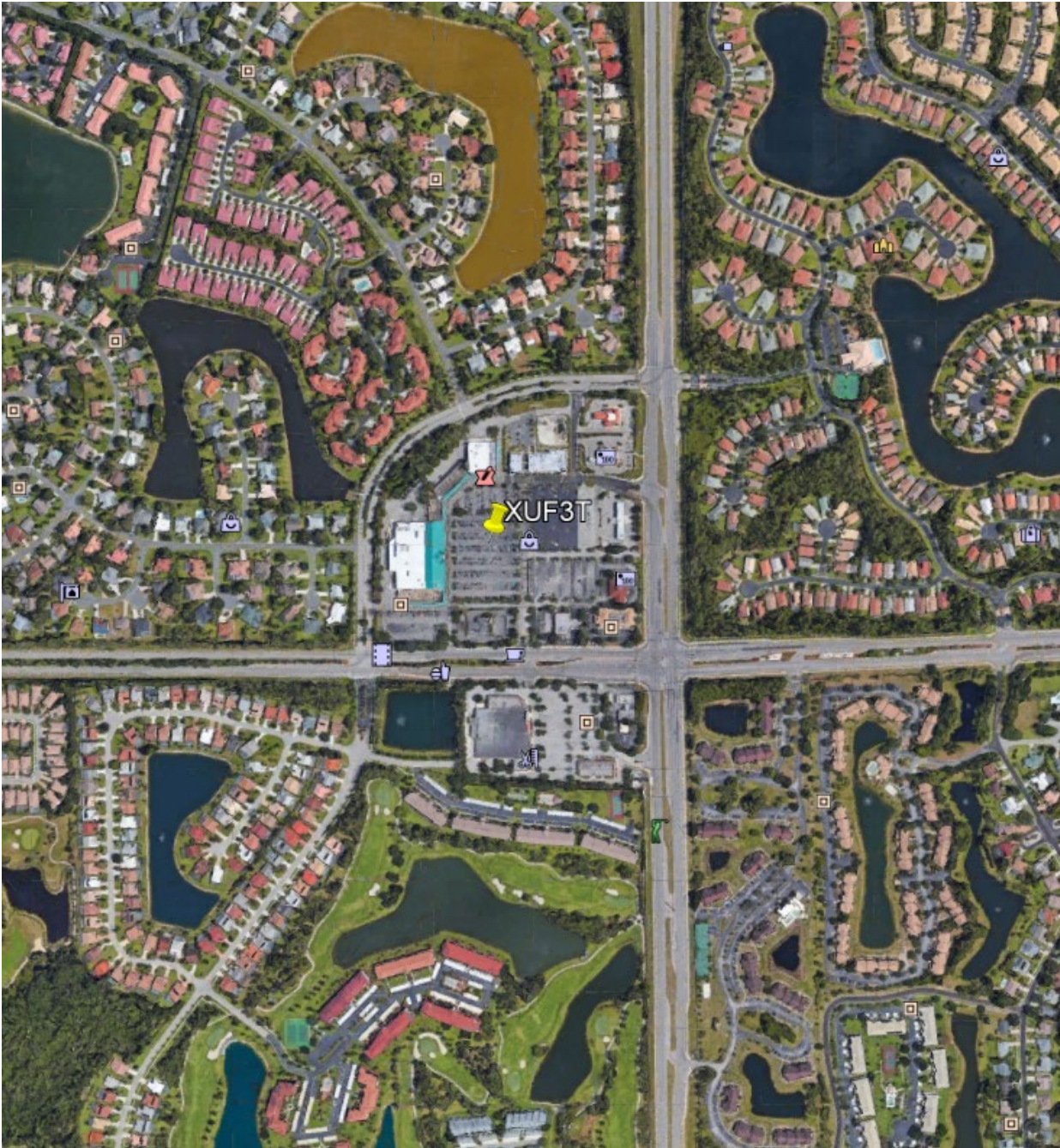


Figure B-4. Aerial image of University of Florida station XUF3T.

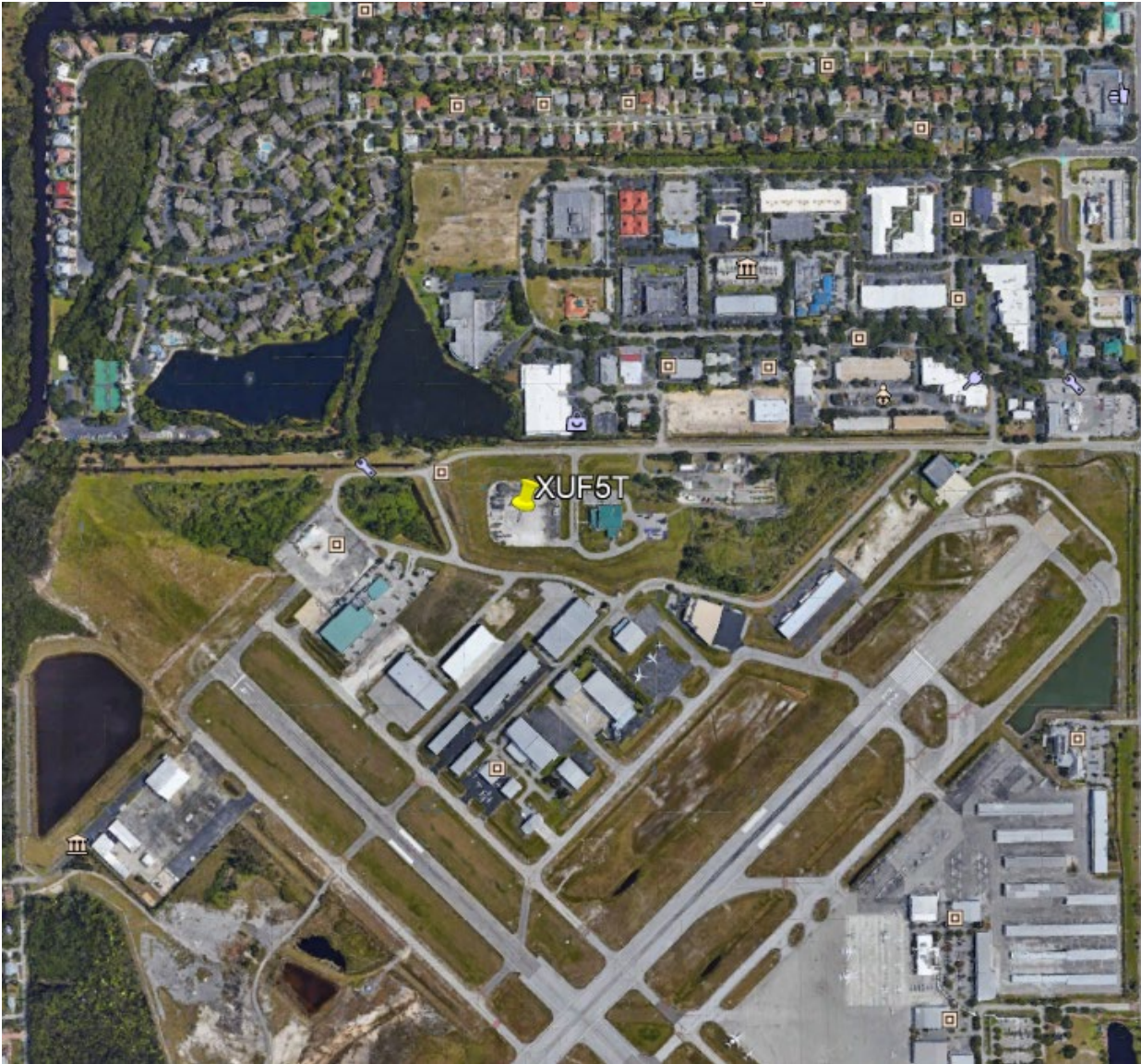
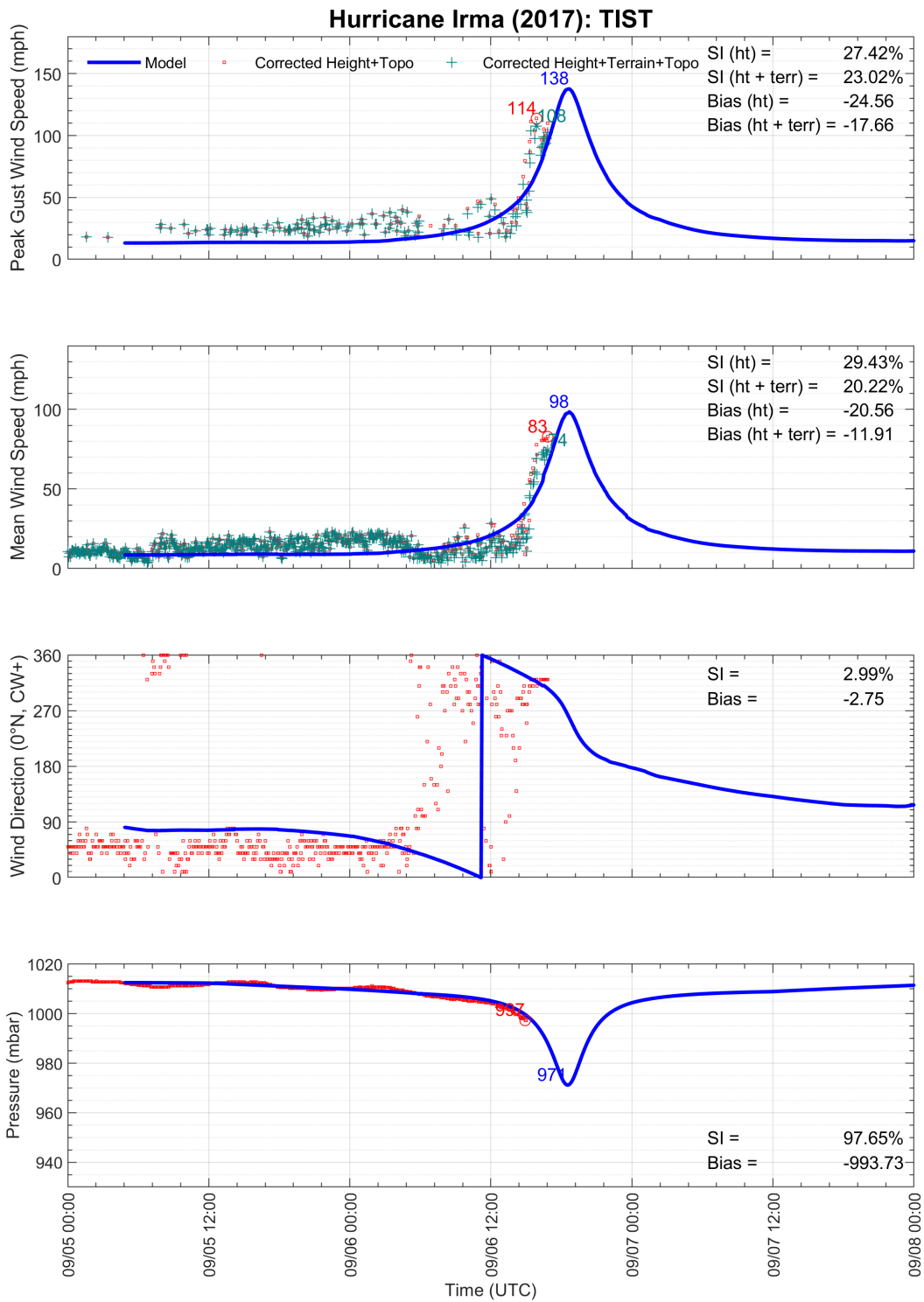


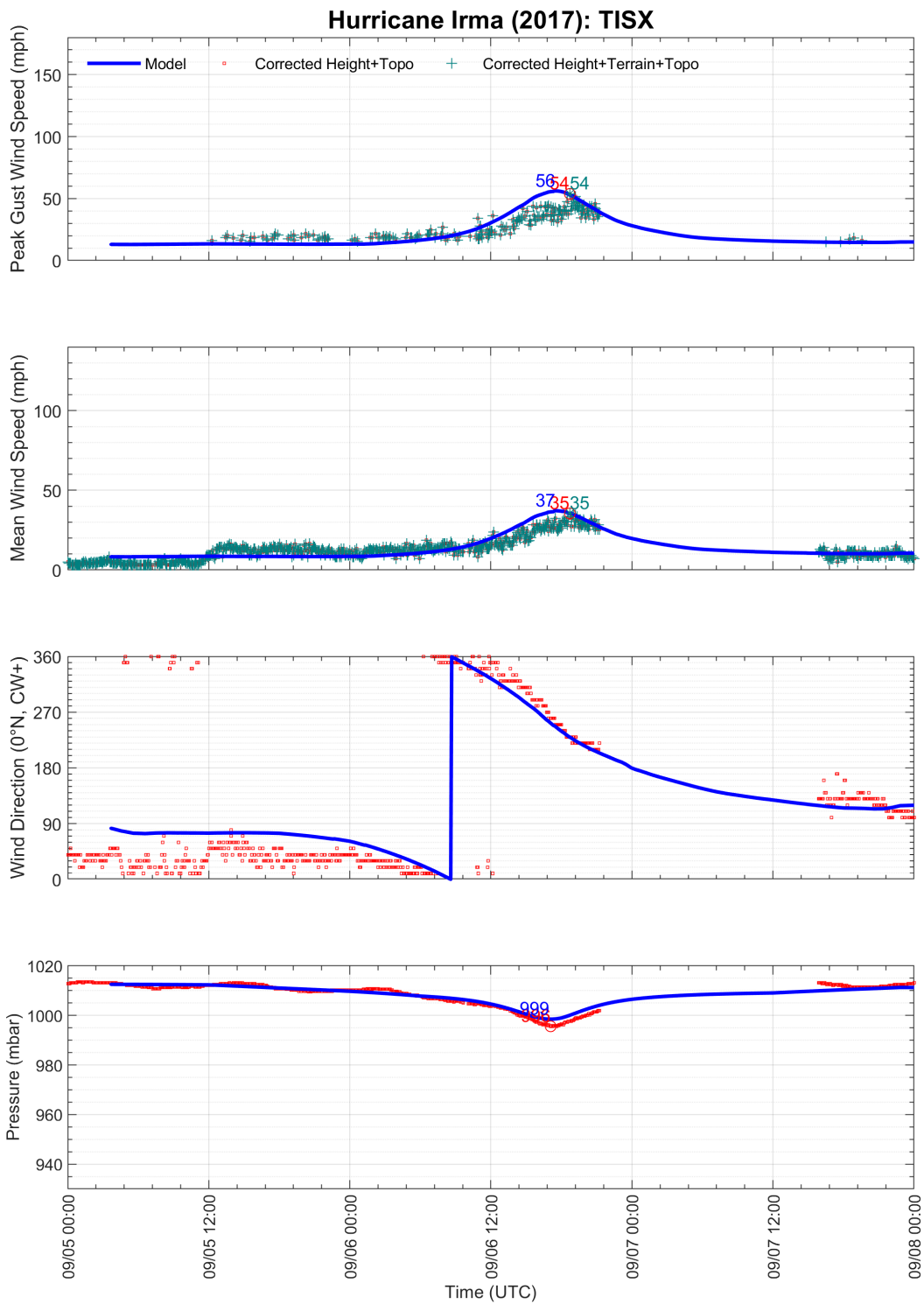
Figure B-5. Aerial image of University of Florida station XUF5T.

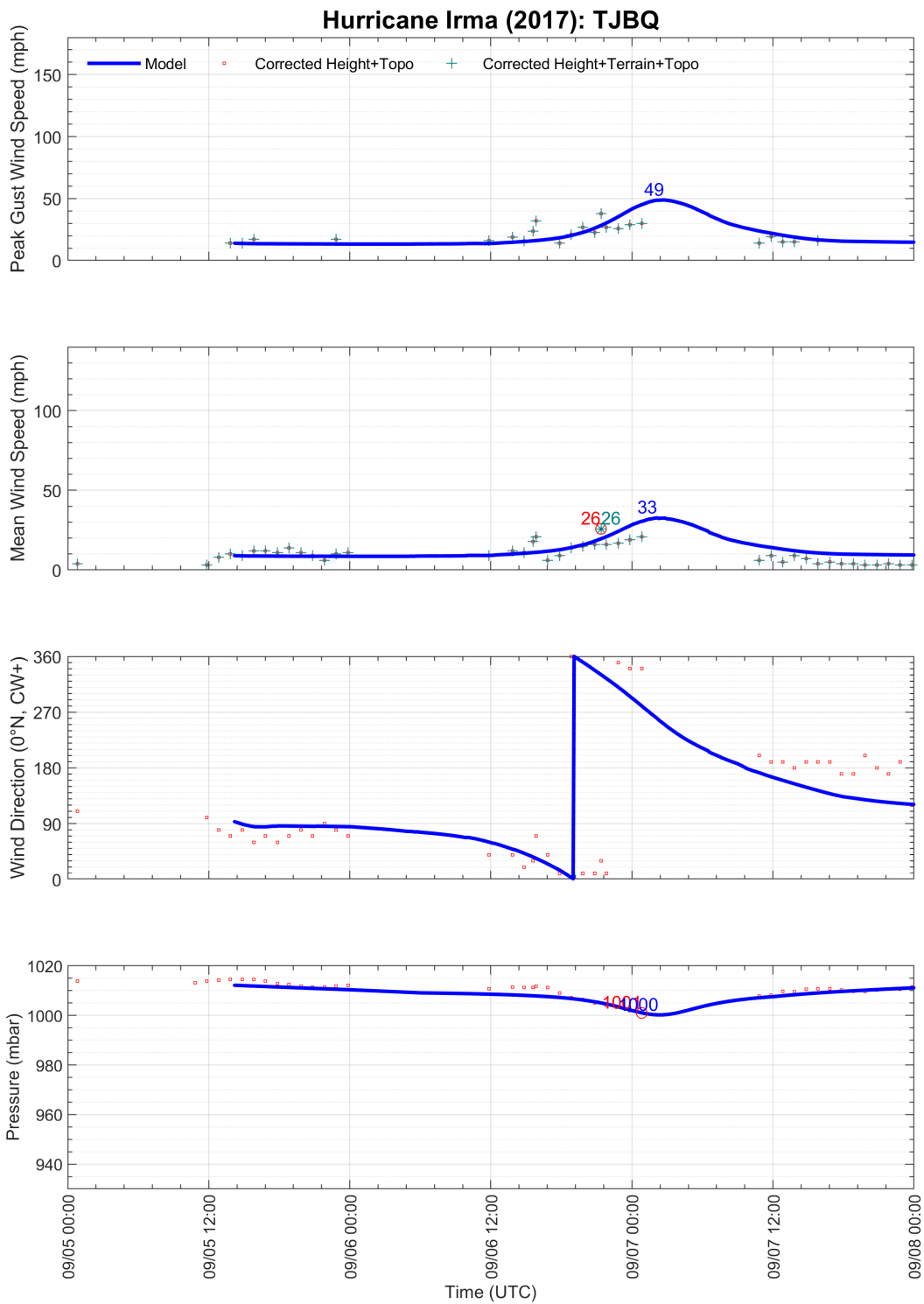
Appendix C. HURRICANE IRMA (OCONUS)

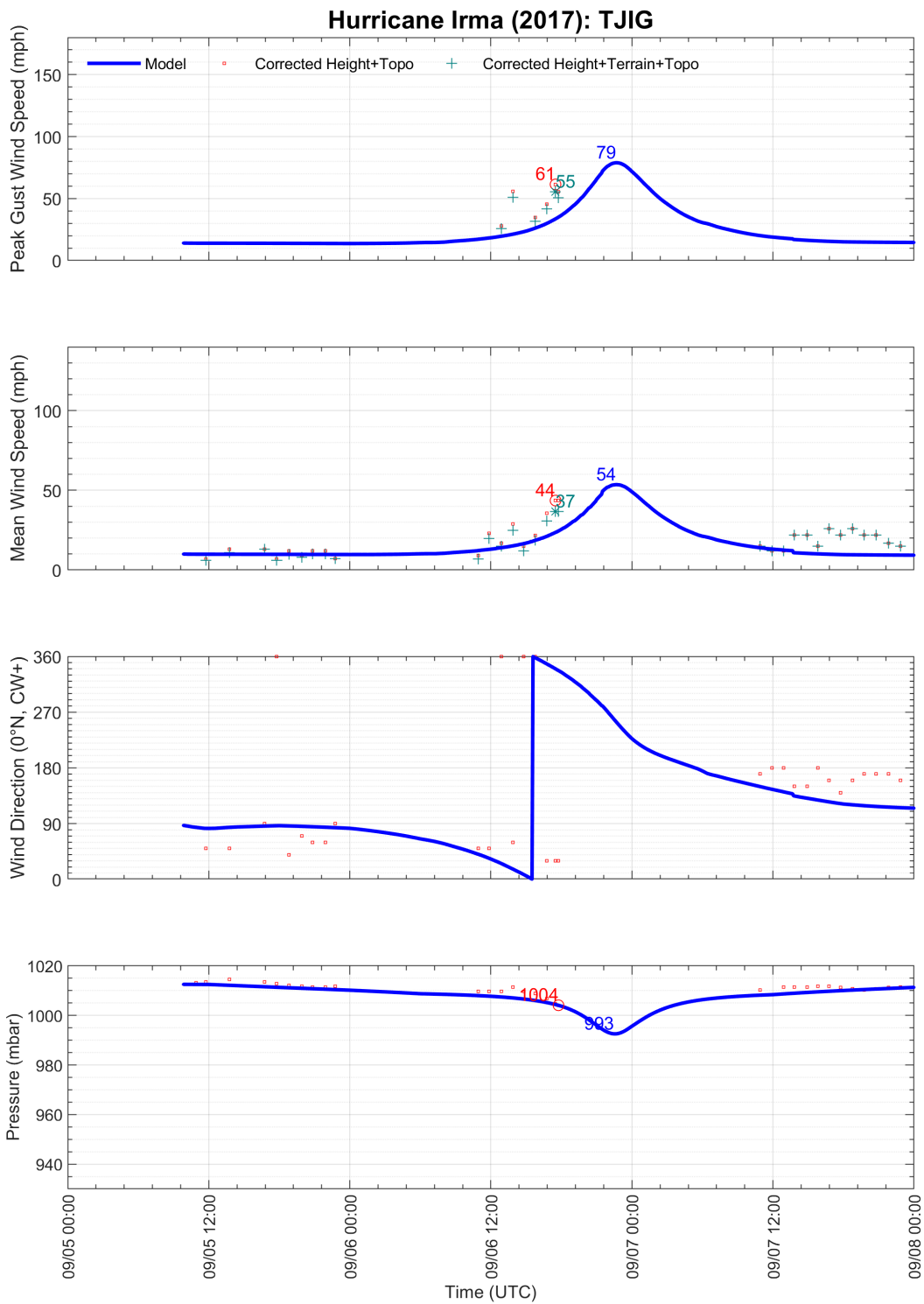
Appendix C.1 SURFACE OBSERVATION STATION DETAILS

Station	Latitude (°N)	Longitude (°W)	Anemometer Height (m)
TIST	18.337	64.973	7.00
TISX	17.700	64.805	17.00
TJBQ	18.495	67.129	72.00
TJIG	18.457	66.098	3.00
TJNR	18.255	65.639	10.00
TJPS	18.008	66.563	9.00
TJSJ	18.433	66.011	3.00
TUPJ	18.445	64.543	10.00
AROP4	18.480	66.702	6.40
CHAV3	18.335	64.920	7.60
CHSV3	17.748	64.699	8.40
ESPP4	18.094	65.471	10.50
FRDP4	18.335	65.631	6.40
IMGP4	17.969	67.044	22.36
LTBV3	17.695	64.754	9.70
MGIP4	17.970	67.046	7.50
MGZP4	18.218	67.159	11.50
PTRP4	18.367	67.251	15.00
SJNP4	18.459	66.116	7.00
VQSP4	18.153	65.444	6.40
YABP4	18.055	65.833	6.40
41052	18.251	64.763	4.00
41053	18.474	66.099	4.00
41056	18.260	65.457	4.00
41058	18.476	65.157	4.00
42085	17.860	66.524	4.00

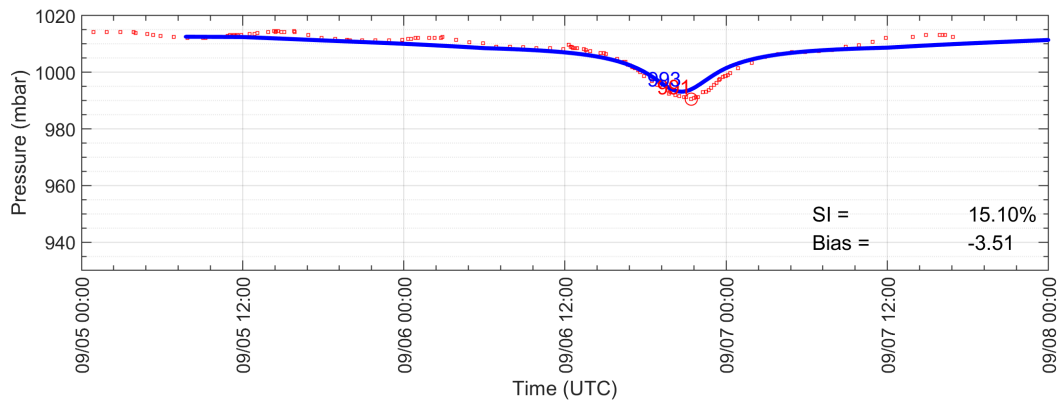
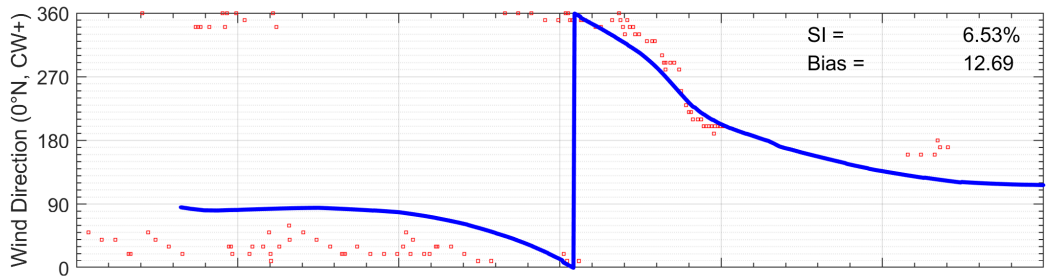
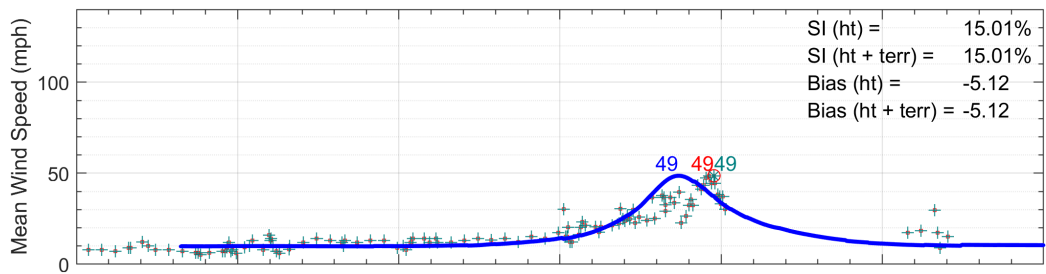
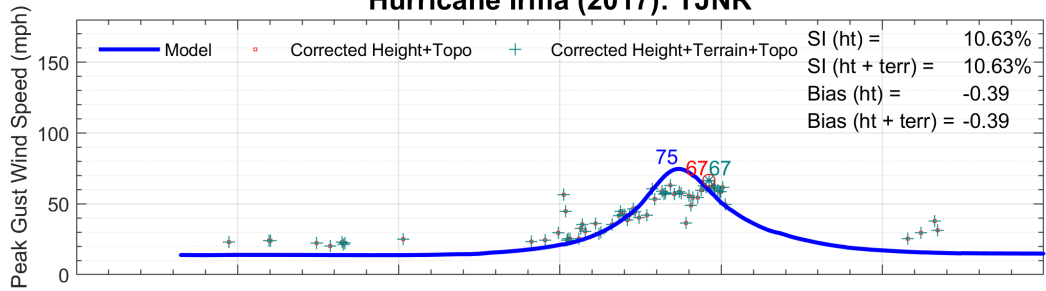




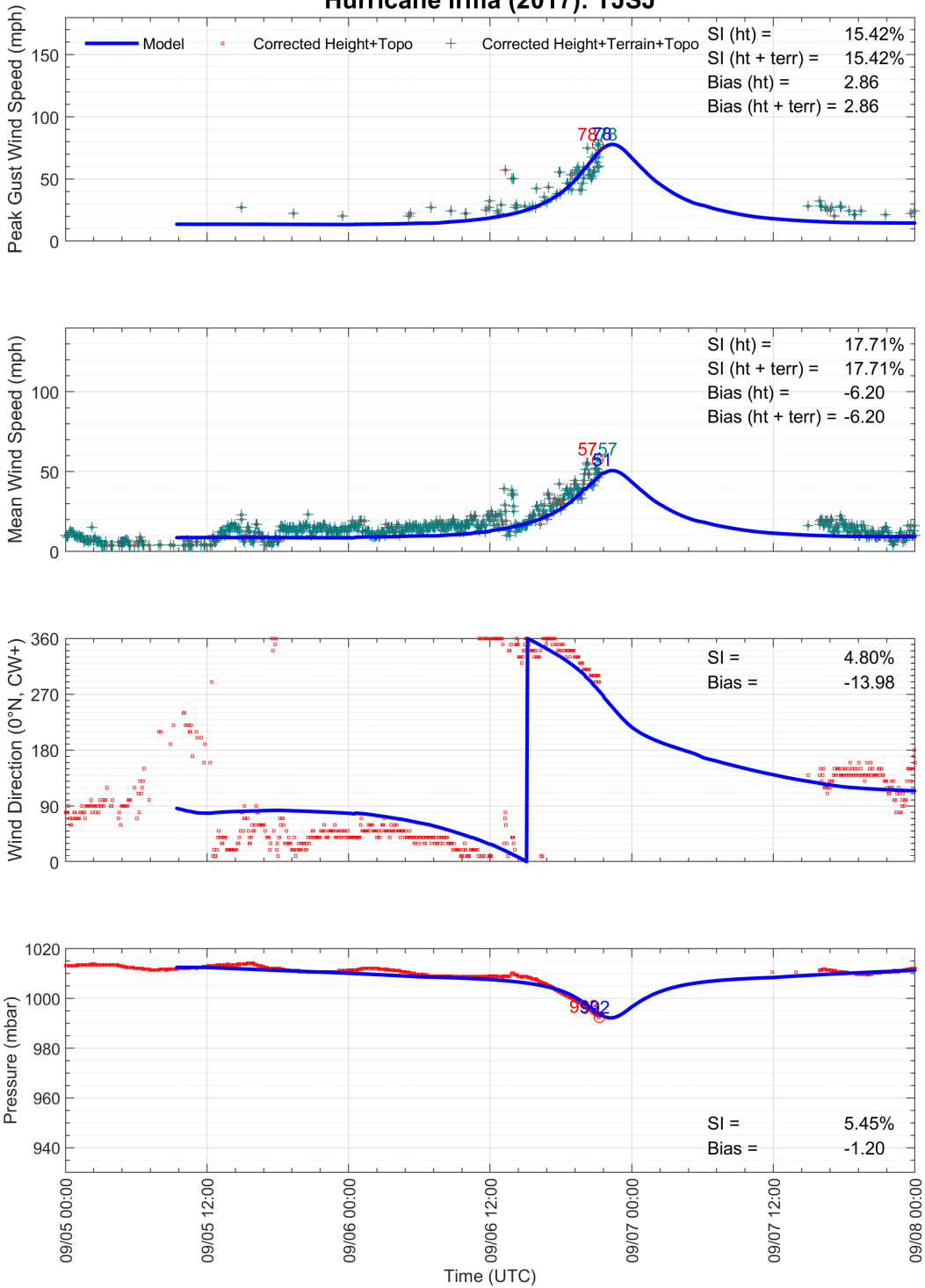




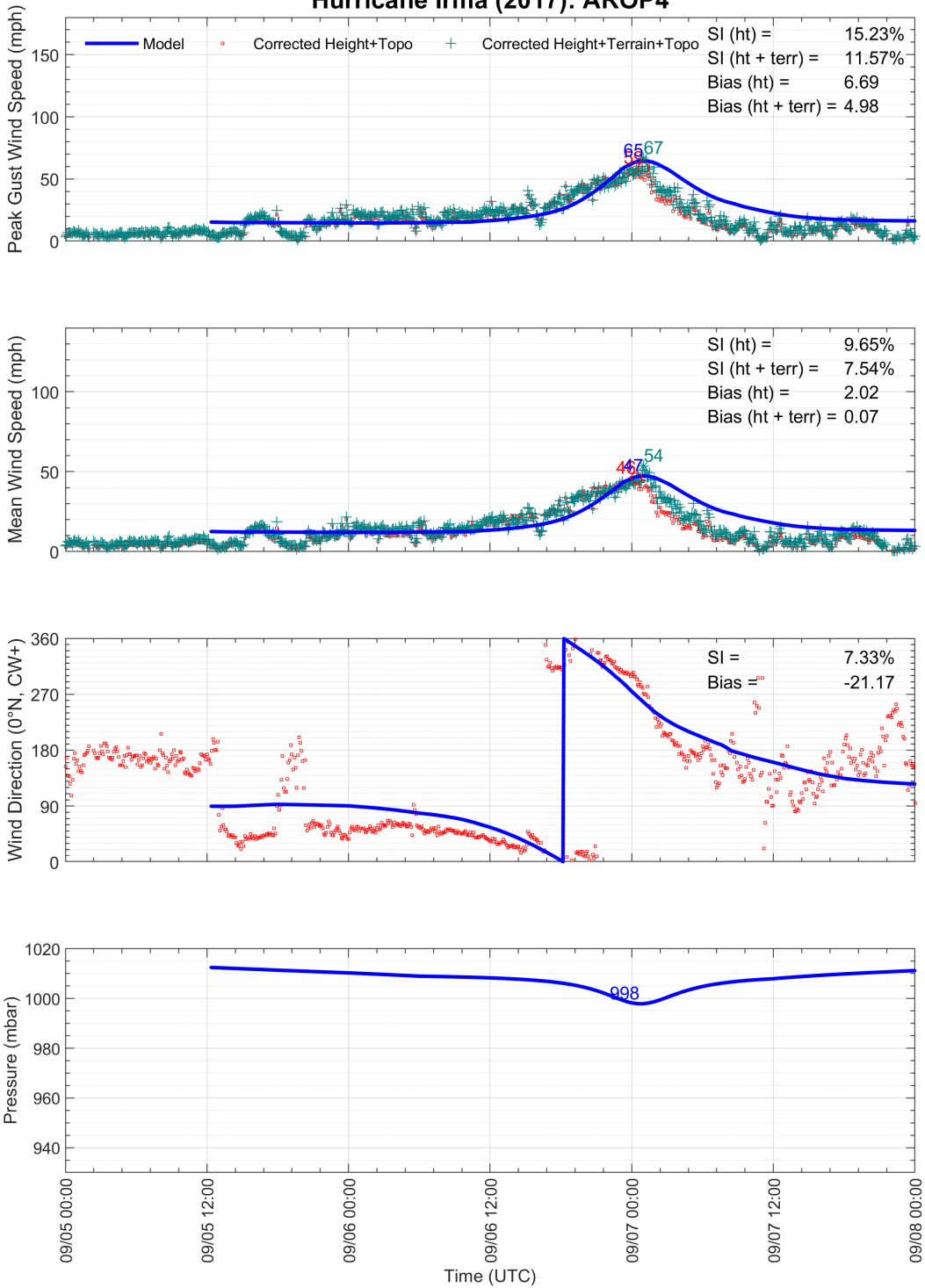
Hurricane Irma (2017): TJNR



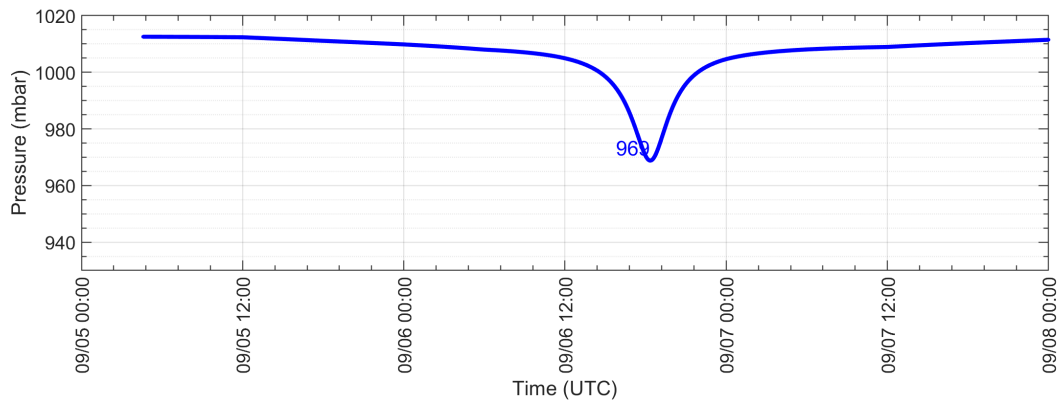
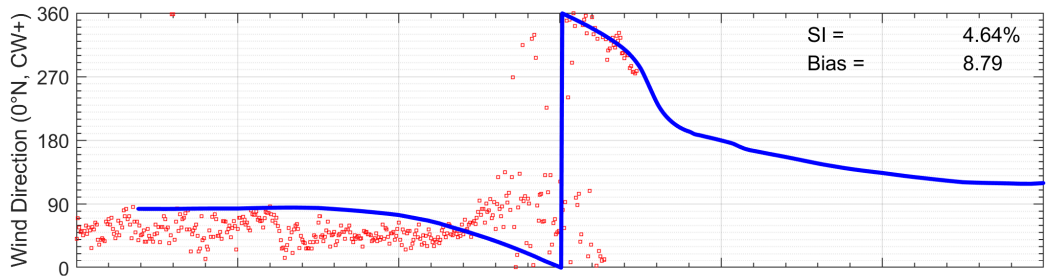
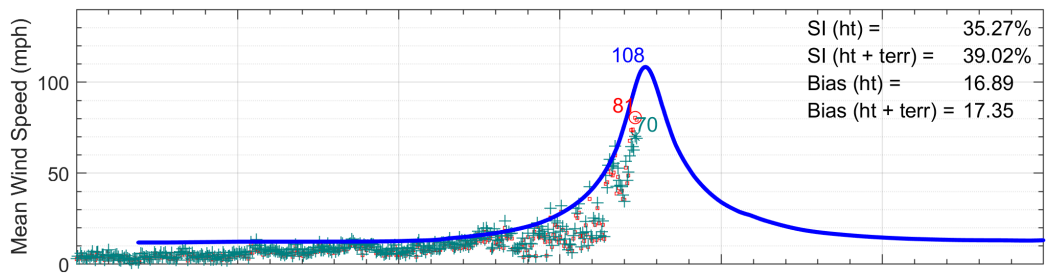
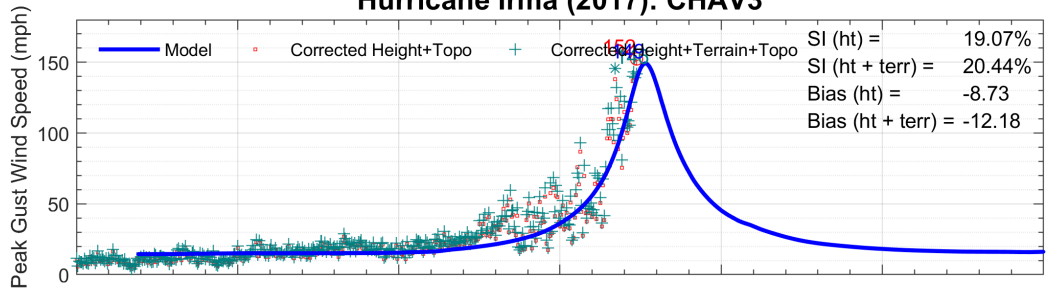
Hurricane Irma (2017): TJSJ



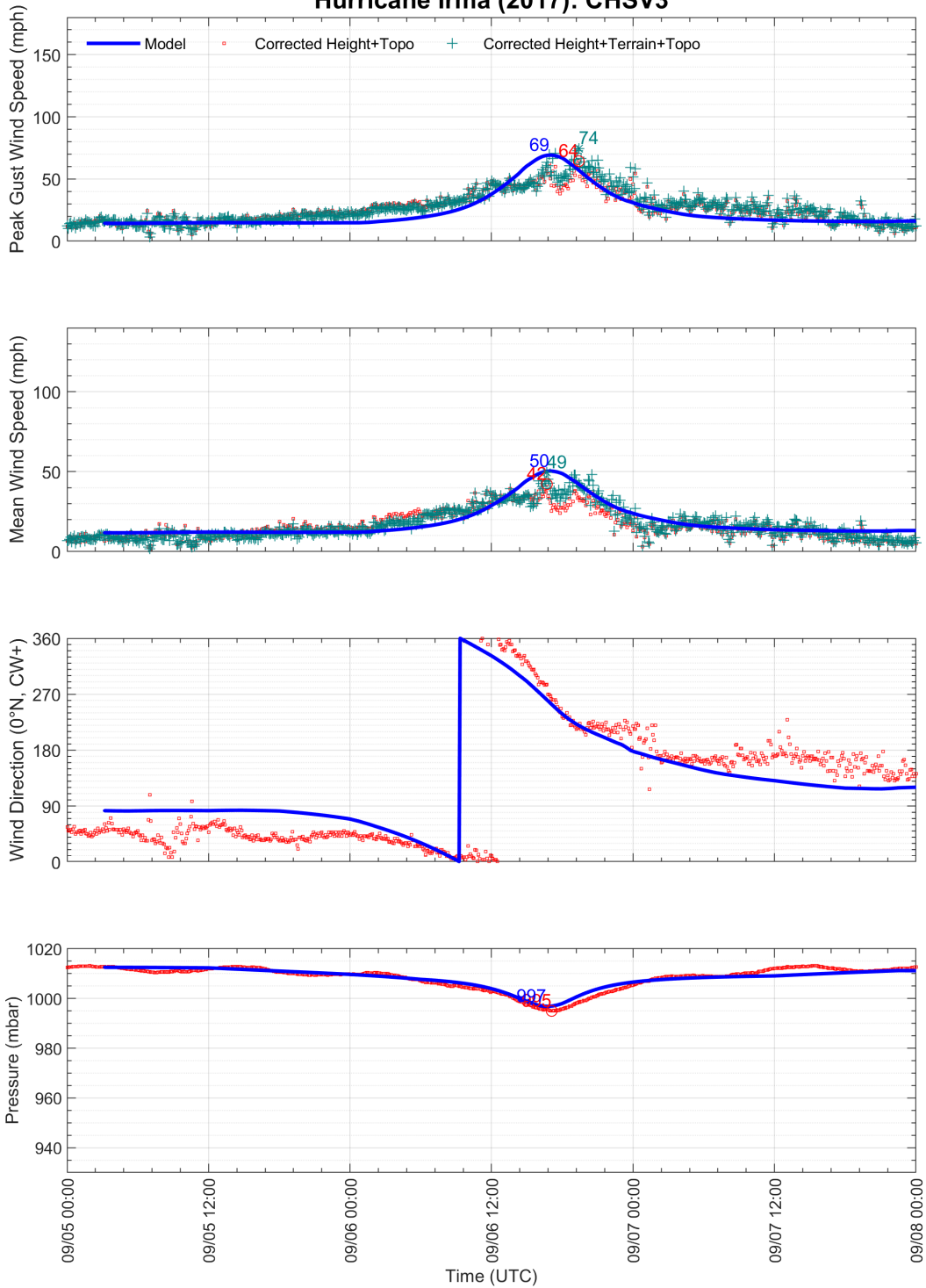
Hurricane Irma (2017): AROP4



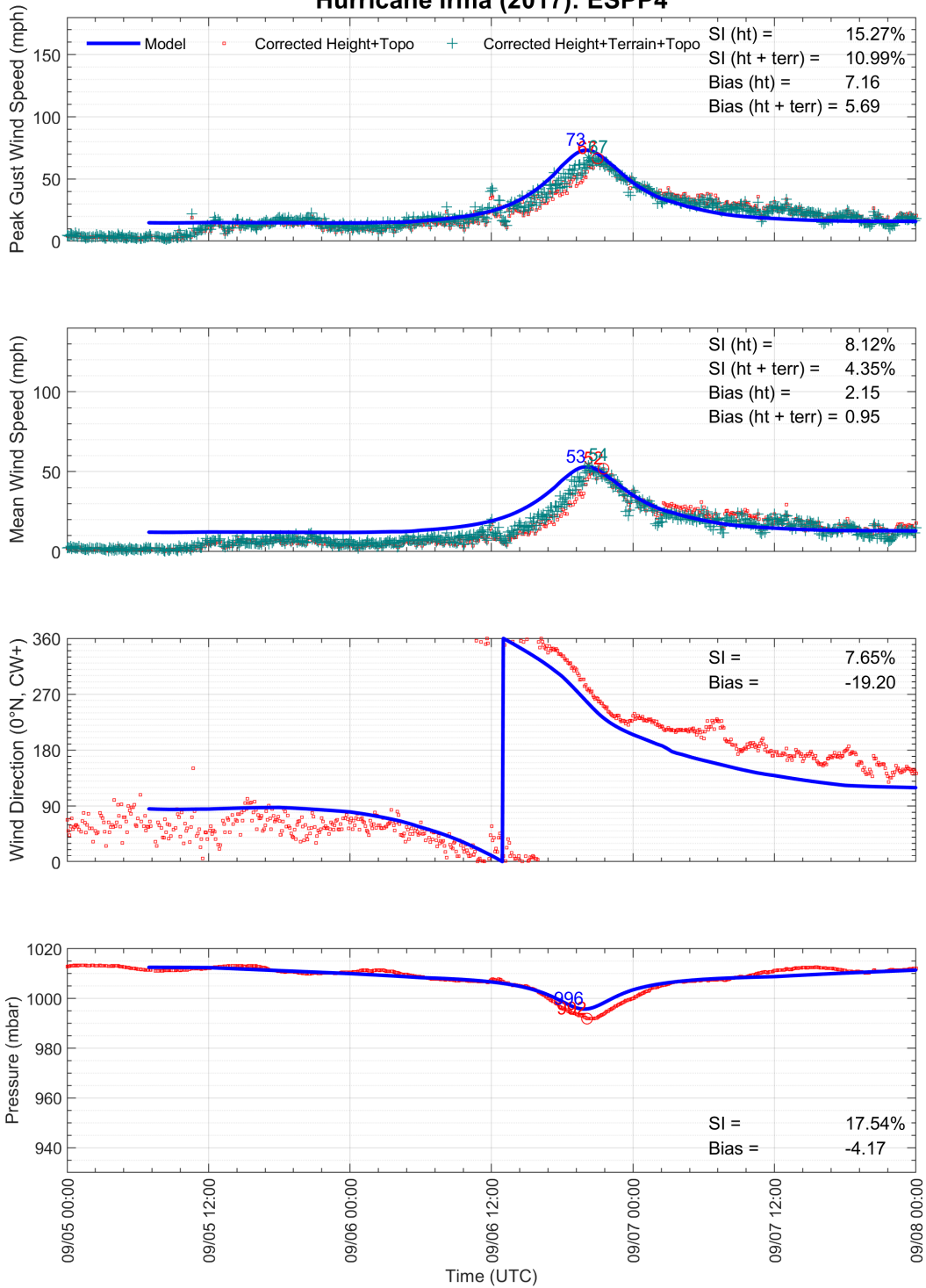
Hurricane Irma (2017): CHAV3



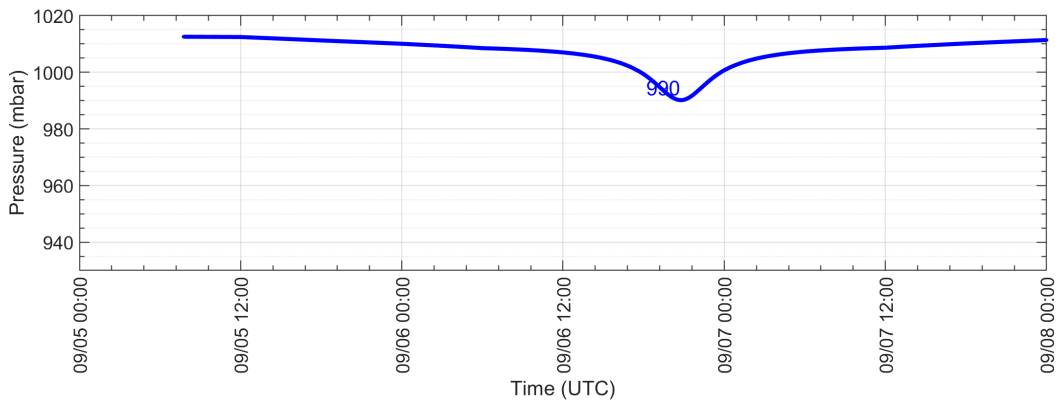
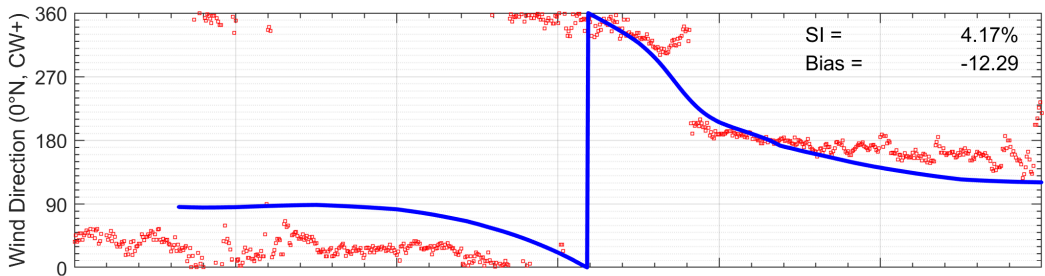
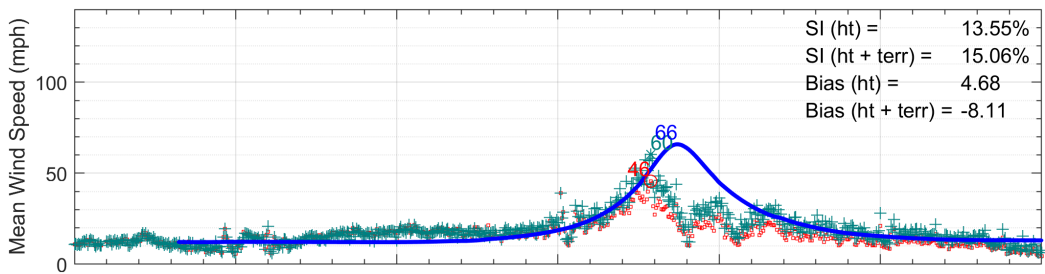
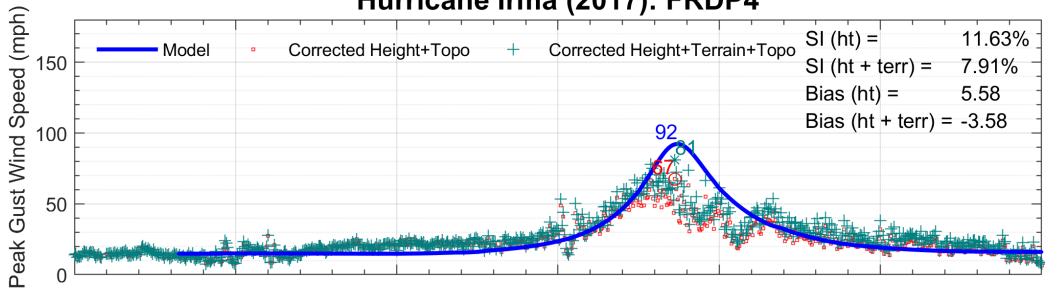
Hurricane Irma (2017): CHSV3



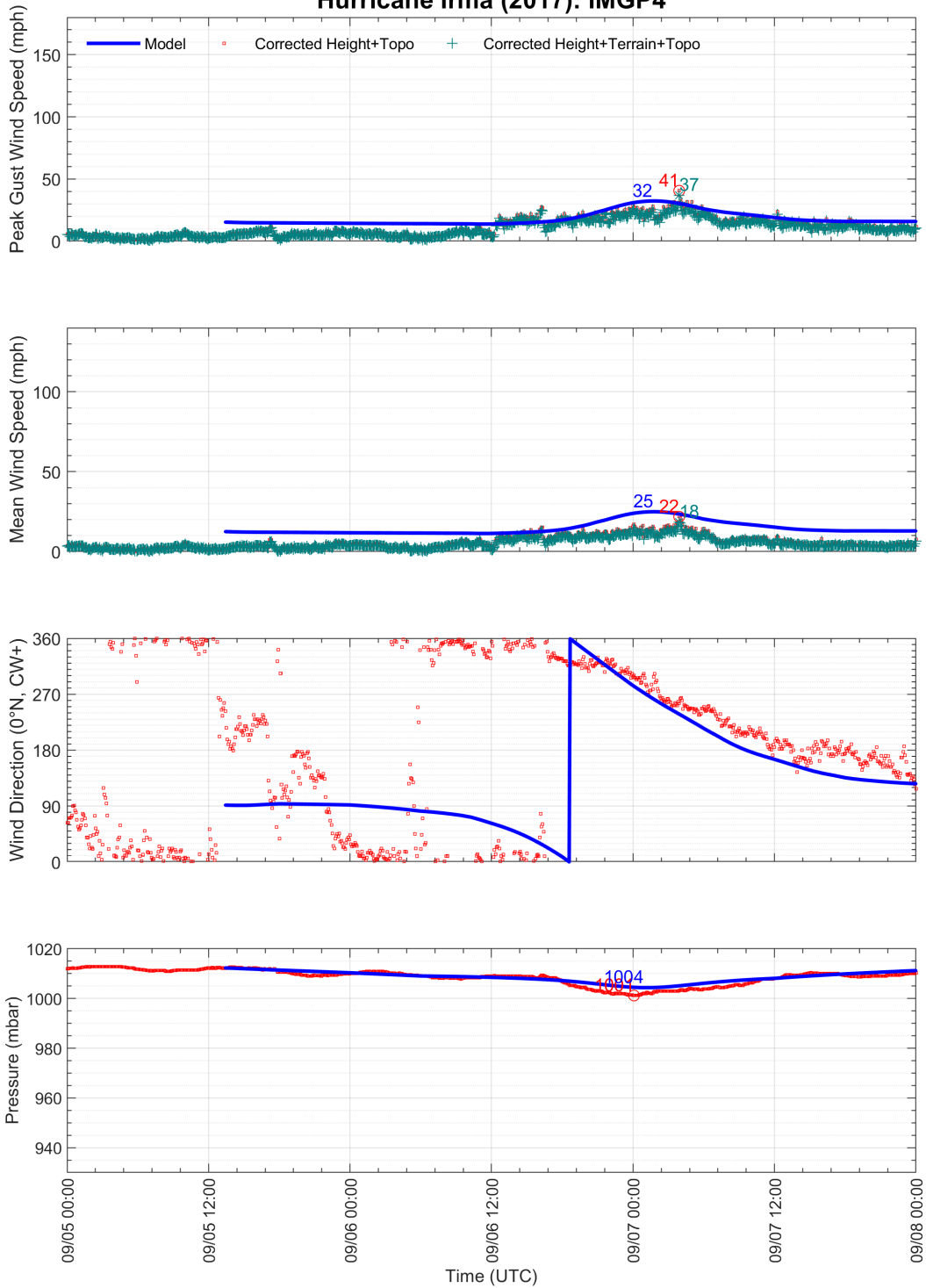
Hurricane Irma (2017): ESPP4



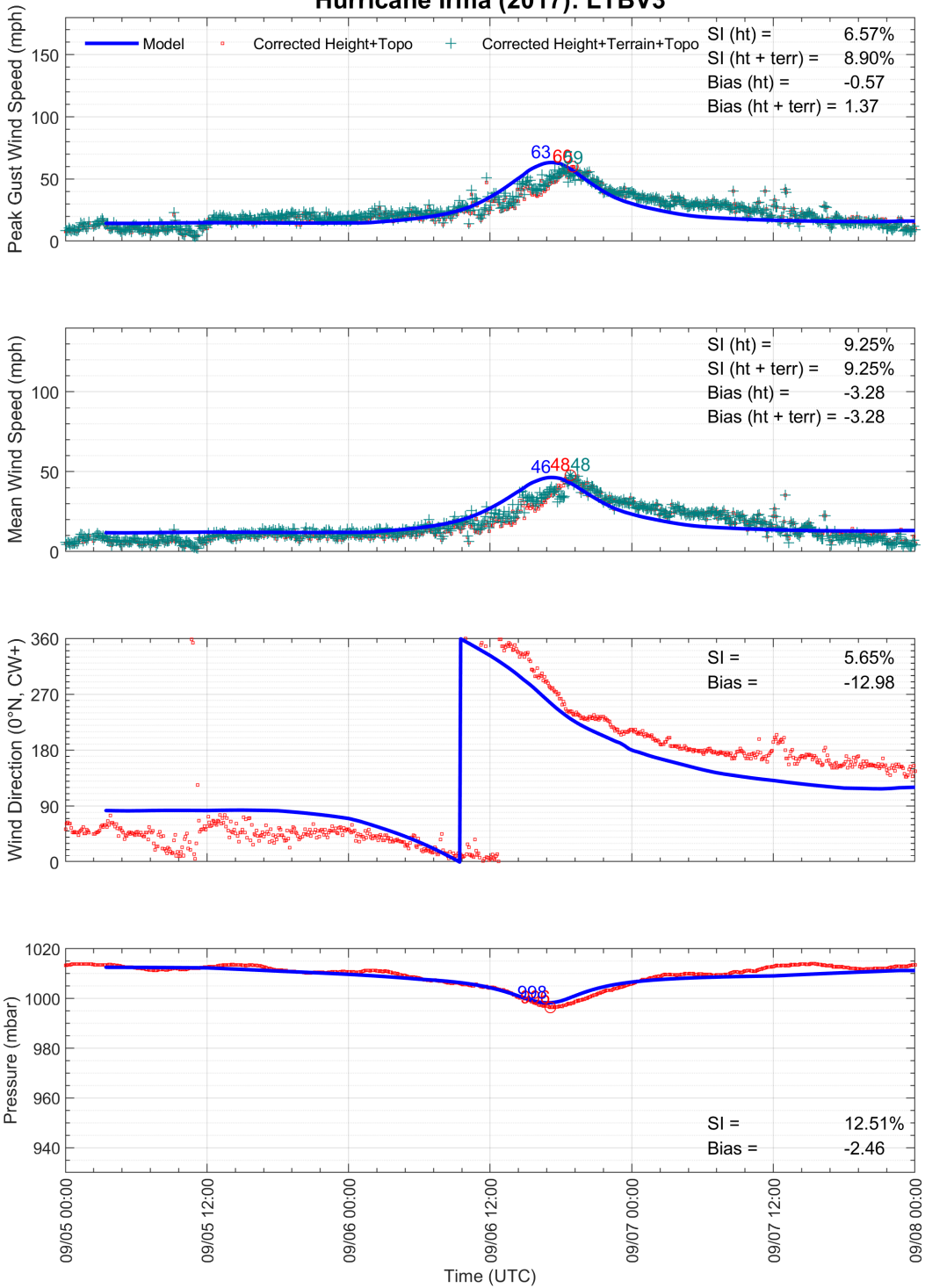
Hurricane Irma (2017): FRDP4



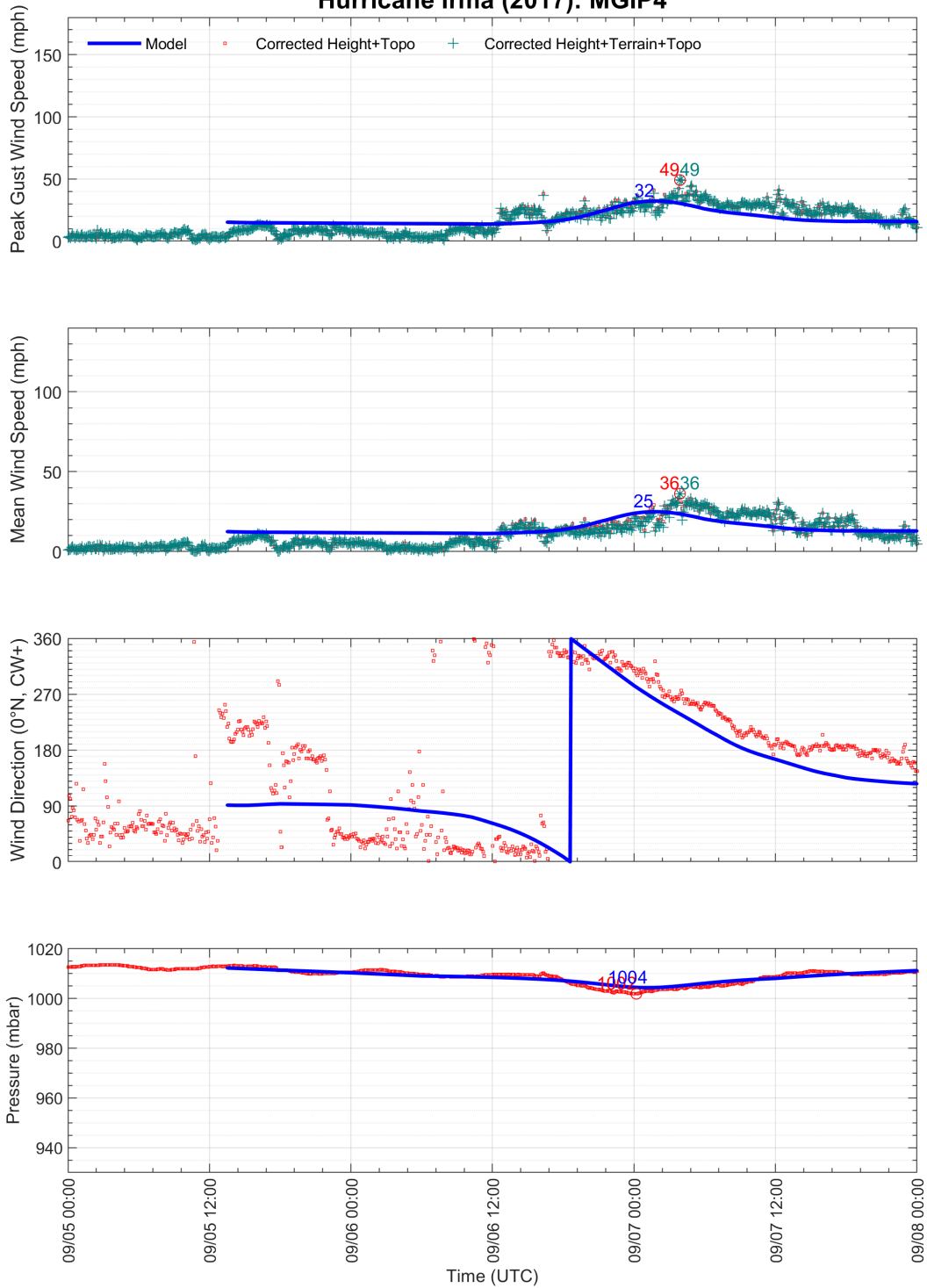
Hurricane Irma (2017): IMGP4

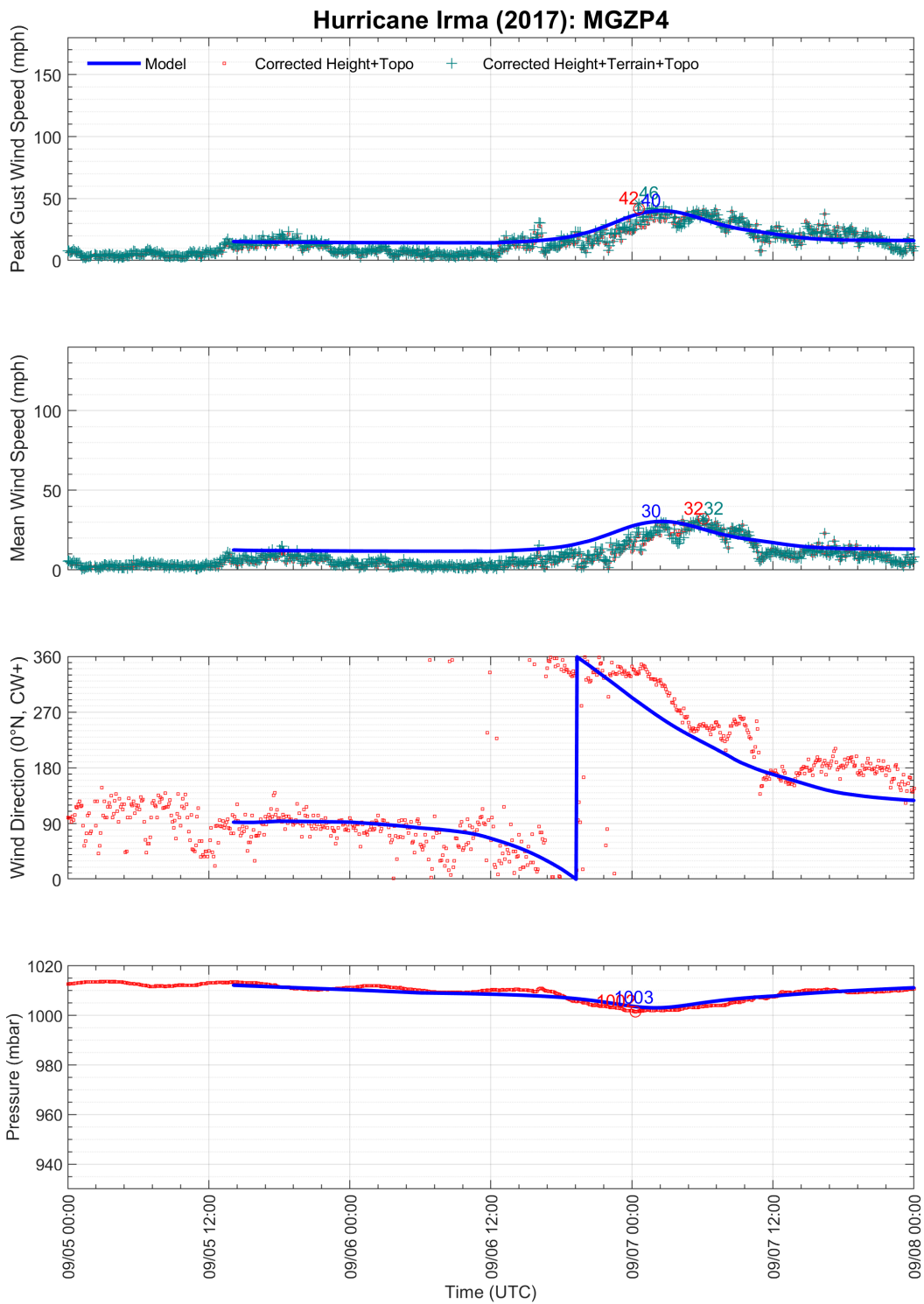


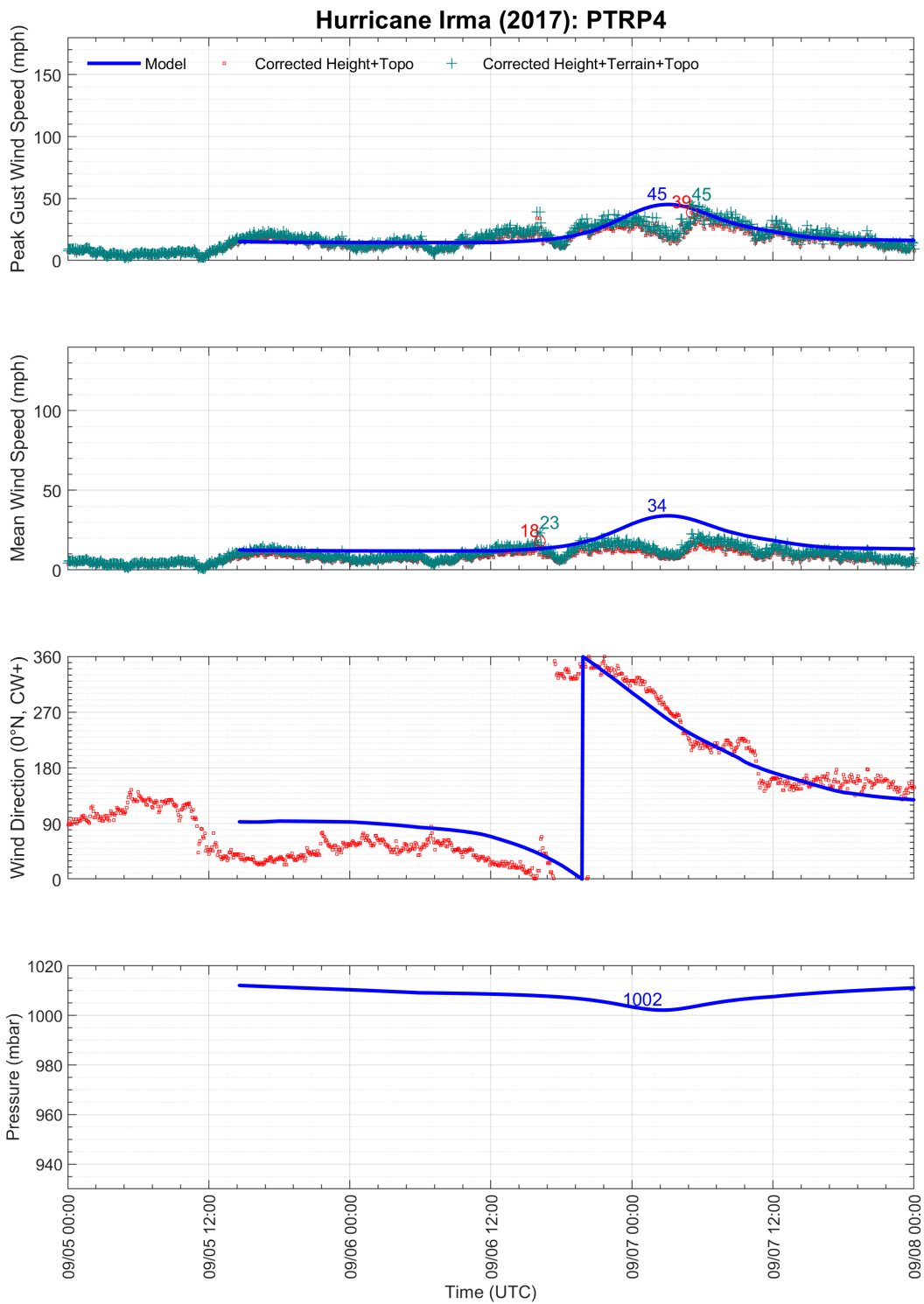
Hurricane Irma (2017): LTBV3



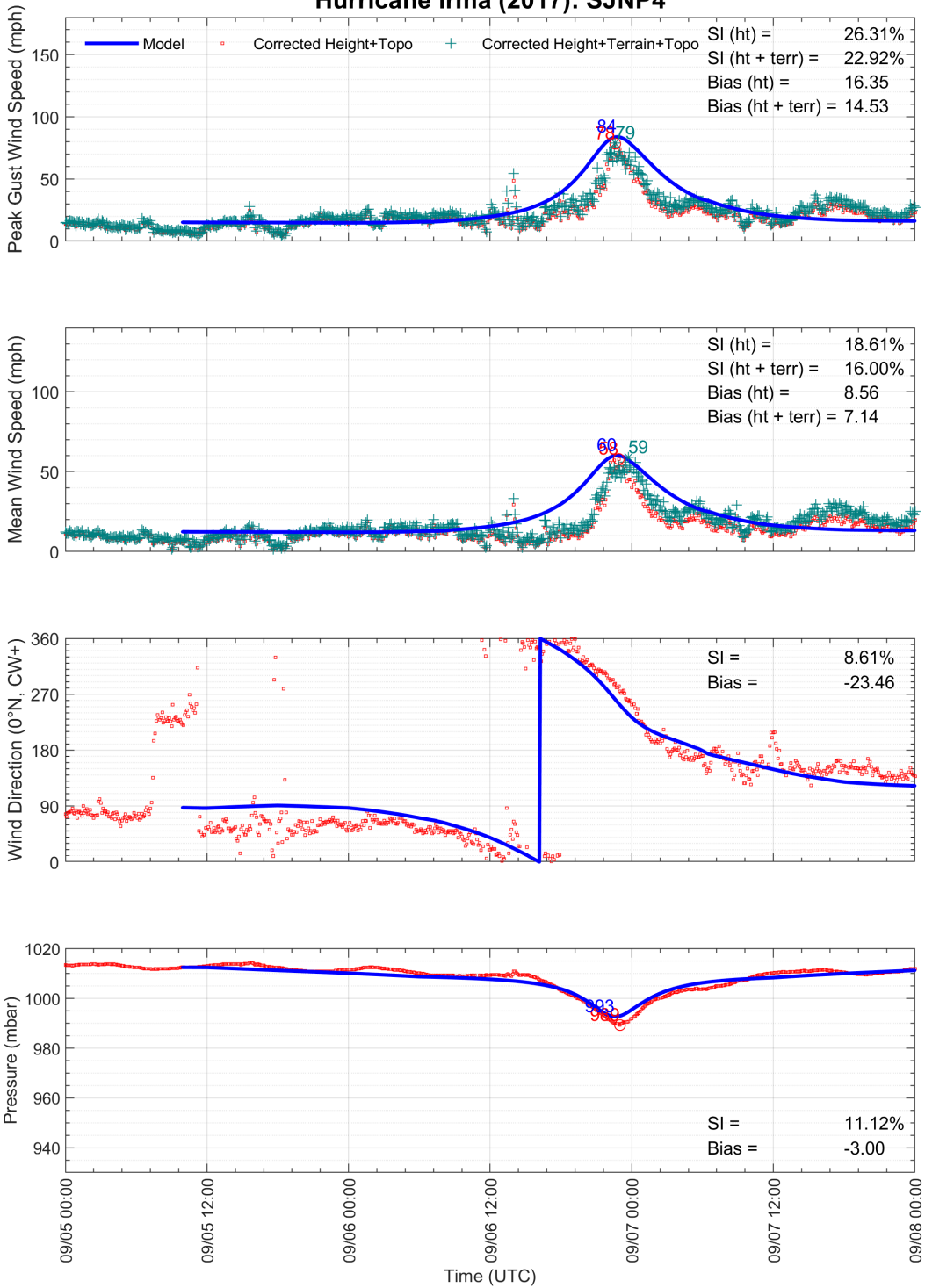
Hurricane Irma (2017): MGIP4



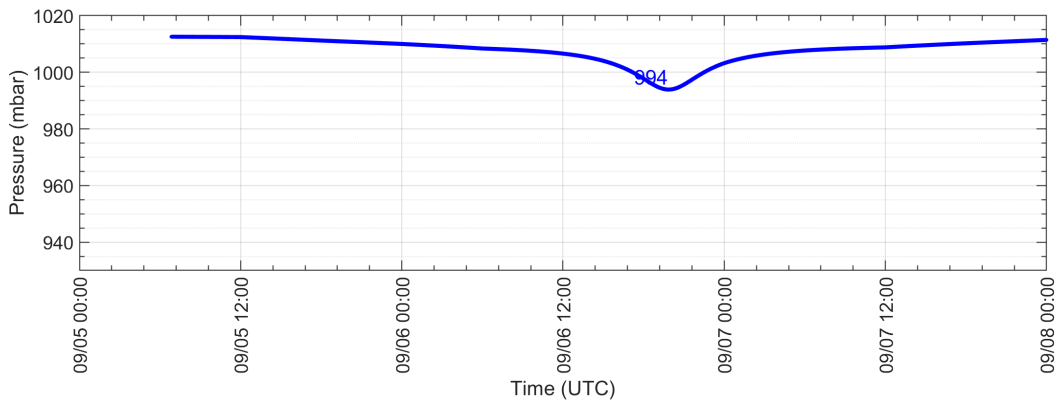
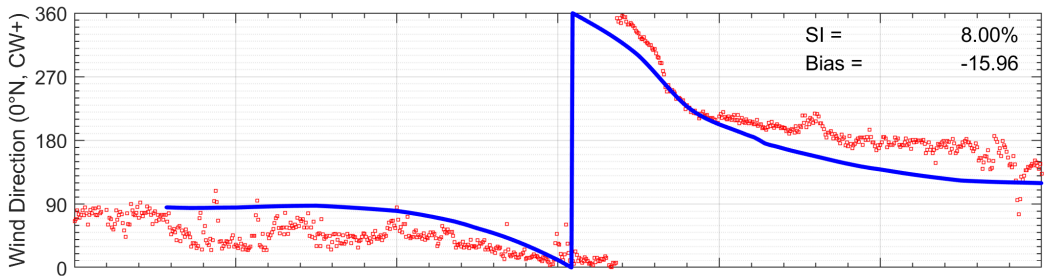
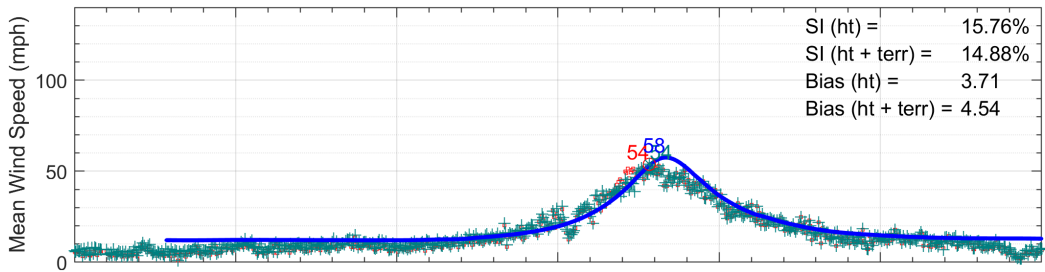
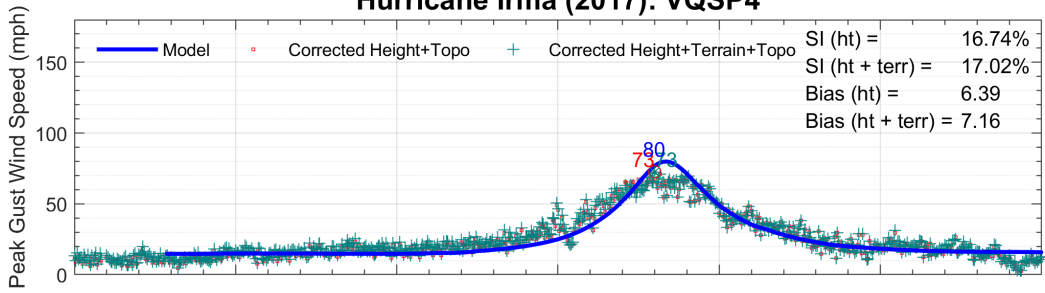


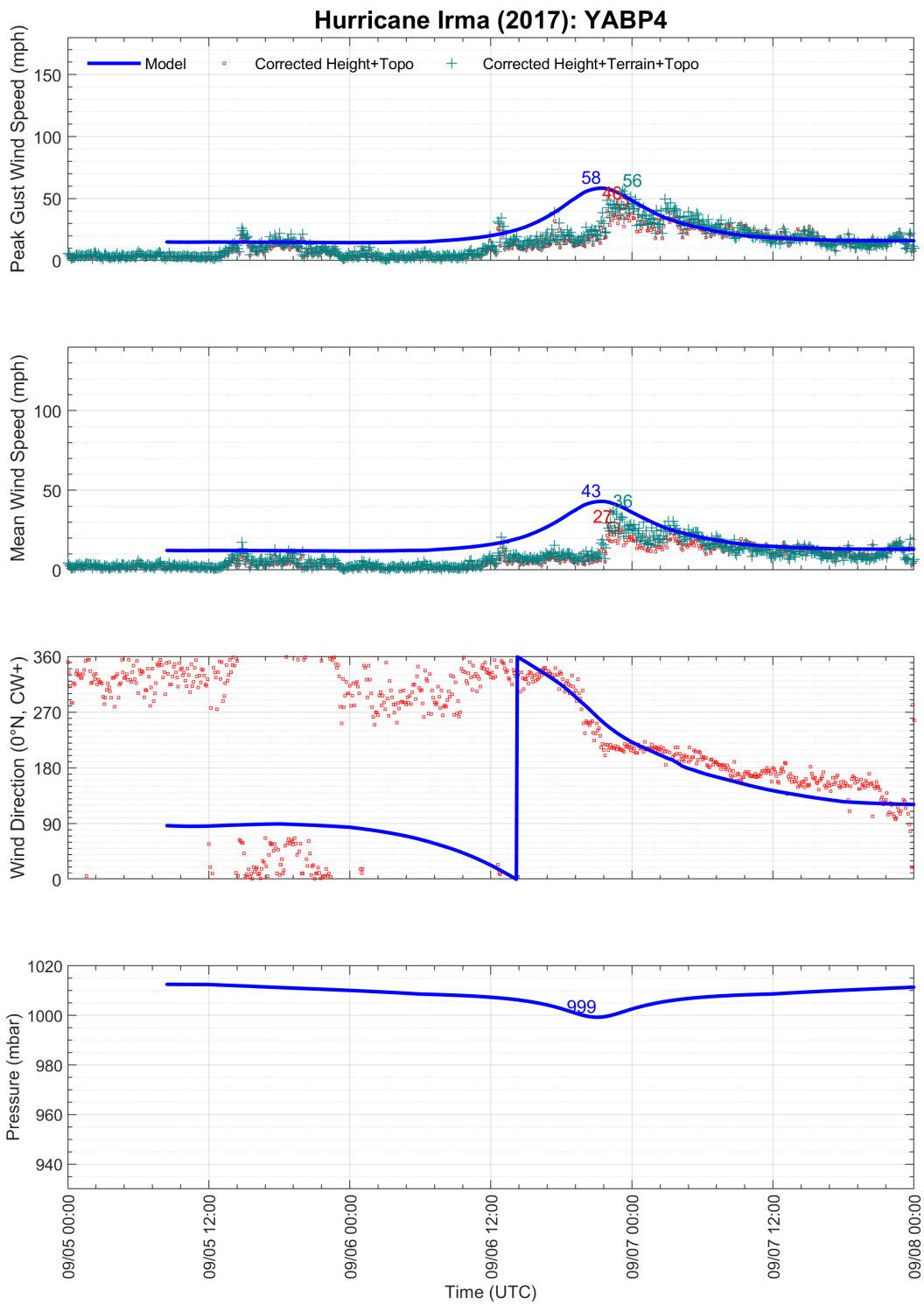


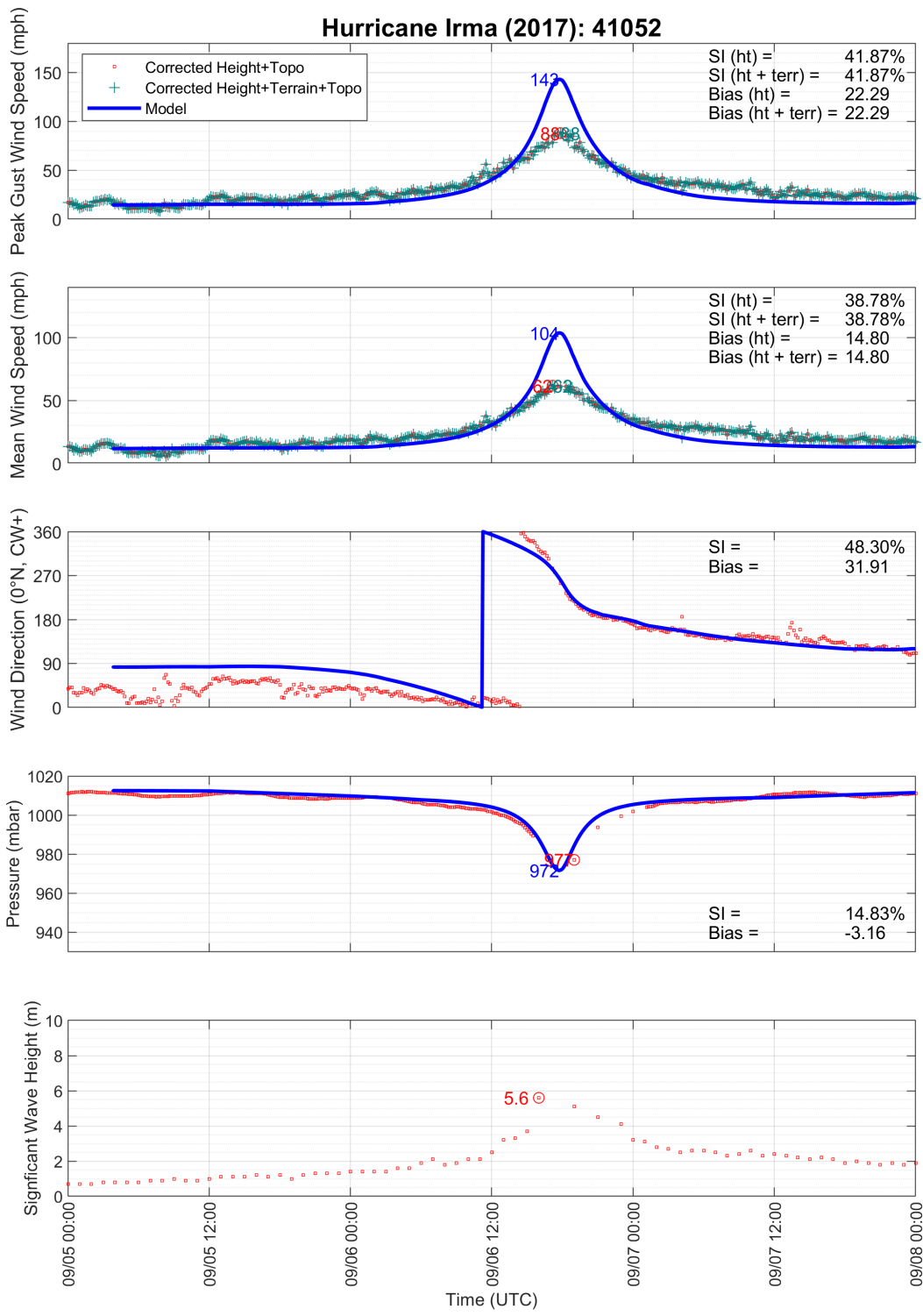
Hurricane Irma (2017): SJNP4

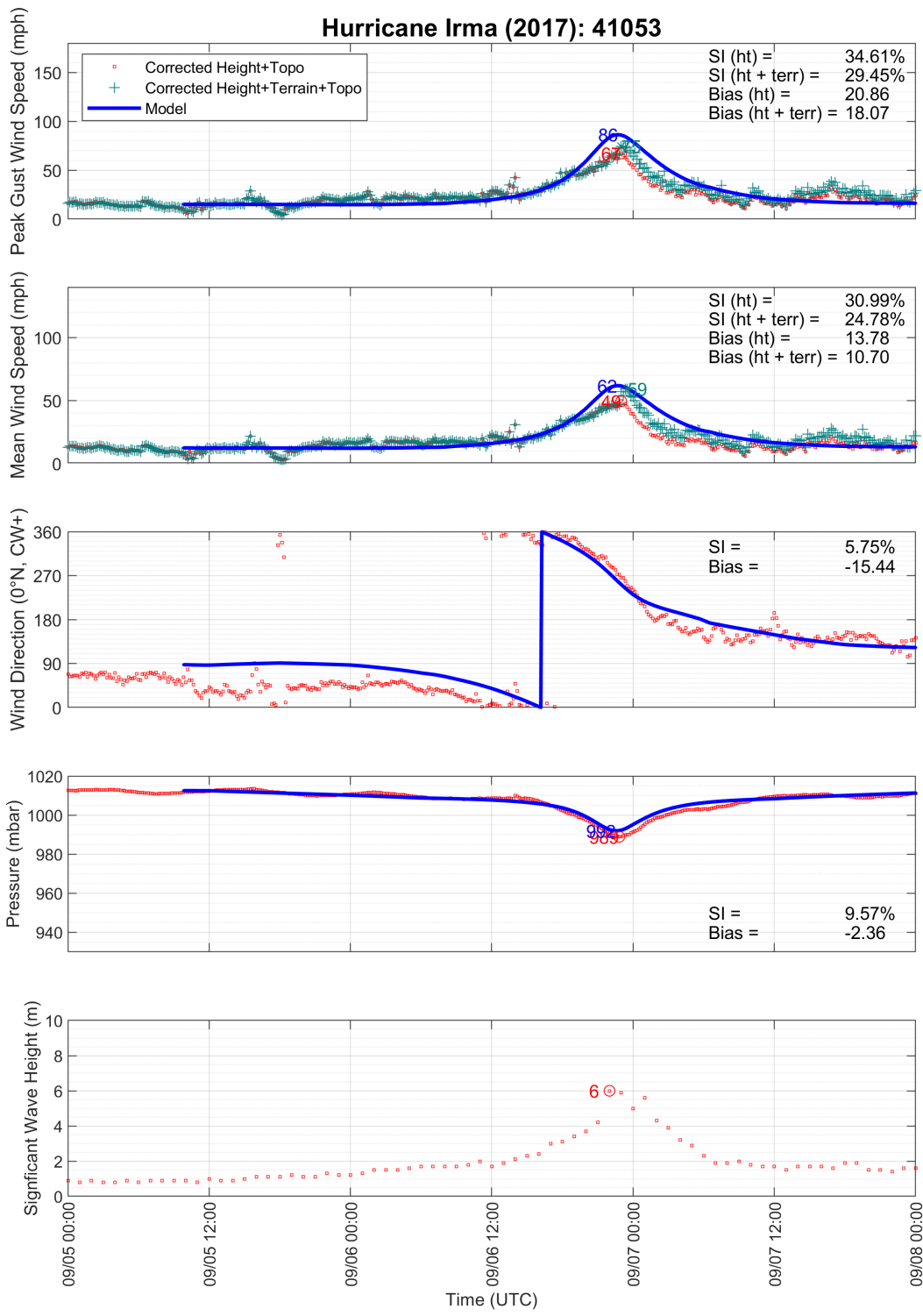


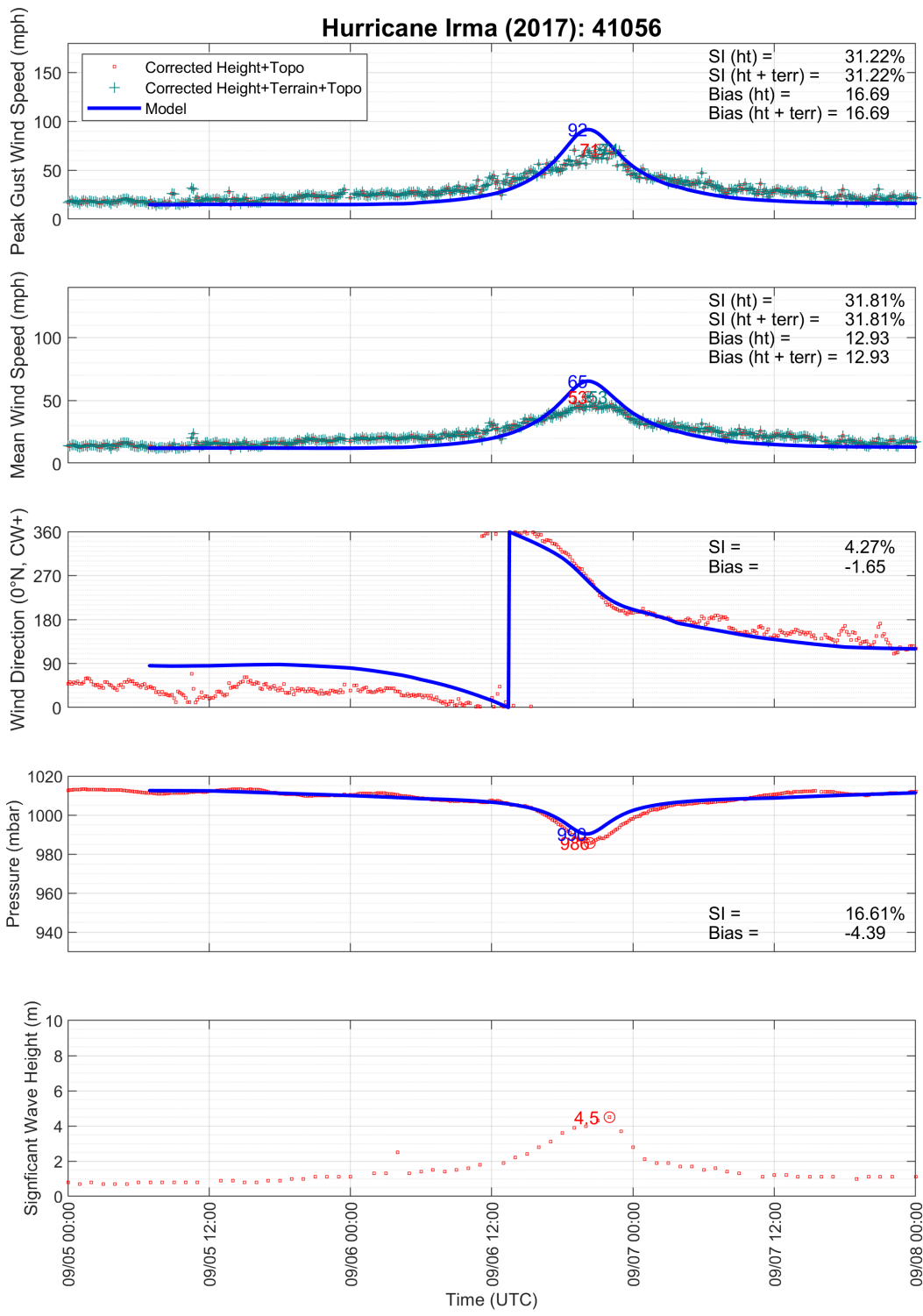
Hurricane Irma (2017): VQSP4

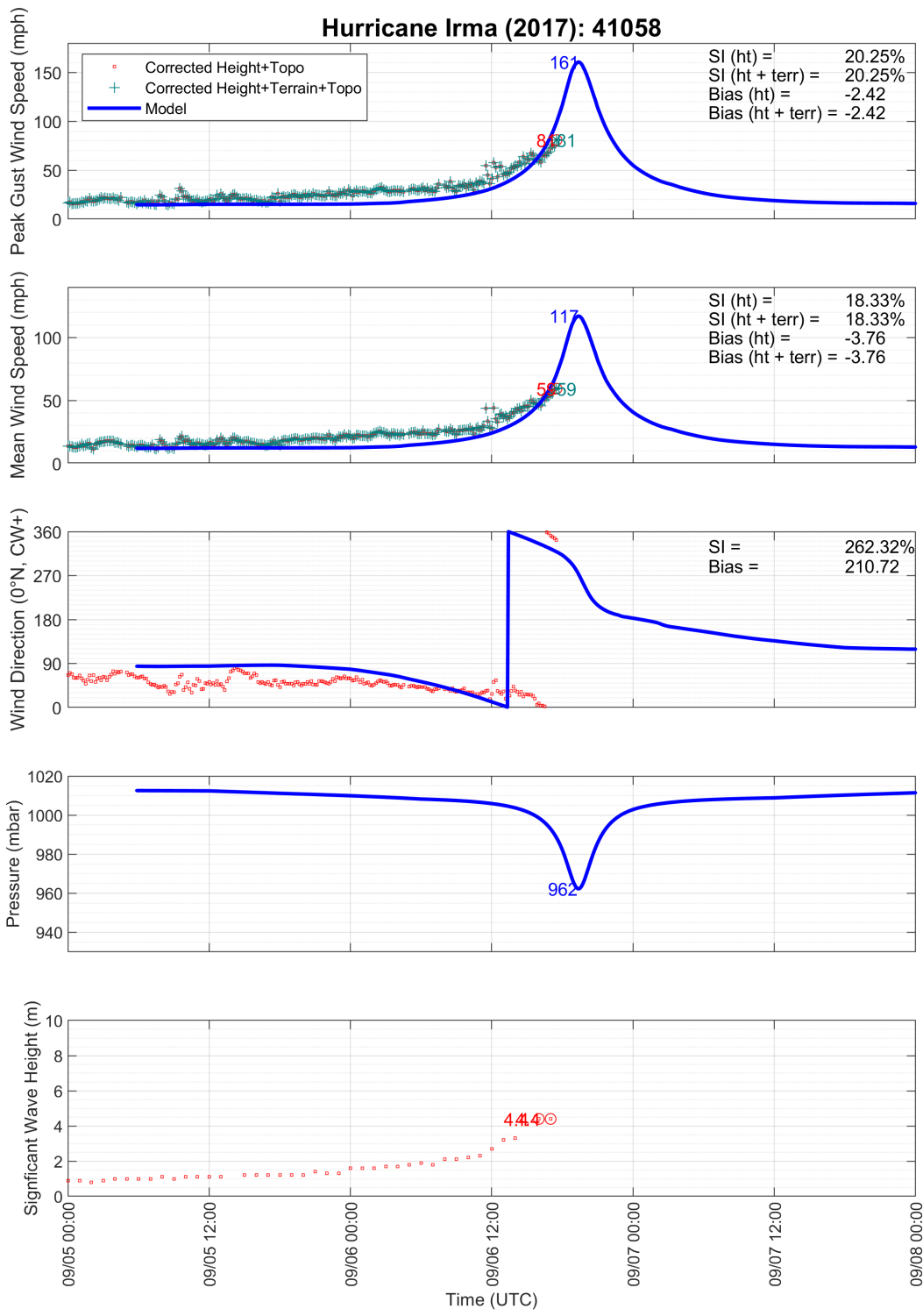


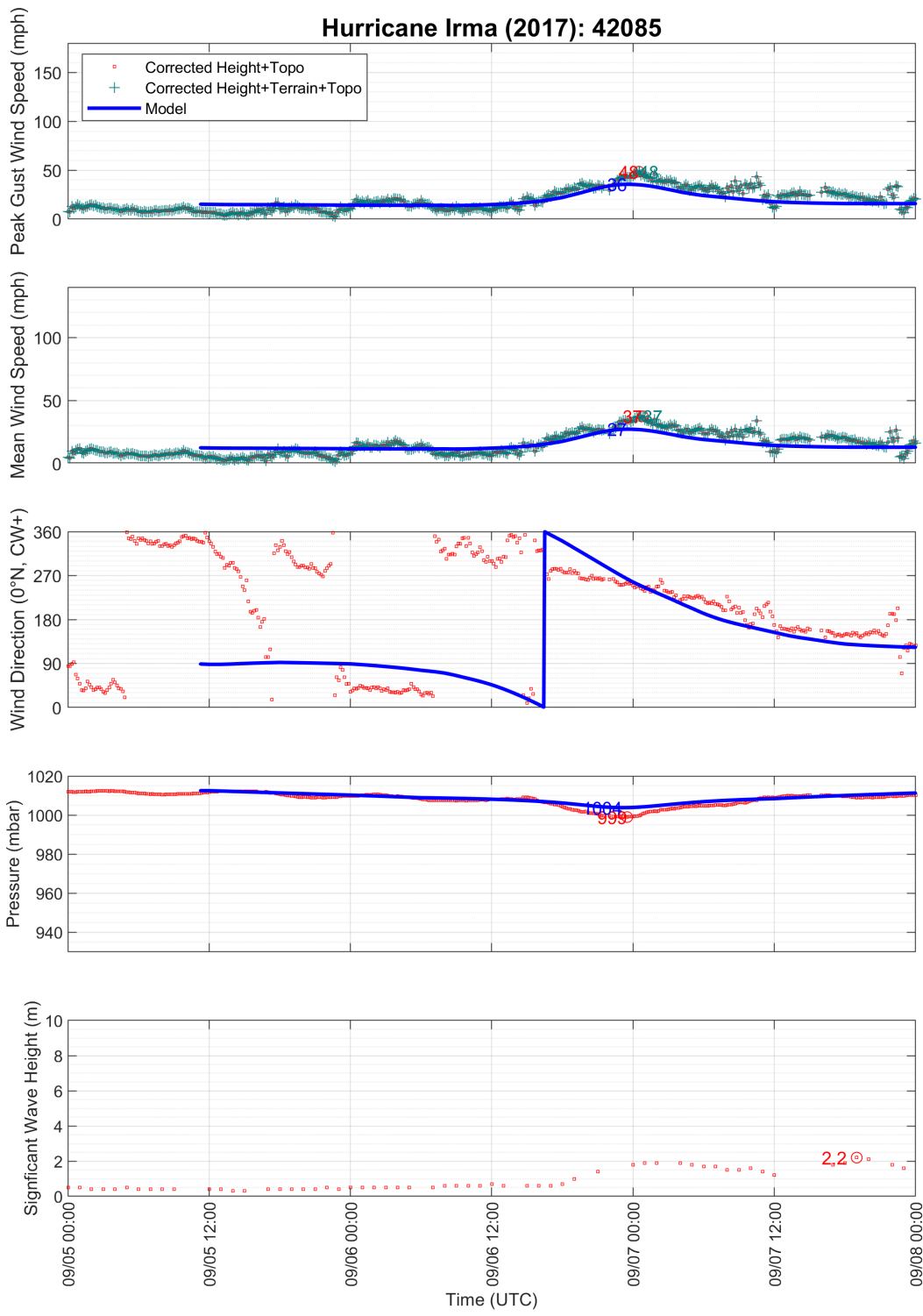












Appendix C.3 STATION DIRECTIONAL SURFACE ROUGHNESS VALUES

Station	Direction (0°N, CW+)															
	0	22.5	45	67.5	90	112.5	135	157.5	180	202.5	225	247.5	270	292.5	315	337.5
TIST	0.0300	0.0300	0.0300	0.0300	0.0300	0.0300	0.0030	0.0030	0.0030	0.0030	0.0030	0.0030	0.0030	0.0030	0.0030	0.0300
TISX	0.0300	0.0300	0.0300	0.0300	0.0300	0.0300	0.0300	0.0300	0.0300	0.0300	0.0300	0.0300	0.0300	0.0300	0.0300	0.0300
TJBQ	0.0300	0.0300	0.0300	0.0300	0.0300	0.0300	0.0300	0.0300	0.0300	0.0300	0.0300	0.0300	0.0300	0.0300	0.0300	0.0300
TJIG	0.0050	0.0050	0.0050	0.0050	0.0300	0.0300	0.0300	0.0300	0.0300	0.0300	0.0300	0.0300	0.0300	0.0300	0.0050	0.0050
TJNR	0.0300	0.0300	0.0300	0.0300	0.0300	0.0300	0.0300	0.0300	0.0300	0.0300	0.0300	0.0300	0.0300	0.0300	0.0300	0.0300
TJPS	0.0300	0.0300	0.0300	0.0300	0.0300	0.0300	0.0300	0.0300	0.0300	0.0300	0.0300	0.0300	0.0300	0.0300	0.0300	0.0300
TJSJ	0.0300	0.0300	0.0300	0.0300	0.0300	0.0300	0.0300	0.0300	0.0300	0.0300	0.0300	0.0300	0.0300	0.0300	0.0300	0.0300
TUPJ	0.0300	0.0300	0.0300	0.0300	0.0300	0.0300	0.0300	0.0300	0.0300	0.0300	0.0300	0.0300	0.0300	0.0300	0.0300	0.0300
AROP4	0.0000	0.0000	0.0500	0.5000	0.5000	0.5000	0.9000	0.9000	0.9000	0.9000	0.9000	0.5000	0.3000	0.0000	0.0000	0.0000
CHAV3	0.1000	0.1000	0.1000	0.1000	0.1000	0.3000	0.3000	0.3000	0.1000	0.0800	0.0500	0.0050	0.0050	0.0050	0.1000	0.1000
CHSV3	0.0000	0.0000	0.0050	0.1000	0.1000	0.1000	0.1000	0.1000	0.1000	0.1000	0.8000	0.8000	0.8000	0.0500	0.0000	0.0000
ESPP4	0.7000	0.7000	0.7000	0.7000	0.5000	0.0500	0.0050	0.0000	0.0000	0.0050	0.0000	0.0000	0.0000	0.5000	0.6000	0.7000
FRDP4	0.0500	0.0000	0.0000	0.0000	0.0000	0.0000	0.3000	0.5000	0.8000	0.8000	0.8000	0.8000	0.8000	0.8000	0.8000	0.1500
IMGP4	0.0100	0.0100	0.0100	0.0100	0.0100	0.0100	0.0100	0.0100	0.0100	0.0100	0.0100	0.0100	0.0100	0.0100	0.0100	0.0100
LTBV3	0.3000	0.1500	0.1500	0.0500	0.0100	0.0100	0.0050	0.0000	0.0000	0.0000	0.0000	0.0000	0.0050	0.1500	0.3000	0.3000
MGIP4	0.0080	0.0080	0.1000	0.1000	0.1000	0.1000	0.0500	0.0000	0.0000	0.0000	0.0000	0.0000	0.0000	0.0050	0.0080	0.0080
MGZP4	0.7000	0.7000	0.7000	0.7000	0.7000	0.7000	0.7000	0.1000	0.0000	0.0000	0.0000	0.0000	0.0000	0.0100	0.1000	0.7000
PTRP4	0.8000	0.8000	0.8000	0.8000	0.8000	0.8000	0.8000	0.8000	0.8000	0.8000	0.8000	0.8000	0.8000	0.8000	0.8000	0.8000
SJNP4	0.9000	0.7000	0.3000	0.1000	0.0100	0.5000	0.5000	0.8000	0.8000	0.7000	0.6000	0.5000	0.0100	0.0100	0.5000	0.9000
VQSP4	0.0100	0.0500	0.1000	0.1000	0.1000	0.1000	0.1000	0.1000	0.0000	0.0000	0.0000	0.0000	0.0000	0.0000	0.0000	0.0000
YABP4	0.9000	0.9000	0.9000	0.9000	0.0000	0.0000	0.0000	0.0000	0.0100	0.9000	0.9000	0.9000	0.9000	0.9000	0.9000	0.9000
41052	0.0000	0.0000	0.0000	0.0000	0.0000	0.0000	0.0000	0.0000	0.0000	0.0000	0.0000	0.0000	0.0000	0.0000	0.0000	0.0000
41053	0.0000	0.0000	0.0000	0.0000	0.0000	0.0000	0.5000	0.8000	0.8000	0.7000	0.6000	0.5000	0.0000	0.0000	0.0000	0.0000
41056	0.0000	0.0000	0.0000	0.0000	0.0000	0.0000	0.0000	0.0000	0.0000	0.0000	0.0000	0.0000	0.0000	0.0000	0.0000	0.0000
41058	0.0000	0.0000	0.0000	0.0000	0.0000	0.0000	0.0000	0.0000	0.0000	0.0000	0.0000	0.0000	0.0000	0.0000	0.0000	0.0000
42085	0.0000	0.0000	0.0000	0.0000	0.0000	0.0000	0.0000	0.0000	0.0000	0.0000	0.0000	0.0000	0.0000	0.0000	0.0000	0.0000



Figure C-1. Aerial image of NDBC station AROP4: Arcibo, PR.

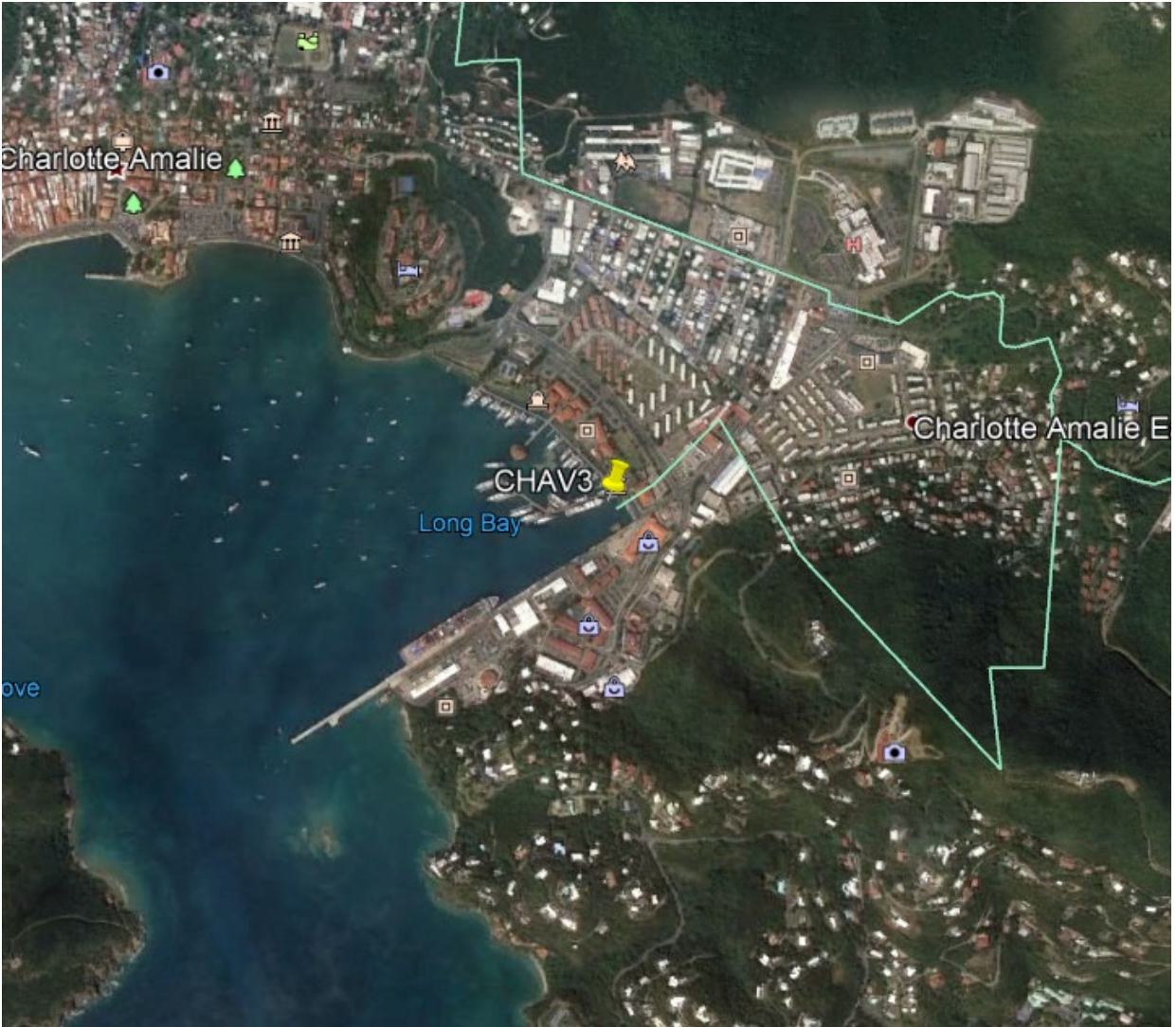


Figure C-2. Aerial image of NDBC station CHAV3: Charlotte Amalie, VI.

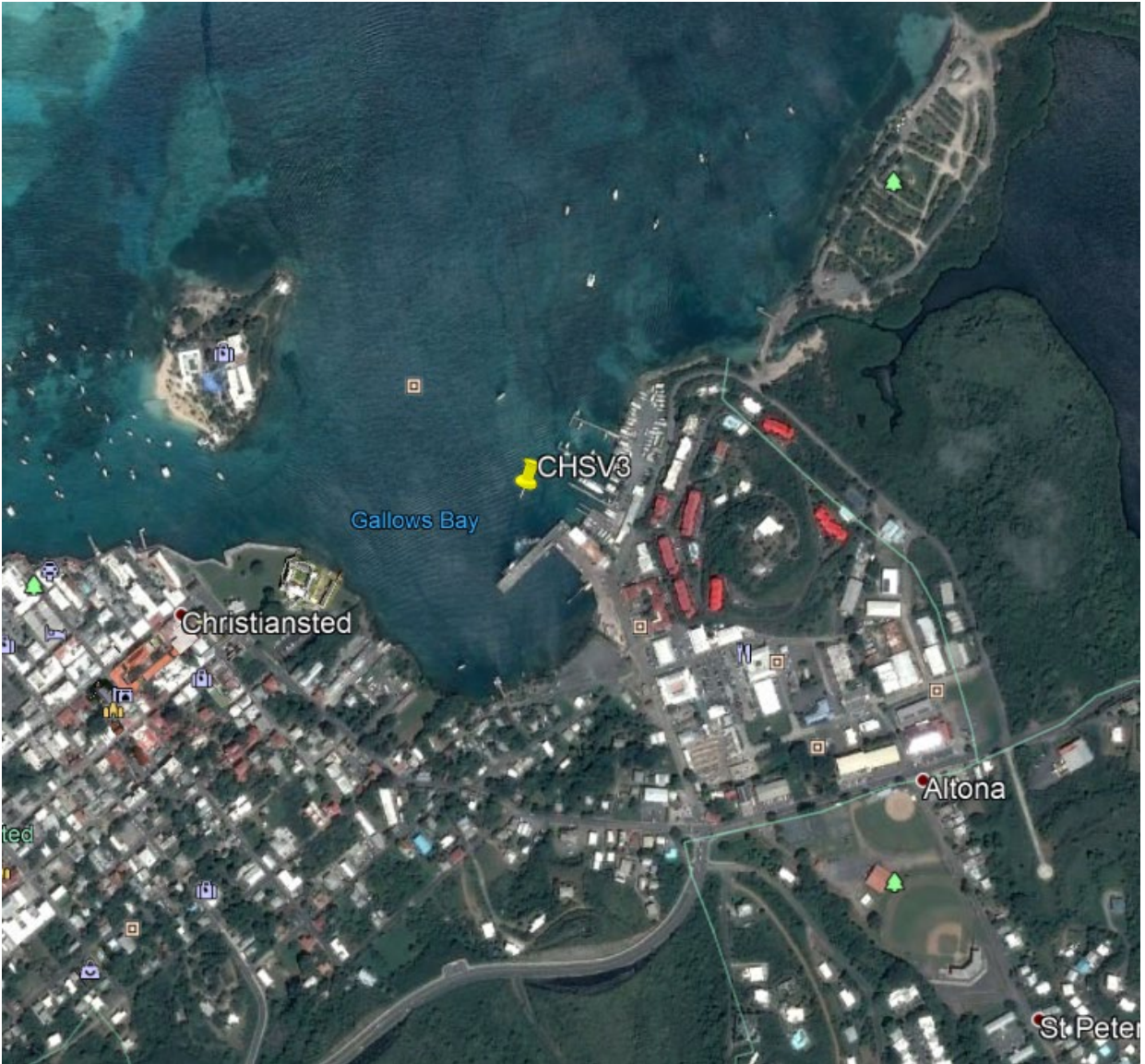


Figure C-3. Aerial image of NDBC station CHSV3: Christiansted Harbor, St, Croix, VI.



Figure C-4. Aerial image of NDBC station ESPP4: Esperanza, Vieques Island, PR.



Figure C-5. Aerial image of NDBC station FRDP4: Fajardo, PR.

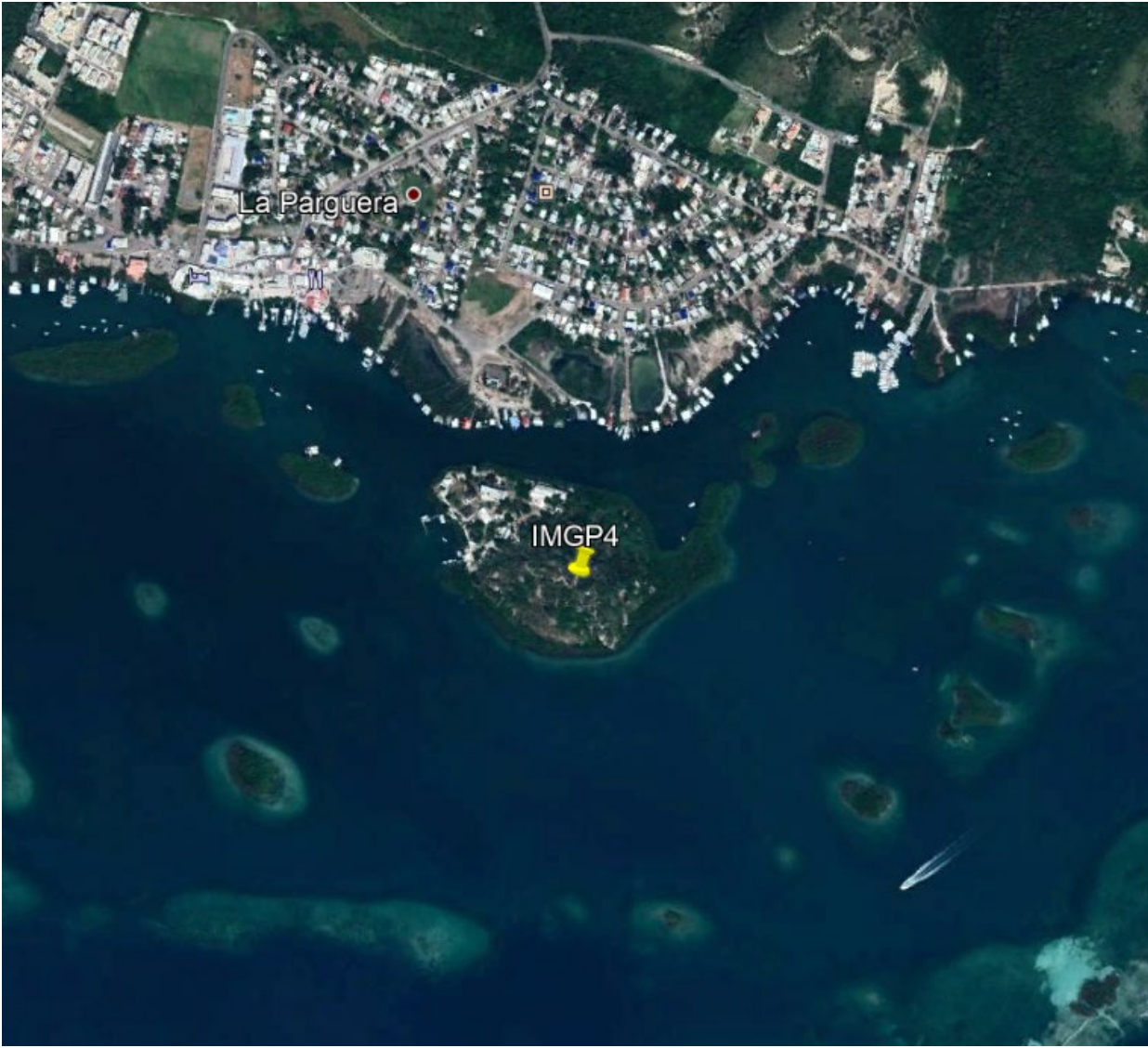


Figure C-6. Aerial image of NDBC station IMGP4: Isla Magueyes, Lajas, PR.

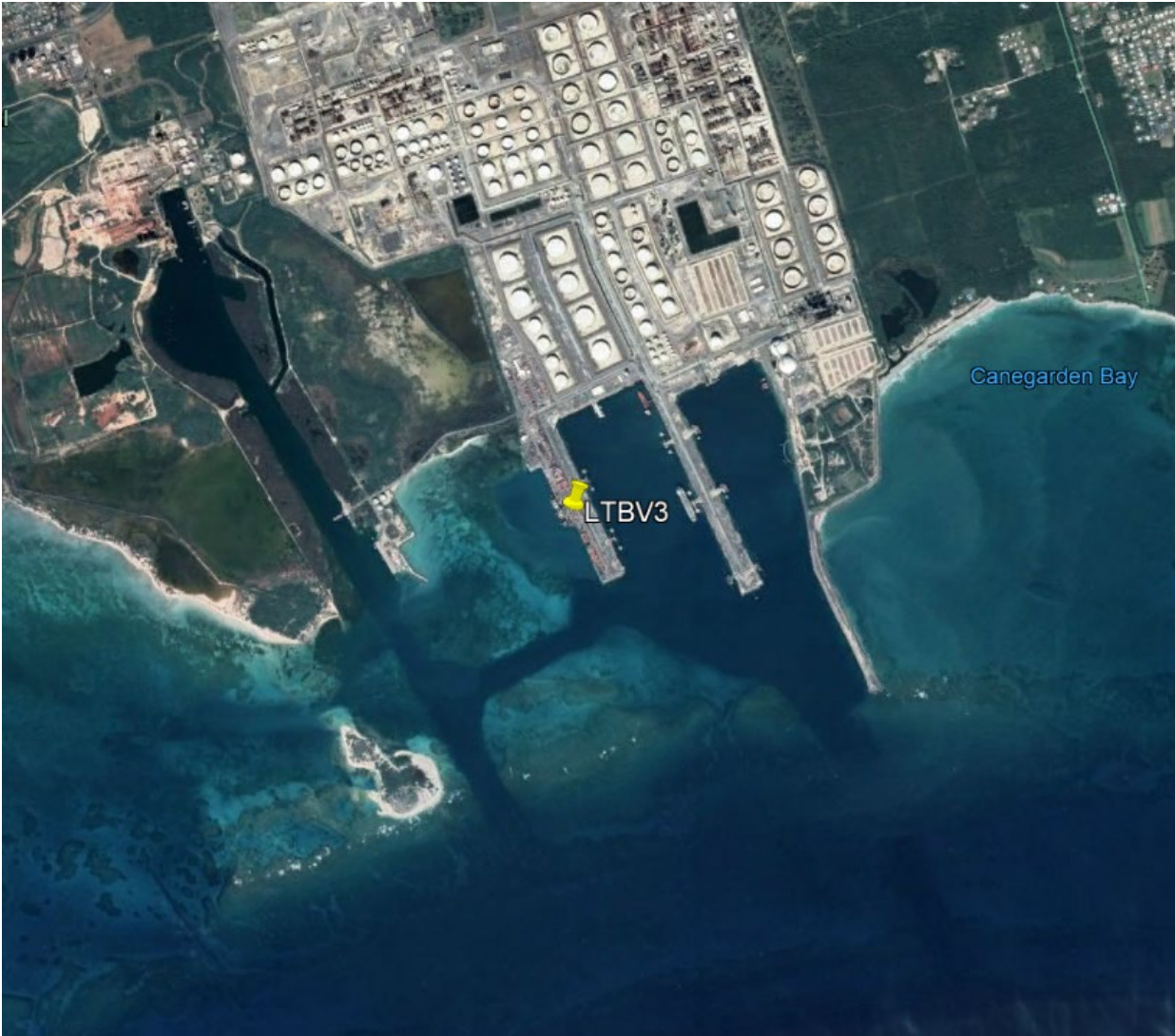


Figure C-7. Aerial image of NDBC station LTBV3: Lime Tree Bay, St. Croix, VI.



Figure C-8. Aerial image of NDBC station MGIP4: Magueyes Islands, PR.



Figure C-9. Aerial image of NDBC station MGZP4: Mayaguez, PR.



Figure C-10. Aerial image of NDBC station PTRP4: Puntas Rincon, PR.

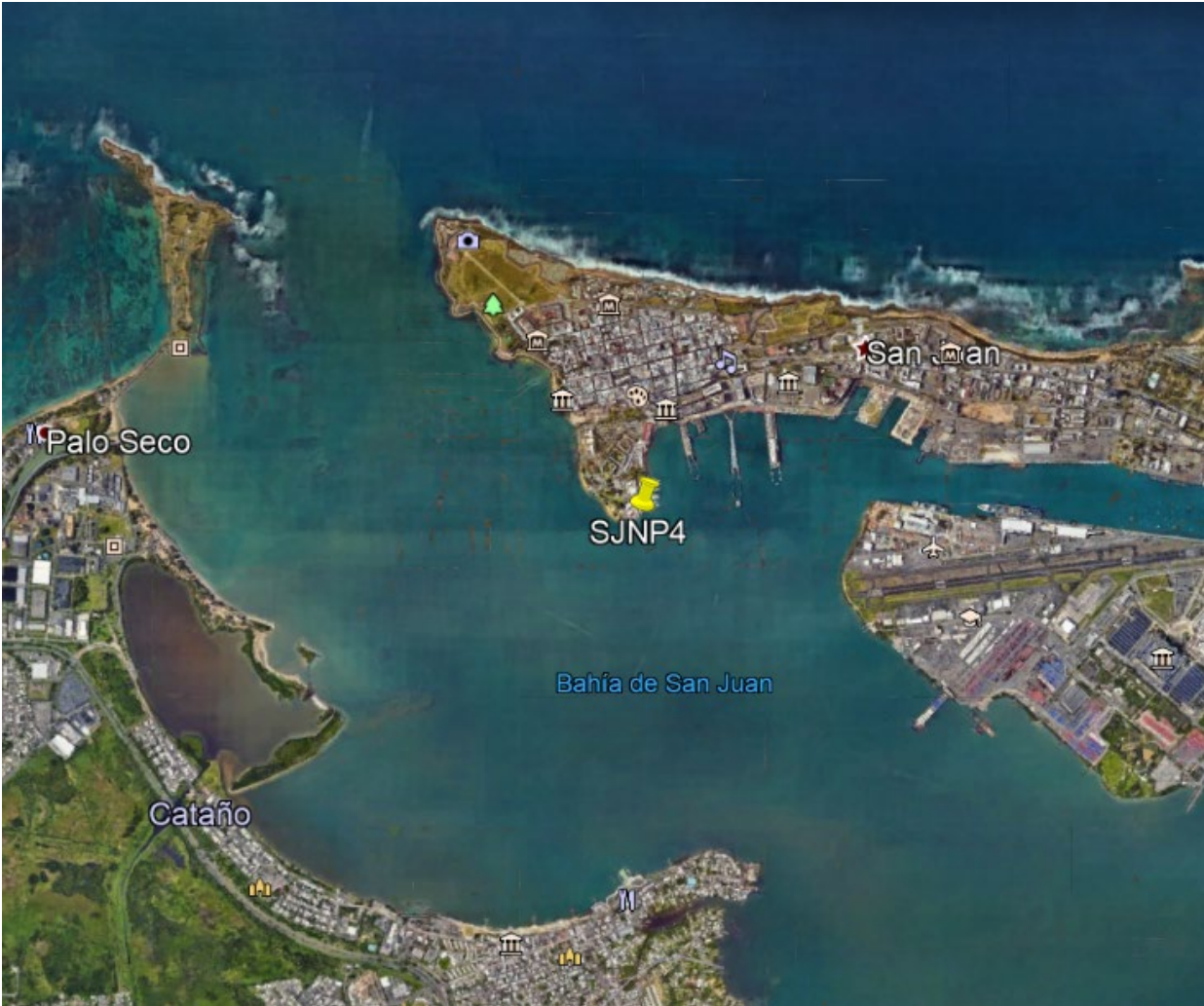


Figure C-11. Aerial image of NDBC station SJNP4: San Juan, La Puntilla, San Juan Bay, PR.



Figure C-12. Aerial image of NDBC station VQSP4: Isabel Segunda, Vieques Island, PR.



Figure C-13. Aerial image of NDBC station YABP4: Yabucoa Harbor, PR.

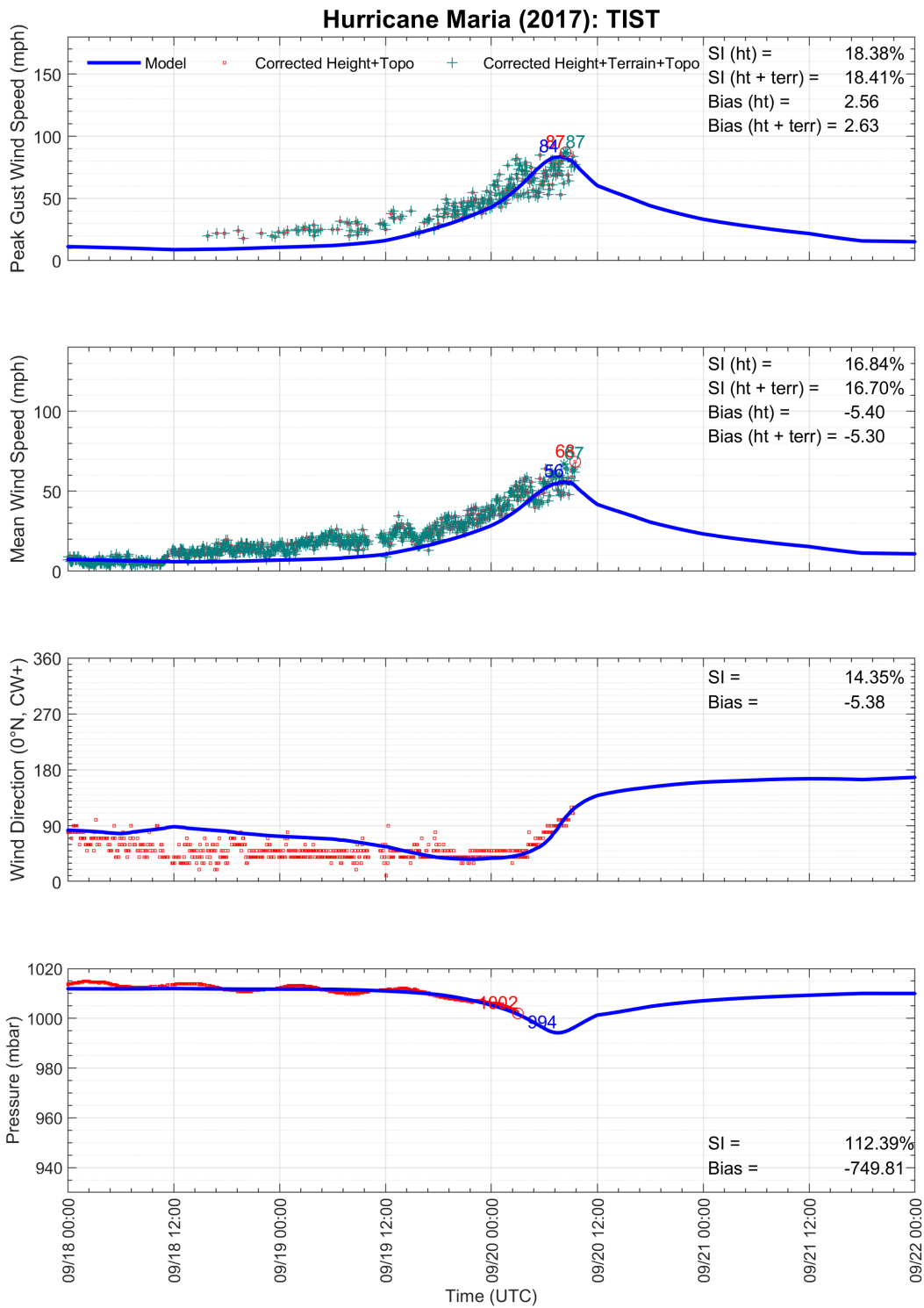
Appendix D. HURRICANE MARIA

Appendix D.1 SURFACE OBSERVATION STATION DETAILS

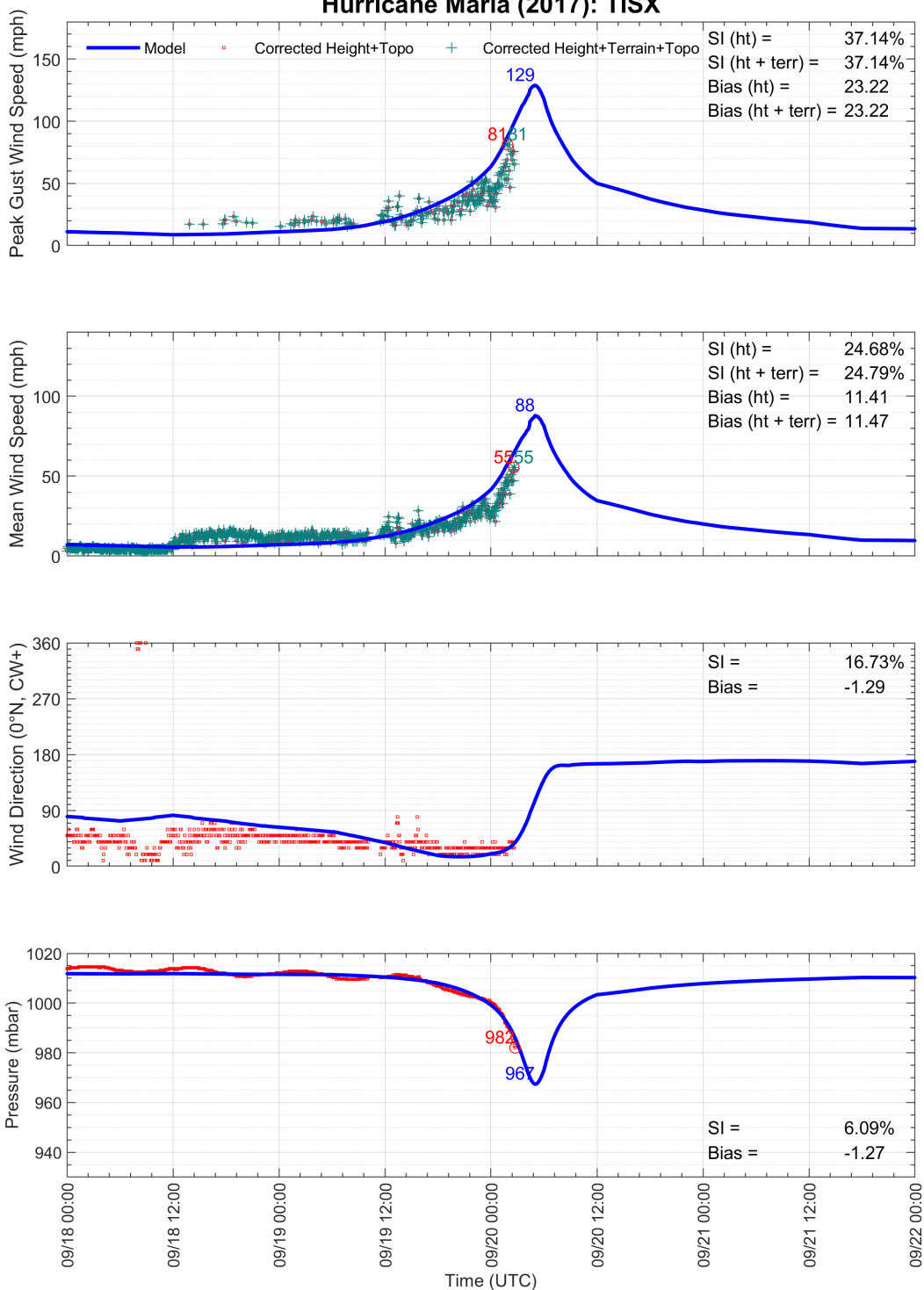
Station	Latitude (°N)	Longitude (°W)	Anemometer Height (m)
TIST	18.337	64.973	7.00
TISX	17.700	64.805	17.00
TJBQ	18.495	67.129	72.00
TJNR	18.255	65.639	10.00
TJSJ	18.433	66.011	3.00
AROP4	18.480	66.702	6.40
CHSV3	17.748	64.699	8.40
ESPP4	18.094	65.471	10.50
FRDP4	18.335	65.631	6.40
IMG4	17.969	67.044	22.36
LTBV3	17.695	64.754	9.70
MGIP4	17.970	67.046	7.50
MGZP4	18.218	67.159	11.50
PTRP4	18.367	67.251	15.00
SJNP4	18.459	66.116	7.00
VQSP4	18.153	65.444	6.40
YABP4	18.055	65.833	6.40
41053	18.474	66.099	4.00
41056	18.260	65.457	4.00
42085	17.860	66.524	4.00

Appendix D.2

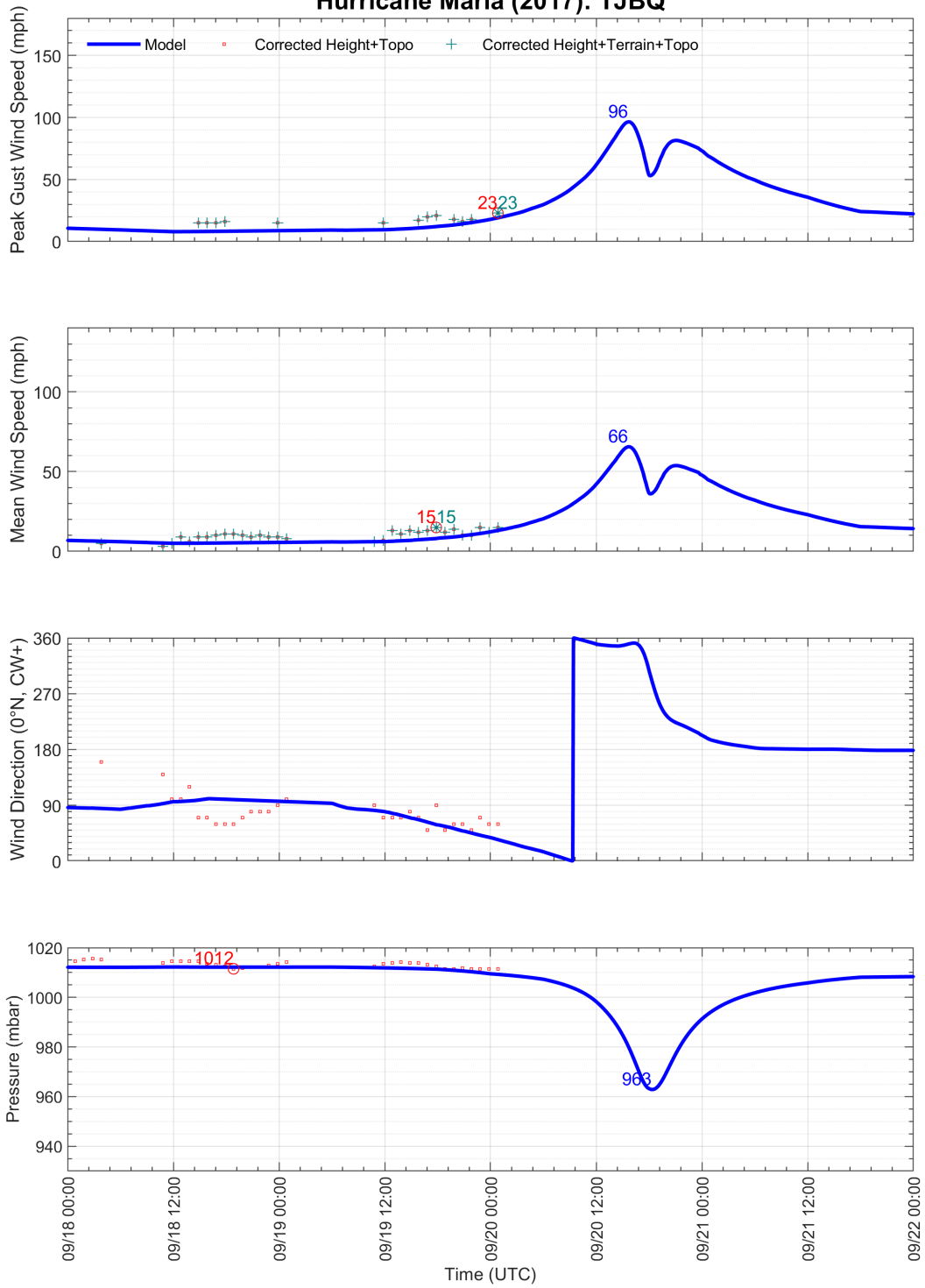
MODELED AND OBSERVED STATION TIME HISTORIES



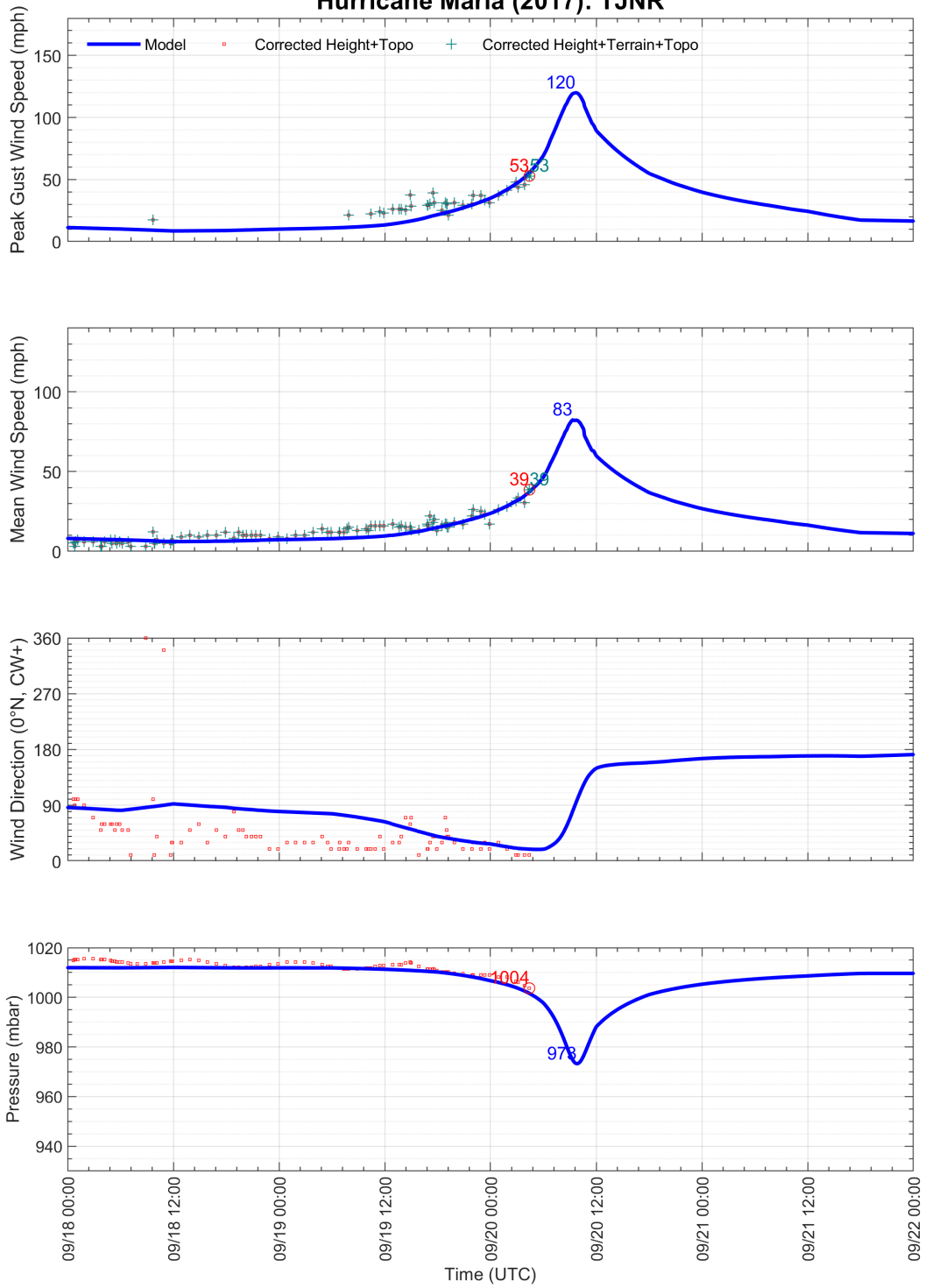
Hurricane Maria (2017): TISX



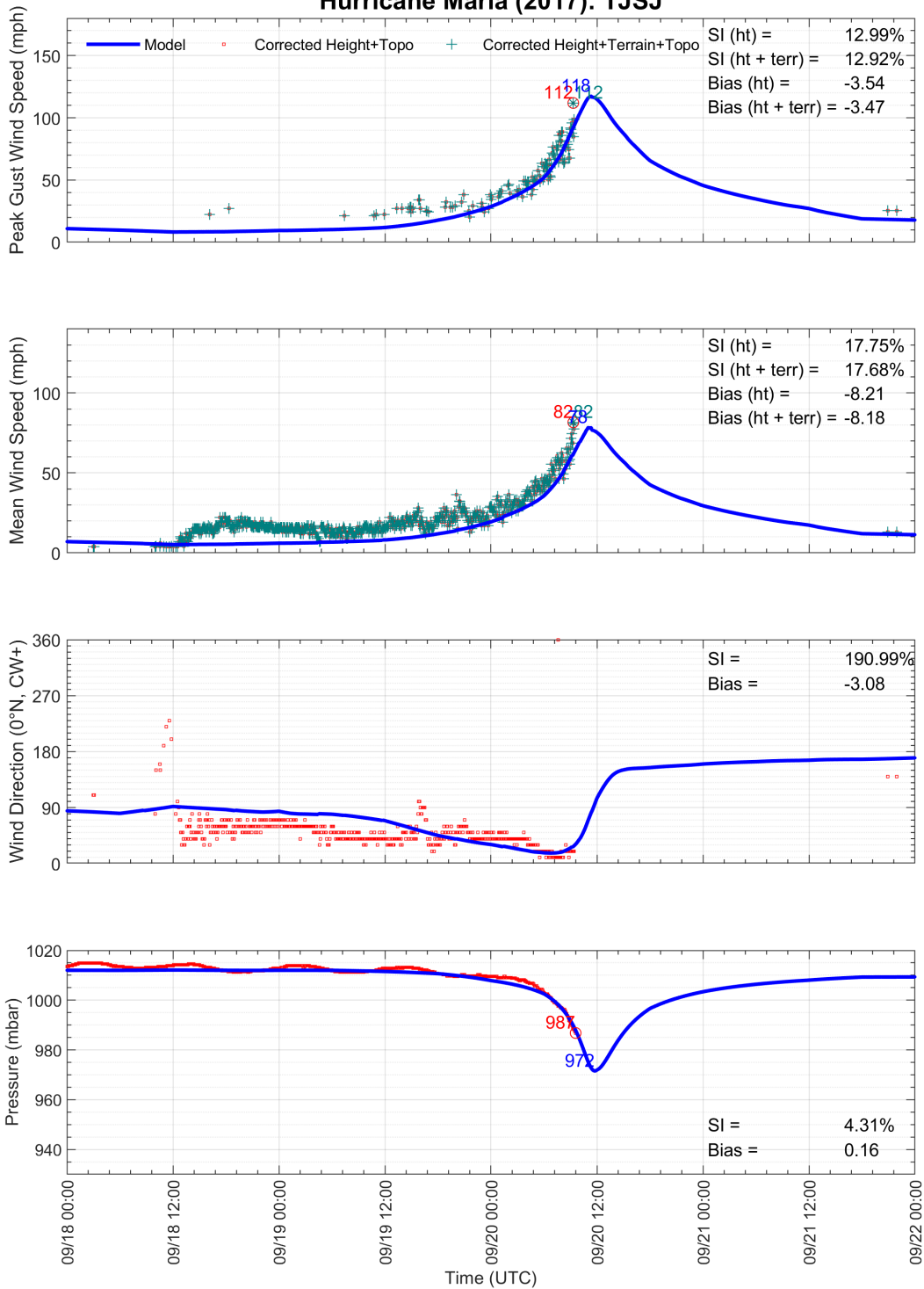
Hurricane Maria (2017): TJBQ



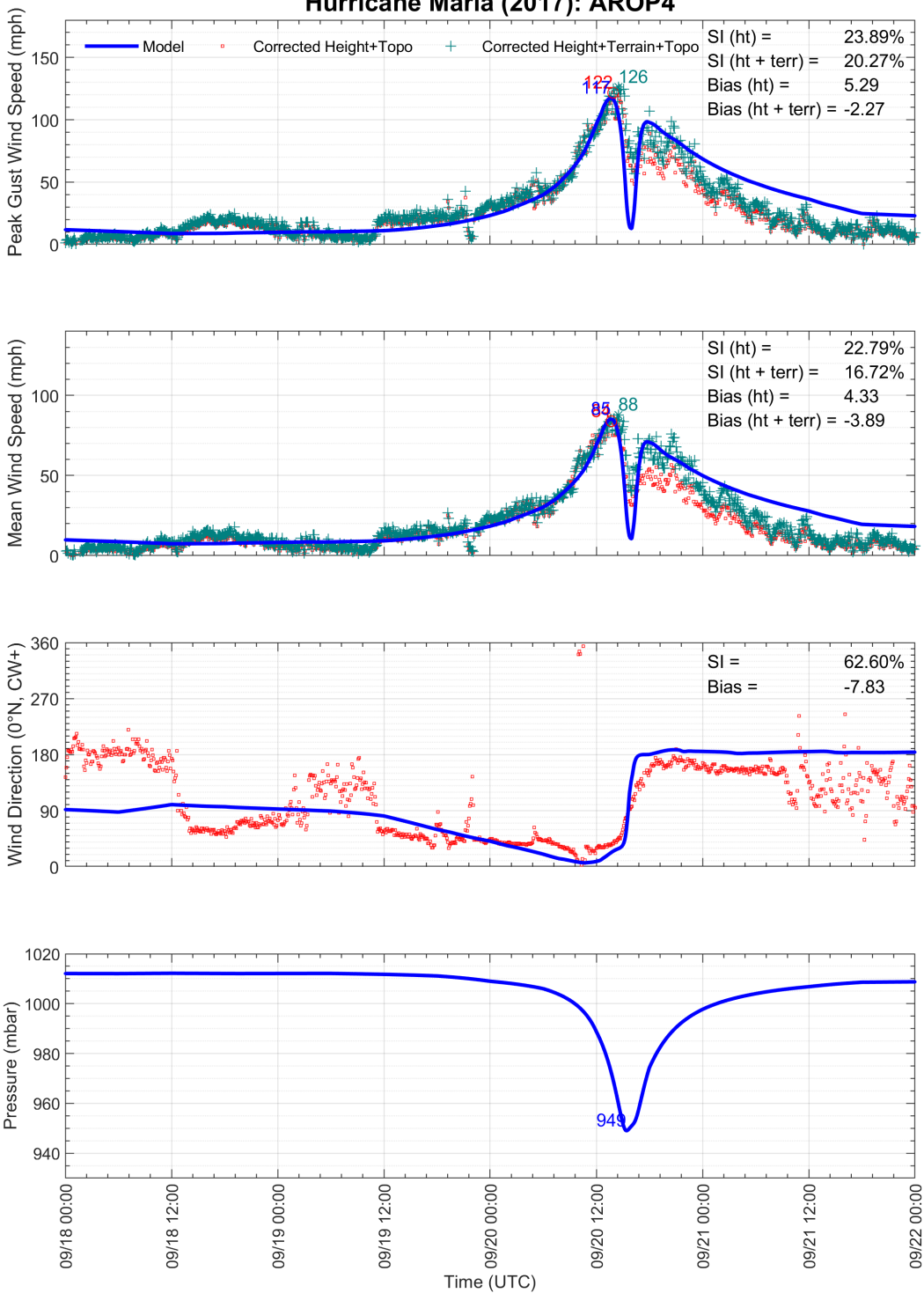
Hurricane Maria (2017): TJNR



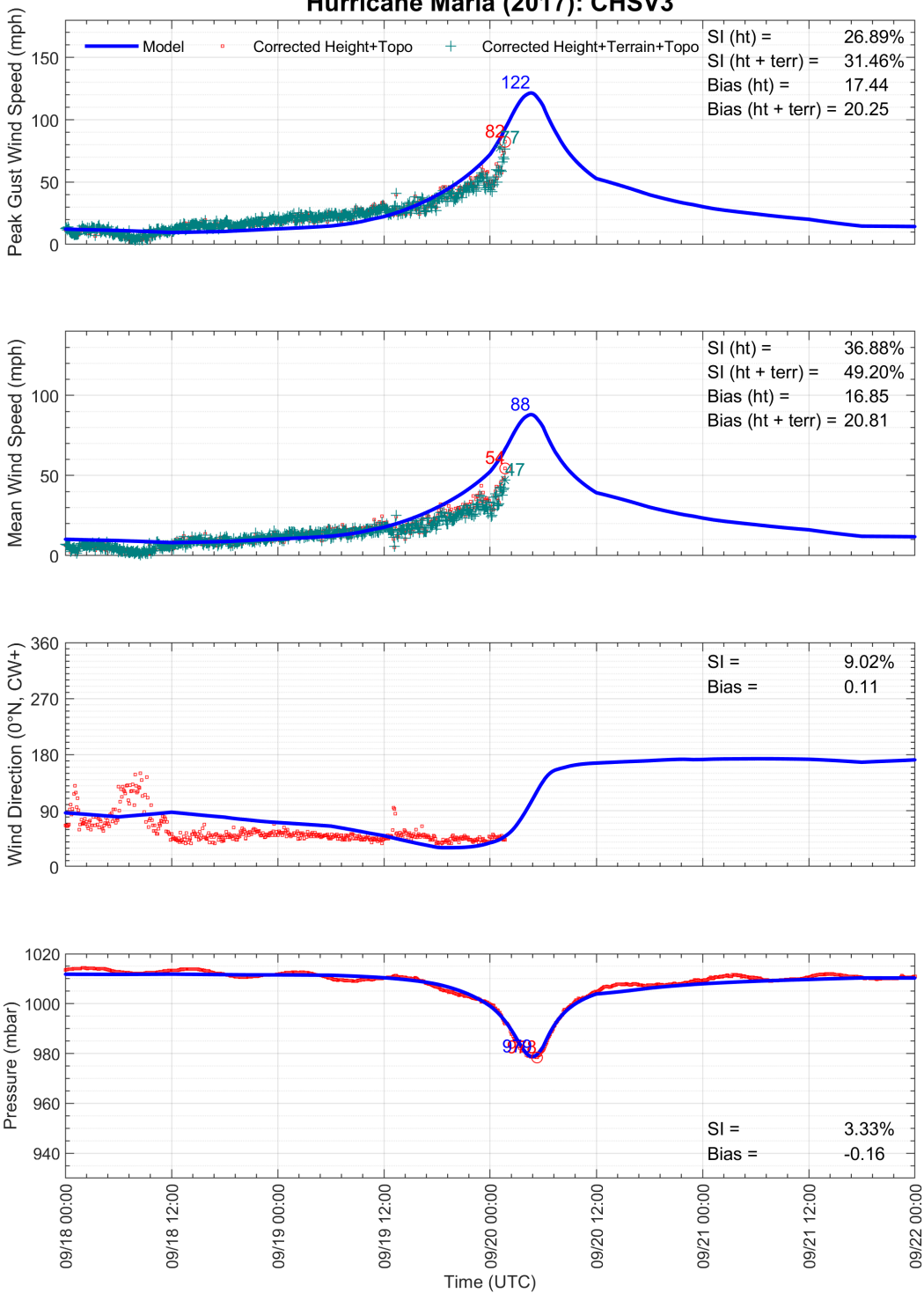
Hurricane Maria (2017): TJSJ

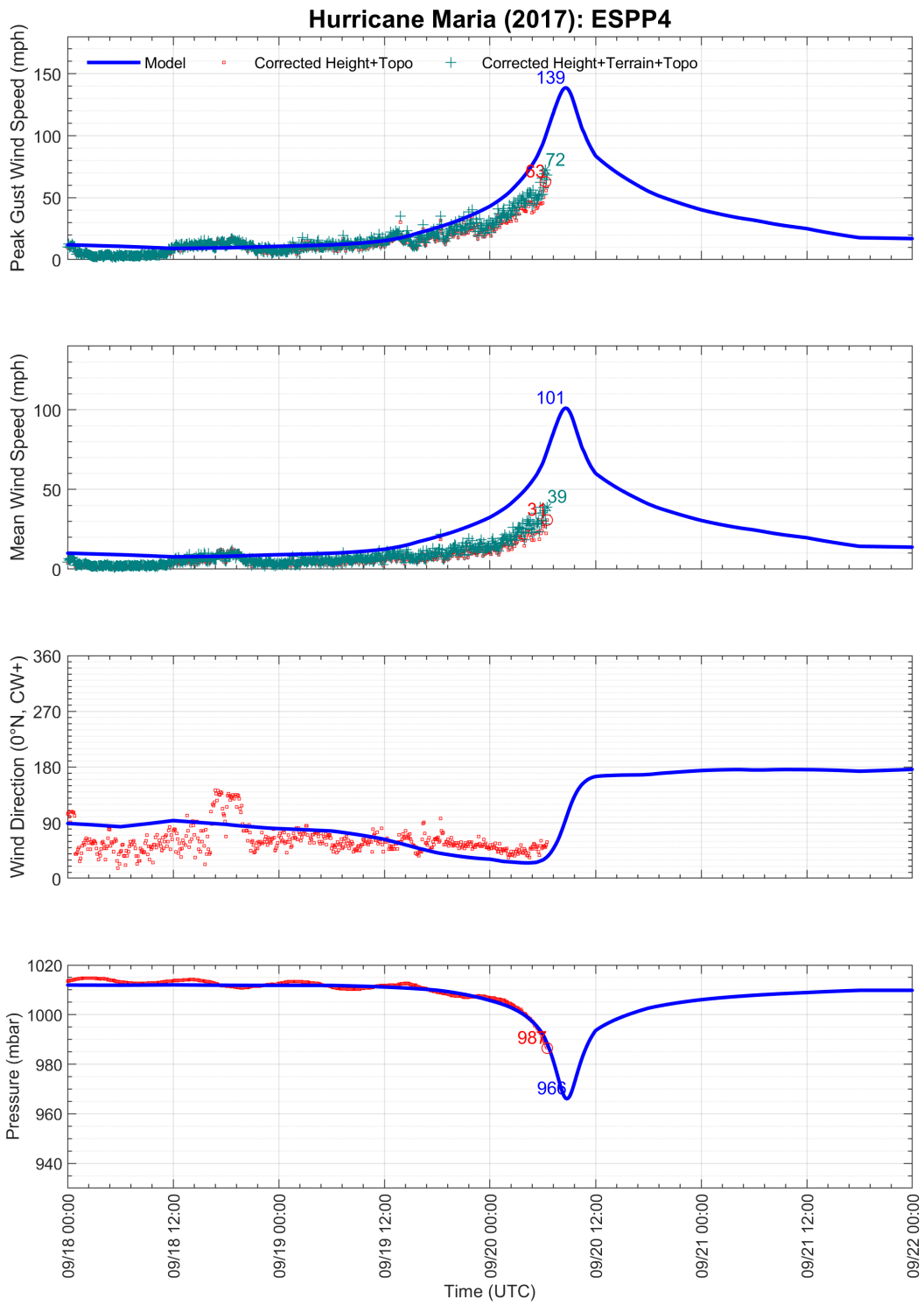


Hurricane Maria (2017): AROP4

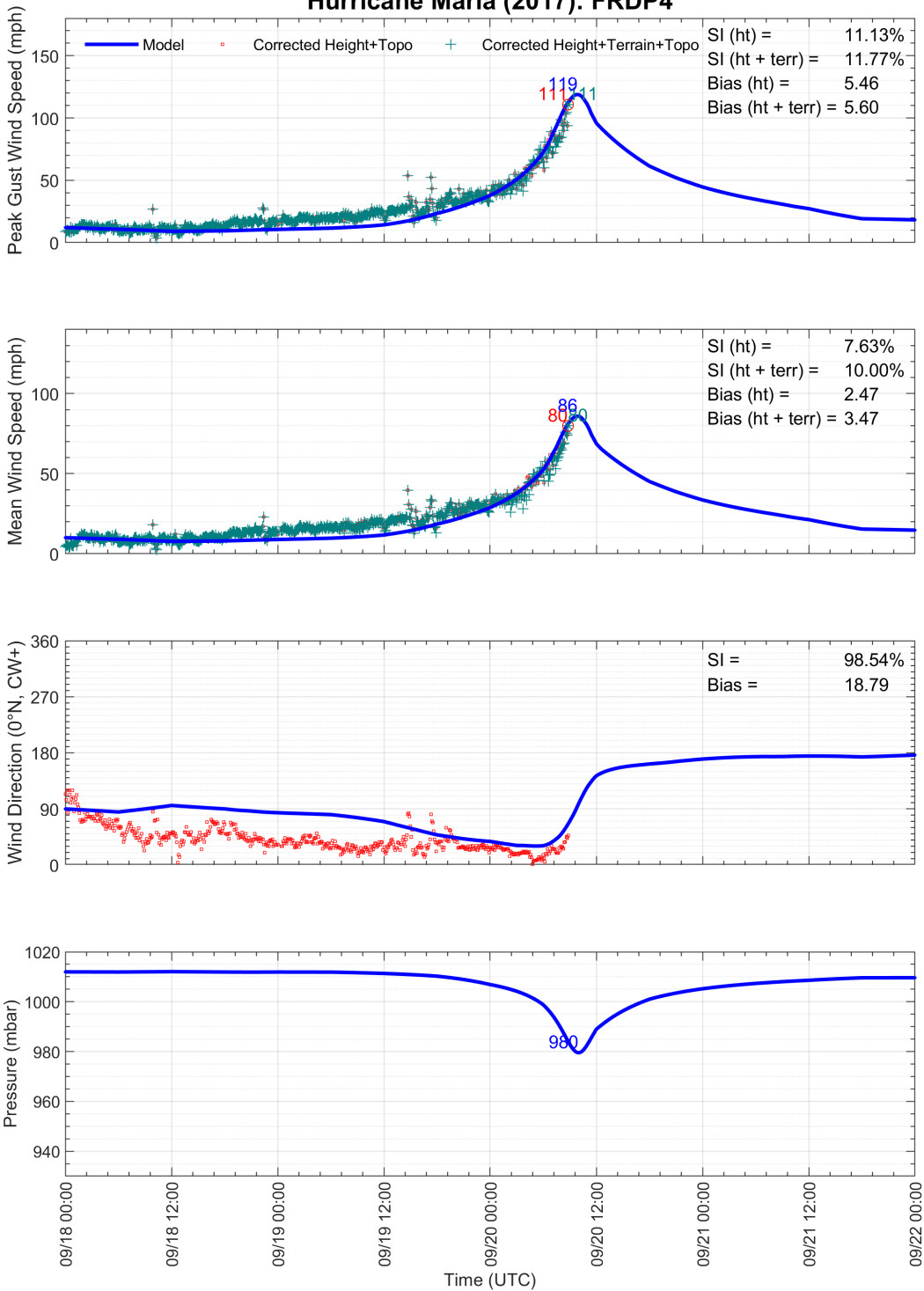


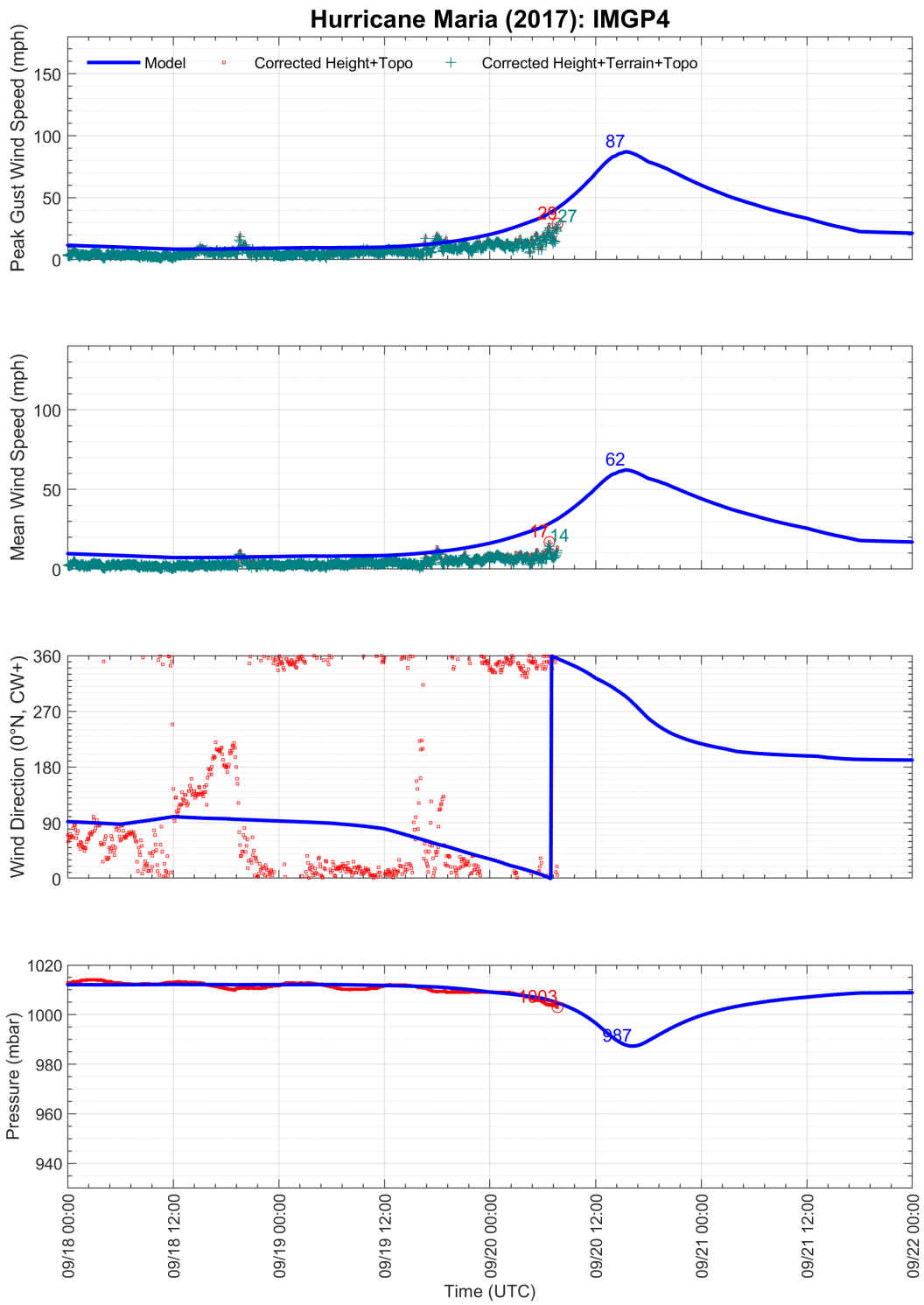
Hurricane Maria (2017): CHSV3



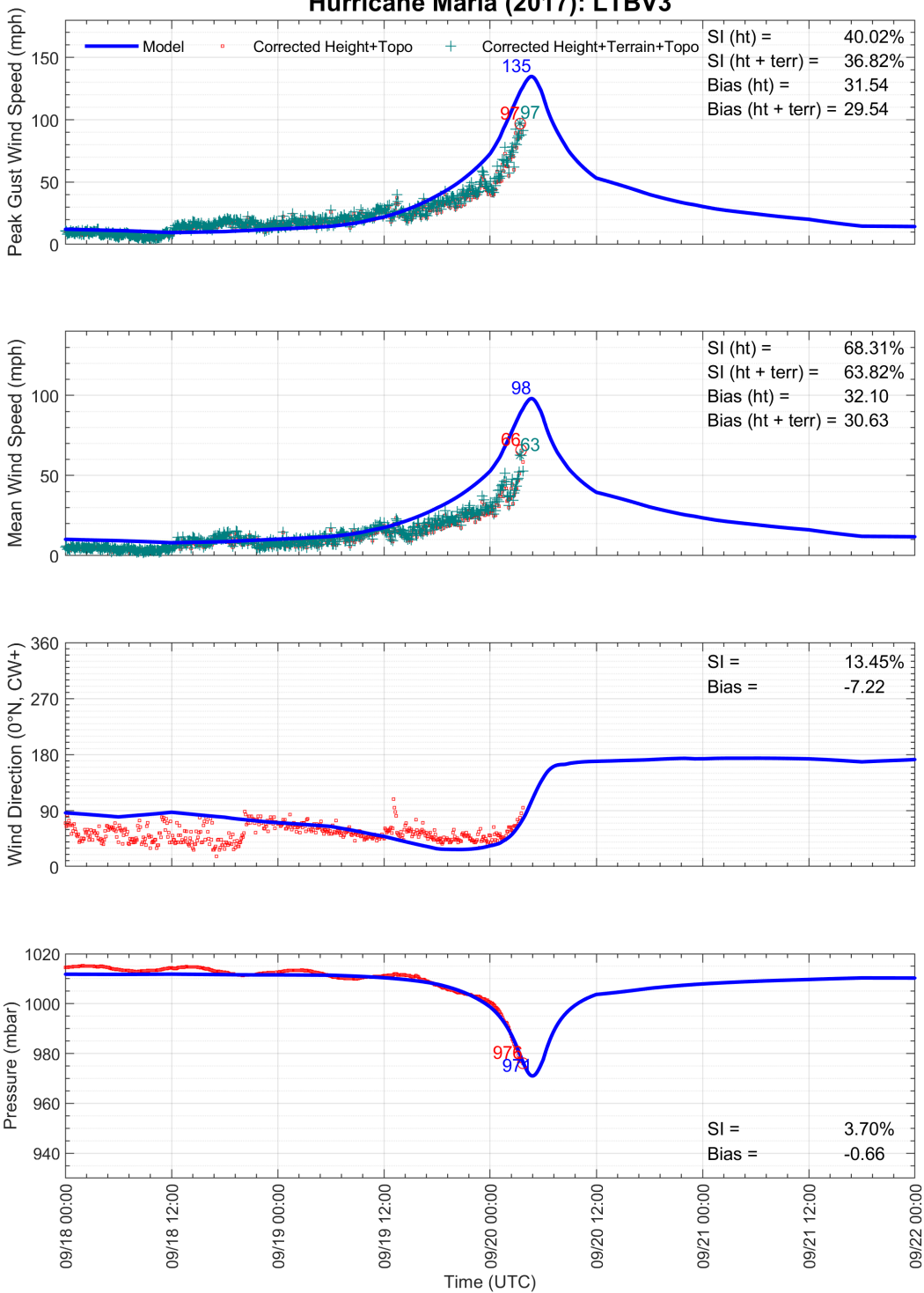


Hurricane Maria (2017): FRDP4

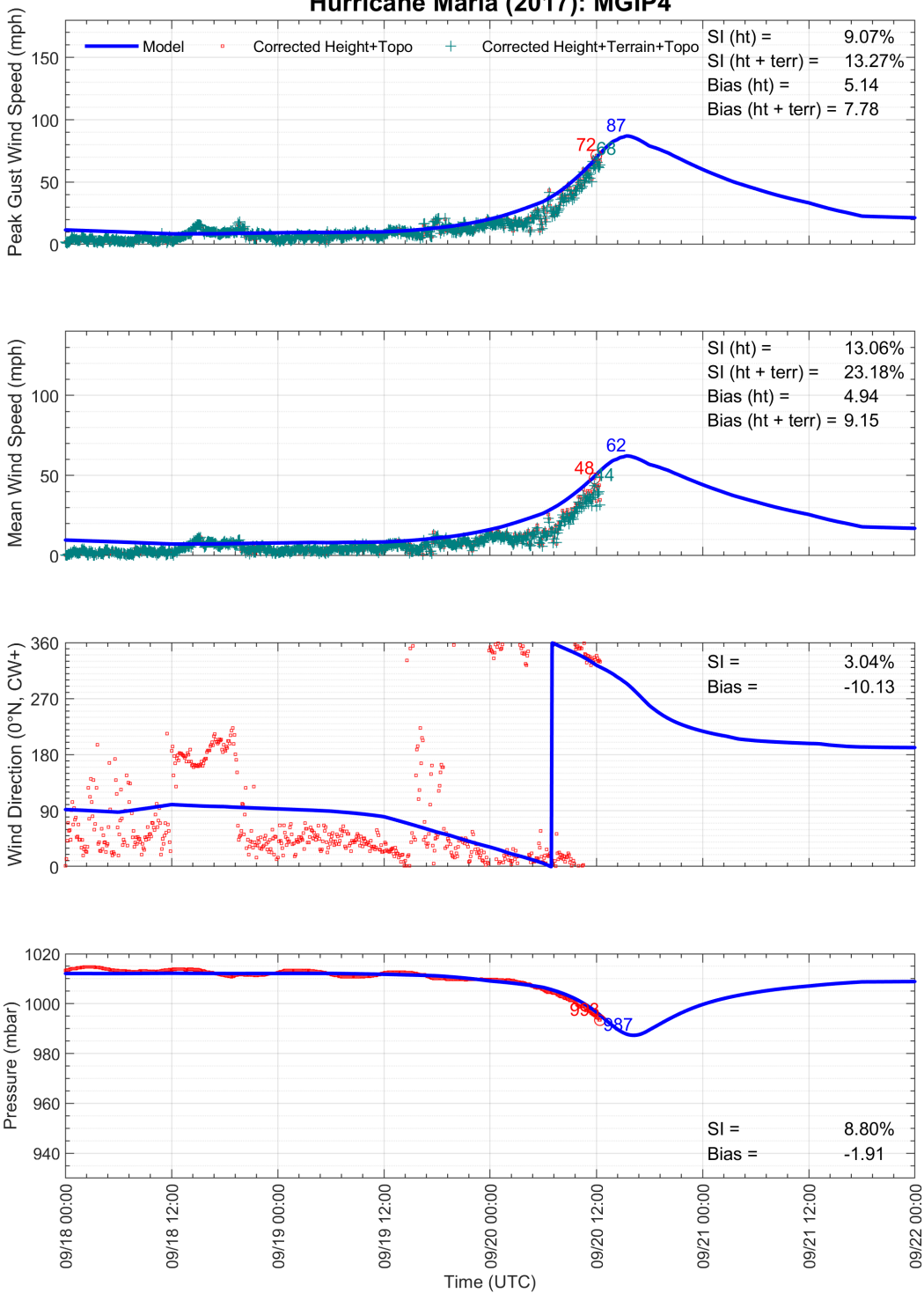




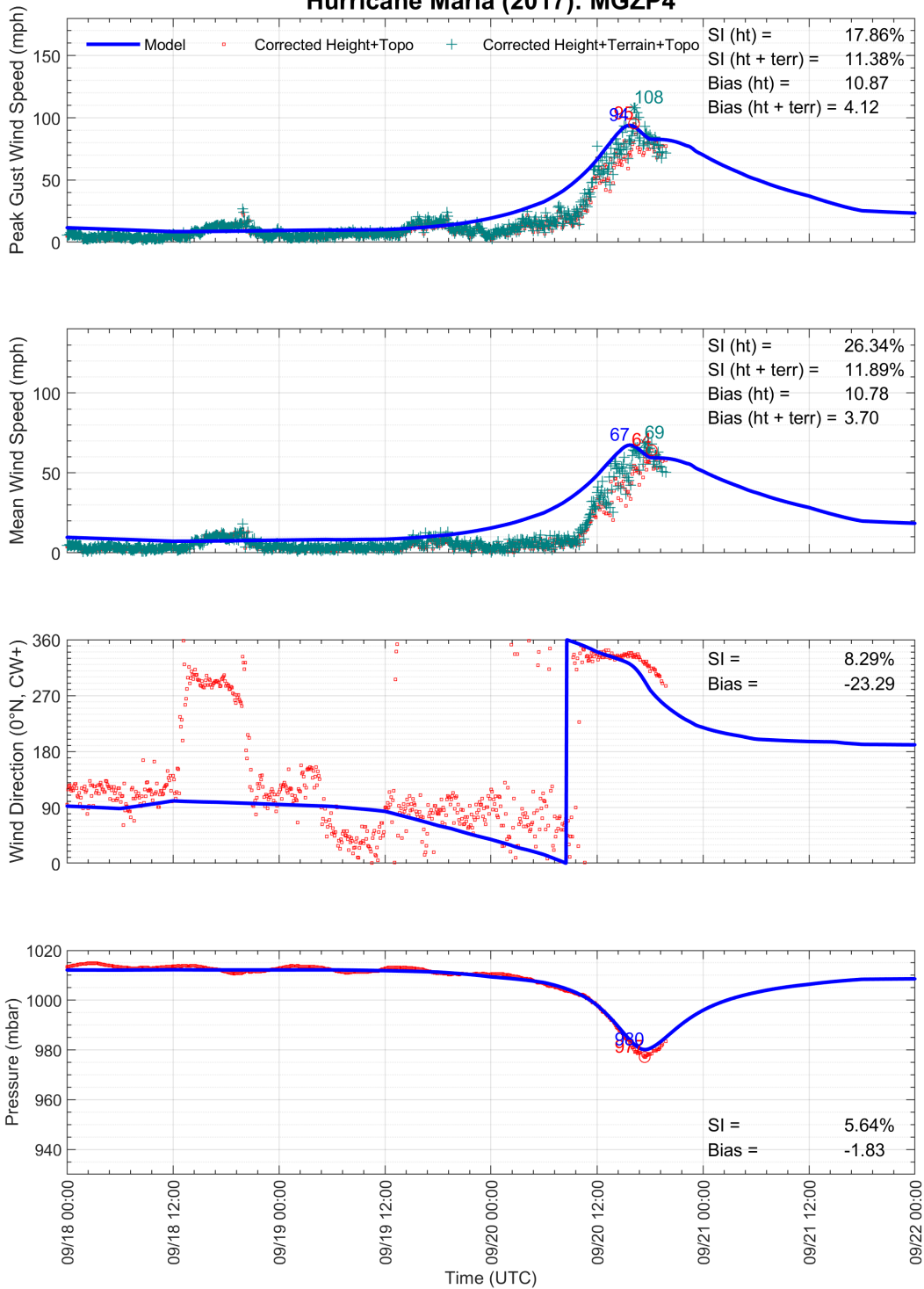
Hurricane Maria (2017): LTBV3

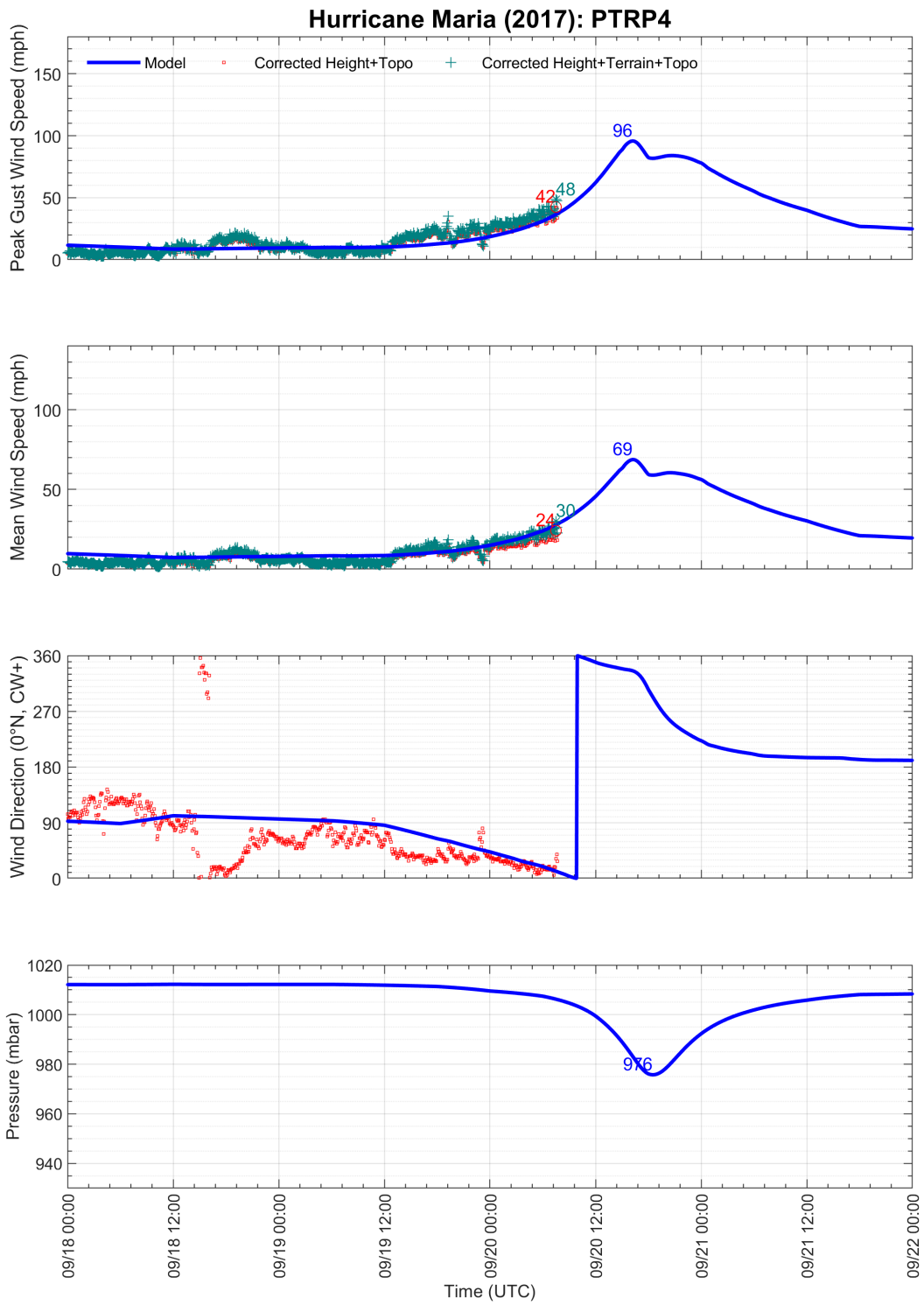


Hurricane Maria (2017): MGIP4

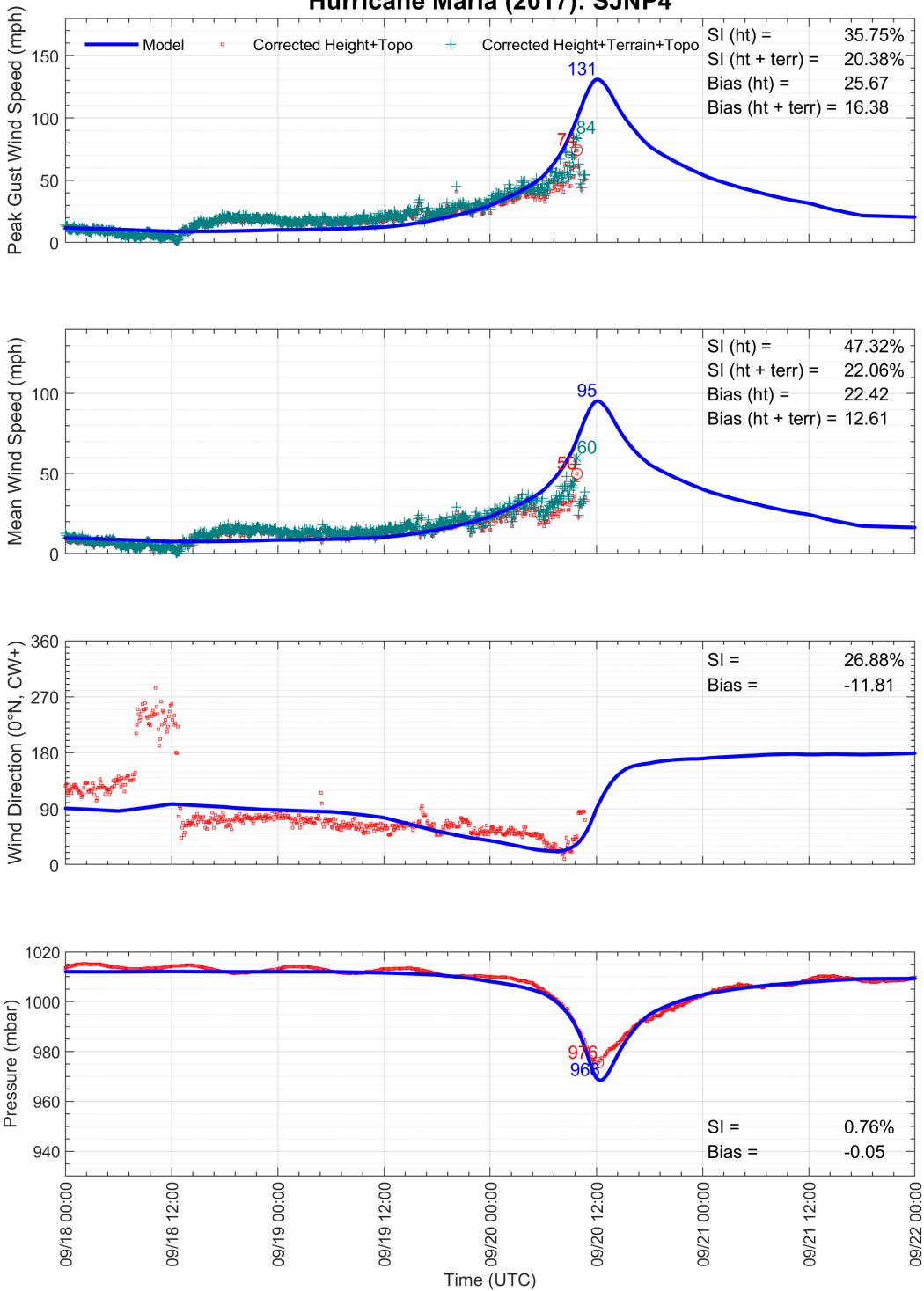


Hurricane Maria (2017): MGZP4

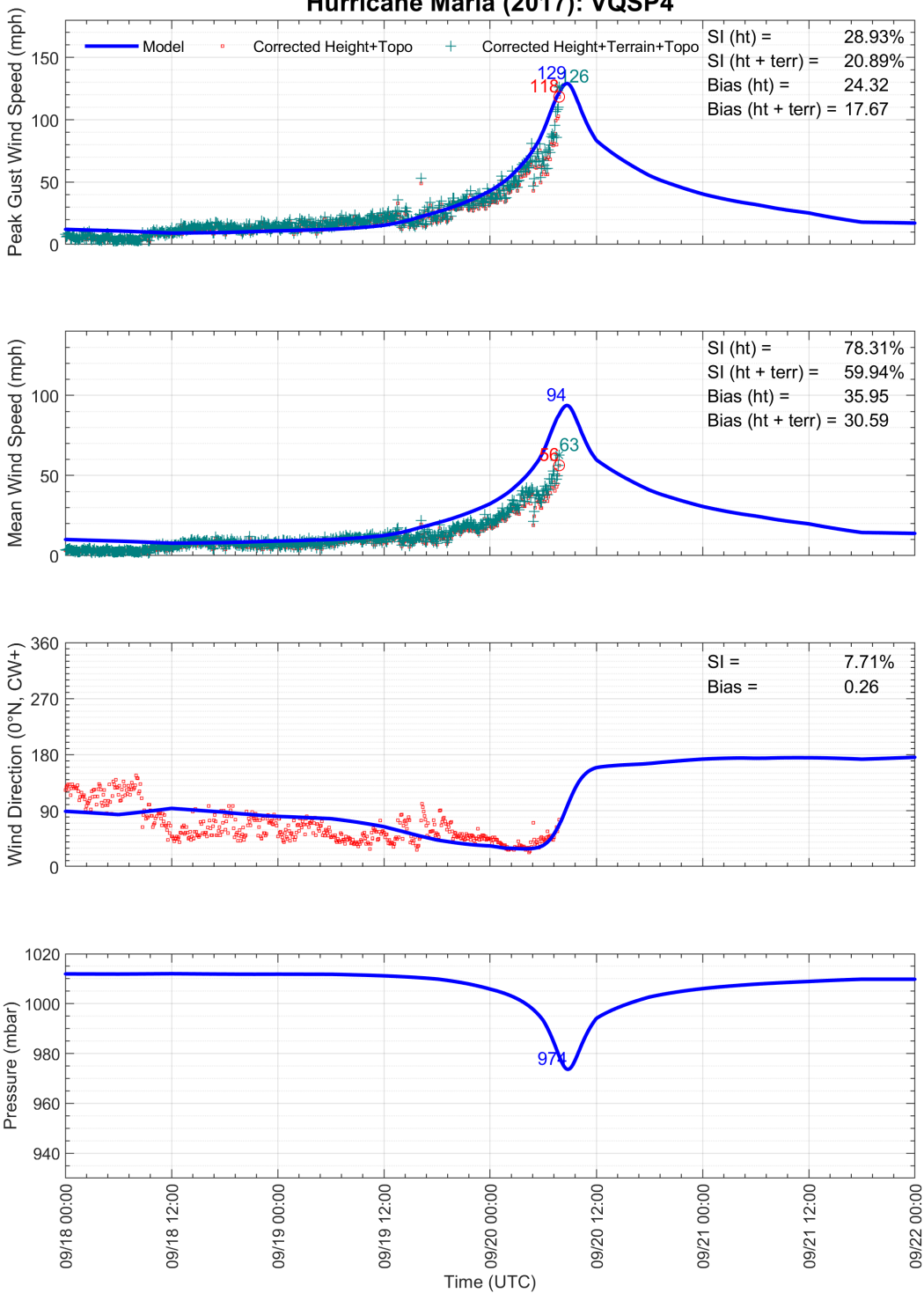


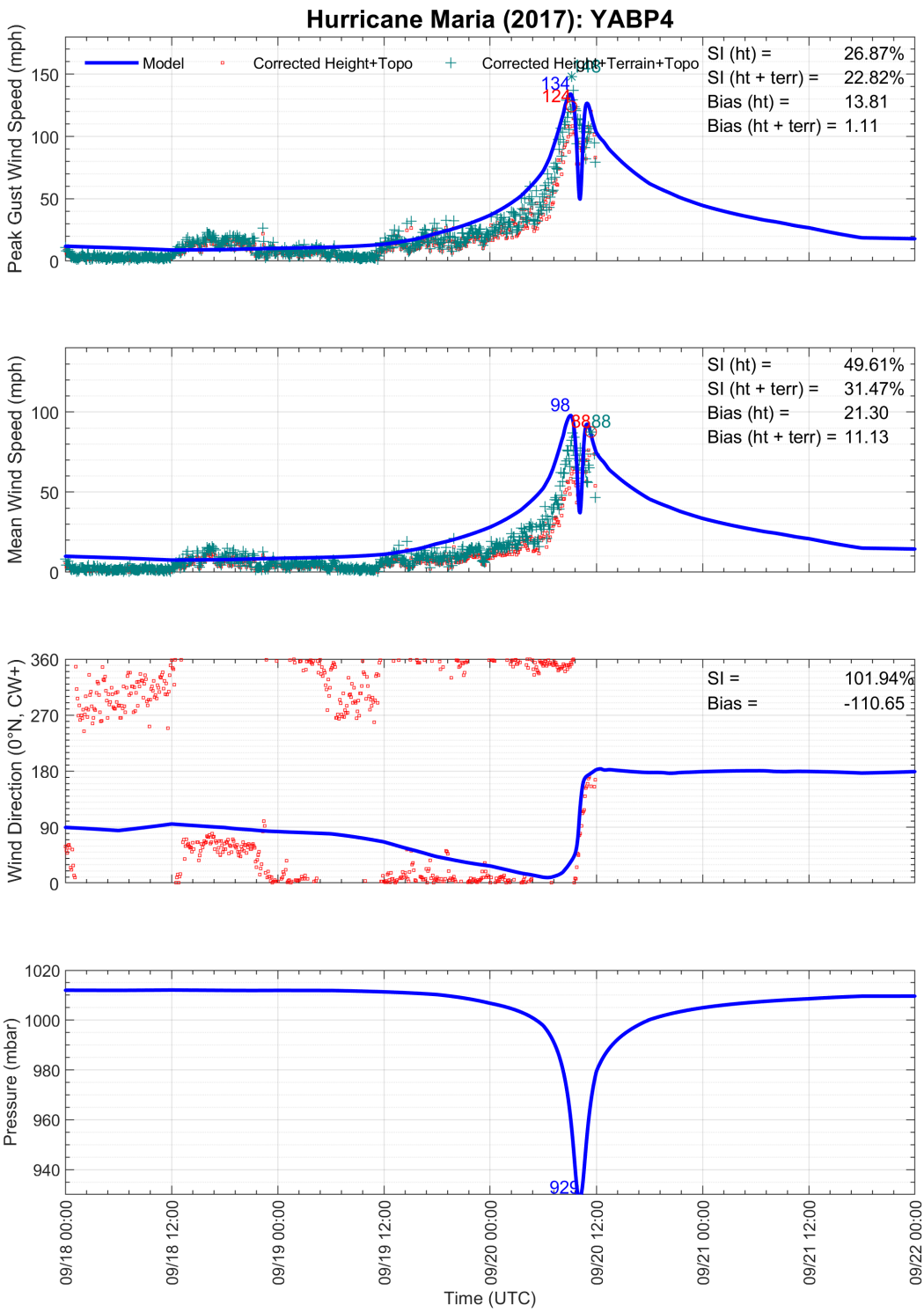


Hurricane Maria (2017): SJNP4



Hurricane Maria (2017): VQSP4





Appendix D.3 STATION DIRECTIONAL SURFACE ROUGHNESS VALUES

Station	Direction (0°N, CW+)															
	0	22.5	45	67.5	90	112.5	135	157.5	180	202.5	225	247.5	270	292.5	315	337.5
TIST	0.0300	0.0300	0.0300	0.0300	0.0300	0.0300	0.0030	0.0030	0.0030	0.0030	0.0030	0.0030	0.0030	0.0030	0.0030	0.0300
TISX	0.0300	0.0300	0.0300	0.0300	0.0300	0.0300	0.0300	0.0300	0.0300	0.0300	0.0300	0.0300	0.0300	0.0300	0.0300	0.0300
TJBQ	0.0300	0.0300	0.0300	0.0300	0.0300	0.0300	0.0300	0.0300	0.0300	0.0300	0.0300	0.0300	0.0300	0.0300	0.0300	0.0300
TJNR	0.0300	0.0300	0.0300	0.0300	0.0300	0.0300	0.0300	0.0300	0.0300	0.0300	0.0300	0.0300	0.0300	0.0300	0.0300	0.0300
TJSJ	0.0300	0.0300	0.0300	0.0300	0.0300	0.0300	0.0300	0.0300	0.0300	0.0300	0.0300	0.0300	0.0300	0.0300	0.0300	0.0300
AROP4	0.0000	0.0000	0.0500	0.5000	0.5000	0.5000	0.9000	0.9000	0.9000	0.9000	0.9000	0.5000	0.3000	0.0000	0.0000	0.0000
CHSV3	0.0000	0.0000	0.0050	0.1000	0.1000	0.1000	0.1000	0.1000	0.1000	0.1000	0.8000	0.8000	0.8000	0.0500	0.0000	0.0000
ESPP4	0.7000	0.7000	0.7000	0.7000	0.5000	0.0500	0.0050	0.0000	0.0000	0.0050	0.0000	0.0000	0.0000	0.5000	0.6000	0.7000
FRDP4	0.0500	0.0000	0.0000	0.0000	0.0000	0.0000	0.3000	0.5000	0.8000	0.8000	0.8000	0.8000	0.8000	0.8000	0.8000	0.1500
IMGP4	0.0100	0.0100	0.0100	0.0100	0.0100	0.0100	0.0100	0.0100	0.0100	0.0100	0.0100	0.0100	0.0100	0.0100	0.0100	0.0100
LTBV3	0.3000	0.1500	0.1500	0.0500	0.0100	0.0100	0.0050	0.0000	0.0000	0.0000	0.0000	0.0000	0.0050	0.1500	0.3000	0.3000
MGIP4	0.0080	0.0080	0.1000	0.1000	0.1000	0.1000	0.0500	0.0000	0.0000	0.0000	0.0000	0.0000	0.0000	0.0050	0.0080	0.0080
MGZP4	0.7000	0.7000	0.7000	0.7000	0.7000	0.7000	0.7000	0.1000	0.0000	0.0000	0.0000	0.0000	0.0000	0.0100	0.1000	0.7000
PTRP4	0.8000	0.8000	0.8000	0.8000	0.8000	0.8000	0.8000	0.8000	0.8000	0.8000	0.8000	0.8000	0.8000	0.8000	0.8000	0.8000
SJNP4	0.9000	0.7000	0.3000	0.1000	0.0100	0.5000	0.5000	0.8000	0.8000	0.7000	0.6000	0.5000	0.0100	0.0100	0.5000	0.9000
VQSP4	0.0100	0.0500	0.1000	0.1000	0.1000	0.1000	0.1000	0.1000	0.0000	0.0000	0.0000	0.0000	0.0000	0.0000	0.0000	0.0000
YABP4	0.9000	0.9000	0.9000	0.9000	0.0000	0.0000	0.0000	0.0000	0.0100	0.9000	0.9000	0.9000	0.9000	0.9000	0.9000	0.9000
41053	0.0000	0.0000	0.0000	0.0000	0.0000	0.0000	0.5000	0.8000	0.8000	0.7000	0.6000	0.5000	0.0000	0.0000	0.0000	0.0000
41056	0.0000	0.0000	0.0000	0.0000	0.0000	0.0000	0.0000	0.0000	0.0000	0.0000	0.0000	0.0000	0.0000	0.0000	0.0000	0.0000
42085	0.0000	0.0000	0.0000	0.0000	0.0000	0.0000	0.0000	0.0000	0.0000	0.0000	0.0000	0.0000	0.0000	0.0000	0.0000	0.0000



Figure D-1. Aerial image of NDBC station AROP4: Arcibo, PR.

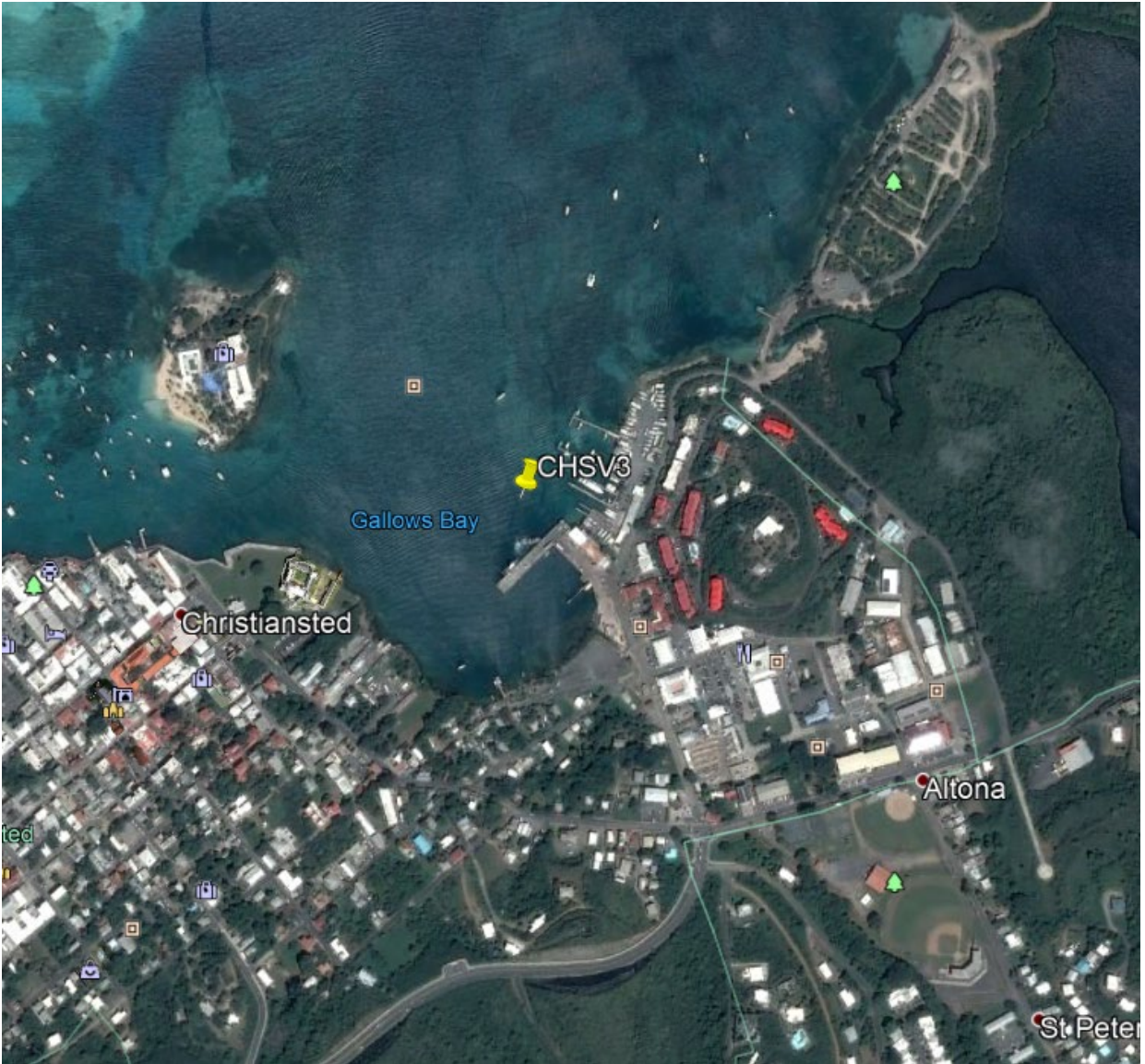


Figure D-2. Aerial image of NDBC station CHSV3: Christiansted Harbor, St, Croix, VI.



Figure D-3. Aerial image of NDBC station ESPP4: Esperanza, Vieques Island, PR.



Figure D-4. Aerial image of NDBC station FRDP4: Fajardo, PR.

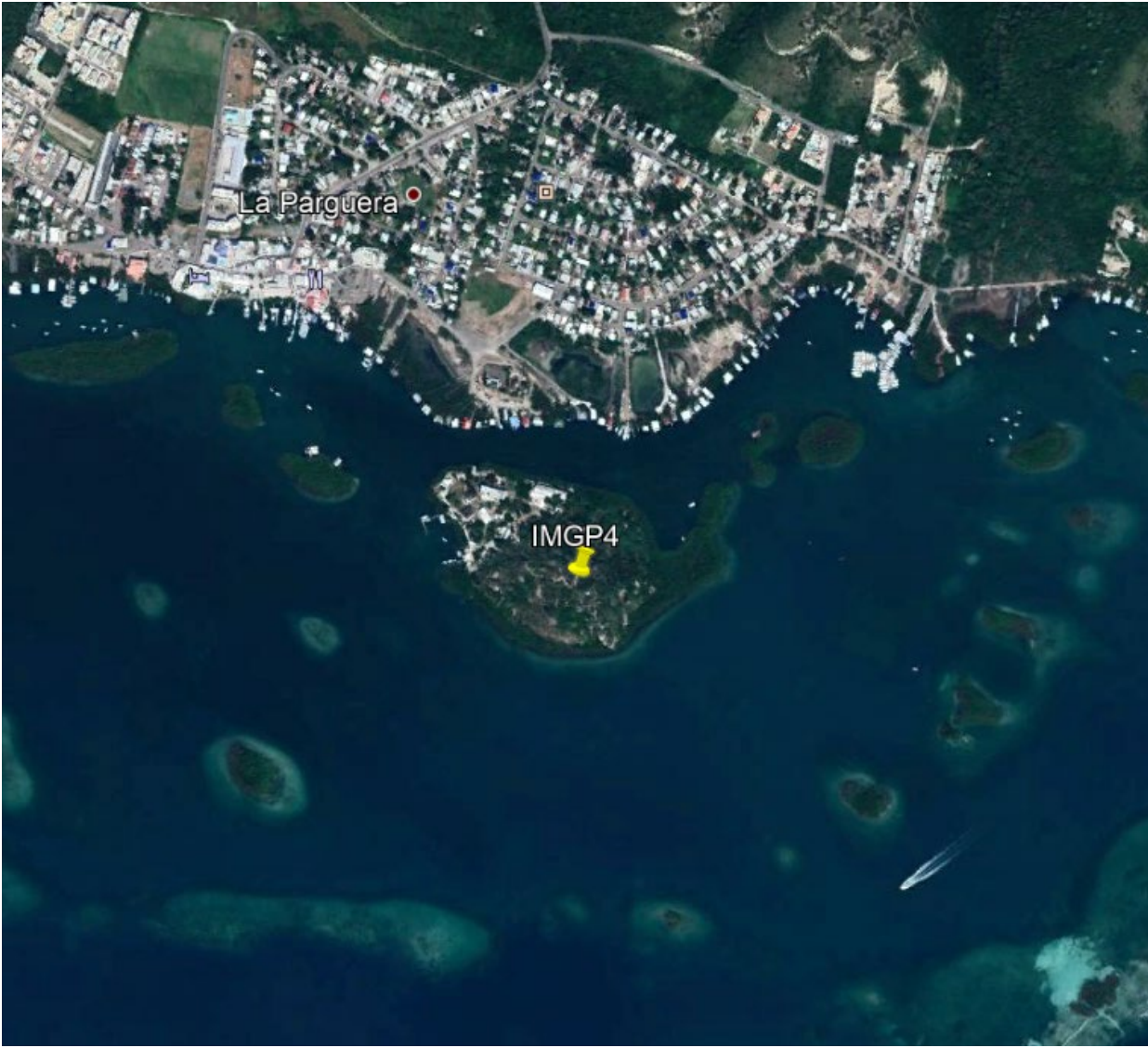


Figure D-5. Aerial image of NDBC station IMGP4: Isla Magueyes, Lajas, PR.

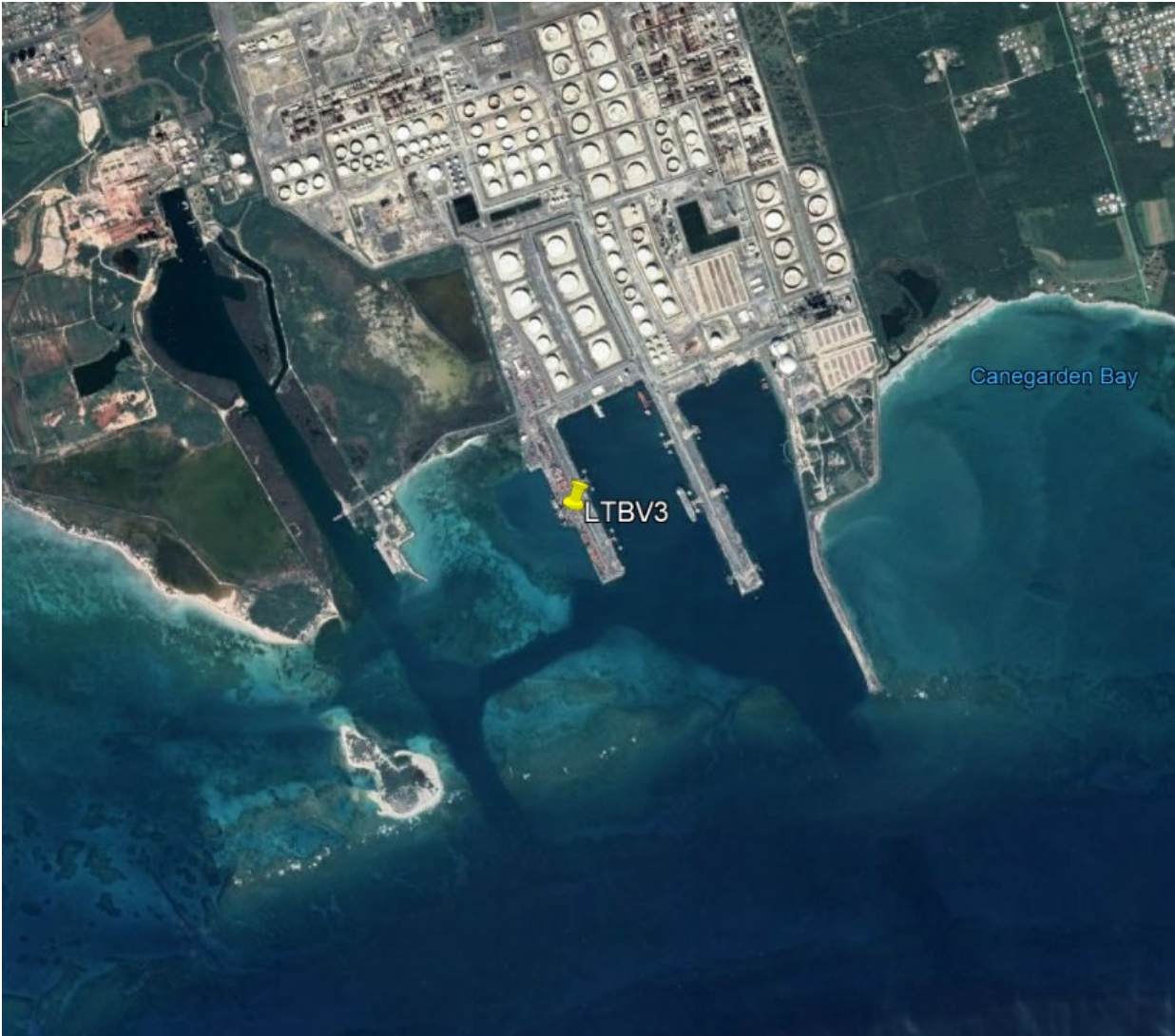


Figure D-6. Aerial image of NDBC station LTBV3: Lime Tree Bay, St. Croix, VI.

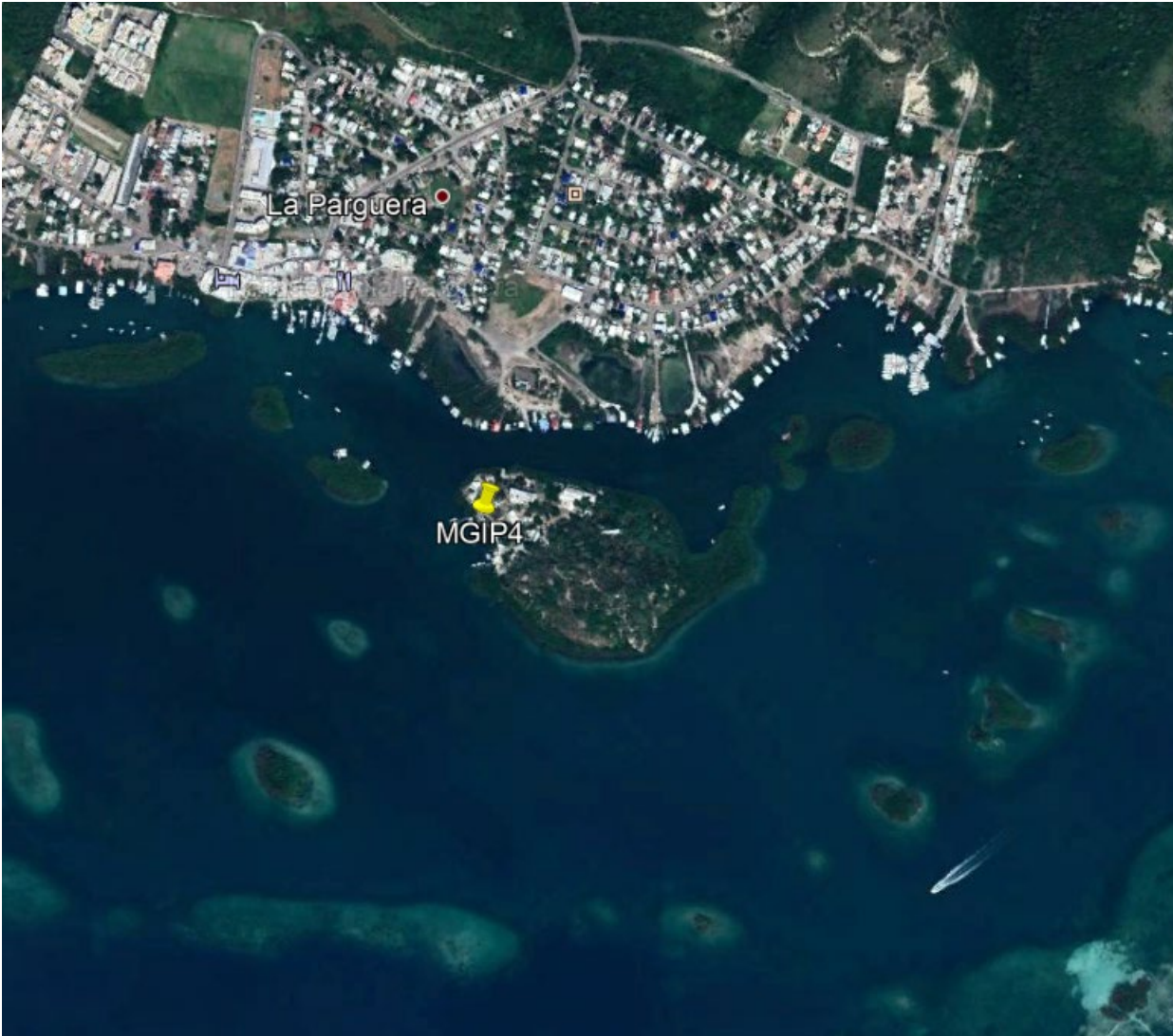


Figure D-7. Aerial image of NDBC station MGIP4: Magueyes Islands, PR.



Figure D-8. Aerial image of NDBC station MGZP4: Mayaguez, PR.



Figure D-9. Aerial image of NDBC station PTRP4: Puntas Rincon, PR.

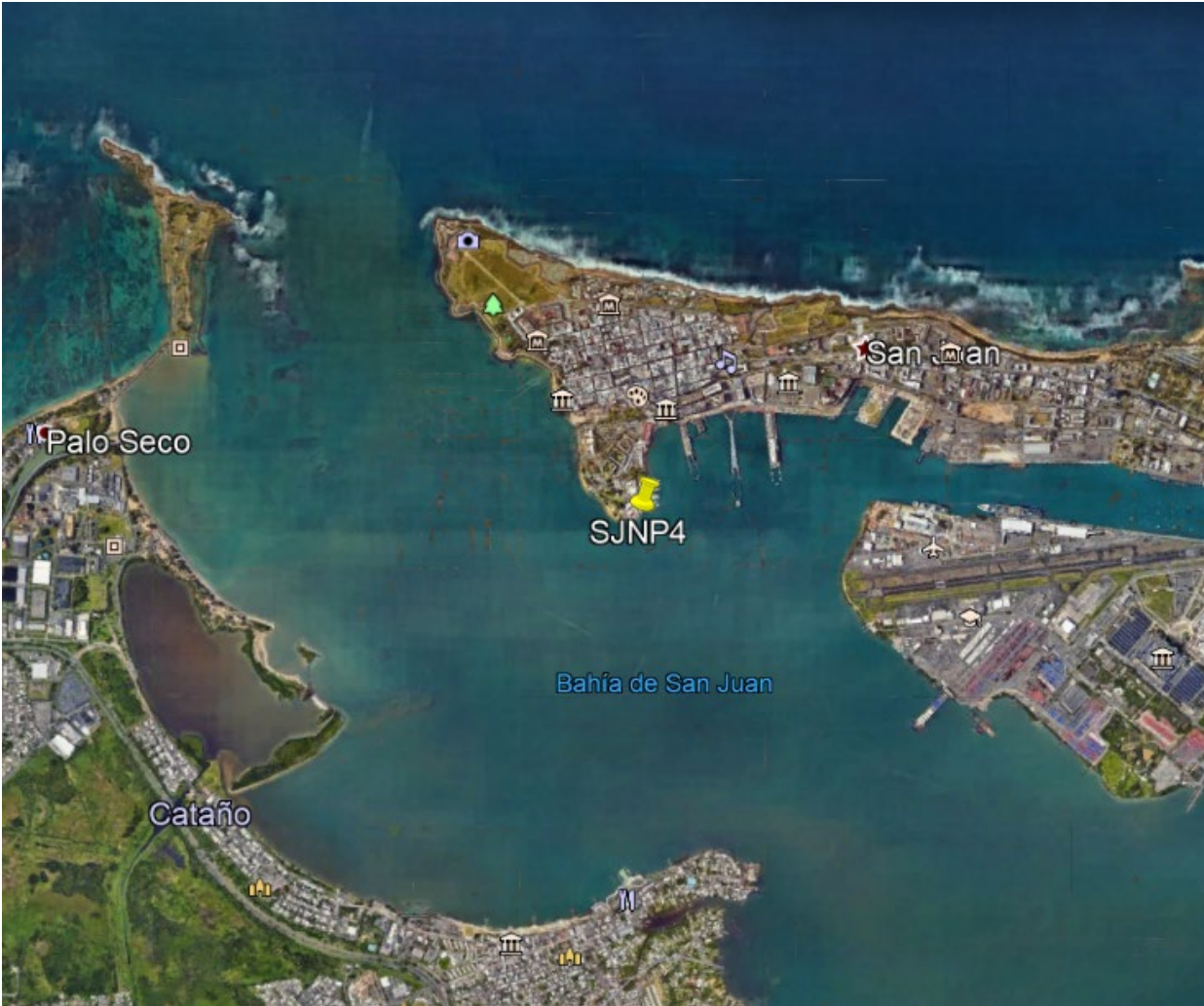


Figure D-10. Aerial image of NDBC station SJNP4: San Juan, La Puntilla, San Juan Bay, PR.



Figure D-11. Aerial image of NDBC station VQSP4: Isabel Segunda, Vieques Island, PR.



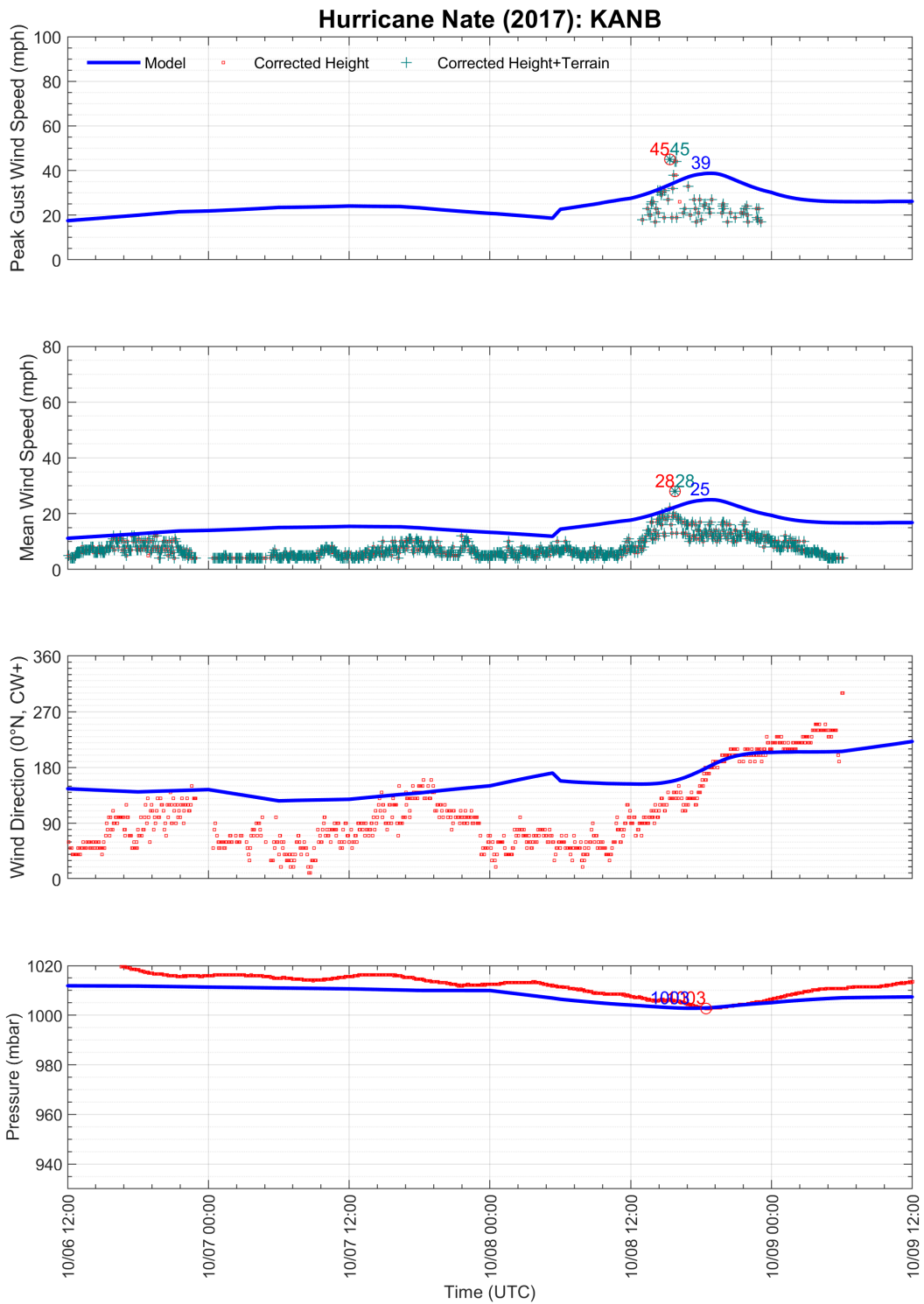
Figure D-12. Aerial image of NDBC station YABP4: Yabucoa Harbor, PR.

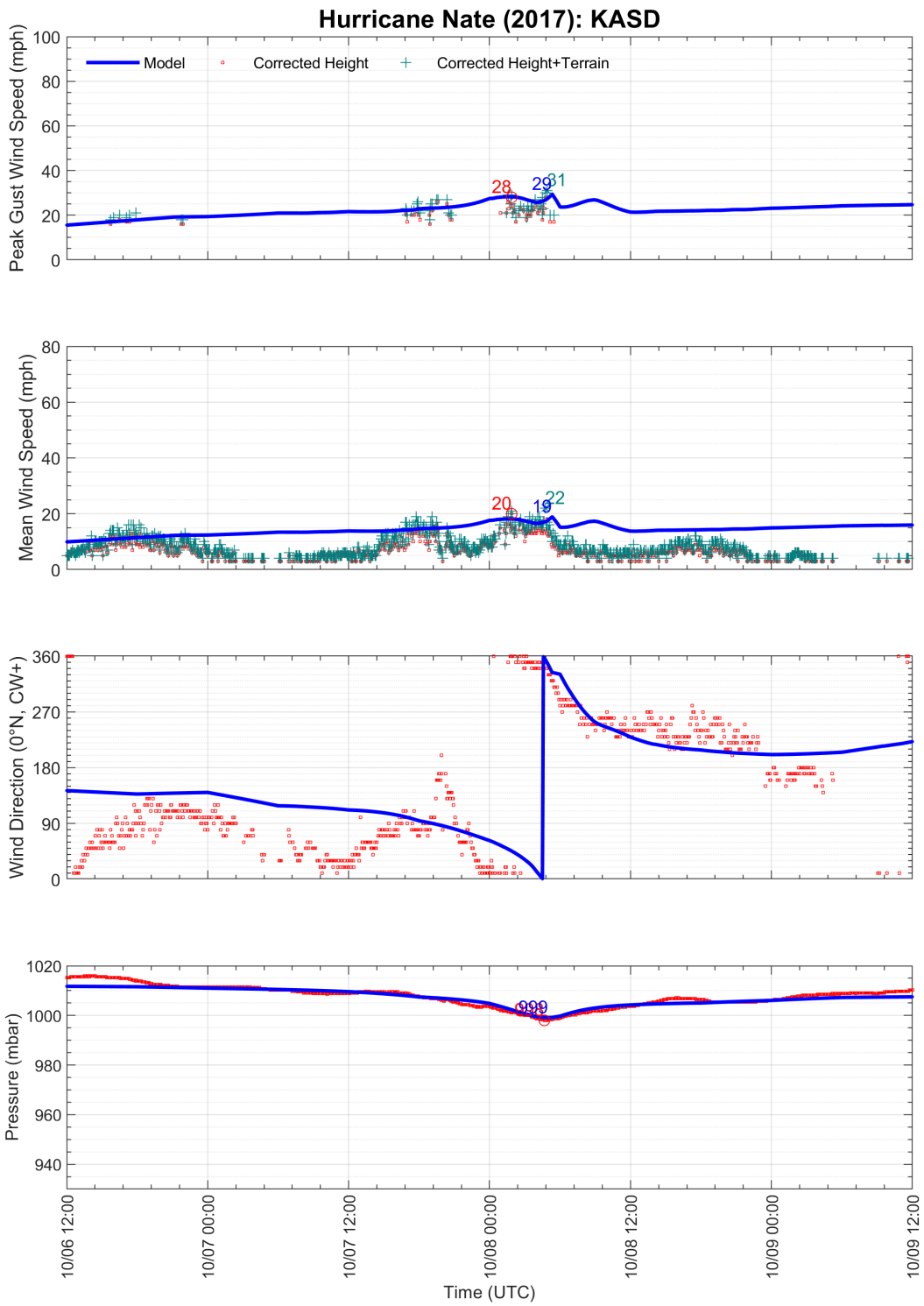
Appendix E. HURRICANE NATE

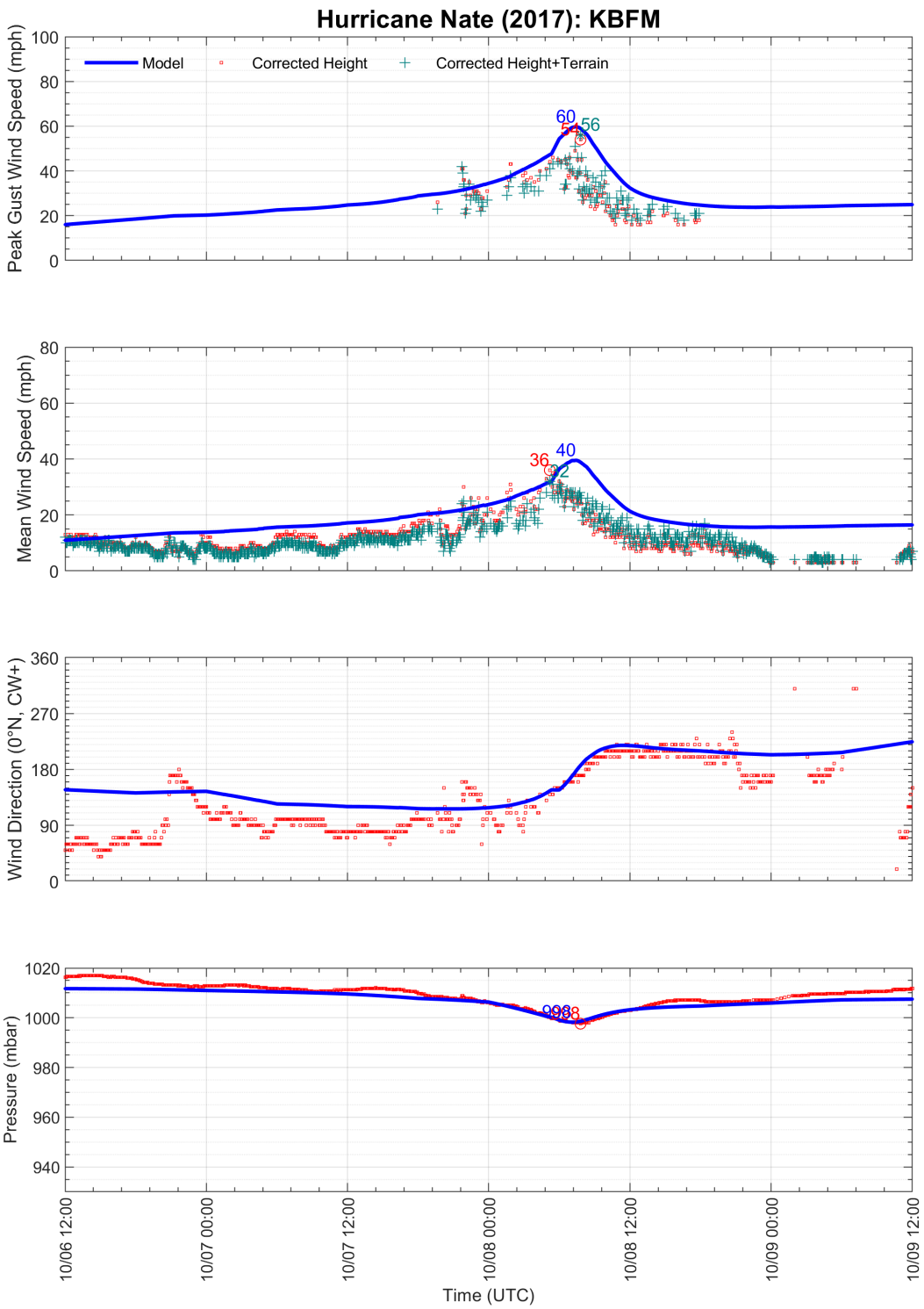
Appendix E.1 SURFACE OBSERVATION STATION DETAILS

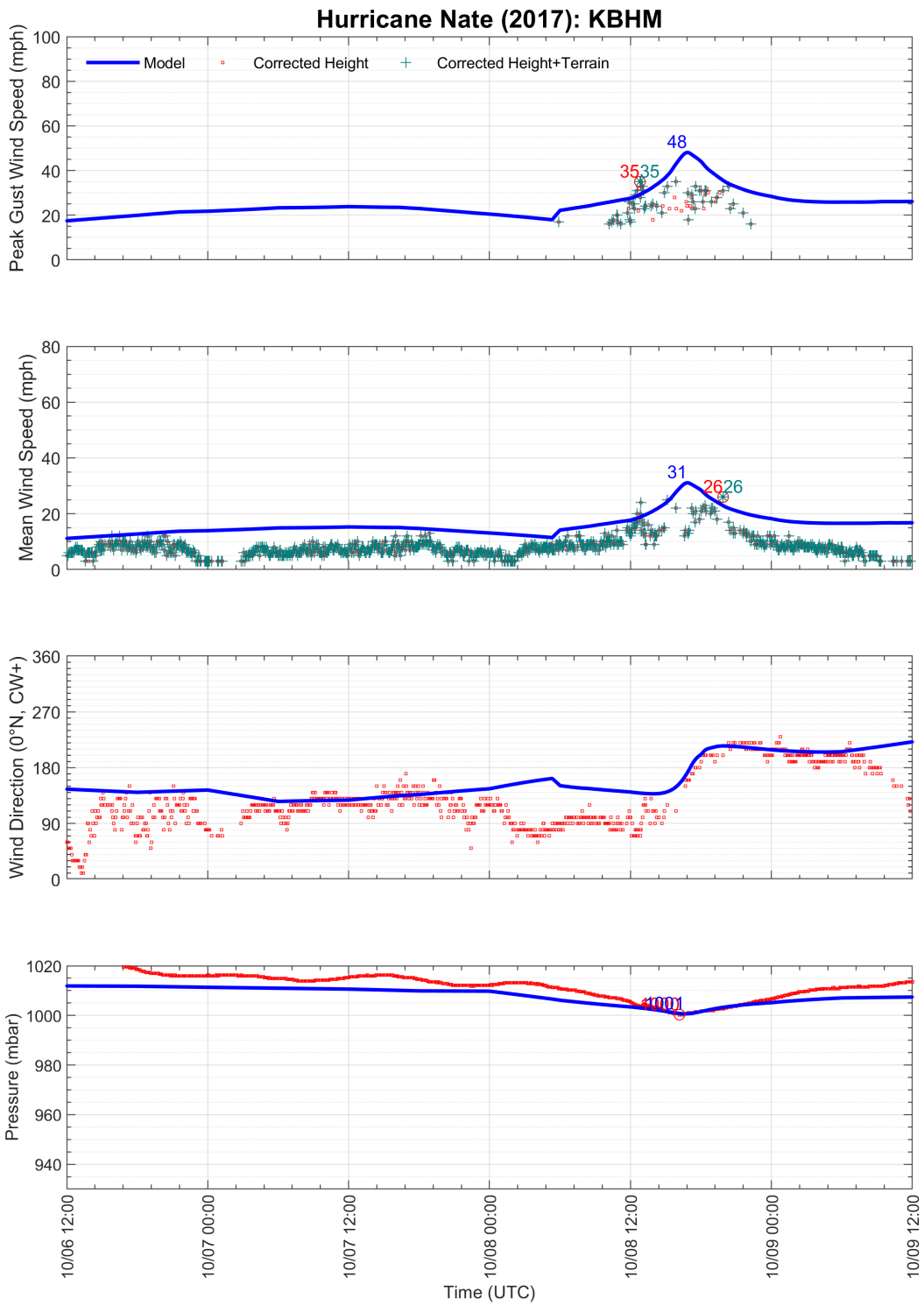
Station	Latitude (°N)	Longitude (°W)	Anemometer Height (m)
KANB	33.588	85.858	8.00
KASD	30.345	89.821	10.00
KBFM	30.626	88.068	10.00
KBHM	33.564	86.754	10.00
KBTR	30.537	91.147	10.00
KBVE	29.350	89.407	10.00
KCEW	30.780	86.522	10.00
KCHA	35.033	85.200	10.00
KDCU	34.652	86.945	10.00
KDTS	30.400	86.472	8.00
KEET	33.178	86.782	10.00
KFFC	33.355	84.567	10.00
KFTY	33.779	84.521	8.00
KGPT	30.407	89.070	10.00
KGZH	31.416	87.044	10.00
KHBG	31.265	89.253	10.00
KHKS	32.335	90.222	10.00
KHSV	34.644	86.786	10.00
KJAN	32.320	90.078	10.00
KMEI	32.333	88.751	10.00
KMGM	32.301	86.394	10.00
KMOB	30.688	88.246	10.00
KMSL	34.745	87.610	10.00
KNEW	30.043	90.028	8.00
KPNS	30.473	87.188	10.00
KPQL	30.464	88.532	8.00
KRMG	34.348	85.161	10.00
KTCL	33.212	87.616	10.00
KTOI	31.861	86.012	10.00
KTUP	34.261	88.771	10.00
KVPC	34.123	84.849	10.00
AMRL1	29.450	91.338	11.00
BURL1	28.905	89.428	38.00
DKCM6	30.356	88.567	8.40
EINL1	29.373	91.384	10.00
FMOA1	30.228	88.024	38.20
FREL1	30.106	90.422	14.00
GISL1	29.265	89.958	9.30
NWCL1	30.027	90.113	11.60
PILL1	29.179	89.259	11.80
PSTL1	28.932	89.407	23.90

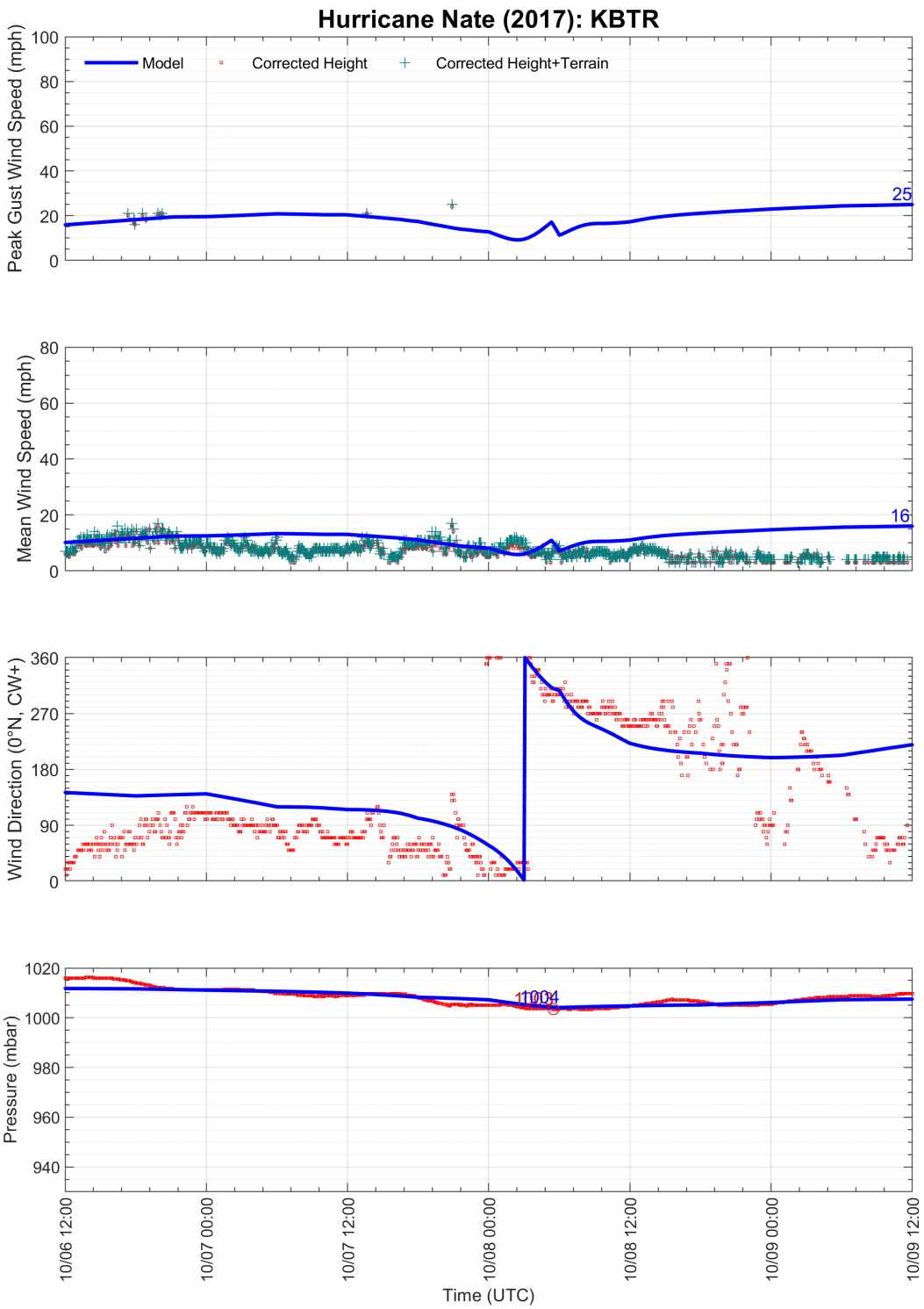
Station	Latitude (°N)	Longitude (°W)	Anemometer Height (m)
RARM6	30.343	88.511	22.90
SHBL1	29.868	89.673	15.60
SPLL1	28.867	90.483	10.00
TESL1	29.668	91.237	12.50
WYCM6	30.326	89.326	9.90
42001	25.897	89.668	3.60
42012	30.064	87.551	5.00
42040	29.208	88.226	4.00
42360	26.672	90.471	3.00
42395	26.404	90.792	3.00

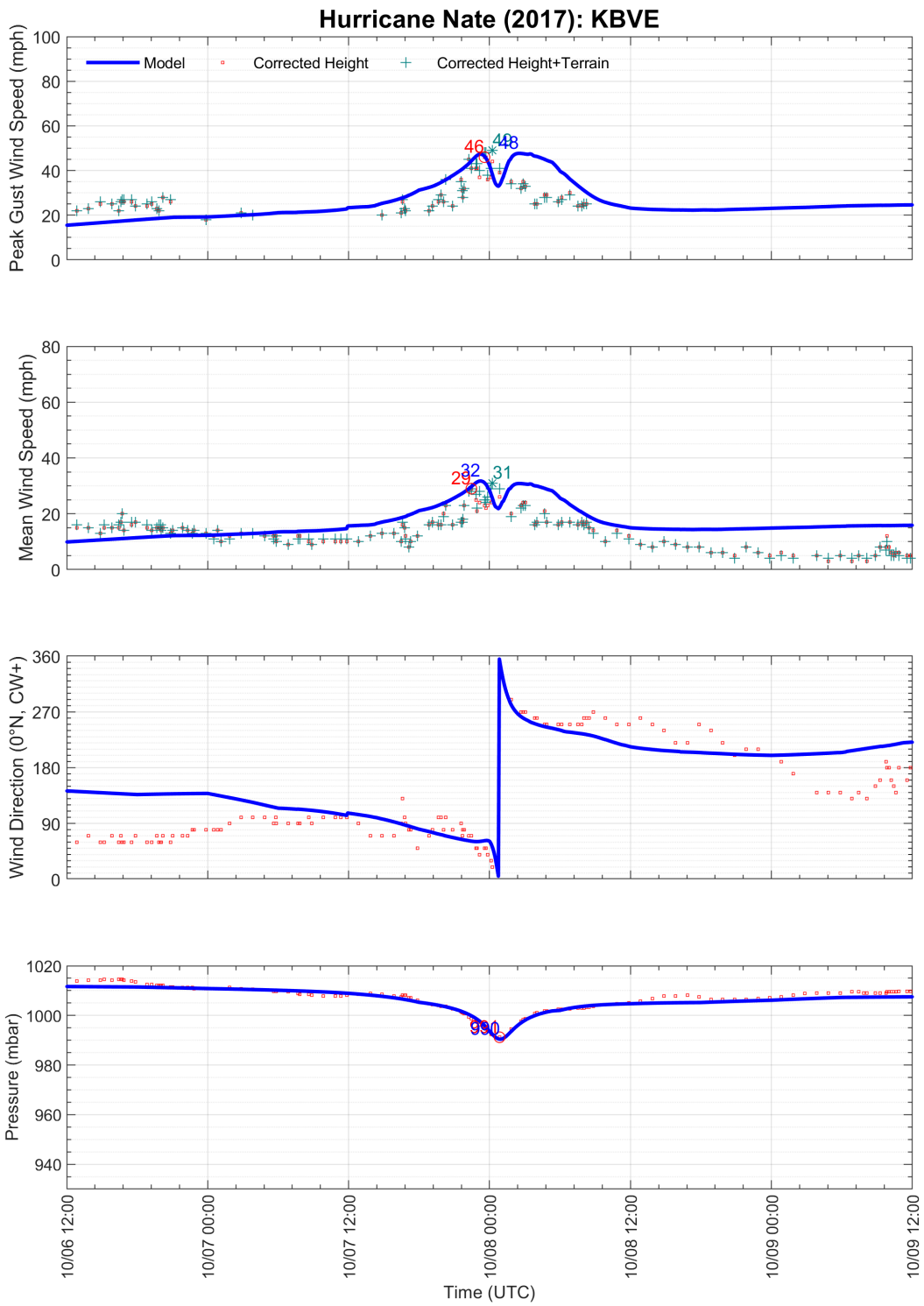


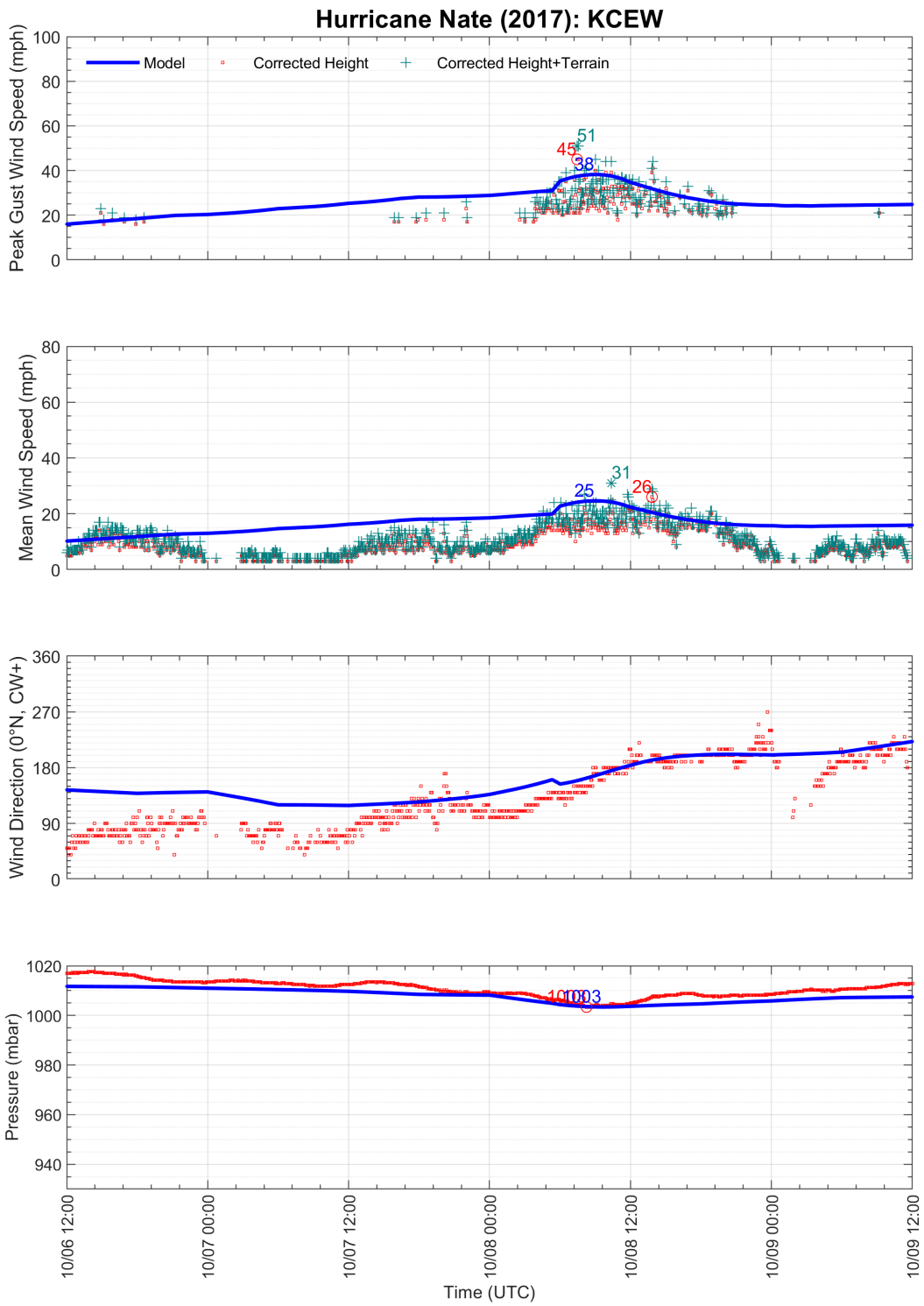


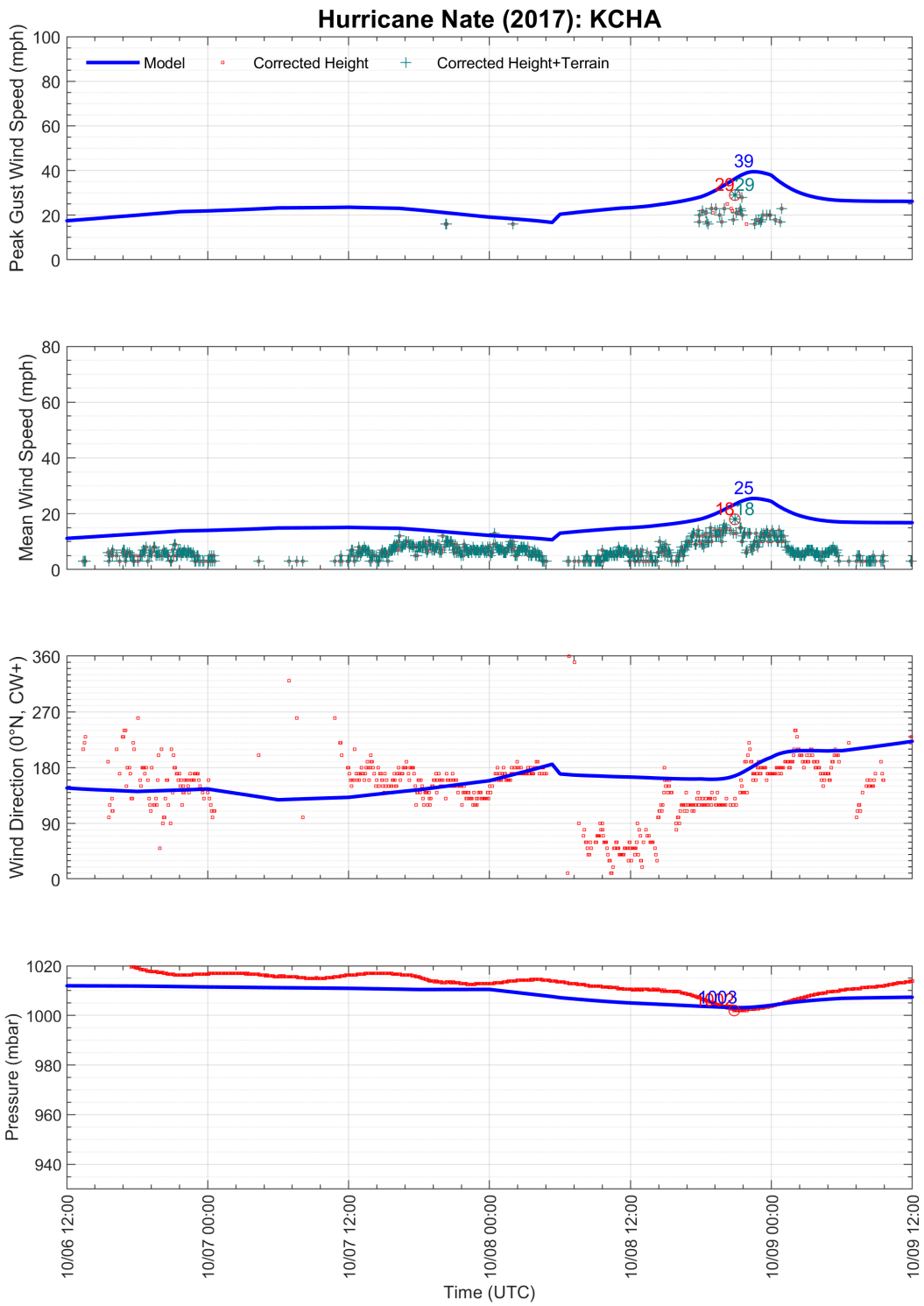


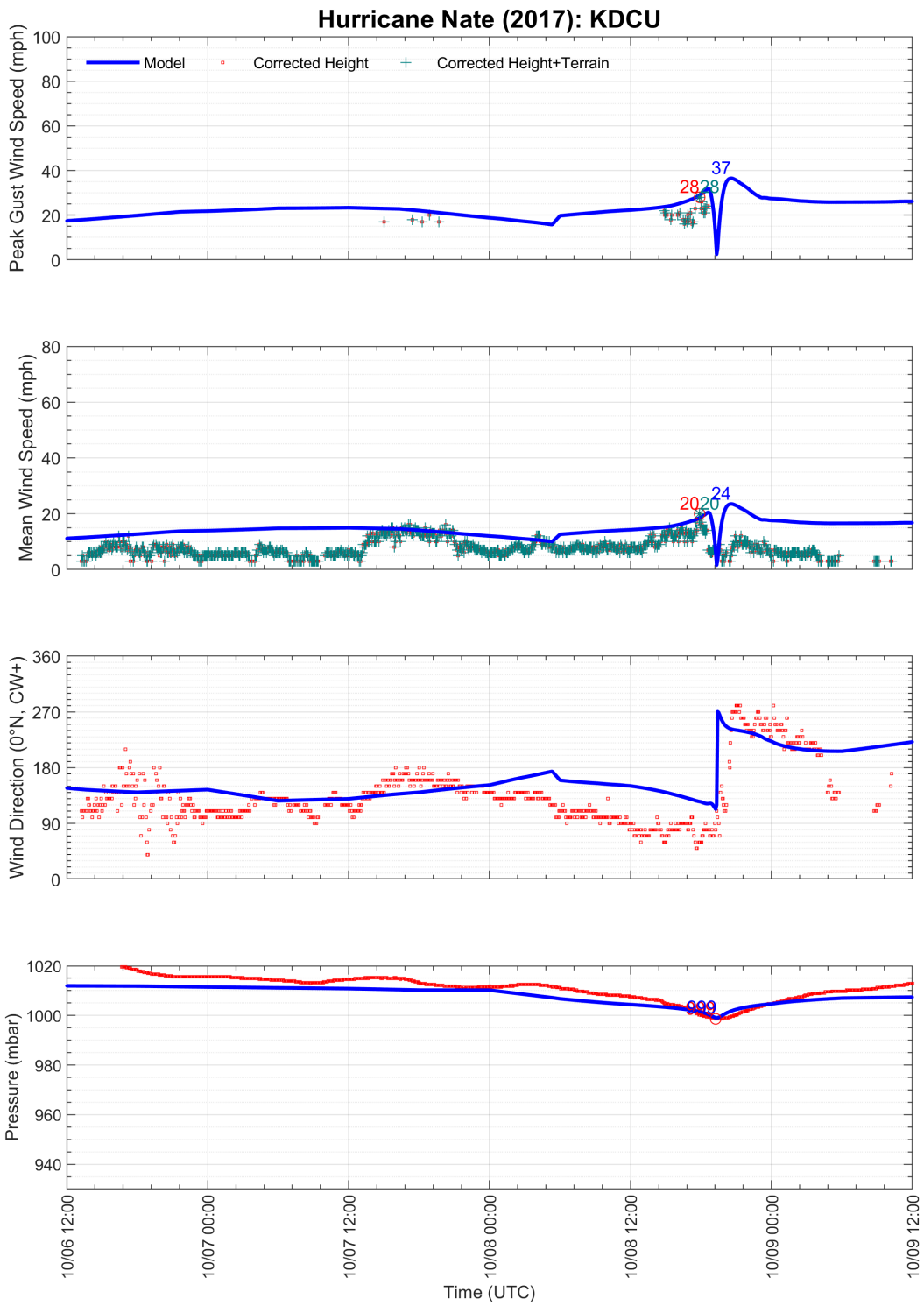


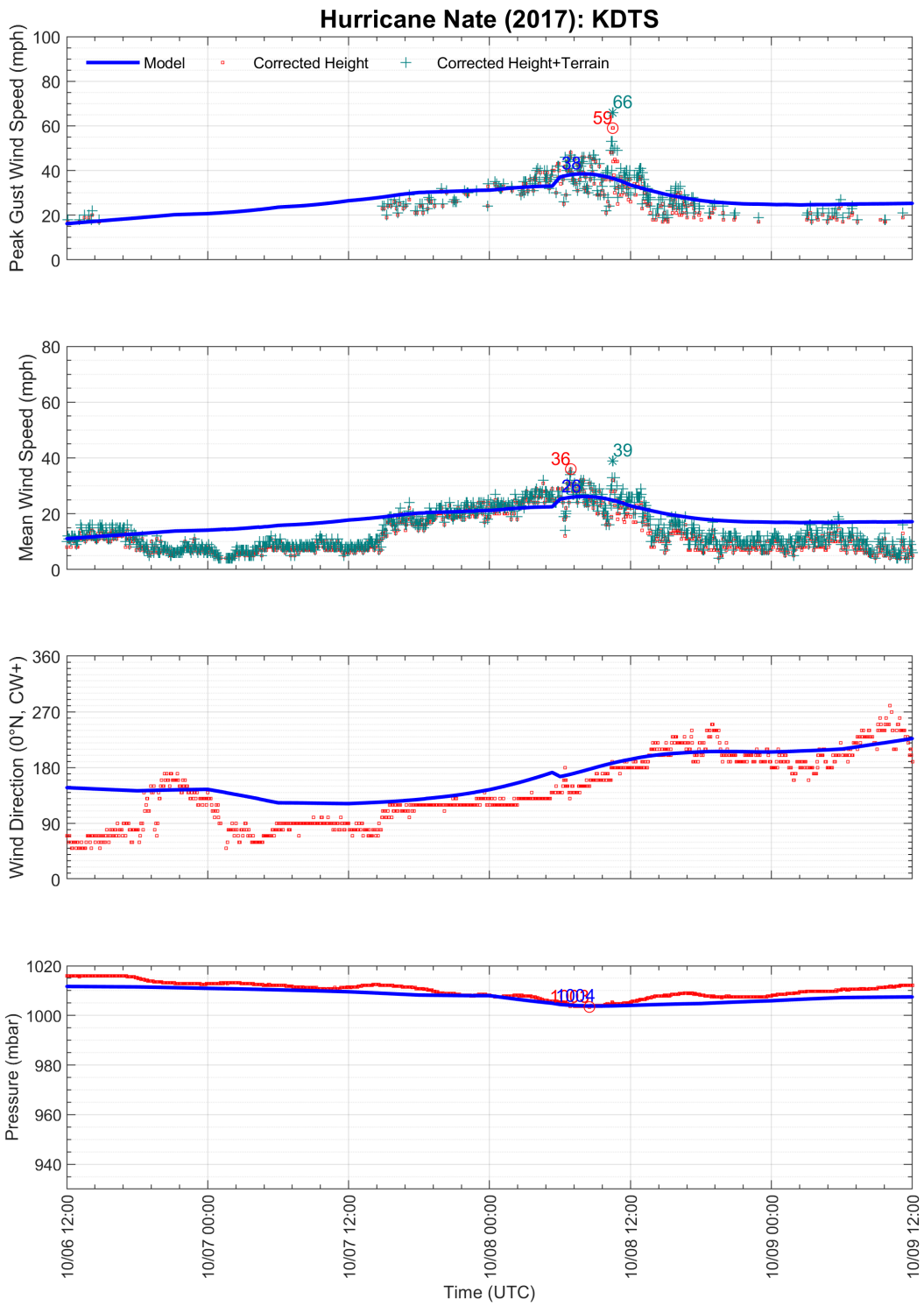


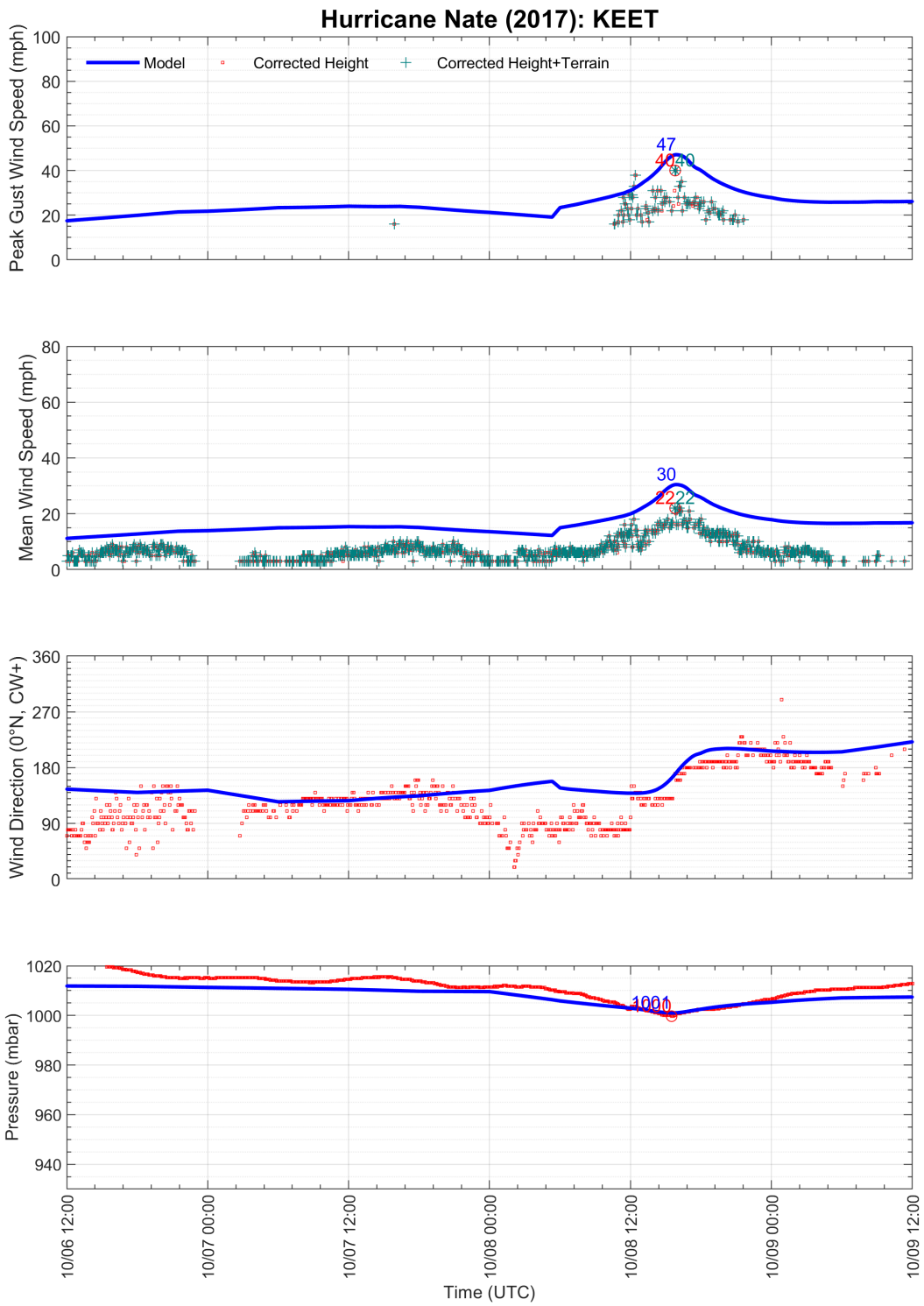


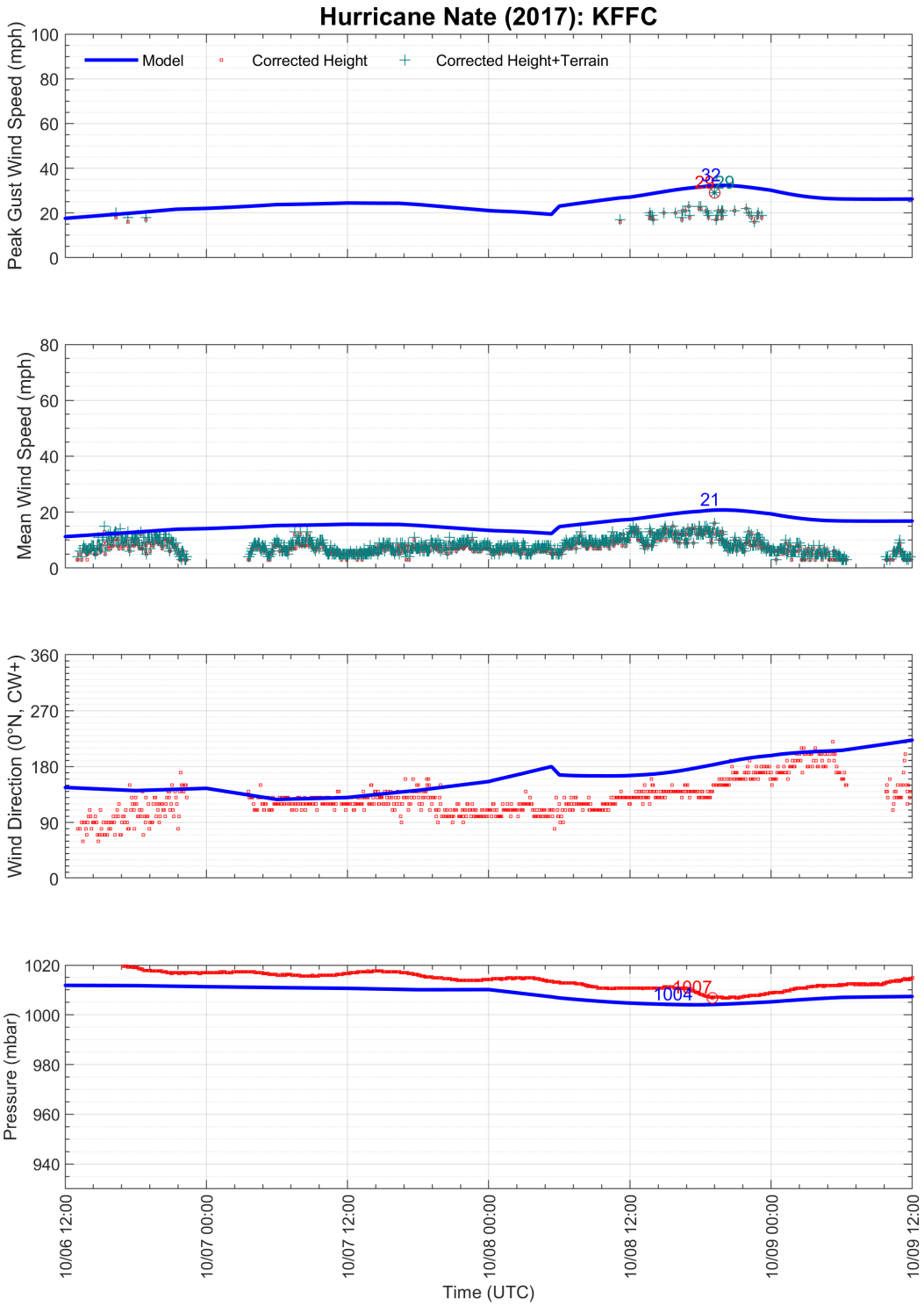


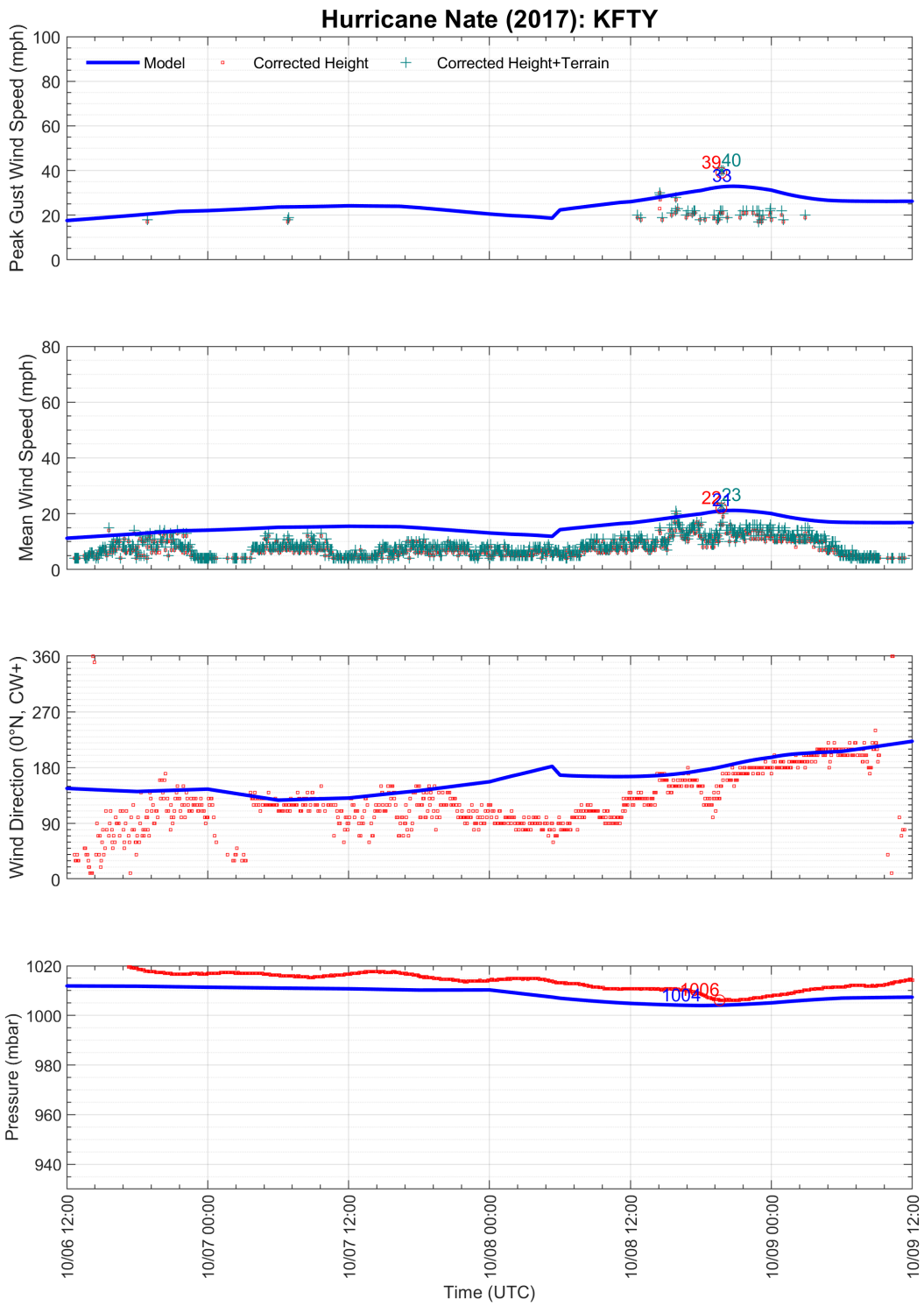


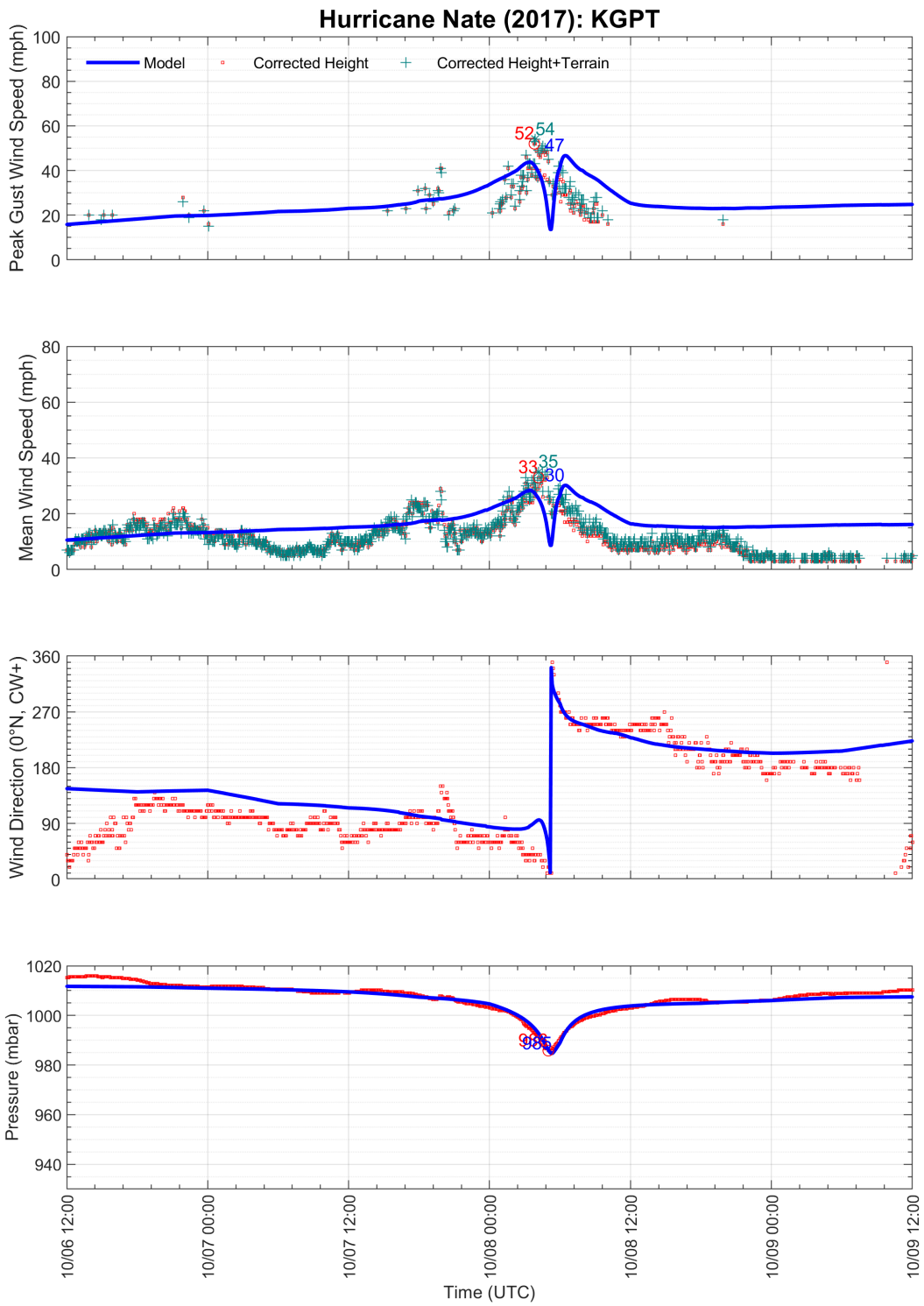


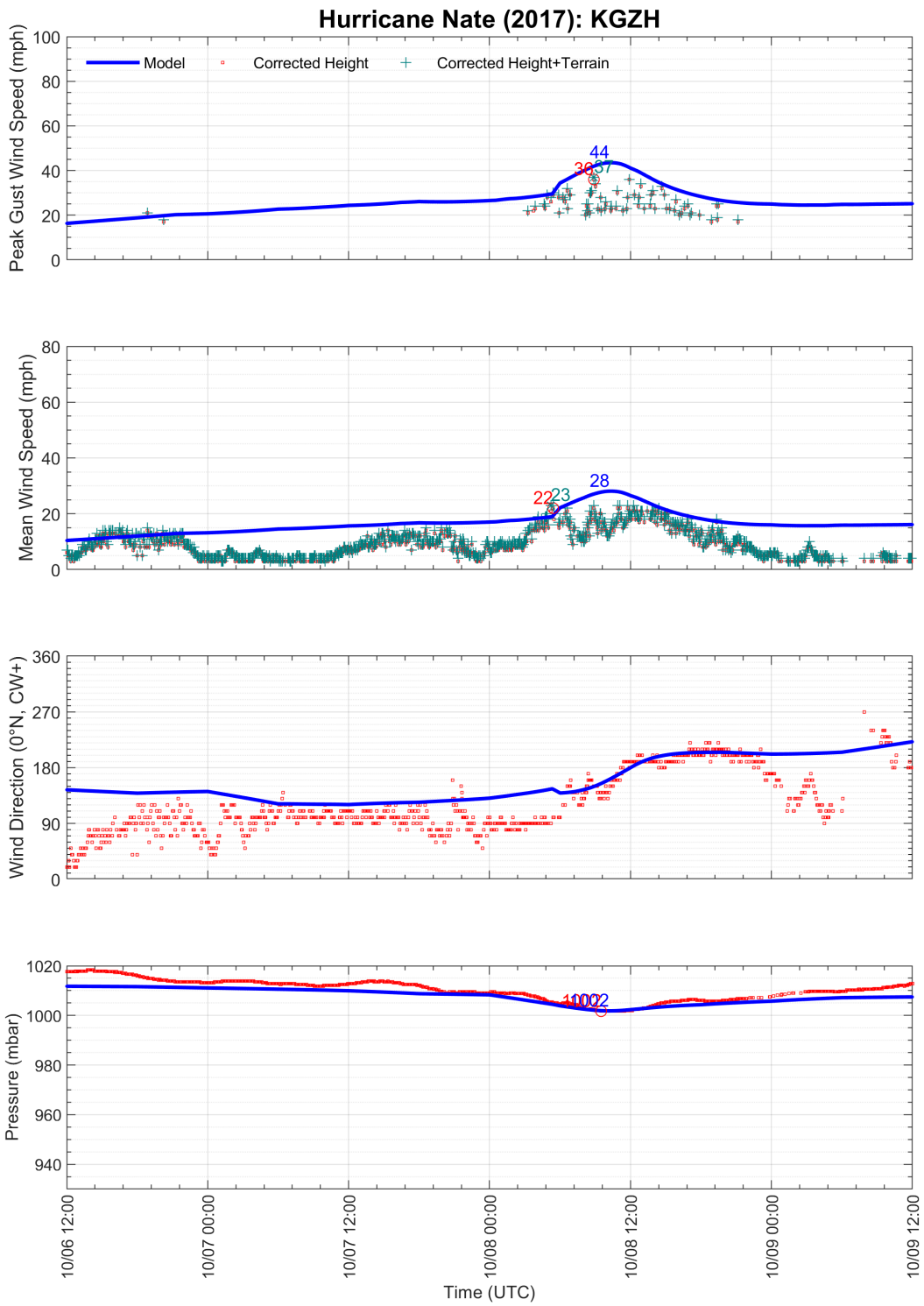


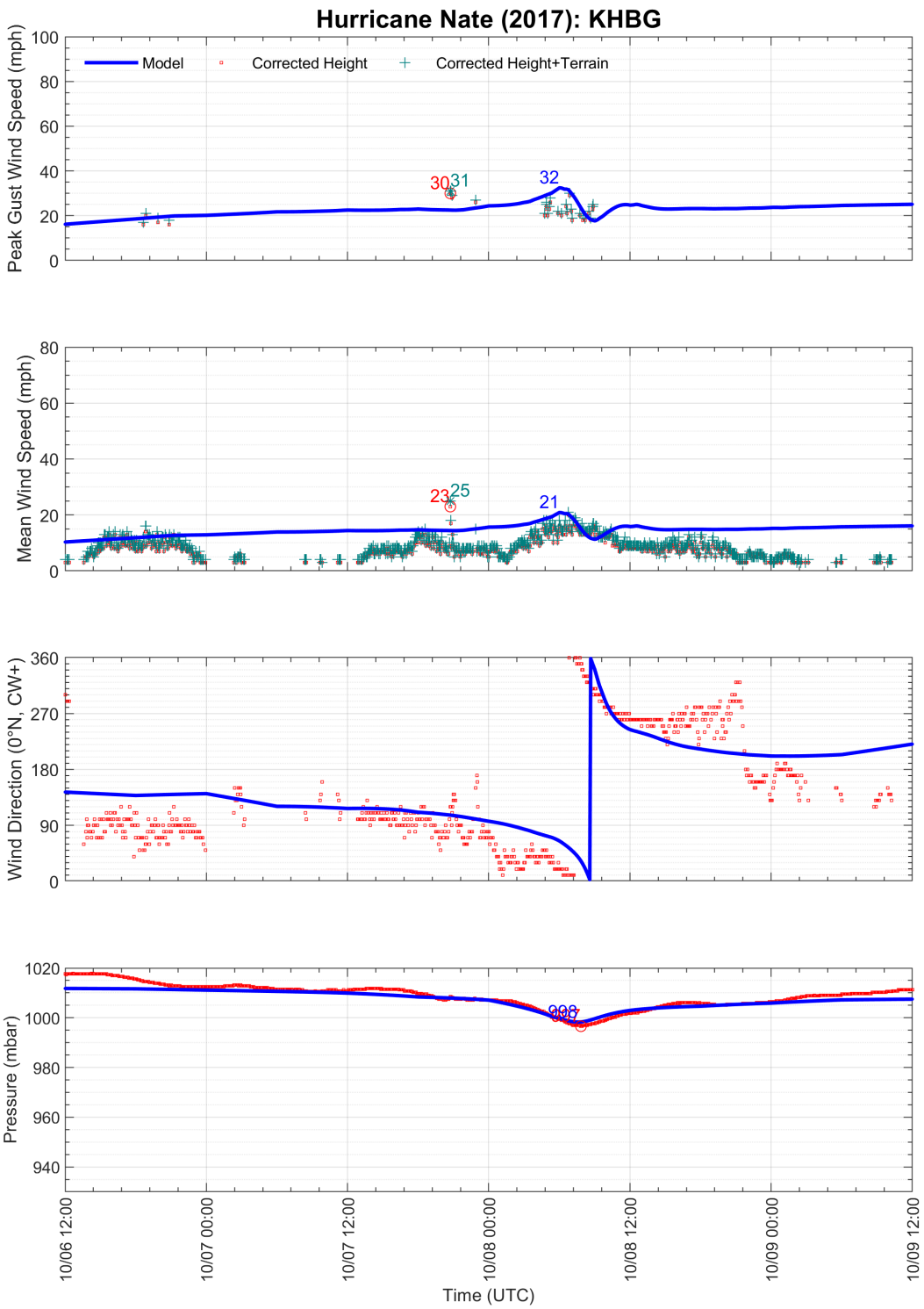


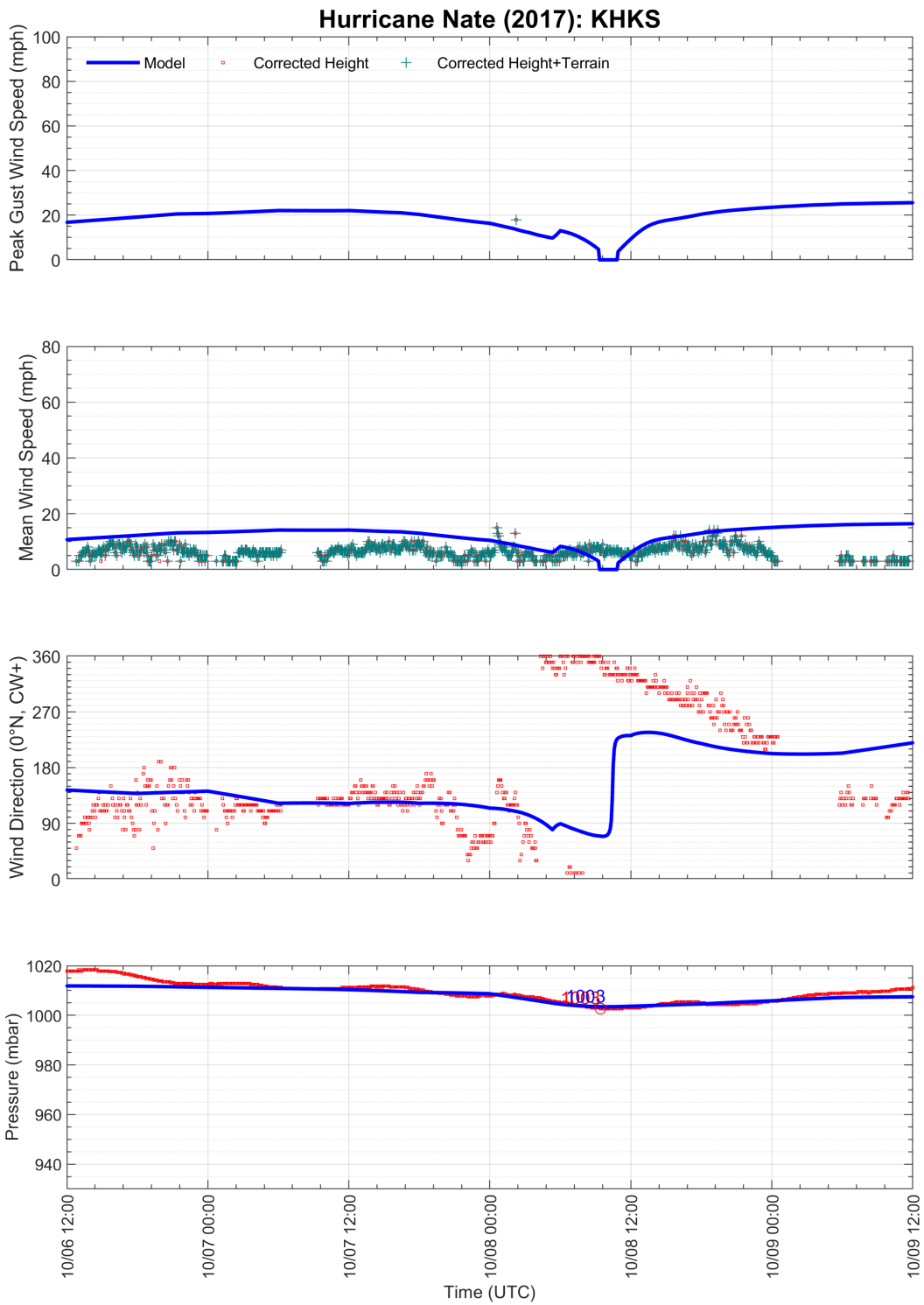


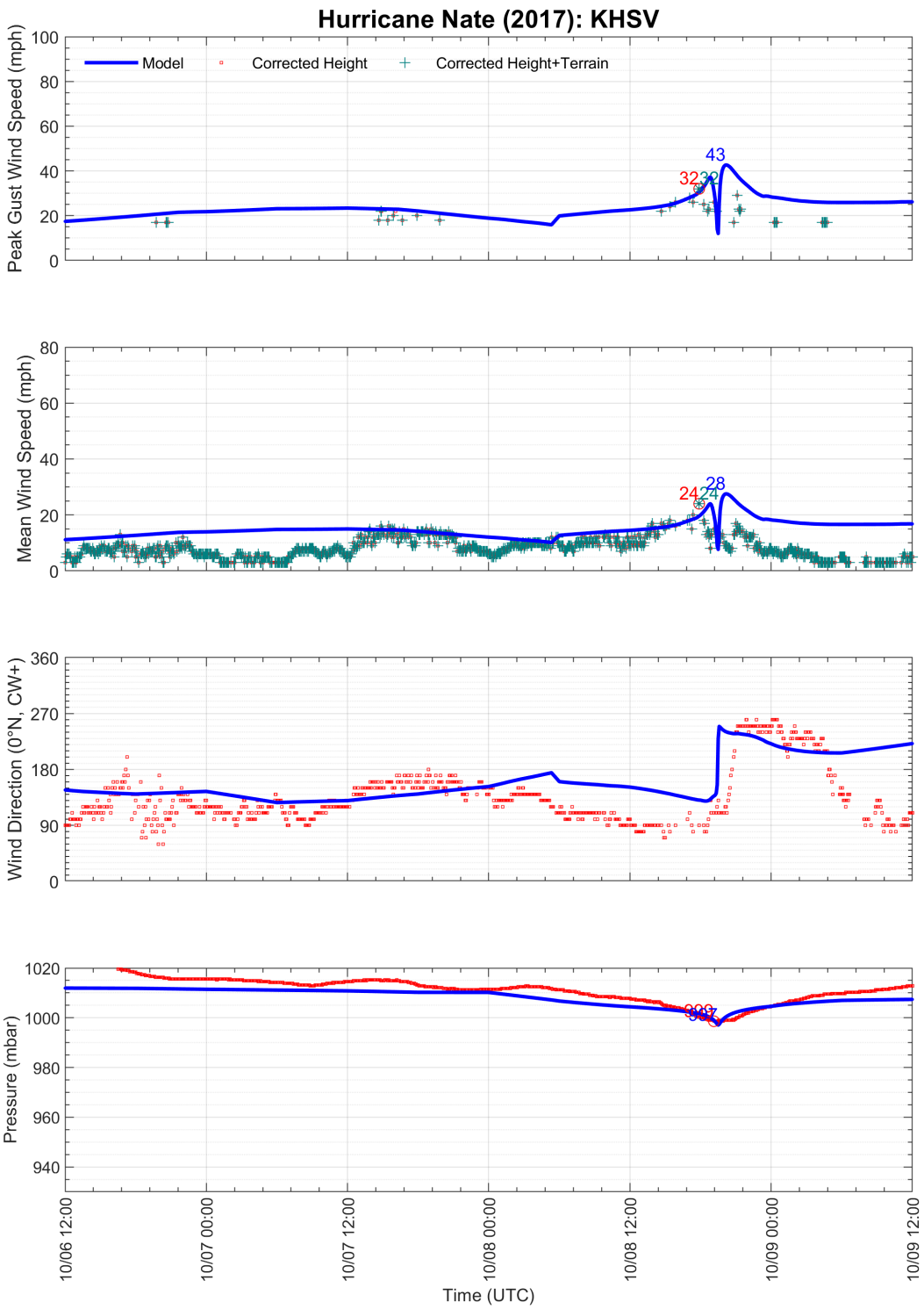


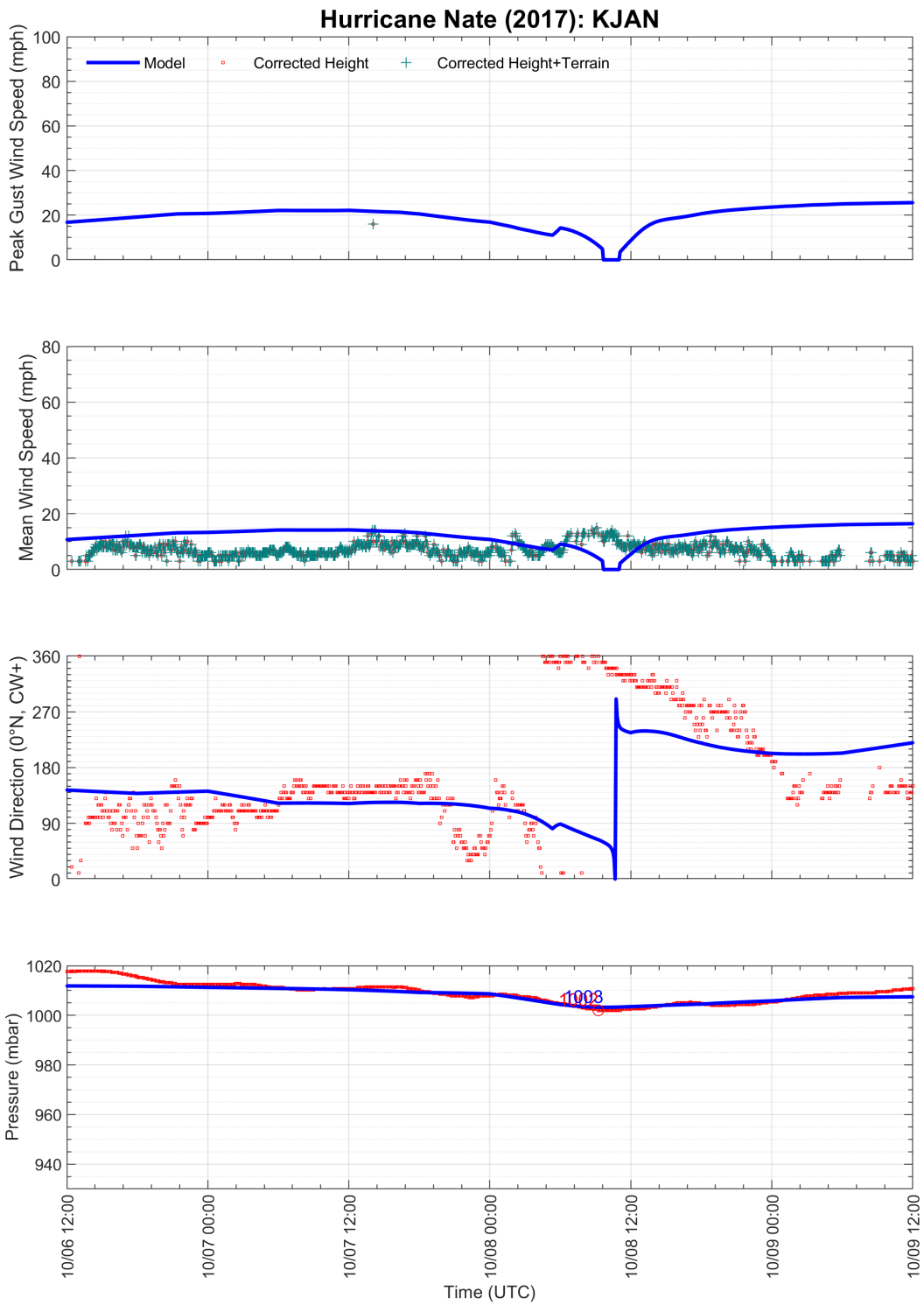


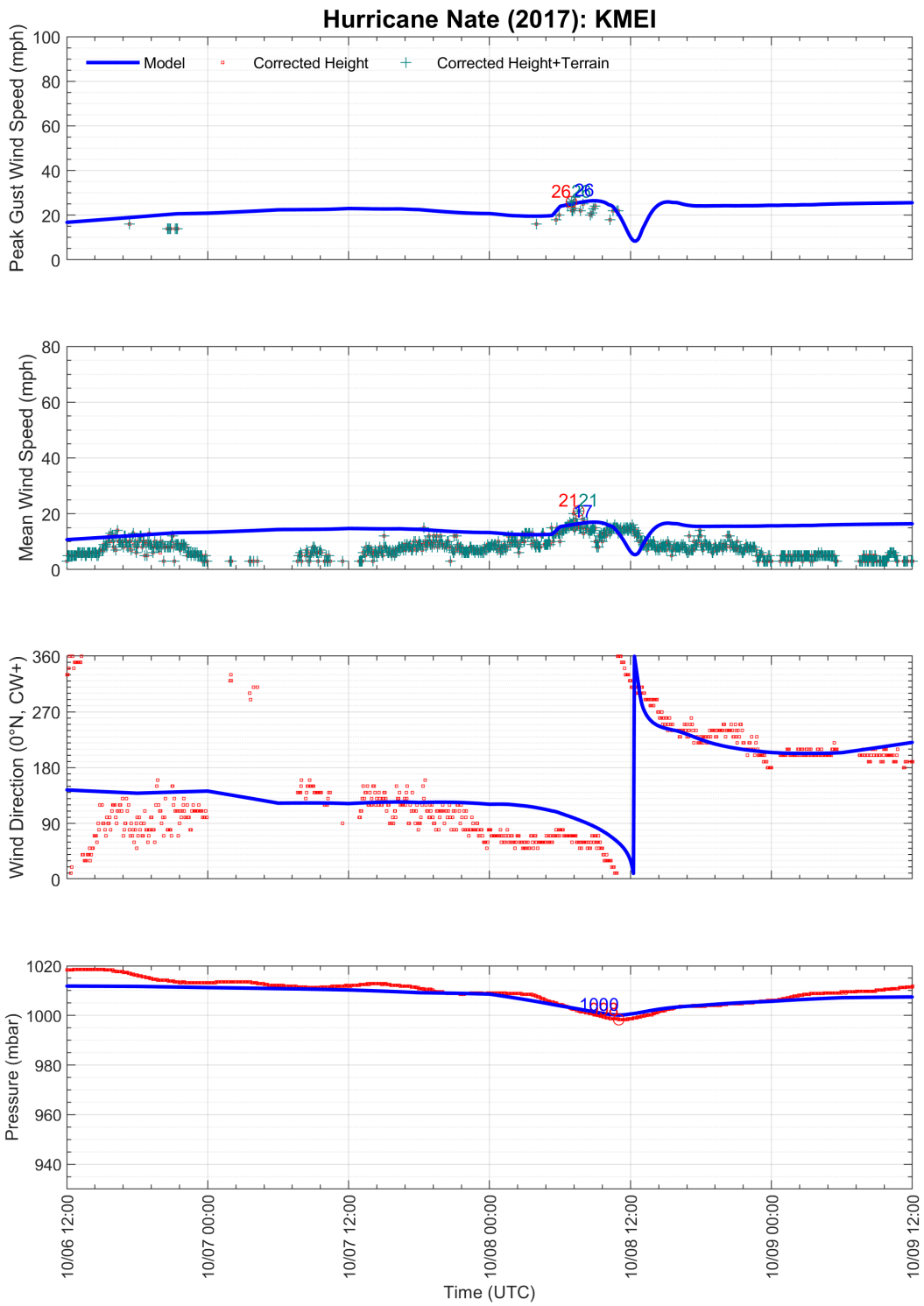


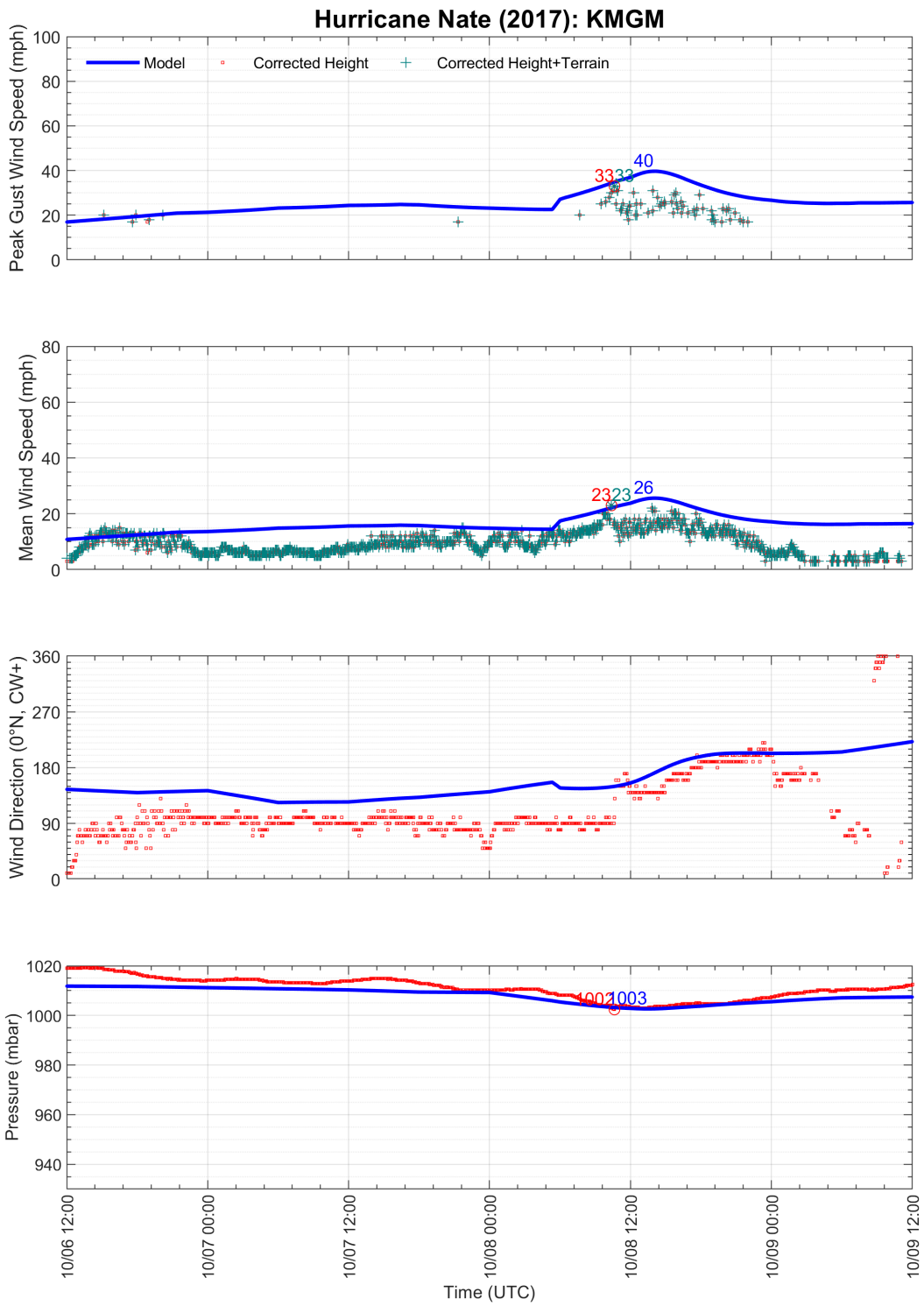


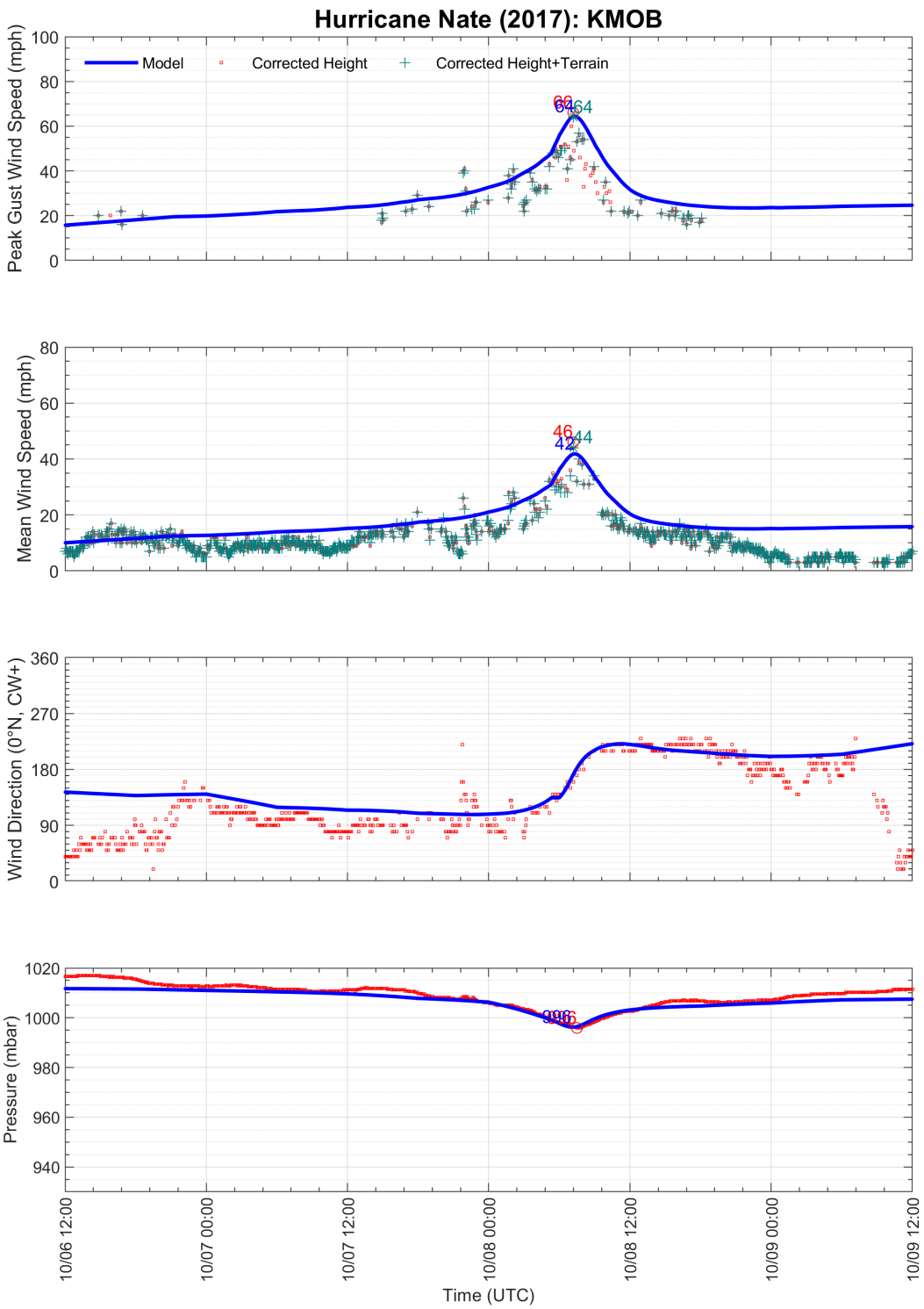


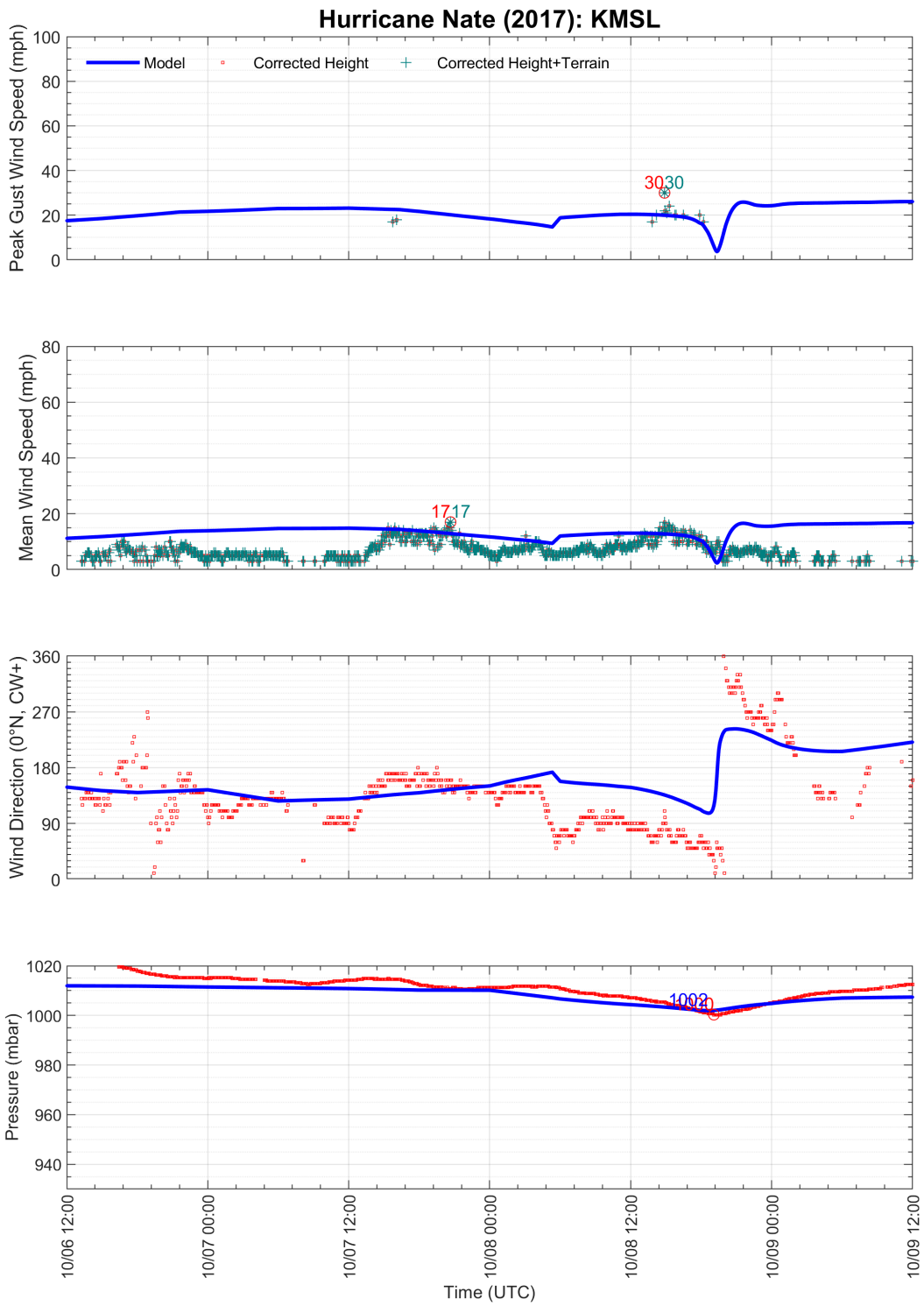


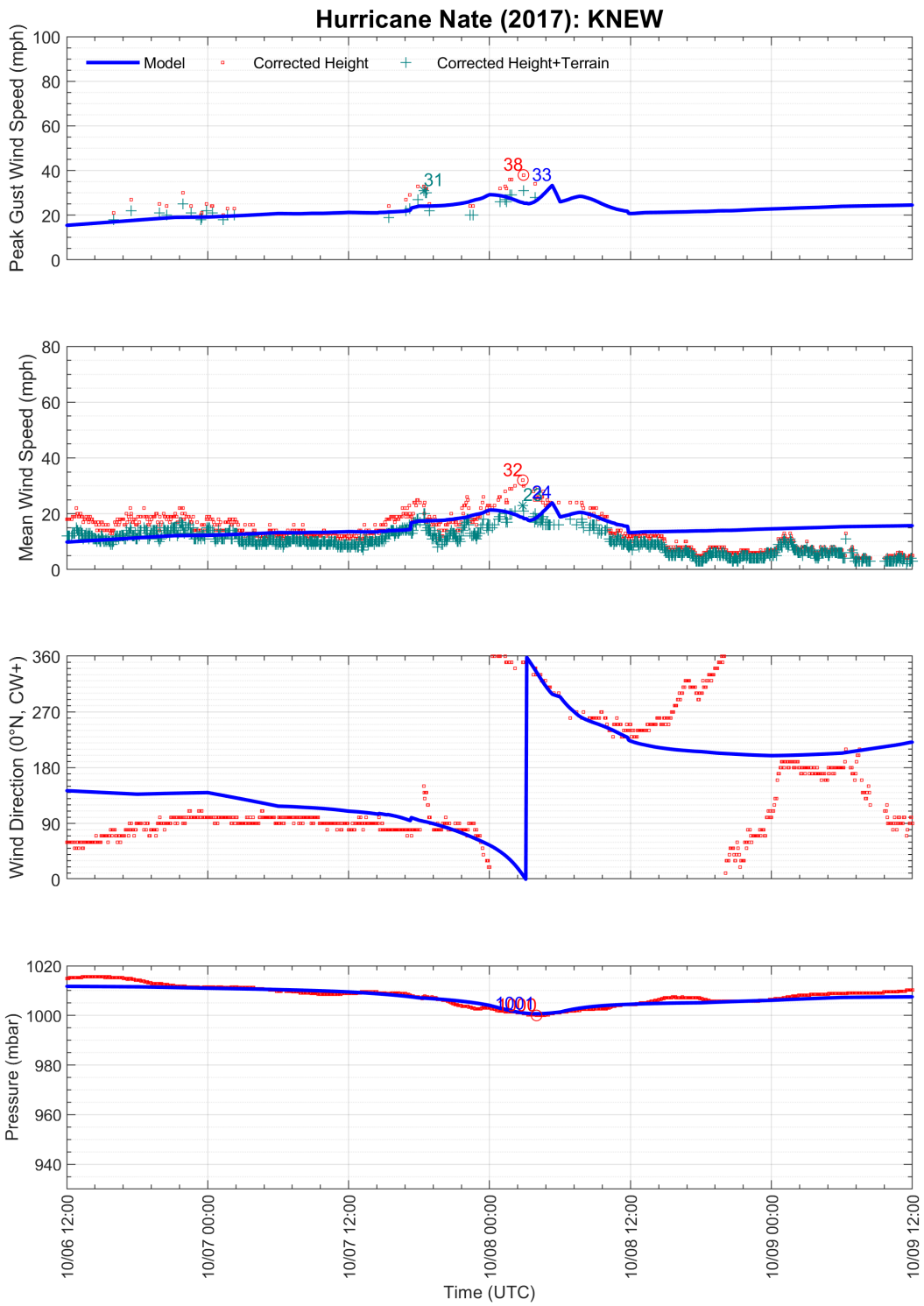


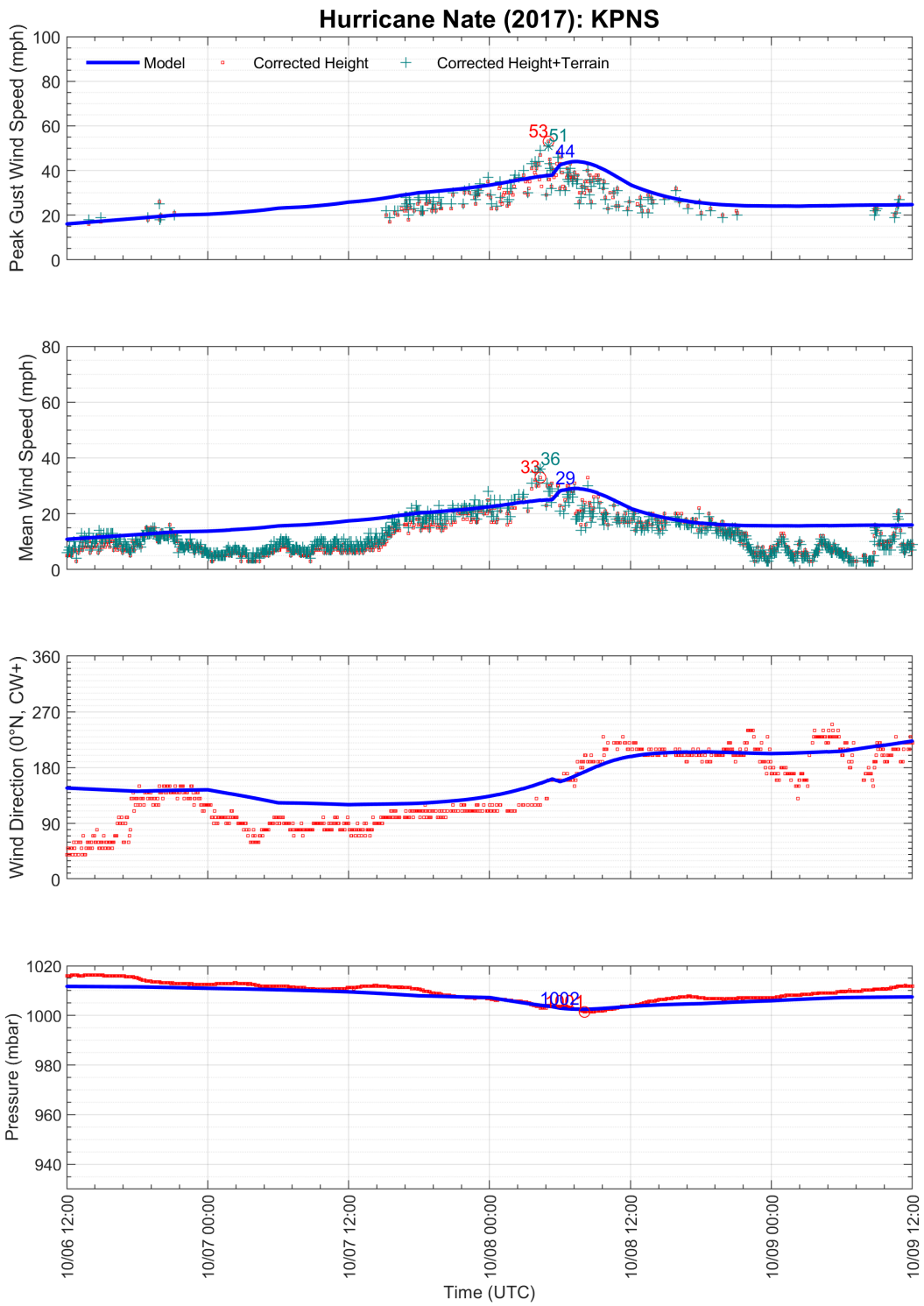


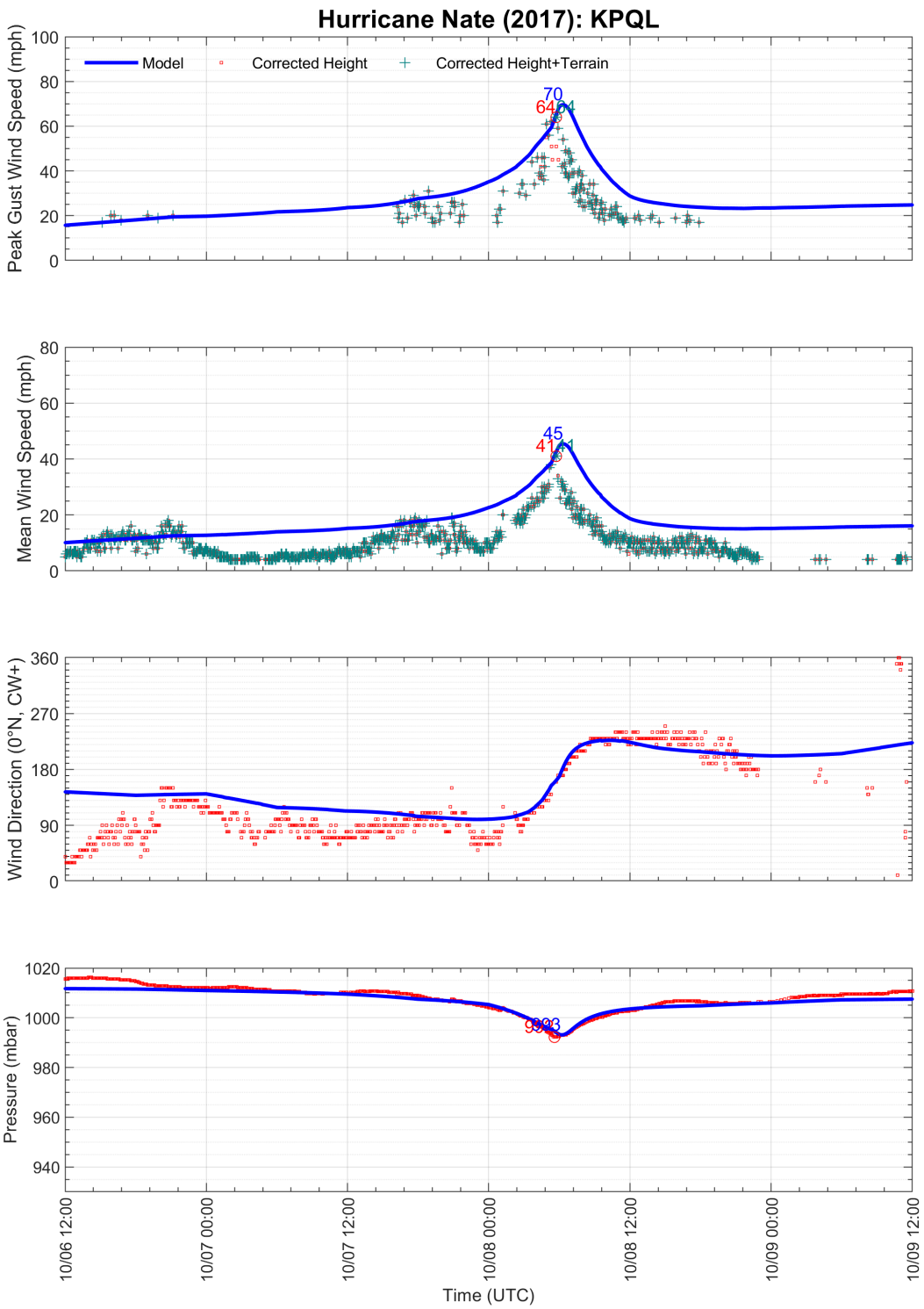


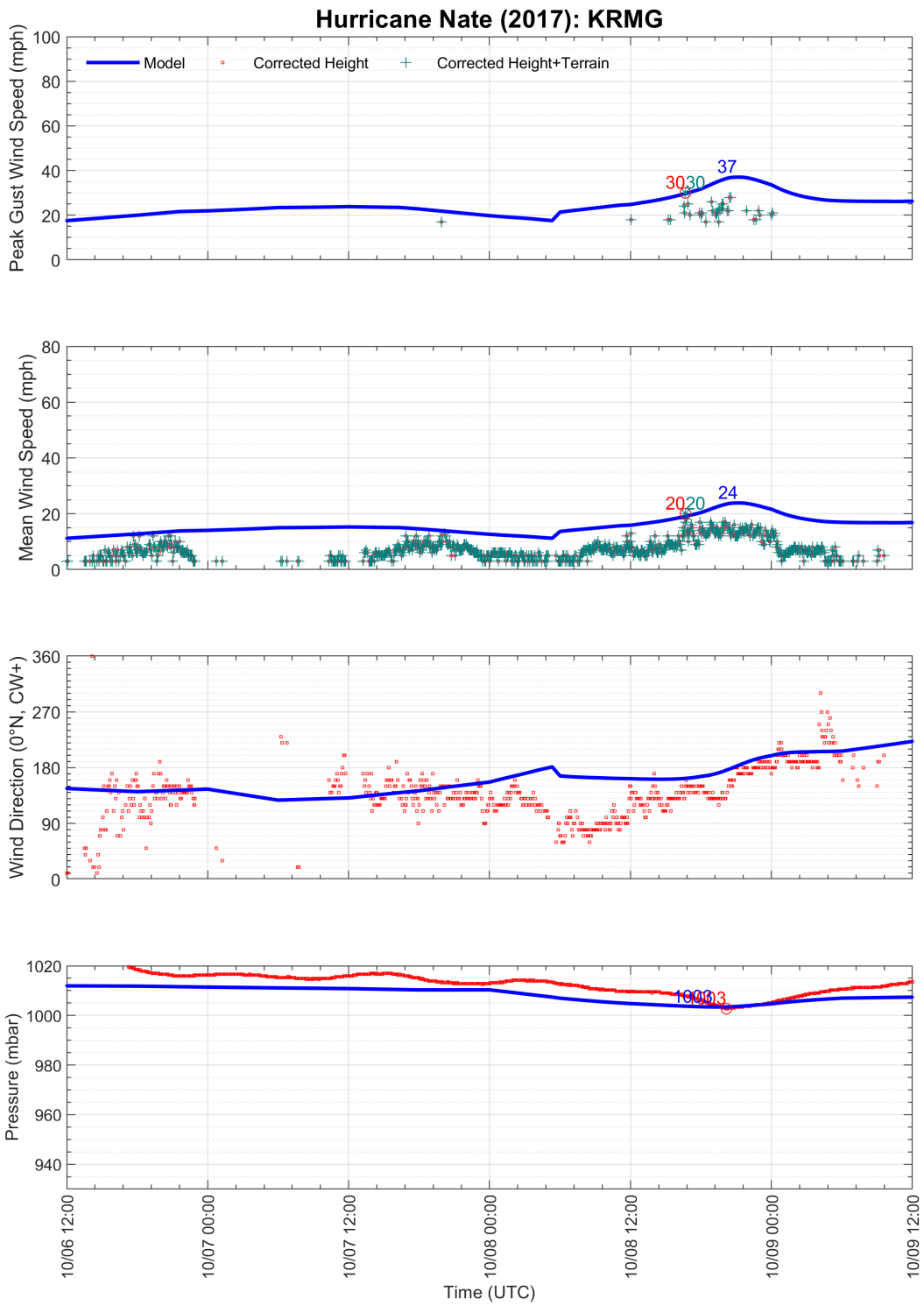


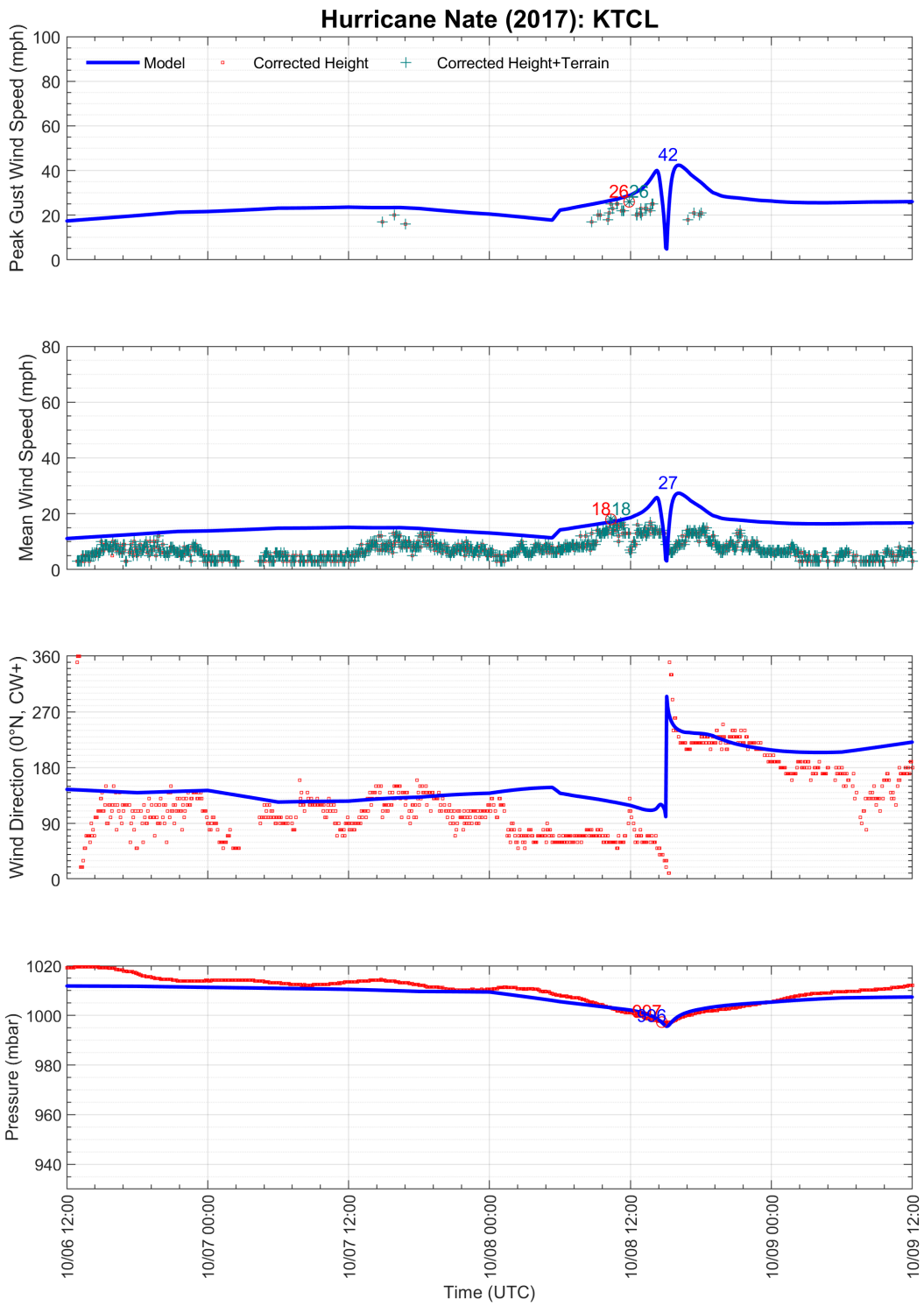


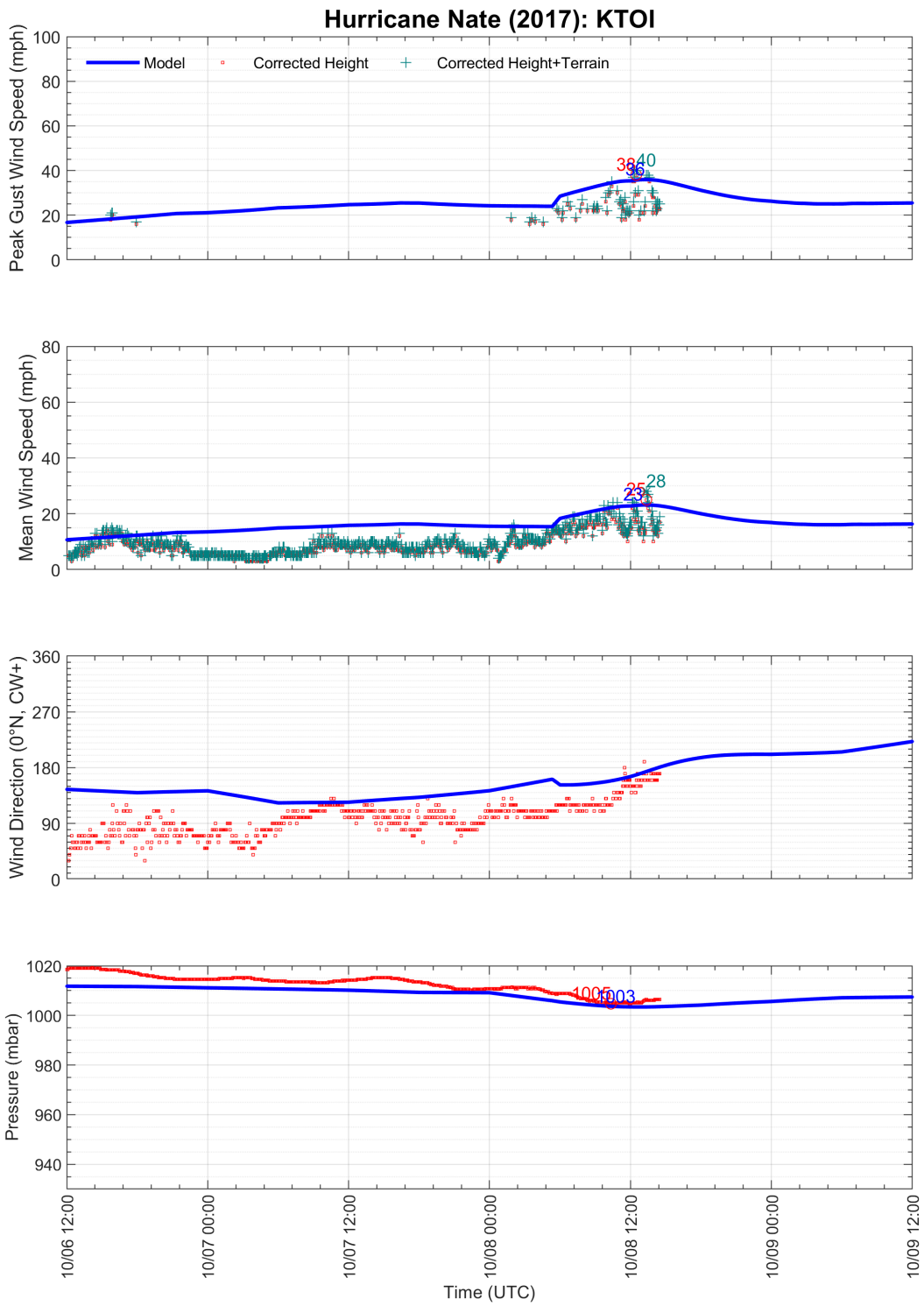


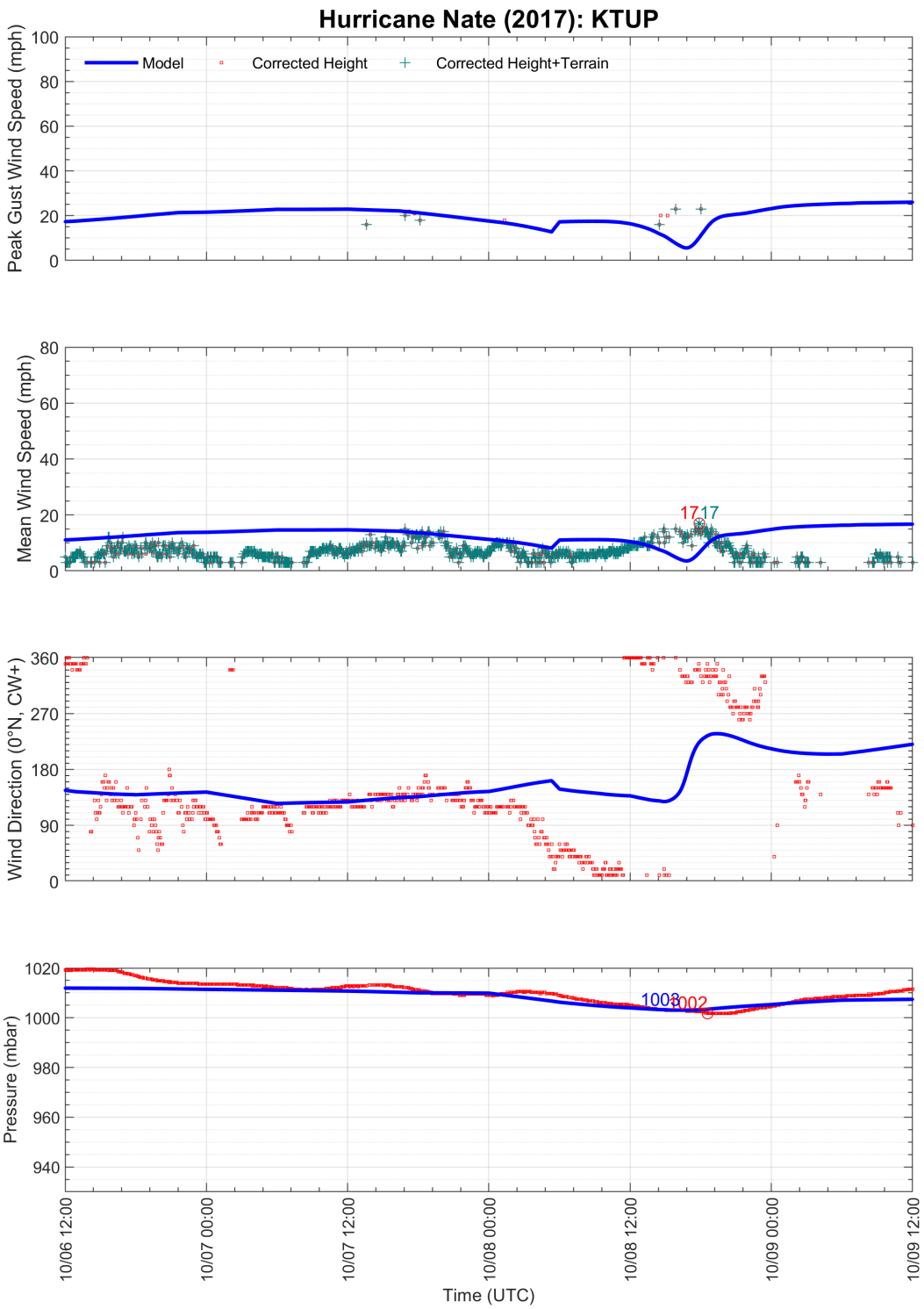


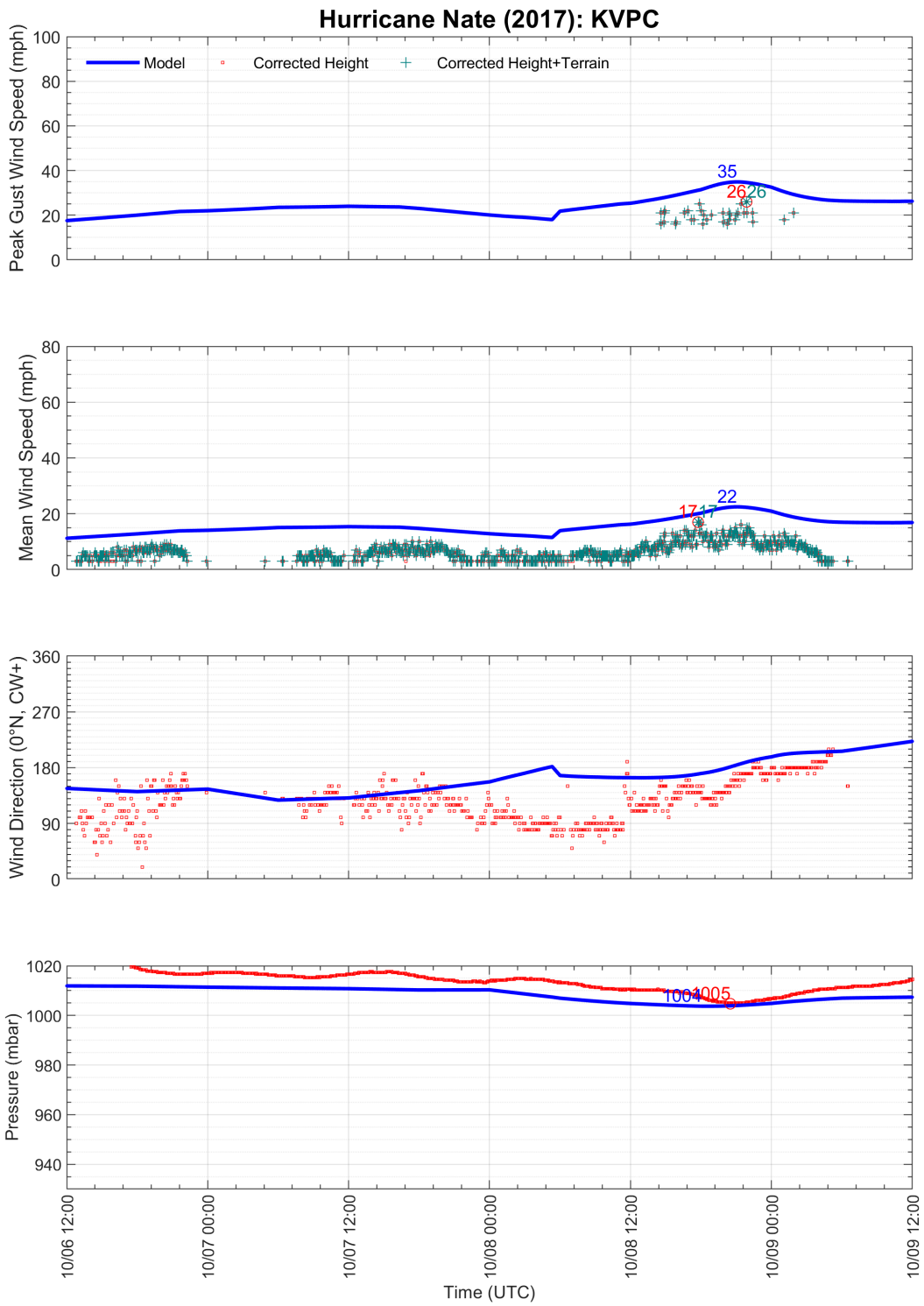


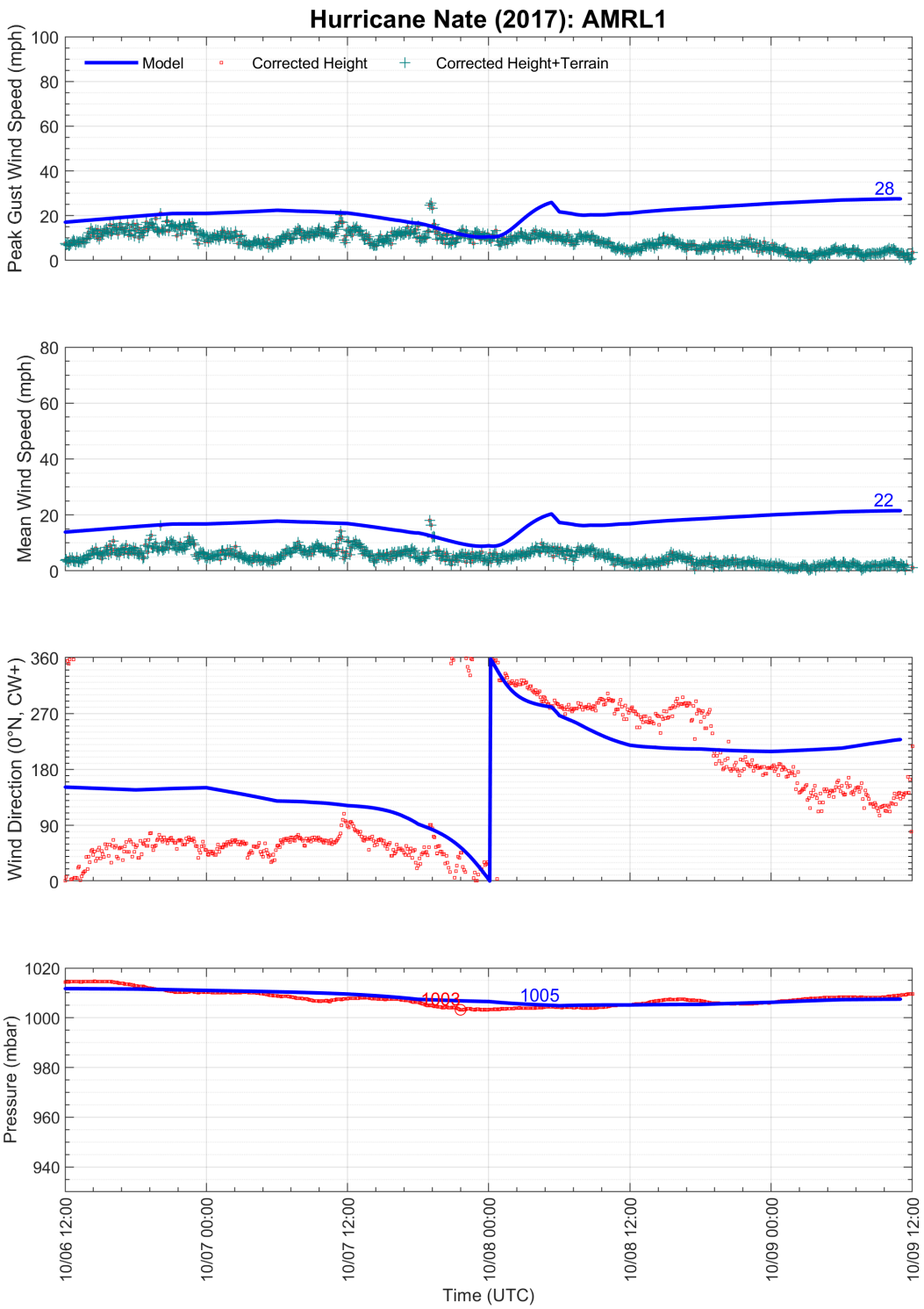




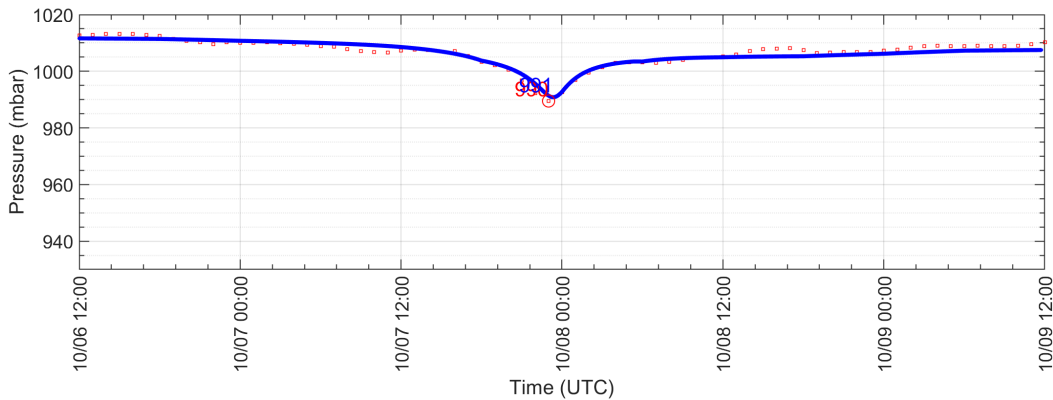
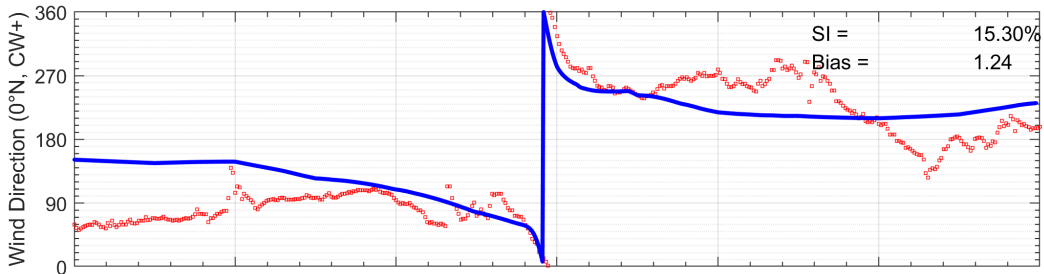
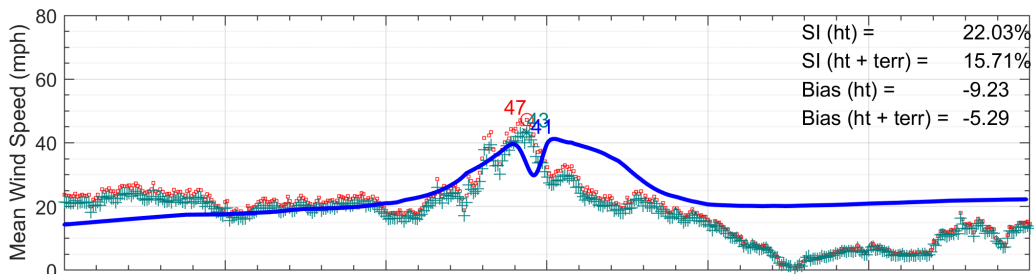
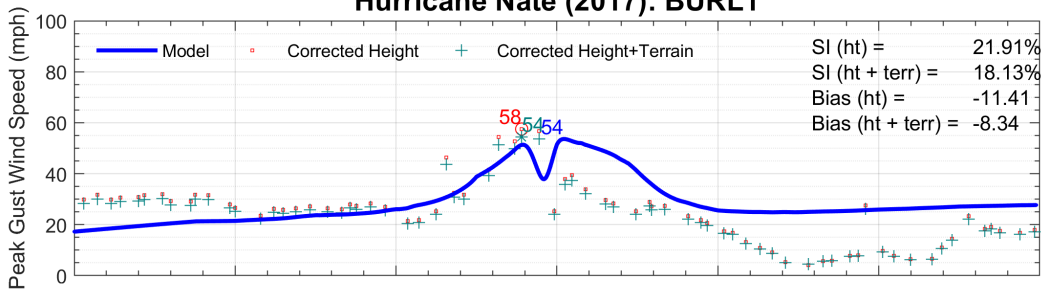




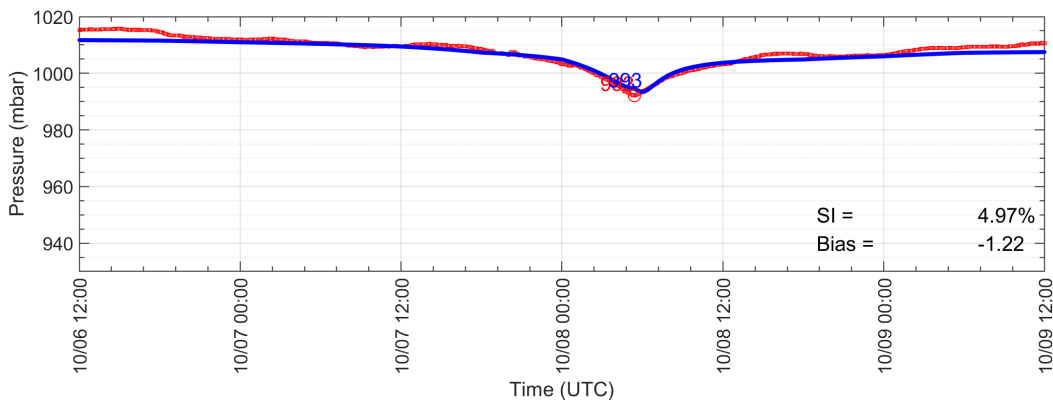
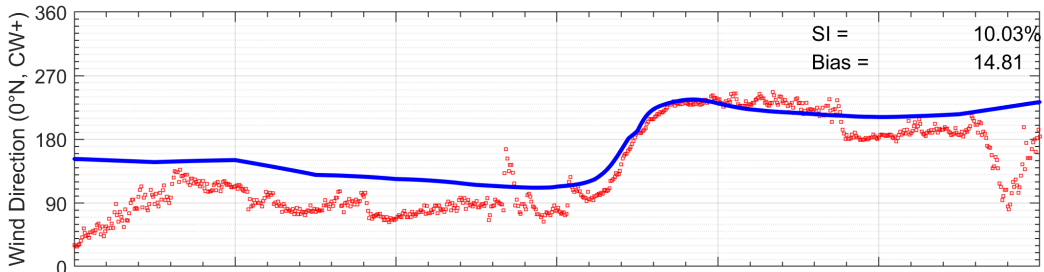
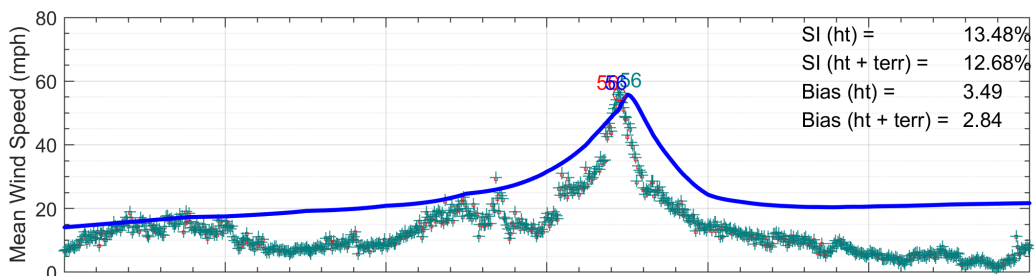
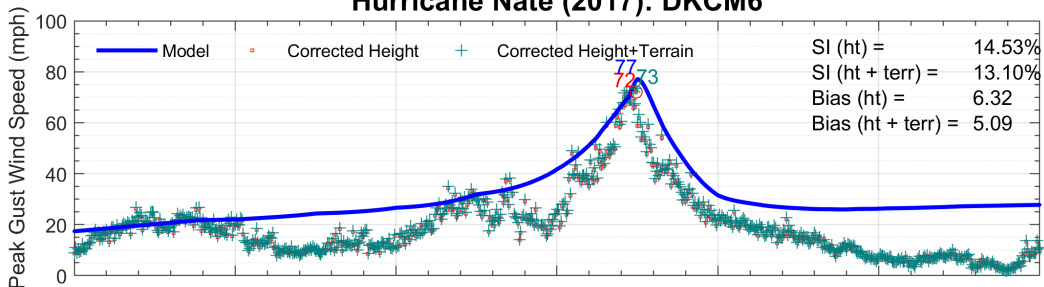


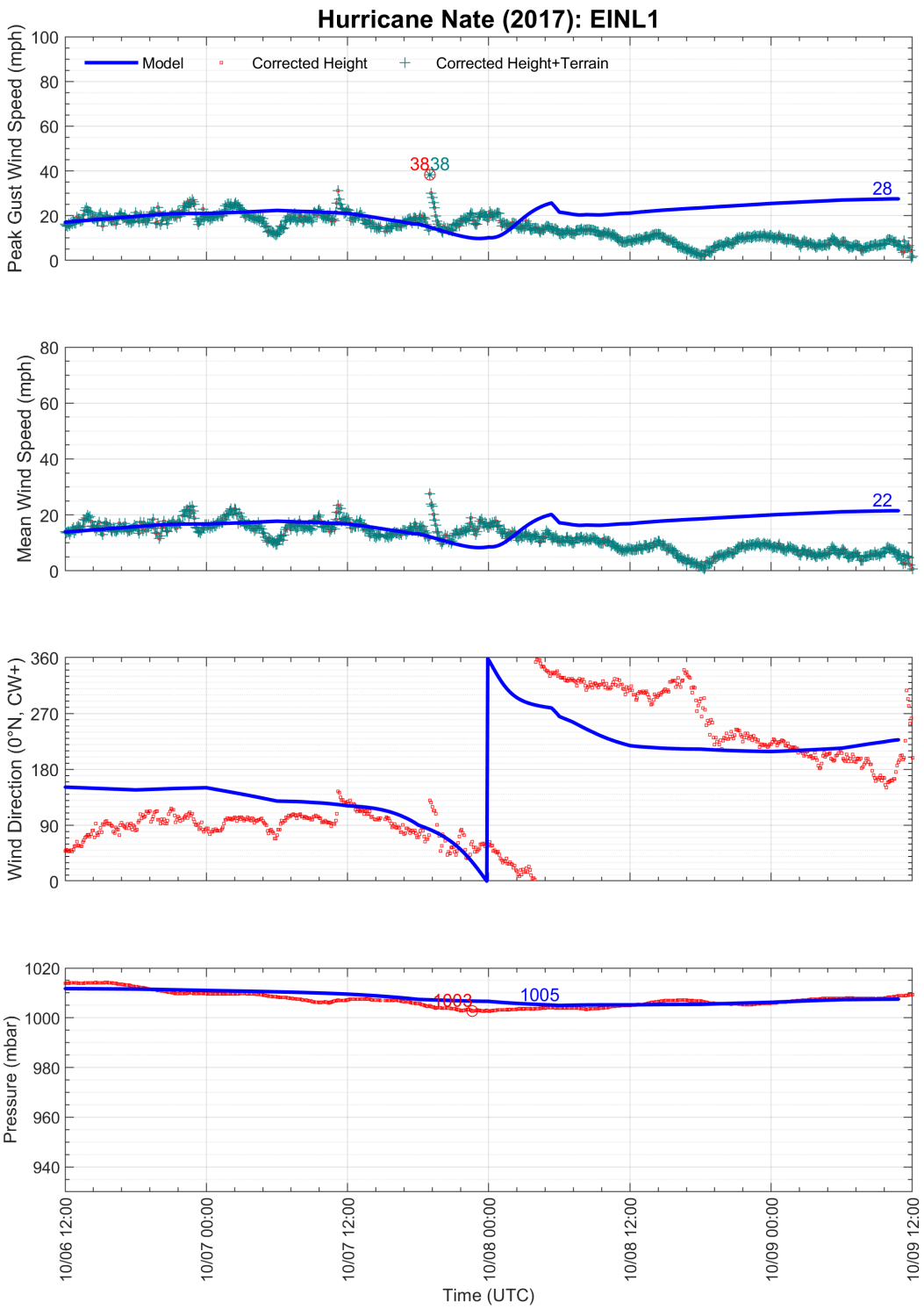


Hurricane Nate (2017): BURL1

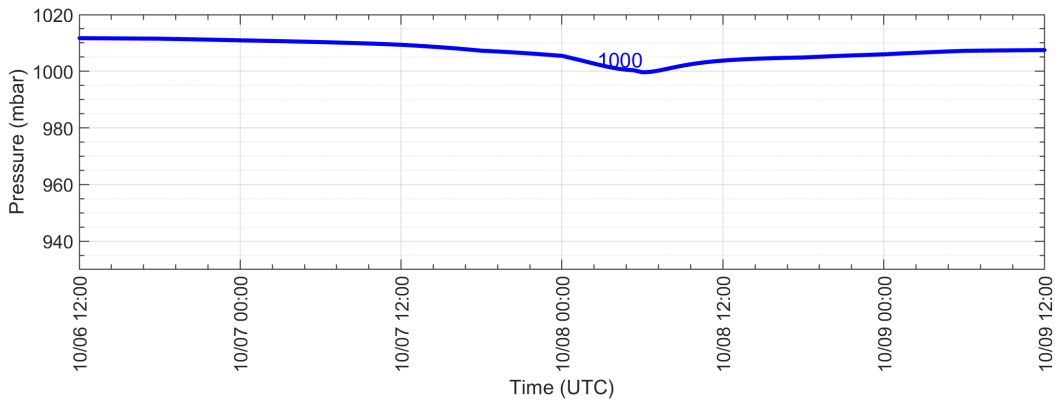
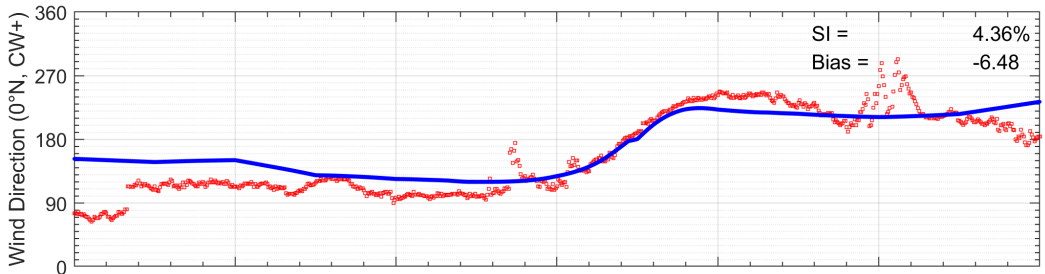
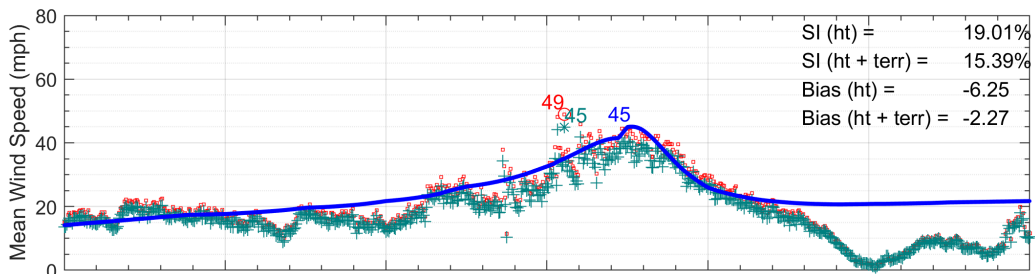
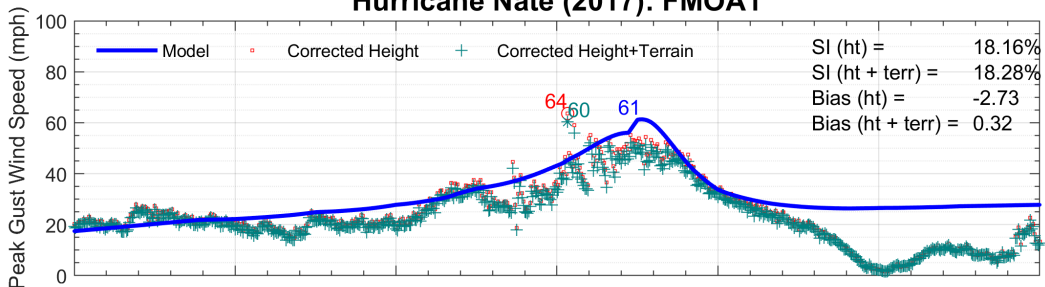


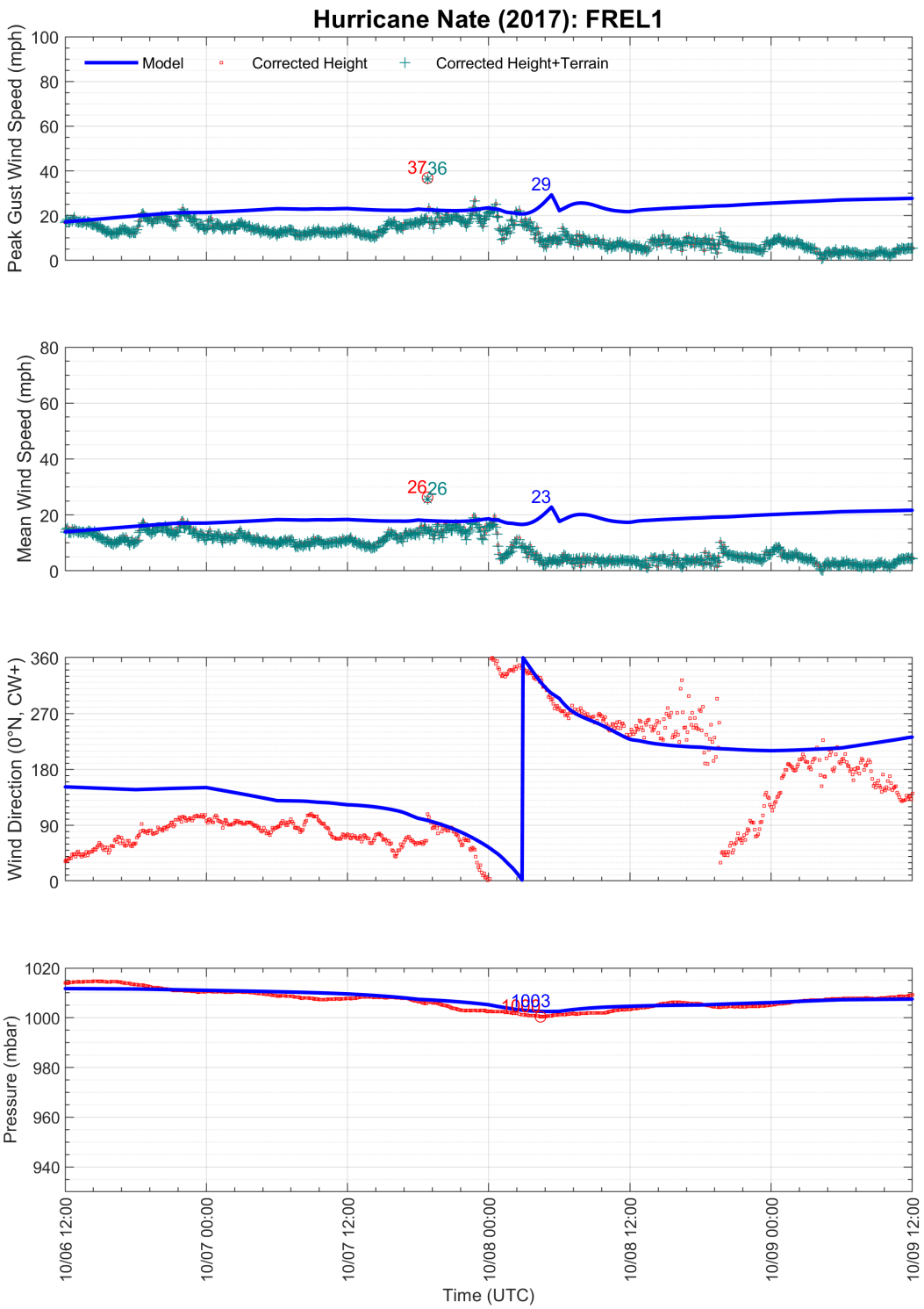
Hurricane Nate (2017): DKCM6

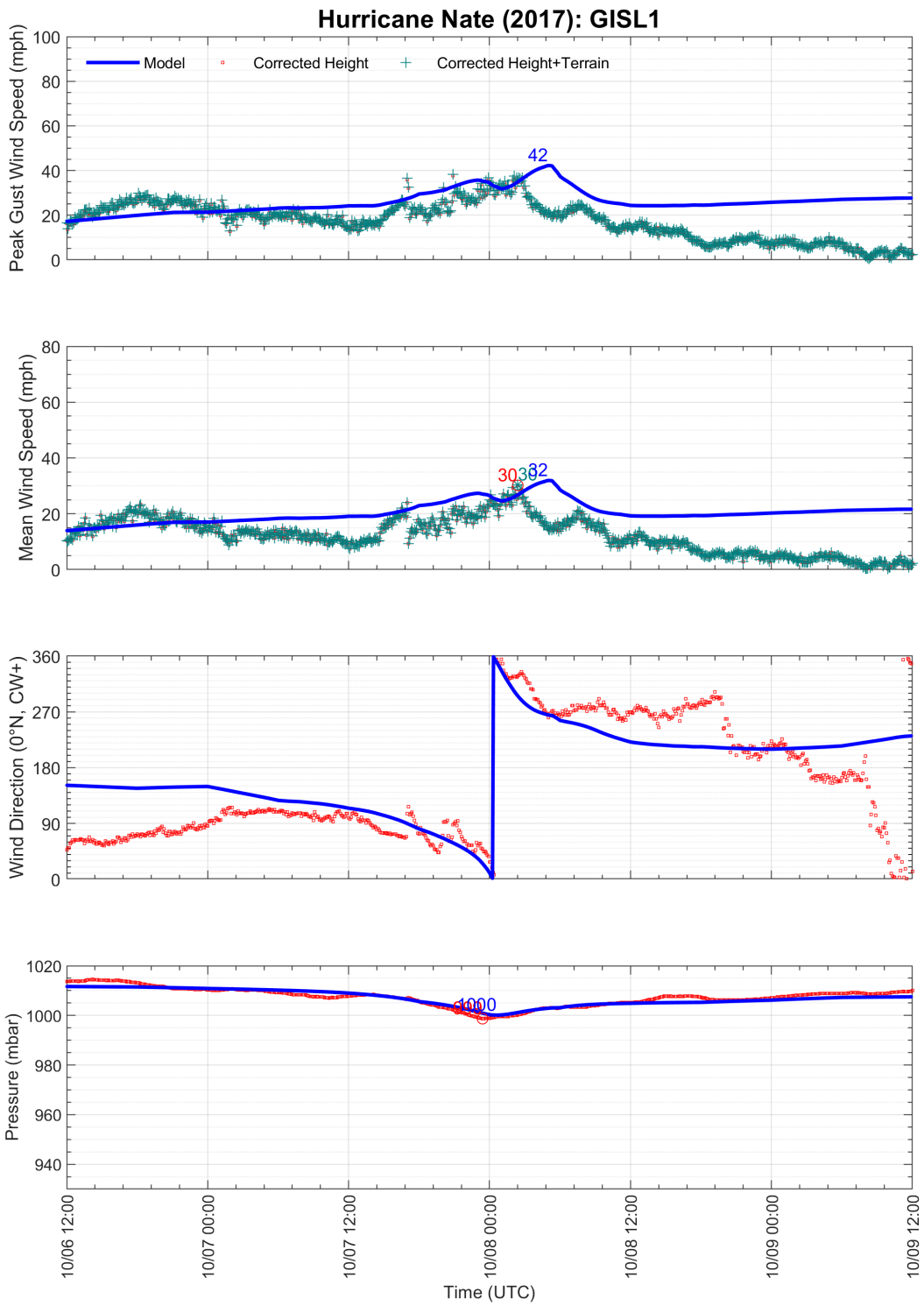


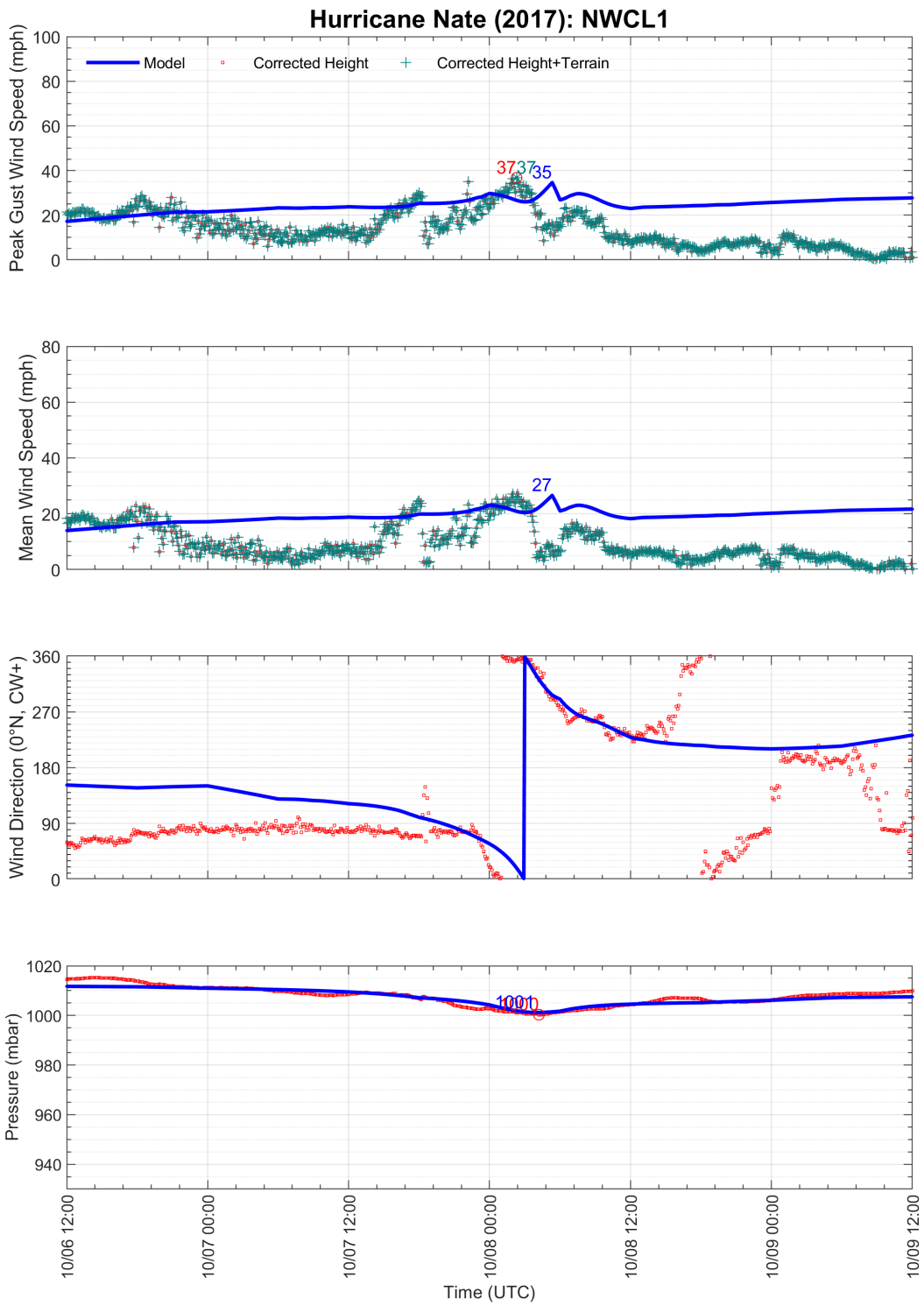


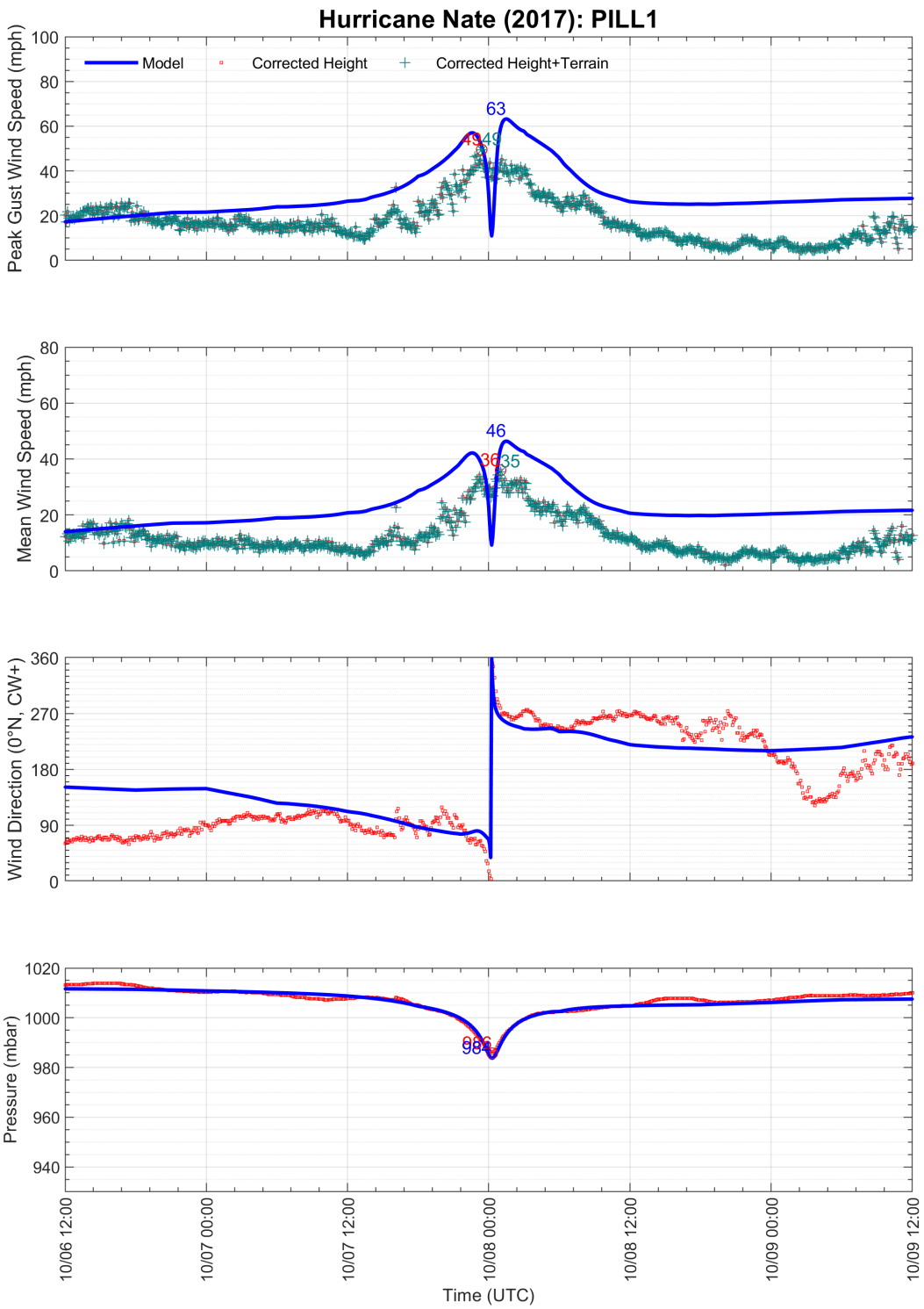
Hurricane Nate (2017): FMOA1



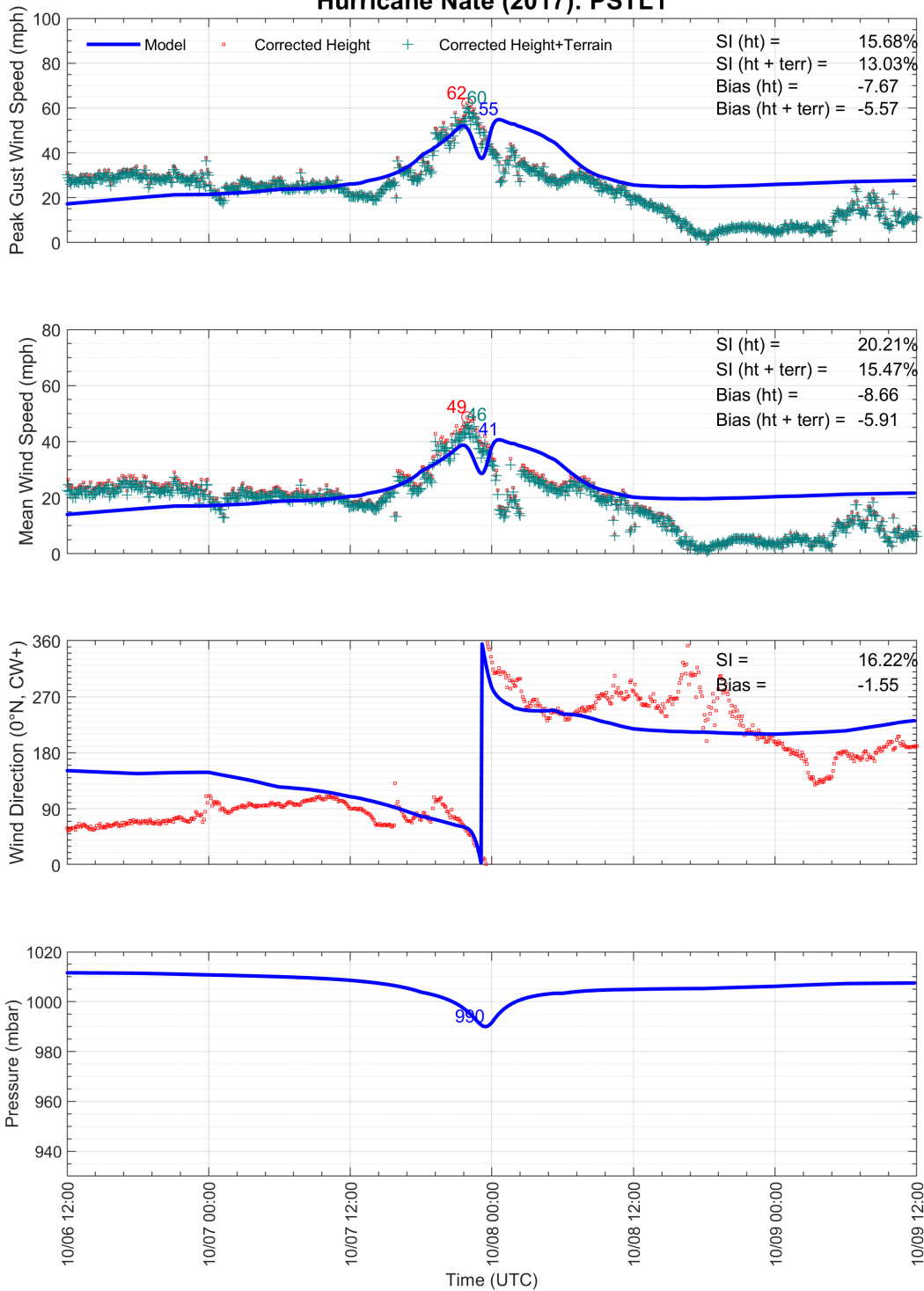




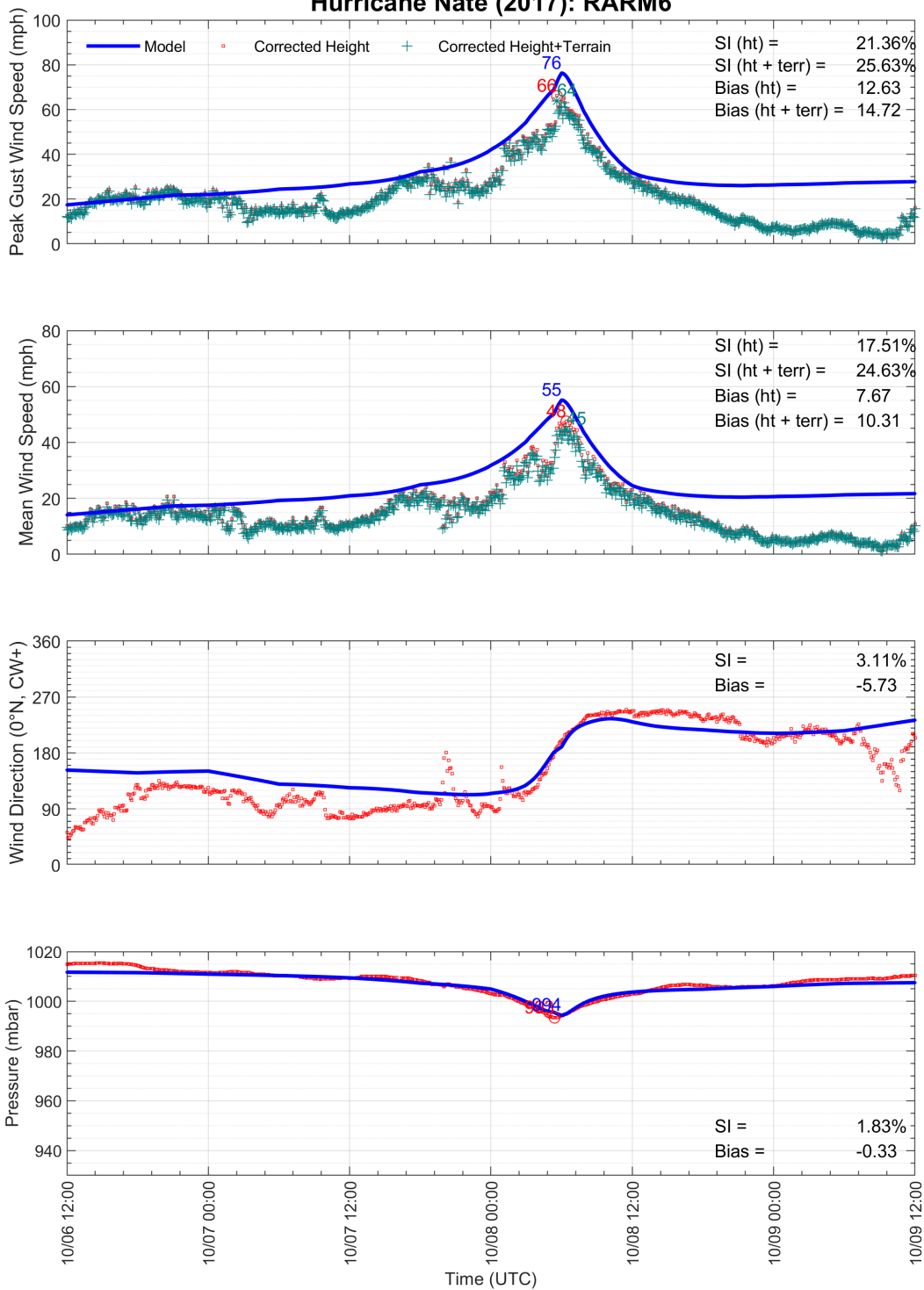


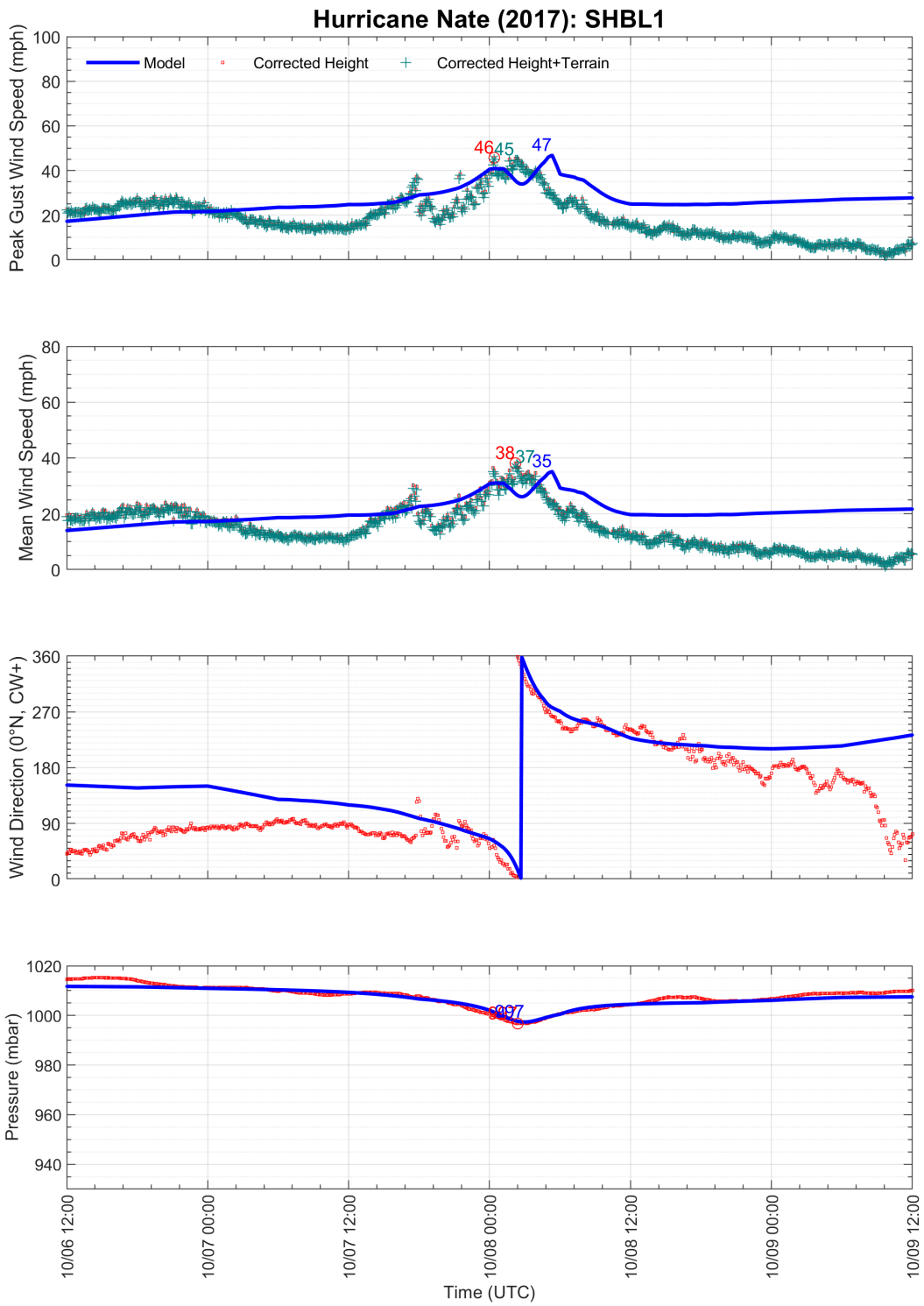


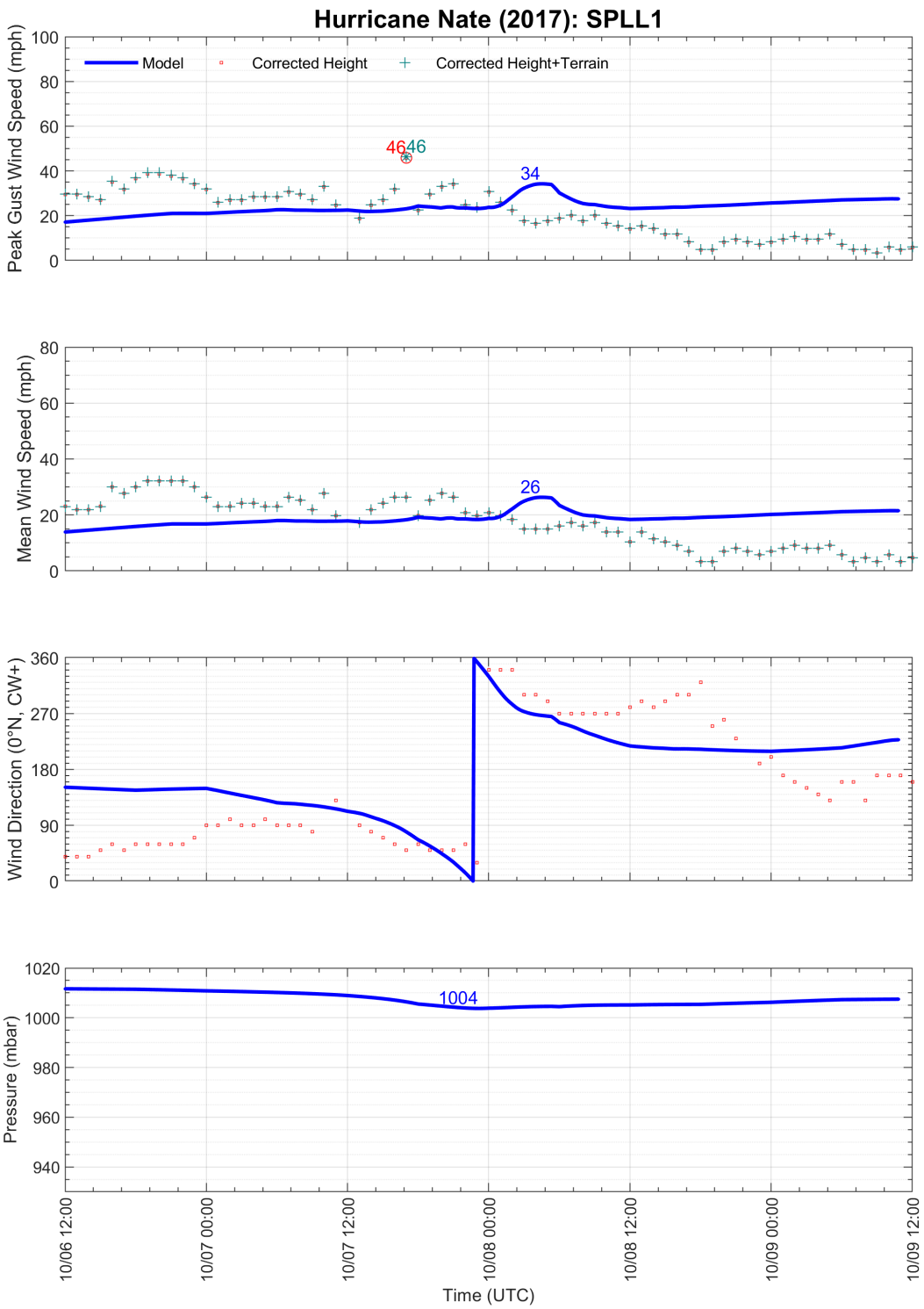
Hurricane Nate (2017): PSTL1

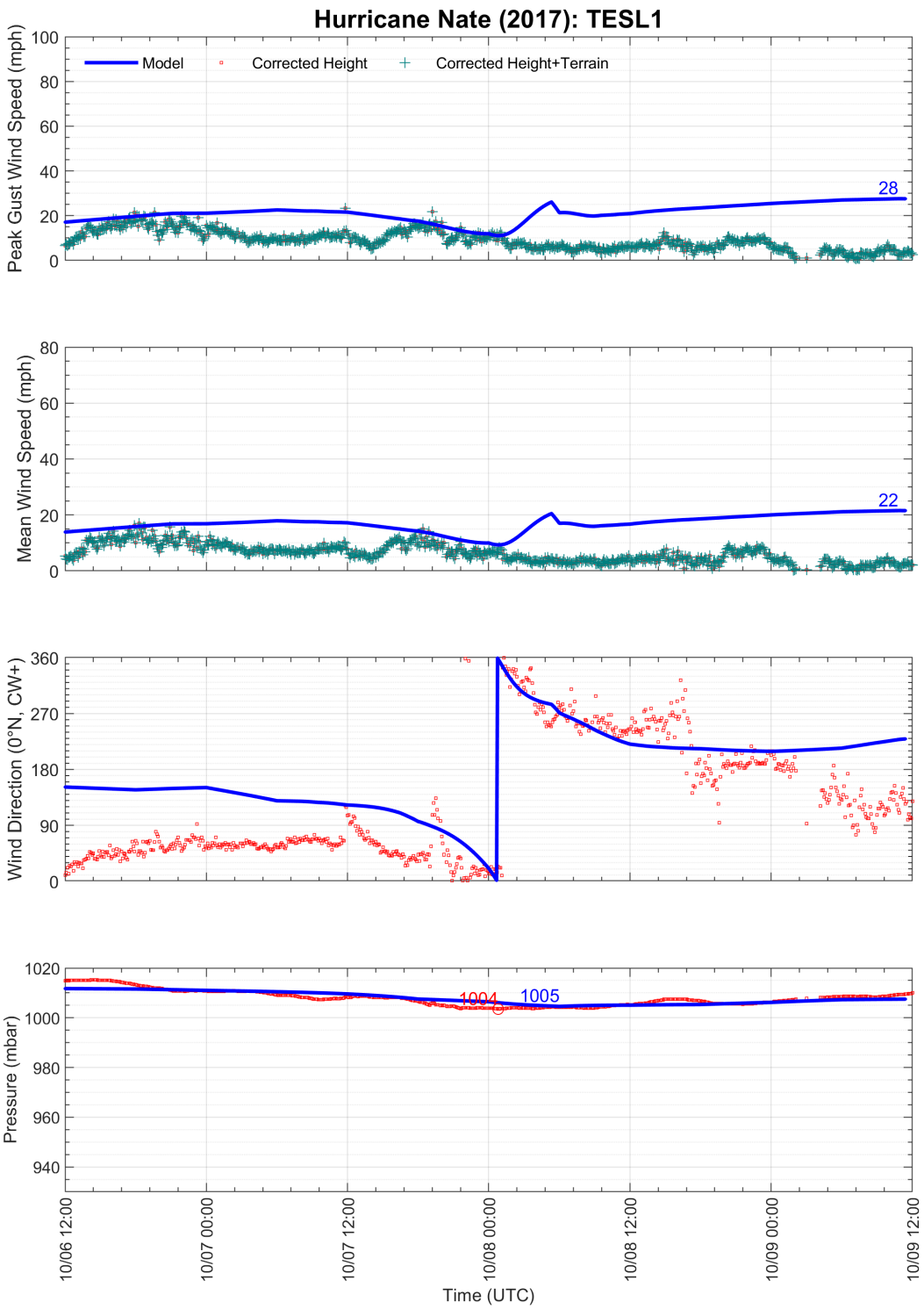


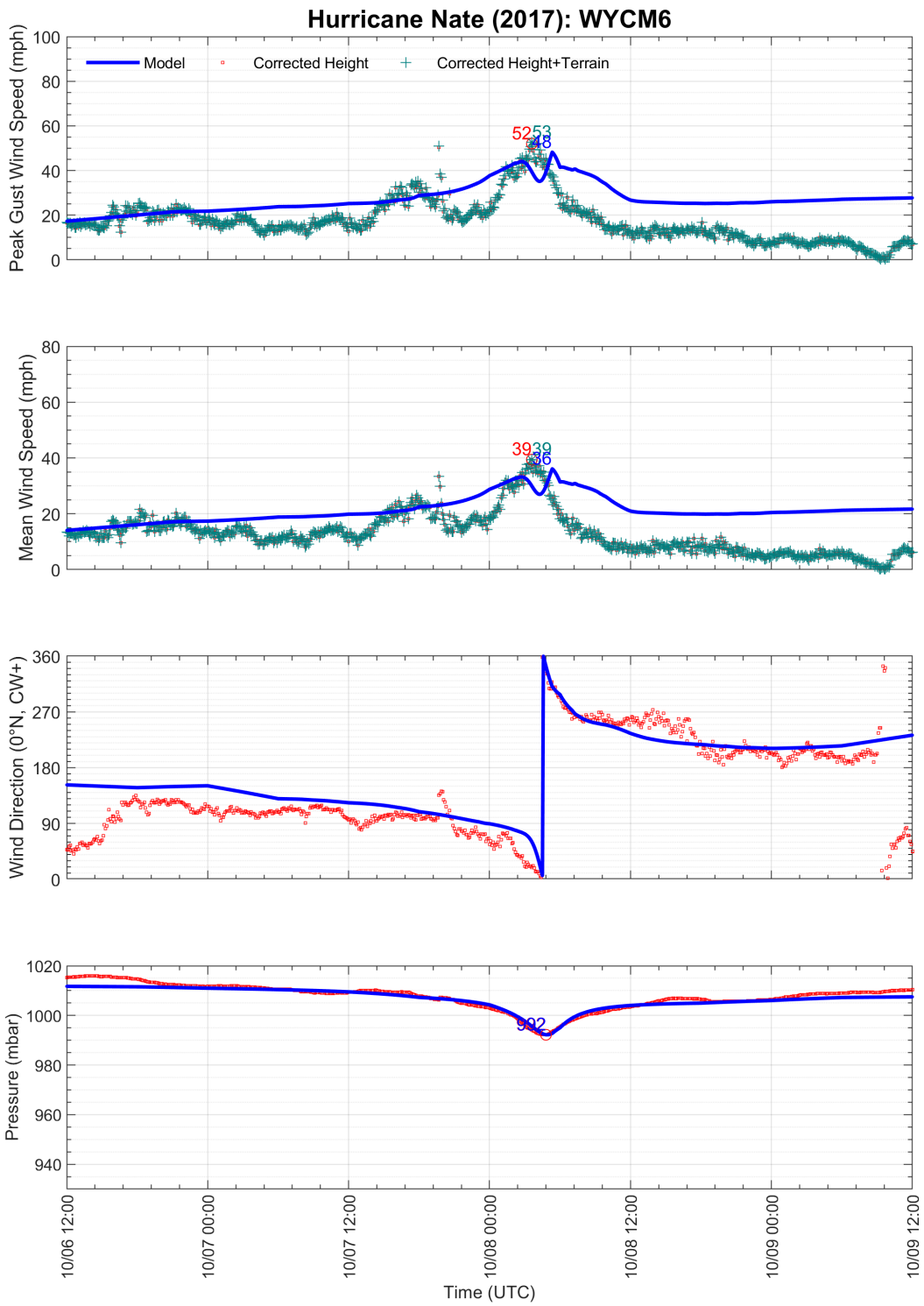
Hurricane Nate (2017): RARM6

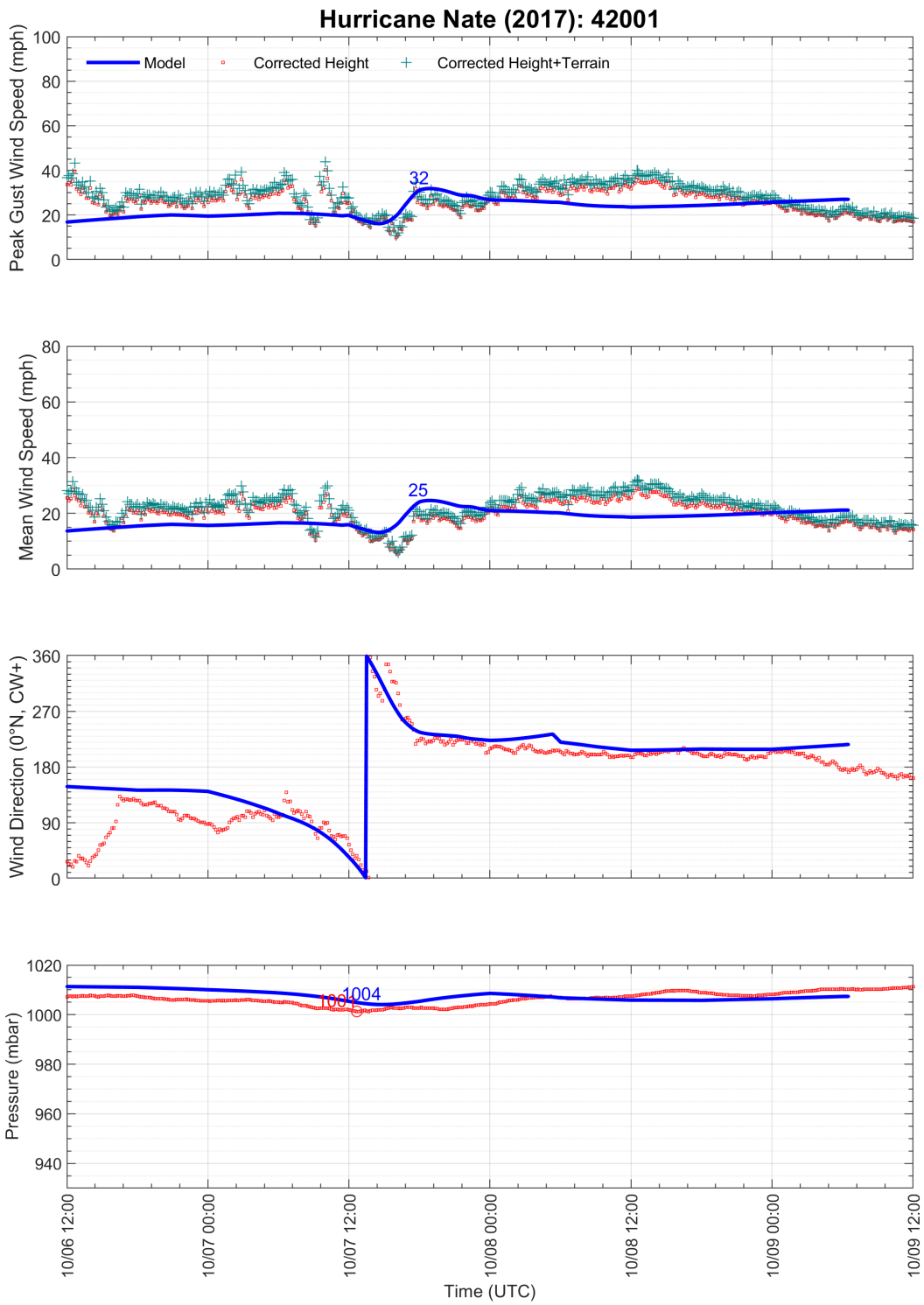




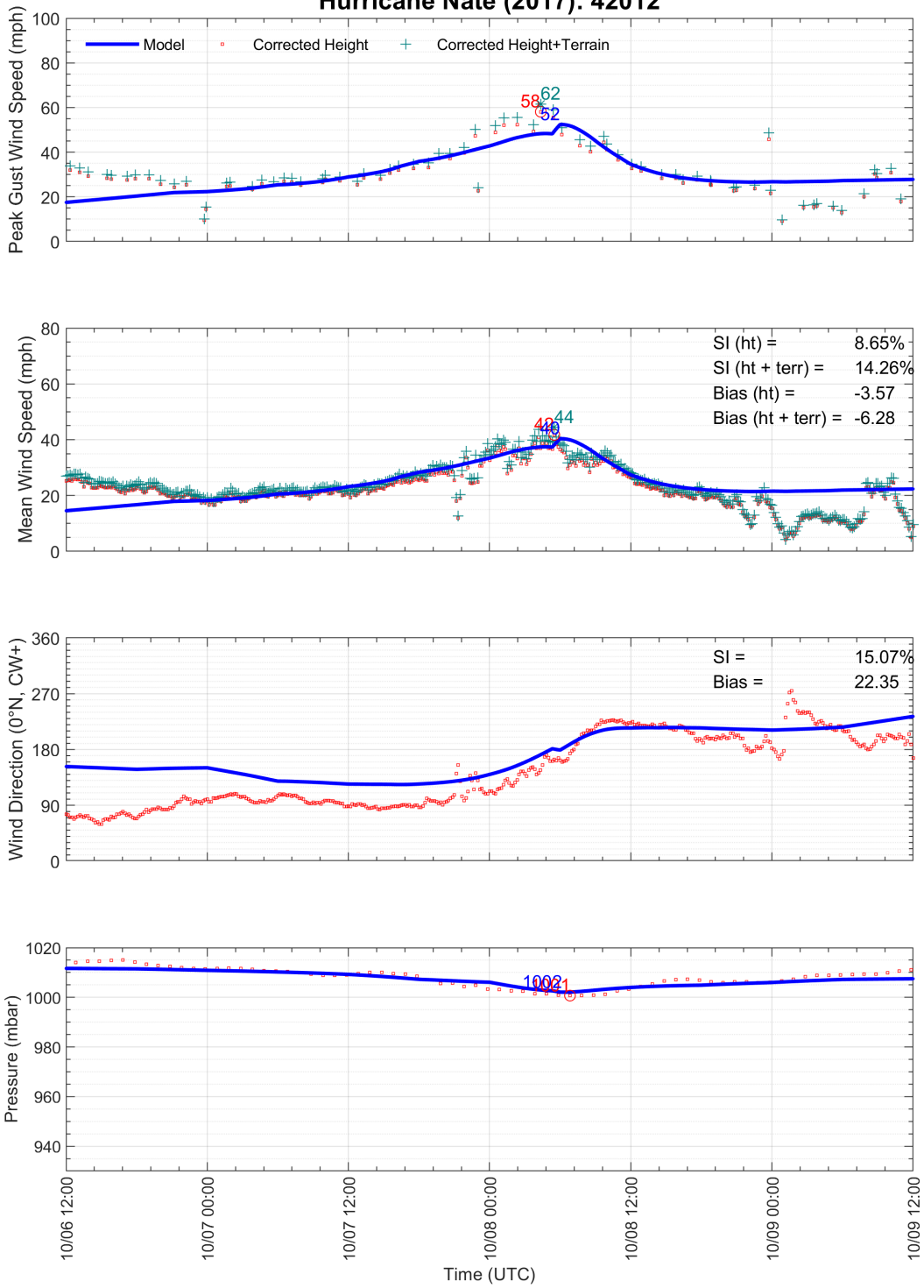




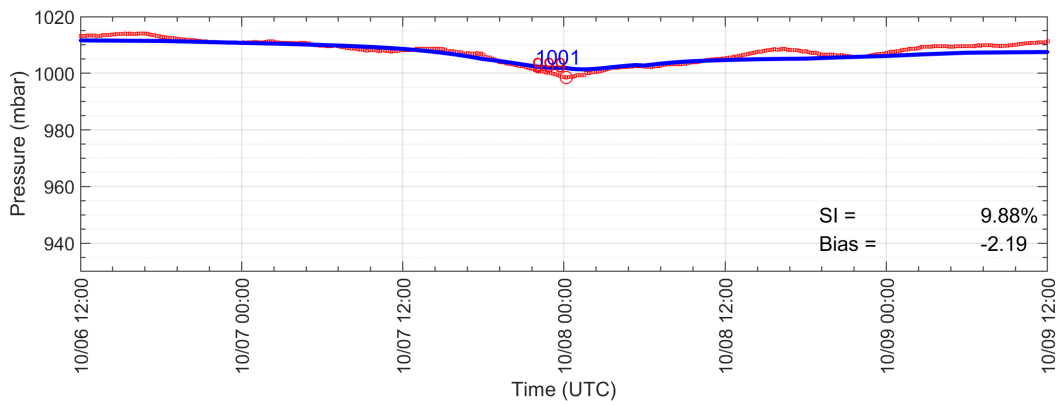
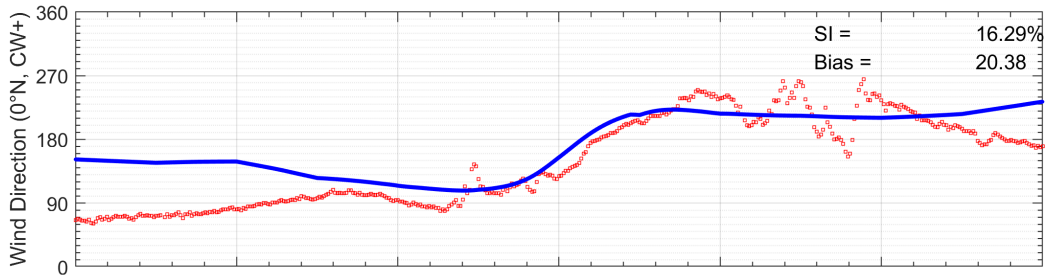
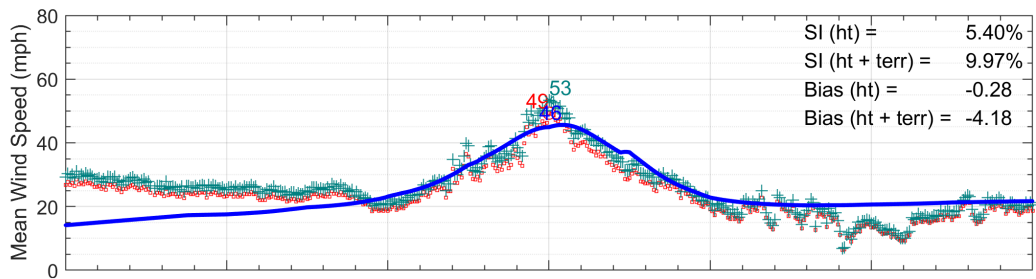
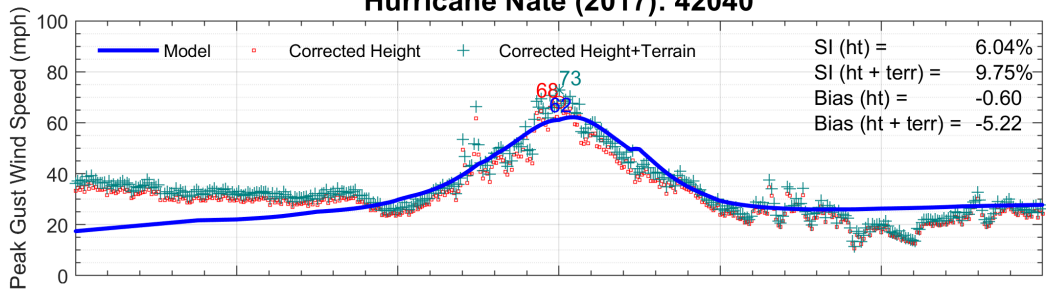


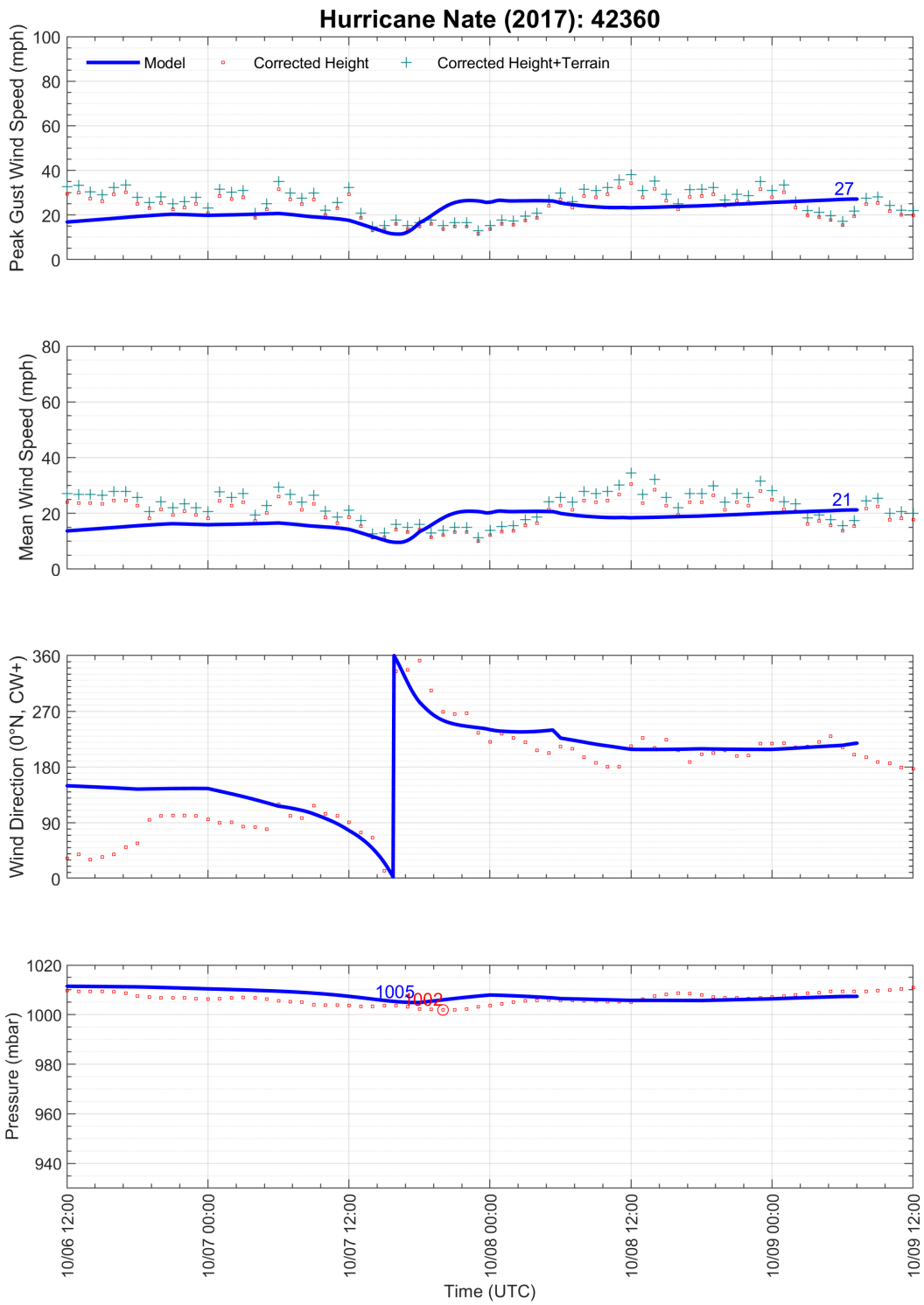


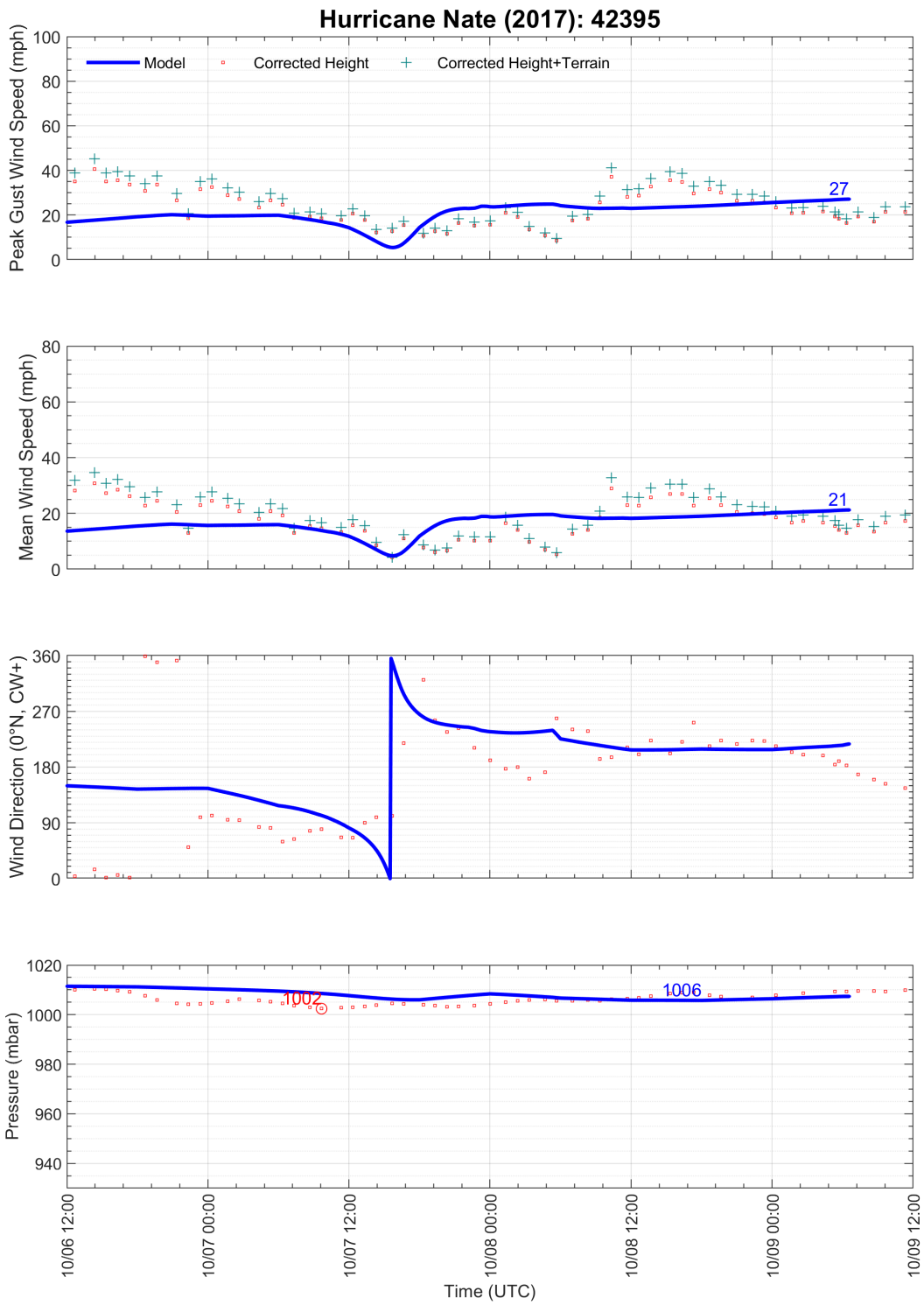
Hurricane Nate (2017): 42012



Hurricane Nate (2017): 42040







Appendix E.3 STATION DIRECTIONAL SURFACE ROUGHNESS VALUES

Station	Direction (0°N, CW+)															
	0	22.5	45	67.5	90	112.5	135	157.5	180	202.5	225	247.5	270	292.5	315	337.5
KANB	0.0300	0.0300	0.0300	0.0300	0.0300	0.0300	0.0300	0.0300	0.0300	0.0300	0.0300	0.0300	0.0300	0.0300	0.0300	0.0300
KASD	0.1130	0.0404	0.1461	0.5000	0.7058	0.4782	0.1945	0.0852	0.0406	0.1121	0.4448	0.8840	0.8157	0.7474	0.6791	0.6108
KBFM	0.0354	0.0508	0.0120	0.0099	0.0016	0.0012	0.0056	0.0266	0.1257	0.6780	0.9238	0.8111	0.6985	0.5858	0.1325	0.0208
KBHM	0.0300	0.0300	0.0300	0.0300	0.0300	0.0300	0.0300	0.0300	0.0300	0.0300	0.0300	0.0300	0.0300	0.0300	0.0300	0.0300
KBTR	0.4377	0.4178	0.3980	0.0395	0.0421	0.0776	0.0952	0.0700	0.0321	0.0223	0.0205	0.0251	0.0261	0.0739	0.3910	0.4575
KBVE	0.5333	0.5178	0.1361	0.0308	0.0263	0.0621	0.0680	0.0207	0.0047	0.0144	0.0318	0.0221	0.0225	0.0195	0.0267	0.0814
KCEW	0.6042	0.5590	0.5138	0.4686	0.4234	0.4635	0.5036	0.5437	0.4809	0.0774	0.0843	0.0735	0.1048	0.1433	0.0819	0.1263
KCHA	0.0300	0.0300	0.0300	0.0300	0.0300	0.0300	0.0300	0.0300	0.0300	0.0300	0.0300	0.0300	0.0300	0.0300	0.0300	0.0300
KDCU	0.0300	0.0300	0.0300	0.0300	0.0300	0.0300	0.0300	0.0300	0.0300	0.0300	0.0300	0.0300	0.0300	0.0300	0.0300	0.0300
KDTS	0.0755	0.1020	0.1955	0.2230	0.1583	0.1111	0.0246	0.0318	0.4051	0.5141	0.4197	0.3253	0.9999	0.9999	0.7167	0.0507
KEET	0.0300	0.0300	0.0300	0.0300	0.0300	0.0300	0.0300	0.0300	0.0300	0.0300	0.0300	0.0300	0.0300	0.0300	0.0300	0.0300
KFFC	0.2000	0.2500	0.3000	0.5000	0.4000	0.2000	0.0500	0.0300	0.1000	0.1500	0.1500	0.0800	0.0800	0.0300	0.0300	0.1500
KFTY	0.0300	0.0300	0.0300	0.0300	0.1500	0.1500	0.1500	0.0300	0.2000	0.2500	0.2000	0.2000	0.0500	0.0300	0.0300	0.0300
KGPT	0.0568	0.0599	0.0917	0.0740	0.0410	0.0100	0.0062	0.0317	0.1703	0.3689	0.5711	0.5013	0.4315	0.3617	0.2919	0.0554
KGZH	0.3109	0.2081	0.1139	0.1249	0.1359	0.0317	0.0400	0.0754	0.0452	0.0721	0.1161	0.2052	0.6000	0.5516	0.5033	0.4549
KHBG	0.1246	0.1237	0.1700	0.2162	0.2625	0.1067	0.0488	0.0290	0.0579	0.0786	0.1311	0.1254	0.2442	0.0998	0.1072	0.1576
KHKS	0.0300	0.0300	0.0300	0.0300	0.0300	0.0300	0.0300	0.0300	0.0300	0.0300	0.0300	0.0300	0.0300	0.0300	0.0300	0.0300
KHSV	0.0300	0.0300	0.0300	0.0300	0.0300	0.0300	0.0300	0.0300	0.0300	0.0300	0.0300	0.0300	0.0300	0.0300	0.0300	0.0300
KJAN	0.0300	0.0300	0.0300	0.0300	0.0300	0.0300	0.0300	0.0300	0.0300	0.0300	0.0300	0.0300	0.0300	0.0300	0.0300	0.0300
KMEI	0.0300	0.0300	0.0300	0.0300	0.0300	0.0300	0.0300	0.0300	0.0300	0.0300	0.0300	0.0300	0.0300	0.0300	0.0300	0.0300
KMGM	0.1000	0.0800	0.0300	0.0300	0.0300	0.0300	0.0300	0.0300	0.0300	0.0300	0.0300	0.0300	0.0300	0.0300	0.1000	0.1000
KMOB	0.0378	0.0265	0.0265	0.0346	0.0576	0.0203	0.0160	0.0192	0.0365	0.0365	0.0607	0.1652	0.2107	0.2561	0.2288	0.0737
KMSL	0.0300	0.0300	0.0300	0.0300	0.0300	0.0300	0.0300	0.0300	0.0300	0.0300	0.0300	0.0300	0.0300	0.0300	0.0300	0.0300
KNEW	0.0002	0.0001	0.0001	0.0001	0.0003	0.0032	0.0053	0.0072	0.0051	0.0039	0.0022	0.0008	0.0001	0.0001	0.0001	0.0001
KPNS	0.1012	0.1155	0.5000	0.5000	0.5429	0.1356	0.0167	0.0138	0.0088	0.0140	0.0310	0.0248	0.0473	0.0321	0.0598	0.0276
KPQL	0.0300	0.0300	0.0300	0.0300	0.0300	0.0300	0.0300	0.0300	0.0300	0.0300	0.0300	0.0300	0.0300	0.0300	0.0300	0.0300
KRMG	0.0300	0.0300	0.0300	0.0300	0.0300	0.0300	0.0300	0.0300	0.0300	0.0300	0.0300	0.0300	0.0300	0.0300	0.0300	0.0300
KTCL	0.0300	0.0300	0.0300	0.0300	0.0300	0.0300	0.0300	0.0300	0.0300	0.0300	0.0300	0.0300	0.0300	0.0300	0.0300	0.0300
KTOI	0.0654	0.0719	0.0900	0.1800	0.1749	0.1268	0.1002	0.1755	0.2010	0.1302	0.1275	0.1925	0.2653	0.1946	0.0763	0.0502
KTUP	0.0300	0.0300	0.0300	0.0300	0.0300	0.0300	0.0300	0.0300	0.0300	0.0300	0.0300	0.0300	0.0300	0.0300	0.0300	0.0300

Station	Direction (0°N, CW+)															
	0	22.5	45	67.5	90	112.5	135	157.5	180	202.5	225	247.5	270	292.5	315	337.5
KVPC	0.0300	0.0300	0.0300	0.0300	0.0300	0.0300	0.0300	0.0300	0.0300	0.0300	0.0300	0.0300	0.0300	0.0300	0.0300	0.0300
AMRL1	0.0000	0.0000	0.0000	0.0000	0.0000	0.0000	0.0000	0.0000	0.0000	0.0000	0.0000	0.0000	0.0000	0.0000	0.0000	0.0000
BURL1	0.0000	0.0000	0.0000	0.0000	0.0000	0.0000	0.0000	0.0000	0.0000	0.0000	0.0000	0.0000	0.0000	0.0000	0.0000	0.0000
DKCM6	0.0000	0.0000	0.0000	0.0000	0.0000	0.0000	0.0000	0.0000	0.0000	0.0000	0.0000	0.0000	0.0000	0.0000	0.0000	0.0000
EINL1	0.0000	0.0000	0.0000	0.0000	0.0000	0.0000	0.0000	0.0000	0.0000	0.0000	0.0000	0.0000	0.0000	0.0000	0.0000	0.0000
FMOA1	0.0000	0.0000	0.0000	0.0000	0.0000	0.0000	0.0000	0.0000	0.0000	0.0000	0.0000	0.0000	0.0000	0.0000	0.0000	0.0000
FREL1	0.0000	0.0000	0.0000	0.0000	0.0000	0.0000	0.0000	0.0000	0.0000	0.0000	0.0000	0.0000	0.0000	0.0000	0.0000	0.0000
GISL1	0.0000	0.0000	0.0000	0.0000	0.0000	0.0000	0.0000	0.0000	0.0000	0.0000	0.0000	0.0000	0.0000	0.0000	0.0000	0.0000
NWCL1	0.0000	0.0000	0.0000	0.0000	0.0000	0.0000	0.0000	0.0000	0.0000	0.0000	0.0000	0.0000	0.0000	0.0000	0.0000	0.0000
PILL1	0.0000	0.0000	0.0000	0.0000	0.0000	0.0000	0.0000	0.0000	0.0000	0.0000	0.0000	0.0000	0.0000	0.0000	0.0000	0.0000
PSTL1	0.0000	0.0000	0.0000	0.0000	0.0000	0.0000	0.0000	0.0000	0.0000	0.0000	0.0000	0.0000	0.0000	0.0000	0.0000	0.0000
RARM6	0.0000	0.0000	0.0000	0.0000	0.0000	0.0000	0.0000	0.0000	0.0000	0.0000	0.0000	0.0000	0.0000	0.0000	0.0000	0.0000
SHBL1	0.0000	0.0000	0.0000	0.0000	0.0000	0.0000	0.0000	0.0000	0.0000	0.0000	0.0000	0.0000	0.0000	0.0000	0.0000	0.0000
SPLL1	0.0000	0.0000	0.0000	0.0000	0.0000	0.0000	0.0000	0.0000	0.0000	0.0000	0.0000	0.0000	0.0000	0.0000	0.0000	0.0000
TESL1	0.0000	0.0000	0.0000	0.0000	0.0000	0.0000	0.0000	0.0000	0.0000	0.0000	0.0000	0.0000	0.0000	0.0000	0.0000	0.0000
WYCM6	0.0000	0.0000	0.0000	0.0000	0.0000	0.0000	0.0000	0.0000	0.0000	0.0000	0.0000	0.0000	0.0000	0.0000	0.0000	0.0000
42001	0.0000	0.0000	0.0000	0.0000	0.0000	0.0000	0.0000	0.0000	0.0000	0.0000	0.0000	0.0000	0.0000	0.0000	0.0000	0.0000
42012	0.0000	0.0000	0.0000	0.0000	0.0000	0.0000	0.0000	0.0000	0.0000	0.0000	0.0000	0.0000	0.0000	0.0000	0.0000	0.0000
42040	0.0000	0.0000	0.0000	0.0000	0.0000	0.0000	0.0000	0.0000	0.0000	0.0000	0.0000	0.0000	0.0000	0.0000	0.0000	0.0000
42360	0.0000	0.0000	0.0000	0.0000	0.0000	0.0000	0.0000	0.0000	0.0000	0.0000	0.0000	0.0000	0.0000	0.0000	0.0000	0.0000
42395	0.0000	0.0000	0.0000	0.0000	0.0000	0.0000	0.0000	0.0000	0.0000	0.0000	0.0000	0.0000	0.0000	0.0000	0.0000	0.0000